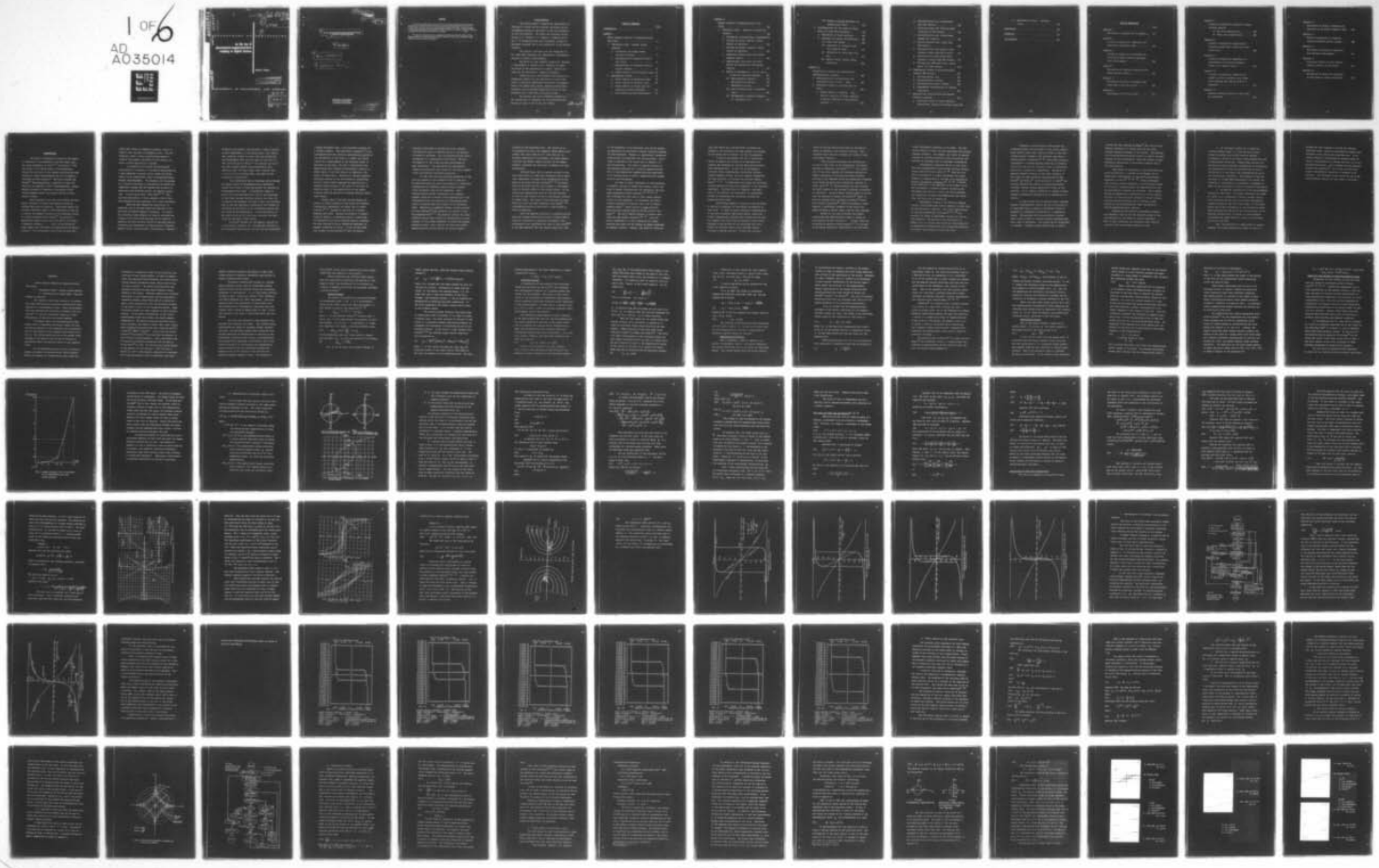
AD-A035 014 CALIFORNIA UNIV LOS ANGELES DEPT OF ENGINEERING F/G 20/2
ON THE USE OF PIEZOELECTRIC-MAGNETOSTRICTIVE COUPLING IN DIGITA--ETC(U)
AUG 62 A A BORSEI NONR-233(52)
UNCLASSIFIED UCLA62-37 NL

1 OF 6
AD
A035014



ADA035014

Code 688A
cm
689B

AUGUST 1962

DEPARTMENT OF ENGINEERING

on the use of piezoelectric-magnetostrictive coupling in digital devices

ARTHUR A. BORSEI

REPORT NO. 62-37

DISTRIBUTION STATEMENT A
Approved for public release;
Distribution Unlimited

UNIVERSITY OF CALIFORNIA, LOS ANGELES

DDC
RECEIVED
JAN 31 1977
A

(14) UCLA
Report No. 62-37
Aug 62
(11)
(12) 524 p.

(6) ON THE USE OF PIEZOELECTRIC-MAGNETOSTRICTIVE COUPLING IN DIGITAL DEVICES.

(10) Arthur A. Borsei

(15) Nonr-233(52)

(9) Doctoral thesis,

DEPARTMENT OF ENGINEERING
UNIVERSITY OF CALIFORNIA
LOS ANGELES 24, CALIFORNIA

DISTRIBUTION STATEMENT A
Approved for public release;
Distribution Unlimited

072260

FOREWORD

The research described in this report, *On the Use of Piezoelectric-Magnetostrictive Coupling in Digital Devices*, by Arthur A. Borsei, was carried out under the technical direction of G. Estrin, C. T. Leondes and M. Aoki and is part of the continuing program in Digital Technology. This report is based on a dissertation submitted in partial satisfaction of the requirements for the degree of Doctor of Philosophy in Engineering at the University of California, Los Angeles.

The project is conducted under the sponsorship of the Department of the Navy, Office of Naval Research and the Atomic Energy Commission, Division of Research. This report is submitted in partial fulfillment of Contract Number Nonr-233(52).

ACKNOWLEDGMENT

The writer wishes to express his appreciation to Professor G. Estrin for his constant assistance and encouragement during all the phases of the work presented in this dissertation. The advice and criticism of Professors R. S. Elliott, T. A. Rogers, I. Rudnick and of Mr. C. R. Viswanathan have been invaluable in many experimental problems and in the preparation of the written material.

The skillful assistance and the suggestions of Mr. James Bibb throughout the experimental investigation deserves a grateful acknowledgment.

The writer is also indebted to Messrs J. Distaso, H. Reichenbach, E. Russell and P. Schaefer for their assistance in the preparation of digital computer programs and the operation of computing equipment.

Thanks are due to the National Cash Register Co. (Hawthorne, Calif.) for the deposition of part of the films, to the Space Technology Laboratories (El Segundo, Calif.) for making their analog computing installation available, and to the UCLA Computing Facility for the extensive use of their data processing system.

The delicate and expert machining required in the construction of equipment for the preparating and testing of films is due to Mr. Eric Lehman.

Letter on file

A

TABLE OF CONTENTS

	Page
INTRODUCTION.	1
CHAPTER I	
Static magnetic behavior of magnetostrictive thin films.	15
1. Theoretical model - General energy equation.	15
a. Assumptions for simple model, existing solutions.	15
b. Determination of hysteresis loop by root locus.	31
c. Determination of hysteresis loop by digital computer.	54
d. Stress effects on film critical curve	66
2. Experimental studies.	74
a. Stress effects on hysteresis loops.	76
b. Stress effects on critical curve. .	104
c. Stress effects on domain wall configurations (Bitter patterns) . . .	116
d. Film magnetostriction measurements.	133

CHAPTER II

Dynamic behavior of magnetostrictive thin films. 136

1. Theoretical model - Equation of Landau and Lifshitz 136

a. Preliminary considerations, assumptions 136

b. Solution by analog computer, stress effects on switching 146

c. Solution by digital computer, stress effects on switching 164

d. Comparison between analog and digital computer results 166

e. Computational flow charts for integration and plotting of film dynamic response 169

f. Effects of parameters α , β , δ , ϕ_o, λ. on the film switching response. . . 180

(1) Film switching response 180

Non-destructive pulsing 180

Destructive pulsing 181

(2) Inverse peaking time vs. switching field 228

(3) Ferromagnetic resonance frequency vs. switching field 237

(4) Dynamic switching threshold vs. perpendicular field. 247

2. Instrumentation for the study of stress effects on thin film switching. 255

a. Description of instrumentation. . . . 256

b. Operation and design considerations . 266

(1) Strip line design. 269

(2) Estimation of available strip line magnetic field. 274

(3) Estimation of film pickup voltage. 277

(4) Mercury relay, coaxial cables, connectors 280

CHAPTER III

Piezoelectric crystals and piezoelectric-magnetostrictive coupling 286

1. Characteristics of piezoelectric and electrostrictive crystals. Table 287

2. Theoretical models of piezoelectric behavior 289

a. General method of analysis, piezoelectric equations of state, equation of motion, magnitude of piezoelectric constant d 289

b. Electrostrictive bar, longitudinal mode (DC strains) 292
c. Electrostrictive bar, thickness mode (transient and DC strains). 294
d. Electrostrictive bar, bending mode, bimorph (DC strains). 301
e. Electrostrictive disc, radial mode (DC strains). 306
f. Electrostrictive thin walled closed cylinder, radial mode (DC strains). . 310
g. Electrostrictive thin walled split cylinder, flexural mode (DC strains). 312
h. Piezoelectric ADP plate X-cut, quartz plate Y-cut (DC strains). 317
3. Experimental studies on electrostrictive ceramics (DC strains) 321
a. Electrostrictive disc 321
b. Electrostrictive cylinder 322
c. Electrostrictive split cylinder . . . 322
d. Experimental determination of coupling coefficient 327
4. Piezoelectric (electrostrictive)-magnetostrictive coupling. 329
a. Theoretical model of static behavior-Piezoelectric uniaxial & isotropic stress 329

b. Experimental studies. Isotropic stress. 334

CONCLUSIONS 339

APPENDICES 351

BIBLIOGRAPHY. 442

LIST OF APPENDICES

	Page
Appendix 1	
Derivation of equation (25) in Chapter I	351
Appendix 2	
Listing of program for computation and plotting of hysteresis loops.	352
Appendix 3	
Listing of program for computation and plotting of static critical switching curve with example.	358
Appendix 4	
Description of substrate bending jig for Bitter pattern studies.	363
Appendix 5	
Description of device for bending film substrates in B-H loop tester	366
Appendix 6	
Description of B-H loop tester.	371

Appendix 7

Listing of program for solution of Landau-Lifshitz equation

a) One curve computer plot. 379

b) Three curve computer plot. 384

Appendix 8

Listing of program for computation of "inverse peaking time" (three curve computer plot). 388

Appendix 9

Listing of program for computation of ferromagnetic oscillation frequency (three curve computer plot). 392

Appendix 10

Listing of program for computation of dynamic critical switching curve (three curve computer plot with ϕ_o or δ as a parameter. 396

Appendix 11

Absolute chemical analysis of thin films by colorimetry 403

Appendix 12

Description of probe to determine the direction of the earth's magnetic field 406

Appendix 13

Method of preparation of magnetite colloid for Bitter pattern studies. . . . 408

Appendix 14

Description of Tolansky's method for film thickness measurements. 410

Appendix 15

Statistical errors in X-ray spectrochemical analysis of thin films. 414

Appendix 16

Description of system for production of thin films by vacuum evaporation . . 438

INTRODUCTION

The effect of mechanical stresses on the magnetic properties of ferromagnetics have been known since the early experiments of Joule[1, 2] and Villari.[3] With the advent of the domain theory of ferromagnetism, during the early part of the century, much work has been carried out toward understanding the role of magnetostriction in bulk materials.[4] The book by Becker and Doring,[23] "Ferromagnetismus", published in 1939, and that of R. M. Bozorth in 1951, "Ferromagnetism", contain detailed accounts of theories of macroscopic interactions between elastic and magnetic forces in ferromagnetic bodies.

These theories do not take into account the reciprocal influence of elastic and magnetic actions in defining the state of materials. They merely define the internal "effective field" by differentiation of the sum of elastic and magnetic energies in an elementary volume. As stated by William Fuller Brown,[77] "occasionally a magnetician becomes uneasy about the effects of strains on magnetic formulas, ... also, an elastician becomes uneasy about the effect of magnetization on elastic formulas." On a microscopic scale it may be said that

nature will deform an elementary magnetic crystal if doing so will decrease its energetic level. This deformation causes a stress redistribution which influences the magnetic anisotropy of the crystal, etc. until a stable equilibrium is reached.

As observed by Brillouin[5] and Sokolnikoff[6] the presence of a magnetic or electrical polarization in a body subjected to elastic forces causes the stress tensors to be asymmetrical, while the magnetostriction becomes shape-dependent. The complexity of the problem in a practical situation is increased by the effects of temperature changes and the unpredictable presence of impurities with different elastic and magnetic properties. In more recent years (1953-1957)[77, 26] more accurate descriptions of elasto-magnetic effects have been proposed but many questions still remain unanswered.

Among the many engineering applications of magnetism, one of the most recent and important is in the field of digital computer technology. The search for two-stable state elements for digital switching and storage is far from being exhausted and the field of magnetics has been the most fertile in providing devices satisfying the requirements of modern digital computers. Magnetic cores, ferrite plates, "transfluxors", "biaxes",

"twistors" and magnetic rods provided a range of devices to meet requirements of low driving power, fast switching, acceptable signal to noise ratio and reliability. The ferromagnetic thin film was added to this list in 1955, with the work of Blois,[21] who proposed the use of this new bistable element which potentially could switch at least 100 times faster than a ferrite core, required much less driving power, and might be more economical to manufacture.

The considerable body of knowledge gained through the domain theory of ferromagnetism was immediately brought into action to study and predict the behavior of ferromagnetic thin films. A considerable number of papers have been published since 1955 on the properties of thin films and many existing theories have been used to describe the phenomena involved in thin film switching. Some of the most important contributions are referred to constantly in the course of the forthcoming chapters and are listed in the bibliography. A brief perspective of the state of the art is given here to present the motivation for the work in this thesis.

As Blois[21] pointed out the magnetic reversal of a film having a thickness of a few thousand angstroms is not affected by eddy currents and the film has essentially

a square hysteresis loop, a very desirable property for a bistable element. From theoretical arguments[12] it may be predicted that the structure energetically possible at film thicknesses of the order of a domain size should consist of a single domain in the direction normal to the plane of the film. For such a configuration the magnetization will reverse by simultaneous rotation of atomic spins, a very fast process as compared to the motion of domain walls. Because of a uniaxial magnetic anisotropy induced in the film during its preparation, the most obvious model suggested by experience was a magnetic moment pivoted at the center of the film, of magnitude equal to the magnetization of the sample, oriented along the direction of minimum intrinsic anisotropy energy.

Energy terms to describe the macroscopic behavior of a film according to this model were obtained from previous expressions for single iron or nickel crystals,[10, 11] applied to the case of a uniaxial magnetic anisotropy. Because the presence of magnetostrictive effects, as mentioned earlier, complicated the theoretical and device problems greatly, attention has been focussed on alloys minimizing dependence of magnetic properties on stress. It was already known from studies of bulk materials[10] that the magneto-

striction coefficient of nickel-iron alloys changes from positive values to negative values as the percent of nickel is increased. The zero magnetostriction point corresponds to a composition of 81% nickel, 19% iron. The behavior of thin films has been investigated by many researchers. The theoretical and experimental studies have generally been divided in two parts, pseudo-static and high-speed switching properties.

In the first case the switching properties of the film are studied at low frequencies (60 to 2500 cps). By differentiating the total free energy for a particular configuration of externally applied fields a pseudo-static hysteresis loop can be determined. These external fields include a switching, low frequency magnetic field and a constant field perpendicular to the alternating field, the direction of easy magnetization being at a preset angle with respect to the switching field. Analytical or graphical methods already existing for bulk materials[10] were modified and applied to thin film magnetization.[8, 9] The graphical methods are rather laborious because they consist of superposition of polar diagrams of free energy components to obtain the minimum energetic states. Also, they do not take into account magnetostriction and the effects of initial angular

position of the anisotropy axis. The results of an investigation to find a new graphical method which could predict the static behavior of a thin film for all possible combinations of parameters, including magnetostriction and initial angular position of the magnetization, constitute the first part of Chapter I of this dissertation.

Although domain walls in planes parallel to the film cannot exist in films with thicknesses below domain size, observation of domain walls perpendicular to the plane of the film have been predicted[51, 52] and widely observed by Bitter patterns and by means of instruments based on the Kerr effect or the Faraday effect. At low frequencies magnetization reversal has been observed to occur by wall motion and not by simultaneous rotation of atomic spins. The value of field necessary to cause motion of a wall has been determined from theory[51, 52] and experiment and have been found to agree within an order of magnitude.

Since the magnetic properties of magnetostrictive films are strongly affected by internal stresses (which cannot be controlled or predicted accurately) a few investigators have considered the study of such films.[27,47] It has been observed[5] that the coercive force of a film

or the squareness of its hysteresis loop may be changed by application of anisotropic stresses induced by bending the film substrate. However, no quantitative correlation between model and experiment has been performed. Such a study is reported in the second part of Chapter I of this dissertation. The effect of applied stresses on the switching threshold of a positive magnetostriction film is investigated and compared with the predictions of an existing model in which a magnetostriction energy term has been introduced.

In order to obtain information on the mechanisms of magnetic reversal by domain wall motion, visual displays of domain configurations are obtained by the well-known technique of Bitter patterns.[10, 42, 46, 47] This technique has been used to study domain configurations in bulk materials, to investigate the metallurgical properties of special steels and to display magnetic marks.[4] Stress effects in <u>bulk</u> materials have also been studied using the Bitter pattern technique.[42] The use of Bitter patterns to observe thin films has been highly successful.[46, 47] since the surface conditions of a film evaporated on a glass substrate are ideal for the display of domain boundaries by magnetic colloids. However, the effect of stress on

thin film domain wall configurations is however neglected in the literature and some studies are included in the second part of Chapter I of this dissertation.

In many investigations the use of theoretical models to predict the outcome of an experiment presupposes the knowledge of constant which must be determined experimentally. In the case of non-magnetostrictive films, magnetization, anisotropy constant, dynamic damping constant, and also chemical composition and film thickness are obtained by auxiliary experiments.[6, 7, 41] In magnetostrictive films the anisotropy constant measured by the usual technique[7] is not obviously applicable. Therefore Part 2 of Chapter I includes a study of the validity and limitations of conventional methods of determining the anisotropy constant for magnetostrictive films.

Insufficient emphasis is placed in the literature on the use of computers to investigate the behavior of thin films. In order to permit extensive experimentation on the multi-parameter theoretical models, analog and digital computational programs were constructed and used. For example, thin film critical switching curves corresponding to any position of the anisotropy axis with respect to switching field can be obtained readily utilizing a digital computer. Closed form solutions

cannot be derived analytically owing to the implicit nature of parameters and variables involved. This situation holds even more strongly in studies of thin film dynamic behavior.

After having investigated the switching properties of thin films at low frequencies, the dynamic behavior is generally considered.[5, 6, 7] This second part of the study examines the switching mechanism at higher frequencies of driving field with attention directed to the behavior during and immediately following state change resulting from simultaneous reversal of atomic spins.[29, 30] Existing models for bulk material are again adapted to the uniaxial anisotropy encountered in thin films. The most widely accepted model is derived from the equation of Landau and Lifshitz[18] (1935) or from its modified form, proposed by Gilbert[19] (1955). More recently Harrington[80] (1958) has proposed a model based on a variational treatment of the total free energy in which a kinetic energy term has been included.

Because of its wide acceptance and general verification the Landau-Lifshitz model is chosen for investigation in this dissertation. A stress term, not considered in previous investigations,[6, 7] is included in the energy expression substituted in the non-linear

scalar differential equations of the model. The predicted effects of stress are then determined from digital computer solutions. For example, the effect of applied stresses on switching threshold under any possible combination of parameters may be thoroughly investigated.

Ferromagnetic resonance effects in thin films have been experimentally observed when external driving forces cause the film to switch.[6, 61] When the film does not switch but is simply "disturbed" the output signal in a sensing wire is too weak to be observed by present instrumental techniques.[41, 61, 62] A theoretical prediction of the magnitude of the signal and of the ferromagnetic resonant frequency excited by the disturbing field pulse as stress and other parameters are changed has not been previously reported and constitutes the first part of Chapter II.

Experimental studies of the effect of applied stresses on the high-speed dynamic behavior of films have not been previously reported. Only minor modifications of existing experimental techniques[61, 62, 70] are necessary to design an experiment suitable for such an investigation. The purpose of the second part of Chapter II is to discuss the design and construction of an experimental configuration for studying the effect of anisotropic and isotropic stresses on films.

Attention is now directed to the methods for producing stresses and the type of stress which results. Prior stress studies have induced a strain in the film through surface coupling to the substrate upon which a bending moment is impressed.[5, 50] With proper mechanical arrangements a constant bending moment may be obtained across the film and the resulting stress is anisotropic and can be a tension or a compression. The effect of applied isotropic stresses on the static behavior of thin films has been considered theoretically by MacDonald[25] and Blades.[27] More recently D. O. Smith[81] has actually observed the effects of temperature-induced isotropic stresses during deposition of films by evaporation. It is, however, difficult to control a stress induced by mechanical deformation or by temperature variation.

A closer control may be obtained from a coupling between a piezoelectric crystal and the film because it is relatively easy to control a polarizing voltage as compared to a mechanical deformation or a temperature change. Piezoelectric and electrostrictive crystals offer a wide variety of available strains depending upon their mode of excitation. The strains may be alternating or constant. Coupling of pure nickel films to quartz

crystals has been reported by Bömmel[76] who excited ferromagnetic resonance in a nickel film from the piezoelectric resonant frequency of the crystal. The specific use of electrically-polarized crystals to induce isotropic stresses in thin ferromagnetic films had however not been previously reported and is discussed in Chapter III of this dissertation.

Description of piezoelectric and electrostrictive modes and materials is carried out in Chapter III together with a presentation of applicable piezoelectric equations of state.[89, 90, 91, 92] Strains obtainable from selected standard geometries are derived and studies of the actual coupling between the magnetostrictive and the piezoelectric elements are described. These studies include an experimental investigation of surface characteristics of polycrystalline elements of Barium Titanate and Lead Zirconate Titanate and of isotropic stress effects on thin film hysteresis loops through piezoelectric-magnetostrictive coupling.

Fundamental and auxiliary experimental methods and components required for the different phases of the investigation are the object of several appendices. Most of these techniques are standard in this field of research, with the possible exception of two:

1. An instrument capable of: a) imposing a constant bending moment to a film substrate placed inside two pickup coils at 90° from one another; b) applying a DC and an AC fields along perpendicular and interchangeable directions. Compensating circuits are provided for making identical calibrations as alternating and perpendicular fields are switched from one set of driving coils to the other, thus eliminating the use of two driving power amplifiers. When bending of the film substrate is accomplished mechanically, the elastic deformation is controlled by a micrometric arrangement in order for the instrument to have an acceptable sensitivity.

2. An improved technique for X-ray spectrochemical analysis of thin films. In present techniques the number of counts to be accumulated to reach a certain statistical accuracy does not take into account the impurity contents present in the X-ray tube target, in the sample holder and in the surroundings of the fluorescence meter. When analyzing iron and nickel the contributions, to the observed counting rate, of amounts of these elements surrounding the sample may be as large as the counting rate due to the film.

Also, the analysis of a large number of samples requires fast manual operations in order to keep at a

minimum the time required to perform the analysis. Electronic drift, caused by environmental changes, may introduce errors during long operating runs. A convenient method for determining the minimum number of counts, corresponding to a desired accuracy, is to use precalculated curves. Such a method has been proposed by Mack and Spielberg,[87] but it does not take into account environmental impurities of elements to be analyzed. The derivation of new curves for use in the spectrochemical analysis of thin films is discussed.

CHAPTER I

Static magnetic behavior of magnetostrictive thin films.

1. Theoretical model - General Energy Equation

a. Assumptions for simple model - Existing methods of solution.

The object of this first section is to present the reader with the basic equations governing the static behavior of a ferromagnetic system. These relationships have been developed and discussed at length in the literature[6...13] and will serve here solely as a basic prerequisite for the first and second chapters.

The domain theory of ferromagnetism has been widely used in formulating theoretical models for predicting the behavior of ferromagnetics and in particular that of thin magnetic films prepared from alloys of Ni, Fe, Co. The history which has led to the present understanding of the domain structure may be retraced in describing briefly the physical nature of thin magnetic films.

In the demagnetized state a film is divided in regions of magnetic saturation called "Weiss Domains". Within each domain all uncompensated atomic spins are

oriented by a "molecular field" in one direction, the direction of "easy magnetization". As shown by Heisenberg, the molecular field originates from electrostatic actions between neighboring atoms, which tend to keep the spins parallel. The energy associated with this proximity coupling has been named "exchange energy" because of its origin. Different domains have different directions of easy magnetization and are separated by transition regions called "Bloch Walls" in which the spins rotate progressively from the direction existing in one domain to that in the neighboring domain. These transition regions are small compared to their adjacent domains. If the domain contributions to the overall magnetization cancel one another, the sample appears demagnetized. The energy associated with Bloch walls, their thickness, the manner in which their spins achieve their progressive rotation have been studied by Bloch[14], Lifshitz[15], Néel[16], Lilley[17]. At the same time Landau-Lifshitz[18] and Gilbert[19] have clarified the dynamics of spin rotation in ferromagnetics. This considerable body of theoretical knowledge originated from the work of Pierre Weiss[20] in 1907, and initially was applied mainly to the behavior of bulk material. With the work of Blois[21] in 1955 on the magnetic properties of evaporated thin films the previous body of theoretical and exper-

imental research received a new impetus as thin films showed promise of important engineering applications in digital switching and storage.

The domain configuration assumed by a ferromagnetic material results from the interaction between external forces and the internal atomic and crystalline properties of the material. It is a well-known principle in physics that a system will assume a final configuration which minimizes its total free energy. This principle has been used extensively to study domain size and distribution in ferromagnetic substances since the original work of Bloch in domain walls in 1932. It has been applied to the study of thin films during the last decade.

The total free energy of a thin magnetic film includes the following four terms: the exchange energy representing the degree of alignment between neighboring spins, the anisotropy energy which determines easy and hard direction of magnetization in relation to the crystalline structure of the lattice, the magnetostrictive energy which represents a contribution due to the elastic properties of the material, the magnetostatic energy resulting from the interaction between free magnetic poles at the surface of the material and externally applied magnetic fields. The presence of

free magnetic poles causes demagnetizing effects which depend upon the geometry of the material.

Before discussing the different models which have been proposed for predicting the behavior of thin magnetic films, the expressions for the energies involved in a magnetic system will be presented, following a review by Kittel.[11]

Exchange Energy:

The energy corresponding to interaction between two neighboring atoms, i and j of a ferromagnetic, varies as the scalar product of their spin moments S. This energy is given by the expression:[13, 22]

(1) $$E_{ex_{ij}} = 2 J S^2 (1 - \cos \phi_{ij})$$

where J is the exchange integral[22] relating atoms i and j, ϕ_{ij} is the angle between the direction of their spin moments. For an atom i surrounded by N neighbors expression (1) becomes, neglecting additive terms:

(1') $$\Delta E_{ex_i} = -2JS^2 \sum_{j=1}^{N} \cos \phi_{ij}$$

If two neighboring spins are located within a domain wall the angle ϕ_{ij} is small and expression (1) becomes:

(2) $$E_{ex_{ij}} = J S^2 \phi_{ij}^2$$

Let ϕ be the total spin rotation through N

atoms, across the wall, then the exchange energy density becomes[13]:

$$(3) \qquad E_{ex} = J S^2 \left(\frac{\phi}{N}\right)^2 N = J S^2 \phi^2/N \text{ ergs/ccm}$$

where it is assumed that the angle between one spin and the next is constant. Expression (3) shows that the larger N, the smaller the exchange energy, i.e. the spins will tend to make the thickness of the wall a minimum. The exchange integral J may be obtained experimentally by measuring the Curie temperature. At the Curie temperature the thermal energy becomes equal to the exchange energy.

The exchange energy interacts with other forms of energy which tend to increase N in order to assume a minimum value. The final thickness of the wall is the result of a compromise between conflicting energetic requirements and corresponds to minimizing the sum of all energies involved. In the case of a body centered cubic crystal[13, 18] the exchange energy density (ergs/ccm) may be expressed as

$$(4) \qquad E_{ex} = \frac{2 J S^2}{a} \left[(\nabla \alpha_1)^2 + (\nabla \alpha_2)^2 + (\nabla \alpha_3)^2\right]$$

where a is the lattice constant, α_1, α_2, α_3 the direction cosines of the atomic spin at the center of the cube with respect to the crystalline axes. For iron,

through measurement of the Curie temperature, a simple computation[13] gives:

$$2 J S^2/a = 1.87 \times 10^{-6} \text{ ergs/cm}$$

Anisotropy Energy:

An explanation of the origin of the anisotropy energy has been given by Van Vleck[22], who attributed this ferromagnetic property to a coupling between the orbital and spin momenta. The result of this interaction is the orientation of elementary magnetizations toward preferred crystalline direction called "directions of easy magnetization". In the case of a uniaxial crystal, such as cobalt, there are two easy directions along the hexagonal axis of the crystal.

The anisotropy energy density is only a function of the angle between the easy axis and the magnetization. The series expansion of the sine of this angle may be used to represent this energy density mathematically, where the odd powers have been dropped, since both orientations along an easy axis are possible. For a uniaxial crystal (cobalt), the expression limited to the first two terms is:

(5) $$E_K = K1 \sin^2 \alpha + K2 \sin^4 \alpha$$

In the case of crystals with cubic symmetry (iron, nickel), the anisotropy energy density is expressed by a series expansion of the direction cosines

α_1, α_2, α_3 of the magnetization with respect to the three concurrent axes formed by the edges of the cube. Only even power terms in α_i are allowed due to symmetry relations; the expression must be symmetric with respect to α_i because of the 4-fold symmetry; and the identities:

$$(6) \qquad \sum_{i=1}^{3} \alpha_i^2 = 1 , \qquad \left(\sum_{i=1}^{3} \alpha_i^2\right)^2 = 1$$

must be considered. The result is

$$(7) \quad E_K = K_1 \left(\alpha_1^2\alpha_2^2 + \alpha_2^2\alpha_3^2 + \alpha_3^2\alpha_1^2\right) + K_2 \alpha_1^2\alpha_2^2\alpha_3^2$$

K_1 is positive when the cube edges are easy axes (e.g. iron), K_1 is negative when the cube main diagonals are easy axes (e.g. nickel). K_2 is always positive.

When the free energy has its origin within the crystal lattice, it is convenient to express it in terms of fictitious fields which would give the same effects. These fictitious fields have been called "effective fields" by Landau and Lifshitz[18]. The effective field corresponding to the anisotropy energy has been named "anisotropy field" H_K, and is oriented along the easy direction closest to the magnetization vector. If the crystal is uniaxial (e.g. cobalt) the fourth order term may be neglected and the expression becomes:

$$(8) \qquad E_K = K_1 \sin^2\alpha$$

Similarly, if the crystal has cubic symmetry (e.g. iron), the magnetization is close to the x-axis, α_2 and α_3 are very small, (6) and (7) give:

(8) $$E_K = K_1 \sin^2\alpha$$

A similar expression may be obtained for the cubic symmetry of Nickel.

If α is small the energy of interaction between the effective anisotropy field H_K and the magnetization becomes

$$E_K = - M H_K \cos\alpha = - M H_K \left(1 - \frac{\sin^2\alpha}{2}\right)$$

(9) $$E_K = - M H_K + M H_K \frac{\sin^2\alpha}{2}$$

Equating (8) to (9) and dropping the constant additive term $- M H_K$ gives:

(10) $$H_K = 2 K_1/M$$

The effective anisotropy field will be measured and (10) used to obtain K_1 in the case of thin films and for normalization of energies corresponding to externally applied fields and stresses.

Magnetostrictive Energy:

When a mechanical stress is applied to an elastic ferromagnetic crystal, the strains induced in the crystal deform the lattice and alter its anisotropy energy. This change depends upon the elastic modulus

of the material and causes a rotation of the magnetization in order to minimize the total energy which had been altered by the application of the stress. Conversely, when a magnetic field is applied to an unstressed crystal, elastic deformations of the lattice result, which affect the direction of the magnetization. General expressions for the energy associated with magnetostriction have been derived by Becker and Döring[23], Kittel[11] and Vautier[24]. The case of isotropic magnetostriction will be considered here since it is of special interest in the forthcoming presentation.

If it is assumed that the magnetostrictive constants in the general expression for the magnetostrictive energy are equal, the change in the anisotropy energy caused by the application of the stress is

$$E_\sigma = \frac{3}{2} \lambda_s \sigma \sin^2\alpha \tag{11}$$

where λ_s is the saturation magnetostriction coefficient, σ is the applied tensile or compressive stress, α is the angle between the applied stress and the magnetization.

Equating expressions (8) and (11) the effective field equivalent to magnetostriction may be obtained as,

$$H_\sigma = \frac{3 \lambda_s \sigma}{M} \tag{12}$$

For the purpose of studying the effects of an anisotropic stress on the observed hysteresis loop of a thin Ni-Fe film, the expression (11) is sufficient if it can be assumed that no other stresses are present and the magnetic induced anisotropy resulting from the contribution of the elementary cubic crystal is uniaxial. This is not generally true and, because stress fields in a film have a profound influence on their switching and storage properties, several investigators have suggested more refined models.[25, 26, 27]

MacDonald[25] has recognized the following stresses to be active in a thin film of nickel and iron: a planar isotropic stress due to the difference in thermal expansion coefficients between the metal and substrate, a tensile or a compressive stress of magnetostrictive origin caused by the applied DC magnetic field used to induce a uniaxial anisotropy during evaporation, and a complex system of microstrains originated from impurities and imperfections, whose effects cannot be predicted accurately.

Following the work of Baltzer[26] on single crystals, Blades[27] has considered a film as a random planar distribution of microcrystals and has written a more complete anisotropy energy expression:

(13) $$E_K = (K_1)_{eff} S + (K_2)_{eff} P + E_\sigma + E_\pi$$

where $(K_1)_{eff}$ and $(K_2)_{eff}$ are functions of the intrinsic anisotropy constants discussed earlier, S and P contain the direction cosines of the magnetization with respect to crystallographic axes. E_σ and E_π are expressions for anisotropic and planar stresses, applied or residual and obtained by averaging the contributions of elementary crystals contained in the film.

Since iron and nickel single crystals have their easy magnetizations distributed in three dimensions the resulting total energy given by expression (13) contains angles ϕ and θ which are magnetic spin moment polar coordinate angles referenced to the film plane.

Magnetostatic Energy

This is the energy between a dipole and an applied field. It is given by the scalar product of the magnetization by the field acting on it:

(14) $$E_H = - \vec{M} \cdot \vec{H}$$

In the case of a thin film the magnetization M represents the macroscopic magnetic vector resulting from the contribution of all elementary atomic moments and oriented along the easy direction of induced magnetization. This is an assumption since it considers the film as one domain. In his proposed model mentioned

earlier Blades has computed a new term for the magnetostatic energy of a thin film by averaging the magnetization of a large number of elementary cubic crystals. His expression assumes the form:

(15) $$E_H = - M H f (\phi, \psi)$$

When a uniformly magnetized film is subjected to an external field, the magnetization, initially in the plane of the film tends to approach the applied field by a precessional rotation which, because of the geometry, is a very flat ellipse instead of a cone. During the precession the magnetization moves away from the film plane, thus causing a discontinuity of its normal component at the surface of the film. This discontinuity originates the formation of magnetic poles, which have a strong demagnetizing action as they originate from the very strong molecular Weiss field. The magnitude of the demagnetizing field depends upon the geometry of the film and is proportional to the normal component of the magnetization:

(16) $$H_d = - N M \cos \theta$$

In the emu system of units:

$$N = 4\pi$$

for a circular film with a self field (the demagnetizing field), normal to its plane. The demagnetizing energy becomes then (assuming that any demagnetizing field in

the plane of the film is negligible),

(17) $$E_d = - H_d M \cos \theta = 4\pi M^2 \cos^2 \theta$$

where θ is the angle between the normal to the surface of the film and the magnetization vector precessing around the applied field.

These energy expressions will be used in the following section to present a method for predicting static hysteresis loops under different conditions. This method permits an increase in the number of parameters influencing hysteresis loops without excessive increase in algebraic or graphical labor. In particular initial magnetization angular position and stresses may be specifically introduced.

The modified and more complex expressions introduced by Blades[27] for the magnetostrictive and magnetostatic energies may be used for determining stable states of minimum energy by differentiating the total energy with respect to ϕ and to ψ. However, the simpler expression which assumes uniaxial magnetic properties in the plane of a single domain film which undergoes coherent rotational switching will be used for predicting the static and dynamic behavior under stressed conditions. The expression for the total energy density is simply the sum of terms given by (8), (11), (14), (17), as shown in Chapter II and reference (6):

$$E_t = K \sin^2 (\phi - \gamma) + 3/2 \lambda_s \sigma \cos^2 \phi - M H_p \sin \phi$$
$$- M H_s \cos \phi + 4\pi M^2 \cos^2 \theta$$

Models of flux reversal in thin ferromagnetic films

Mechanisms of flux reversal in thin film have been the object of considerable study in recent years[28, 29, 30, 31]. Despite the fundamental role of film imperfections in the reversal process, it has not been reasonable to include accurate specification of these imperfection properties of the material in a thin ferromagnetic film. This fact and the complexity of computation in a general solution of the problem have prevented the formulation of an accurate model for thin film flux reversal. However, three models have been proposed which describe fairly well the processes of reversal under specified experimental conditions.

If the magnetization in a thin film is reversed by a pulse of increasing magnitude and if the inverse of the switching time[29] is observed, a curve is obtained which shows three distinct regions. In the case of a non-magnetostrictive permalloy film Gyorgy[29] has observed the results illustrated by the curve in Fig. 1. The three regions in the curve correspond to three different mechanisms of magnetization reversal:

For low values of switching field amplitude, in excess of the coercive force the reversal takes place

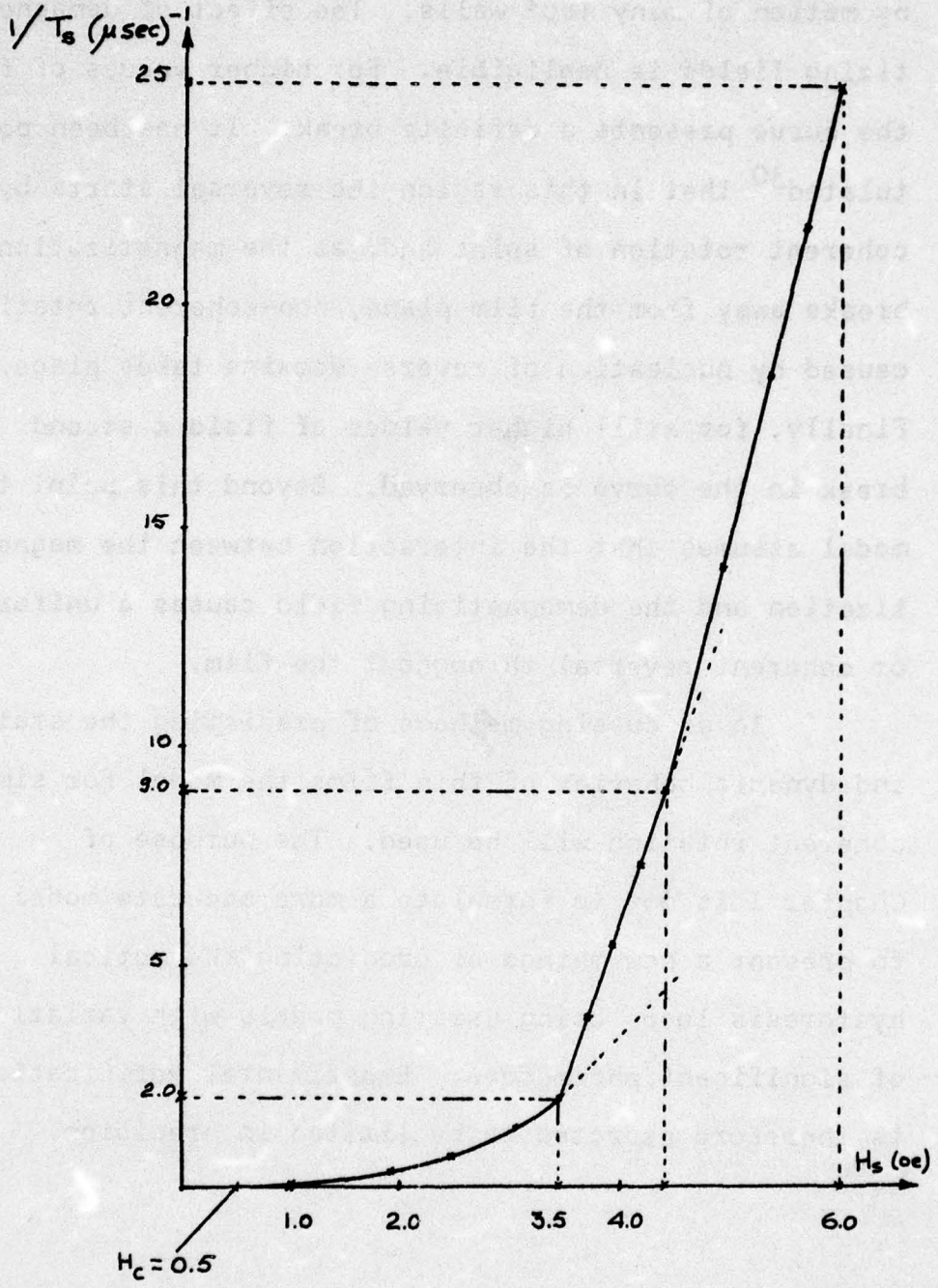


FIG. 1 INVERSE SWITCHING TIME VS. SWITCHING FIELD, 3500Å PERMALLOY FILM, (AFTER GYORGY).

by motion of many 180° walls. The effect of demagnetizing fields is negligible. For higher values of field the curve presents a definite break. It has been postulated[30] that in this region the reversal starts by coherent rotation of spins and, as the magnetization breaks away from the film plane, non-coherent rotation caused by nucleation of reverse domains takes place. Finally, for still higher values of field a second break in the curve is observed. Beyond this point the model assumes that the interaction between the magnetization and the demagnetizing field causes a uniform or coherent reversal throughout the film.

In discussing methods of predicting the static and dynamic behavior of thin films the model for simple coherent rotation will be used. The purpose of Chapter I is not to formulate a more accurate model but to present a new method of predicting theoretical hysteresis loops using existing models with variation of significant parameters. Experimental verification is therefore expected to be limited in precision.

b. Determination of hysteresis loop by root locus.

It is assumed that the uniaxial thin film switches by coherent rotation according to the simple model previously mentioned (p. 25). The total energy density associated with the film may be written as:

(18) $E_t = K \sin^2(\phi-\gamma)+\frac{3}{2} \lambda_s \sigma \cos^2\phi - MH_p \sin\phi - MH_s \cos\phi$

where:

$K \sin^2 (\phi - \gamma)$ is the magnetic anisotropy energy of induced uniaxial magnetization, K being the anisotropy constant.

$3/2\ \lambda_s \sigma \cos^2 \phi$ is the magnetostriction energy of a stress applied along the y-axis, λs being the magnetostriction constant at saturation.

$M H_p \sin \phi$ is the magnetostatic energy associated with a biasing magnetic field H_p applied along the x-direction and called the "perpendicular field", M being the saturation magnetization.

$M H_s \cos \phi$ is the magnetostatic energy associated with a magnetic field applied along the y-direction and called the "switching field".

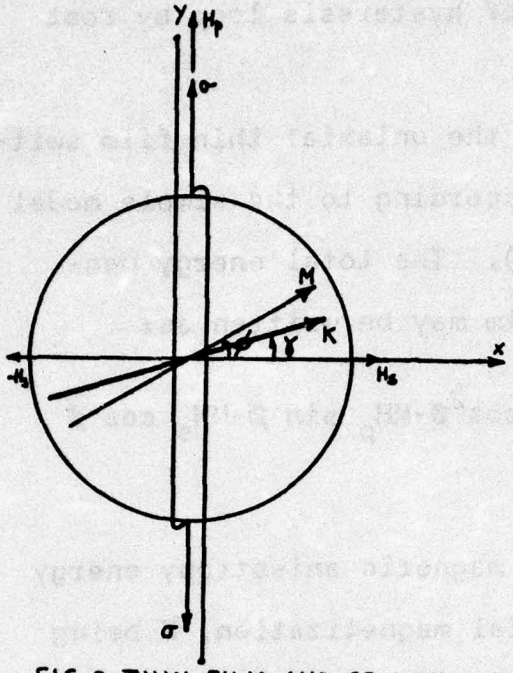


FIG. 2 THIN FILM AND SENSING WIRE FOR LONG. HYSTERESIS LOOP

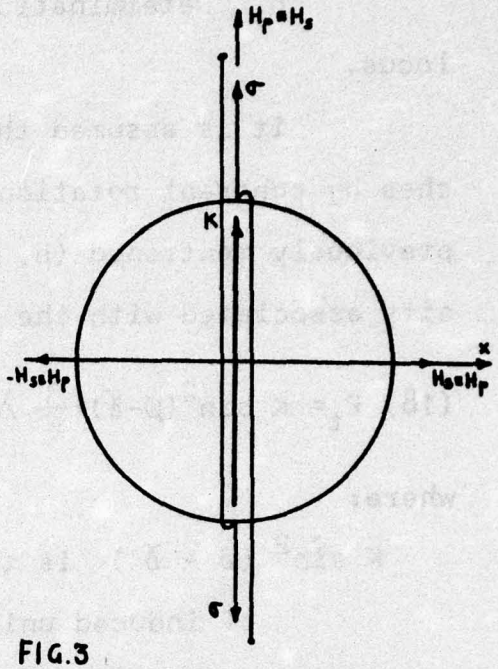


FIG. 3
THIN FILM AND SENSING WIRE FOR TRANSV. HYSTERESIS LOOP

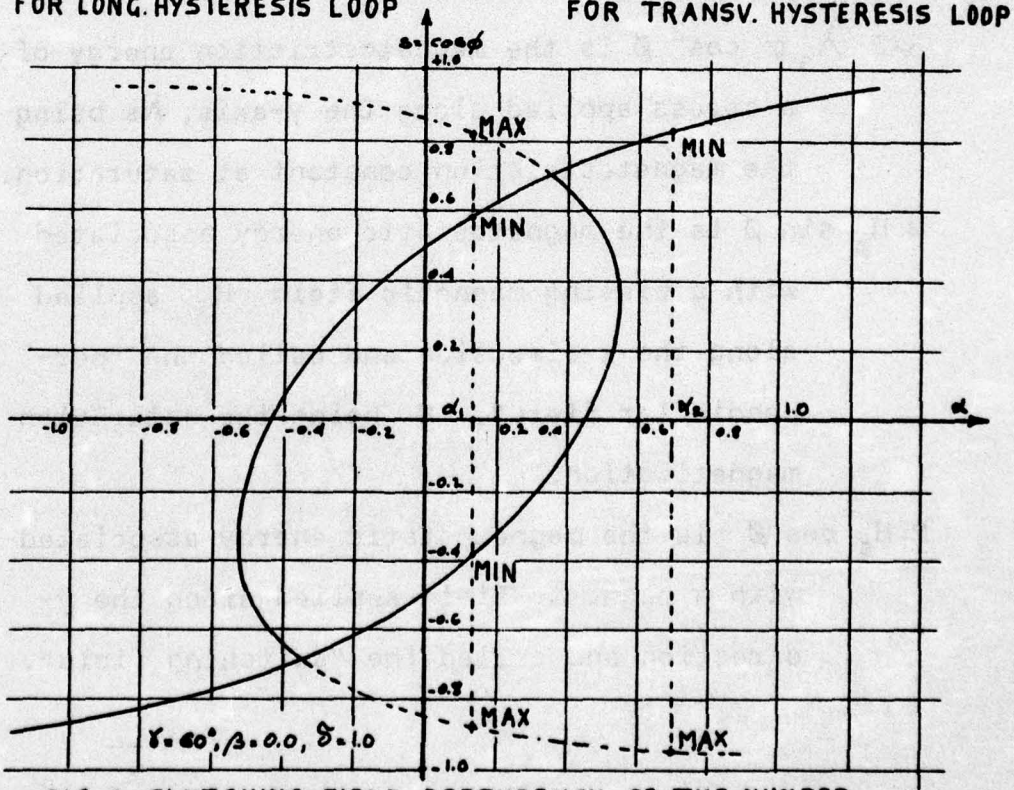


FIG. 4 SWITCHING FIELD DEPENDENCY OF THE NUMBER OF REAL ROOTS

ϕ is the angle between the magnetization vector and the x-reference axis for any combination of magnetic energies.

γ is the initial angle made by the axis of easy magnetization with the direction of the applied switching field H_s.

The relative magnitude of the driving forces applied to the film and its intrinsic anisotropic properties affect the shape of the hysteresis loop and the switching time of the magnetization, from one remanent point to the other. It is assumed that the film is subjected to a constant stress, a constant perpendicular field, and a sinusoidal low frequency (of the order of a few thousands cps) longitudinal switching field.

If a sensing loop is placed around the film, as shown in Fig. 2, as the magnetization vector rotates under the drive of H_s, the x-component of M will change and an emf will be induced in the loop. The plot of $M \cos \phi$ vs. H_s is the "longitudinal" hysteresis loop. If the film is rotated by 90° as shown in Fig. 3, then the roles of H_s and H_p are interchanged, H_s becomes a perpendicular field acting on the hard direction of magnetization. The emf induced in the sense loop in these conditions originates from the change in $M \sin \phi$. The plot of $M \sin \phi$ vs H_p for $H_s = 0$ is

the "transverse" hysteresis loop.

In order to find the values of ϕ at which the magnetization will come to rest upon the application of a switching field H_s, for constant H_p and σ, the energy equation (18) is differentiated with respect to ϕ and the positions of minimum energy are determined from:

$$dE_t/d\phi = 0 \tag{19}$$

and

$$d^2 E_t/d\phi^2 > 0 \tag{20}$$

From equation (19)

$$2K \sin(\phi - \delta) \cos(\phi - \gamma) - 3\lambda_s \sigma \sin\phi \cos\phi - M H_p \cos\phi + M H_s \sin\phi = 0 \tag{21}$$

In equation (21) let $H_s = 0$, $\sigma = 0$, $\delta = 0$, the transverse loop is then obtained from:

$$\sin\phi = M H_p/2K$$

At $\sin\phi = 1$ saturation is reached for

$$2K = M H_p \tag{22}$$

This value of H_p is called the "anisotropy field".

Equation (21) is usually normalized to the anisotropy field by dividing it by 2 K:

$$\sin(\phi - \gamma) \cos(\phi - \gamma) - \delta \sin\phi \cos\phi - \beta \cos\phi + \alpha \sin\phi = 0 \tag{23}$$

where

(24) $\alpha = M H_s/2K \quad \beta = M H_p/2K \quad \delta = 3\lambda_s \sigma /2K$

To obtain the hysteresis loop in the longitudinal direction, $M \cos \phi$ vs α, equation (21) is modified (Appendix 1) and the following polynomial in $S = \cos \phi$ is obtained:

$$(25)\ S^4\left[1 + \delta^2 - 2\delta(\cos^2\gamma - \sin^2\gamma)\right] +$$
$$+ S^3\left[4\beta \sin\gamma \cos\gamma + 2\ (\cos^2\gamma - \sin^2\gamma - \delta)\right] -$$
$$- S^2\left[1 + \delta^2 - 2\delta(\cos^2\gamma - \sin^2\gamma) - \alpha^2 - \beta^2\right] -$$
$$- S\left[2\beta \sin\gamma \cos\gamma + 2\alpha(\cos^2\gamma - \sin^2\gamma - \delta)\right] -$$
$$-\alpha^2 + \sin^2\gamma \cos^2\gamma = 0$$

This polynomial may have four real roots or two imaginary and two real roots. In the first case two roots correspond to values of $\cos \phi$ for which E_t is a maximum, and in the second case one real root also corresponds to a maximum energy condition. These roots are discarded using the inequality (20).

Let the coefficients of the polynomial (25) be A, B, C, D, E in decreasing powers of s. The polynomial becomes then

$$(26)\quad A S^4 + B S^3 + C S^2 + D S + E = 0$$

Inequality (20) may be written:

$$\frac{d\ (d E_t/d \phi)}{d \cos \phi} \cdot \frac{d \cos \phi}{d \phi} > 0$$

or:

$$\frac{d\,(d\,E_t/d\,\phi)}{ds}\ \sin\phi < 0 \tag{27}$$

which leads to:

$$(4\,A\,S^3 + 3\,B\,S^2 + 2\,C\,S + D)\sin\phi < 0 \tag{28}$$

$$\text{for } 0° < \phi < 180°$$

and to:

$$(4\,A\,S^3 + 3\,B\,S^2 + 2\,C\,S + D)\sin\phi > 0 \tag{28'}$$

$$\text{for } 180° < \phi < 360°$$

This change in sign corresponds to the minimum becoming a maximum when the magnetization vector moves from the first and second quadrants into the third and fourth.

In equation (27), for fixed values of β, γ, δ, the roots describe a locus of points in the complex plane as α varies between - 1 and + 1. As α is varied from zero to positive and negative values, it is possible to obtain the two values of s corresponding to the minimum in the case of four real roots and the single value of s for the minimum in the case of two real roots. A plot of $s = \cos\phi$ vs. $\alpha = M\,H_s/2K$ is the longitudinal component of magnetization $M\cos\phi$ with the magnitude of the longitudinal switching field H_s.

Fig. 4 shows qualitatively the two cases for an irreversible hysteresis loop ($\delta = 0$, $\beta = 0$, $\gamma = 60°$). The dotted lines correspond to a maximum condition. For $\alpha = \alpha_1$ there are four real roots, for $\alpha = \alpha_2$

there are two real roots. Complex roots have no physical significance.

The locus of roots is obtained by use of a "Spirule" and by repeated polynomial root extraction on a digital computer.

The locus of roots and the Spirule[32, 33, 34]

When plotting the locus of roots by means of a Spirule, a polynomial must be written in a convenient form. Consider, for example, a polynomial of the fourth order:

$$x^4 + b\,x^3 + c\,s^2 + d\,x + e = 0 \tag{29}$$

b, c, d are assumed constant, e is a parameter whose variation will cause the roots to describe a locus in the complex plane.

Equation (29) is rearranged as follows:

$$\left[x^3 + b\,(x^2 + \frac{c}{b}\,x + \frac{d}{b})\right] x = -\,e \tag{30}$$

The cubic in the square bracket may be written:

$$x^3 + b\,(x^2 + \frac{c}{b}\,x + \frac{d}{b}) = 0$$

The roots of the quadratic are found and the cubic becomes

$$b\,\frac{(x - r_1)\,(x - r_2)}{x^3} = -\,1 \tag{31}$$

Equation (31) is in convenient form for Spirule use. The roots of the cubic, r_3, r_4, r_5 are found and equation (30) becomes:

$$(x - r_3)\,(x - r_4)\,(x - r_5)\,x = -e$$

which may be written conveniently:

$$(32) \qquad e\,\frac{1}{(x - r_3)\,(x - r_4)\,(x - r_5)\,x} = -1$$

The roots r_6, r_7, r_8, r_9, of equation (32) are found by root locus by means of a Spirule. Equation (29) may then be factored:

$$(33) \qquad (x - r_6)\,(x - r_7)\,(x - r_8)\,(x - r_9) = 0$$

Any coefficient of the polynomial may be chosen as a parameter. In general equations (31) and (32) have the form:

$$(34) \qquad 1 + \frac{(x + r_1)\,(x + r_2)\ldots.\,(x + r_n)}{(x + r_1')\,(x + r_2')\ldots.\,(x + r_n')} = 0$$

where the roots r_i, r_i' may be real or complex. Identifying x with s in the complex plane, the complex numbers $(s + r_i)$ and $(s + r_i')$ may be written in exponential form:

$$(35) \qquad 1 + K\,\frac{R_1\,e^{j\phi_1}\,R_2\,e^{j\phi_2}\ldots.\,R_n\,e^{j\phi_n}}{R_1'\,e^{j\phi_1'}\,R_2'\,e^{j\phi_2'}\ldots.\,R_n'\,e^{j\phi_n'}} = 0$$

or

$$(36) \qquad 1 + M\,e^{j\phi} = 0$$

where

$$(37) \qquad M = K \frac{R_1 \; R_2 \; \ldots\ldots \; R_n}{R_1' \; R_2' \; \ldots\ldots \; R_n'}$$

$$(38) \qquad \phi = \phi_1 + \phi_2 + \ldots\ldots + \phi_n - (\phi_1' + \phi_2' + \ldots\ldots \phi_n')$$

Equation (36) may be written:

$$(37) \qquad M \, e^{j\phi} = e^{j\pi(2K+1)}$$

Satisfying this equation involves a phase condition and a magnitude condition:

$$(38) \qquad \phi_1 + \phi_2 + \ldots\ldots + \phi_n - \phi_1' - \phi_2' - \ldots\ldots - \phi_n' = (2K+1)\pi$$

$$(39) \qquad K \frac{R_1 \; R_2 \; \ldots\ldots \; R_n}{R_1' \; R_2' \; \ldots\ldots \; R_n'} = 1$$

The points of the plane which satisfy (38) and (39) may be found by means of a Spirule. The phase condition is satisfied by determining the locus of roots for which the difference $\phi_n - \phi_n'$ is equal to 180° (direct root locus) or to 0° (inverse root locus). Points on the locus satisfying equation (39) are found by means of a logarithmic spiral printed on the Spirule. Vector lengths are multiplied or divided by adding or subtracting their logarithms.

Application to thin film magnetization

The root locus method is now applied to find

the roots of the fourth order polynomial at the left-hand side of equation (25). The parameter which is to be varied as gain is α, representing the normalized switching field, and appearing in four coefficients of the polynomial.

In order to obtain a form suitable for root locus technique, equation (25) is rearranged as follows:

$$(40) \quad -4\beta \sin\gamma\cos\gamma\, s^3 - \beta^2 s^2 + 2\beta \sin\gamma\cos\gamma\, s - \sin^2\gamma\cos^2\gamma = \left[1 + \delta^2 - 2\delta(\cos^2\gamma - \sin^2\gamma)\right]$$

$$s^4 + 2\alpha(\cos^2\gamma - \sin^2\gamma - \delta)\, s^3 - \left[1 + \delta^2 - 2\delta(\cos^2\gamma - \sin^2\gamma) - \alpha^2\right] s^2 - 2\alpha(\cos^2\gamma - \sin^2\gamma - \delta)\, s - \alpha^2$$

The left-hand side is a cubic in s and its roots are found independently from the right-hand side:

$$(41) \quad 4\beta \sin\gamma\cos\gamma\, s^3 + \beta^2 s^2 - 2\beta \sin\gamma\cos\gamma + \sin^2\gamma\cos^2\gamma = 0$$

Finally

$$(42) \quad 1 = \frac{1}{2} \frac{s - \dfrac{\sin\gamma\cos\gamma}{}}{s^2\left(s + \dfrac{\beta}{4\sin\gamma\cos\gamma}\right)}$$

This equation is solved by an "inverse auxiliary" root locus, with a gain $K = 1/2$, it has a double pole at the origin, one at $-\beta/(4\sin\gamma\cos\gamma)$ and a zero at $(\sin\gamma\cos\gamma)/2\beta$. Let the roots be α_1, α_2,

α_3, equation (41) may then be written as follows:

(43) $4\beta \sin\gamma \cos\gamma (S-\alpha_1)(S-\alpha_2)(S-\alpha_3) = 0$

The roots of the right-hand side of equation (40) must now be found. Let this second polynomial be written as follows, for brevity:

(44) $M S^4 + 2\alpha N S^3 - (M-\alpha^2) S^2 - 2\alpha N S - \alpha^2 = 0$

where: (45) $M = 1 + \delta^2 - 2\delta(\cos^2\gamma - \sin^2\gamma)$

(46) $N = \cos^2\gamma - \sin^2\gamma - \delta$

Equation (44) does not require a root locus for its solution, since it may be factored as follows:

(47) $(S^2-1)\left[S-(-\alpha\frac{N}{M}+\frac{\alpha}{M}\sqrt{N^2-M})\right]\left[S-(-\alpha\frac{N}{M}-\frac{\alpha}{M}\sqrt{N^2-M})\right] = 0$

It is easy to verify that:

(48) $N^2 - M = 4\sin^2\gamma\cos^2\gamma$

Equation (48) shows that equation (44) will always have two complex roots.

Through the following step equation (40) is modified, using equations (43) and (47), in order to find equation (50), which is a convenient form for plotting the final root locus:

(49) $-\left[M S^4 + 2\alpha N S^3 - (M-\alpha^2) S^2 - 2\alpha N S - \alpha^2\right] =$

$= 4\beta \sin\gamma \cos\gamma (S-\alpha_1)(S-\alpha_2)(S-\alpha_3)$

(50) $-1 = \frac{2\beta \sin 2\gamma}{(1+\delta^2-2\delta\cos 2\gamma)(S^2-1)} \frac{(S-\alpha_1)(S-\alpha_2)(S-\alpha_3)}{\left[S+\frac{\alpha(\cos 2\gamma - \delta \pm j\sin 2\gamma)}{1+\delta^2-2\delta\cos 2\gamma}\right]}$

By using equation (50) the locus of roots for any normalized perpendicular field β, any initial angle γ and any applied normalized uniaxial stress δ, may be plotted. If the stress is isotropic or two dimensional the same method may be used to reach an equation similar to (50) from a polynomial in S.

Equation (50) does not lead to a standard root locus in which the poles and the zeros are fixed and the gain varies. The rules usually followed in sketching root loci do not apply to sketching the locus obtained from equation (50), when an hysteresis loop is desired. The gain is independent of α whose variation causes the roots to move in the complex plane. For given values of β, γ, δ the gain is fixed, the roots α_1, α_2, α_3 obtained from the auxiliary root locus are fixed, only α varies and the two complex poles in the denominator of the right-hand side of equation (50) move along two straight lines passing through the origin, at an angle with the real axis, given by

$$\Psi = \tan^{-1} \frac{\sin 2\gamma}{\cos 2\gamma - \delta} \tag{51}$$

Thus, each time α is advanced the two complex poles must be advanced along these two lines. The complex branches of the root locus need not be plotted as the information necessary to plot hysteresis loops is

given by the real branches. If for a given value of α there are four, two must be rejected. The selection of the roots corresponding to a minimum energy condition is done at $\alpha = 0$, using equation (28) or (28'). The roots selected at $\alpha = 0$ are then followed on the locus of roots as α is advanced towards ± 1. Plotting these roots vs the normalized switching field α gives the hysteresis loop.

Example 1:

Let $\beta = 0.6 \qquad \gamma = 60° \qquad \delta = 0$

Equation (41) for the auxiliary loop gives

$$\beta\sqrt{3}\, s^3 + \beta^2 s^2 - \beta\frac{\sqrt{3}}{2} s + \frac{3}{16} = 0$$

which is changed into the following equation, according to equation (42):

$$1 = \frac{1}{2} \frac{s - 0.362}{s^2 (s + 0.346)}$$

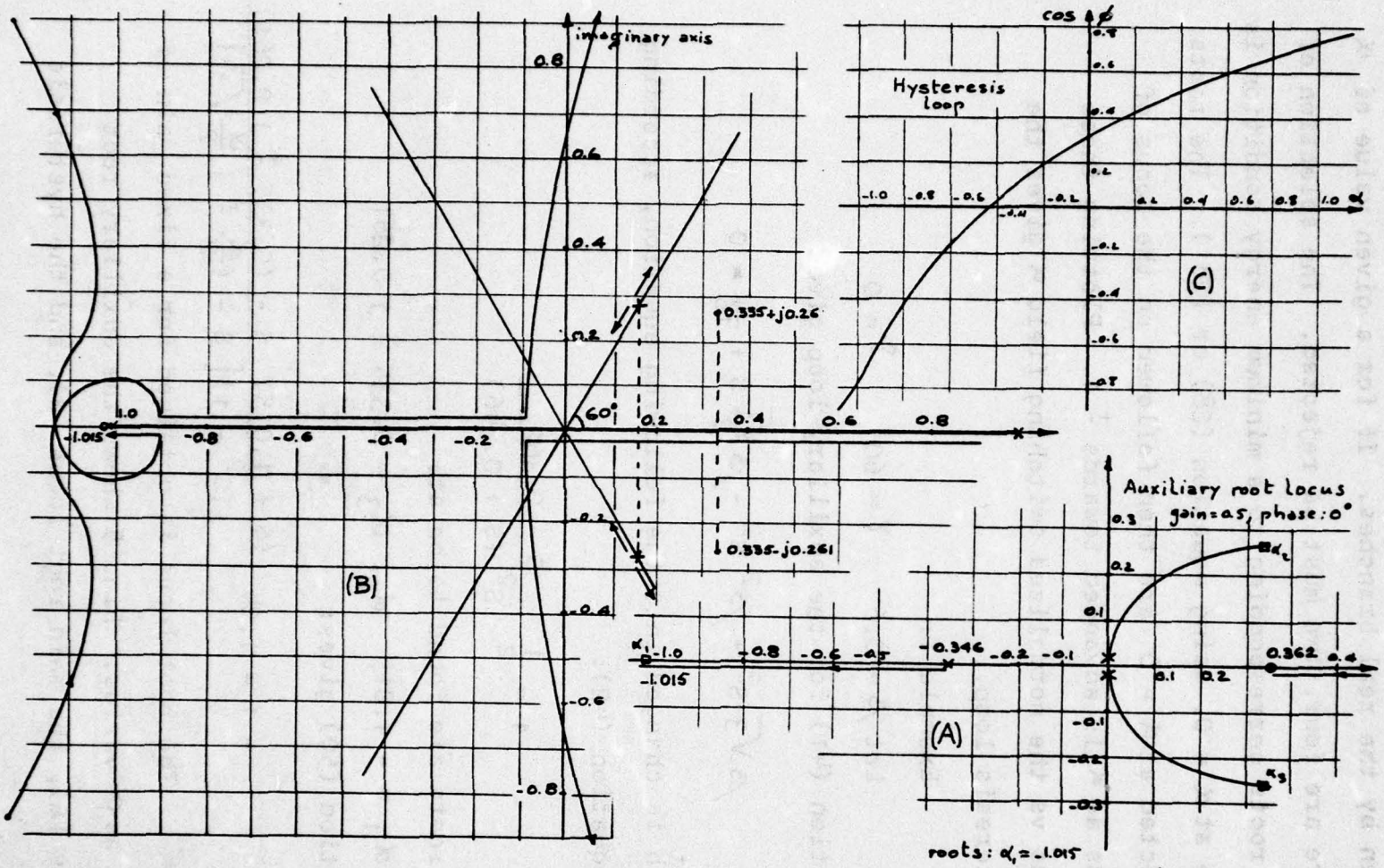
The roots are found to be at:

$$\alpha_1 = -1.015 \quad \alpha_2, \alpha_3 = 0.335 \pm j\, 0.261$$

Equation (50) gives:

$$-1 = 1.04 \frac{(s + 1.015)\; s - (0.335 \pm j\, 0.261)}{(s^2 - 1)\left[s - \left(\frac{\alpha}{2} \pm j \frac{\alpha}{2}\sqrt{3}\right)\right]}$$

The root locus is obtained for a fixed gain of 1.04 as α varies. Fig. 5 shows the auxiliary root locus (A), the main root locus (B), and the hysteresis



roots: $\alpha_1 = -1.015$

$\alpha_2, \alpha_3 = 0.335 \pm j\,0.261$

FIG. 5 LOCUS OF ROOTS FOR $\beta = 0.6$, $\gamma = 60°$, $\delta = 0.0$

loop (C). Only two real roots are found at $\alpha = 0$, one is discarded and the other is followed as the two complex poles move along two lines making an angle $\psi = 60°$ with the real axis, as given by equation (51). The hysteresis loop is reversible with the chosen parameters. Fig. 6 shows four hysteresis loops, corresponding to $\beta = 0.6$, $\gamma = 0$ and $\delta = 0.0, 0.3, 0.5, 0.7$. The squareness deteriorates as the stress increases and the loop closes for a value of δ between 0.3 and 0.5. Since the magnetostriction coefficient may be positive or negative, for a given tensile stress, loops for negative values of δ should be compared to those shown in Fig. 6, where δ was taken as positive. Fig. 7 shows four hysteresis loops corresponding to $\beta = 0$, $\gamma = 60°$, $\delta = 0.0, 0.3, 0.7, 1.0$.

The hysteresis loops shown in Figs. 4, 5, 6 have been obtained also from a digital computer. The digital computer program is discussed in Section c.

Some interesting analogies between the locus of roots and a hysteresis loop may be made, such as real axis break-away points and minimum value of longitudinal field for film switching (cfr Fig. 7) which reduces to the film coercive force for $\gamma = 0°$ (cf. Fig. 6). At such points two real roots become complex and correspondingly there is only one value of magne-

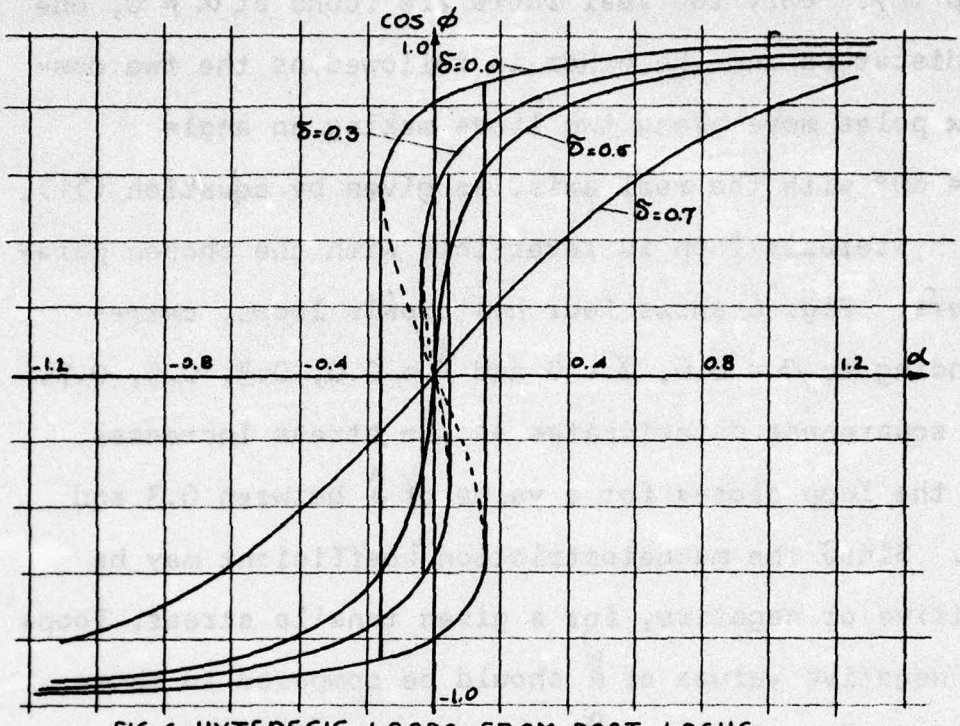


FIG. 6 HYTERESIS LOOPS FROM ROOT LOCUS
$\beta = 0.6$, $\gamma = 0°$, δ varying

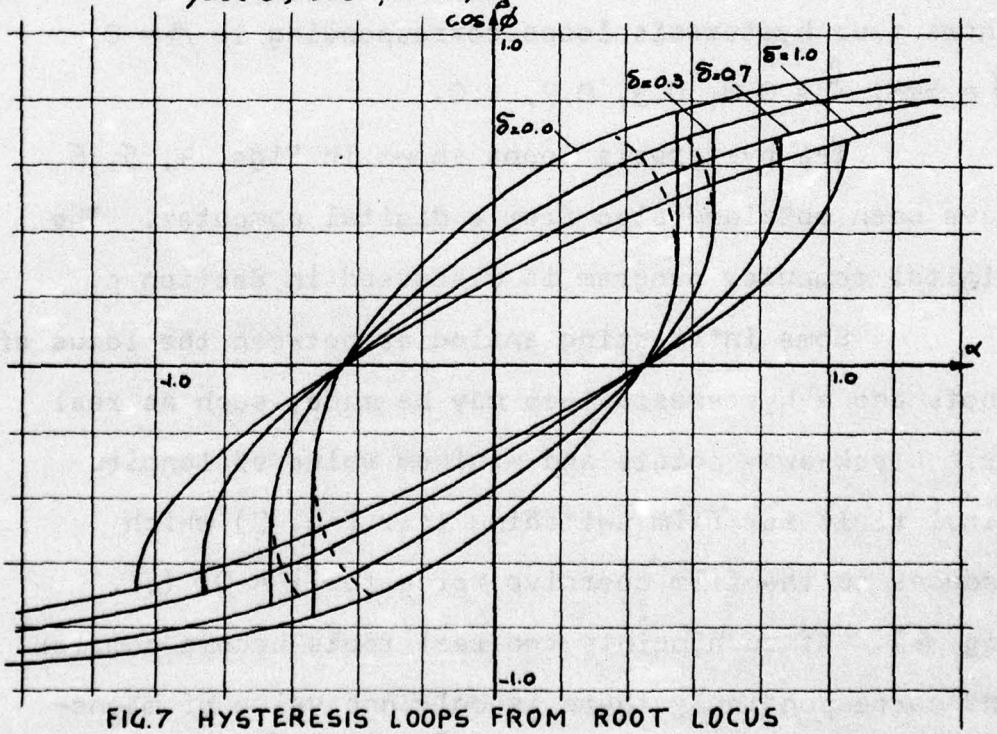


FIG. 7 HYSTERESIS LOOPS FROM ROOT LOCUS
$\gamma = 60°$, $\beta = 0.0$, δ varying

tization for a value of applied switching field.

Example 2:

As it is easily verified, equation (50) cannot be readily applied to the case when $\gamma = 0$, $\delta = 0$. For such a condition equation (40) becomes:

$$(52) \qquad -\beta^2 s^2 = s^4 + 2\alpha s^3 - (1 - \alpha^2) s^2 - 2\alpha s - \alpha^2$$

The right-hand side of this equation may be factored:

$$-\beta^2 s^2 = (s^2 - 1)(s + \alpha)^2$$

which may be conveniently written for root locus plot:

$$(53) \qquad -1 = \frac{1}{\beta^2} \frac{(s^2 - 1)(s + \alpha)^2}{s^2}$$

Hysteresis loops corresponding to several values of perpendicular field β when no stress is applied and the magnetization coincides initially with the direction of the switching field, have been plotted by other graphical methods[35, 36, 37]. A Spirule plot from equation (53) leads to identical results. Fig. 8 shows root loci for five values of β. Figs. 9 through 12 show four hysteresis loops corresponding respectively to $\beta = 0.23, 0.45, 0.68, 0.9$. The abscissa of the root locus break-away points corresponds to the coercive force and when $\beta = 0$ the break away points move to ± 1. For $\alpha = 0$ equation (53) gives:

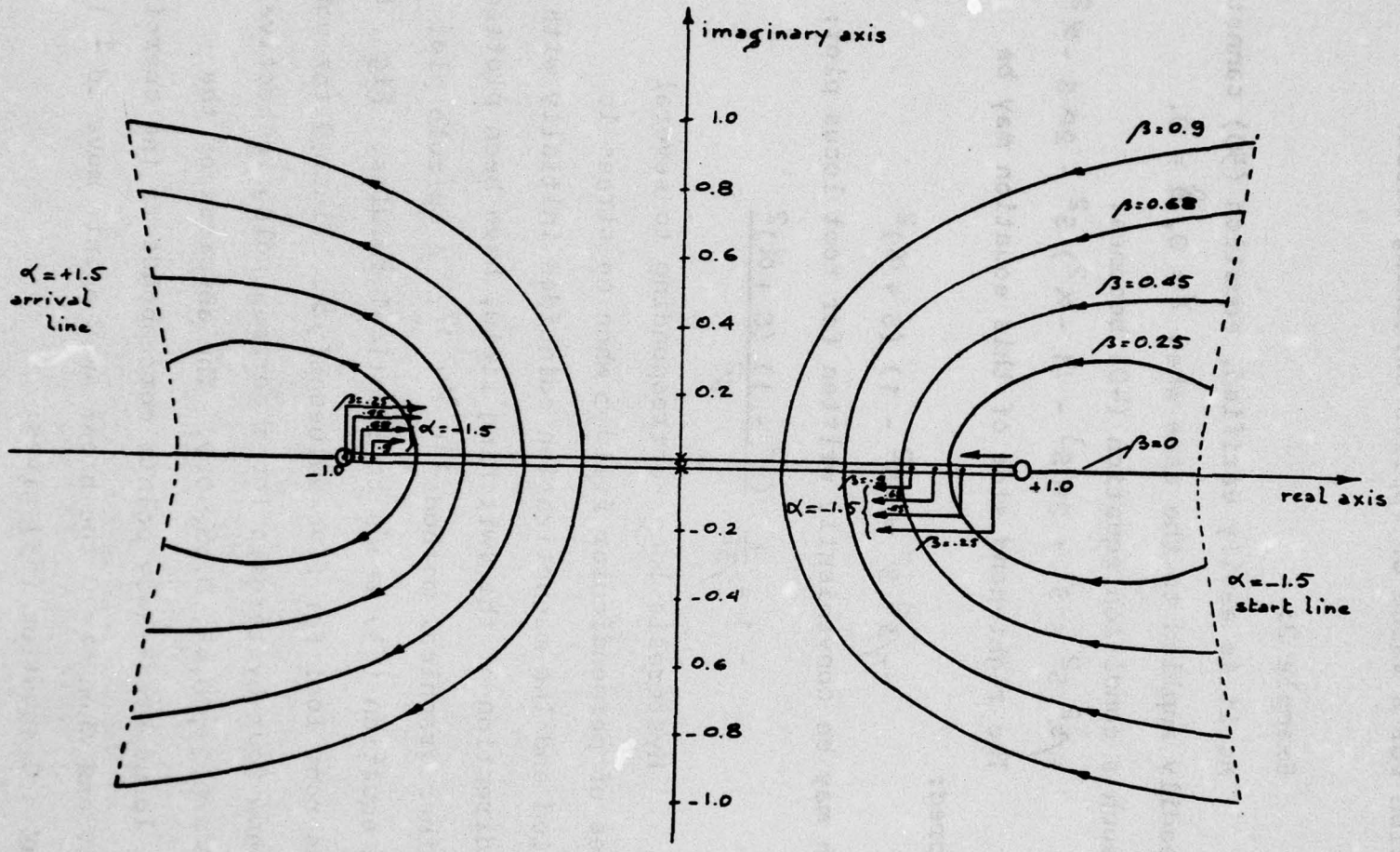


FIG. 8 LOCUS OF ROOTS FOR $\gamma = 0°$, $\delta = 0.0$

(54) $$S = \pm (1 - \beta^2)^{1/2}$$

This expression shows that for $\beta = 0$ the remanent points are ± 1. From these considerations one concludes that the hysteresis loop is a perfect square when $\beta = 0$. For increasing values of β from zero to one remanence decreases from ± 1 to zero, as shown by equation (54) and by Figs. 9 through 12. For fixed values of α the effect of varying β may be investigated by a standard root locus from equation (53).

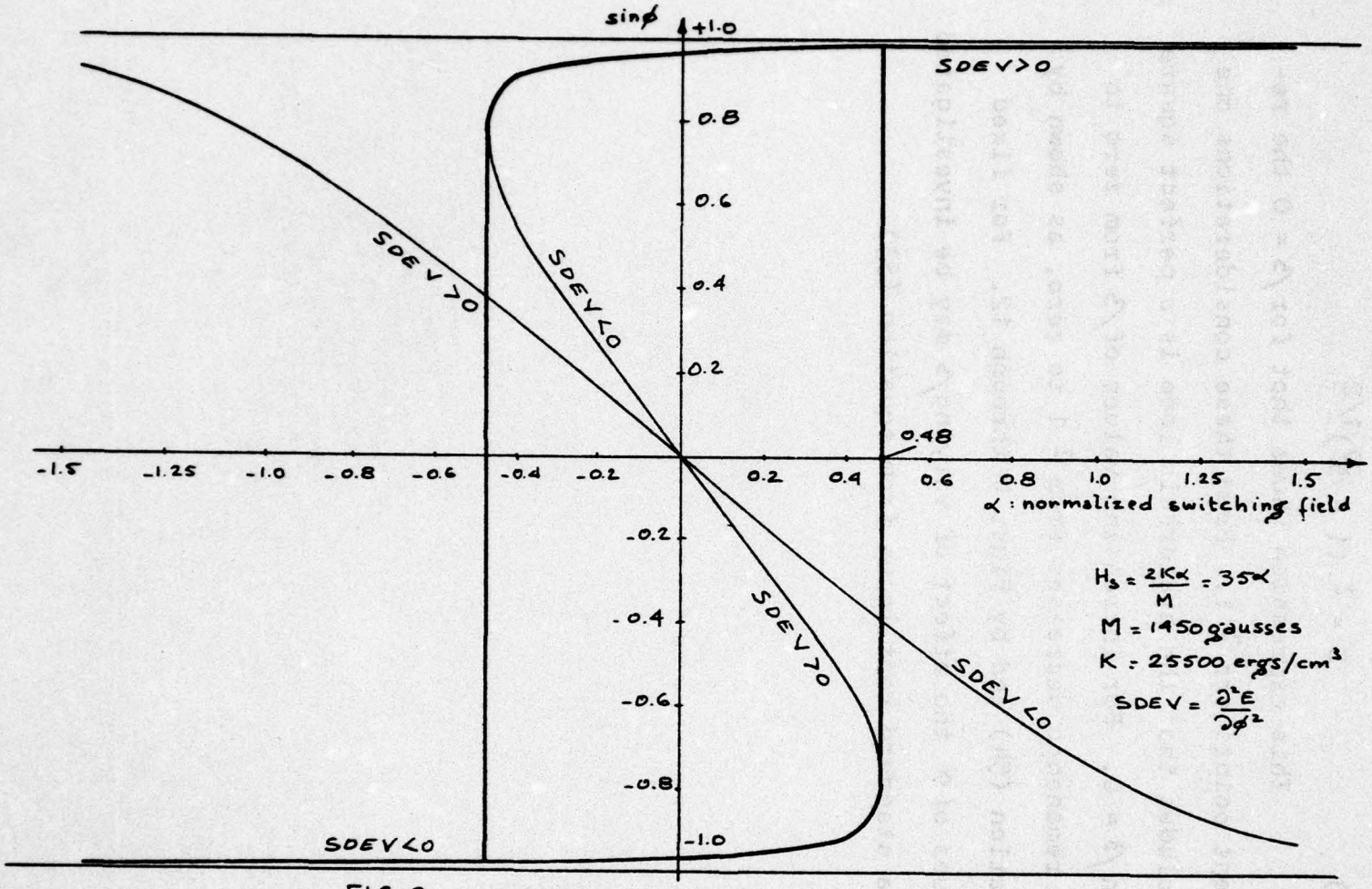


FIG. 9 HYSTERESIS LOOP FOR $\beta = 0.23$, $\gamma = 0$, $\delta = 0$
(longitudinal direction)

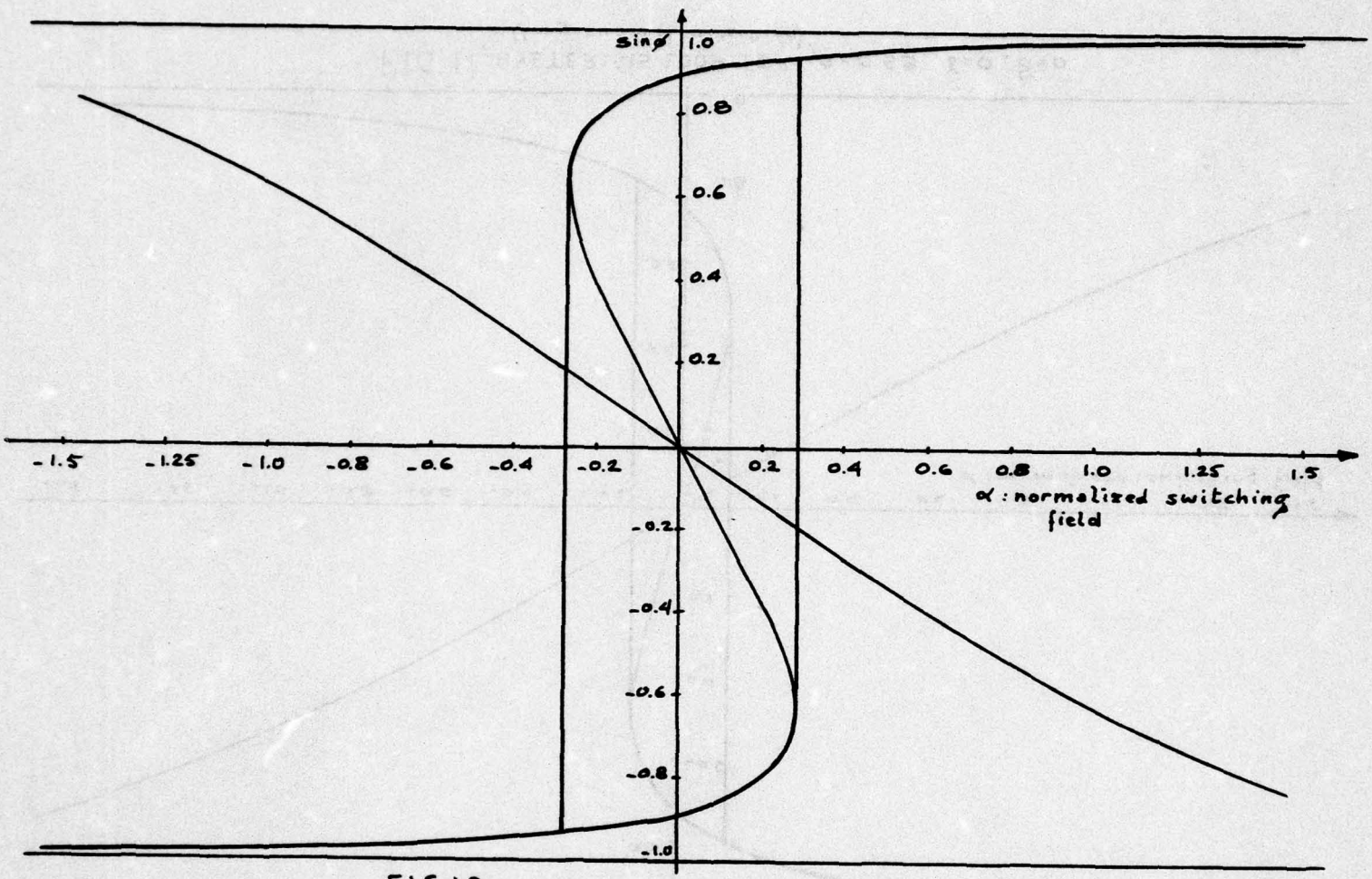


FIG. 10 HYSTERESIS LOOP FOR $\beta = 0.45$, $\gamma = 0$, $\delta = 0$
(longitudinal direction)

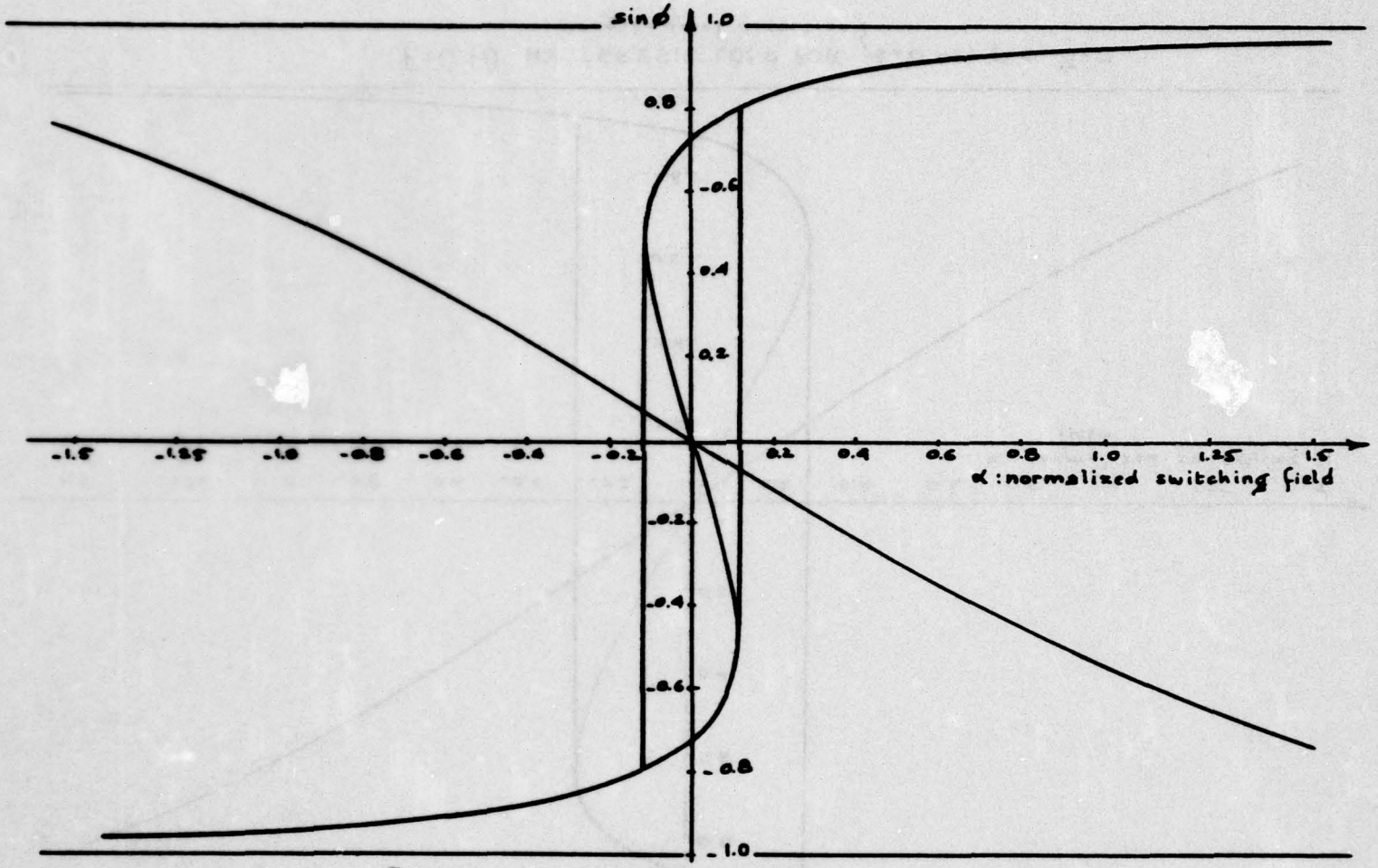


FIG. 11 HYSTERISIS LOOP FOR $\beta = 0.68$, $\gamma = 0$, $\delta = 0$
(longitudinal direction)

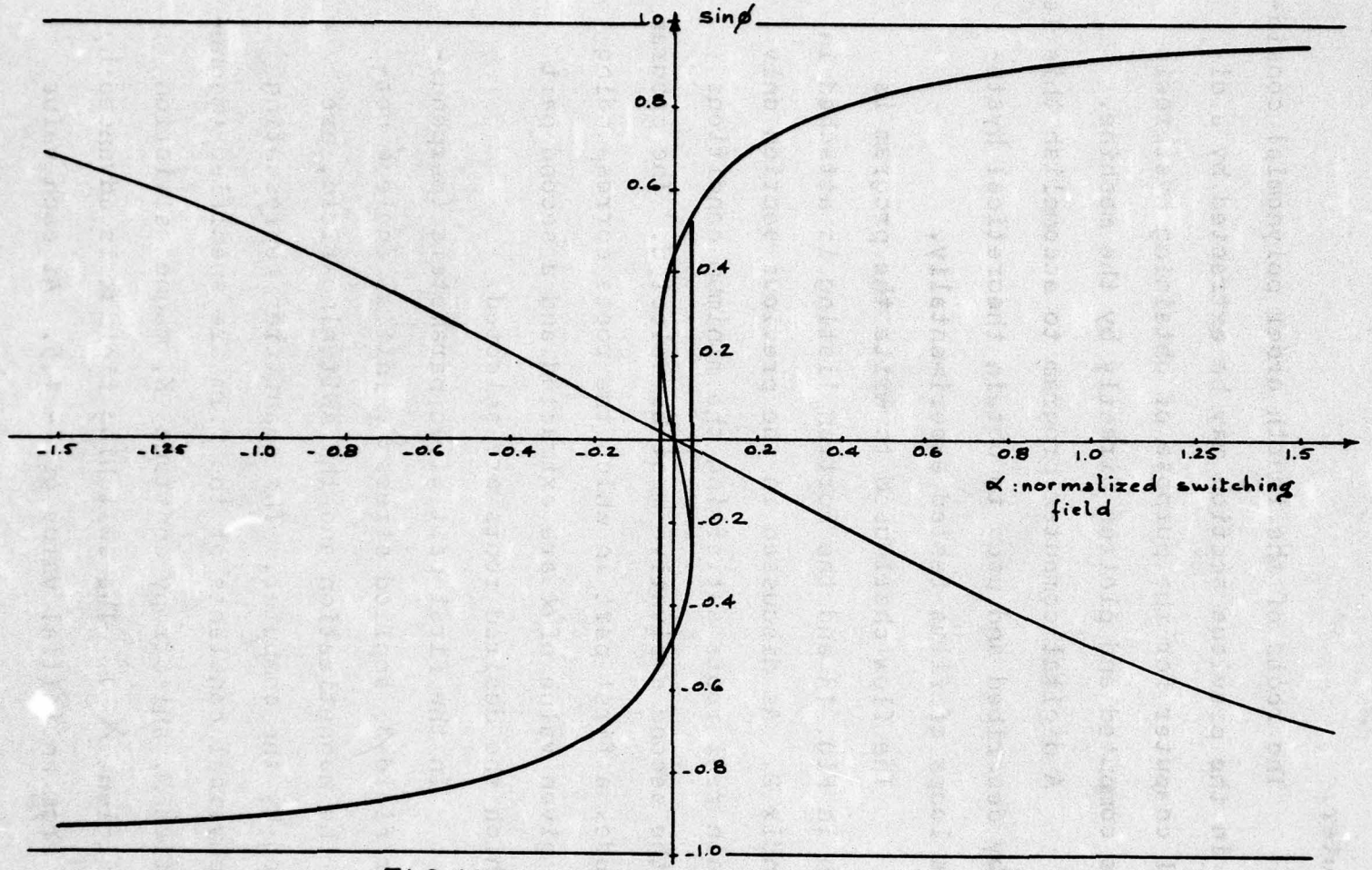


FIG. 12 HYSTERESIS LOOP FOR $\beta = 0.9$, $\gamma = 0$, $\delta = 0$
(longitudinal direction)

c. Determination of hysteresis loop by digital computer.

The roots of the fourth order polynomial considered in the previous section may be extracted by a digital computer for the purpose of obtaining hysteresis loops computed and plotted directly by the machine.

A digital computer program to accomplish this is hereby described and used to obtain theoretical hysteresis loops of films tested experimentally.

The flow chart used to write the program is shown in Fig. 13 and the Fortran listing is attached in Appendix 2. As discussed in the previous section only certain real roots satisfying the minimum conditions for the second derivative must be selected. The program includes a first part in which the roots corresponding to a given value of α are extracted and a second part in which the desired roots are selected.

In the first part given parameters (perpendicular field β, applied stress δ, initial angle γ between the magnetization and the switching field, are stored by the computer. The quantities representing the physical constants of the film are specified (magnetization M, anisotropy constant K, magnetostriction coefficient λ_s). The switching field α is advanced by $\Delta\alpha$ from an initial value of - 1.5. At each value

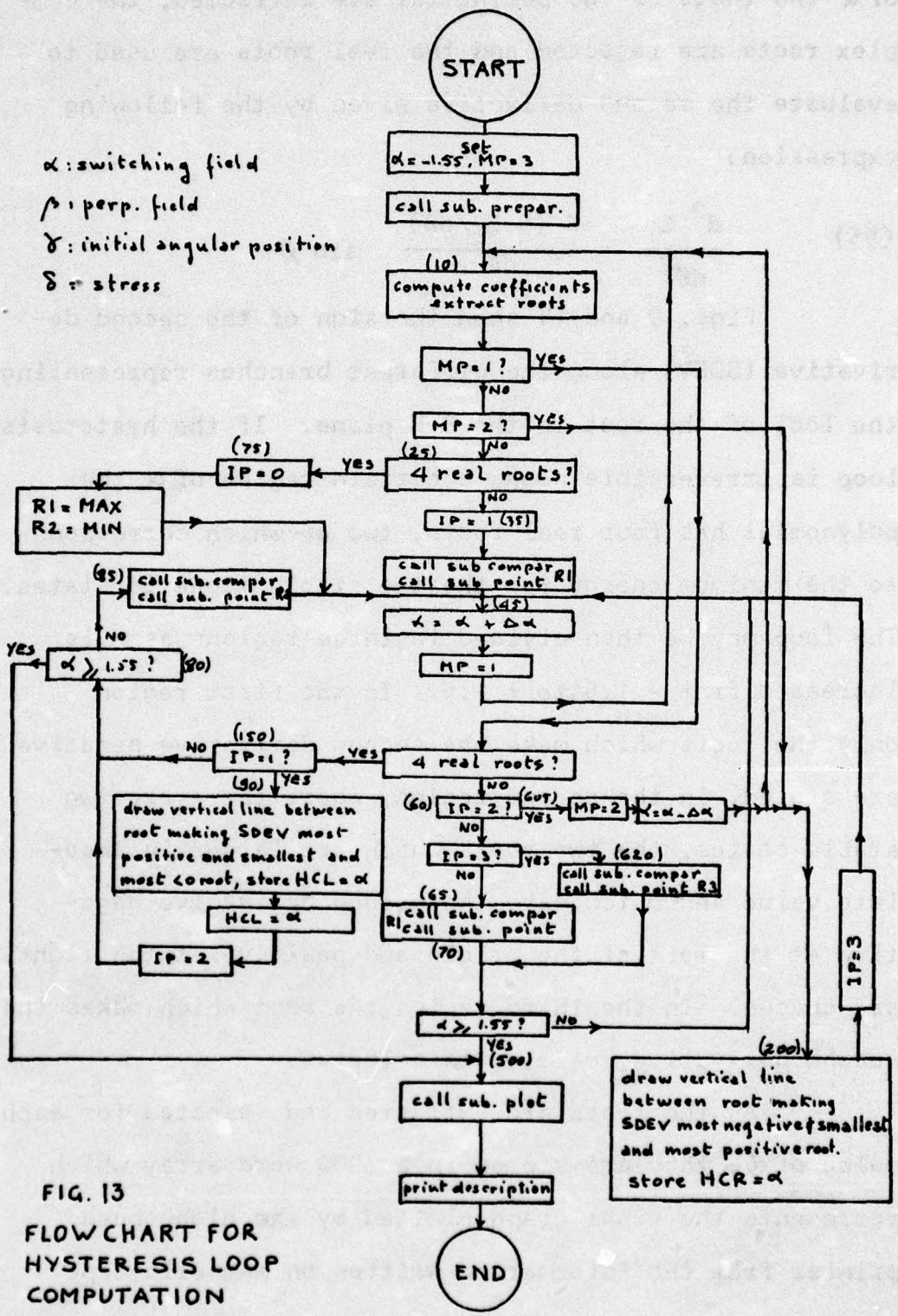


FIG. 13

FLOW CHART FOR HYSTERESIS LOOP COMPUTATION

of α the roots of the polynomial are extracted, the complex roots are rejected and the real roots are used to evaluate the second derivative given by the following expression:

$$(55) \qquad \frac{d^2 E_t}{d\phi^2} = \frac{d\,(d\,E_t/d\phi)}{ds} \quad \sin \phi$$

Figs. 9 and 14 show the sign of the second derivative (SDEV) along the different branches representing the loci of the root in the S-H plane. If the hysteresis loop is irreversible along a certain region of α the polynomial has four real roots, two of which correspond to the minimum energy for the two stable magnetic states. The loop may be then divided in three regions as α is increased from - 1.5 to + 1.5. In the first region only the roots which make the second derivative negative are stored, in the second region, where there are two stable states, the two roots which are larger in absolute value and which make the second derivative negative at the left of the origin and positive at the right, are chosen. In the third region the root which makes the second derivative positive is selected.

As the roots are extracted and selected for each value of α, they are stored in a 3000 word array which represents the final graph plotted by the high-speed printer from the information written on magnetic tape

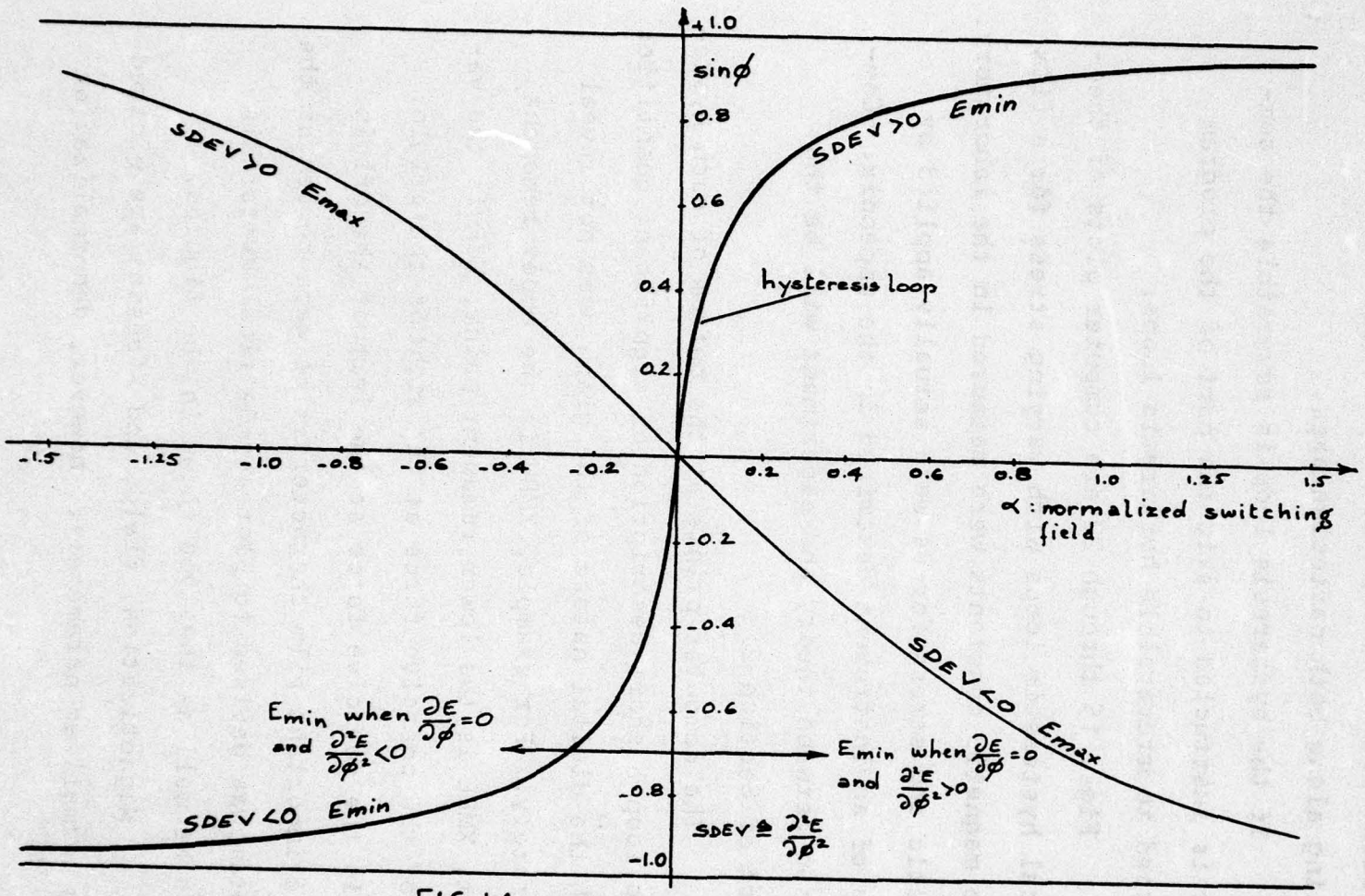


FIG. 14 HYSTERESIS LOOP FOR $\beta=0.6, \gamma=0, \delta=0.5$
(longitudinal direction)

subroutine transfers the array onto tape, with proper labeling along both cartesian axes.

If the hysteresis loop is reversible the computer is instructed to skip the part of the program reversed to irreversible hysteresis loops.

Figs. 15 through 20 are computer plots of theoretical hysteresis loops with varying stress for a film whose magnetic constants were measured in the laboratory. Magnetic and stress forces were actually applied by means of an instrument described in the appendix. Comparison between theory and experiment will be the object of Section 2.

The computer prints at the bottom of each hysteresis loop a short description of significant quantities which the digital nature of the graph does not reveal accurately. For example, XMRU is the upper remanent point, XMRL is the lower remanent point, HCR is the value of the coercive force at the right of the origin. HCL is the coercive force at the left of the origin. These important film characteristics were chosen as the program was devised to plot asymmetrical hysteresis loops as well as the type shown in the figures.

Magnetization, fields and stresses are plotted from normalized parameters; however, denormalization

factors for conversion into physical units are given in the plot description.

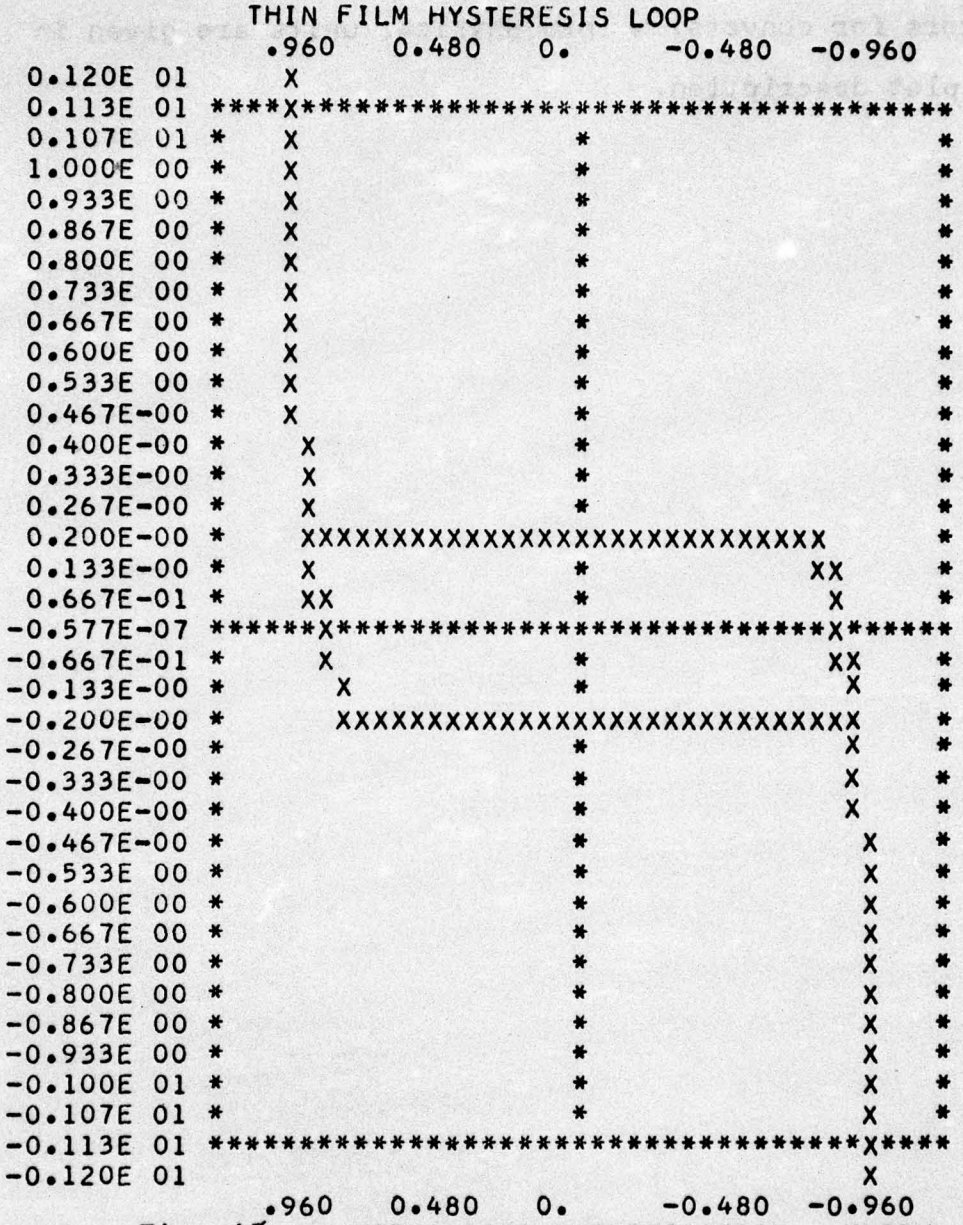


Fig. 15. NORMALIZED MAGNETIZATION = MNORM

MAGNETIZATION (GAUSSES) = (MNORM) 1450.
HSWCH (OERSTEDS) = ALPHA(2K/M) = (ALPHA)35.17
BETA = 0.590 DELTA = -0.132
GAMMA(INITIAL PHI) = -0 M (SATURATION) = 1450.
K(ERGS/CCM) = 25500. LAMBDAS(MAGSTRICTION)=0.20E-04
HPERP = (BETA)35.17 SIGMA(DYN/SCM)=(DELTA)0.85E 09
XMRU = 0.8534 XMRL = -0.8534
HCR = 0.2250 HCL = -0.2250

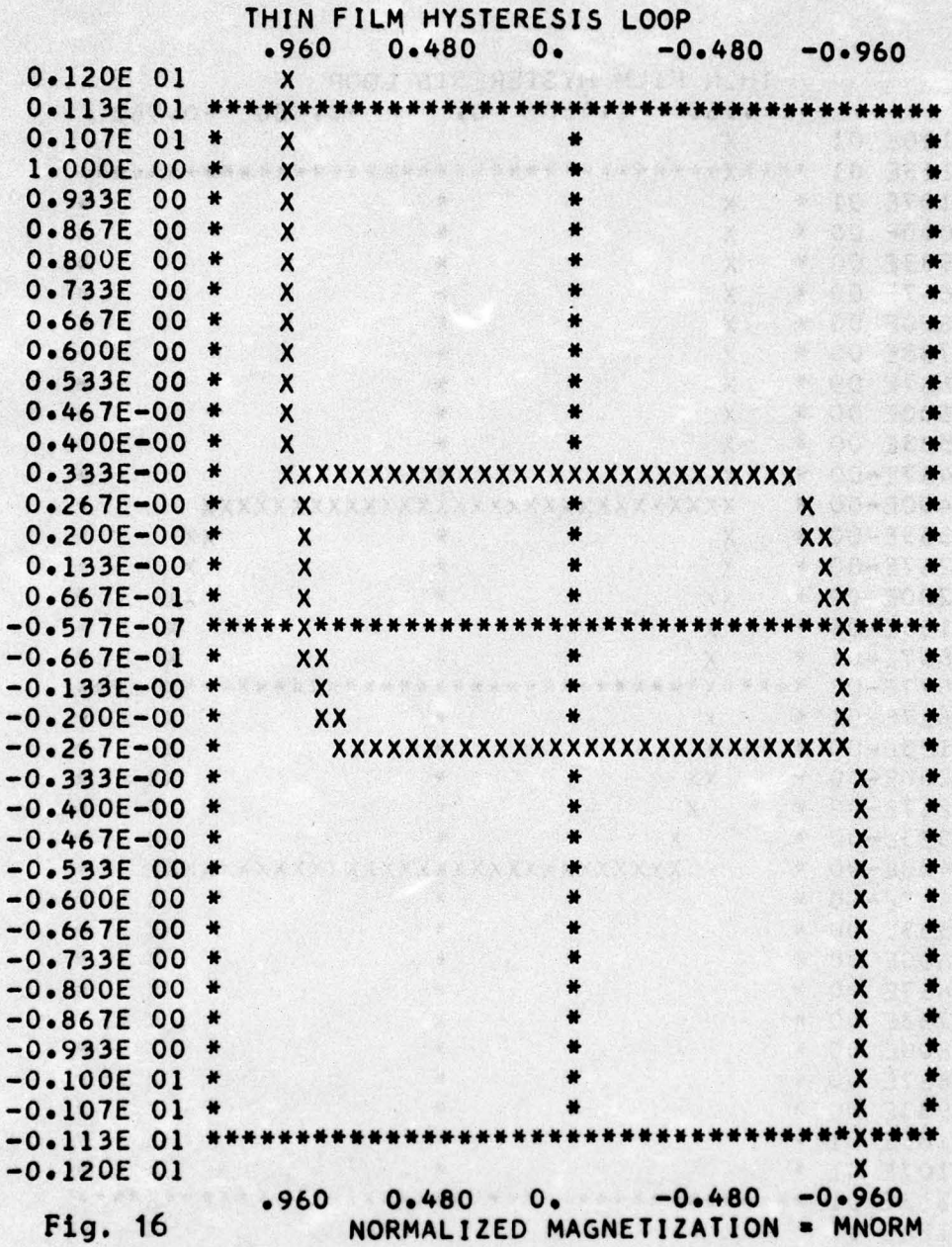


Fig. 16

MAGNETIZATION (GAUSSES) = (MNORM) 1450.
HSWCH (OERSTEDS) = ALPHA(2K/M) = (ALPHA)35.17
BETA = 0.590 DELTA = -0.266
GAMMA(INITIAL PHI) = -0 M (SATURATION) = 1450.
K(ERGS/CCM) = 25500. LAMBDAS(MAGSTRICTION)=0.20E-04
HPERP = (BETA)35.17 SIGMA(DYN/SCM)=(DELTA)0.85E 09
XMRU = 0.8848 XMRL = -0.8848
HCR = 0.3000 HCL = -0.3000

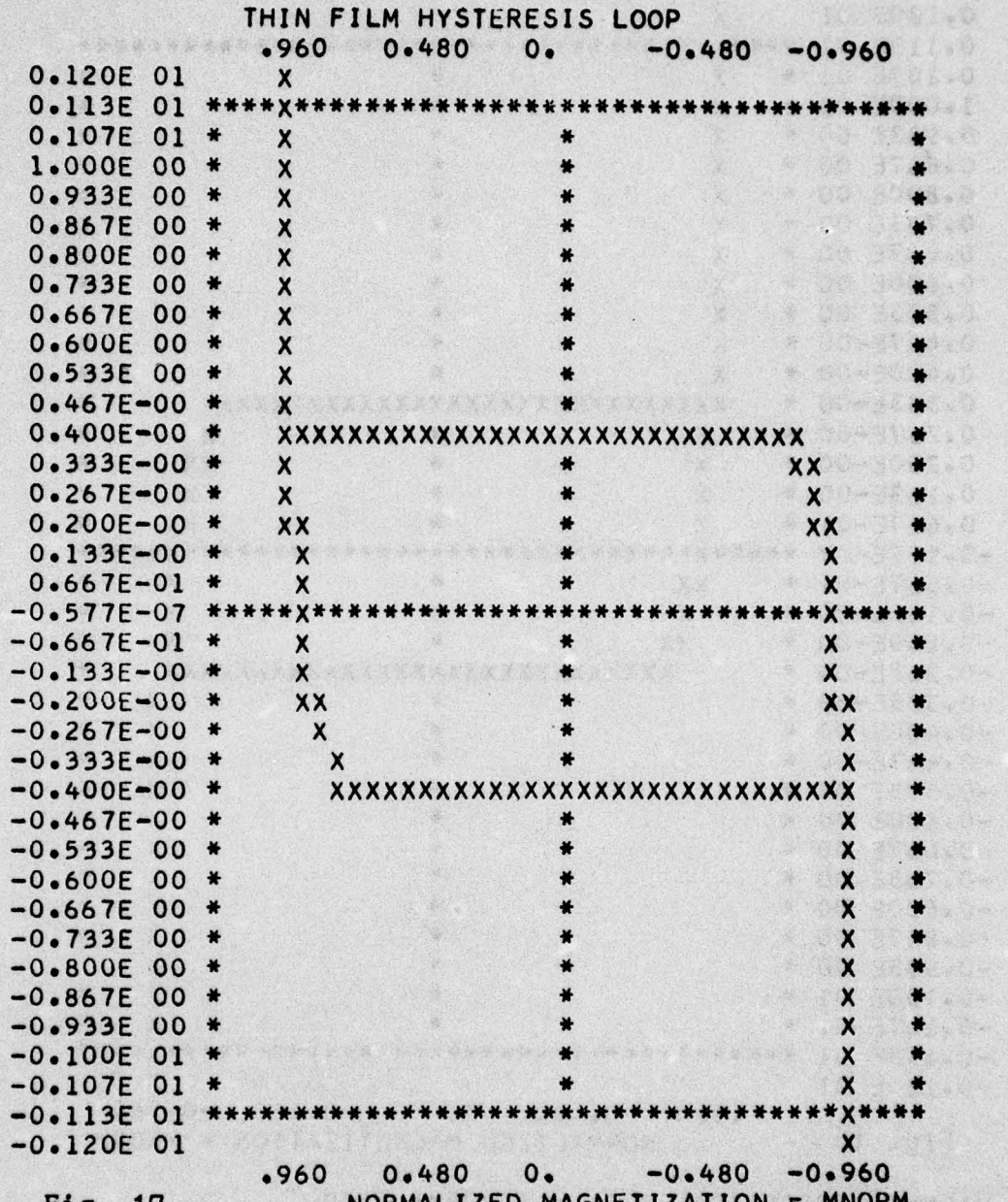


Fig. 17

MAGNETIZATION (GAUSSES) = (MNORM) 1450.
HSWCH (OERSTEDS) = ALPHA(2K/M) = (ALPHA)35.17
BETA = 0.590 DELTA = -0.400
GAMMA(INITIAL PHI) = -0 M (SATURATION) = 1450.
K(ERGS/CCM) = 25500. LAMBDAS(MAGSTRICTION)=0.20E-04
HPERP = (BETA)35.17 SIGMA(DYN/SCM)=(DELTA)0.85E 09
XMRU = 0.9069 XMRL = -0.9069
HCR = 0.4000 HCL = -0.4000

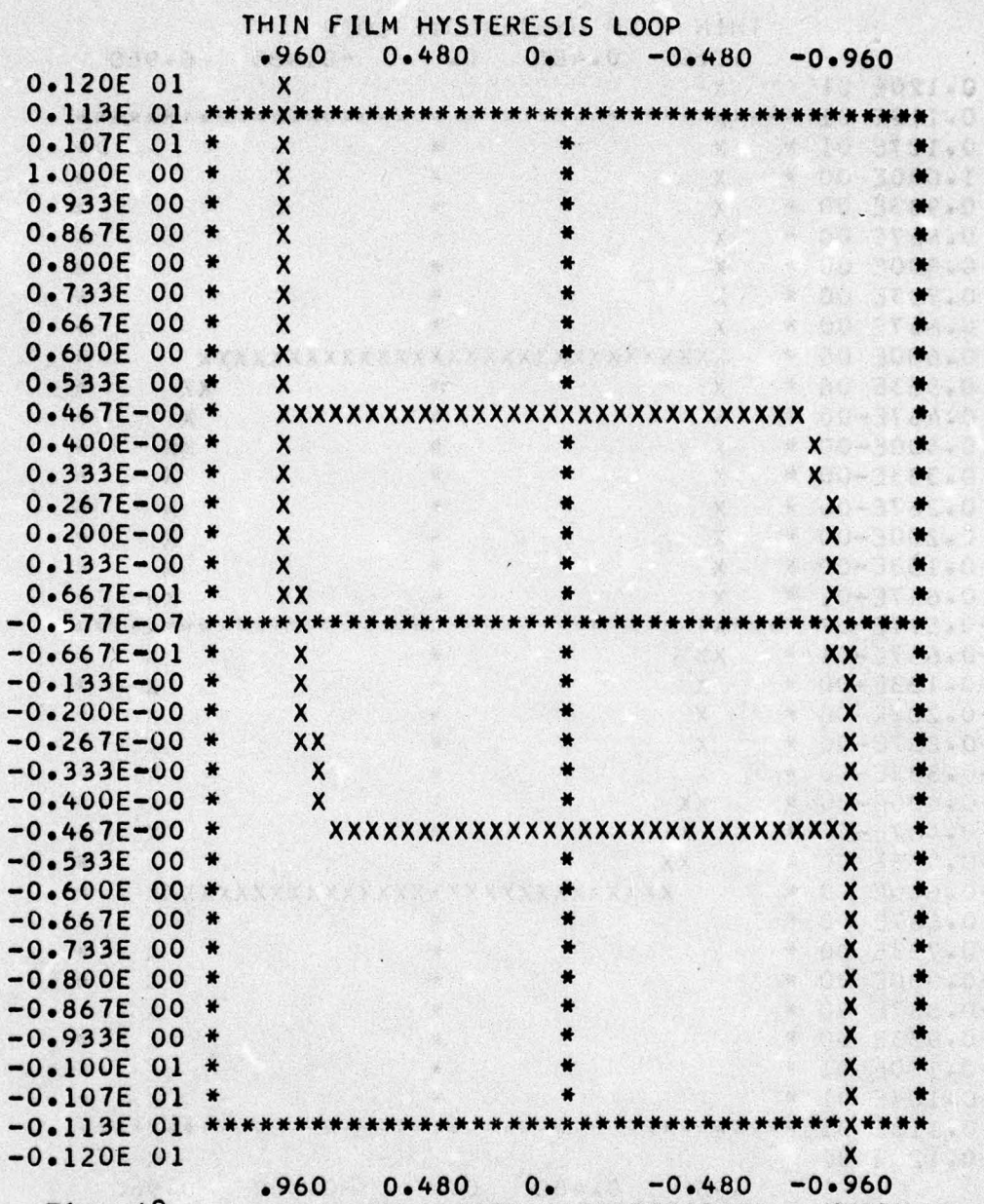


Fig. 18

MAGNETIZATION (GAUSSES) = (MNORM) 1450.
HSWCH (OERSTEDS) = ALPHA(2K/M) = (ALPHA)35.17
BETA = 0.590 DELTA = -0.532
GAMMA(INITIAL PHI) = -0 M (SATURATION) = 1450.
K(ERGS/CCM) = 25500. LAMBDAS(MAGSTRICTION)=0.20E-04
HPERP = (BETA)35.17 SIGMA(DYN/SCM)=(DELTA)0.85E 09
XMRU = 0.9229 XMRL = -0.9229
HCR = 0.4750 HCL = -0.4750

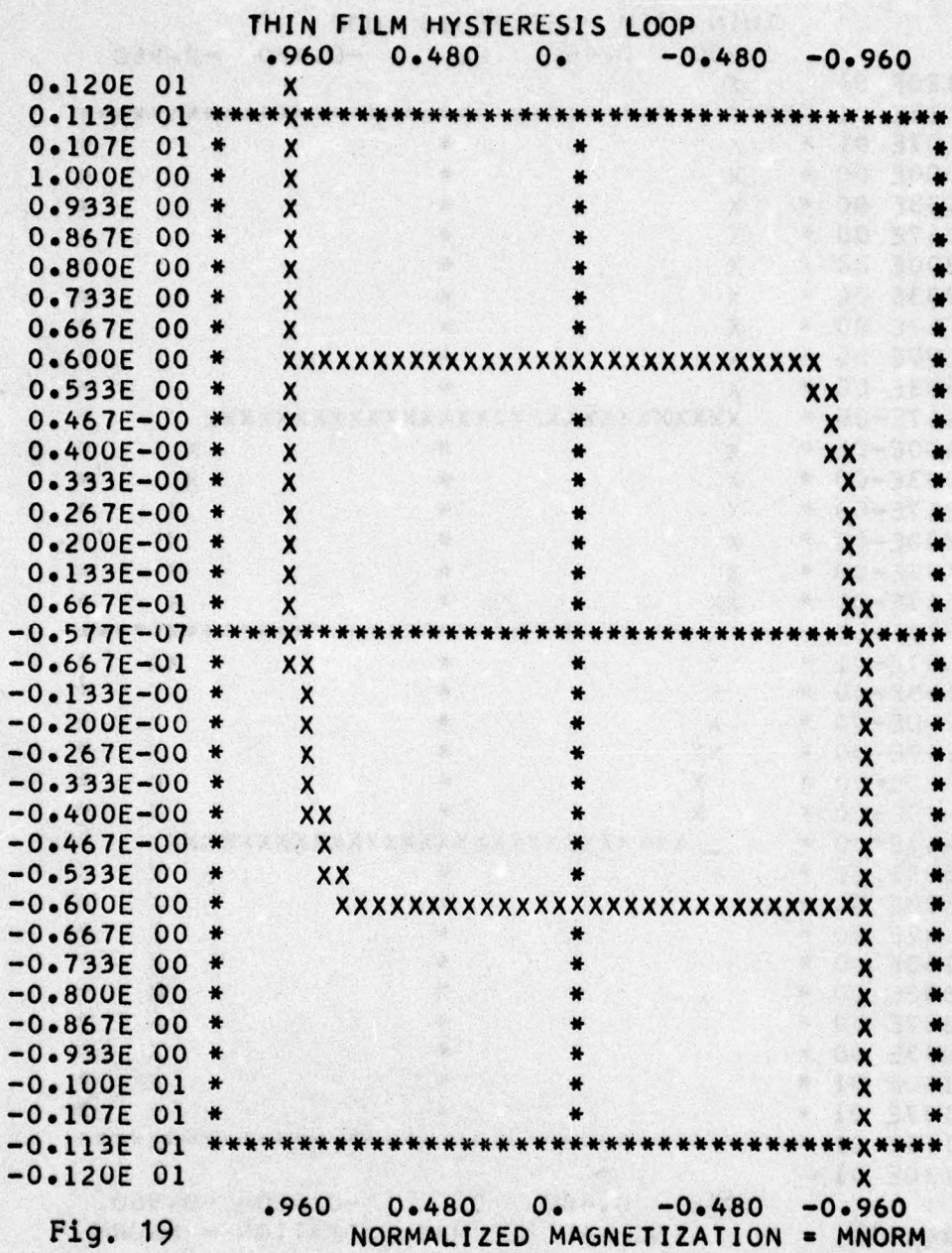


Fig. 19

MAGNETIZATION (GAUSSES) = (MNORM) 1450.
HSWCH (OERSTEDS) = ALPHA(2K/M) = (ALPHA)35.17
BETA = 0.590 DELTA = -0.664
GAMMA(INITIAL PHI) = -0 M (SATURATION) = 1450.
K(ERGS/CCM) = 25500. LAMBDAS(MAGSTRICTION)=0.20E-04
HPERP = (BETA)35.17 SIGMA(DYN/SCM)=(DELTA)0.85E 09
XMRU = 0.9350 XMRL = -0.9350
HCR = 0.5750 HCL = -0.5750

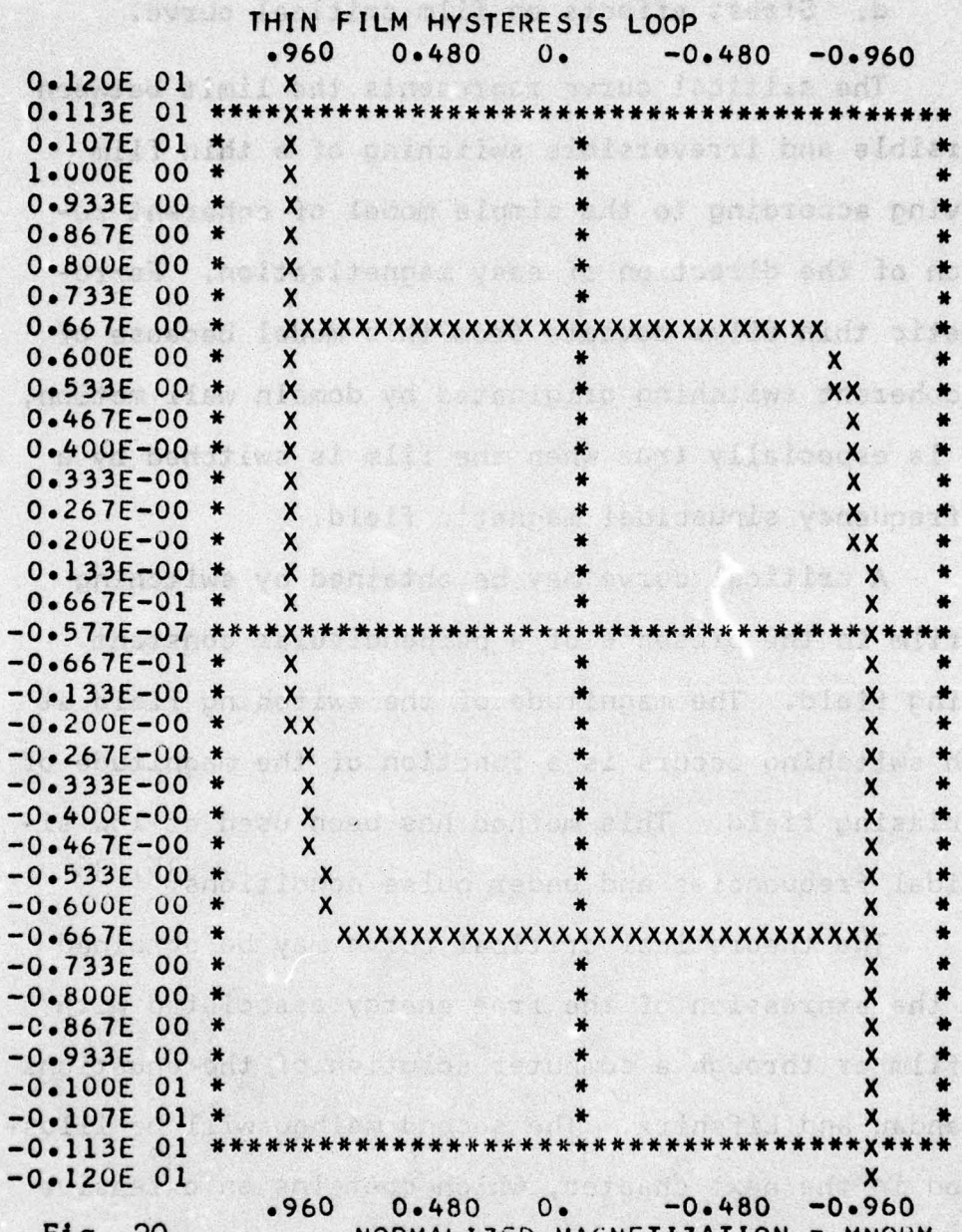


Fig. 20

MAGNETIZATION (GAUSSES) = (MNORM) 1450.
HSWCH (OERSTEDS) = ALPHA(2K/M) = (ALPHA)35.17
BETA = 0.590 DELTA = -0.796
GAMMA(INITIAL PHI) = -0 M (SATURATION) = 1450.
K(ERGS/CCM) = 25500. LAMBDAS(MAGSTRICTION)=0.20E-04
HPERP = (BETA)35.17 SIGMA(DYN/SCM)=(DELTA)0.85E 09
XMRU = 0.9445 XMRL = -0.9445
HCR = 0.6750 HCL = -0.6750

d. Stress effects on film critical curve.

The critical curve represents the limit between reversible and irreversible switching of a thin film behaving according to the simple model of coherent rotation of the direction of easy magnetization. Ferromagnetic thin films deviate from this model because of non-coherent switching originated by domain wall motion, This is especially true when the film is switched by a low frequency sinusoidal magnetic field.

A critical curve may be obtained by switching the film in the presence of a perpendicular constant biasing field. The magnitude of the switching field at which switching occurs is a function of the magnitude of the biasing field. This method has been used at low sinusoidal frequencies and under pulse conditions.[35, 36]

The theoretical critical curve may be obtained from the expression of the free energy associated with the film or through a computer solution of the equations of Landau and Lifshitz. The second method will be illustrated in the next chapter, which contains an extensive analog and digital study of these first order non-linear equations.

The free energy equation when no stress is applied to the film and in the assumption of coincidence between

the anisotropy axis and the switching field may be expressed by:

(56) $$E_t = K \sin^2 \phi - M H_p \sin \phi - M H_s \cos \phi$$

The conditions for irreversible switching of the film are:

(57) $$\frac{d E_t}{d\phi} = 0 \quad \frac{d^2 E_t}{d\phi^2} = 0$$

These conditions give:

(58) $$\frac{H_K}{2} \sin 2\phi - H_p \cos \phi + H_S \sin \phi = 0$$

(59) $$H_K \cos 2\phi + H_p \sin \phi + H_S \cos \phi = 0$$

where

(60) $$H_K = \frac{2K}{M}$$

Solving (58) for H_p and substituting in (59) gives:

(61) $$H_S = - H_K \cos^3 \phi$$

Substituting H_S in (59) gives:

(62) $$H_p = H_K \sin^3 \phi$$

From (61) and (62):

(63) $$\left(\frac{H_S}{H_K}\right)^{2/3} = \cos^2 \phi \qquad \left(\frac{H_p}{H_K}\right)^{2/3} = \sin^2 \phi$$

By adding equations (63) the equation of the critical curve is obtained

(64) $$H_p^{2/3} + H_S^{2/3} = H_K^{2/3}$$

This is the equation of a hypocycloid with four cusps also called "astroid" and it represents the envelope of a diameter of a circle of radius H_K rolling without slipping inside a fixed circle of diameter $4\ H_K$.

The region inside the astroid corresponds to reversible switching, while the outside contains points where switching is irreversible. If anisotropic stresses are applied to the film the anisotropy constant is changed by the magnetostrictive property of the film. The total free energy E_t contains then an additional stress term:

$$E_s = \frac{3}{2}\ \lambda_s\ \sigma\ \cos^2 \phi \tag{65}$$

Equation (56) may then be written:

$$E_t = K' \sin^2 \phi - M\ H_p \sin \phi - M\ H_s \cos \phi + \frac{3}{2}\lambda_s\sigma \tag{66}$$

where

$$K' = K - \frac{3}{2}\ \lambda_s\sigma \tag{67}$$

Conditions (56) for the minimum energy give then:

$$H_s^{2/3} + H_p^{2/3} = H_K'^{2/3} \tag{68}$$

where:

$$H_K' = \frac{2}{M}\ \left(K - \frac{3}{2}\ \lambda_s\sigma\ \right) \tag{69}$$

Equation (68) becomes:

$$H_s^{2/3} + H_p^{2/3} = \left(H_K - \frac{3\lambda_s \sigma}{M}\right)^{2/3}$$

This equation shows that the diameter of the hypocycloid fixed circle is increased when:

1. The film has a negative magnetostriction coefficient and a compressive stress is applied along H_s or a tensile stress is applied along H_p.

2. The film has a positive magnetostriction coefficient and a tensile stress is applied along H_s or a compressive stress is applied along H_p.

In all other cases the diameter of the fixed circle is decreased. Fig. 21 illustrates these conclusions.

Unless the magnetization is at an initial angle γ different from zero with respect to the longitudinal field, the combination of the stress and the longitudinal field, in the absence of a perpendicular field, cannot cause the film to switch. For a given value of stress the relationship between this angle of initial position of magnetization with H_s may be obtained by finding pairs of values of γ and H_s, which satisfy both equations (57) simultaneously. Under these conditions it seems impossible to eliminate ϕ between the two equations and express the relationship between and H_s explicitly.

The methods presented in section b of this chapter for plotting hysteresis loops by root locus, using a Spirule or a digital computer from the energy equation, may be used readily to obtain critical curves relating γ and H_s in the presence of applied stresses.

1. Root locus method by the Spirule

The roots of the fourth order polynomial obtained from the first of equations (57) are extracted for $H_s = 0$ ($\alpha = 0$, if normalized fields are used). If only two real roots are obtained it is concluded immediately that there is only one remanent point and the search for a critical curve has no further interest. If the four real roots are found at $H_s = 0$ the two roots corresponding to the minimum, which are in most cases the two closest to the origin, are followed until the value of H_s corresponding to the coercive force is found. This value coincides with the point at which two real roots become complex as previously explained in section b of this chapter. If this procedure is repeated for successive values of γ the curve $\gamma = f(\alpha_{sc})$ may be plotted for any value of applied stress.

2. Root locus method by digital computer.

In the digital computer program illustrated in section b of this chapter the computer is instructed to start extracting the roots of the polynomial at $\alpha = 0$

and to count the number of real roots by examining the complex parts of all the roots. If only two real roots are detected at $\alpha = 0$ the computation is terminated and the computer prints that the hysteresis loop has only one remanent point. If four real roots are found α is increased by $\Delta\alpha$ and the machine extracts new roots. The procedure is repeated until the number of real roots becomes two. The computer backs up one step in α and stores the value of the coercive force. A new value of γ is given by stepping up γ by $\Delta\gamma$ and the same procedure is reiterated. Values of α_c and γ are stored in an array until γ has reached its maximum allowed limit, at which point the array is transferred onto tape for plotting on the high-speed printer.

It is relevant to point out that the second derivative condition for the minimum need not be used to obtain the critical curve from the Spirule or from the digital computer program.

A simplified flow chart is shown in Fig. 22 for computing the critical curve $\gamma = f(\alpha_c)$. The astroid curve may also be obtained by setting $\gamma = 0$ and replacing γ by β in the program. A program listing for such a computation is given in Appendix 3.

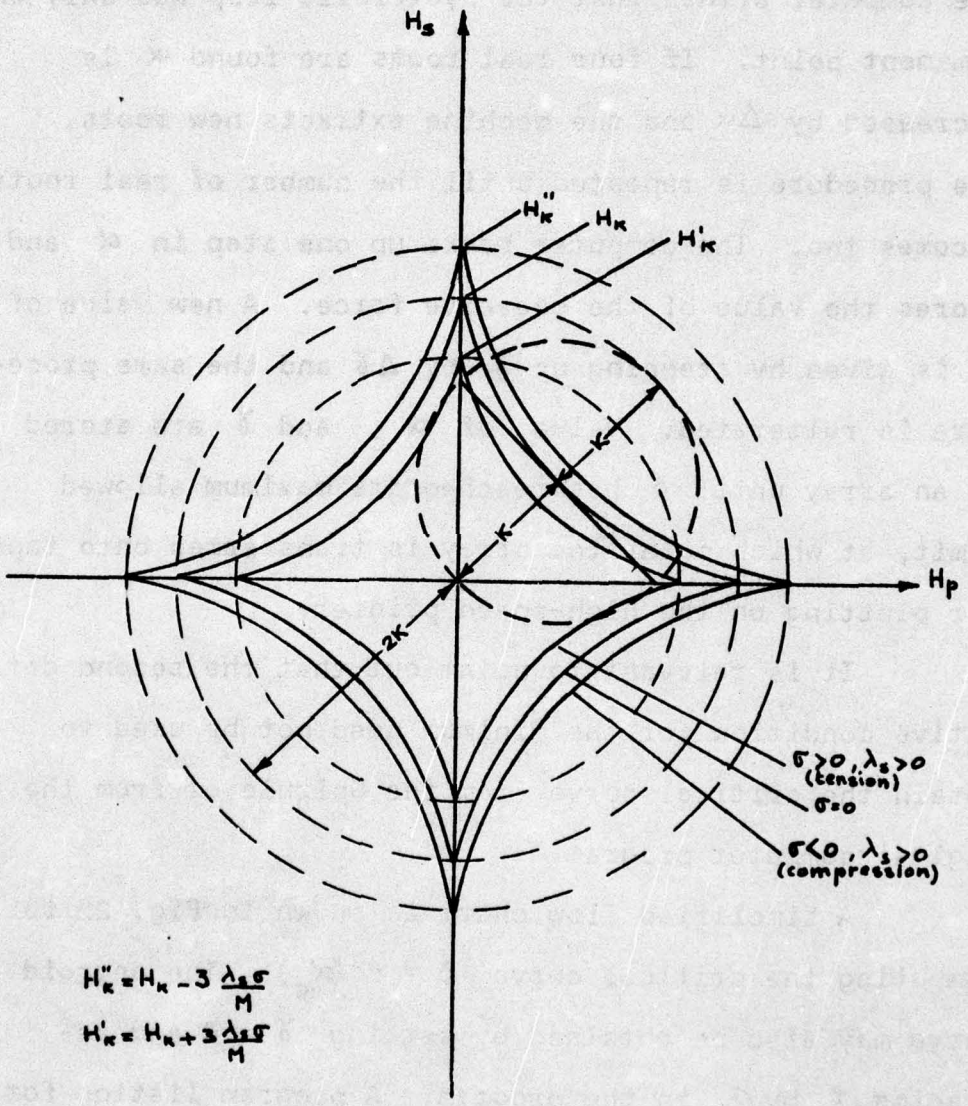
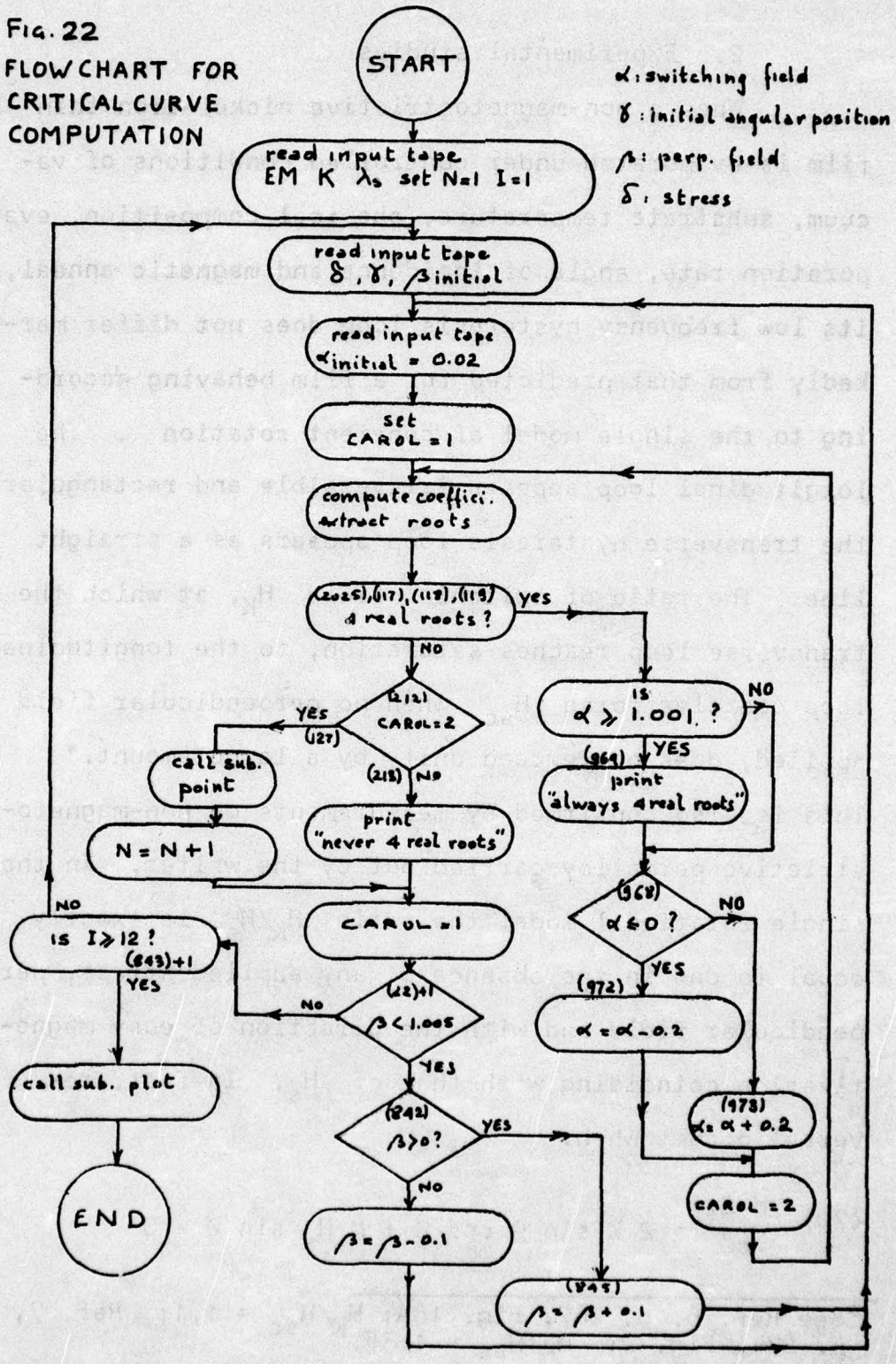


FIG. 21 EFFECTS OF ANISOTROPIC STRESS ON CRITICAL CURVE

Fig. 22
FLOW CHART FOR CRITICAL CURVE COMPUTATION



2. Experimental studies

When a non-magnetostrictive nickel-iron thin film is evaporated under controlled conditions of vacuum, substrate temperature, chemical composition, evaporation rate, angle of incidence and magnetic anneal, its low frequency hysteresis loop does not differ markedly from that predicted for a film behaving according to the single model of coherent rotation . The longitudinal loop appears irreversible and rectangular, the transverse hysteresis loop appears as a straight line. The ratio of switching field H_K, at which the transverse loop reaches saturation, to the longitudinal loop coercive force H_{sc} when no perpendicular field is applied, does not exceed unity by a large amount.* This is also confirmed by measurements on non-magnetostrictive permalloy carried out by the writer. In the single rotational model the ratio H_K/H_{sc} is exactly equal to one in the absence of any applied stress, perpendicular field and with the direction of easy magnetization coinciding with that of H_s. In fact, reversal occurs when:

$$(70) \quad \frac{d E_t}{d\phi} = 2 K \sin \phi \cos \phi + M H_s \sin \phi = 0$$

*See Ref. 6, p. 267, Fig. 16A: $H_K/H_{sc} = 1.1$; Ref. 7, p. 274, Fig. 2: $H_K/H_{sc} = 1.35$.

The two stable states correspond to $\emptyset$ = 0 degrees and $\emptyset$ = 180 degrees. The magnetization is reversed when the energy $M H_s$, contributed by the applied magnetic field, exceeds the anisotropy energy 2 K. The corresponding value of H_s is then:

(71) $$H_{sc} = 2 K/M$$

By rotating the film 90 degrees the equation for the transverse loop is obtained:

(72) $$\frac{d E_t}{d\emptyset} = 2 K \sin \emptyset \cos \emptyset - M H_p \cos \emptyset = 0$$

The value H_K of the perpendicular field at which saturation is reached corresponds to a 90 degrees rotation of the magnetization away from the easy axis. Equality between intrinsic and applied energy gives:

(73) $$H_p = H_K = 2 K/M$$

From (71) and (73):

(74) $$H_K/H_{sc} = 1$$

As the chemical composition of the permalloy is changed toward regions of higher magnetostriction, larger deviations between experiment and simple rotational theory are observed. The magnetic structure becomes more sensitive to the complex system of residual strains. The observed hysteresis loops reveal the existence of magnetic anisotropy dispersion in certain regions of the film. The transverse loop becomes irreversible and the longitudinal loop loses its square-

ness.

This type of film hysteretic behavior has been reported in the literature[39, 40] and a model based on the assumption of a minor easy direction of magnetization along the main hard axis has been attributed to the presence of Neel type walls directed along the main easy axis.[39]

Studies of the effects of stresses on hysteresis loops and on domain configurations as observed by Bitter patterns are however meager in the literature and were therefore the subject of the following experiments.

Permalloy films having a chemical composition ranging between 0 and 100% iron in the melt and thicknesses of approximately 1000 Å were evaporated and measurements were carried out on the following characteristic film constants: anisotropy constant, magnetization, magnetostriction coefficient, chemical composition (in the film), and thickness.

a. Stress effects on hysteresis loops.

The film chosen for this study presented a high magnetostrictive effect and had a composition of 44% nickel, 56% iron $\pm$ 1%, as read from an experimental curve obtained from X-ray spectrochemical analysis.

The following magnetic and physical

properties were measured:

anisotropy constant:

$K = 15500$ ergs/ccm (unstressed film) $\pm$ 10%

saturation magnetization:

$M = 1450$ gauss $\pm$ 5%

magnetostriction coefficient:

$\lambda_s = 19.10^{-6}$ (in/in) oe $\pm$ 15%

thickness:

1290 $\mathring{A}$ $\pm$ 5%

Other constants were taken from published data for bulk nickel-iron alloys:

Young's modulus[4]: $E = 13 \times 10^{11}$ dynes/scm

Poisson's ratio[4]: $\nu = 0.28$

The film is placed in a hysteresis loop tester capable of providing a switching field of about 70 oe at 2500 cps and a constant field of approximately the same magnitude, along the direction perpendicular to the first. The drives may be switched from one set of coils to the other in order to observe both hysteresis loops while the film is being stressed. The applied stress is controlled by a micrometer and is initially set to zero by means of a measuring microscope.* The stress induced in the film substrate by mechanical bending is transmitted to the film by adherence.

*See Appendix 4

In addition to the differences between theoretical and experimental loops due to the inherent simplicity of the model, hysteresis loops displayed on the oscilloscope deviate from rectangularity as affected by the time response of the instrument. A perfectly square hysteresis loop is obtained if a perfect square wave originated from the electronic integration of the emf induced in the sensing coil at each film reversal is displayed vs. a voltage exactly proportional to the reversing magnetic field and with the proper phase relationship. In experimental instrumentations, such as reported here, however, the circuitry necessary for integration simplification and filtering of the signal causes the corners of the square wave to be rounded and the sides to deviate from the vertical. In addition, the difference between the signal representing B and that representing H is frequency dependent and for a fixed frequency depends upon the magnitude of the drive. Variations in the apparent loop coercive force result as the drive is changed. This apparent variation in coercive force may be eliminated by a phase compensation circuit introduced along the path of the signal representing H just before the oscilloscope. The proper phase adjustment is obtained when the intersections of the vertical sides of the loop with the H-axis (i.e. H_c) remain fixed as

the drive is changed. For rotational thin film switching, vertical lines passing through such intersection points are the true sides of the experimental hysteresis loops when over two stable states exist.

Hysteresis loops shown in Figs. 25 to 32 have the same horizontal and vertical calibration:

Horizontal: 1 cm = 6.68 oersteds

Vertical: 1 cm = 550 gausses

A description of a compensating circuit for making calibrations with both pairs of driving coils identical is given in Appendix 6.

Figs. 23 and 24 show the configuration of magnetic and mechanical forces applied to the film in the experiment and in the rotational model.* In Fig. 2, representing the conditions of drive for the model, the stress was assumed to be a tension parallel to the perpendicular field H_p and corresponding to a term:

$$(75) \qquad \frac{3}{2} \lambda_s \sigma \cos^2 \phi$$

In the experiment the film substrate is bent to induce a tension parallel to the switching field. The configuration of the model reduces to that of the experiment if the sign of σ (or δ) is changed in expression (75) or in equation (25), respectively, since:

*See also figures 2 and 3.

$$(75') \quad \frac{3}{2}\lambda_s\sigma\cos^2\phi = \frac{3}{2}\lambda_s\sigma + \frac{3}{2}\lambda_s(-\sigma)\sin^2\phi$$

The additive constant in the energy expression (75') may be disregarded.

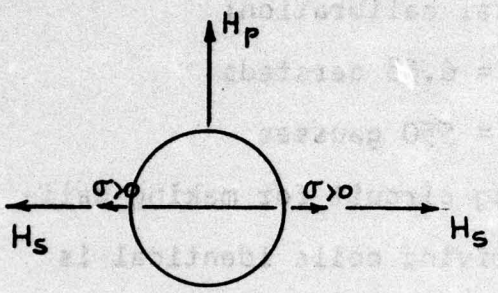


FIG. 23
EXPERIMENTAL CONFIGURATION

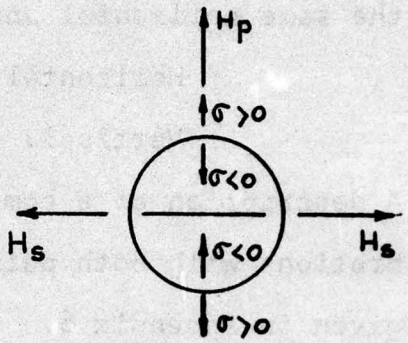


FIG. 24
ROTATIONAL MODEL CONFIG.
$\sigma<0$ equivalent to Fig. 23.
(Cfr. Figs. 2,3)

The film substrate is bent by the action of a glass bar which is moved vertically, remaining parallel to a horizontal plane. The edges of the bar impress a pure bending moment in the region of the substrate occupied by the film, thus giving a constant unidirectional stress across the film. The vertical displacement of the bar, expressed in thousandths of an inch on a micrometer is related to the strain induced in the substrate and in the film by the expression (cf. appendix 5).

(76) $$\varepsilon = (7.8 + 72.4d)\ 10^{-6}$$

The corresponding stress is:

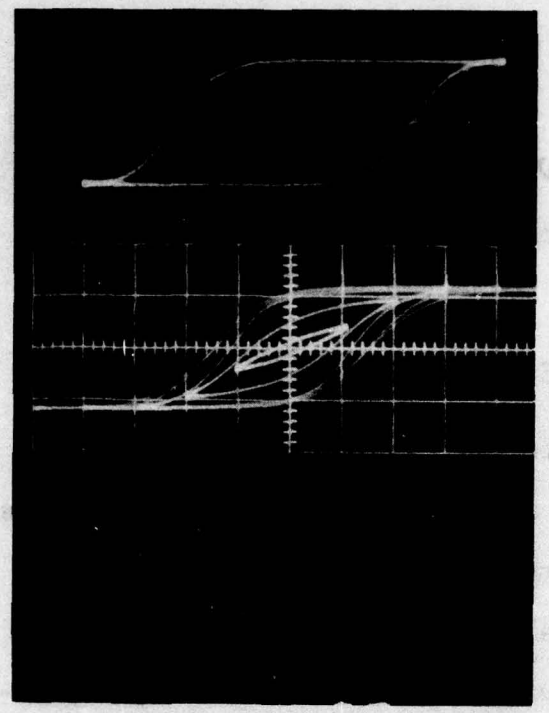
$$\sigma = \varepsilon E (1 + \nu) = 16 \times 10^3 \varepsilon \text{ Kg/mm}^2$$

The normalized stress in the film is related to the strain ε by:

(77) $$\delta = 3 \frac{\lambda_s}{2K} E (1 + \nu) \varepsilon$$

Hysteresis loops in the longitudinal and in the perpendicular directions, in the absence of a transverse field H_p and applied stress δ are shown in Figs. 25A and B. Several transverse loops have been recorded, corresponding to several values of drive in the longitudinal direction. Figs. 26A to F show the effect of applying an increasing transverse field on the longitudinal loop. The coercive force decreases from 15.4 oe to zero as the perpendicular field is increased from zero to 4.75 Kg/mm^2, the longitudinal coercive force increases from 15.4 to 17 oe, in the absence of perpendicular field, as is shown by Figs. 25 and 27. The transverse loop becomes more elongated and its coercive force decreases from 10.7 oe to 6.68 oe. The application of a perpendicular field of increasing magnitude up to 57.6 oe causes the longitudinal loop coercive force to decrease to zero.

Further increase in stress does not cause



A. LONG. LOOP, $H_p = 0$ oe
$H_c = 15.4$ oe

B TRANSV. LOOPS

FIG. 25
H : 1cm = 6.68 oe.
V : 1cm = 550 Gausses
$\sigma = 0$ kg/mm^2

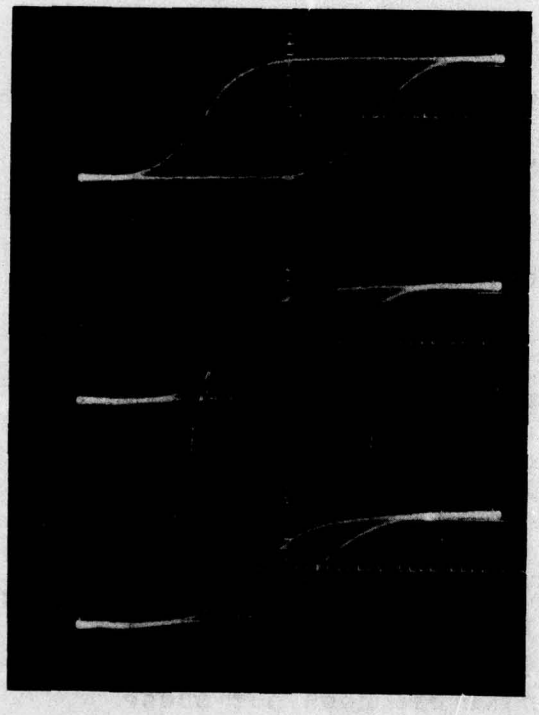
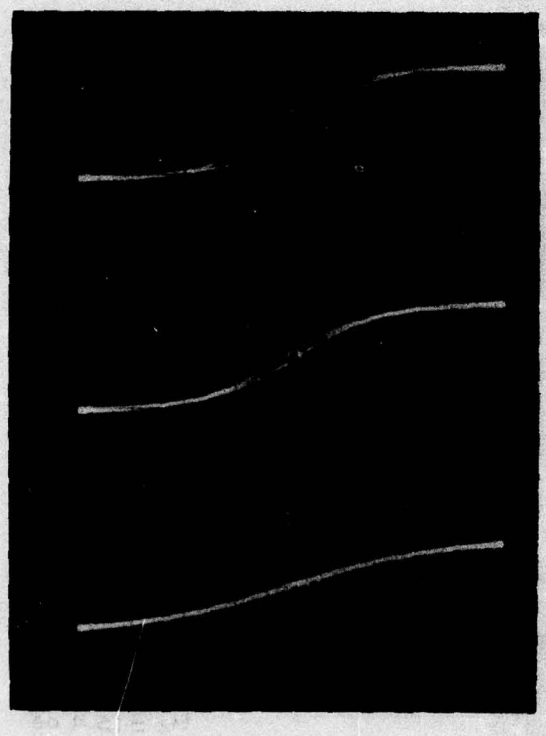


FIG. 26
H : 1cm = 6.68 oe
V : 1cm = 550 Gausses
$\sigma = 0$ kg/mm^2

A LONG. LOOP, $H_p = 6.7$ oe
$H_c = 11.0$ oe

B LONG. LOOP, $H_p = 13.42$ oe
$H_c = 6.5$ oe

C LONG. LOOP, $H_p = 20$ oe
$H_c = 3.8$ oe

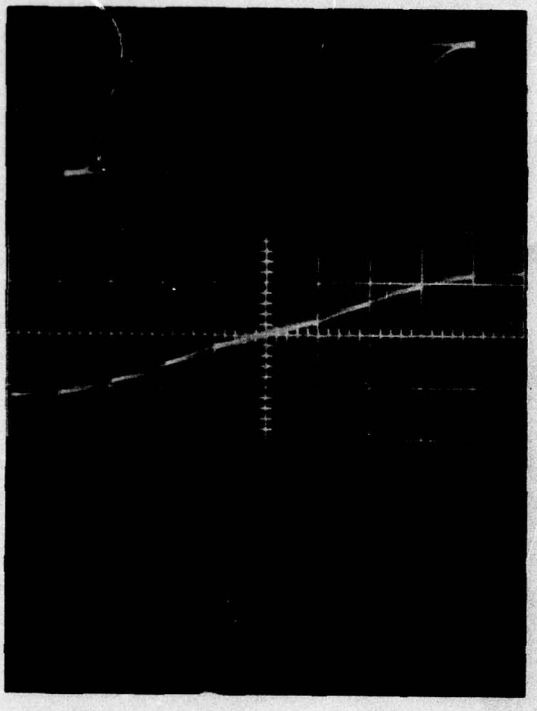


D LONG. LOOP, H_p = 26.8 oe
H_c = 2 oe

E LONG. LOOP, H_p = 33.5 oe
H_c = 0.85 oe

F LONG. LOOP, H_p = 57.6 oe
H_c = 0.0

FIG. 26 (CONT.)
H : 1 cm = 6.68 oe
V : 1 cm = 550 Gausses
σ = 0 kg/mm^2



A. LONG. LOOP, $H_p = 0$
$H_c = 17$ oe

B. TRANSV. LOOPS

FIG. 27
H : 1cm = 6.68 oe
V : 1cm = 550 gausses
$\sigma = 4.75$ KG/mm^2
$\varepsilon = 297 \cdot 10^{-6}$

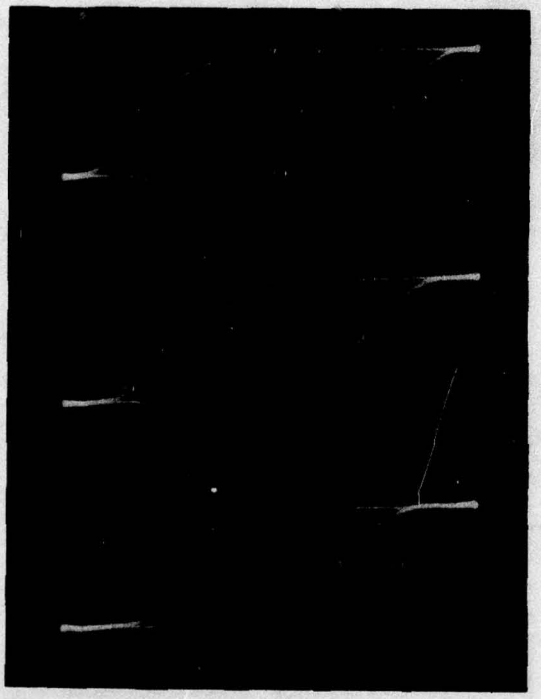


FIG. 28
H : 1cm = 6.68 oe
V : 1cm = 550 gausses
$\sigma = 4.75$ KG/mm^2

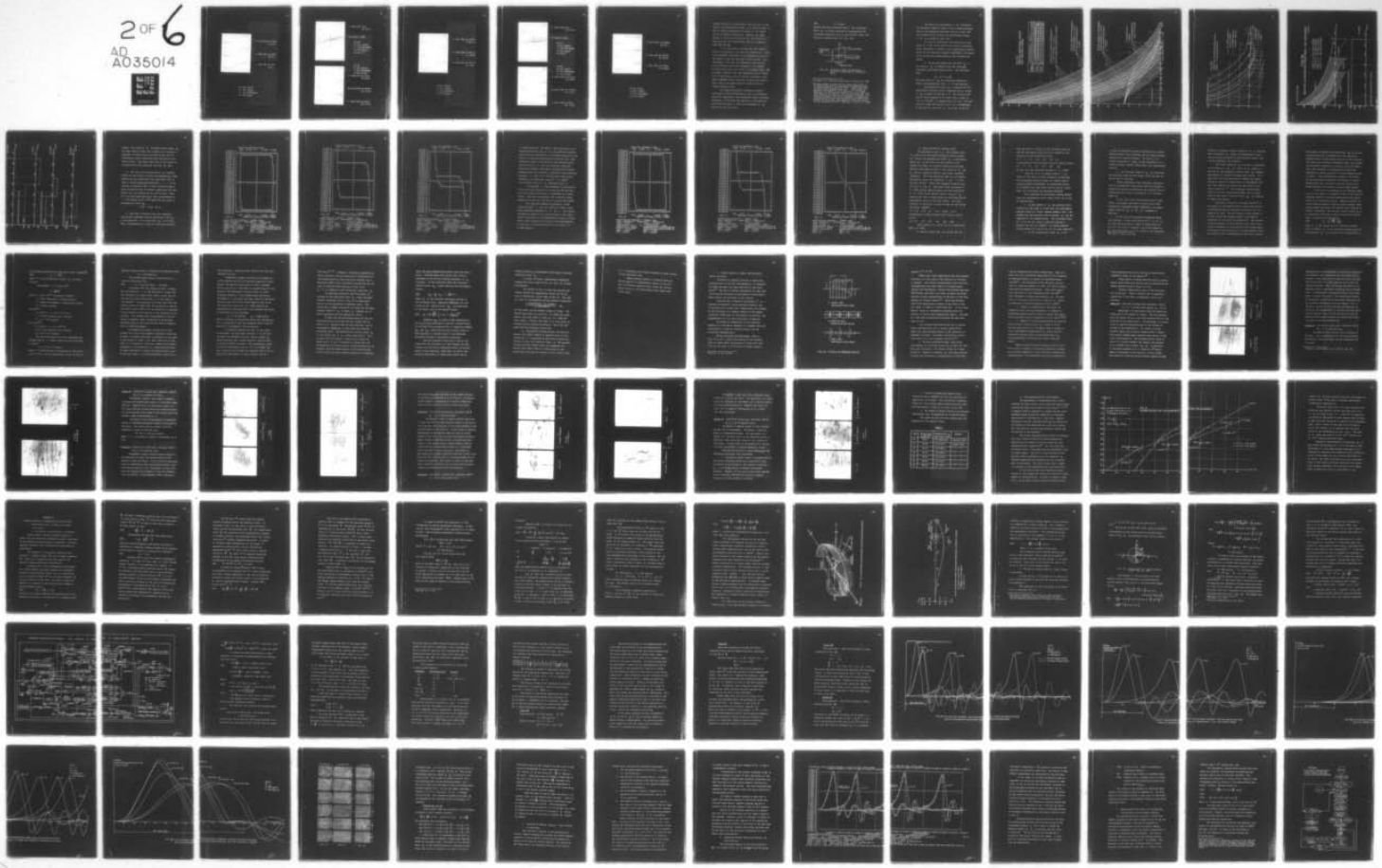
A. LONG. LOOP, $H_p = 6.71$ oe
$H_c = 15.4$ oe

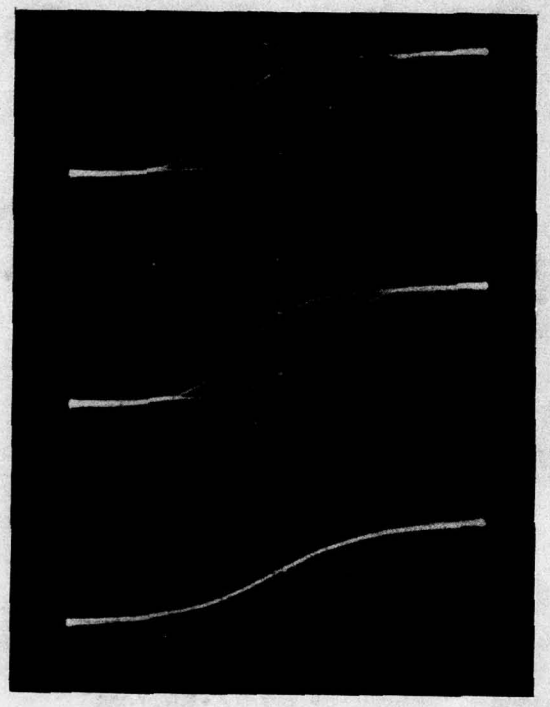
B. LONG. LOOP, $H_p = 13.42$ oe
$H_c = 6.5$ oe

C. LONG. LOOP, $H_p = 20$ oe
$H_c = 3.8$ oe

AD-A035 014 CALIFORNIA UNIV LOS ANGELES DEPT OF ENGINEERING F/G 20/2
ON THE USE OF PIEZOELECTRIC-MAGNETOSTRICTIVE COUPLING IN DIGITA--ETC(U)
AUG 62 A A BORSEI NONR-233(52)
UNCLASSIFIED UCLA62-37 NL

2 OF 6
AD
A035014



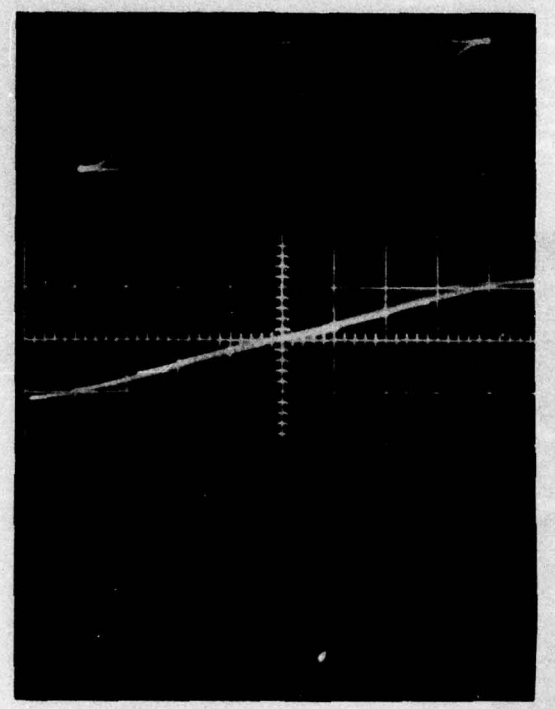


D LONG. LOOP, $H_p = 26.8$
$H_c = 6.0$

E LONG. LOOP, $H_p = 33.5$
$H_c = 4.3$

F LONG. LOOP, $H_p = 57.6$
$H_c = 0$

FIG. 28 (CONT.)
H: 1 cm = 6.68 oe
V: 1 cm = 550 gausses
$\sigma = 4.75$ KG/mm^2



A. LONG. LOOP, $H_p = 0$

$H_c = 17.4$ oe

B. TRANSV. LOOPS

FIG. 29

H : 1cm = 6.68 oe

V : 1cm = 550 Gausses

$\sigma = 7.07$ KG/mm^2

$\varepsilon = 442 . 10^{-6}$

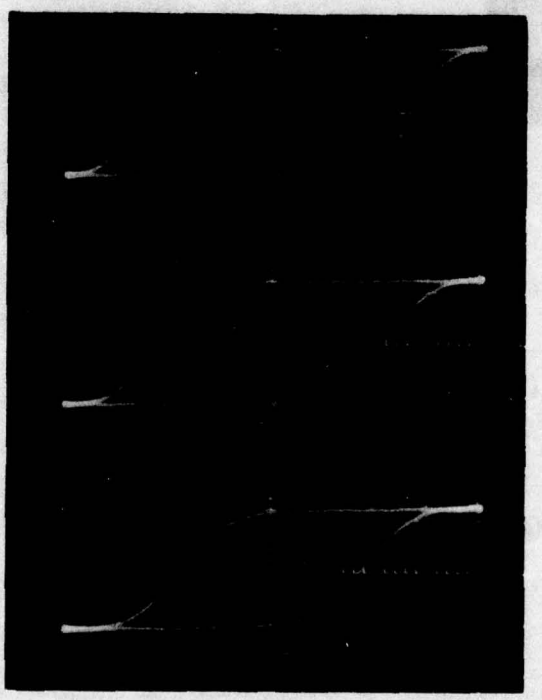


FIG. 30

H : 1cm = 6.68 oe

V : 1cm = 550 Gausses

$\sigma = 7.07$ KG/mm^2

A. LONG. LOOP, $H_p = 6.71$ oe

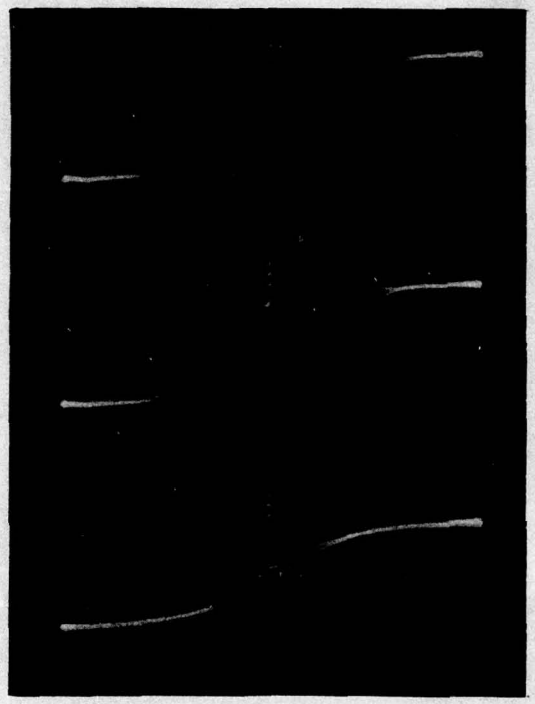
$H_c = 16.2$ oe

B. LONG. LOOP, $H_p = 13.42$ oe

$H_c = 14.5$ oe

C LONG. LOOP, $H_p = 20$ oe

$H_c = 11.4$ oe

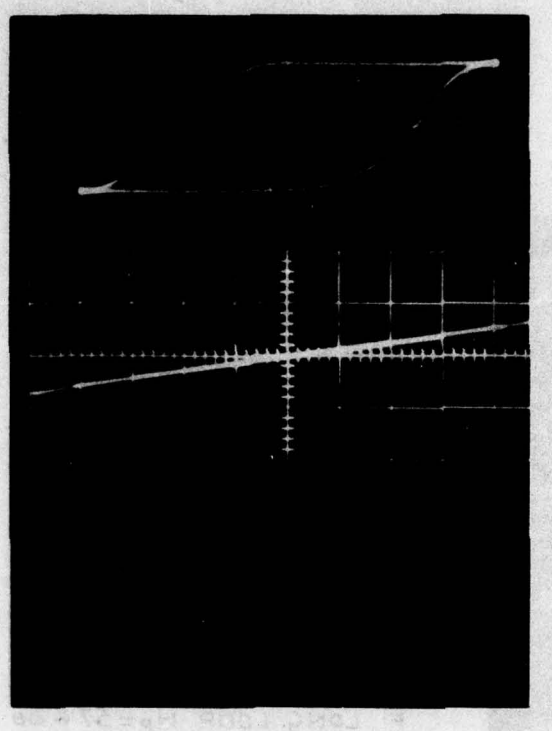


D LONG. LOOP, $H_p = 26.8$ oe
$H_c = 8.6$ oe

E LONG. LOOP, $H_p = 33.5$ oe
$H_c = 6.68$ oe

F LONG. LOOP, $H_p = 57.6$ oe
$H_c = 1.2$ oe

FIG. 30 (CONT.)
H : 1 cm = 6.68 oe
V : 1 cm = 550 gausses
$\sigma = 7.07$ Kg/mm^2.



A LONG. LOOP, $H_p = 0$
$H_c = 17.4$ oe

B TRANSV. LOOPS

FIG. 31
H : 1 cm = 6.68 oe
V : 1 cm = 550 Gausses
$\sigma = 15.17$ KG/mm^2
$\varepsilon = 948 . 10^{-6}$

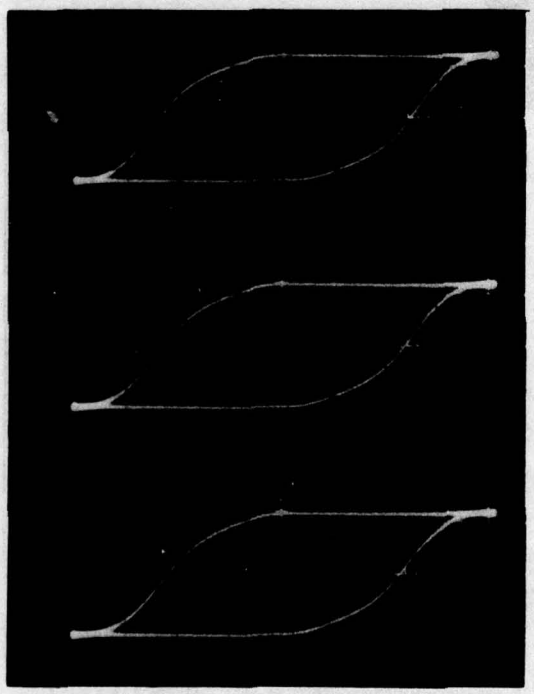
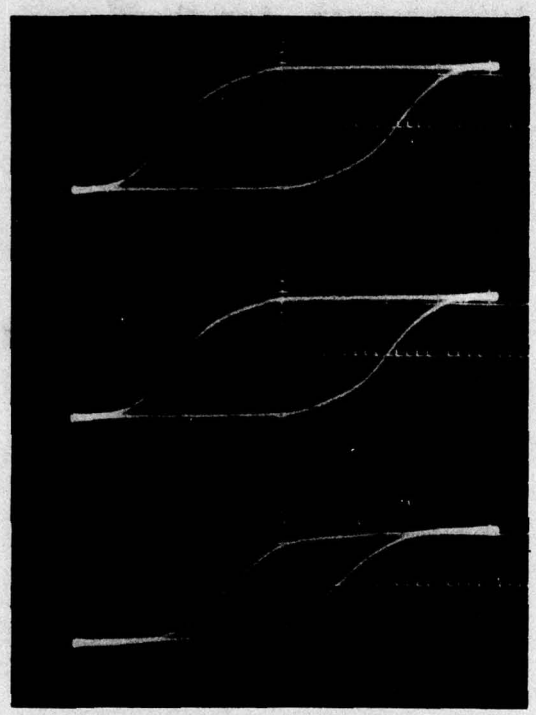


FIG. 32
H : 1 cm = 6.68 oe
V : 1 cm = 550 Gausses
$\sigma = 15.17$ KG/mm^2

A LONG. LOOP, $H_p = 6.71$ oe
$H_c = 16.8$ oe

B LONG. LOOP, $H_p = 13.42$ oe
$H_c = 16.2$ oe

C LONG LOOP, $H_p = 20$ oe
$H_c = 14.7$ oe



D LONG. LOOP, $H_p = 26.8$ oe
$H_c = 14$ oe

E LONG. LOOP, $H_p = 33.5$ oe
$H_c = 13.3$ oe

F LONG. LOOP, $H_p = 57.6$ oe
$H_c = 6.68$ oe

FIG. 32 (CONT.)
H : 1 cm = 6.68 oe
V : 1 cm = 550 Gausses
$\sigma = 15.17$ KG/mm^2

further increase in longitudinal coercive force in the absence of perpendicular field, as is shown by Figs. 29 and 31, which correspond to stresses of 7.07 Kg/mm^2 and 15.17 Kg/mm^2 respectively. However, for these values of stress an increase in H_p up to 57.6 oe does not close the longitudinal loop as is shown by Figs. 30F and 32F.

It is reasonable to assume that the limiting value of longitudinal coercive force reached at a stress of 4.75 Kg/mm^2 corresponds to an alignment of most of the domains along the direction of the tension. The experimental fact that the transverse loop coercive force continues to decrease beyond σ = 4.75 Kg/mm^2 to reach practically zero at σ = 7.07 Kg/mm^2 (Figs. 27B and 29B), indicates that the transverse loop is sensitive to the presence of any residual transverse anisotropy component beyond the point at which the longitudinal loop is no longer affected significantly by further applied stress.

For films presenting a negligible magnetic anisotropy in the hard direction, such as non-magnetostrictive composition films evaporated under controlled conditions, it has been the practice to determine the anisotropy constant, K, from the measurement of H_K and use of the expression

(78) $$K = M H_K/2$$

derived from the rotational model.* The anisotropy field H_K is usually measured by extrapolating the reversible transverse loop to saturation**, under conditions of reduced drive (cf. Fig. 33).

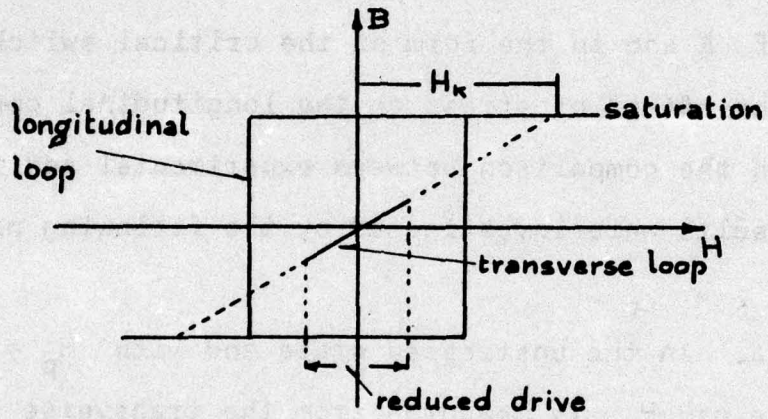


Fig. 33: Graphical method for measuring H_K from an experimental transverse loop.

---

*See Ref. 7, p. 276 and bottom trace in Fig. 2, p. 275.

**Another method of measuring the anisotropy field is to subject the film to ferromagnetic resonance at microwave frequencies with the film oriented along the two directions between which the desired degree of magnetic anisotropy is to be measured. At a fixed frequency, as the applied field is increased, the voltage induced in a pick-up coil reaches a maximum. The difference between the field magnitudes to reach the maximum with the easy axis oriented at 0° and 90° with respect to the field, corresponds to twice the value of the anisotropy field[41]. (See Ref. 6, Fig. 7, p. 269).

The method for measurement of H_K introduces an uncertainty whenever there exists an open hysteresis loop in the transverse direction such as in Fig. 25B. This problem exists because the relationship between K and H_K assumes an ideal film.

In order to investigate the difference in the values of K and in the form of the critical switching curve, the effect of stress on the longitudinal coercive force and the comparison between experimental and theoretical results were investigated by the following procedure.

a. In the unstressed state and with $H_p = 0$ the value of H_K is measured from the transverse hysteresis loop under reduced drive. Fig. 25B gives then:

$$H_K = 21 \text{ oe} \pm 10\%.$$

With this value of H_K, the anisotropy constant is found, using expression (77): K = 15,500 ergs/ccm.

A perpendicular field H_p is applied and the longitudinal coercive force is measured for six values of H_p, as shown in Figs 26A to F. The stress on the film is then increased in 13 steps until a value of $\sigma = 15.17 \text{ Kg/mm}^2$ is reached (Figs. 31, 32). For each value of stress the coercive force H_c corresponding to the same six values of H_p as in Fig. 26 are re-

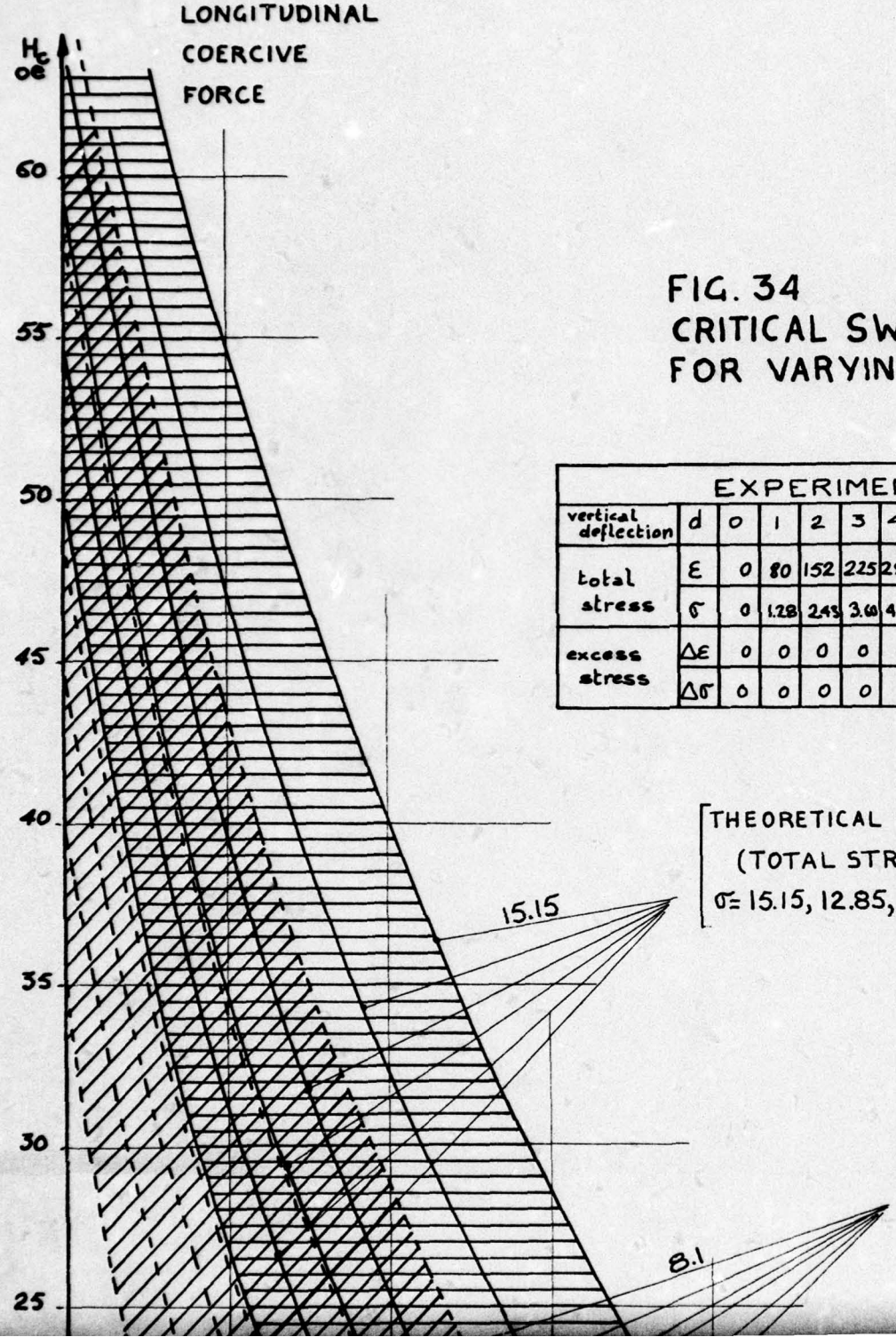


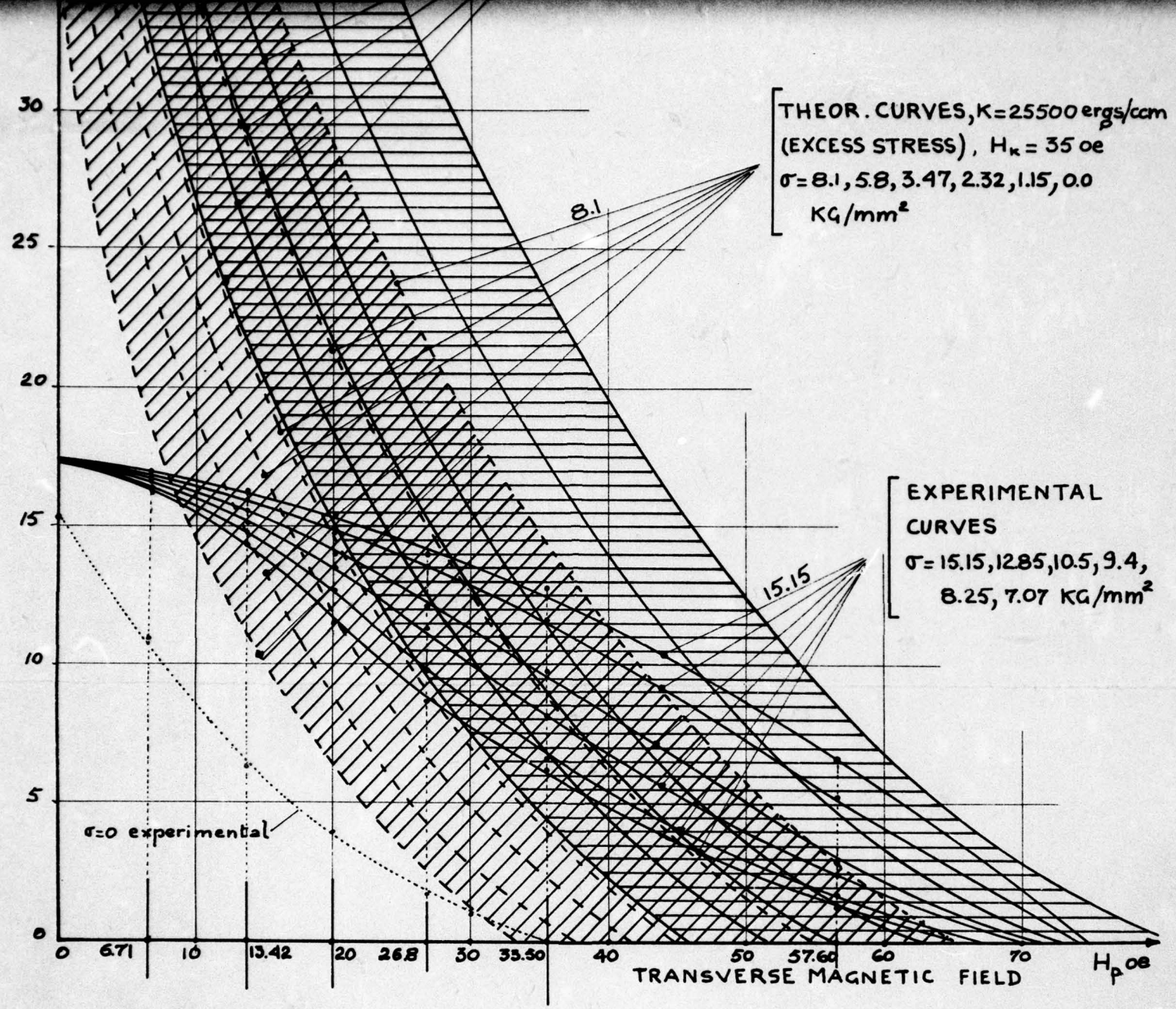
FIG. 34
CRITICAL SWITCHING CURVES
FOR VARYING STRESS

EXPERIMENTAL DATA

vertical deflection	d	0	1	2	3	4	5	6	7	8	9	10	11	12	13	$\times 10^{-3}$ in.
total stress	ε	0	80	152	225	297	370	442	514	587	659	732	804	876	948	$\times 10^{-6}$
	σ	0	1.28	2.43	3.60	4.85	6.15	7.07	8.25	9.40	10.5	11.7	12.85	14.0	15.15	$\frac{kg}{mm^2}$
excess stress	$\Delta\varepsilon$	0	0	0	0	0	0	0	72	144	213	284	362	433	505	$\times 10^{-6}$
	$\Delta\sigma$	0	0	0	0	0	0	0	1.15	2.32	3.47	4.63	5.8	6.9	8.1	$\frac{kg}{mm^2}$

THEORETICAL CURVES, K = 15500 ergs/ccm
(TOTAL STRESS), H_K = 21 oe
σ = 15.15, 12.85, 10.5, 9.4, 8.25, 7.07, KG/mm²

THEOR. CURVES, K = 25500 ergs/ccm
(EXCESS STRESS), H_K = 35 oe
σ = 8.1, 5.8, 3.47, 2.32, 1.15, 0.0
KG/mm²


THEOR. CURVES, K=25500 ergs/ccm
(EXCESS STRESS), H_K = 35 oe
σ = 8.1, 5.8, 3.47, 2.32, 1.15, 0.0
KG/mm²
8.1
EXPERIMENTAL
CURVES
σ = 15.15, 12.85, 10.5, 9.4,
8.25, 7.07 KG/mm²
15.15
σ=0 experimental
30
25
20
15
10
5
0
0
6.71
10
13.42
20
26.8
30
35.50
40
50
57.60
60
70
H_p oe
TRANSVERSE MAGNETIC FIELD

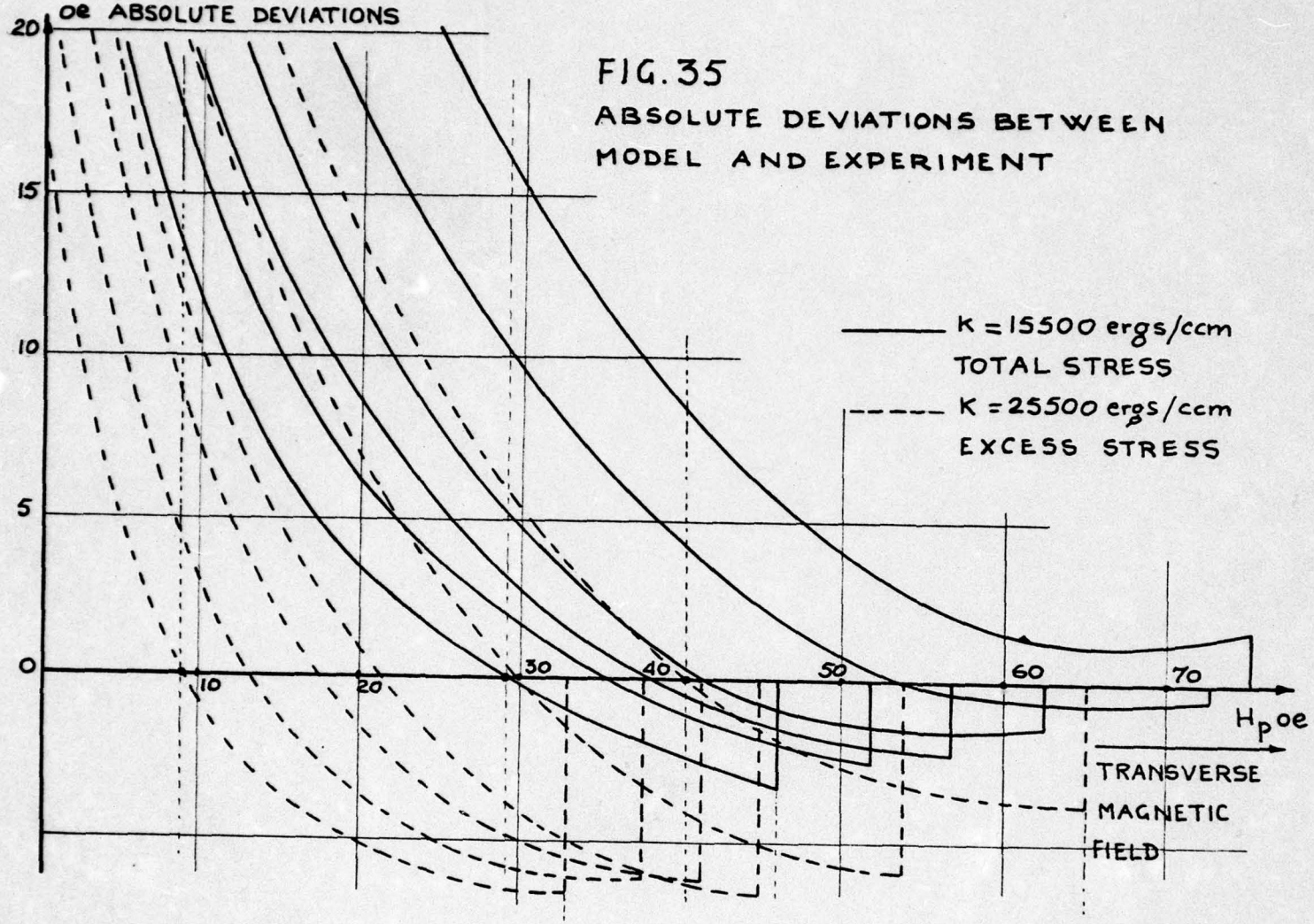
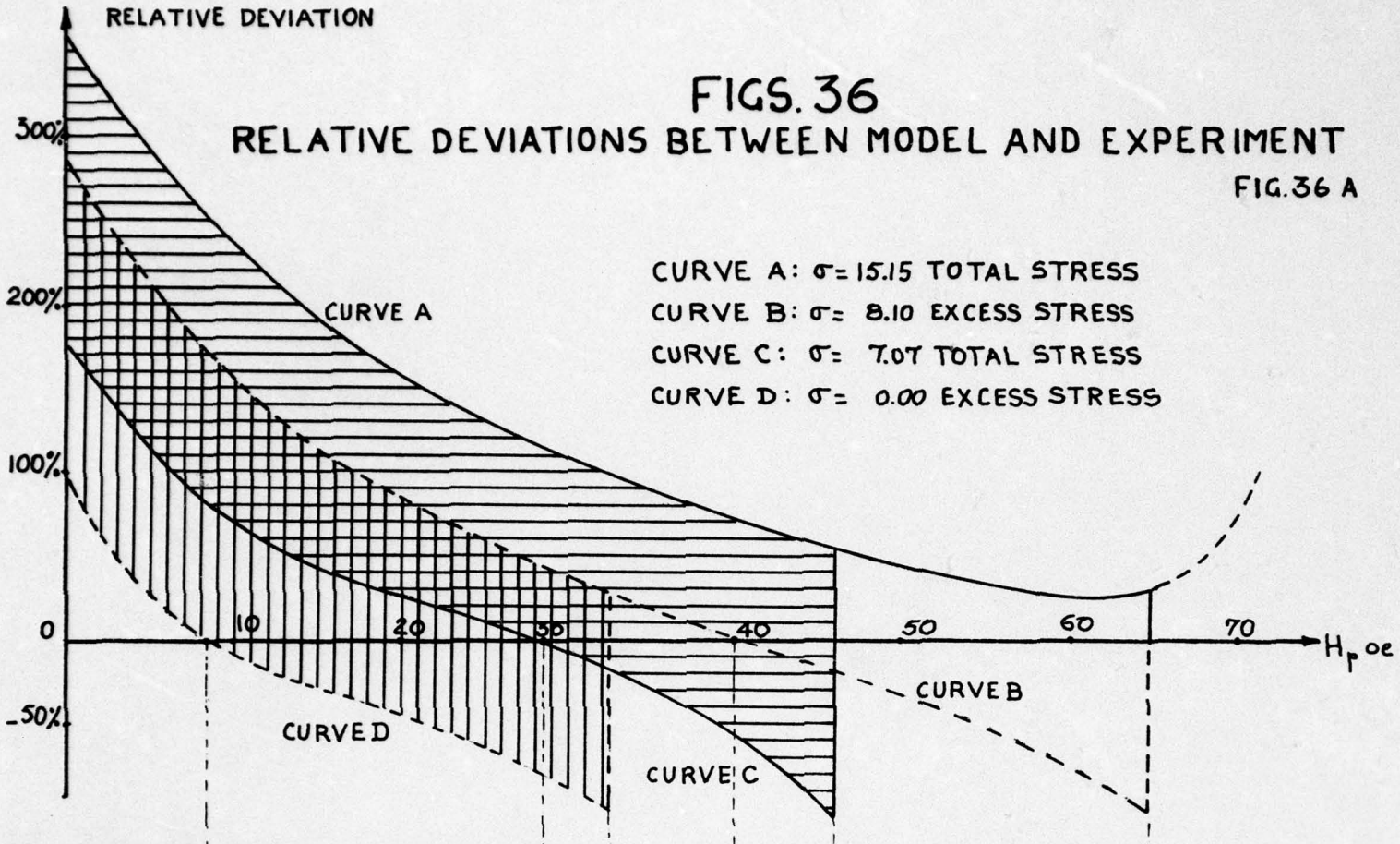


FIG. 35

ABSOLUTE DEVIATIONS BETWEEN MODEL AND EXPERIMENT

FIGS. 36
RELATIVE DEVIATIONS BETWEEN MODEL AND EXPERIMENT

FIG. 36 A



CURVE A: σ = 15.15 TOTAL STRESS
CURVE B: σ = 8.10 EXCESS STRESS
CURVE C: σ = 7.07 TOTAL STRESS
CURVE D: σ = 0.00 EXCESS STRESS

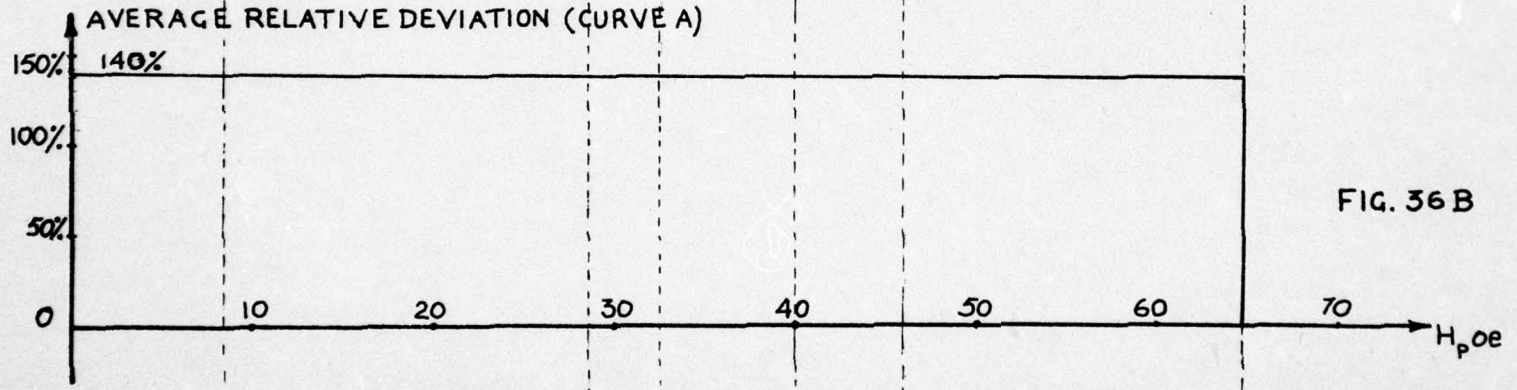
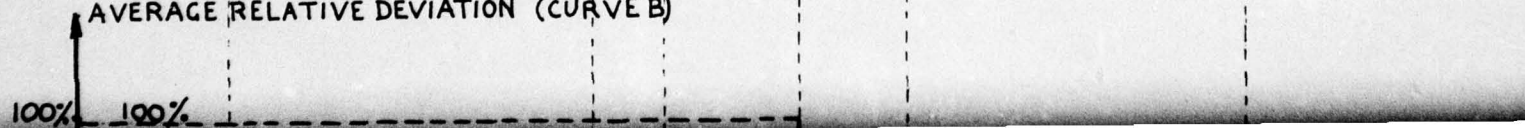


FIG. 36 B



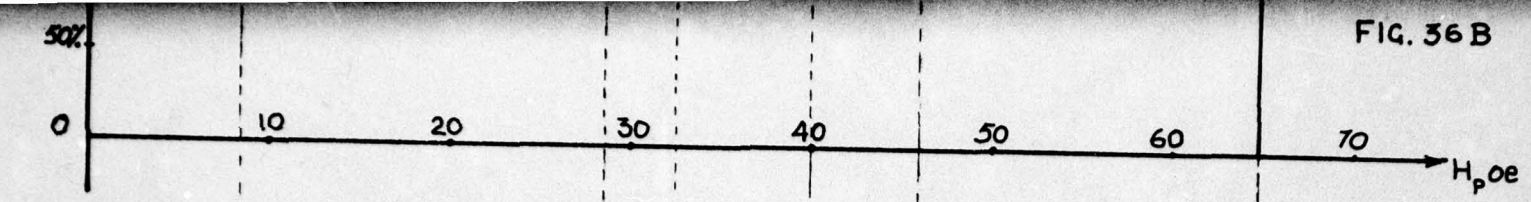


FIG. 36 B

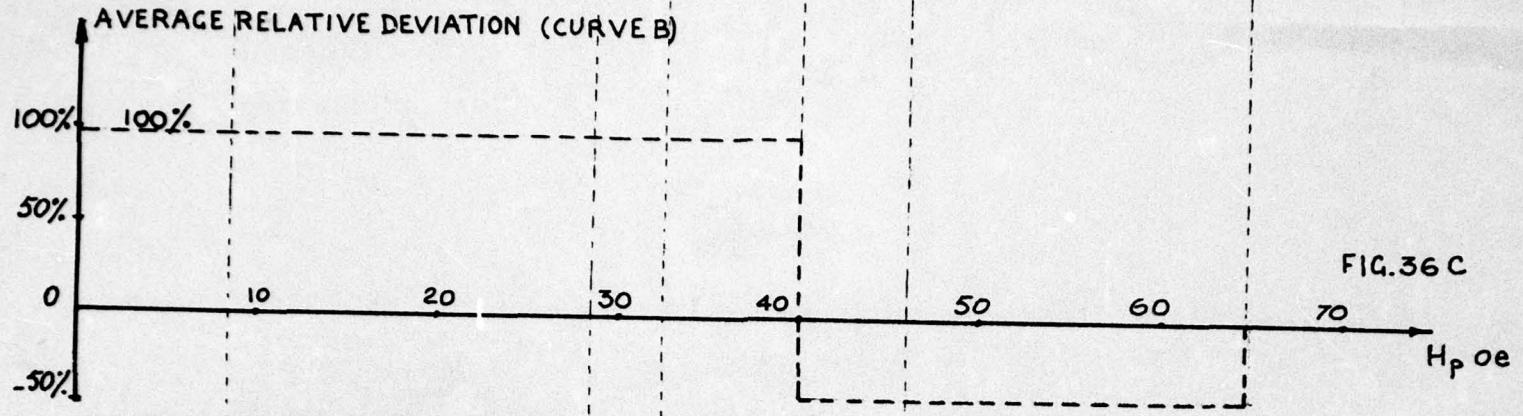


FIG. 36 C

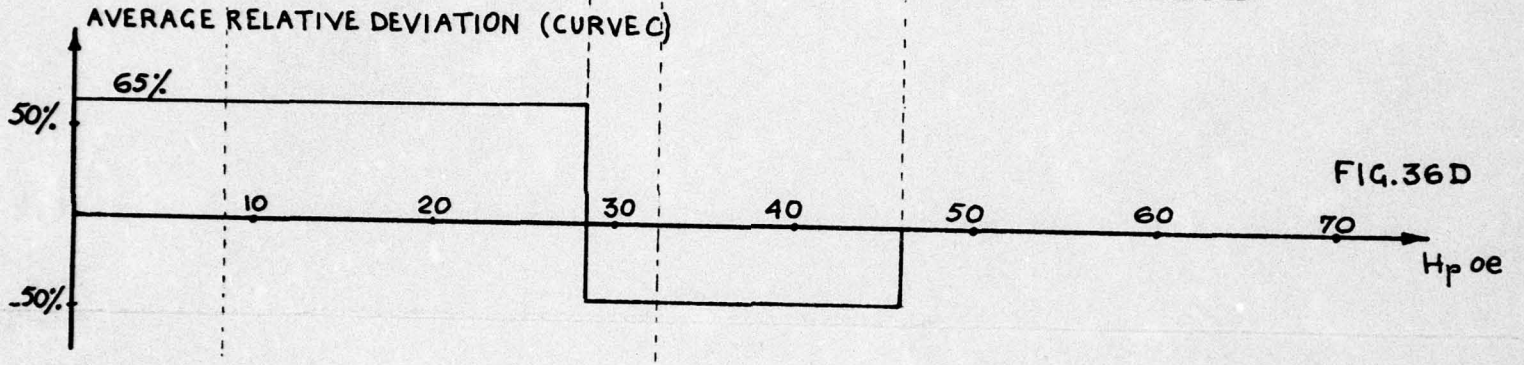


FIG. 36 D

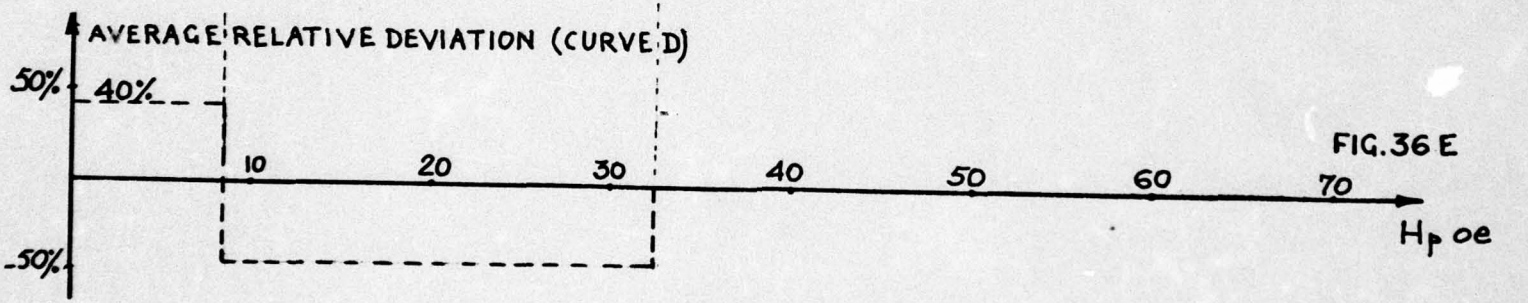


FIG. 36 E

corded. The values of H_c are then plotted versus H_p for each value of stress and a family of 13 curves is obtained. Of these six are plotted in Fig. 34, the experimental points shown have been connected by continuous lines. The figure shows that as the stress is increased the curves move away from the H_p axis.

b. The value of anisotropy field H_K obtained (15500 oe) and values of stress and perpendicular field applied are now substituted into expressions (24) in order to obtain normalized parameters λ, β, ζ to be inserted in equation (25) to obtain predicted theoretical hysteresis loops by digital computation (the graphical root locus method may be used as well). Figs. 37 to 39 show three hysteresis loops corresponding to σ = 7.07 Kg/mm^2 (7.07 x 10^8 dynes/cm^2) and values of perpendicular field H_p:

12.5, 21.38, 36 oe.

c. The film is stressed until the transverse loop becomes reversible and the anisotropy field H_K is then measured. It is found that H_K = 35 oe (Fig. 29B), corresponding to a value of anisotropy constant:

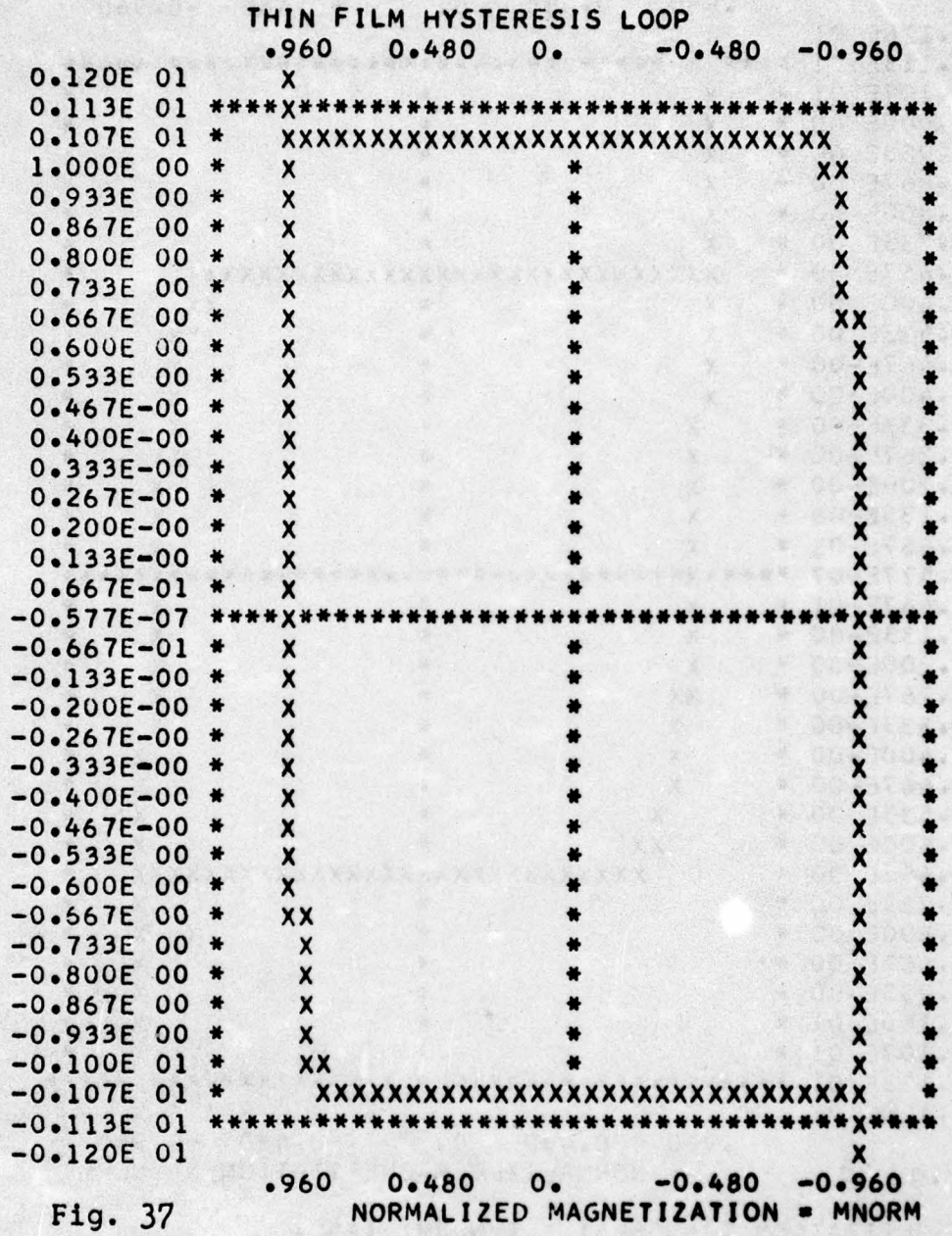


Fig. 37

MAGNETIZATION (GAUSSES) = (MNORM) 1450.
HSWCH (OERSTEDS) = ALPHA(2K/M) = (ALPHA)21.38
BETA = 0.590 DELTA = -1.330
GAMMA(INITIAL PHI) = -0 M (SATURATION) = 1450.
K(ERGS/CCM) = 15500. LAMBDAS(MAGSTRICTION)=0.20E-04
HPERP = (BETA)21.38 SIGMA(DYN/SCM)=(DELTA)0.52E 09
XMRU = 0.9674 XMRL = -0.9674
HCR = 1.0750 HCL = -1.0750

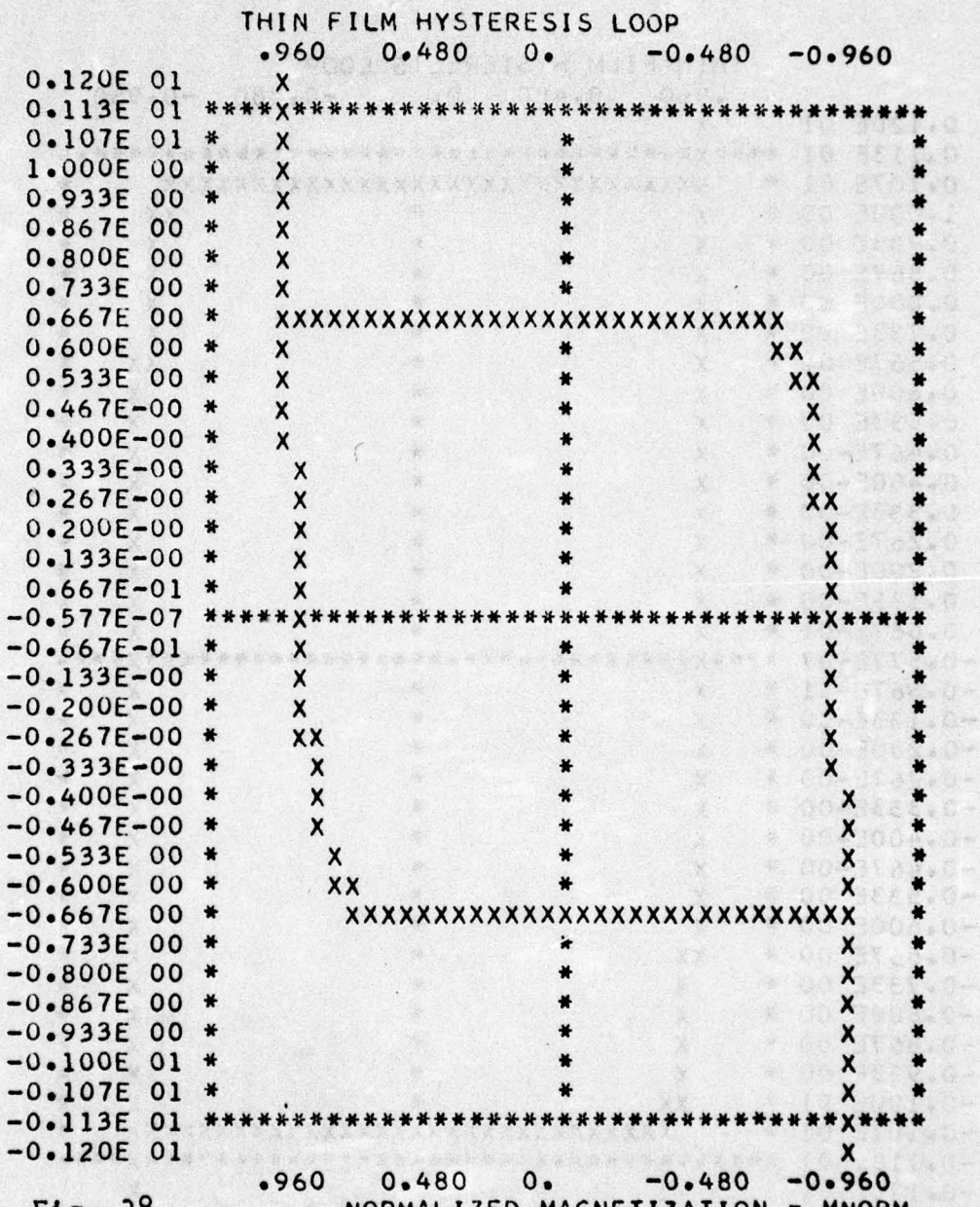


Fig. 38

MAGNETIZATION (GAUSSES) = (MNORM) 1450.
HSWCH (OERSTEDS) = ALPHA(2K/M) = (ALPHA)21.38
BETA = 1.000 DELTA = -1.330
GAMMA(INITIAL PHI) = -0 M (SATURATION) = 1450.
K(ERGS/CCM) = 15500. LAMBDAS(MAGSTRICTION)=0.20E-04
HPERP = (BETA)21.38 SIGMA(DYN/SCM)=(DELTA)0.52E 09
XMRU = 0.9032 XMRL = -0.9032
HCR = 0.6500 HCL = -0.6500

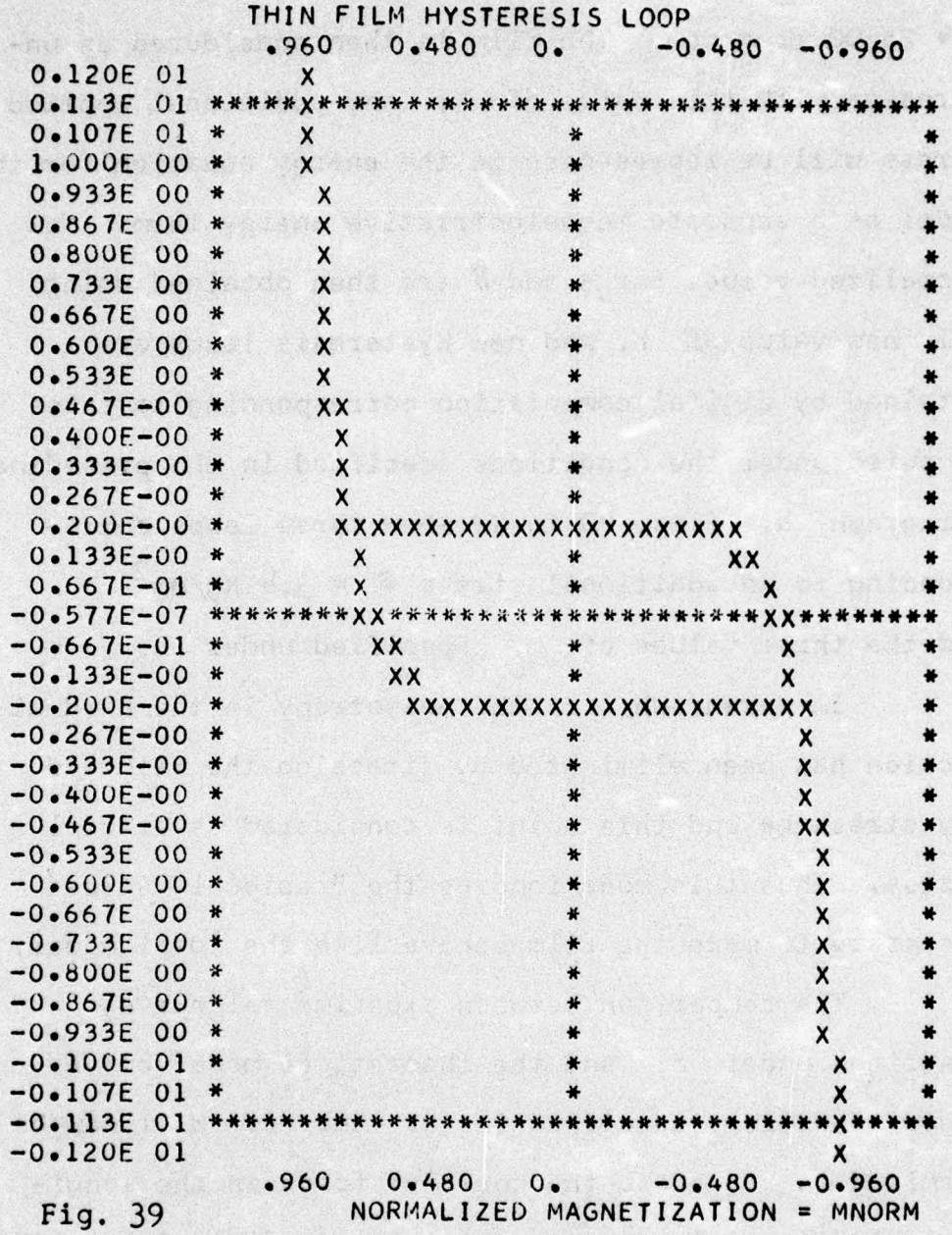


Fig. 39

MAGNETIZATION (GAUSSES) = (MNORM) 1450.
HSWCH (OERSTEDS) = ALPHA(2K/M) = (ALPHA)21.38
BETA = 1.700 DELTA = -1.330
GAMMA(INITIAL PHI) = -0 M (SATURATION) = 1450.
K(ERGS/CCM) = 15500. LAMBDAS(MAGSTRICTION)=0.20E-04
HPERP = (BETA)21.38 SIGMA(DYN/SCM)=(DELTA)0.52E 09
XMRU = 0.6839 XMRL = -0.6839
HCR = 0.1875 HCL = -0.1875

K = 25500 ergs/ccm. The film is then considered as unstressed with this value of K; any additional applied stress will be represented in the energy equation for the model as a separate magnetostrictive energy term. New normalized values for β and δ are then obtained using this new value of K, and new hysteresis loops are obtained by digital computation corresponding to those computed under the conditions specified in the preceding paragraph b. Figs. 40 to 42 show three loops corresponding to an additional stress σ = 3.4 Kg/mm^2 and the three values of H_p specified under b.

In paragraph c. the anisotropy in the hard direction has been eliminated by stressing the film and any stress beyond this point is considered as a total stress. Thus this mode ignores the "residual" stress necessary to make the film behave like the ideal model.

The comparison between experimental curves described under a. and the theoretical model curves under conditions specified in b. and c. will now be examined in regard to the coercive force in the longitudinal direction, as the perpendicular field is varied. These curves represent the critical switching behavior of the film as discussed theoretically in Part 1 d. of this chapter.

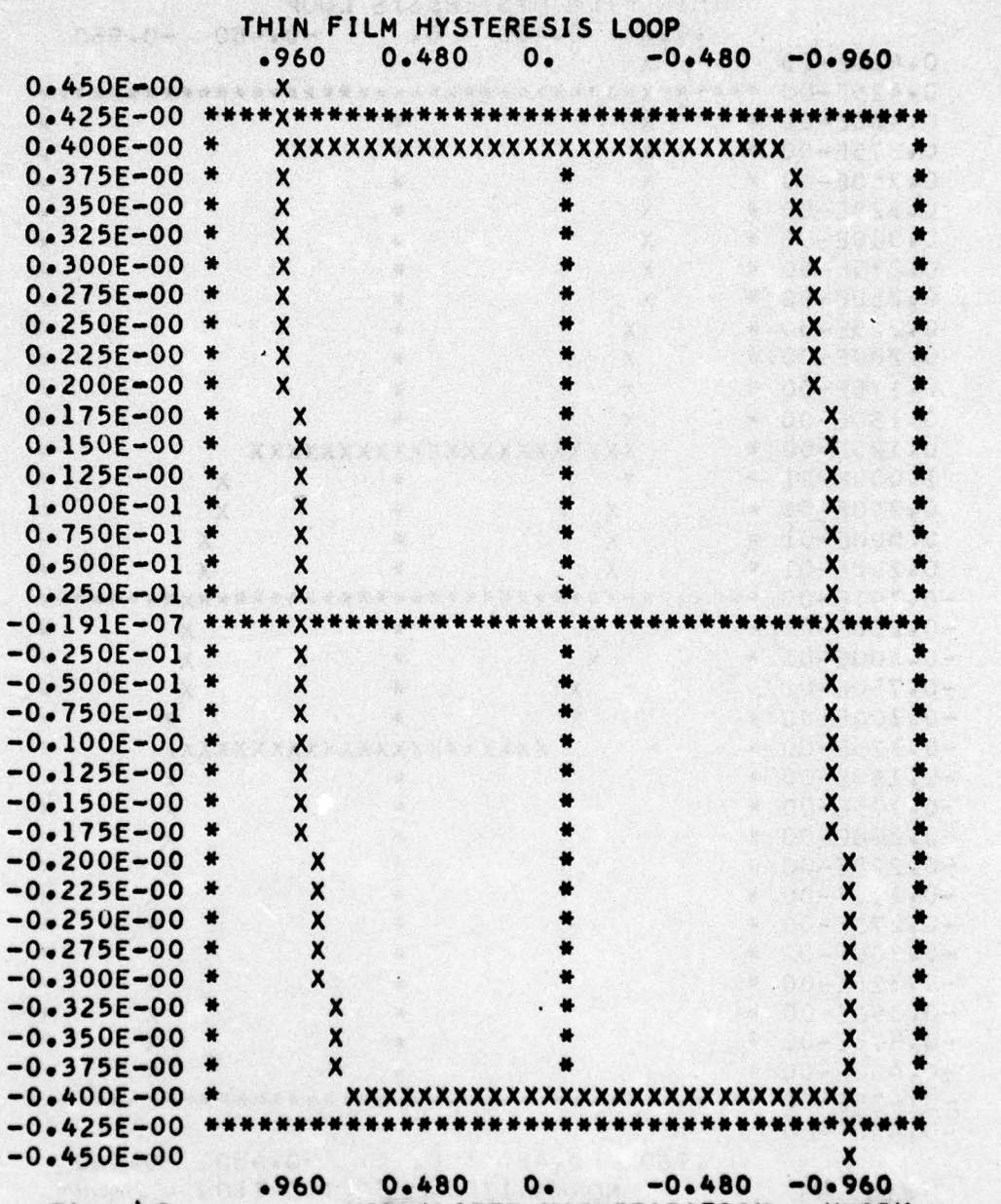


Fig. 40

MAGNETIZATION (GAUSSES) = (MNORM) 1450.
HSWCH (OERSTEDS) = ALPHA(2K/M) = (ALPHA)35.17
BETA = 0.590 DELTA = -0.400
GAMMA(INITIAL PHI) = -0 M (SATURATION) = 1450.
K(ERGS/CCM) = 25500. LAMBDAS(MAGSTRICTION)=0.20E-04
HPERP = (BETA)35.17 SIGMA(DYN/SCM)=(DELTA)0.85E 09
XMRU = 0.9069 XMRL = -0.9069
HCR = 0.4000 HCL = -0.4000

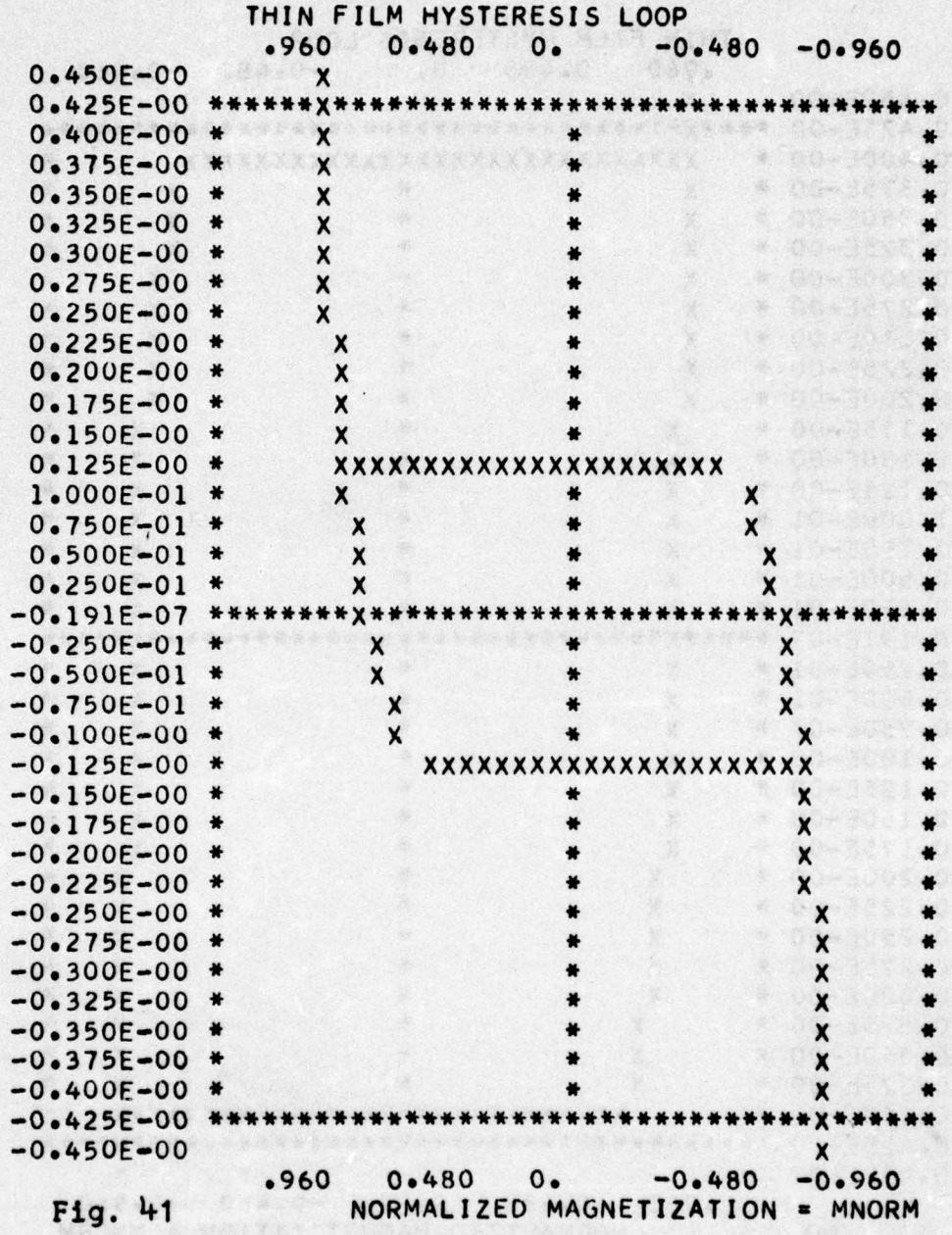


Fig. 41

MAGNETIZATION (GAUSSES) = (MNORM) 1450.
HSWCH (OERSTEDS) = ALPHA(2K/M) = (ALPHA)35.17
BETA = 1.000 DELTA = -0.400
GAMMA(INITIAL PHI) = -0 M (SATURATION) = 1450.
K(ERGS/CCM) = 25500. LAMBDAS(MAGSTRICTION)=0.20E-04
HPERP = (BETA)35.17 SIGMA(DYN/SCM)=(DELTA)0.85E 09
XMRU = 0.6999 XMRL = -0.6999
HCR = 0.1250 HCL = -0.1250

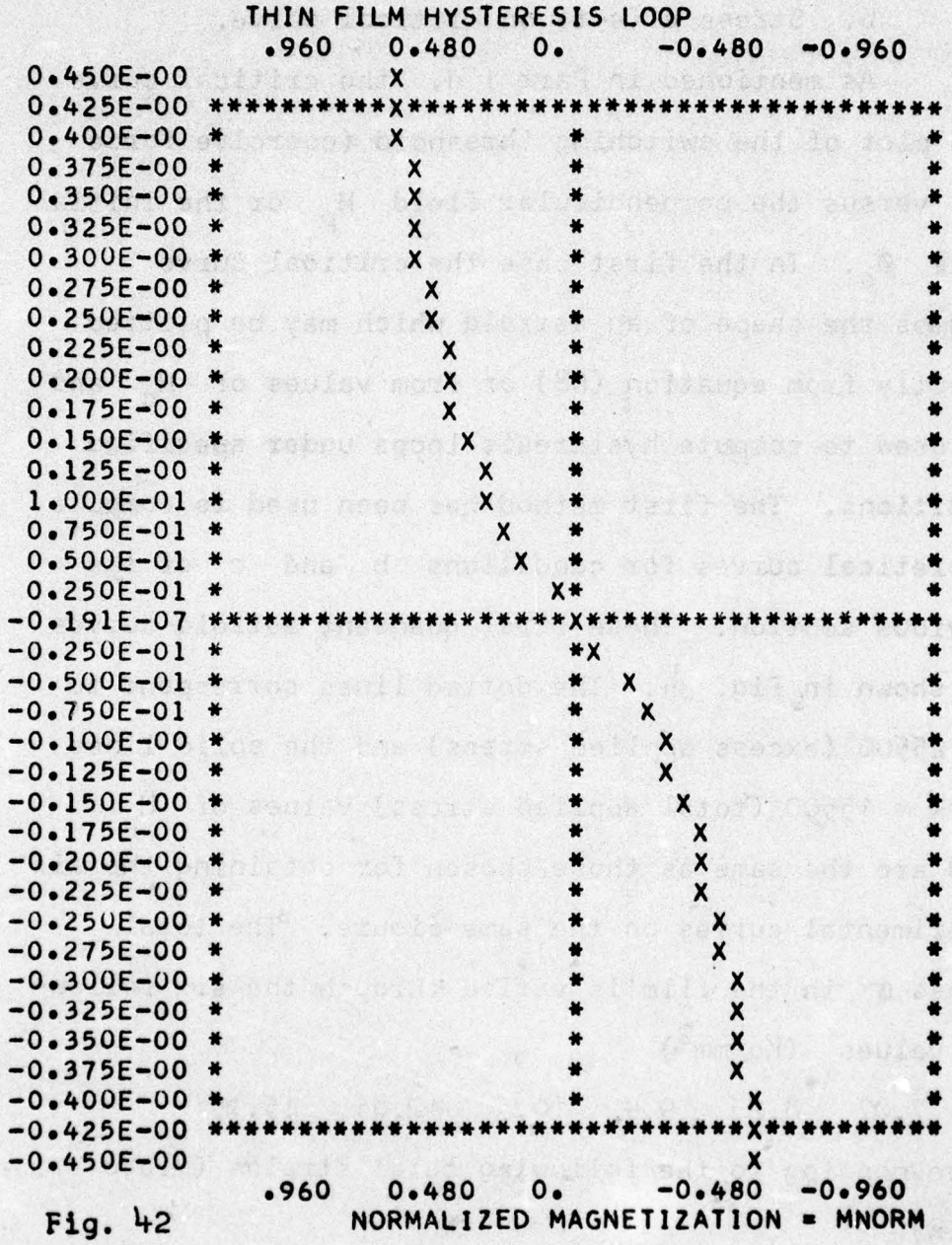


Fig. 42

MAGNETIZATION (GAUSSES) = (MNORM) 1450.
HSWCH (OERSTEDS) = ALPHA(2K/M) = (ALPHA)35.17
BETA = 1.700 DELTA = -0.400
GAMMA(INITIAL PHI) = -0 M (SATURATION) = 1450.
K(ERGS/CCM) = 25500. LAMBDAS(MAGSTRICTION)=0.20E-04
HPERP = (BETA)35.17 SIGMA(DYN/SCM)=(DELTA)0.85E 09
XMRU = 0. XMRL = 0.
HCR = 0. HCL = 0.

b. Stress effects on critical curve.

As mentioned in Part 1 d. the critical curve is a plot of the switching threshold (coercive force H_c) versus the perpendicular field H_p or the initial angle ϕ_o. In the first case the critical curve assumes the shape of an astroid which may be plotted directly from equation (68) or from values of H_c and H_p used to compute hysteresis loops under specified conditions. The first method has been used to compute theoretical curves for conditions b and c of the previous section. These first quadrant astroid curves are shown in Fig. 34. The dotted lines correspond to K = 25500 (excess applied stress) and the solid lines to K = 15500 (total applied stress) values of H_p used are the same as those chosen for obtaining the six experimental curves on the same figure. The total stress σ in the film is varied through the six following values (Kg/mm^2)

σ : 7.07 8.25 9.4 10.5 12.85 15.15

corresponding to the following total strains (micro in/in)

ε : 442 514 587 659 804 948

These values of σ and ε are to be associated with K = 15500.

If excess stresses $\Delta\sigma$ and strains $\Delta\varepsilon$ be-

yond the point of closure of the transverse loop are used the following values are to be inserted in the equation for the theoretical curve:

σ : 0 1.15 2.32 3.47 5.8 8.1

corresponding to the following values of excess strains:

ε : 0 72 145 217 362 505

In this case the anisotropy constant is K = 25500.

From Fig. 34 it is evident that if K is chosen at the value of stress necessary to eliminate the transverse anisotropy there is a better general overlap between experimental and theoretical curves. It is evident also that stress may be used as a parameter for controlling the switching threshold.

From examining the differences between theoretical and experimental curves shown in Fig. 34, it may be observed that:

1. In the absence of H_p the coercive force predicted by the model is larger than the experimental coercive force by a factor ranging between 2 and 5, depending upon the procedure used to measure H_K and the magnitude of the applied stress. The experiment shows H_c = 17 oe for all values of applied stresses σ between 7.07 and 15.15 Kg/mm^2; the theory predicts values between 35 oe and 75 oe, for the same range of σ.

2. As the perpendicular field H_p is in-

creased the difference between theoretical and experimental coercive force decreases and the latter becomes sensitive to applied stresses. The slope of the curves, expressed by H_c/H_p, in the assumption of coherent rotation, differs considerably from experimental results.

3. As very high values of H_p are approached the coercive forces and the slopes of the two sets of curves tend to converge.

These observations find reasonable interpretation by considering in more detail the role played by domain wall motion in determining the coercive force of magnetostrictive films at frequencies of a few thousands cps.

In the case of the non-magnetostrictive composition, information published in recent years shows satisfactory agreement between theoretical and experimental curves of H_c vs H_p* at a frequency of 1000 cps.

In the case of the positive magnetostriction film reported in this study the curve of H_s vs H_p for zero applied stress is shown in dotted lines in Fig. 34. As stress is applied, H_c, in the absence of H_p, increases from 15 oe to 17 oe and as the transverse

*See Ref. 6, Fig. 4, p. 266

field is increased a larger increase in H_c is observed. This increase in H_c brings the experimental curves closer to those predicted by the rotational model, but a large difference still remains.

The limit reached by H_c as stress is increased, in the absence of H_p, at a value of H_s equal to a fraction of the rotational coercive force H_K, suggests the presence of reversal by domain wall motion. It is known that the field necessary to reverse the magnetization by motion of domain walls is considerably less than that required to achieve the same result by coherent rotation.[6, 51] The following considerations, based on the work of Kersten and Néel, give an upper bound to the value of coercive force H_{wc} for reversal by domain wall motion.

According to Kersten's inclusion theory,[53] in the absence of any applied field a domain wall remains in equilibrium when its position corresponds to a minimum of its area. The wall energy is then minimum as it must include the maximum number of non-magnetic inclusions of given size and periodicity. The increase in energy necessary to move the wall away from its position corresponds to an increase in wall energy equal to the work to be performed by a driving magnetic field. The coercive force corresponding to this wall displace-

ment energy is however much higher than H_K, as Kersten neglected the work corresponding to the setting of magnetic poles on the internal surface of the inclusion. This theory was therefore reviewed by Néel, who assumed the formation of domains of reversal around the inclusion, thus obtaining a configuration in which the magnetostatic energy necessary to create magnetic poles is absent. This assumption was proved to be correct by the experimental observation of domains of reverse magnetization near inclusions observed in thin film Bitter patterns, and called at present "Néel spikes".

If the film is considered to be uniformly magnetized by the action of a magnetic field, as the field is reversed, domains of reverse magnetization near inclusions act as nucleation centers. Beyond a critical value of reversed magnetic field the walls bounding these domains sweep the entire film surface until complete reversal is achieved. This critical value of field is to be considered as the wall coercive force and in Néel's model is given by the expression:

$$H_c = \frac{5}{4} \sqrt{\frac{\pi^3}{8}} \frac{E_w}{d\, M_s} \tag{79}$$

where d is the average size of inclusions assumed cubic in shape; M_s is the saturation magnetization of the material; E_w is the surface wall energy given by

the following expression in the case of cubic crystals[13]:

(80) $$E_w = 2\sqrt{A\,K}$$

where K is the anisotropy constant K_1 for cubic crystals.

The quantity A is given by[13]:

$$A = \frac{3\,k\,T_c}{n\,a}$$

where $k = 138 \times 10^{-18}$ Boltzmann's constant

T_c = Curie temperature in degrees Kelvin

n = number of neighbors in the crystal lattice

a = lattice constant.

For iron[13]:

$T_c = 1043°$ K, $a = 28.6 \times 10^{-9}$ cm

$n = 8$ (body centered cubic lattice)

$A = 1.9 \times 10^{-6}$ ergs/cm

For nickel[55]:

$T_c = 630°$ K, $a = 35 \times 10^{-9}$ cm,

$n = 6$ (face centered cubic lattice)

$A = 1.24 \times 10^{-6}$ ergs/cm

For the 50-50 nickel-iron film considered the average value of A between those for iron and nickel is chosen:

$$A = 1.57 \times 10^{-6} \text{ ergs/cm}$$

Using $K = 25500$ ergs/ccm, corresponding to the lowest value of stress for the experimental curves in Fig. 34,

the wall surface energy is obtained from expression (80):

$$E_w = 0.40 \text{ ergs/scm}$$

The corresponding value of coercive field is given by expression (79):

(81) $$H_s = 6.7/d \text{ (microns)}, \quad \text{oersteds.}$$

Expression (79) was computed by Neel, assuming that the dimension d of the inclusion is larger than the thickness of a domain wall, which, in the case of iron and its alloys with nickel, is of the order of 0.12 micron[13]. For inclusion size below this value the coercive force is higher than that predicted by expression (79), since in this case the formation of secondary closure domains in the vicinity of the inclusion is not possible. The configuration corresponding to the formation of magnetic poles corresponds to the minimum energetic state in this case and the value of coercive force is therefore higher.

As pointed out by Néel, in the case of bulk material the size of non-magnetic inclusions consisting of holes or foreign impurities is generally of the order of one micron or larger. Very small inclusions of the order of 0.1 microns or below are caused by solid phase segregation or precipitation or a supersaturated phase. It seems reasonable to assume film imperfections to be of the first type, e.g. having dimensions larger than a

wall thickness; expression (81) derived from (79) will therefore be used

Assuming an average inclusion size between two (0.24 microns) and ten (1.2 microns) domain wall thicknesses, the coercive force given by (79) is between 28.0 oe and 5.6 oe. The value of coercive force (17 oe) shown by the experimental curves in Fig. 34, under stressed conditions, falls between these two values. Furthermore, if the upper and lower values of rotational coercive force (50 oe and 75 oe) shown in Fig. 34 by the theoretical curves for $K = 15500$ ergs/ccm are substituted in expression (81), the following two values of inclusion size are obtained:

$$d_u = 0.104 \text{ microns} \qquad d_l = 0.069 \text{ microns}$$

which correspond to sizes below domain wall thicknesses and in disagreement with the assumption made on the dimensions of non-magnetic film inclusions.

It should be pointed out that, as the stress is increased, the anisotropy constant K of the film increases and therefore the wall surface energy E_w should increase, thus causing the wall coercive force as given by (79) to increase. The experimental curves in Fig. 34 show however that at $\sigma = 7.07$ Kg/mm^2 the wall coercive force reaches the limiting value of 17 oe. Expression (79) applies to cubic crystals and for

180° walls[13, 52]. Although a theoretical expression in better agreement with the experimental observations on thin magnetostrictive films should be derived, use of expression (79) is still justified in explaining the low value of coercive force reported in Fig. 34 at $H_p = 0$, as compared to the theoretical rotational H_c.

As mentioned earlier in this discussion, an increase in the transverse field H_p causes the experimental switching curves in Fig. 34 to behave more closely to the theoretical rotational curves. The curves show a higher sensitivity to stress and the experimental values of H_p at which H_c vanishes are in better agreement with the theoretical curves.

In this case the anisotropy forces and the perpendicular field act at 90° from one another and the role of H_c, applied along the easy direction, may be visualized as weakening or reinforcing the effective anisotropy field. The magnetization rotates toward H_p or back toward H_K as H_s varies sinusoidally. This rotation does not involve a translational motion of domain walls, as it is reasonable to assume that the configuration of closure domains around inclusions is rearranged about the imperfections as the magnetization rotates within the film, without giving rise to magnetic

poles and high demagnetizing fields inside the inclusions. Although domain wall motion still occurs, switching of the film by rotation increases as H_p increases. In the rotational model the rotational coercive force H_{KC} varies linearly with the applied stress:

$$(82) \qquad H_{KC} = \frac{2}{M} \left(K_i + 3 \frac{\lambda_s}{2} \sigma\right),$$

where K_i is the intrinsic anisotropy constant of the unstressed film. Expression (80) shows that the predicted wall coercive force H_{wc} is proportional to the square root of the applied stress:

$$(83) \qquad H_{wc} = \frac{5}{4} \sqrt{\frac{\pi^3}{2}} \left[A \left(K_i + 3 \frac{\lambda_s \sigma}{2}\right)\right]^{1/2}$$

Although H_{wc}, as given by this expression is not an accurate prediction of the wall coercive force for the thin film considered here, a comparison between H_{KC} and H_{wc} shows that the film coercive force is more sensitive to applied stress if the switching mechanism involved is prevalently rotational.

From the foregoing discussion it may be concluded that the difference in slope between the experimental and theoretical switching curves, at the frequency of the experiment (2500 cps), is tied to the relative contribution of domain wall motion and co-

herent rotation, as determined by the value of the perpendicular field H_p.

In order to obtain a quantitative comparison between the curves shown in Fig. 34, Figs. 35, 36 have been plotted.

The diagram in Fig. 35 shows the absolute deviation between the experimental curves and the two sets of theoretical curves shown in Fig. 34. Fig. 36A is a plot of corresponding percent relative deviations:

$$\frac{H_c \text{ (experiment)} - H_c \text{ (theory)}}{H_c \text{ (experiment)}} \quad 100,$$

for the lowest and the highest values of stress. The dotted lines refer to curves for $K = 25500$ and excess stress, the solid lines to cases for $K = 15500$ and total stress. Finally, Figs 36B, C, D, E are plots of average percent relative deviations; these four diagrams show the following conclusions:

1. The positive average percent deviation decreases from 100% to 40% if no applied stress is considered but K is measured at the value of stress necessary to close the transverse loop. 2. The positive average deviation between model and experiment decreases from 140% to 65% if a stress equal to the excess above the point of closure is used, with a value

of K measured at the stress necessary to reach closure of the transverse loop.

Bitter pattern studies of stressed films will now be reported as experimental support of the fact that a previously applied stress brings the film behavior closer to that prescribed by the simple rotational model.

c. Stress effects on domain configurations (Bitter patterns)

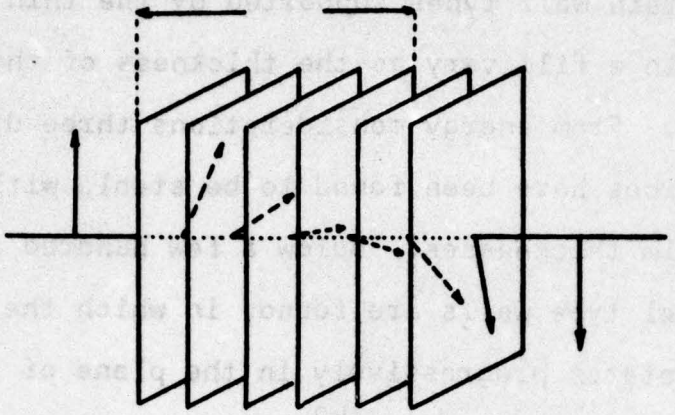
The effect of applied stresses on domain wall configurations of the bulk ferromagnetics, as displayed by Bitter patterns, has been described in the literature.[42] The lack of similar information for thin film structures has motivated an experimental investigation whose results are presented in this section.

From the work of Dijkstra and Martius,[42] as reported by Cochardt*, Bitter patterns indicate that in stressed bulk silicon iron, domain walls are oriented in the direction of an applied tension if the magnetostriction coefficient of the material is positive, and perpendicular to it if the coefficient is negative.

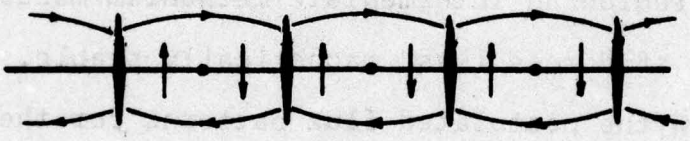
The method of preparation of the colloidal magnetite is included in Appendix 13, together with the description of a special stressing device and the microscope technique used.

Before discussing the photographs shown in Figs. 44 to 50, a brief illustration of the different kinds of domain walls encountered in nickel-iron thin film will be given, from the work of several investi-

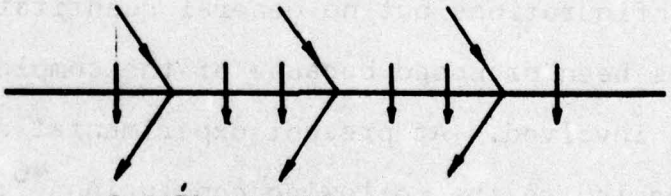
*See Ref. 4, pp. 253-255.



A. BLOCH WALL
ROTATION IN WALL PLANE



B. CROSS TIE WALL
ROTATION IN FILM PLANE



C. NÉEL WALL
ROTATION IN FILM PLANE

FIG. 43 TYPES OF DOMAIN WALLS

gators[43, 44, 45, 46].

Domain wall types supported by the thin magnetic structure in a film vary as the thickness of the film is changed. From energy considerations three different configurations have been found to be stable within certain film thicknesses. Below a few hundred Angstroms (500 Å) Neel type walls are found, in which the magnetization rotates progressively in the plane of the film, between two adjacent domains[43]. Above approximately 1500 Å the magnetization rotates in the plane of the wall which is known as a Bloch-type wall. In the intermediate region an intermediate mechanism makes the presence of "cross ties" magnetically stable. Figs.43A, B, C show the postulated flux patterns for the three types of wall.

Flux patterns have been postulated to explain domain configurations but no general quantitative theory has been proposed because of the complexity of phenomena involved. At present experimental observations have led to the following conclusions[46]:

1. Positive magnetostriction compositions show regions of anisotropy dispersion in which the easy direction fluctuates a few degrees around an average direction. Regions of negative H_K have been observed in which the anisotropy is perpendicular to the direc-

tion of annealing field during evaporation. These regions have been considered responsible for the formation of labyrinth domains or regions of unswitched magnetization[46]. The photograph in Fig. 49 shows the presence of labyrinth domains in an 80 - 20 film of nickel-iron (positive magnetostriction). Films with composition very close to zero magnetostriction (81-19)[47] show a minimum of regions with negative H_K. The presence of anisotropy dispersion or negative H_K cannot be predicted in negative magnetostrictive films[46].

2. Regions of magnetization "buckling" are formed just prior to film switching or in regions of unswitched magnetization in order to explain the formation of parallel lines of magnetite in such cases[47,39,46].

3. Regions of locked magnetization are found in which the wall coercive force H_w (value of field applied antiparallel to a one-domain film to change it into a multidomain configuration) is larger than the rotational coercive force or anisotropy field H_K. Films presenting such effects are called "inverted films".

When a reversing field is applied partial rotations occur in region of anisotropy dispersion, causing the colloidal magnetite to form filiform or needle-like configurations. Such formations have been attributed to

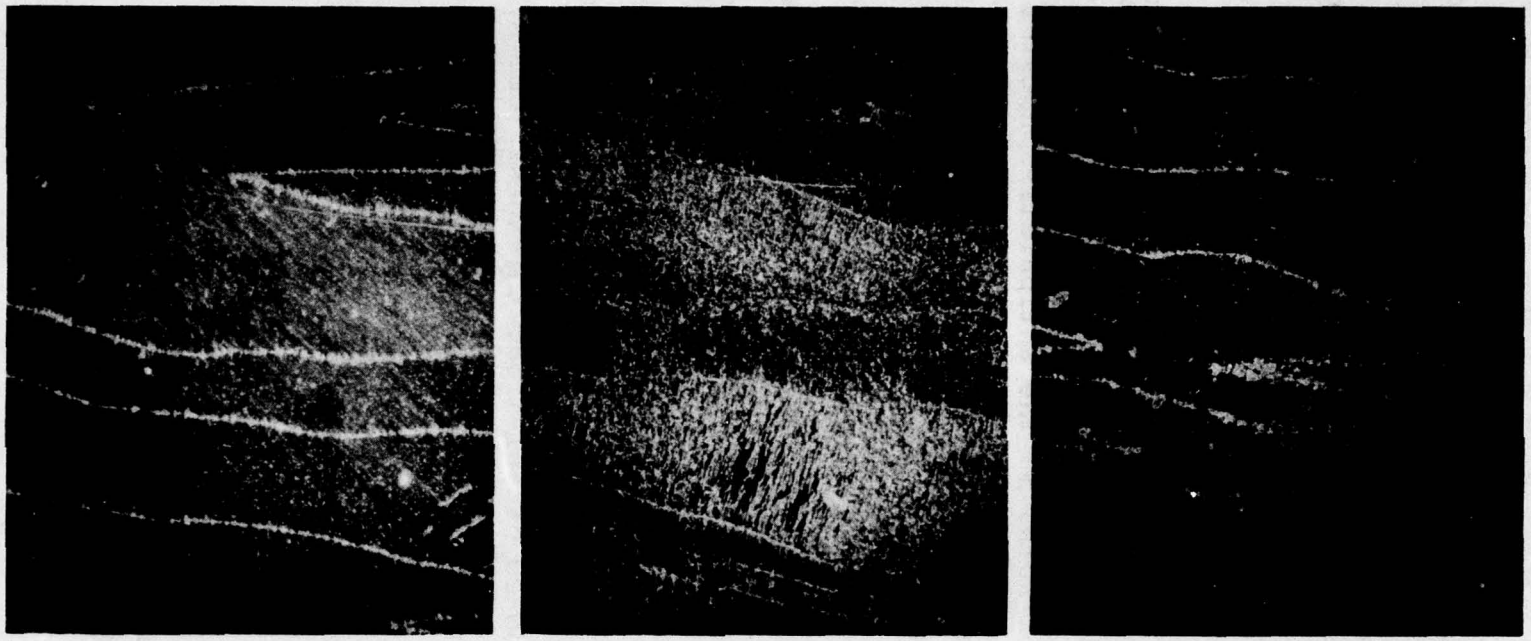
strong demagnetizing effects caused by magnetization components normal to the needles.[48]

These models of domain behavior based on experimental observations will now be used in interpreting the domain patterns shown in Figs. 44 to 50.

Chemical compositions given in the discussion are in the melt. Table I contains the corresponding composition in the film, as measured by X-ray fluorescence.

Figure 44 - Film 90-10 nickel-iron, thickness: 1300 Å, $\lambda_s < 0$ 10 oe DC field applied, H_c = 40 oe.

Photograph 1 in the figure shows the domain configuration in the absence of stress. The film displays cross tie walls and has a very high coercive force in the direction of the domain walls. In photograph 2 a tensile stress is applied perpendicularly to the average direction of the domain walls. For values of stress reaching almost the substrate breaking point a needle-like pattern appears which vanishes upon removal of the stress (photograph 3). The filiform pattern seems to appear in alternate domains and suggests the presence of an inverted film in which $H_w > H_K$. On the basis of the model proposed by D. O. Smith et al[48] photograph 2 corresponds to the film in a "locked state". The colloid is attracted along filiform regions of high



1
STRESS $\sigma=0$

DC FIELD DIRECTION:
H ← 10oe

2
DIRECTION OF σ: ↕
H ← 10oe

3
σ REMOVED
H ← 10oe

FIG.44
Ni-Fe 90-10, $H_c = 40$oe

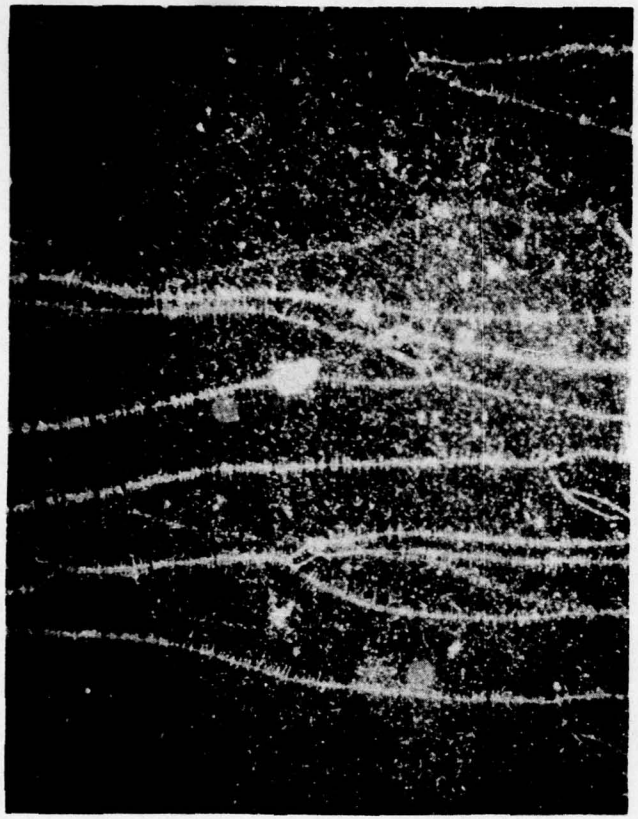
demagnetizing field originated by anisotropy dispersion.* The Helmholtz coils mounted on the microscope did not provide a sufficient field to move the walls, the film had to be placed in a more powerful set of coils to complete reversal. Fig. 44 displays the effect of an applied stress on rotational switching for an inverted film. In photograph 1 the applied field is not sufficient to rotate the spins in the antiparallel domains by the amount allowed by the anisotropy dispersion and the filiform configuration does not appear. If a tension is applied in the direction perpendicular to the walls the magnetization is favored along the direction of the walls ($\lambda_s < 0$) and the effect of the DC applied field becomes stronger and causes the colloid to assume a filiform distribution.

Figure 45 - Film 80-20 nickel-iron, thickness 1000 Å, $\lambda_s > 0$, no applied field.

An applied stress normal to the direction of the walls causes disappearance of the domain pattern. Photograph 2 shows one domain and two remaining film scratches.

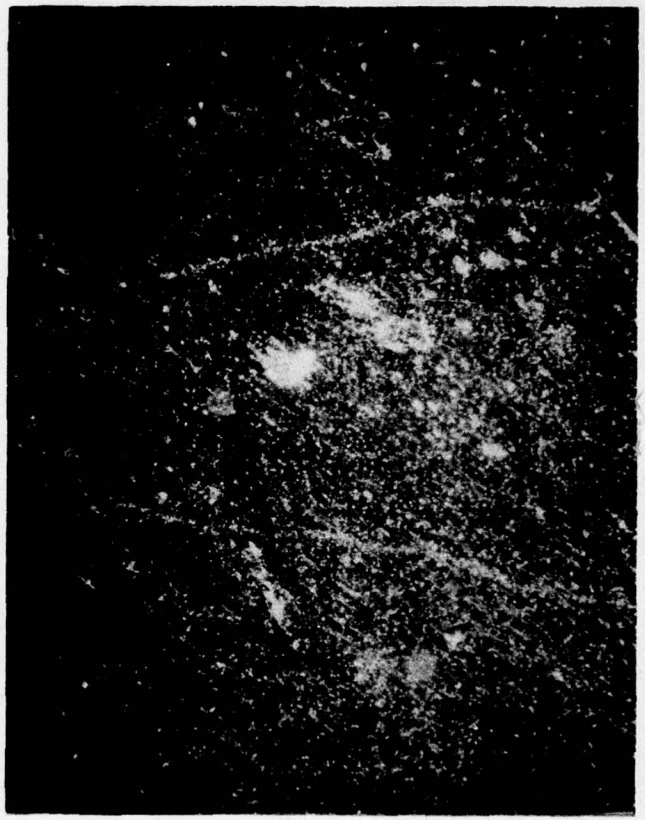
---

*Compare to photograph 1 b, p. 297S of Ref. 48.



1

d=0 ε=0



2

ε :

FIG. 45
Ni-Fe 80-20

Figure 46 - Film 90-10 nickel-iron, thickness 1000 Å, $\lambda_s < 0$, no applied DC field.

Photograph 1 shows a very compact labyrinth configuration representing regions of unswitched magnetization. Application of an increasing stress at a 20° angle from the average domain wall direction (along the double-pointed arrow shown in the figure) gives the patterns shown in photographs 2, 3.

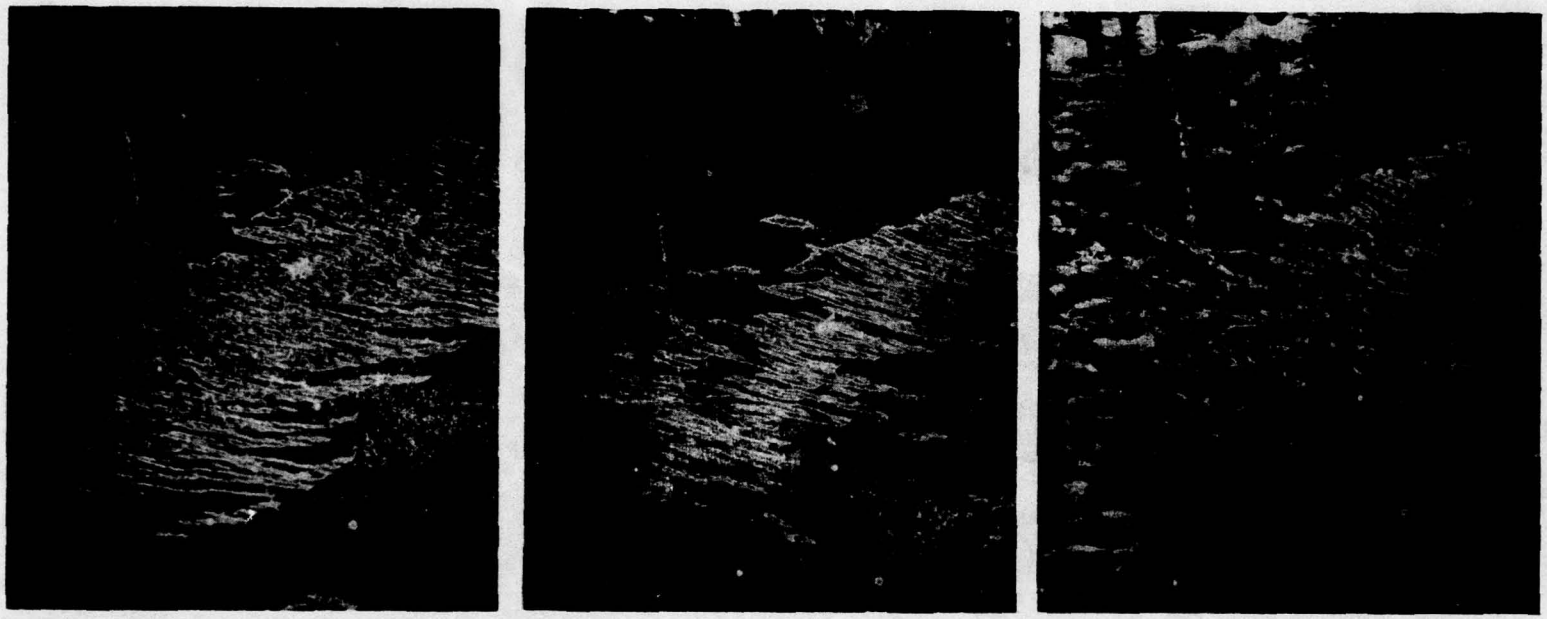
The stress causes disappearance of unswitched regions by providing sufficient energy to move part of the walls. The maximum strain reached caused the substrate to break and had the value

$$\varepsilon = 68\ d = 1220 \text{ micro in/in}$$

where d is a micrometer reading in thousandths of an inch.

Figure 47 - Film 90-10 nickel-iron, thickness 1000 Å, $\lambda_s < 0$, no applied field.

Photograph 1 shows filiform domains normal to the direction of stress and larger domains at 90° bounded by cross tie walls. As the tension is increased along the direction of the double-pointed arrow, filiform domains grow ($\lambda_s < 0$). Photograph 2 shows an interesting interlacing of domains in the two perpendicular directions. In photographs 3 and 4 the cross

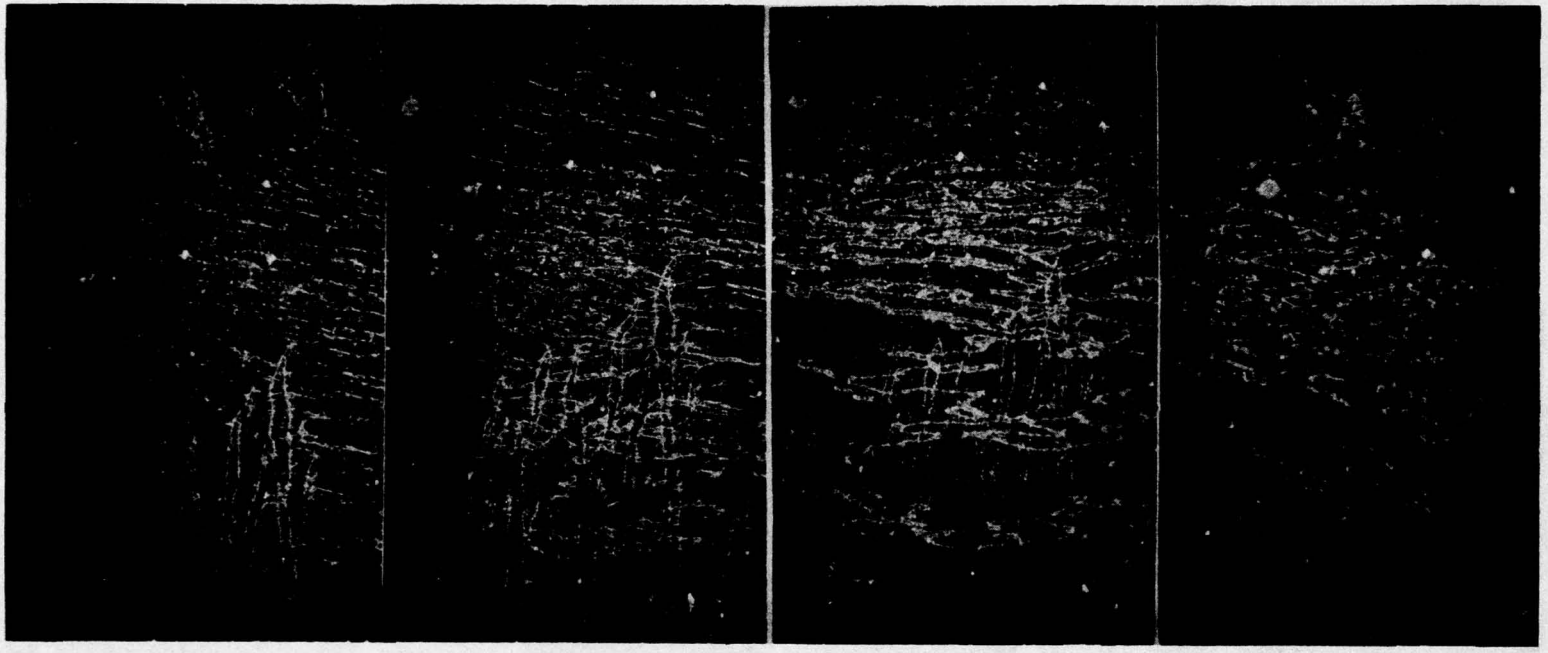


1
d=0 ε=0

2
d=0.005", ε=340μin/in

3
d=0.018", ε=μin/in

FIG. 46
Ni-Fe 90-10



1 d=0 ε=0

2 d=0.002" ε=120 μin/in

3 d=0.009" ε=610 μin/in

4 d=0.013" ε=810 μin/in

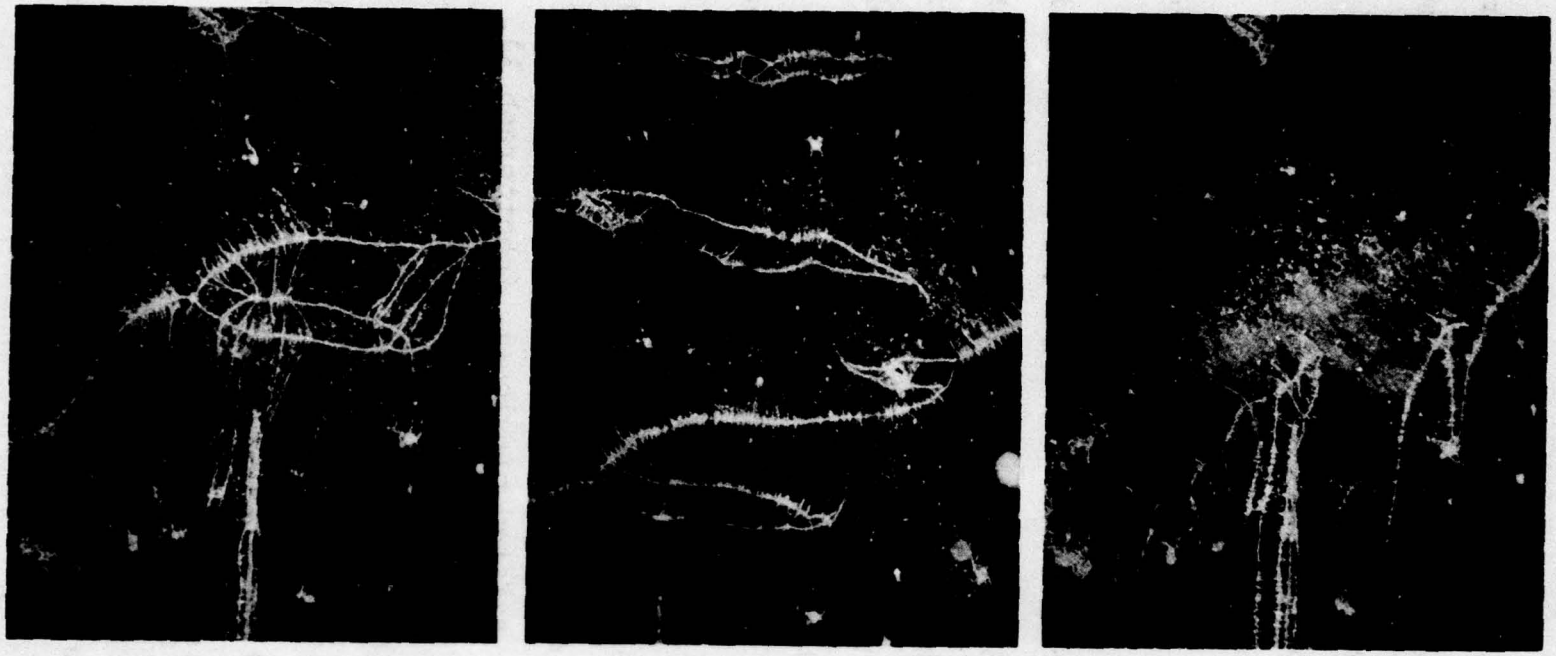
FIG. 47
Ni-Fe 90-10

ties have disappeared and most of the domain structure is directed perpendicularly to the stress. The maximum stress reached corresponded to a strain of 880 micro in/in and the substrate broke at 1225 micro in/in.

Figure 48 - Film 80-20 nickel-iron, thickness 1000 Å, $\lambda_s > 0$, no applied field.

Photograph 1 shows a complex pattern consisting of cross tie walls in the direction normal to the stress to be applied (the direction of the double-pointed arrow) and 180° walls at 90° from it. As the stress is applied (photograph 2) the pattern seems to clear up as the length of the cross ties and their periodicity decrease. When a strain of 340 micro in/in is reached the walls normal to the applied stress vanish suddenly (the unsettled Bitter pattern appears then as a cloud where cross ties walls existed previously (photograph 3). New domain walls appear along the direction of the stress and cross ties form on them in increasing number as the stress is increased. The effect of stress on the energetic conditions favoring cross tie walls has not been reported and deserves further investigation.

Figure 49 - Film 80-20 nickel-iron, thickness 1000 Å, $\lambda_s > 0$, no DC applied field.

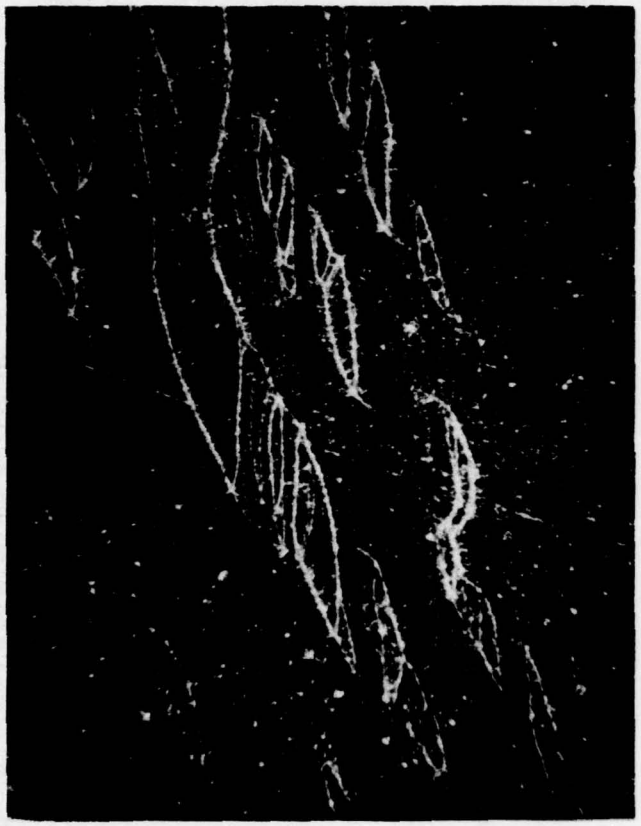


1
d=0 , ε=0

2
d=0.0035", ε=248 μin/in

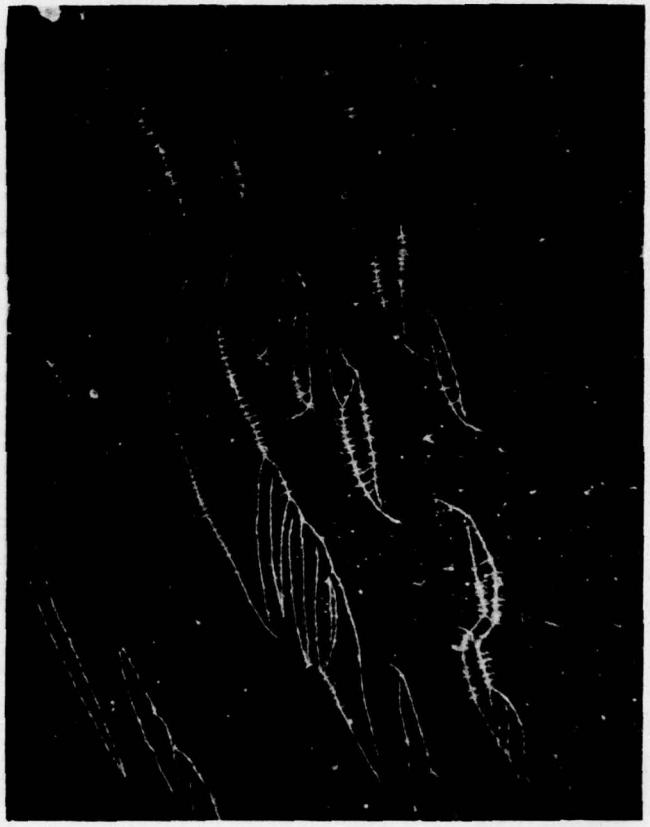
3
d=0.0050", ε=340 μin/in

FIG. 48
Ni-Fe 80-20



2

d = 0.0015" ε = 304 μin/in



1

d = 0 ε = 0

FIG. 49
Ni-Fe 80-20

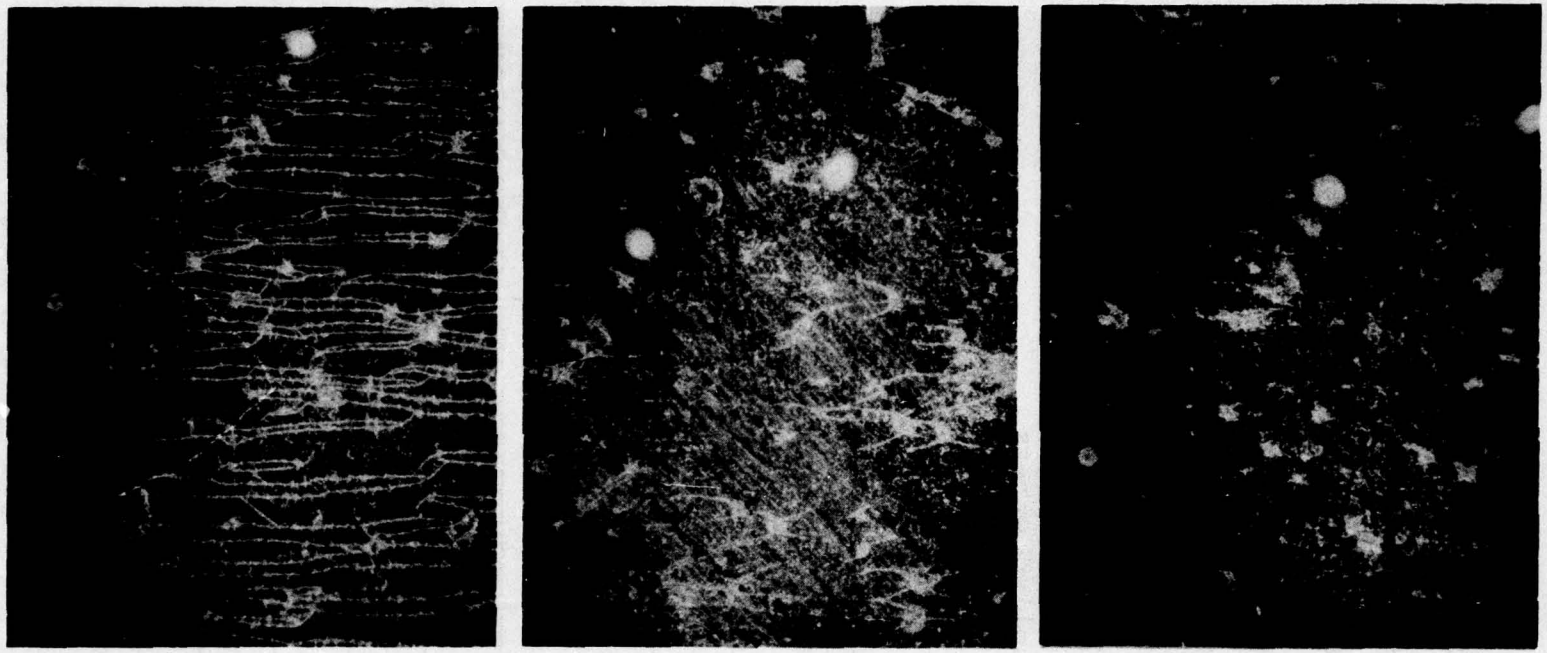
Photograph 1 shows very clear labyrinth walls connected to cross tie walls. The application of stress along the direction of the domain walls does not affect the labyrinth distribution. However, the effect on cross ties is apparent (photograph 2) at a strain ε = 304 micro in/in.

Figure 50 - Film 80-20 nickel-iron, thickness 1000 Å, $\lambda_s > 0$, no DC applied field.

The effect of applied stress is very striking in this set of photographs. Photograph 1 shows the film in a demagnetized state. The application of a strain ε = 136 micro in/in in the direction normal to the walls leaves only Neel spikes in the vicinity of inclusions. If the strain is increased to ε = 272 micro in/in the pattern is almost completely cleared.

From the illustration of these photographs the following conclusions seem reasonable:

1. An applied stress causes a reorganization of the domain structure, which may be explained by the nucleation of new domains in the regions of negative H_K or the disappearance of domains unfavorably oriented. However, if the value of the strain applied is not excessive (100-200 micro in/in) a general clearing up of the pattern is obtained.



1
d=0 ε=0

2
d=0.002 , ε=136 μin/in

3
d=0.004 , ε=272 μin/in

FIG. 50
Ni-Fe 80-20

2. Regions of unswitched magnetization (labyrinth walled domains) are not very sensitive to application of stresses. The sensitivity is however higher for films having higher magnetostriction (compare photographs in Fig. 46 to those in Fig. 49).

3. The degree of domain locking in an inverted film depends upon the magnitude of an applied stress.

The length of the cross ties depends upon the magnitude of the applied stress.

TABLE I

Fig. #	Composition in the melt Ni-Fe %	Composition in the film ±0.5%	Remarks
44	90-10	not measured	inverted film
45	80-10	77.5-22.5	normal film
46	90-10	10.7-89.3	" "
47	90-10	10.7-89.3	" "
48	80-20	77.5-22.5	" "
49	80-20	77.5-22.5	" "
50	80-20	77.5-22.5	" "

d. Film magnetostriction measurements.

The measurement of magnetostriction in bulk material has been carried out by using the direct magnetostrictive effect also known as Joule effect[1, 10, 49]. A magnetic field is applied to a sample and the corresponding change in physical dimensions is measured. Application of such method to a thin film requires separation from the substrate which may be carried out by floating a film evaporated on a rock salt crystal. The film would be relieved from residual strains upon dissolution of the substrate.

The reverse magnetostrictive effect has however been used (Villari effect[3]) for investigating the magnetostrictive behavior of films around the zero magnetostriction composition[50]. For such films the transverse loop is reversible and the longitudinal loop is fairly square. The film is then stressed and the applied strain is plotted versus the change in H_K obtained graphically by extrapolating the transverse loop to saturation. The slope of the curve is taken as a measure of the magnetostriction coefficient λ_s.

In the 44-56 nickel-iron composition investigated in this chapter the transverse loop has a large degree of irreversibility. In order to obtain a value of λ_s to be used in other studies presented in this

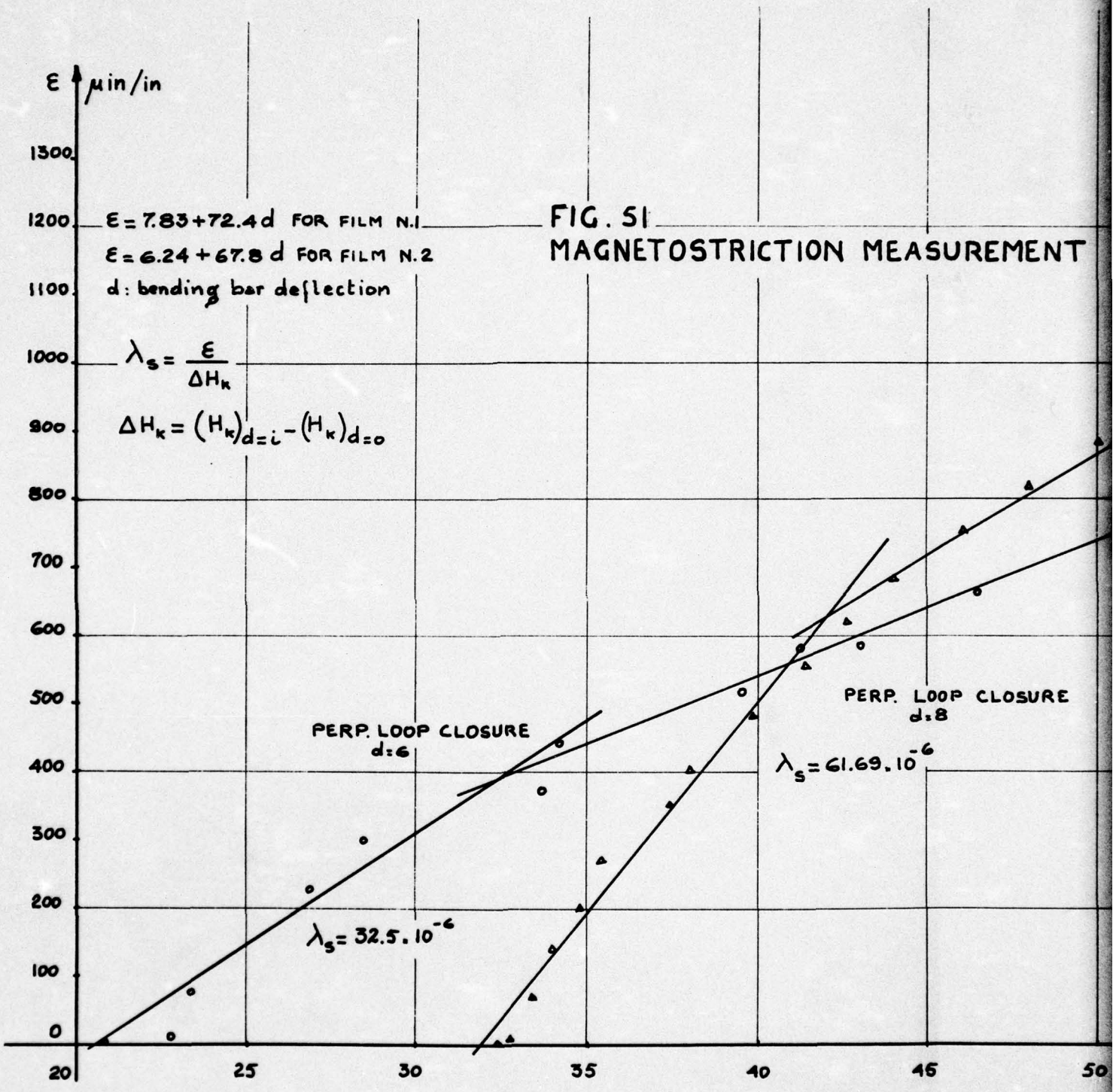
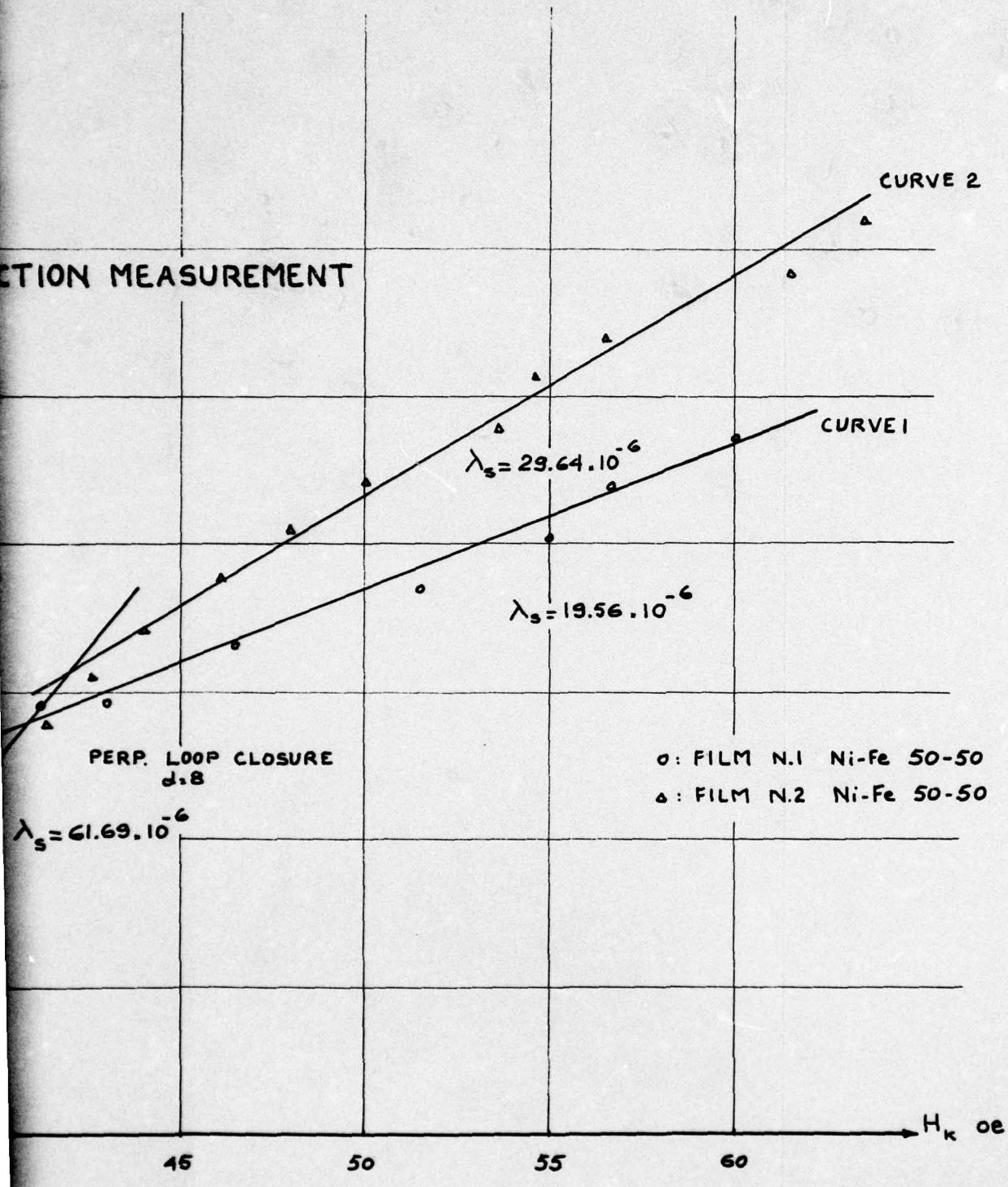


FIG. 51
MAGNETOSTRICTION MEASUREMENT


CTION MEASUREMENT
CURVE 2
CURVE 1
$\lambda_s = 29.64 \cdot 10^{-6}$
$\lambda_s = 19.56 \cdot 10^{-6}$
PERP. LOOP CLOSURE
d.8
$\lambda_s = 61.69 \cdot 10^{-6}$
o: FILM N.1 Ni-Fe 50-50
Δ: FILM N.2 Ni-Fe 50-50
H_k oe
45
50
55
60

chapter λ_s has been measured using the same method reported in Ref. 50 but with a different experimental configuration (Appendix 5).

Two 44-56 nickel-iron films from different evaporations were selected and the resulting plots of ε vs H_K are shown in Fig. 51. A best fit of experimental points by the method of least squares shows a break in the curve near the point of closure of the transverse loop. Curve 1 refers to the same film discussed so far in this chapter, it is apparent that the break occurs in the neighborhood of $H_K = 35$ oe. The value of λ_s above the break is 19.56×10^{-6} in/in/oe and 32×10^{-6} in/in/oe below the break.

Because of the inaccuracy of measuring H_K by this method the possible error is of the order of 20%. The design of a more sophisticated experiment is recommended for measuring the magnetostriction coefficient of thin films, which are more closely represented by the model. For those films which have open hysteresis loops in both "easy" and "hard" directions the discrepancy between experiment and prediction of the simple model outswamps the error in measurement of H_K.

CHAPTER II

Dynamic behavior of magnetostrictive thin films

1. Theoretical model - Equation of Landau and Lifshitz

a. Preliminary considerations, assumptions.

Modern physics explains magnetic effects of matter from the properties conferred to atomic structures by the orbital and spin motions of electrons. In ferromagnetic substances the contribution of spin motion is outstanding.

The spinning of an electron around its axis generates a magnetic moment $\vec{M}_e$ and an angular momentum $\vec{m}_e$. These are in opposite directions owing to the negative charge possessed by the particle.

Assuming that a thin ferromagnetic film behaves as a single domain, the atomic moments are maintained parallel by the molecular field, and, on a macroscopic scale, a magnetic moment $\vec{M}$ and an angular momentum $\vec{m}$ may be attributed to the film. The ratio of these two moments is a constant of the material and is known as the gyromagnetic ratio:

(84) $$\gamma = - |\vec{M}| / |\vec{m}|$$

Because of its angular momentum the electron acts as an elementary gyroscope in the presence of a magnetic field

$\vec{H}$: The axis of spinning precesses about the direction of the field and the torque $\vec{T}$ resulting from interaction between $\vec{M}$ and $\vec{H}$ is equal to the rate of change of $\vec{m}$ with respect to time:

$$\frac{d\vec{m}}{dt} = \vec{T} = \vec{M} \times \vec{H} \tag{85}$$

Substituting $\vec{m}$ from (84) into (85) yields:

$$-\frac{1}{\gamma} \frac{d\vec{M}}{dt} = \vec{T} \tag{86}$$

From the vectorial equation (86) motion along the coordinates of a spherical reference frame may be obtained and the angular velocity of precession is derived:[13]

$$\omega_o = \gamma H \tag{87}$$

Equation (86) is used in studying ferromagnetic resonance: a DC field $\vec{H}$ and a weak rf field $\vec{h}$ with angular velocity ω are impressed on a sample. If $\omega < \omega_o$ the magnetization precesses around $\vec{H}$, forming an elliptical cone with major axis of cross-sectional ellipses parallel to the direction of $\vec{h}$; if $\omega = \omega_o$ the cone becomes circular and for higher frequencies the major axes of all ellipses on the cone are oriented perpendicularly to the direction of the rf field. Polder[57] has solved equation (86) applied to this case and has derived the components of magnetization in cartesian coordinates, the permeability and the susceptibility.

The DC field $\vec{H}$ results from the combined effects of applied fields and effective fields. As mentioned in Ch. 1 in the case of a thin film these fields include the switching field $\vec{H}_s$, the perpendicular field $\vec{H}_p$, the effective field corresponding to applied or residual stresses, the anisotropy field, and, following Kittel,[54] eventual demagnetizing fields. In order to introduce these contributions to the torque $\vec{T}$ appearing in equation (86), one may consider the generalized force[6] $\vec{F}$ and a radius vector in the direction of $\vec{M}$. The force $\vec{F}$ is computed taking the gradient of the free total energy containing terms corresponding to all applied and intrinsic forces:

(88) $$\vec{T} = \vec{M} \times \vec{H} = \vec{r} \times \vec{F} = - \vec{r} \times \nabla E$$

In order to introduce in equation (86) a term corresponding to the damping effect of losses originating from eddy currents (negligible in the case of films) or hysteresis, Landau and Lifshitz added a term introduced in a purely phenomenological manner. Equation (86) becomes then:[13, 55]

(89) $$- \frac{1}{\gamma} \frac{d\vec{M}}{dt} = \vec{M} \times \vec{H} - \frac{\lambda}{M\gamma} \frac{\vec{M}}{M} \times (\vec{M} \times \vec{H})$$

The form of the damping term introduced in equation (89) is suggested by the spiraling motion of $\vec{M}$ at it approaches $\vec{H}$. The driving torque $\vec{M} \times \vec{H}$ is perpendicular to the plane $(\vec{M}, \vec{H})$, and only the presence of a torque directed toward $\vec{H}$ would cause a spiraling precessional motion. Such a torque would precisely be expressed vectorially by the double vector product $K \vec{M} \times (\vec{M} \times \vec{H})$, as suggested by Landau and Lifshitz. The proportionality constant K includes a damping coefficient λ. In the case of thin film switching the field $\vec{H}$ is the resultant $\vec{H}_t$ (Cf. Fig. 52) of the switching field $\vec{H}_s$ and the perpendicular field $\vec{H}_p$. A graphical illustration of the damping torque is given in Ref. 13.

Equation (89) is known as the equation of Landau and Lifshitz and, as recognized by Gilbert[56], is a valid description of gyromagnetic behavior only if the damping constant λ satisfies: $\lambda << \gamma M$. For large λ the damping torque becomes larger than the applied torque $\vec{T}$ and the magnetization moves only along the direction of the damping torque $(\lambda / \gamma M^2)\ \vec{M} \times \vec{T}$. Reversal time of a thin film would then decrease as λ is increased, becoming zero for λ infinite instead of zero.[58]

As shown by Smith[6] the condition $\lambda << \gamma M$ corresponds to natural gyromagnetic phenomena. In the case of thin ferromagnetic films reported by D. O. Smith in Ref. 6 the following experimental conditions were encountered:

For a 83-17 nickel-iron thin film 2500 Å thick:

$$\gamma M/\lambda \cong 150$$

where* $\lambda = 10^8$ cps, $\gamma = 1.76 \times 10^7$ (oe cps)$^{-1}$,

$M = 860$ gausses

For the case of a 44-56 nickel-iron thin film 1300 Å thick:

$$\gamma M/\lambda \cong 260$$

where λ has been taken as 10^8 cps. Data for λ as a function of nickel-iron composition is not available at present; however, even if the value of λ for the 44-56 composition is assumed to be 10 times that for the 83-17 composition the ratio $\gamma M/\lambda$ becomes equal to 26, still in the range of validity of the Landau-Lifshitz

*See Ref. 6, p. 135.

equation.

Equation (89) is written as follows for subsequent derivations:

$$(90) \quad -\dot{\vec{M}} = \gamma \vec{T} - \frac{\lambda}{M^2} \vec{M} \times \vec{T} \quad \text{with} \quad \vec{T} = -\vec{r} \times \nabla E$$

Following standard derivations[6] to obtain scalar equations along coordinates r, θ, one has

TABLE II

	r component	θ component	ø component
$-\dot{\vec{M}}$	$\frac{dM}{dt}$	$-M\dot{\theta}$	$-M \sin\theta \dot{\phi}$
$\vec{T}$	0	$\frac{\gamma}{\sin\theta} \frac{\partial E}{\partial \phi}$	$-\gamma \frac{E}{\theta}$
$-\frac{\lambda}{M^2} \vec{M} \times \vec{T}$	0	$\frac{\lambda}{M} \frac{\partial E}{\partial \theta}$	$\frac{\lambda}{M} \frac{1}{\sin\theta} \frac{\partial E}{\partial \phi}$

Since the magnetization remains close to the plane of the film θ is replaced by its complement ψ.

Fig. 52 shows the coordinate system to which the film is referenced, together with applied magnetic and stress forces. The magnetization vector is initially oriented along the x-axis assumed as the direction of easy magnetization. A stress $\pm \sigma$ is applied along the y-axis and at time t = 0 a step field H_s is impressed along the - x direction. Since at time t = 0 the torque $\vec{M} \times \vec{H}_s$ acting on $\vec{M}$ is zero, it is necessary to provide a small constant perpendicular field $\vec{H}_p$, or to start

with the direction of easy magnetization making a finite angle with $\vec{H}_s$.

The precessional motion of $\vec{M}$ starts at time $t = 0$ and $\vec{M}$ moves along ϕ and away from the xy-plane. As Ψ increases the action of the demagnetizing field increases and impedes further deviation from the plane xy (Ψ remains within 1°). The motion along the direction of increasing ϕ continues as $\vec{M}$ approaches $\vec{H}$ in a damped oscillatory motion. The approach trajectory is a flattened elliptical spiral because of the high demagnetizing field normal to the xy-plane. Fig. 52 shows a sketch of the trajectory of the extremity of $\vec{M}$ along a cylindrical sheet of radius M oriented along z; Fig. 53 shows an actual trajectory for the following conditions:

$M = 860$ gausses, $K = 1290$ ergs/cm,

$\alpha = -1$, $\beta = 0.08$, $\sigma = 0$, $\delta = 0$, $\phi_0 = 0$,

where normalized values of applied fields and stresses are used. The maximum value of the coordinate angle is 0.85 degrees.

From coordinate components appearing in Table I, setting $\Psi = \frac{\pi}{2} - \theta$, the equation of Landau and Lifshitz becomes in scalar form:

$$M \cos\Psi \frac{d\phi}{dt} = -\gamma \frac{\partial E}{\partial \Psi} - \frac{\lambda}{M} \frac{1}{\cos\Psi} \frac{\partial E}{\partial \phi}$$

(91)

$$-M \frac{d\Psi}{dt} = -\gamma \frac{1}{\cos\Psi} \frac{\partial E}{\partial \phi} + \frac{\lambda}{M} \frac{\partial E}{\partial \Psi}$$

where E includes the demagnetizing energy for a circular thin film geometry.

The simultaneous solution of the two nonlinear equations (91) requires the use of a computer, unless experimental conditions encountered justify further model simplifications such as the viscous flow approximation discussed by D. O. Smith[6]. Digital computer solutions of the Landau-Lifshitz and the Gilbert equations have been reported in the literature[6, 7] without introduction of stress energy terms for magnetostrictive compositions. The following section b will illustrate how an analog computer may be used to solve equations (91). Section c will describe the programming of the IBM 7090 to obtain direct computer plots of the solution of equations (91). In addition other digital computer programs will be illustrated to show how direct plots of switching time, ferromagnetic resonant frequency, dynamical critical curves may be obtained for any combination of applied magnetic fields, stress, or initial angle ϕ_o.

The computation of the voltage induced in a sensing loop, as the magnetization reverses is of primary

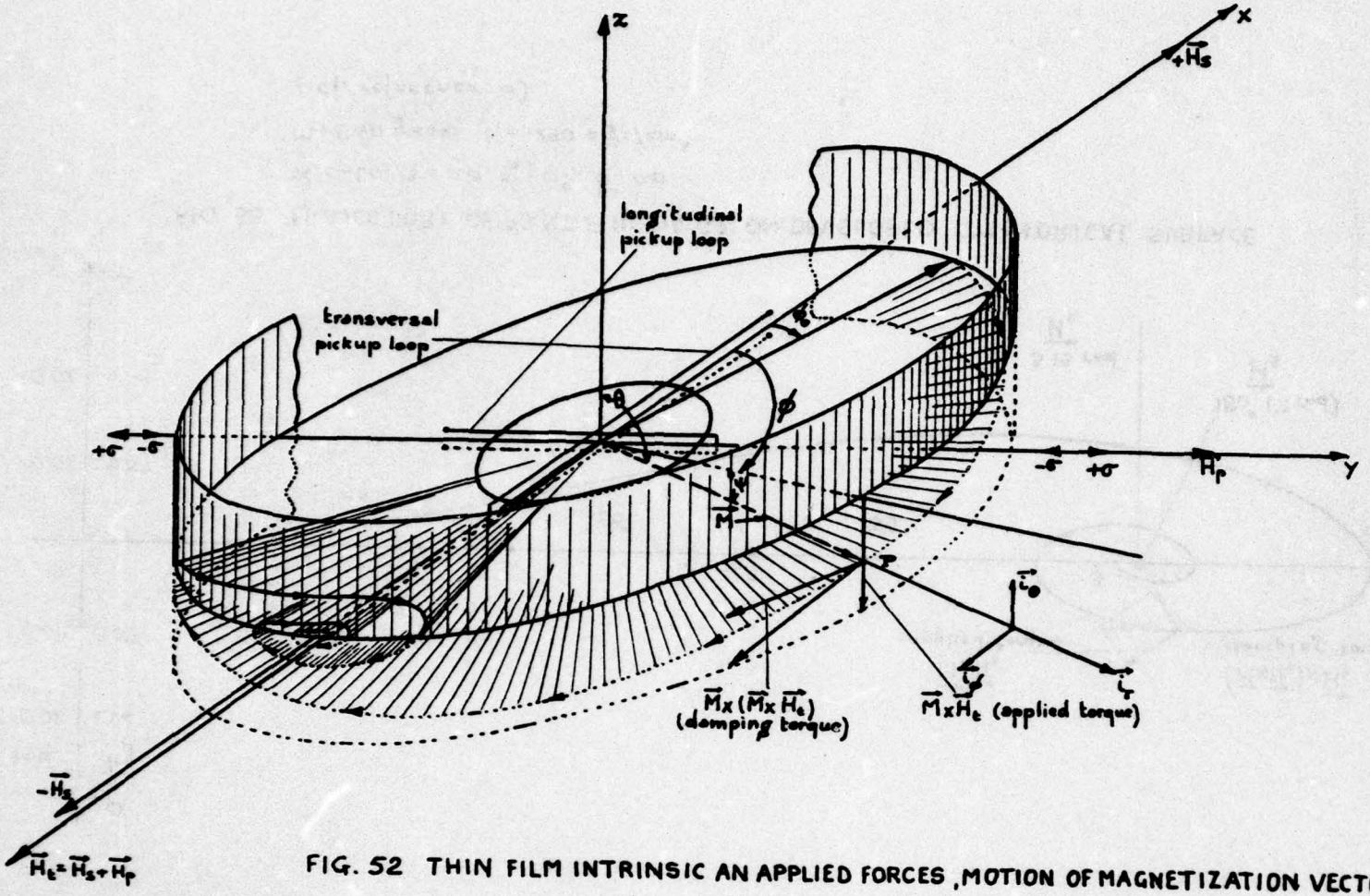


FIG. 52 THIN FILM INTRINSIC AN APPLIED FORCES, MOTION OF MAGNETIZATION VECTOR

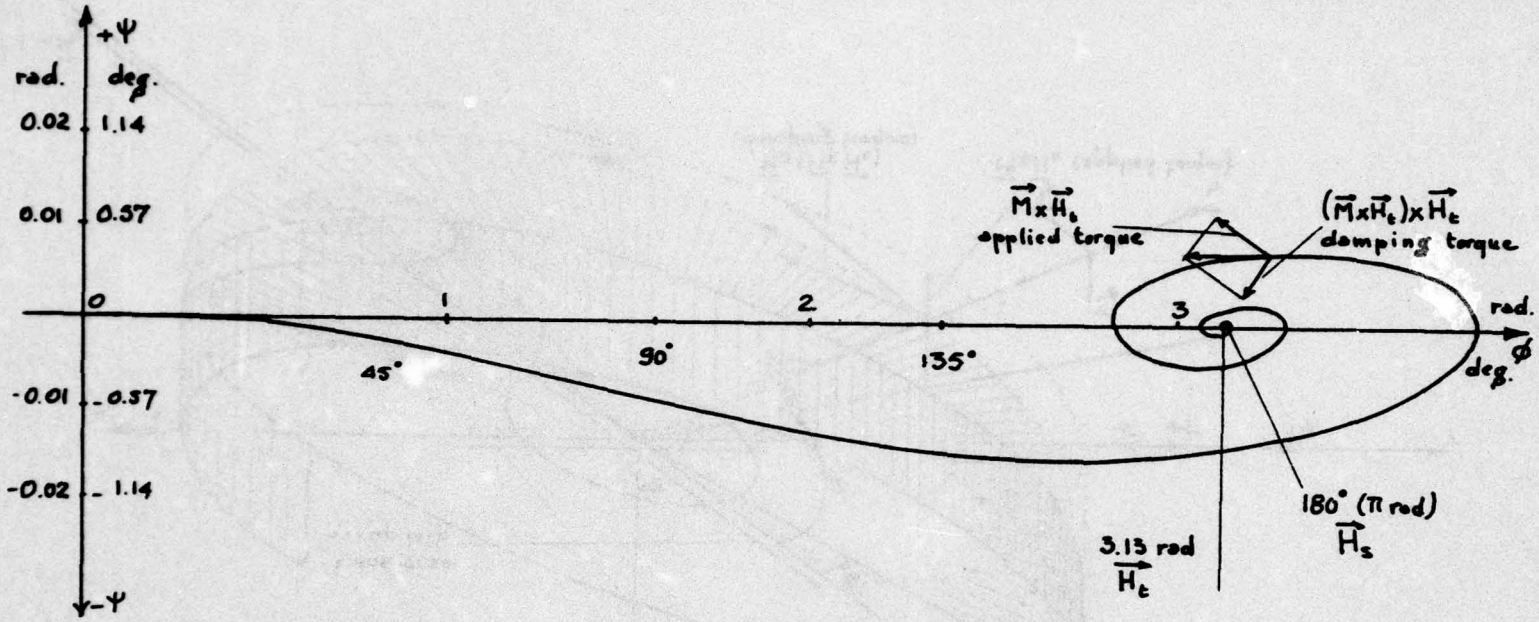


FIG. 53 : TRAJECTORY OF POINT P IN FIG. 62 ON DEVELOPED CYLINDRICAL SURFACE

$\alpha = -1.0, \beta = 0.0, \phi_0 = 0°, \delta = 0.0$

$M = 860$ gauss $K = 1290$ ergs/cm^3

(cf. reference 6)

interest in preparing an analog computer circuit diagram or a program for a digital computer. Fig. 52 shows a sketch of two wires linking the film in the perpendicular and longitudinal directions. The longitudinal pickup loop is sensitive to the component $M \cdot \cos \cdot \phi$ of the magnetization. The voltage induced in the loop is:

$$e = - \frac{d\Phi}{dt} = K M \frac{d\phi}{dt} \sin \phi \tag{92}$$

where K is a constant of the film

The convention used to define switching time will be taken from that used by other investigators[6], as being the time necessary for the voltage e to reach its maximum. Since this is not exactly the time of reversal it will be called "peaking time".

b. Solution by analog computer, stress effects on switching.

In this section a description of an analog computer circuit diagram is given and the solutions obtained are presented.*

The expression for the free energy to be introduced in equations (91) is:

---

*The analog computer installation was made available through the courtesy of Dr. George Bekey and the Space Technology Laboratories, El Segundo, California.

$$E = K \sin^2 (\phi - \phi_o) - H_s M \cos\psi \cdot \cos\phi -$$

(93)

$$-H_p M \cos\psi \cdot \sin\phi + 4\pi M^2 \sin^2\psi + \frac{3}{2}\lambda_s \sigma \cos\psi \sin^2\phi$$

corresponding to the configuration of driving forces shown in Fig. 52 , and repeated in Fig. 54 for clarity:

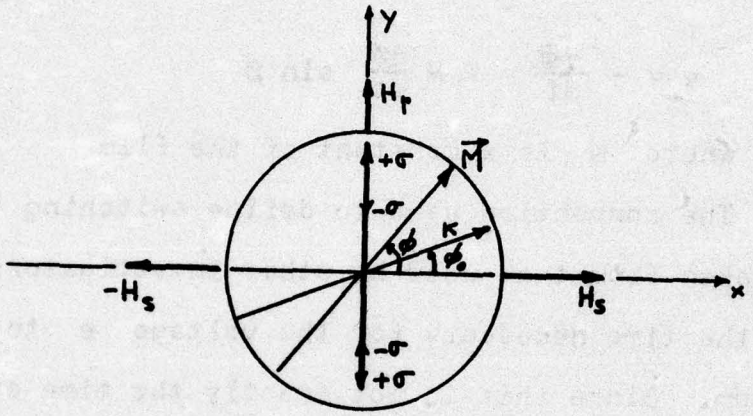


Fig. 54: Configuration of applied driving forces (Cf. Fig. 52)

Substituting E from equation (93) into equation (91), differentiating and normalizing all applied energies with respect to the anisotropy energy yields:

$$\frac{d\phi}{dt} = \frac{2K}{M}\left[\frac{\sin 2(\phi - \phi_o)}{2\cos} + \frac{\delta}{2}\sin 2\phi + \right.$$

$$\left. + \alpha \sin\phi - \beta\cos\phi\right] -$$

(94)

$$- \frac{2K}{M^2}\sin\psi\left[\alpha\cos\phi + \beta\sin\phi - \frac{\delta}{2}\sin^2\phi\right] -$$

$$- \frac{2K\lambda}{M^2}\varepsilon\left[\sin\psi\cos\psi\right]$$

$$\cos\psi \frac{d\phi}{dt} = -\frac{2K\lambda}{M^2}\left[\frac{\sin 2(\phi - \phi_o)}{2\cos\psi} + \frac{\delta}{2}\sin 2\phi + \right.$$

$$\left. + \alpha \sin\phi - \beta\cos\phi\right] -$$

(94)

$$-\frac{2K\gamma}{M}\sin\psi\left[\alpha\cos\phi + \beta\sin\phi - \frac{\delta}{2}\sin^2\phi\right] -$$

$$-\frac{2K\gamma}{M}\varepsilon\left[\sin\psi\cos\psi\right]$$

where:

$$\alpha = H_s M/2K, \quad \beta = H_p M/2K, \quad \delta = 3\lambda_s\sigma/2K,$$

$$\varepsilon = 8\pi M^2/2K$$

In order to check the accuracy of the analog solution as compared to a digital solution, the results published by D. O. Smith* were duplicated. Film constants used in this investigation were as follows:**

(95)

$$M = 860 \text{ gausses}, \quad K = 1290 \text{ ergs/ccm},$$

$$\lambda = 10^8 \text{ cps}, \quad \gamma = 1.76 \times 10^7 \text{ (oe.sec)}^{-1}$$

Applied driving forces were: normalized switching field $\alpha = -1$ (the minus sign is necessary to cause the magnetization originally directed along the x-axis (cf. Fig. 54) to reverse; normalized transverse field $\beta = 0.02, 0.08, 0.5$; direction of easy magnetization coinciding with the x-axis ($\phi_o = 0$). The applied nor-

*See Ref. 6, p. 271.

**Private communication by Dr. Smith.

malized stress δ on switching was not considered in Ref. 6, it is included in the present study; the normalized stress δ is therefore set to zero in order to check the results of the analog computer with those of the reference cited.

It is known that the magnetization of a thin film reverses in a fraction of a nanosecond under the action of a step magnetic field having a very short rise time (of the order of 0.25 nanoseconds)[6, 7]. A real time of 10 nanoseconds will then be allowed for obtaining a solution and, if a scaling of 10^9 is chosen the computer solution will last 10 seconds. During this time it is assumed that drift in chopper stabilized amplifiers and multipliers is negligible.

Let τ be computer seconds, t real seconds

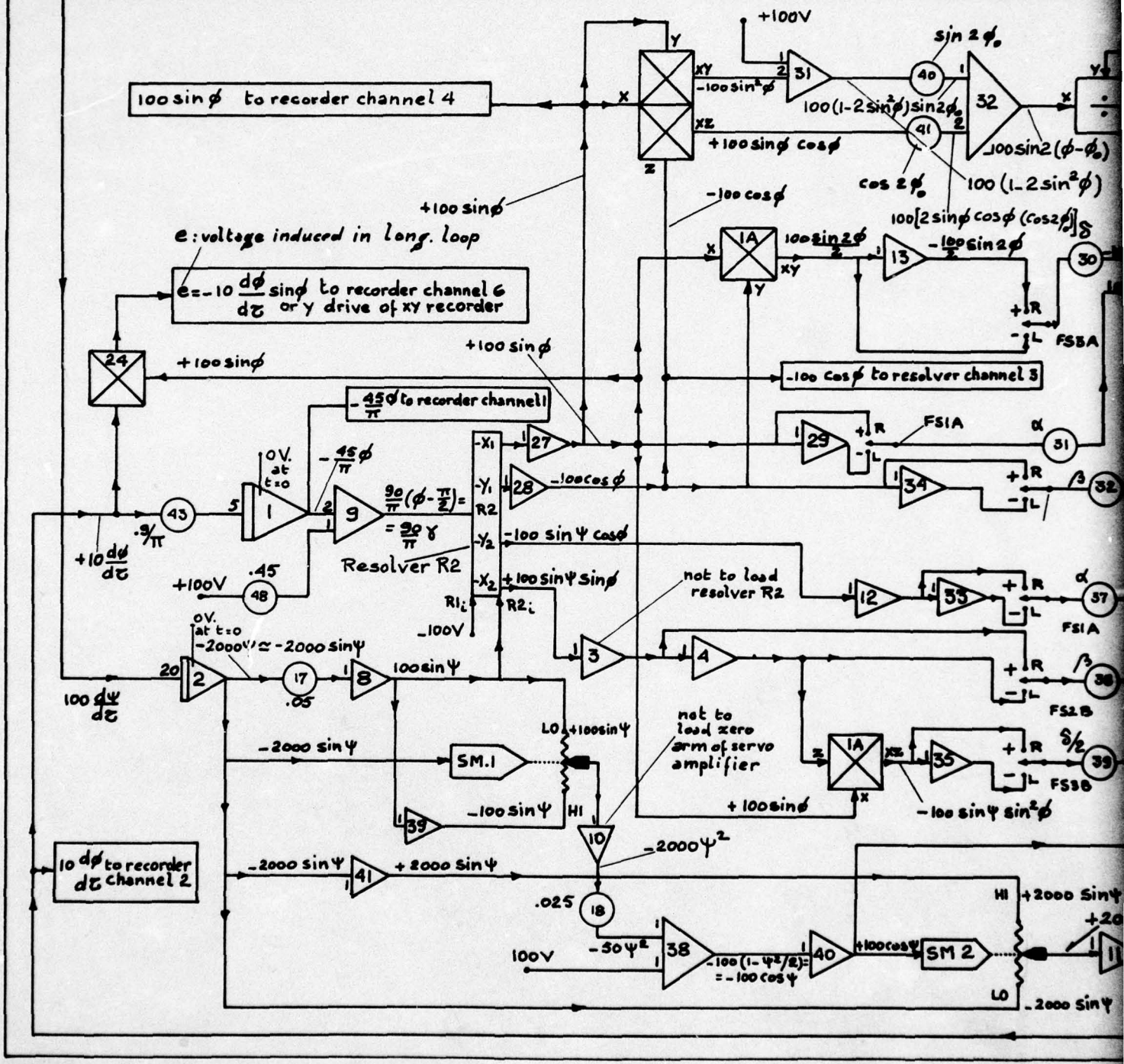
$$\tau = 10^9 t, \quad d\tau = 10^9 dt, \quad \frac{1}{dt} = \frac{10^9}{d\tau} \tag{96}$$

with the film constants chosen in (95), the constants in front of the brackets in equations (94) become:

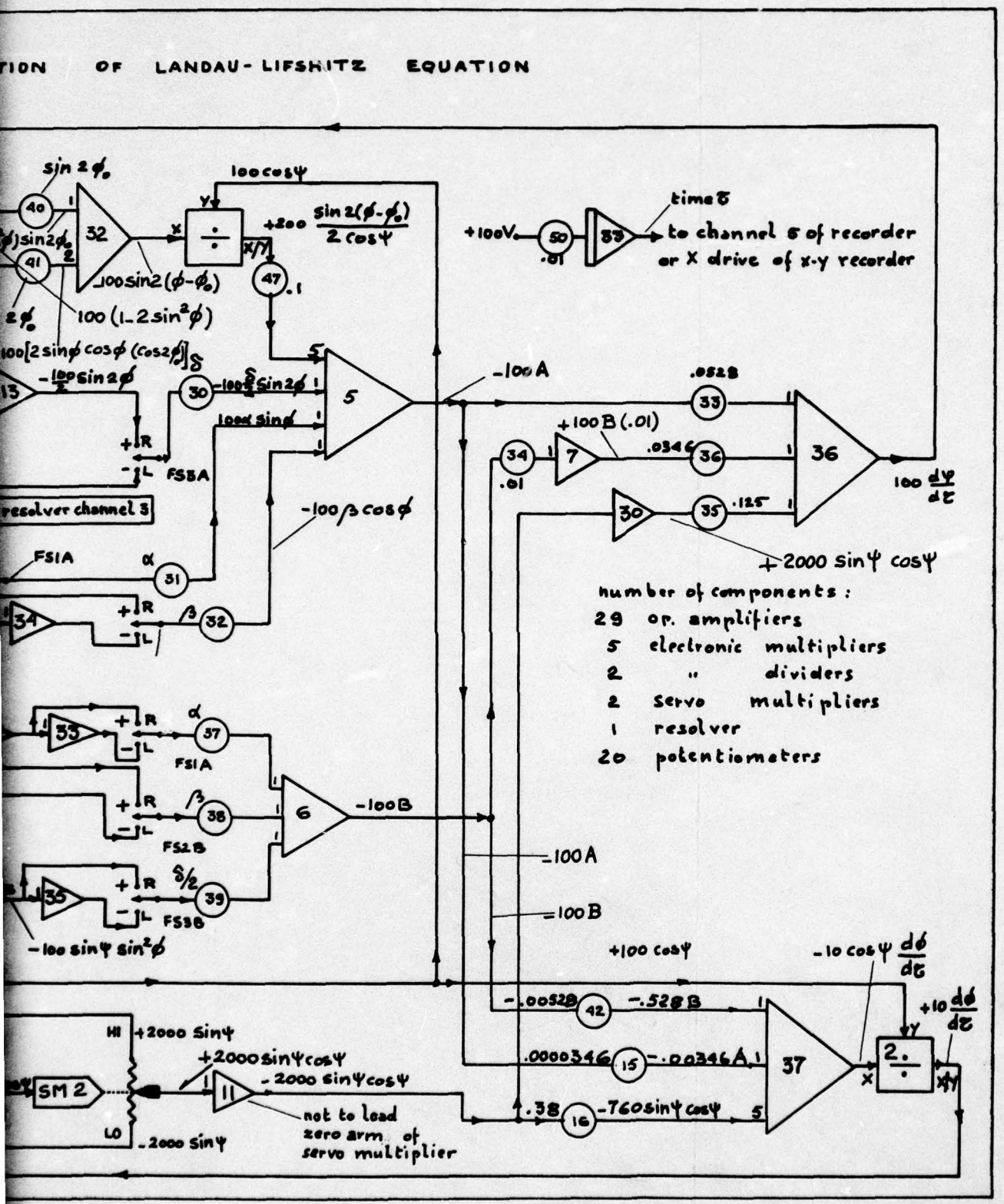
$$2K\gamma/M = 52.8 \times 10^6, \quad 2K\lambda/M^2 = 3.46 \times 10^5$$
$$2K\gamma\varepsilon/M = 380 \times 10^9, \quad 2K\lambda\varepsilon/M^2 = 2.50 \times 10^9 \tag{97}$$

Substituting the quantities given by (96) and (97) into equations (94) gives the computer equations:

FIG. 55 ANALOG COMPUTER CIRCUIT DIAGRAM FOR SOLUTION OF LANDA



TION OF LANDAU-LIFSHITZ EQUATION



$$\frac{d\psi}{d\tau} = 528 \times 10^{-4} A - 3.46 \times 10^{-4} B - 2.50 \sin\psi . \cos\psi$$

(98)

$$\cos\psi \frac{d\phi}{d\tau} = -3.46 \times 10^{-4} A - 528 \times 10^{-4} B - 380 \sin\psi . \cos\psi$$

A further and final modification of these equations is necessary as potentiometers have settings less than unity:

$$-100 \frac{d\psi}{d\tau} = -100 A (.0528) + 100 B (.01)$$

(99)

$$(.0346) + 2000 (.125) \sin\psi . \cos\psi$$

$$10 \cos\psi \frac{d\phi}{dt} = -100 B (.00528) - 100 A$$

$$(.0000346) - 2000 (5) (.38) \sin\psi . \cos\psi$$

where:

$$100 B = 100 (\sin\psi . \cos\phi)\alpha +$$

(100)

$$+ 100 (\sin\psi . \sin\phi)\beta - 100 (\sin\psi . \sin^2\phi) \frac{\delta}{2}$$

$$100 A = 100 \frac{\sin 2(\phi - \phi_o)}{2 \cos\psi} -$$

(101)

$$- 100 \frac{\delta}{2} \sin 2\phi + 100 \alpha \sin\phi - 100 \beta \cos\phi$$

The computer circuit diagram is shown in Fig.55, and is described hereafter.

The resolver R2 provides the following quantities:

$$-100 \sin\phi, + 100 \cos\phi, - 100 \sin\psi . \cos\phi,$$

$$+ 100 \sin\psi . \sin\phi$$

As the angle ϕ increases by 180° during reversal it is necessary that the input to the resolver does not sweep

through an angle larger than 90°, if the proper trigonometric functions are to be obtained. Larger angular displacements would cause the resolver shaft to hit limit stops, thus giving erroneous values at its output.

If the input to the resolver is made equal to

$$\Omega = \frac{90}{\pi} (\phi - \frac{\pi}{2})$$

as ϕ increases from 0 to 180°, Ω increases from - 45° to + 45°. The function sin $2 (\phi - \phi_o)$ appearing in the numerator of the first term in equation (101) is mechanized after performing the following transformation:

$\sin 2 (\phi - \phi_o) = \sin 2\phi \cos 2\phi_o - \sin 2\phi_o \cos 2\phi =$

$= 2 \sin \phi \cos \phi (\cos 2\phi_o) - (1 - 2 \sin^2 \phi) (\sin 2\phi_o)$

The multiplication by the two constants $\cos 2\phi_o$ and $\sin 2\phi_o$ is performed by potentiometers 40 and 41.

Since the angle ψ remains always below 1°, its sine and cosine will be mechanized using the following approximations:

$$\begin{aligned} \sin\psi &\cong \psi \\ \cos\psi &\cong 1 - \frac{\psi^2}{2}, \end{aligned} \tag{102}$$

which eliminates the need for an additional resolver.

The first equation (99) is mechanized at the grid of amplifier 36. The right-hand side of the second equation is formed at the grid of amplifier 37 and 10 $\frac{d\phi}{d\tau}$ is obtained by a subsequent division by $\cos\psi$.

The terms 100A and 100B entering in equations (99) are formed at the grids of amplifiers 5 and 6 respectively. The last terms in equations (99) correspond to the demagnetizing energy and are formed by the two servo multipliers, SM1, SM2, and additional components using approximations (102).

The parameters to be varied may be set by the following potentiometers:

Parameter	Potentiometer #	Setting
α	31, 37	- 1.0
β	32, 38	0.02, 0.08, 0.5 ...
δ	30	0
$\delta/2$	39	0
sin 2 ϕ_o	40	0
cos 2 ϕ_o	41	1
time	50	0.01

Potentiometer 15 is shown to be set at 0.0000346. This setting should be considered as zero; it has been indicated only for the purpose of illustrating how the second of equations (99) is mechanized. Amplifiers 3, 10, 11, 27, 28, 12 are not necessary to the computation, but avoid loading the resolver or the arm of the servo amplifiers. Switches FS3A, FS2A, FS1A, FS2B, FS3B have been provided to change the signs of α , β , δ

according to the desired settings on these parameters. Points to be connected to a six channel recorder or an x-y recorder are indicated in solid boxes. The following six variables have been selected for recording on a Sanborn recorder:

Channel:	1	2	3	4	5	6
Variable:	ϕ	$\frac{d\phi}{dt}$	$\cos\phi$	$\sin\phi$	t	$\left[\frac{d\phi}{dt}\sin\phi\right]$

The variable at channel 6 represents the voltage induced in the longitudinal pickup loop. When the film switches from $\phi = 0$ to $\phi = 180°$, $\cos\phi$ as recorded at channel 3, changes from + 1 to - 1.

The initial voltage across the plate of the feedback capacitors at integrators 1 and 2 is set to zero, since at $t = 0$: $\phi(0) = 0$, $\Psi(0) = 0$.

The results of the analog computation are shown by the curves in Figs. 56, 57, 58, 59, which are plots of the variable e obtained on an x-y recorder. The output of the six channel recorder is shown in Figs. 60, 61, 62. A short discussion of these recordings follows:

Figure 56:

Film constants: $M = 860$ gausses $\quad \lambda = 10^8$

$K = 1290$ ergs/ccm

Driving forces: $\alpha = -1$, $\delta = 0$

$\beta = 1.0, 0.5, 0.08, 0.02.$

The initial position of the magnetization coincides with the direction of the switching field α. The figure shows in solid lines the curves obtained from the analog computation and, in dotted lines, those obtained in Ref. 6 by D. O. Smith from a digital computation for the same conditions. The analog curves have the same general shape, but the switching delay due to the presence of the perpendicular field β is larger and the damping is smaller in the results of the analog computation. These differences may be attributed to the presence of electronic drift, a common occurrence in analog computer circuits. Because of the high sensitivity of the switching delay on β, at low values of perpendicular field, slight changes in H_p, caused by drift, may change the switching delay considerably. However, since no detailed information is available on the digital computation mentioned in Ref. 6, the final discussion on the accuracy of the analog computation is included in the next section c., and presented with the digital computation obtained by the writer.

On the analog computer circuit, parameters α, β, δ, $\emptyset$, M, K, λ_s, λ may be changed readily by simply setting a potentiometer. Any desired variable may be tapped off from the circuit and an immediate display on a recorder may be obtained.

Figure 57:

Same film constants as Fig. 56, the film is magnetostrictive and the magnetostriction coefficient is included in δ

Driving forces: $\alpha = -1$, $\delta = 3\lambda_s\sigma/2K = -.25$

$\beta = 1.0, 0.5, 0.08$

$\phi_o = 0$

The figure shows the effect of an applied negative stress δ along the direction of the perpendicular field. This stress is a compression acting on a film having a positive magnetostriction coefficient, and values of M and K identical to that of the film referred to in Fig. 56. A negative stress along β is equivalent to a positive stress along α and will increase the anisotropy of the film in that direction.

Fig. 57 shows that the effect of stress is to decrease the switching delay corresponding to a particular value of β. For example, at $\beta = 0.02$ the peaking time occurs at 3.8 nanosec. when $\delta = 0$, while the peak is shifted to 2.6 nanosec. if $\delta = -0.25$. A detailed quantitative study of the different parameters affecting switching is given in the next section, in which it is shown how a digital computer may be programmed to study the dynamics of film switching.

Figure 58

Film constants: same film constants as those specified for Fig. 56.

$\alpha = -1.0$

$\beta = .02$

$\phi_o = 0$

$\delta = -1.0, -0.8, -0.4, -0.2, -01, -0.04$

The curves show how peaking time decreases with increasing stress. It should be pointed out that if $\beta = 0$ the film should not switch since there is theoretically no starting switching torque. However, in the analog computer solution, electronic drift causes the film to switch after several seconds, even in these conditions. For this reason it is important to keep solution time as small as possible.

Figure 59

Film constants: same film constants as those specified for Fig. 56.

$\alpha = -1.0$

$\phi_o = 30°$

conditions for β and δ are marked on the figure. A comparison between the curve for $\beta = 1.0$, $\delta = -1.0$ in Fig. 59 and that for the same β and δ in Fig. 57 shows that the effect of changing ϕ_o is to decrease

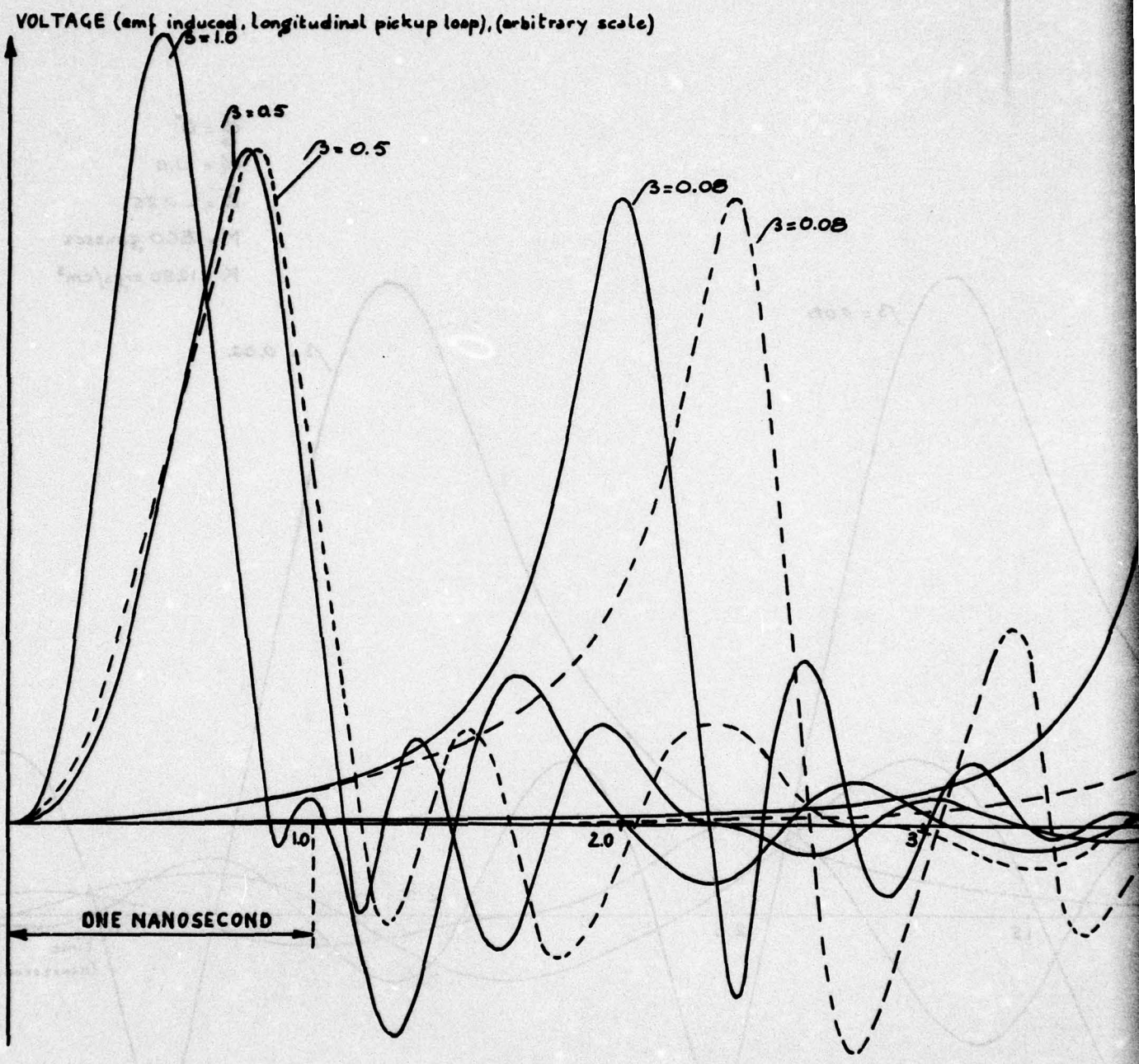
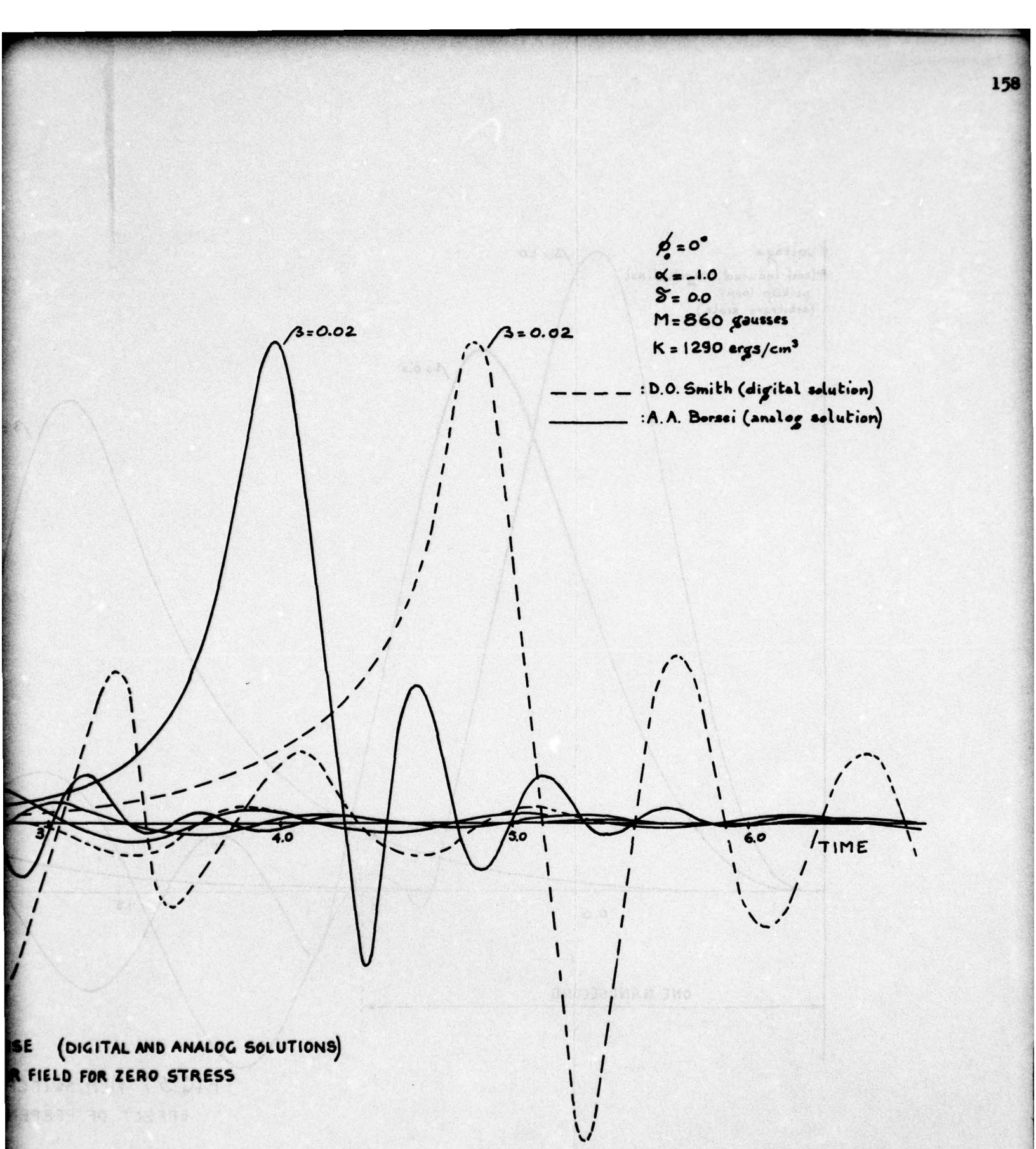


FIG. 56 FILM SWITCHING RESPONSE (DIGITAL AND ANAL
EFFECT OF PERPENDICULAR FIELD FOR ZERO STRE



SE (DIGITAL AND ANALOG SOLUTIONS)
R FIELD FOR ZERO STRESS

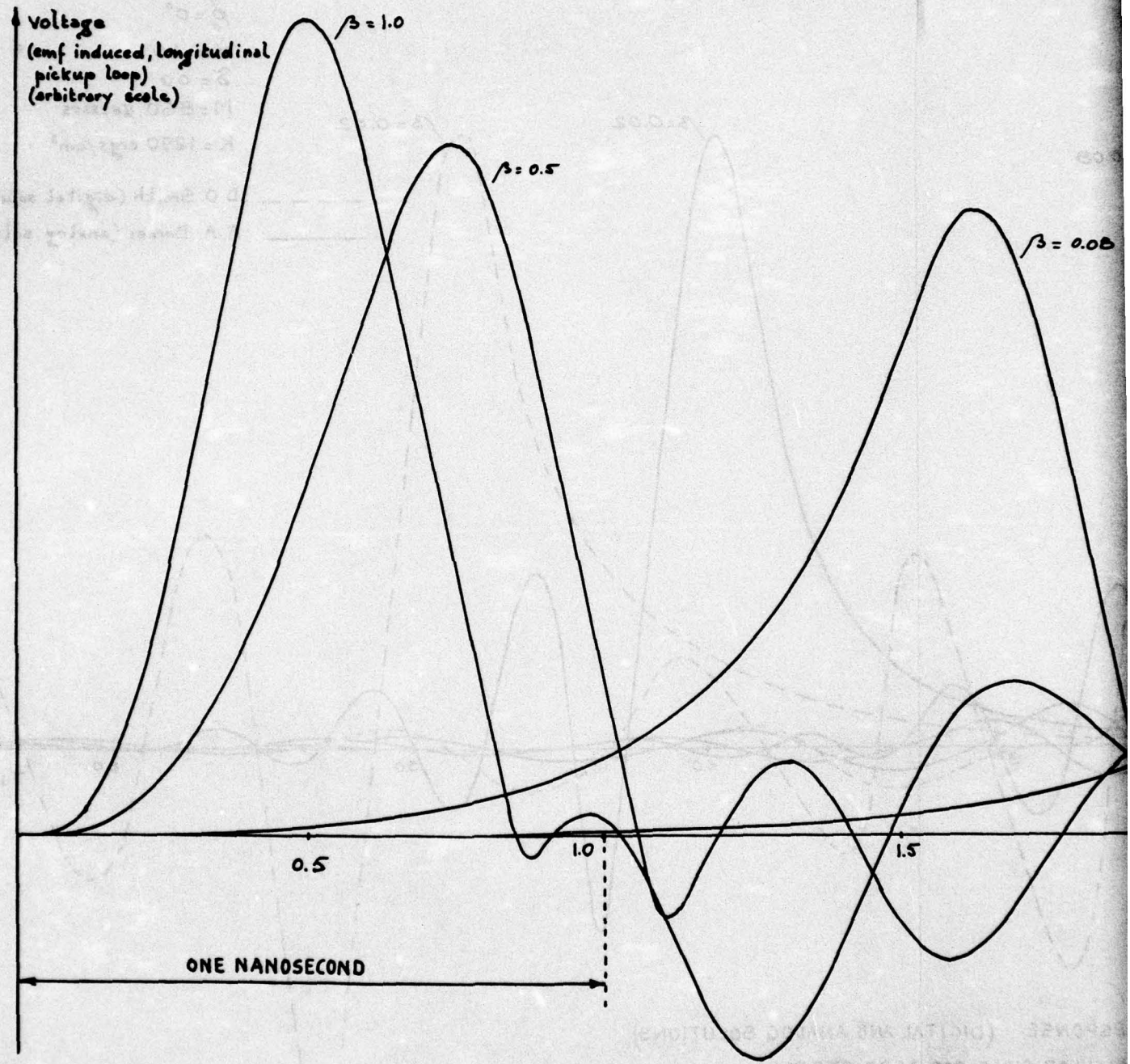
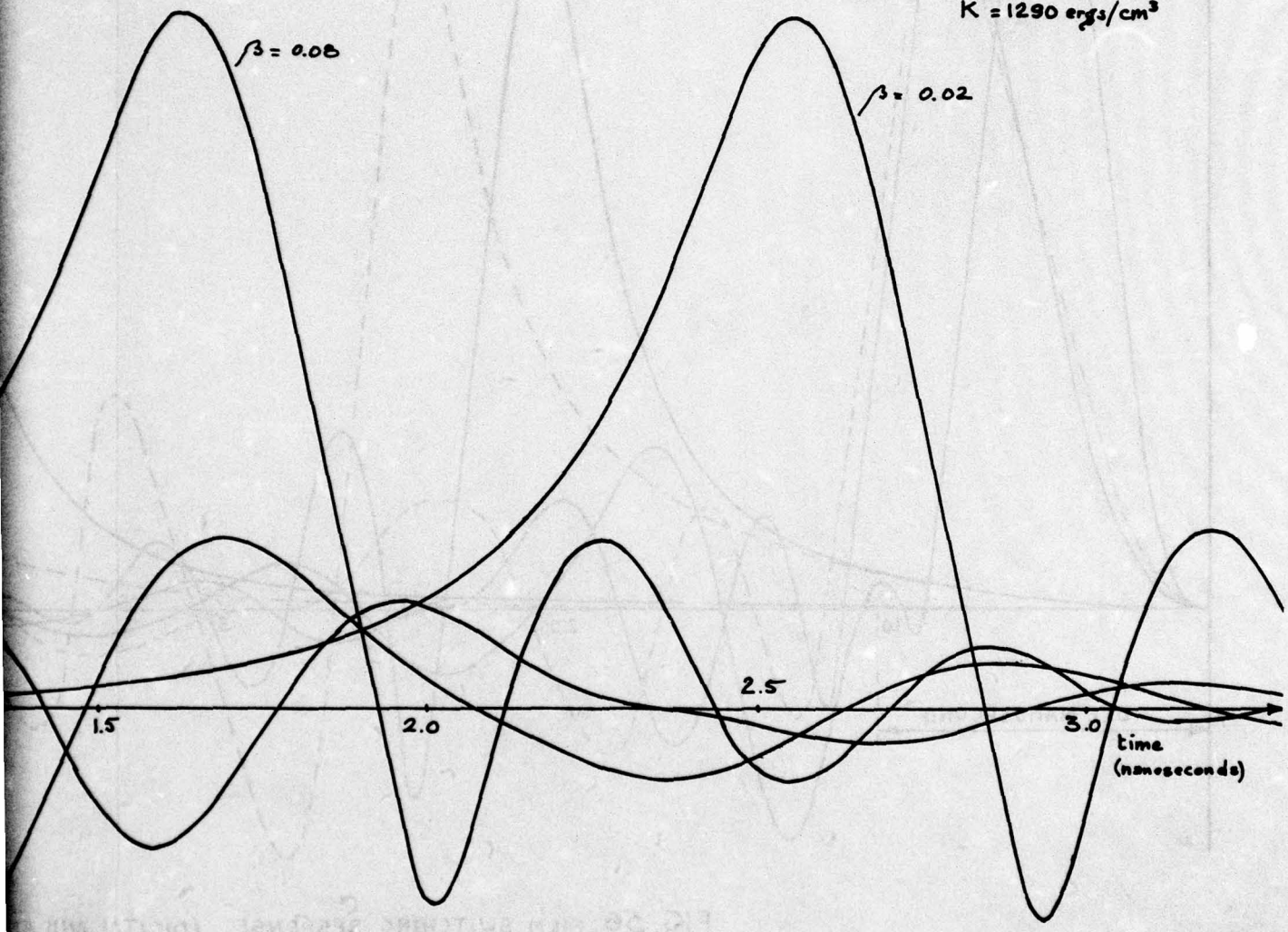


FIG. 57 FILM SWITCHING
EFFECT OF PERPENDICUL



5.57 FILM SWITCHING RESPONSE (ANALOG COMPUTER SOLUTION)
EFFECT OF PERPENDICULAR FIELD FOR CONSTANT STRESS

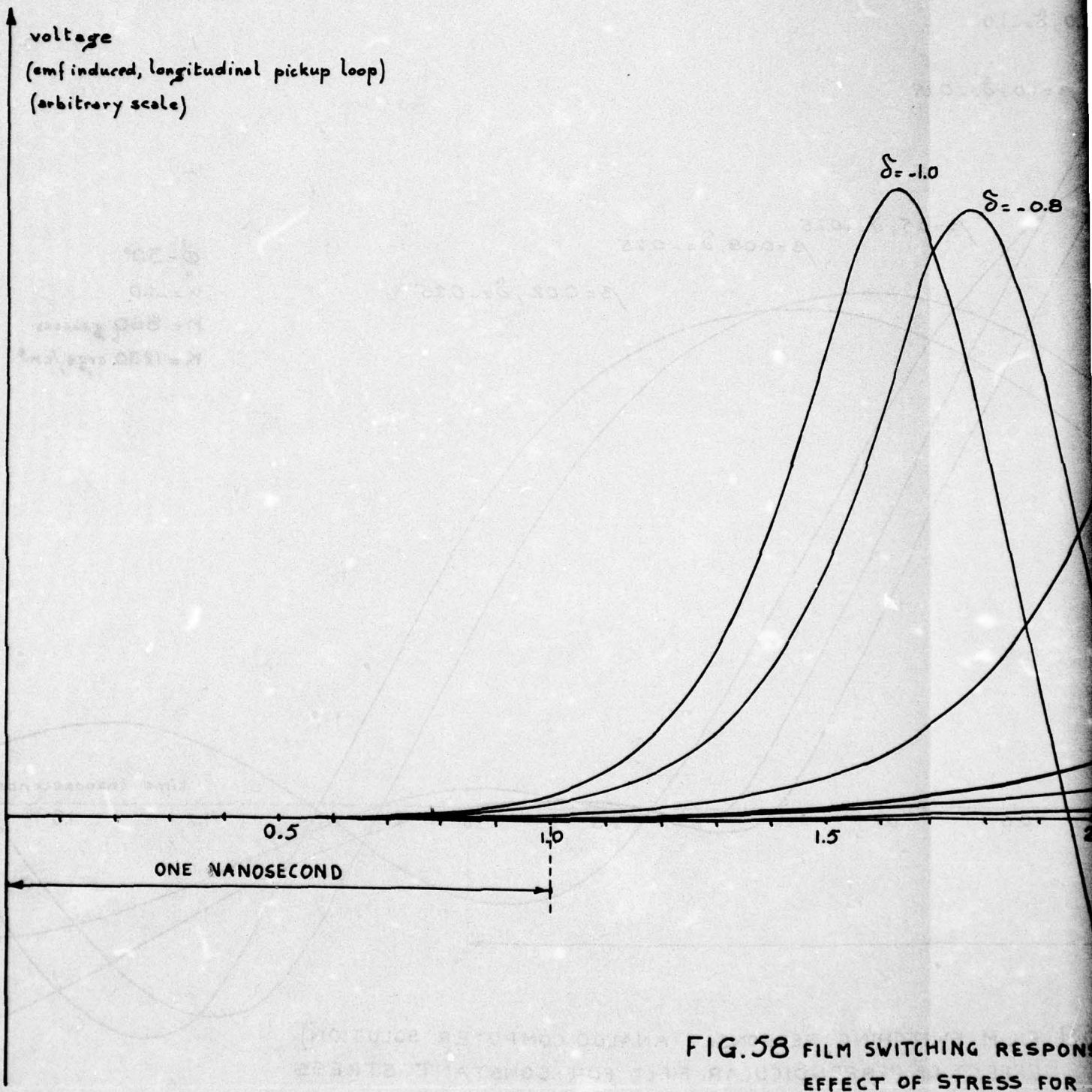
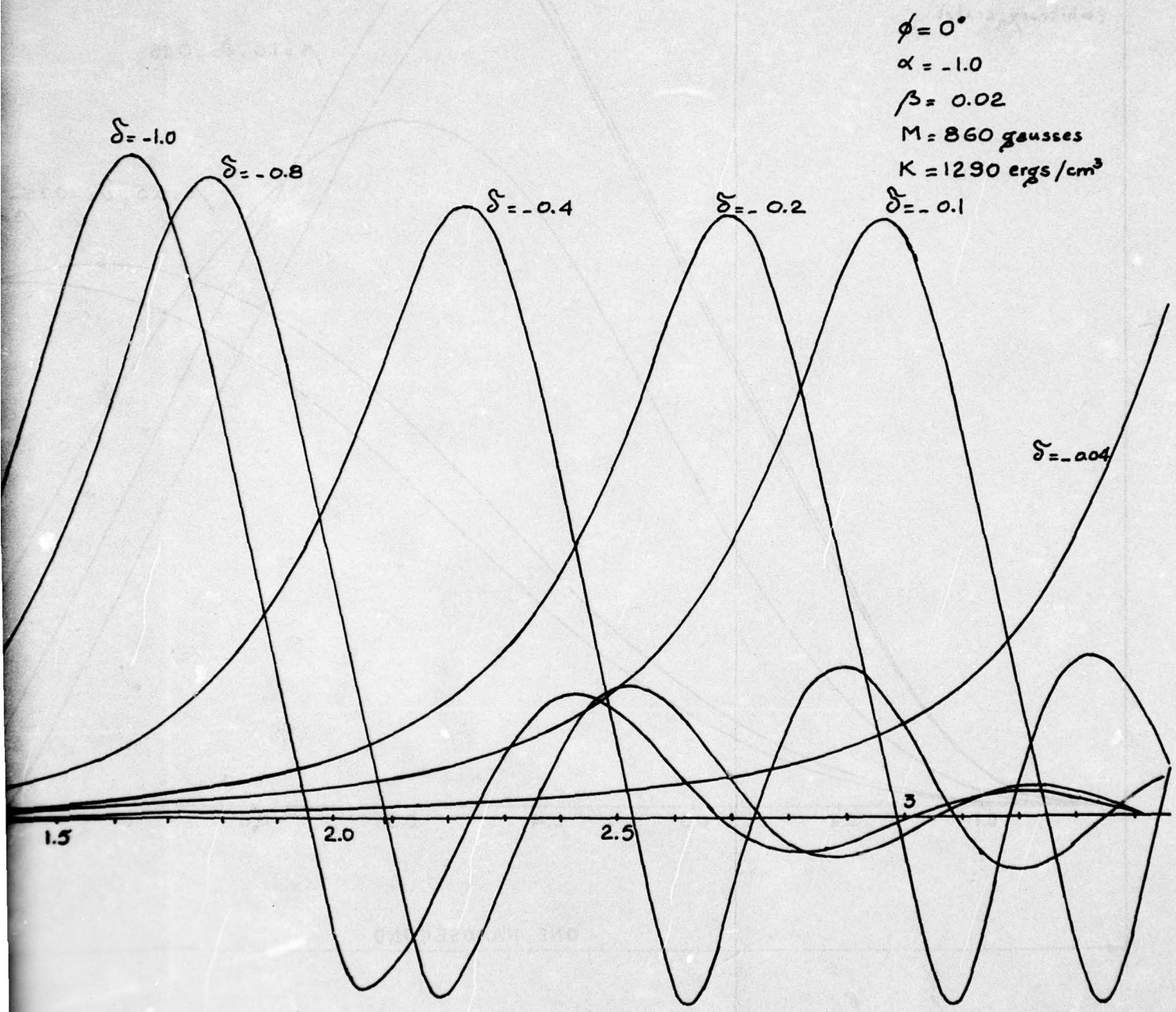


FIG. 58 FILM SWITCHING RESPONS
EFFECT OF STRESS FOR



FILM SWITCHING RESPONSE (ANALOG COMPUTER SOLUTION)
EFFECT OF STRESS FOR CONSTANT PERPENDICULAR FIELD

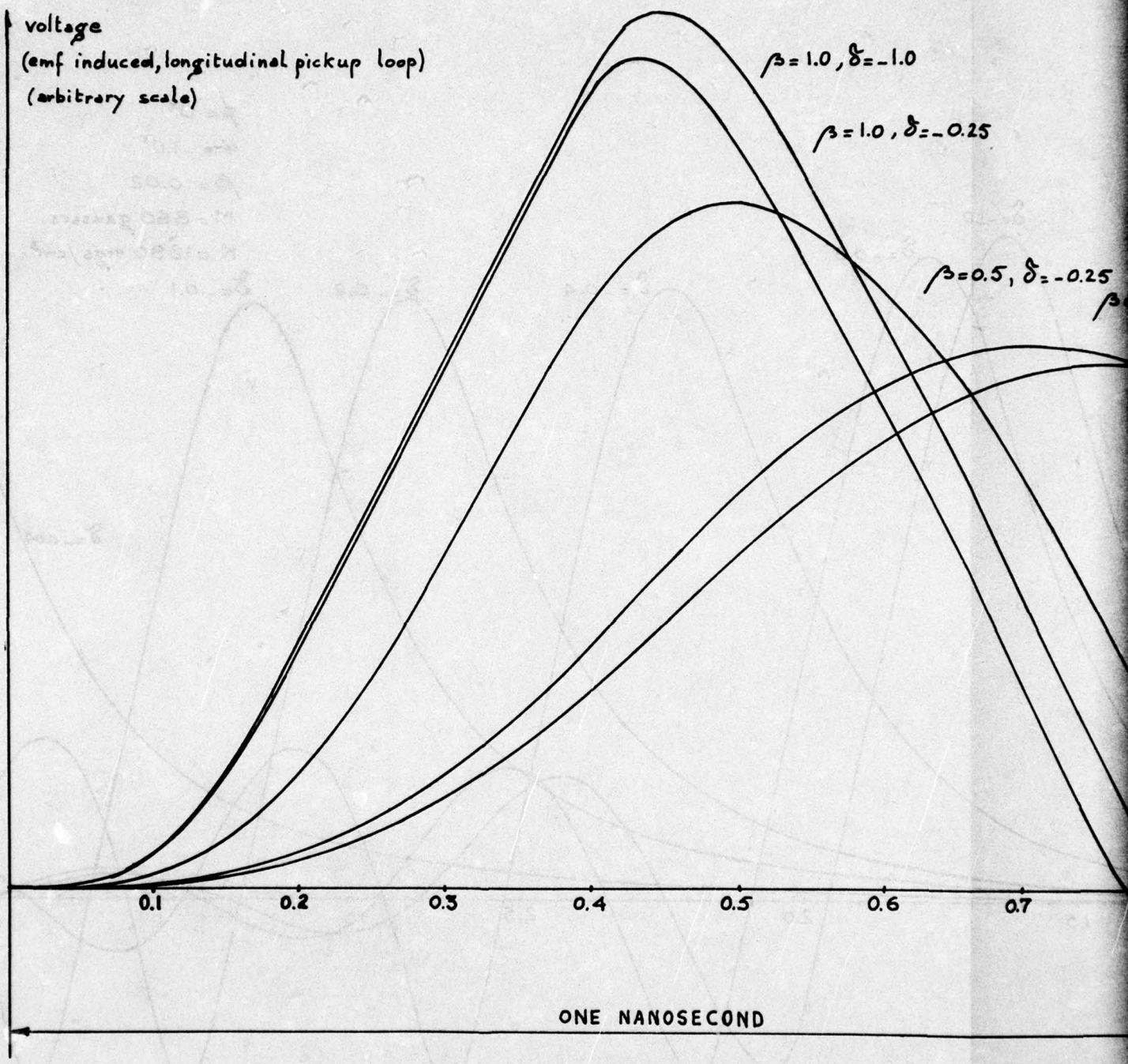
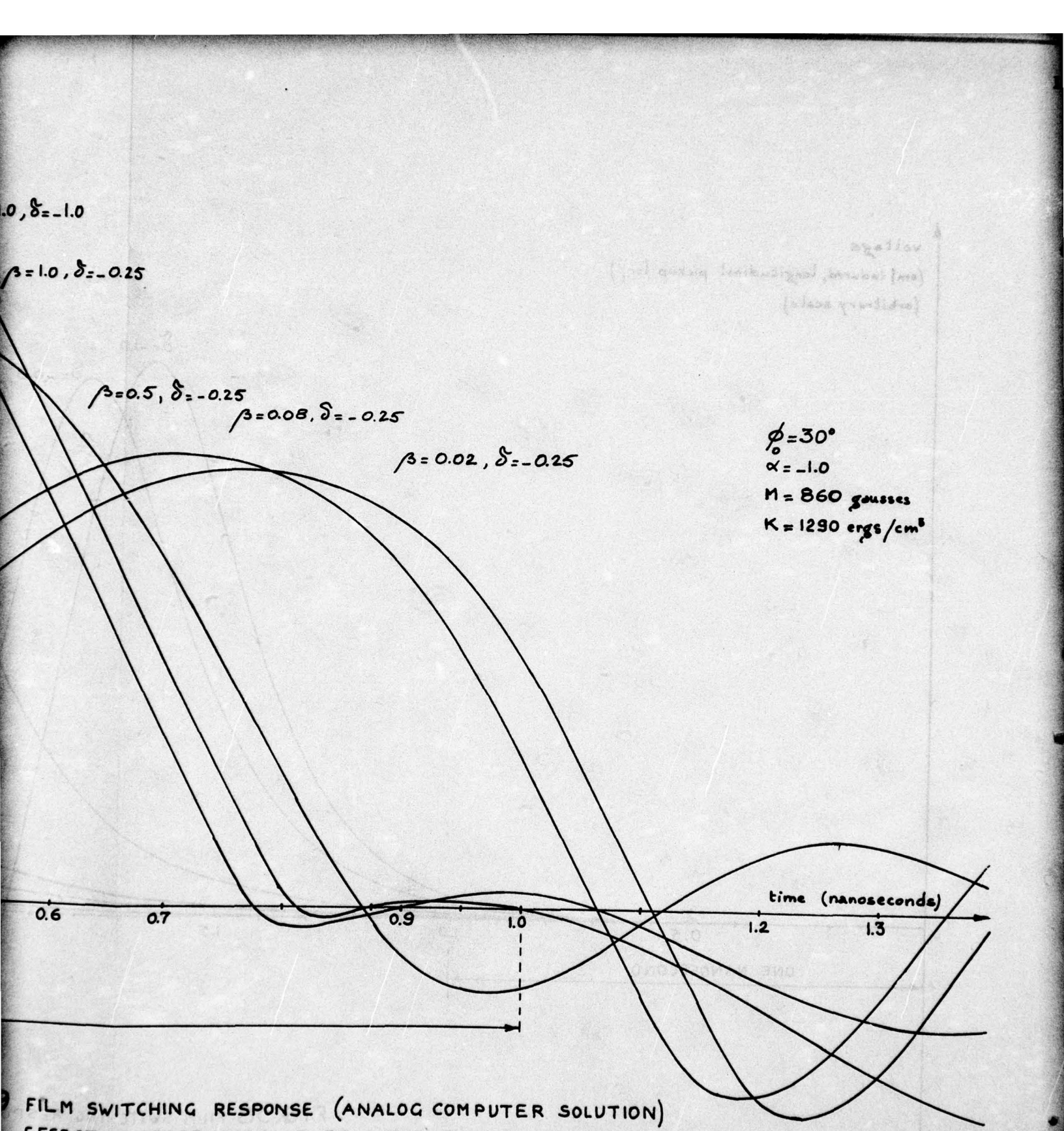


FIG. 59 FILM SWITCHING RES
EFFECT OF PERPENDIC



FILM SWITCHING RESPONSE (ANALOG COMPUTER SOLUTION)
EFFECT OF PERPENDICULAR FIELD FOR CONSTANT STRESS

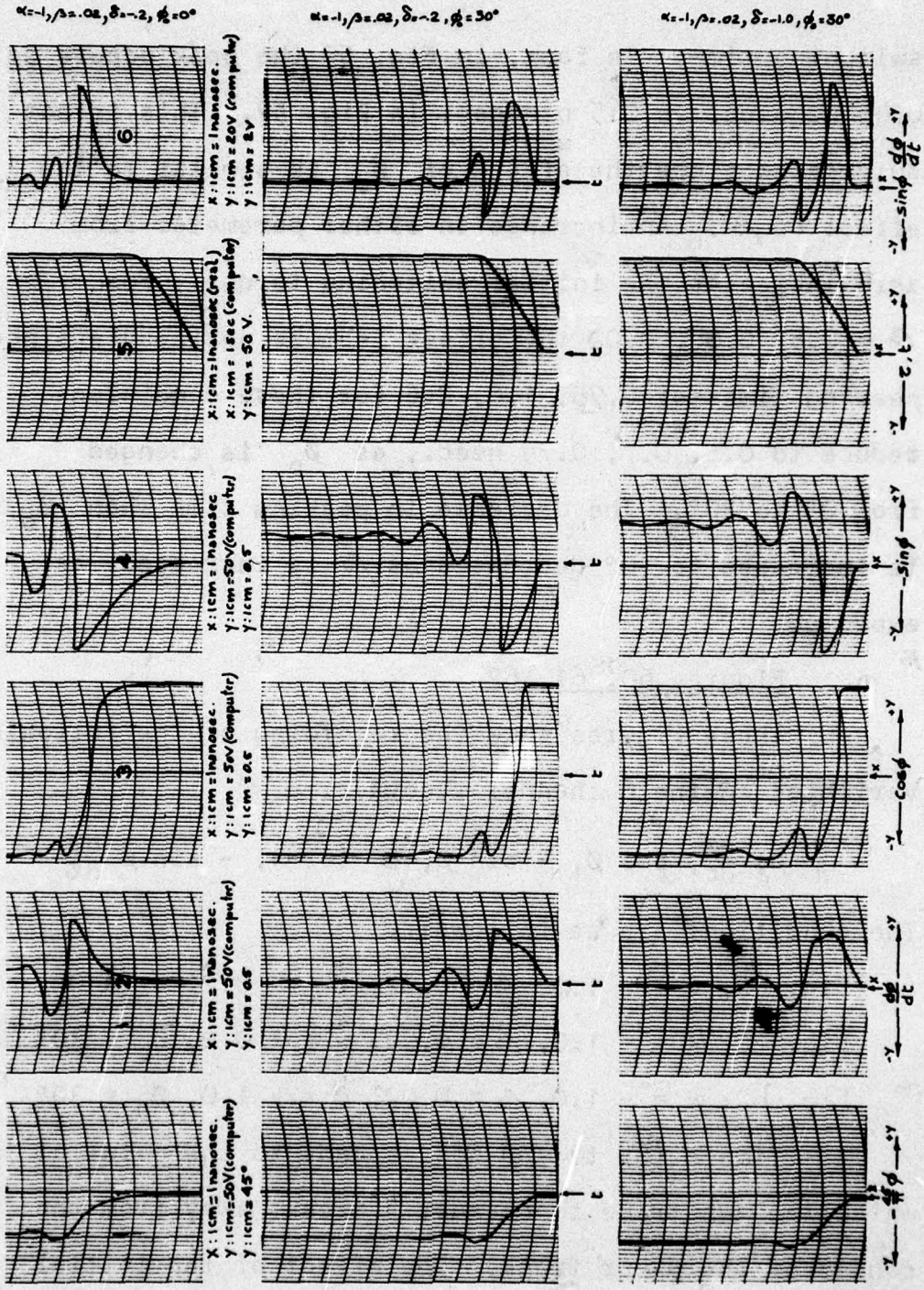


Fig. 60 Fig. 61 Fig. 62

switching time. In fact, in Fig. 59 the peak occurs at 0.45 nanosec. vs 0.5 nanosec. in Fig. 57. This is not surprising since the effect of ϕ_o is similar to the effect of β. An increase in either parameter from zero increases the initial switching torque. For β = 0.5, 0.08, 0.02 the effect is more noticeable since peaking times of 0.75, 1.6, 2.6 for these conditions reduce to 0.5, 0.7, 0.75 nsec., as ϕ_o is changed from 0° to 30°. The decrease in peaking time when ϕ_o is increased to 30° decreases as β is increased, as expected.

Figures 60, 61, 62

These figures show the recording of the following variables on the 6 channel recorder:

$$-\frac{45}{\pi}\phi,\ \frac{d\phi}{d\tau},\ \cos\phi,\ -\sin\phi,\ \tau\ (\text{or } t),\ -\sin\phi\,\frac{d\phi}{d\tau}$$

The conditions are as follows:

Fig. 60: $\alpha = -1.0$, $\beta = 0.02$, $\delta = -0.2$, $\phi_o = 0°$

Fig. 61: $\alpha = -1.0$, $\beta = 0.02$, $\delta = -0.2$, $\phi_o = 30°$

Fig. 62: $\alpha = -1.0$, $\beta = 0.02$, $\delta = -1.0$, $\phi_o = 30°$

Time τ (or t) = 0 corresponds to the point at which the pen trace in channel 5 breaks away from the center of the paper track. The effect of the initial angle ϕ_o on the switching delay is evidenced by comparing the traces in channels 6 for Figs. 60 and 61.

Switching occurs by 180° reversal for both cases as the traces corresponding to cos ϕ move from + 1 to - 1 (cf. channel 3) and the traces for $-\frac{45}{\pi}\ \phi$ display a 45° shift. Comparing traces in channel 2 shows that in the case of Fig. 61 the variable $\frac{d\phi}{d\tau}$ increases more rapidly than in Fig. 60. This may be interpreted by considering that in the case of Fig. 61 the larger delay is due to the smaller starting torque.

Comparing Figs. 61 and 62 shows the effect of an applied stress on the magnetization reversal: traces in channel 6 ($-\sin\phi\ \frac{d\phi}{dt}$) display faster switching as well as traces in channel 3 (cos ϕ). The ferromagnetic oscillation is more pronounced (cf. cos ϕ) when the stress is higher and the time rate of increase of ϕ reaches its maximum sooner if the stress is higher (cf. channel 1 for $d\phi/dt$).

c. Solution by digital computer - Stress effect on switching.

This section is devoted to the description of digital computer programs for solving the Landau Lifshitz equation as the parameters influencing the dynamic response of the film are varied stepwise. The results of the computations are displayed directly in the form of

printer plots and give the following information:

1. The switching response of the film: e (volts) vs. time (nanosec.)
2. The inverse of the peaking time vs. the magnitude of the switching field with the normalized perpendicular field β or the applied normalized stress δ as parameters.
3. The ferromagnetic resonant frequency vs. the magnitude of the switching-field, with β or δ as parameters.
4. The dynamic critical switching curve, that is, the value of the switching magnetic field at which reversal occurs under dynamic conditions (dynamic switching threshold) vs. the normalized perpendicular field β, with ϕ_o or δ as parameter.

These computations were performed for two specimens. The first is the specimen discussed in Ch. I possessing the following characteristics: composition nickel-iron 44-56, saturation magnetization $M_s = 1450$, magnetostriction coefficient $\lambda_s = 19 \times 10^{-6}$. The second has the assumed properties of the film used by D. O. Smith in the investigation reported in Ref. 6. The 44-56 nickel-iron film is considered prestressed at the value of $K = 25500$ ergs cm^3, corresponding to closure of its transverse loop. Any applied stress is considered as

an excess stress in the sense adopted in Ch. I, Part 2 (experimental studies).

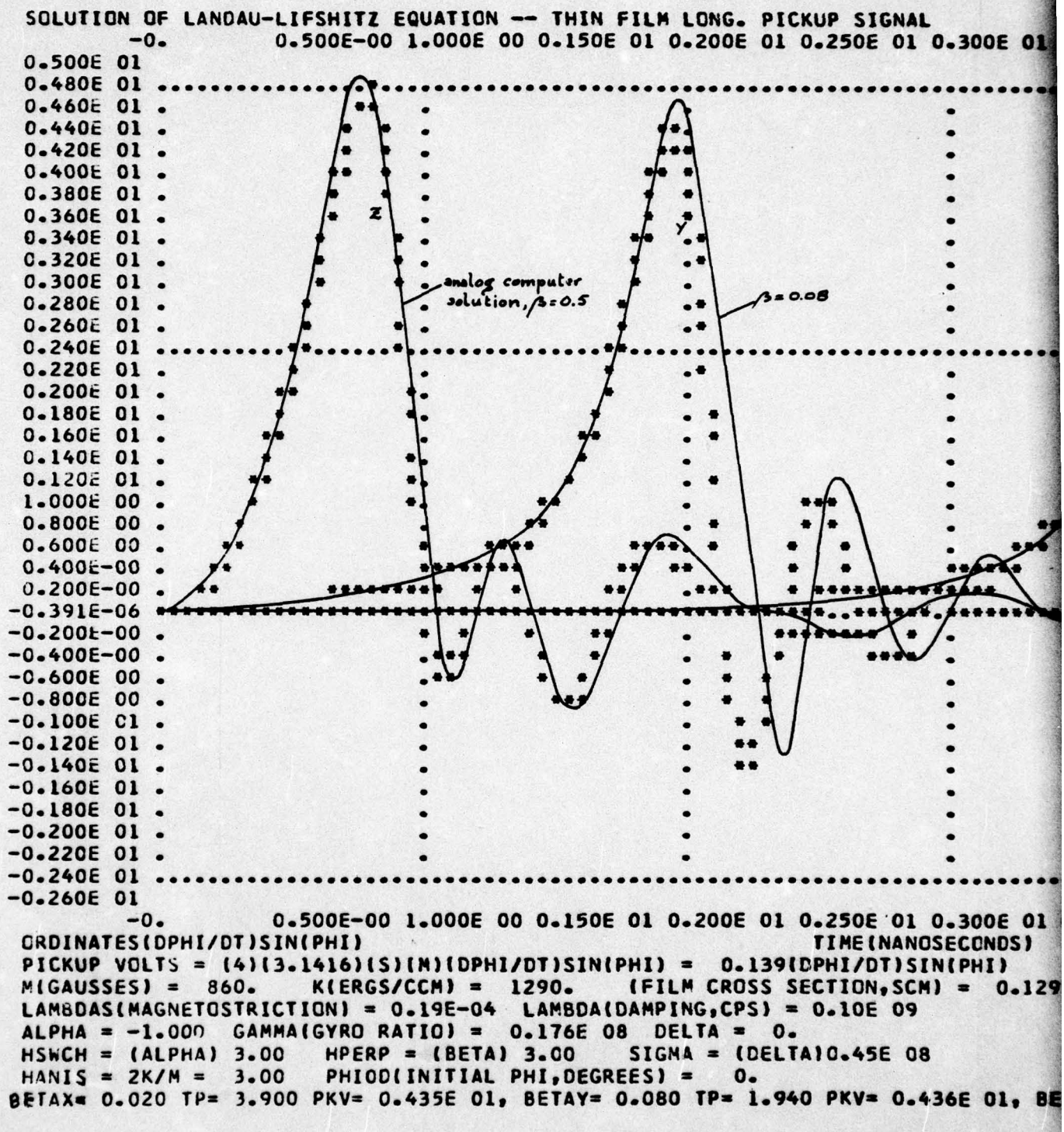
A duplication of the results contained in Ref. 6 is first presented in order to check the results of the digital computer solution with published information and with the results of the analog computer solution presented in the previous section. The film characteristics adopted in this comparative study have been specified in the preceding section.

The digital computer program is then used to obtain the switching response of the 44-56 nickel-iron film and other digital computer programs applied to perform a more thorough computer study of film dynamics.

Because of the discrete character of a digital plot the curves obtained give only the overall shape of the response. However, values of variables at points of interest are stored by the computer as the computation progresses and are printed at the bottom of the page with the accuracy desired, together with other pertinent data on the film or on the particular combination of parameters being investigated.

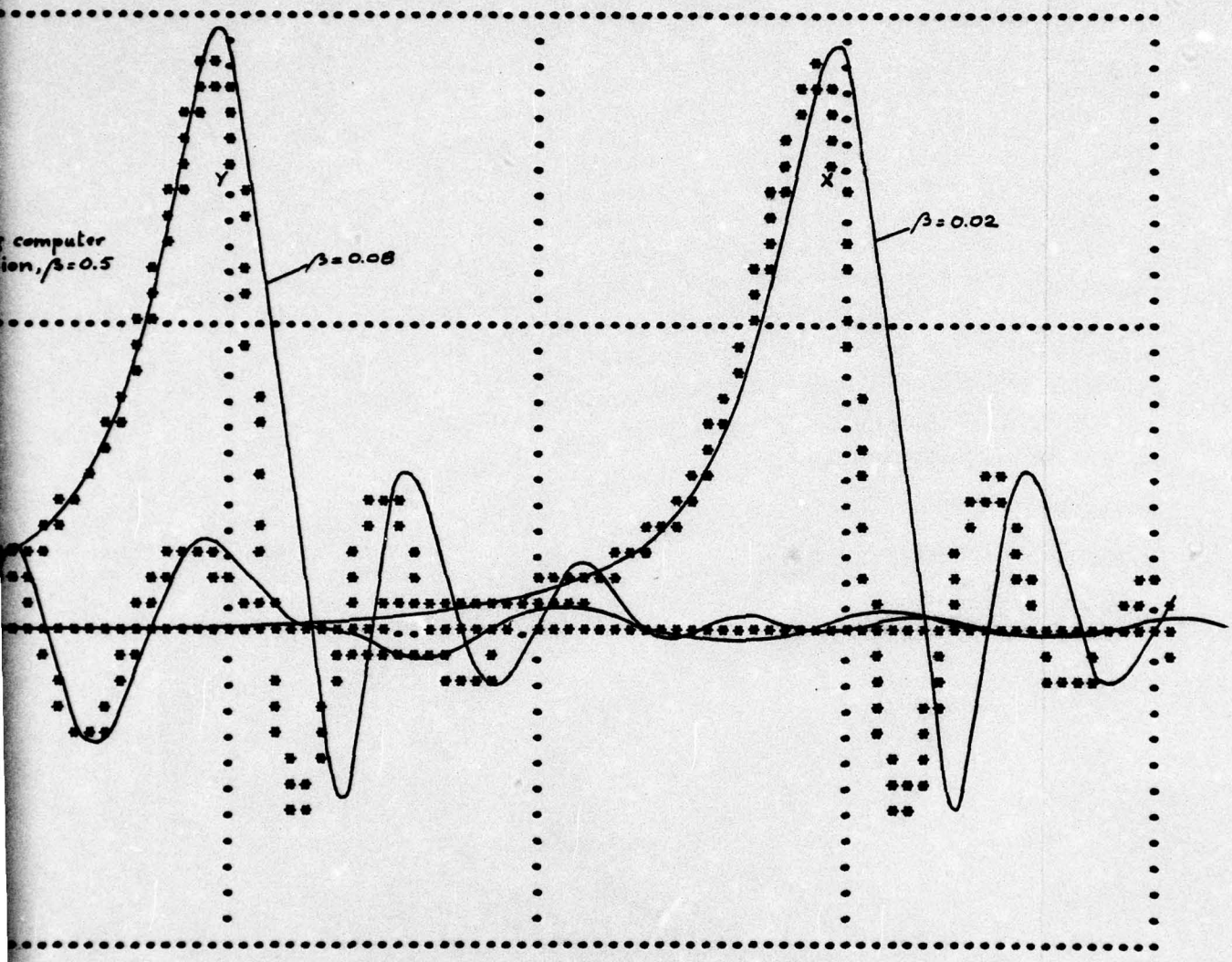
d. Comparison between analog and digital computer results:

The switching response of the film studied in Ref. 6 is shown in Fig. 63, as obtained from the analog



PICKUP VOLTS = (4)(3.1416)(S)(M)(DPHI/DT)SIN(PHI) = 0.139(DPHI/DT)SIN(PHI)
M(GAUSSES) = 860. K(ERGS/CCM) = 1290. (FILM CROSS SECTION,SCM) = 0.129
LAMBDAS(MAGNETOSTRICTION) = 0.19E-04 LAMBDA(DAMPING,CPS) = 0.10E 09
ALPHA = -1.000 GAMMA(GYRO RATIO) = 0.176E 08 DELTA = 0.
HSWCH = (ALPHA) 3.00 HPERP = (BETA) 3.00 SIGMA = (DELTA)0.45E 08
HANIS = 2K/M = 3.00 PHIOD(INITIAL PHI,DEGREES) = 0.
BETAX= 0.020 TP= 3.900 PKV= 0.435E 01, BETAY= 0.080 TP= 1.940 PKV= 0.436E 01, BE

N -- THIN FILM LONG. PICKUP SIGNAL
00 0.150E 01 0.200E 01 0.250E 01 0.300E 01 0.350E 01 0.400E 01 0.450E 01 0.500E 01



00 0.150E 01 0.200E 01 0.250E 01 0.300E 01 0.350E 01 0.400E 01 0.450E 01 0.500E 01
TIME(NANOSECONDS)

I/DT)SIN(PHI) = 0.139(DPHI/DT)SIN(PHI)
1290. (FILM CROSS SECTION,SCM) = 0.129E-04
LAMBDA(DAMPING,CPS) = 0.10E 09
0.176E 08 DELTA = 0.
3.00 SIGMA = (DELTA)0.45E 08
PHI,DEGREES) = 0.
BETAY= 0.080 TP= 1.940 PKV= 0.436E 01, BETAZ= 0.500 TP= 0.780 PKV= 0.471E 01

Fig. 63

and digital computation. The results of the analog computations are plotted in solid line. The results of the digital computations are represented by the asterisks.

In the light of the minor differences shown in comparing the analog and the digital solutions in this study, it may be assumed that the digital solutions in the forthcoming presentation are reasonably free of errors originated from the iterative process performed by the machine during integration, and that the analog solution already presented is reasonably free from electronic drift. The differences existing between the digital solution reported in Ref. 6 and the two types of solutions presented here cannot be explained because of incomplete information on the digital solution cited in Ref. 6.

The description at the bottom of Fig. 63 gives the denormalizing factors which are multiplied by the normalized forces α , β , δ in order to obtain the magnetic fields H_s, H_p in oersteds and the stress in dynes/cm^2. The last line in the description is divided in three parts separated by commas. In each part the following information on the graph is given from the computation:

BETA (x or y or z): Value of normalized, transverse field β.

TP: Peaking time (chosen as switching time)

PKV: Peaking volts: maximum value of voltage induced in the longitudinal pickup loop: $\left[\sin \phi \, (d\phi/dt)\right]_{max}$.

The listing of the program for obtaining three curves in one graph is given in Appendix 7a. The flow chart is illustrated briefly in the course of the forthcoming presentation on the dynamic response of the 44-56 nickel-iron film.

e. Computational flow charts for integration and plotting of film dynamic response.

The computational path followed to obtain the dynamic response of the film is shown in Fig. 64 and the corresponding listing is included in Appendix 7b. Scaling of the equations as for the analog computer solution is unimportant since the digital computation is performed in floating point arithmetic. The scaled equations (98) have been used in the program and the abscissas of the plot express time in seconds. The labeling of the time axis is however shown in "nanoseconds" corresponding to real time t, since 1 sec

computer time = 10^{-9} seconds real time.

The description printed below the plot gives the values of variables and parameters in normalized and physical form as well as the film constants. The ordinates are expressed in "pickup volts" induced in the longitudinal loop by reversal of the magnetization component $N \cos \phi$. The emf induced is:

$$e = - \frac{d \Phi}{dt} = 4\pi M S \frac{d\phi}{dt} \sin \phi, \tag{103}$$

since

$$\Phi = B S = 4\pi S \left[M \cos \phi \right] \tag{104}$$

where S is the cross-sectional area of the film in cm^2.

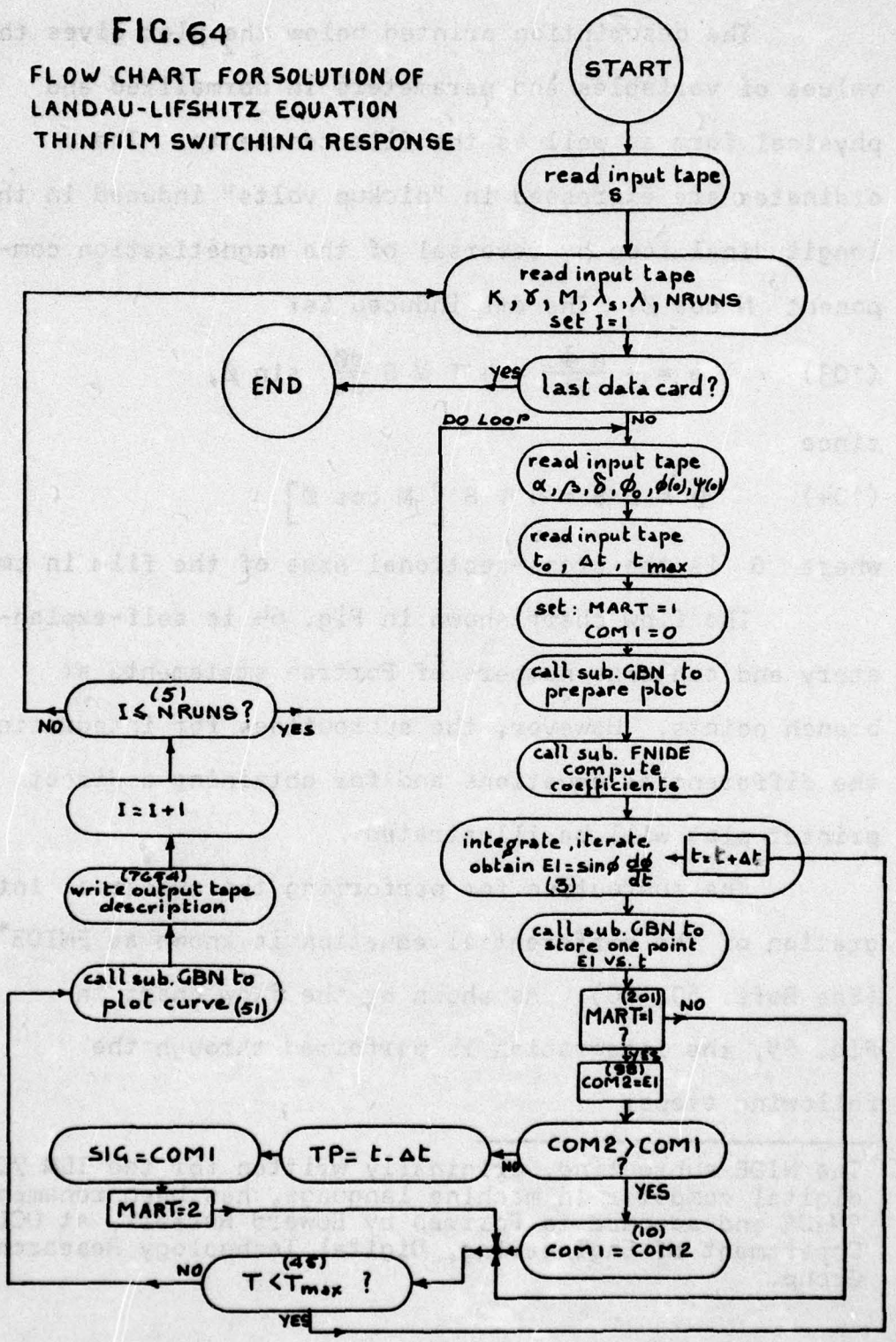
The flow chart shown in Fig. 64 is self-explanatory and contains numbers of Fortran statements at branch points. However, the subroutines for integrating the differential equations and for obtaining a direct printer plot will be illustrated.

The subroutine for performing the numerical integration of the differential equation is known as FNIDE* (See Refs. 59, 60). As shown by the flow chart in Fig. 65, the integration is performed through the following steps:

*The NIDE subroutine, originally written for the IBM 704 digital computer in machine language, has been renamed FNIDE and adapted to Fortran by Edward Russell, at UCLA, Department of Engineering, Digital Technology Research Group.

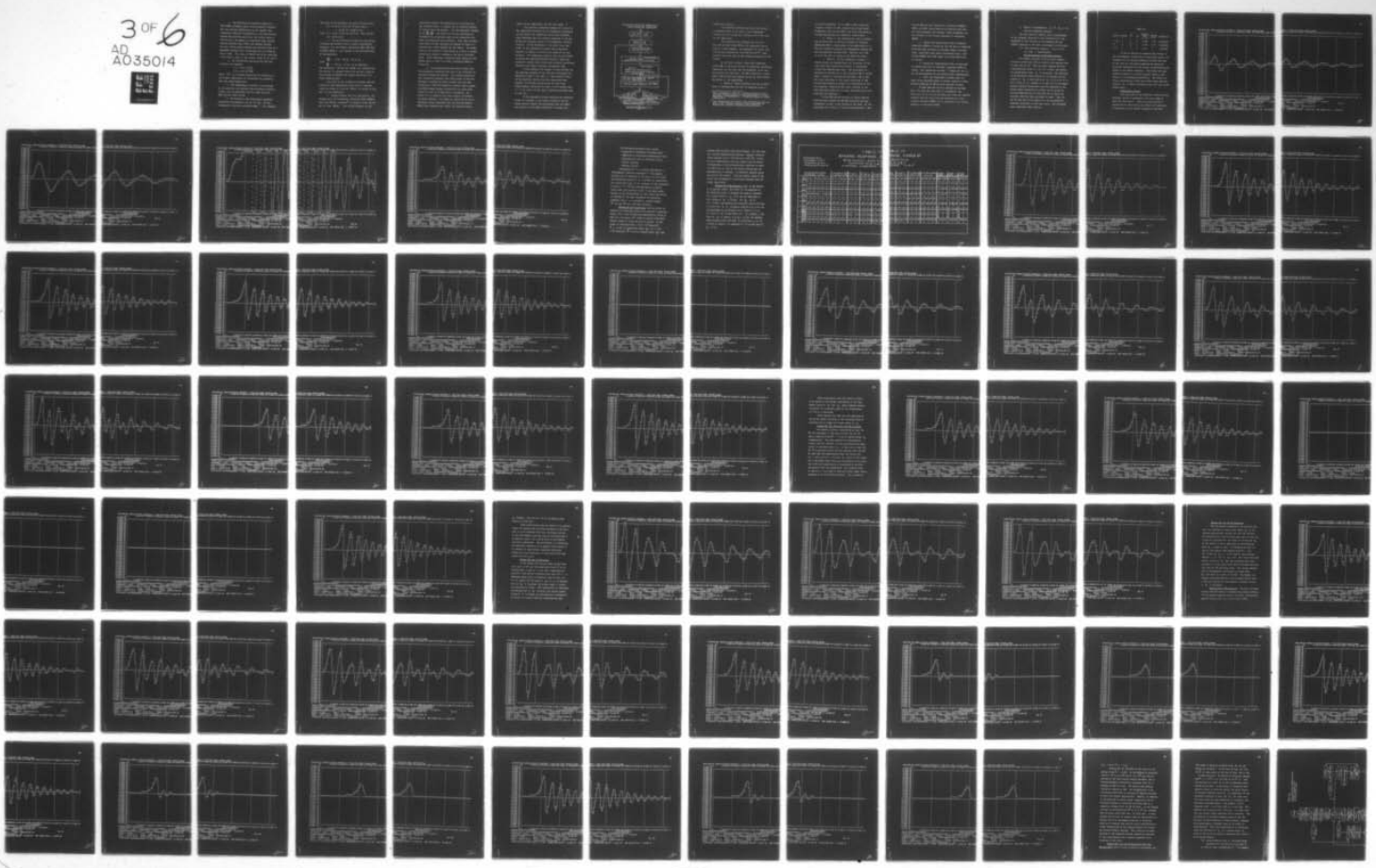
FIG. 64

FLOW CHART FOR SOLUTION OF LANDAU-LIFSHITZ EQUATION THIN FILM SWITCHING RESPONSE



AD-A035 014 CALIFORNIA UNIV LOS ANGELES DEPT OF ENGINEERING F/G 20/2
ON THE USE OF PIEZOELECTRIC-MAGNETOSTRICTIVE COUPLING IN DIGITA--ETC(U)
AUG 62 A A BORSEI NONR-233(52)
UNCLASSIFIED UCLA62-37 NL

3 OF 6
AD A035014



a. The subroutine is entered by means of a CALL FNIDE statement, whose calling sequence contains: the time interval DELTAT equal to the largest time integration step and corresponding to the time interval between two printing operations, the initial value of time TO (t_o), the number of integration steps desired between printing steps (100), the maximum relative, per unit, error allowed between the predicted value of a dependent variable after integration and its corrected value (.006). The values of DELTAT and TO are read from a data card, as well as the initial values of $\emptyset$ and Ψ.

b. The coefficients involving only the film constants are computed:

$$C\,1 = 2\,K\,\gamma\,10^{-9}/M$$

$$C\,2 = 2\,K\,\lambda\,10^{-9}/M^2$$

where 10^{-9} is a scaling coefficient not necessary in the digital computation but maintained for uniformity with the analog computation.

c. The trigonometric functions to be entered in the equations are obtained from the Fortran function library and are named SPSI (sin Ψ), CPSI (cos Ψ), SPHI (sin $\emptyset$), CPHI (cos $\emptyset$).

d. The factors in the differential equations containing the parameters (α, β, δ, $\emptyset_o$) and the trigonometric functions specified under c are computed.

The value of the parameters are read from data cards.

$$A1 = \alpha \sin \phi - \beta \cos \phi + \delta \, (\sin 2\phi)/2 + \\ + \sin \left[2 \, (\phi - \phi_0)\right]/2 \cos \psi$$

$$(106) \quad A2 = \sin \psi \, (\alpha \cos \phi + \beta \sin \phi - \delta/2 \sin^2 \phi)$$

$$A3 = \sin \psi \cos \psi$$

e. The two differential equations are written following the practice used in digital differential analyzers, e.g. the highest derivatives DPSI ($d\psi/d\tau$) and DPHI ($d\phi/d\tau$) are isolated on the left-hand side of the equations:

$$(107) \quad \frac{d\psi}{d\tau} = C1.A1 - C2.A2 - C2.\varepsilon.A3$$

$$\frac{d\phi}{d\tau} = -(C2.A1 + C1.A2 + C1.\varepsilon.A3)/\cos\psi$$

The derivatives $d\psi/d\tau$ and $d\phi/d\tau$ are evaluated for the initial (or current) value of τ and for a time interval equal to DELTAT, the largest specified, in a first iteration pass.

The value of the variable of interest: the emf induced in the longitudinal pickup loop is computed, using the values of $\sin \phi$ and $d\phi/d\tau$ in storage at this point of the computation.

f. Having obtained the first derivatives, the program calls the integration subroutine (CALL FINTEG), which uses Milne's formulas[59] to obtain ψ from $d\psi/d\tau$ and ϕ from $d\phi/d\tau$. The calling sequence of this

subroutine includes the derivatives of a variable and the variable itself. A special set of starting formulas is used to start the process. For each dependent variable Ψ, ϕ, $\frac{d\phi}{d\tau}$, $\frac{d\Psi}{d\tau}$ two tables are set up containing the information to be operated upon by the integration formulas for prediction and correction. Each table contains seven words and the variables are updated by means of a transfer and a shift between the two tables. The oldest value of the variable at the bottom of a table is dropped and the most recent is entered at the top of the other table. After computing a corrected value, while the predicted value is still in a table, subroutine UPDAT is called for.

g. The updating subroutine works closely with the integration subroutine and acts as the controller of the whole integration process. The calling sequence of this subroutine includes: VAR, which refers to the four dependent variables for which storage space has been allotted by a VAR (12) dimension statement (main program and FNIDE common storage accessibility has been established by means of an equivalence statement); the figure "4", to indicate the index register containing the return address; the symbol L1, which may be set to different values, depending upon the decision made by UPDAT after examining the tables, for further contin-

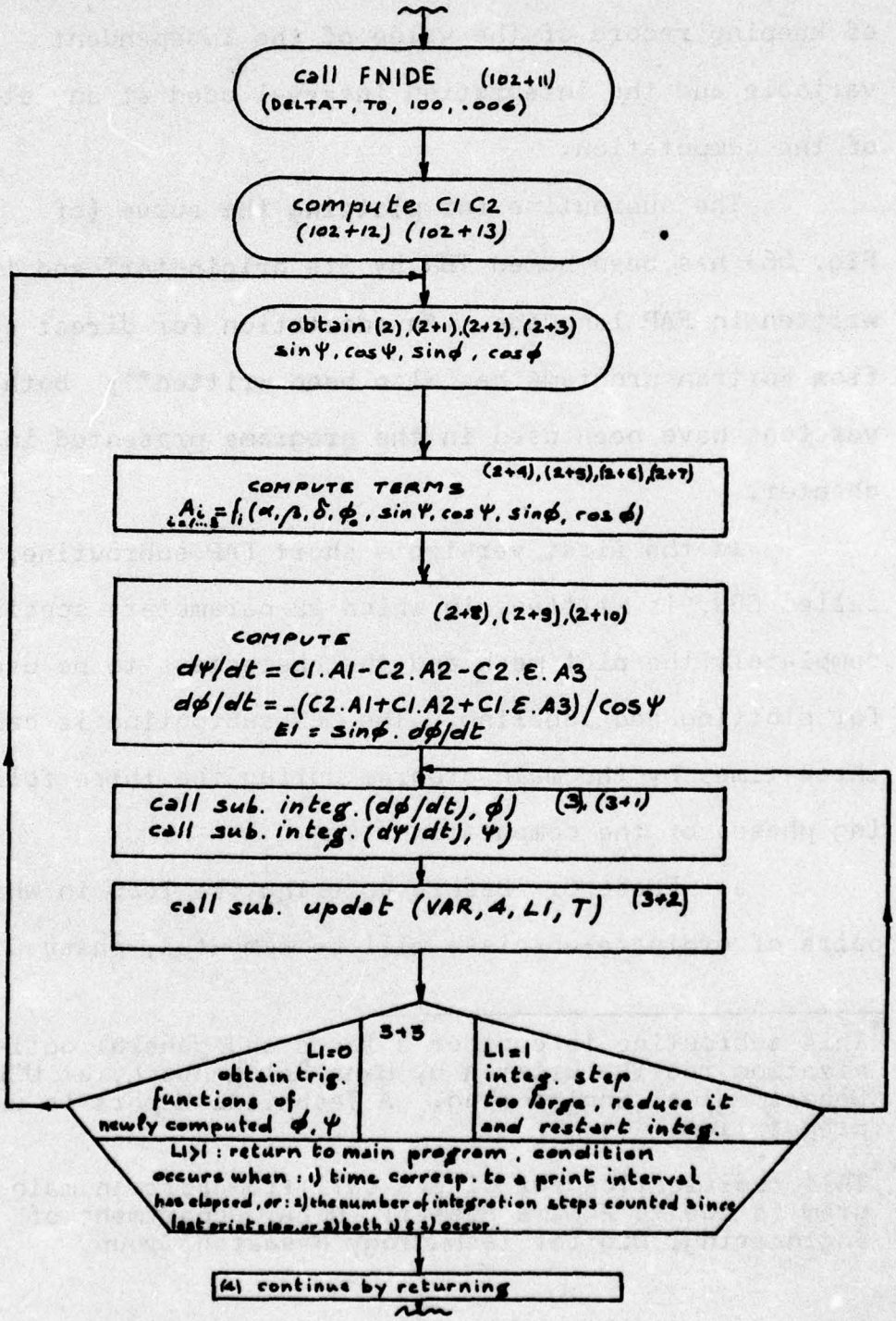
uation of the computation; and the time symbol T.

The updating subroutine examines the results of the computation performed by the integration subroutine and may direct the computation along three different paths depending upon the relative magnitude of the predicted and corrected values of the dependent variables ϕ and ψ. If the difference is too small (less than 1/100 of the specified tolerance) the integration interval is doubled to increase the speed of the computation. The integration interval will not be allowed to exceed the specified printing interval, which was entered in storage from a data card and which constitutes therefore the largest allowable integration step.

It was noticed, for example, in the solution for the switching response of the film with characteristics specified in Ref. 6 (M = 860, K = 1290 ergs/cm^3) that, if the numerical results from the computation were printed, the printed column giving the time steps showed numbers increasing in steps of 0.02 seconds from τ = 0 sec to τ = 10 sec, with a specified printing step of 0.02 sec.

If the agreement between predicted and corrected values of variables is not within tolerance, the updating routine reduces the integration step and transfers control to the INTEG subroutine to restart the

FIG. 65 FLOW CHART FOR OPERATION OF FNIDE INTEGRATING SUBROUTINE



integration process.

The updating subroutine has also the function of keeping record of the value of the independent variable and the integration interval used at any step of the computation.

The subroutine for plotting the curve (cf. Fig. 66) has been named TBN by its originator* and is written in FAP language. An adaptation for direct call from Fortran programs has also been written**; both versions have been used in the programs presented in this chapter.

In the first version a short FAP subroutine, called GBN, is written, in which 22 parameters specifying completely the plot mesh and the characters to be used for plotting and labeling. The GBN subroutine is called three times by the main program during the three following phases of the computation:

a. Phase 0: Before entering the loop in which pairs of ordinate-abscissa will be computed, phase 0

---

*This subroutine is part of a large and general optimization routine written by Hans Reichenbach, at UCLA, Department of Engineering. A Technical Report is under preparation.

**This modification for direct call from Fortran main program is due to Edward Russell, UCLA, Department of Engineering, Digital Technology Research Group.

is set by specifying IA = 0, GBN is then called and transfers control to TBN, transmitting all plot mesh parameters, thus causing TBN to set aside 3000 words of storage representing the completely labeled mesh.

b. Phase 1: The computational loop is entered and the first pair of abscissa-ordinate is obtained. Subroutine GBN is called again, after specifying IA = 1. The call statement contains the independent variable (T) and the dependent variable (EI): GBN will cause TBN to store the pair of values in the 3000 word array.

c. Phase 2: As the independent variable T (time) reaches its maximum value all the points of the curve have been obtained and control is transferred outside the computational loop. The third phase is specified by setting IA = 2 and subroutine GBN is called again. Control is transferred from GBN to TBN to TBP. This last subroutine is the output subroutine of TBN and has been written in Fortran for convenience in output handling. Subroutine TBN causes transfer of the 3000 word array from core to tape, thus making the curve available for printing.

In the TBN version written for direct TBN call from the main program the FAP GBN subroutine has been eliminated, as well as the setting of the index IA for specifying the 3 phases of the plotting operation. Sub-

routine GBN has been replaced by subroutines PREPAR, POINT, and PLOT, which need not be modified each time the mesh parameters are changed. These parameters are now included in the calling sequences of subroutine PREPAR.

a. Before the computational loop is entered, subroutine PREPAR is called for and the mesh is completely specified from estimates of variable ranges, printing steps, characters used, point overlapping rules. Subroutine PREPAR calls TBN, which sets aside 3000 words of storage.

b. During the computational loop, as each pair of ordinate-abscissa is obtained, subroutine POINT is called. This subroutine includes T (time) and EI in its calling sequence for the problem under consideration.

c. After the independent variable reads its final value subroutine PLOT is called, control is transferred to TBN and to TBP for plot transfer to tape.

If more than one curve is desired on the same plot, for more than one value of a parameter, the characters to be used for plotting each curve are supplied together with the input data and specified by a subscripted variable (SYMBOL (I)), included in the calling sequence of subroutine POINT.

f. Effects of parameters α , β , δ , ϕ_o, λ on the film switching response.

The four types of computer plots corresponding to the programs mentioned in the introduction at the beginning of this section are now examined and the dynamic response of the films investigated is discussed.

(1) Film switching response: e $\equiv$ E1 volts vs. time T (nanoseconds)

Non destructive or disturbed pulsing.

The dynamic response of the positive magnetostriction nickel-iron film is shown by the computer plot in Figs. 66, 67, 68. With no stress applied and with a perpendicular field of 7 oe (β = 0.198), the switching longitudinal field H_s is increased. The amplitude of the disturbed signal induced in the pickup loop increases as H_s is increased from H_s = 0.35 oe to 14 oe. For a value of H_s between 14 oe and 17.5 oe the magnetization switches irreversibly and the magnitude of the pickup signal increases by a factor of 10, as may be seen by comparing Fig. 67 with Fig. 69, in which the ordinate scale has been increased 10 times. Figs. 67 and 68 show the pickup signals for the disturbed and switched conditions, in the same scale. The following table summarizes these results:

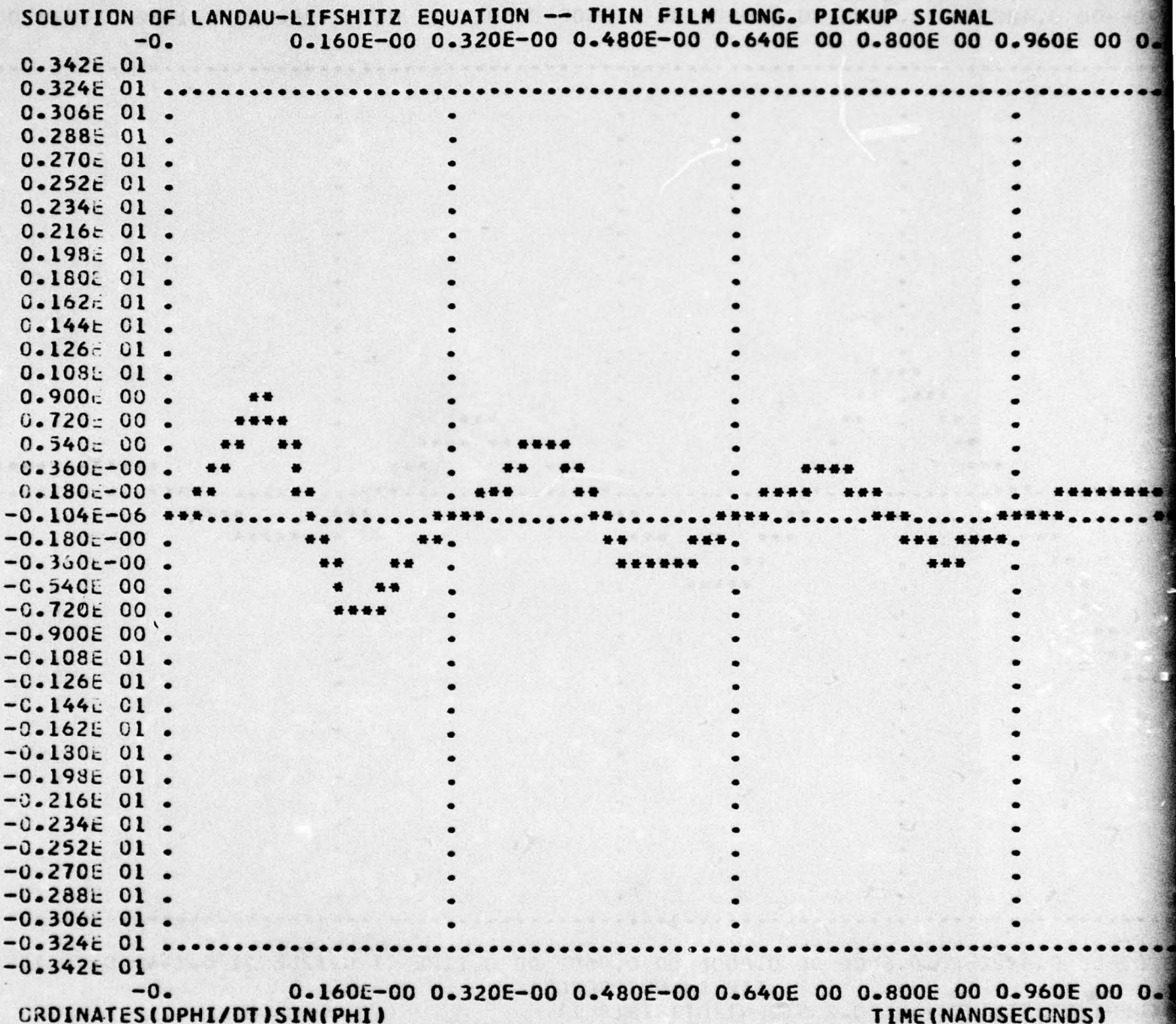
TABLE III

H_s(oe)	H_p(oe)	δ	ϕ_o	Peaking time n. sec.	Pickup volts	Condition:
0.35	7	0	0	0.104	0.19	disturbed
14	7	0	0	0.142	0.41	disturbed
17.5	7	0	0	0.33	4	switched

As may be noticed by comparing the effects of the ferromagnetic oscillation on the pickup signal, the frequency in the switched condition is much less than in the case of a disturbed condition and among the disturbed conditions the one closest to switching corresponds to the lowest frequency. This effect has been studied by means of a special program, which is the object of a forthcoming presentation. The effects of stress, perpendicular field and initial angle upon the value of H_s at which switching occurs will also be reported later.

Destructive pulsing:

From the study of 300 different conditions with different values of parameters, the cases shown in Table IV were chosen. These cases were the most significant in representing the effects of variations of parameters on the dynamic response of the film.



PICKUP VOLTS = (4)(3.1416)(S)(M)(DPHI/DT)SIN(PHI) = 0.235(DPHI/DT)SIN(PHI)

M(GAUSSES) = 1450. K(ERGS/CCM) = 25500. (FILM CROSS SECTION,SCM) = 0.129E-

LAMBDAS(MAGNETOSTRICTION) = 0.20E-04 LAMBDA(DAMPING,CPS) = 0.10E 09

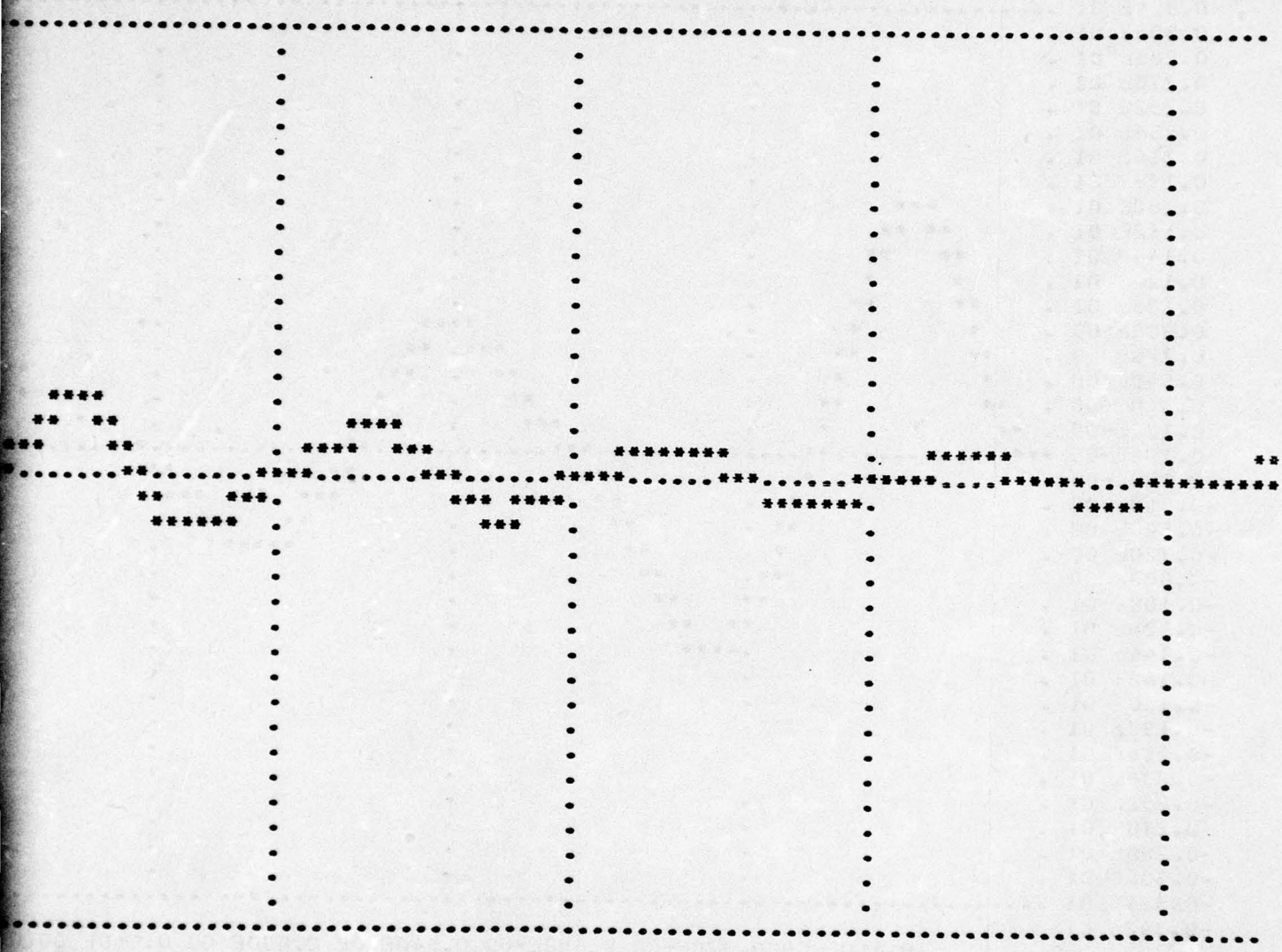
ALPHA = -0.010 BETA = 0.198 DELTA = 0.

HSWCH = (ALPHA)35.17 HPERP = (BETA)35.17 SIGMA = (DELTA)0.85E 09

HANIS = 2K/M = 35.17 PHIOD(INITIAL PHI,DEGREES) = 0.

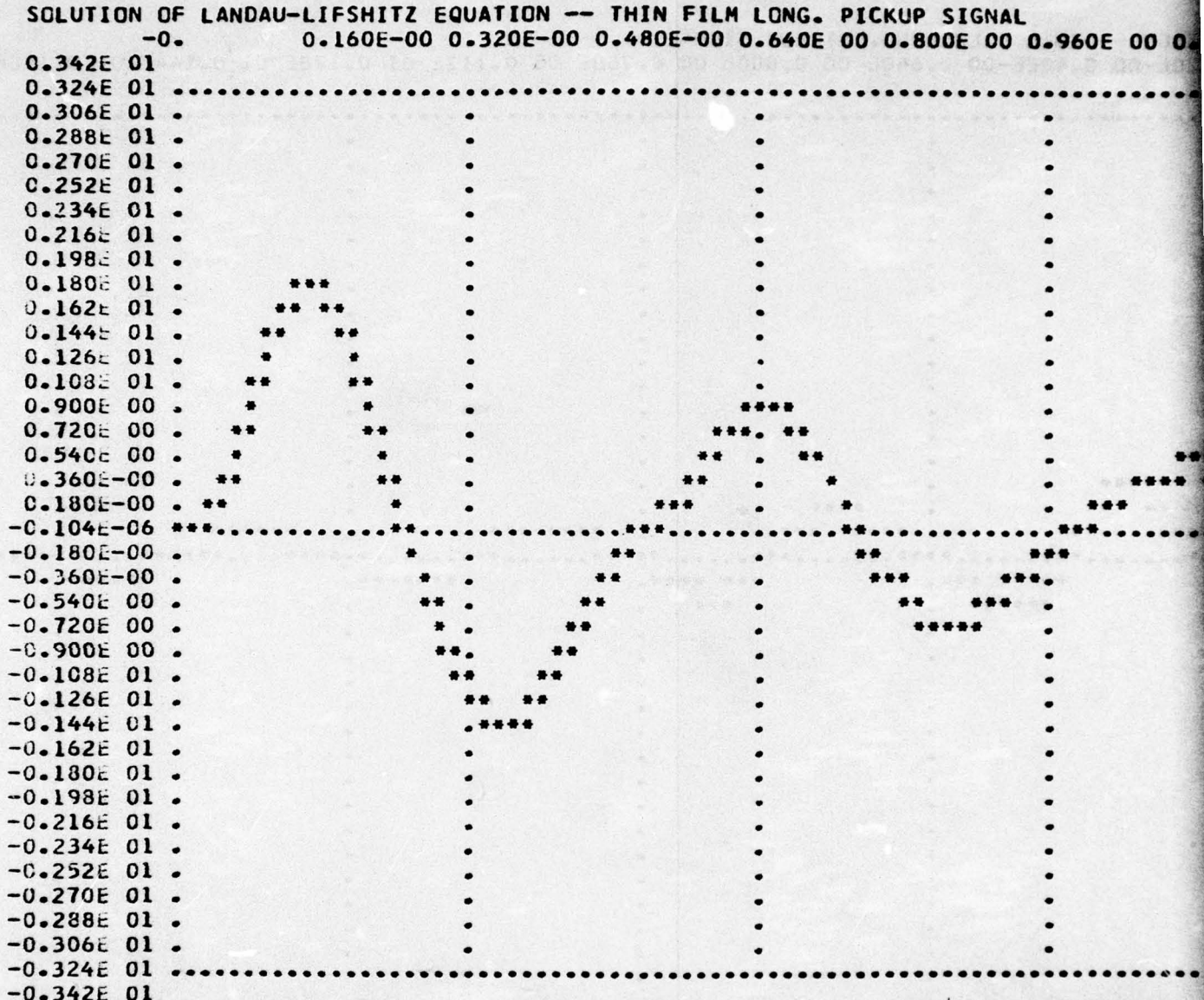
TP(PEAKING TIME,NANOSECONDS) = 0.104 GAMMA(GYRO RATIO) = 0.176E 08 MAX PICKUP

ATION -- THIN FILM LONG. PICKUP SIGNAL
120E-00 0.480E-00 0.640E 00 0.800E 00 0.960E 00 0.112E 01 0.128E 01 0.144E 01 0.160E 01

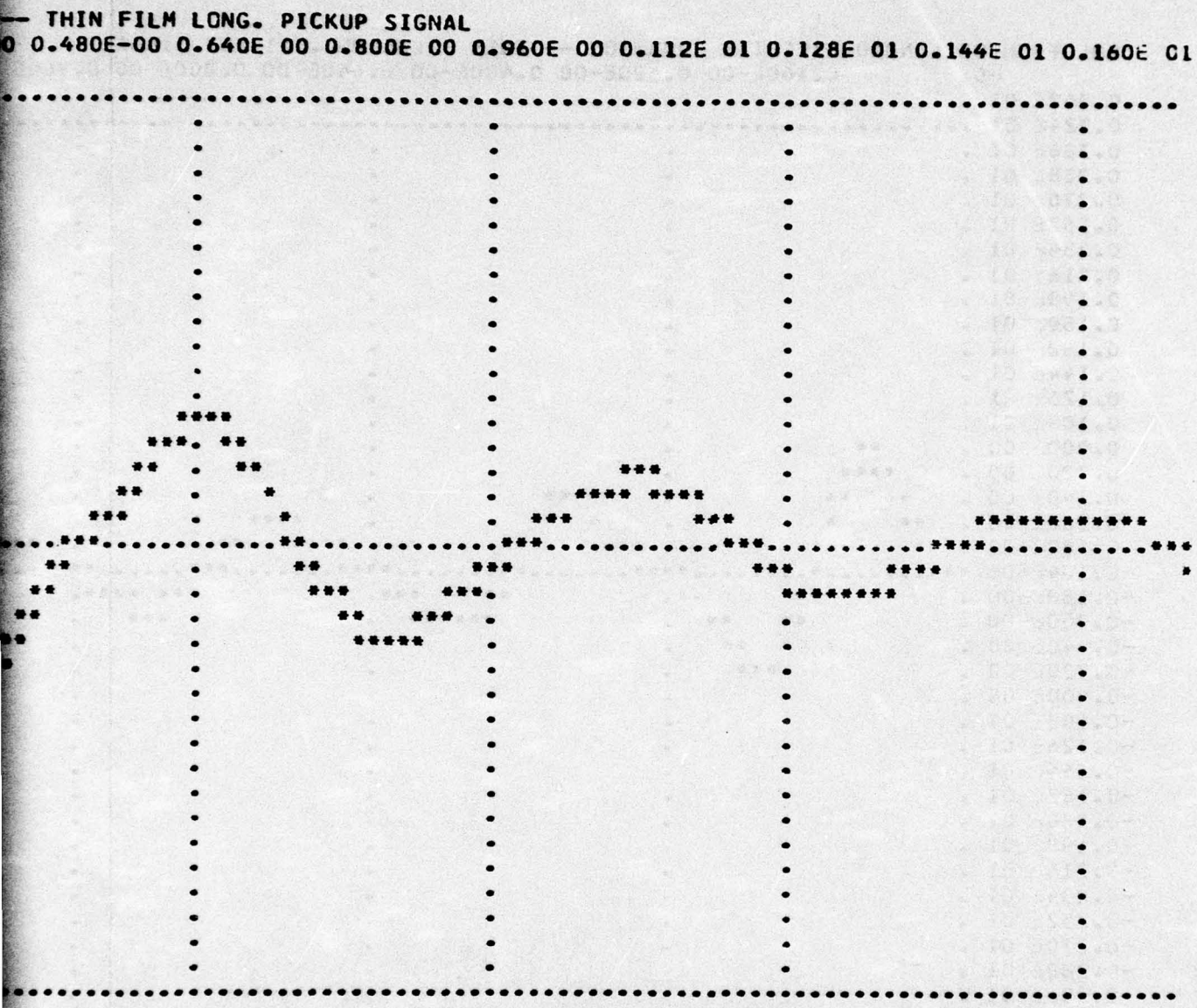


20E-00 0.480E-00 0.640E 00 0.800E 00 0.960E 00 0.112E 01 0.128E 01 0.144E 01 0.160E 01
TIME(NANOSECONDS)
(DPHI/DT)SIN(PHI) = 0.235(DPHI/DT)SIN(PHI)
= 25500. (FILM CROSS SECTION,SCM) = 0.129E-04
-04 LAMBDA(DAMPING,CPS) = 0.10E 09
198 DELTA = 0.
ETA)35.17 SIGMA = (DELTA)0.85E 09
TIAL PHI,DEGREES) = 0.
104 GAMMA(GYRO RATIO) = 0.176E 08 MAX PICKUP SIG. = 0.837E 00

Fig. 66



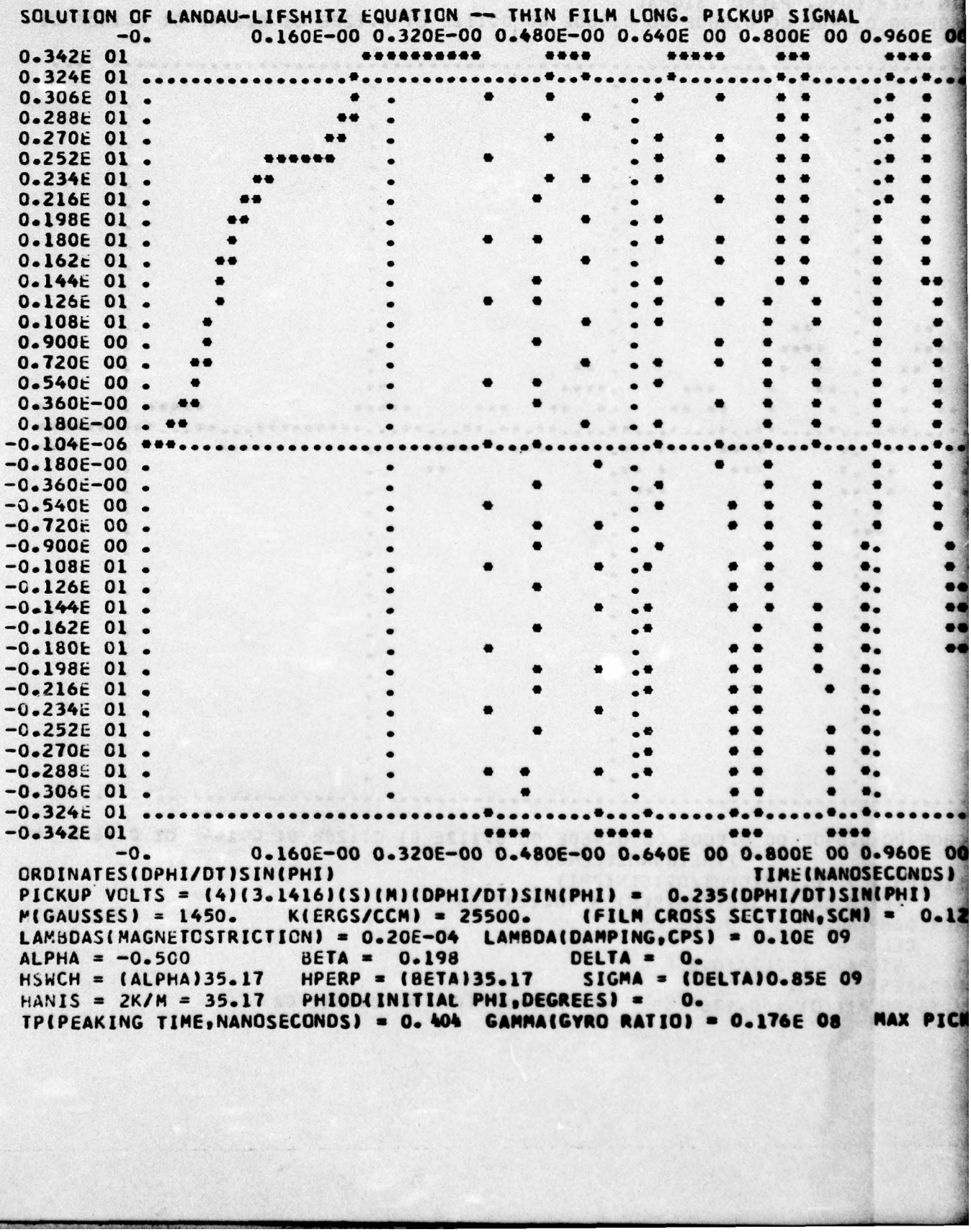
PICKUP VOLTS = (4)(3.1416)(S)(M)(DPHI/DT)SIN(PHI) = 0.235(DPHI/DT)SIN(PHI)
M(GAUSSES) = 1450. K(ERGS/CCM) = 25500. (FILM CROSS SECTION,SCM) = 0.129E-
LAMBDAS(MAGNETOSTRICTION) = 0.20E-04 LAMBDA(DAMPING,CPS) = 0.10E 09
ALPHA = -0.400 BETA = 0.198 DELTA = 0.
HSWCH = (ALPHA)35.17 HPERP = (BETA)35.17 SIGMA = (DELTA)0.85E 09
HANIS = 2K/M = 35.17 PHIOD(INITIAL PHI,DEGREES) = 0.
TP(PEAKING TIME,NANOSECONDS) = 0.142 GAMMA(GYRO RATIO) = 0.176E 08 MAX PICKUP



DT)SIN(PHI) = 0.235(DPHI/DT)SIN(PHI)
500. (FILM CROSS SECTION,SCM) = 0.129E-04
LAMBDA(DAMPING,CPS) = 0.10E 09

Fig. 67

DELTA = 0.
5.17 SIGMA = (DELTA)0.85E 09
HI,DEGREES) = 0.
GAMMA(GYRO RATIO) = 0.176E 08 MAX PICKUP SIG. = 0.176E 01



PICKUP VOLTS = (4)(3.1416)(S)(M)(DPHI/DT)SIN(PHI) = 0.235(DPHI/DT)SIN(PHI)

M(GAUSSES) = 1450. K(ERGS/CCM) = 25500. (FILM CROSS SECTION,SCM) = 0.12

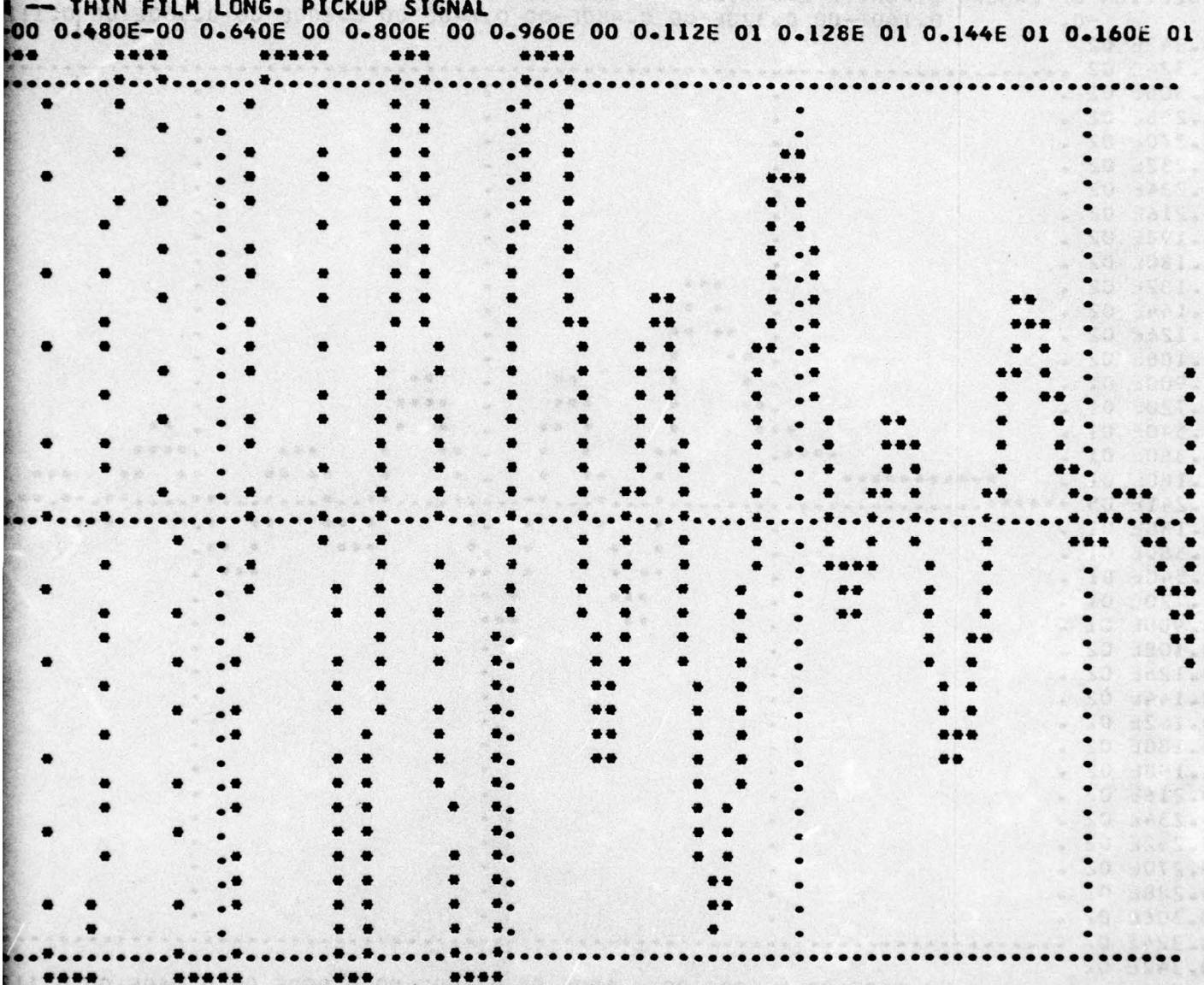
LAMBDAS(MAGNETOSTRICTION) = 0.20E-04 LAMBDA(DAMPING,CPS) = 0.10E 09

ALPHA = -0.500 BETA = 0.198 DELTA = 0.

HSWCH = (ALPHA)35.17 HPERP = (BETA)35.17 SIGMA = (DELTA)0.85E 09

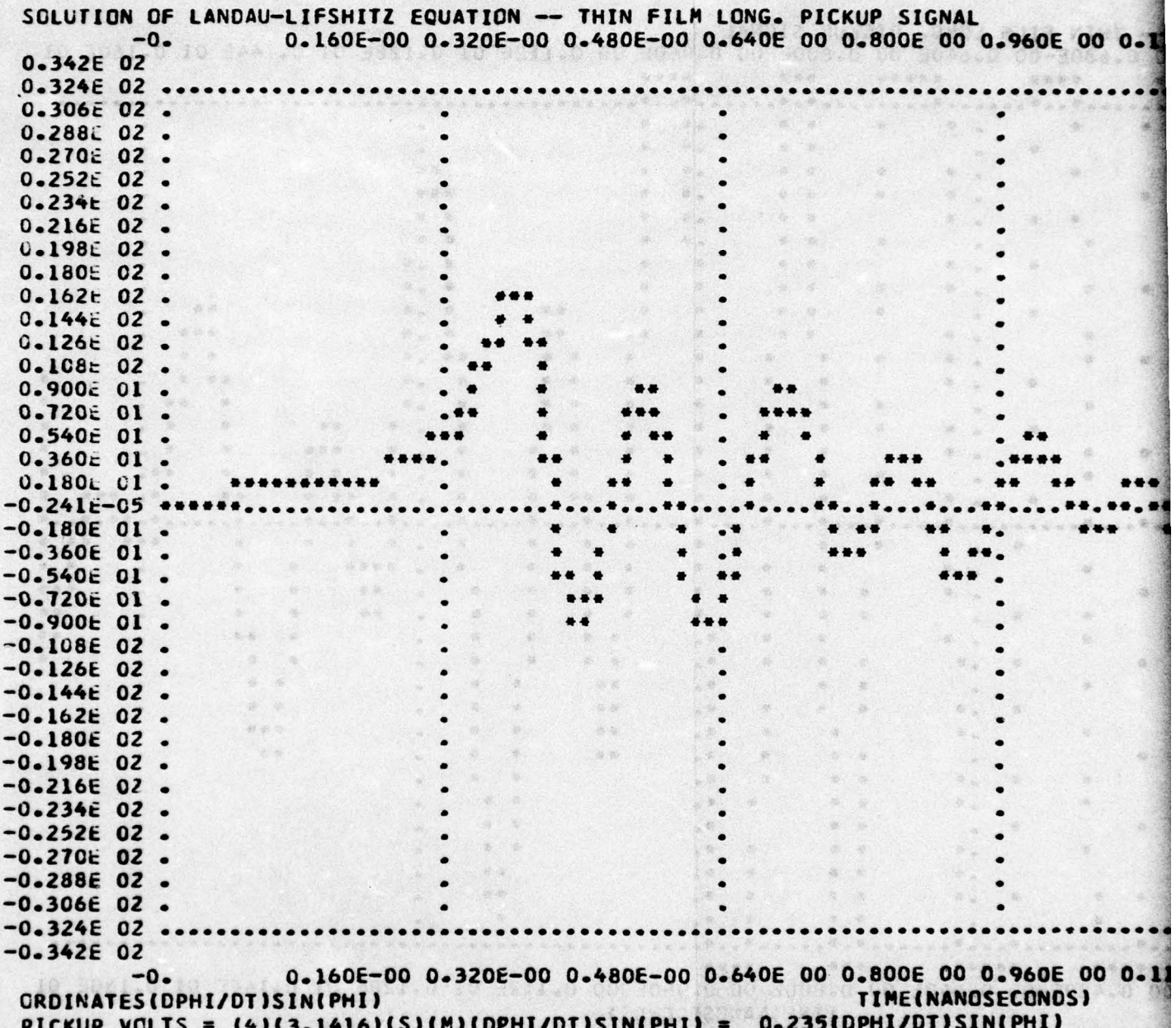
HANIS = 2K/M = 35.17 PHIOD(INITIAL PHI,DEGREES) = 0.

TP(PEAKING TIME,NANOSECONDS) = 0.404 GAMMA(GYRO RATIO) = 0.176E 08 MAX PICK



HI/DT)SIN(PHI) = 0.235(DPHI/DT)SIN(PHI)
25500. (FILM CROSS SECTION,SCM) = 0.129E-04
LAMBDA(DAMPING,CPS) = 0.10E 09
DELTA = 0.
)35.17 SIGMA = (DELTA)0.85E 09
PHI,DEGREES) = 0.
GAMMA(GYRO RATIO) = 0.176E 08 MAX PICKUP SIG. = 0.249E 01

Fig. 68



PICKUP VOLTS = (4)(3.1416)(S)(M)(DPHI/DT)SIN(PHI) = 0.235(DPHI/DT)SIN(PHI)

M(GAUSSES) = 1450. K(ERGS/CCM) = 25500. (FILM CROSS SECTION,SCM) = 0.129E-0

LAMBDAS(MAGNETOSTRICTION) = 0.20E-04 LAMBDA(DAMPING,CPS) = 0.10E 09

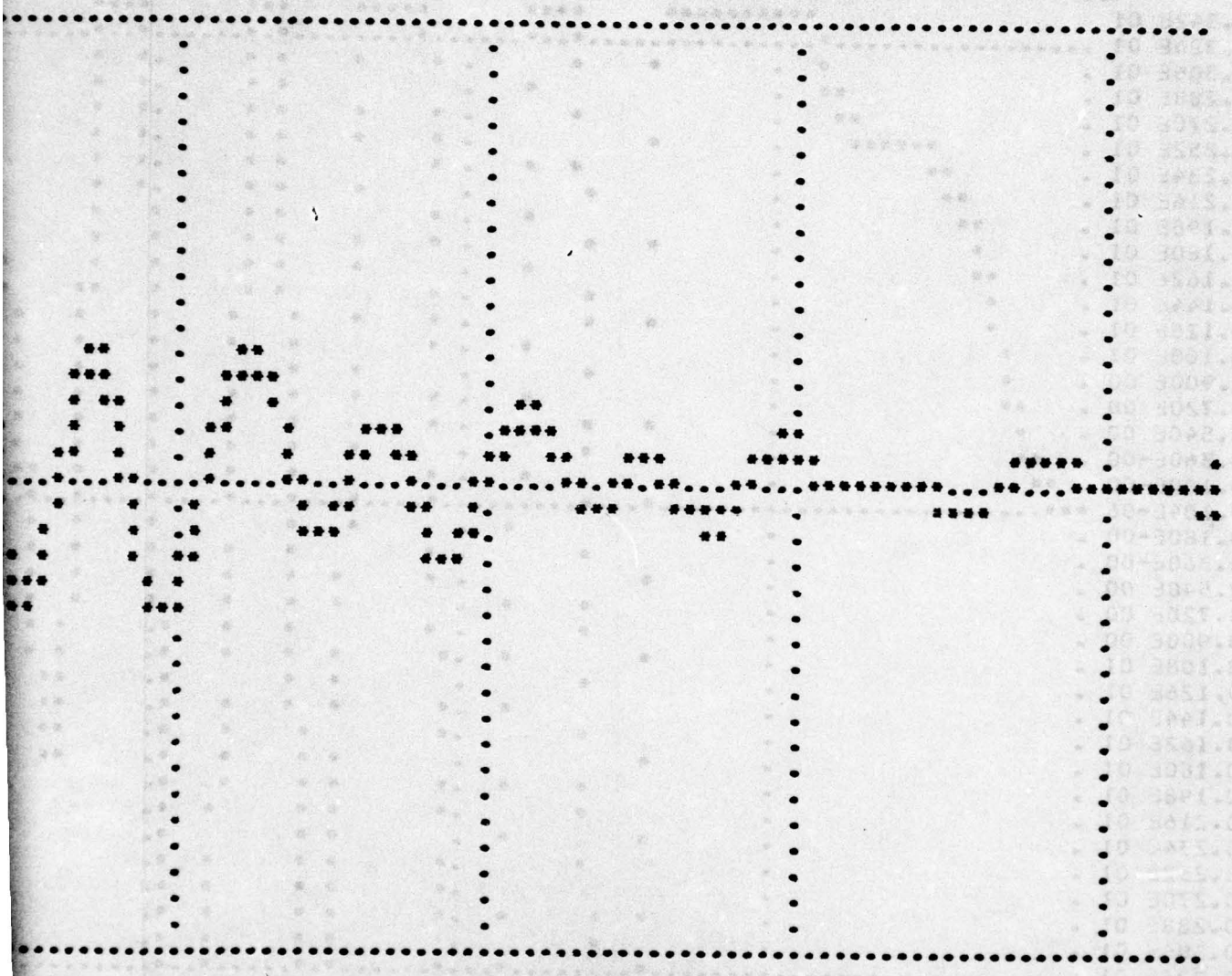
ALPHA = -0.500 BETA = 0.198 DELTA = 0.

HSWCH = (ALPHA)35.17 HPERP = (BETA)35.17 SIGMA = (DELTA)0.85E 09

HANIS = 2K/M = 35.17 PHIOD(INITIAL PHI,DEGREES) = 0.

TP(PEAKING TIME,NANOSECONDS) = 0.404 GAMMA(GYRO RATIO) = 0.176E 08 MAX PICKUP S

- THIN FILM LONG. PICKUP SIGNAL
0.480E-00 0.640E 00 0.800E 00 0.960E 00 0.112E 01 0.128E 01 0.144E 01 0.160E 01



.480E-00 0.640E 00 0.800E 00 0.960E 00 0.112E 01 0.128E 01 0.144E 01 0.160E 01
TIME(NANOSECONDS)
)SIN(PHI) = 0.235(DPHI/DT)SIN(PHI)
0. (FILM CROSS SECTION,SCM) = 0.129E-04
MBDA(DAMPING,CPS) = 0.10E 09
DELTA = 0.
17 SIGMA = (DELTA)0.85E 09
,DEGREES) = 0.
MMA(GYRO RATIO) = 0.176E 08 MAX PICKUP SIG. = 0.164E 02

Fig. 69

The following parameters were varied:

- magnitude of normalized switching field
- magnitude of normalized perpendicular field
- magnitude and sign of normalized stress
- initial angle ϕ_o
- damping constant

Measurement of λ is usually performed by a ferromagnetic resonance experiment.[6] The damping constant was not measured in the course of this study and information giving λ as a function of composition for nickel-iron films is not available in the literature. A value of $\lambda = 10^8$ cps corresponding to an 80-20 nickel-iron film reported in Ref. 6 has been chosen. Because of the arbitrariness of this choice the effect of changing λ has been considered and switching responses with λ as a parameter, varying between 10^8 cps and 10^9 cps, have been obtained.

Figures 70 to 75 inclusive show the effect of applying an increasing stress from negative to positive values, for a case in which the perpendicular field is kept at a low value ($\beta = 0.08$) to provide sufficient initial torque to cause the film to switch. As the stress is increased from -0.79×10^9 dynes/cm^2, $\delta = -0.930$ (a compression along H_p), to $+0.112 \times 10^9$ dynes/cm^2, $\delta = 0.132$ (a tension along H_p), the

peaking time increases from 0.213 nanosec. to 0.361 nanosec. and the magnetization reverses. Beyond a value of stress between 0.112×10^9 and 0.45×10^9 ($\delta = 0.532$), the film magnetization does not reverse and the pickup corresponding to the non-destructive condition is equal to 0.077 volts or 1/75 of the signal induced when the magnetization is reversed. In addition, peaking occurs now after 0.144 nanosec. From the general shape of the curves the ferromagnetic oscillation frequency does not change appreciably.

Figures 76 to 82 inclusive show, in the absence of an applied stress, the effect of the magnitude of the switching field in changing the speed of reversal, for a given value of H_p, (β), and the amplitude of this change as H_p is varied. For $H_p = 21$ oe ($\beta = 0.590$), the peaking time decreases from 0.145 nsec. to 0.127 nsec. as H_s increases from 24.5 oe to 42.5 oe (corresponding to an increase in α from 0.7 to 1.2, (cf. Figs 77, 78, 79 and Table IV). If, however, a low value of H_p is chosen, e.g. $H_p = 1.8$ oe, the peaking time decreases from 0.74 nsec. to 0.275 nsec., i.e. by a factor of almost 3 as compared to 1.14 in the case of $H_p = 21$ oe.

TABLE IV

DYNAMIC RESPONSE C

44-56 NICKEL IRON FIL

PARAMETERS : H_s, H_p, σ, ϕ_o, λ

M = 1450 GAUSSES K = 25500 ERGS/CM^3, λ_s

Denormalization factors :

H_s (oersteds) = $\alpha \cdot 35.17$

H_p (oersteds) = $\beta \cdot 35.17$

σ (dynes/cm) = $\delta \cdot 0.85 \cdot 10^8$

	varying stress δ, $H_s = 35$ oe, $H_p = 2.8$ oe, $\phi_o = 0$, $\lambda = 10^8$ cps						varying H_s, $H_p = 20.5$ oe, $\delta = 0.59$, $\phi_o = 0$, $\lambda = 10^8$ cps				varying H_s, $H_p = 2.8$ oe, $\delta = 0$			varying H_s, $H_p = 2.8$ oe, $\delta < 0$			varying H_s, $H_p = 2.8$ oe, $\delta >$		
Fig. number	70	71	72	73	74	75	76	77	78	79	80	81	82	83	84	85	86	87	8
α (norm)	-1.0	-1.0	-1.0	-1.0	-1.0	-1.0	-0.5	-0.7	-0.8	-1.2	-0.7	-0.8	-1.2	-0.7	-0.8	-1.2	-0.7	-0.8	-1.
β (norm)	0.08	0.08	0.08	0.08	0.08	0.08	0.590	0.590	0.590	0.590	0.08	0.08	0.08	0.08	0.08	0.08	0.08	0.08	0.
δ (norm)	0.930	-0.532	-0.132	0.0	+0.132	+0.532	0.0	0.0	0.0	0.0	0.0	0.0	0.0	-0.132	-0.132	-0.132	0.132	0.132	0.
ϕ_o (deg.)	0	0	0	0	0	0	0	0	0	0	0	0	0	0	0	0	0	0	0
λ cps	10^8	10^8	10^8	10^8	10^8	10^8	10^8	10^8	10^8	10^8	10^8	10^8	10^8	10^8	10^8	10^8	10^8	10^8	10
TP peak time (m.sec)	0.213	0.242	0.291	0.319	0.361	0.144	0.157	0.145	0.140	0.127	0.740	0.421	0.275	0.410	0.350	0.253	0.161	0.195	0.
pickup signal (volts)	6.8	6.3	5.9	5.8	5.7	0.077	4.8	5.7	6.1	7.5	4.8	5	6.5	4.7	5.15	6.65	0.10	0.16	6.
$\pm 180°$ reversal	YES	YES	YES	YES	YES	NO	YES	YES	YES	YES	YES	YES	YES	YES	YES	YES	NO	NO	YE

ABLE IV

PONSE CASES OF

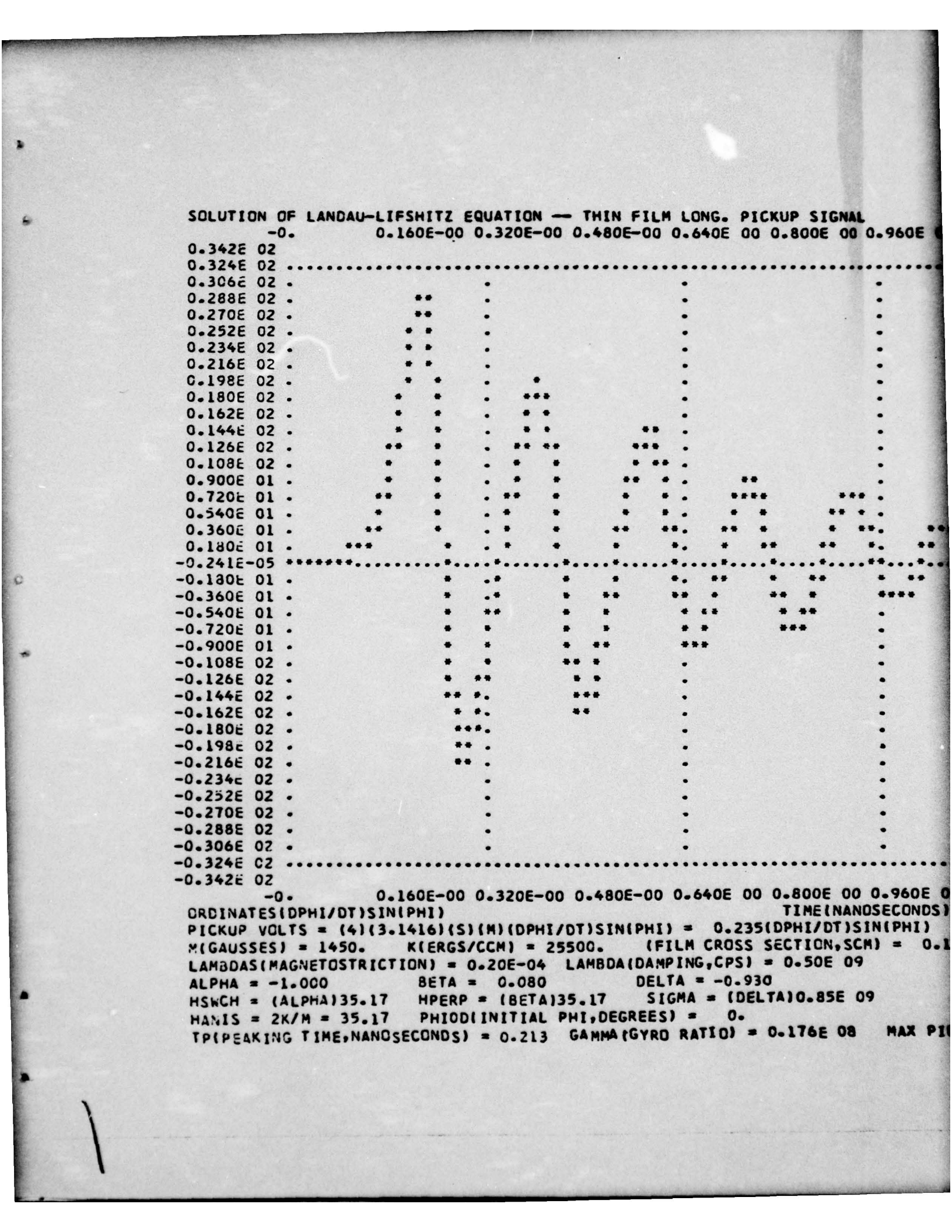
IRON FILM

$H_s, H_p, \sigma, \phi_0, \lambda$

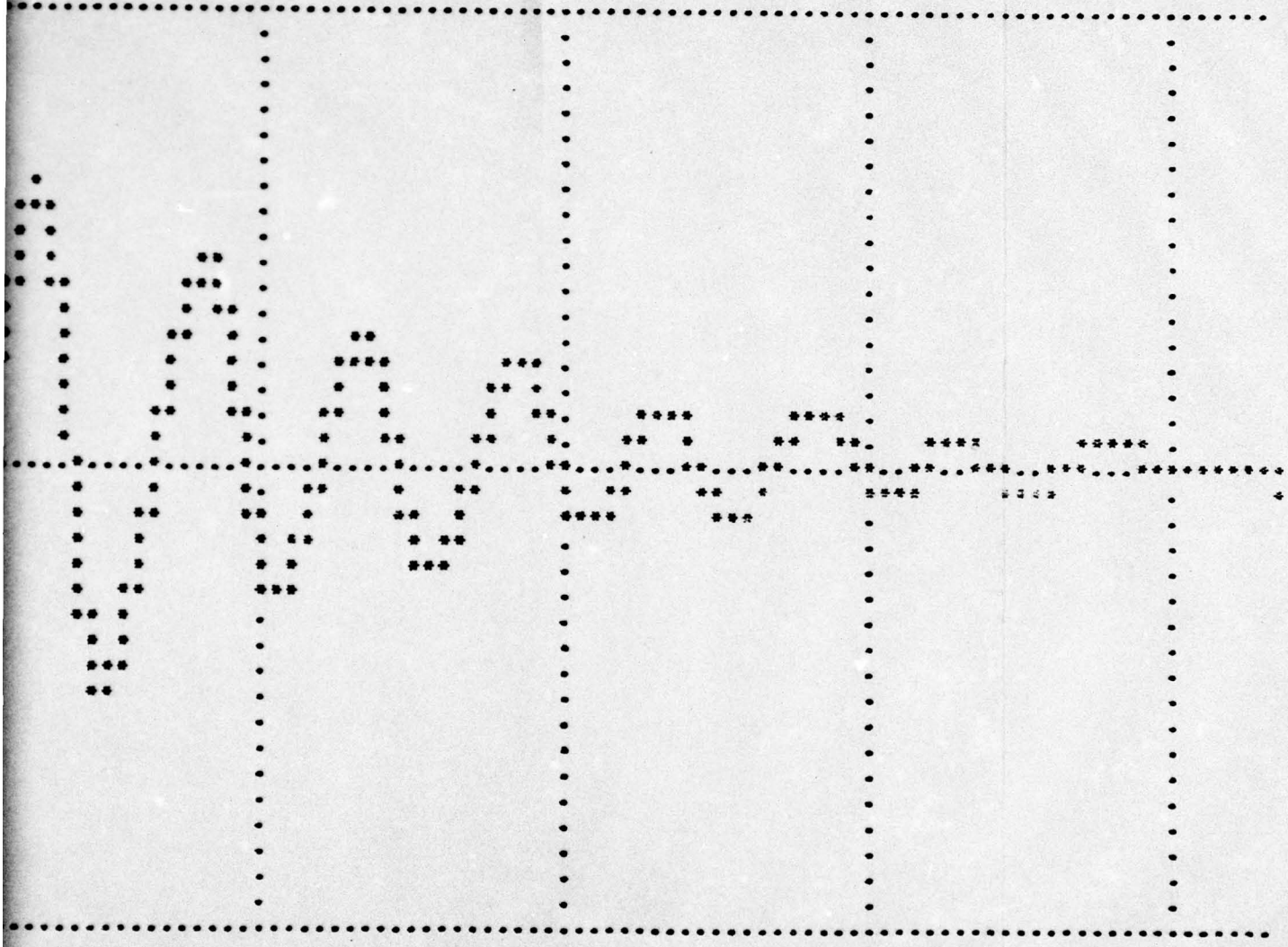
00 ERGS/CM^3, $\lambda_s = 20.10^{-6}$

g H_s e $\delta<0$		varying H_s $H_p=2.8$ oe, $\delta>0$			varying stress $H_s=35$oe, $H_p=2.8$oe			varying ϕ_0 $H_s=35$oe $H_p=0$, $\sigma=0$				varying λ, $\delta<0, \phi=0$, $H_p=2.8$, $H_s=35$oe			varying λ $\delta=0, \phi=0$ $H_p=2.8$, $H_s=35$oe			varying λ $\delta>0, \phi=0$ $H_p=2.8$, $H_s=35$oe		
84	85	86	87	88	89	90	91	92	93	94	95	96	97	98	99	100	101	102	103	104
8	-1.2	-0.7	-0.8	-1.2	-1.0	-1.0	-1.0	-1.0	-1.0	-1.0	-1.0		-1.0	-1.0		-1.0	-1.0		-1.0	-1.0
08	0.08	0.08	0.08	0.08	0.08	0.08	0.08	0.0	0.0	0.0	0.0		0.08	0.08		0.08	0.08		0.08	0.08
132	-0.132	0.132	0.132	0.132	-0.930	-0.532	-0.132	0.0	0.0	0.0	0.0		-0.132	-0.132		0.0	0.0		0.132	0.132
0	0	0	0	0	60	60	60	10	30	45	60		0	0		0	0		0	0
0^8	10^8	10^8	10^8	10^8	10^8	10^8	10^8	10^8	10^8	10^8	10^8		5.10^8	10.10^8		5.10^8	10.10^8		5.10^8	10.10^8
360	0.259	0.161	0.195	0.296	0.102	0.107	0.112	0.245	0.153	0.127	0.122		0.400	0.573		0.460	0.688		0.575	0.424
15	6.65	0.10	0.16	6.45	8.3	7.8	7.3	5.45	5.5	6.12	6.9									
ES	YES	NO	NO	YES	YES	YES	YES	YES	YES	YES	YES		YES	YES		YES	YES		YES	YES

same as Fig. 72 | same as Fig. 73 | same as Fig. 74

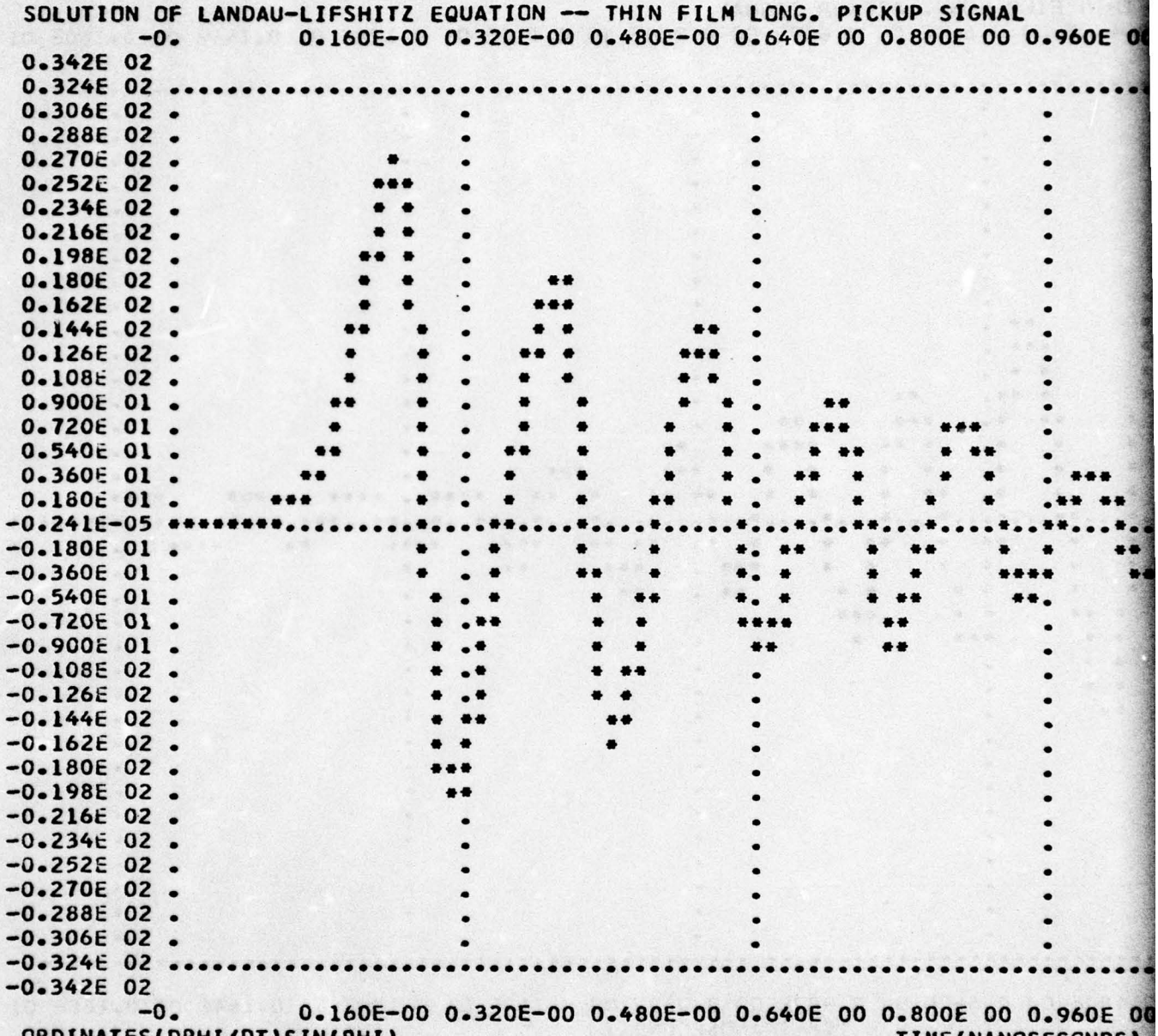

SOLUTION OF LANDAU-LIFSHITZ EQUATION — THIN FILM LONG. PICKUP SIGNAL
-0. 0.160E-00 0.320E-00 0.480E-00 0.640E 00 0.800E 00 0.960E
0.342E 02
0.324E 02
0.306E 02
0.288E 02
0.270E 02
0.252E 02
0.234E 02
0.216E 02
0.198E 02
0.180E 02
0.162E 02
0.144E 02
0.126E 02
0.108E 02
0.900E 01
0.720E 01
0.540E 01
0.360E 01
0.180E 01
-0.241E-05
-0.180E 01
-0.360E 01
-0.540E 01
-0.720E 01
-0.900E 01
-0.108E 02
-0.126E 02
-0.144E 02
-0.162E 02
-0.180E 02
-0.198E 02
-0.216E 02
-0.234E 02
-0.252E 02
-0.270E 02
-0.288E 02
-0.306E 02
-0.324E 02
-0.342E 02
-0. 0.160E-00 0.320E-00 0.480E-00 0.640E 00 0.800E 00 0.960E 0
ORDINATES(DPHI/DT)SIN(PHI)
TIME(NANOSECONDS)
PICKUP VOLTS = (4)(3.1416)(S)(M)(DPHI/DT)SIN(PHI) = 0.235(DPHI/DT)SIN(PHI)
M(GAUSSES) = 1450. K(ERGS/CCM) = 25500. (FILM CROSS SECTION,SCM) = 0.1
LAMBDAS(MAGNETOSTRICTION) = 0.20E-04 LAMBDA(DAMPING,CPS) = 0.50E 09
ALPHA = -1.000 BETA = 0.080 DELTA = -0.930
HSWCH = (ALPHA)35.17 HPERP = (BETA)35.17 SIGMA = (DELTA)0.85E 09
HANIS = 2K/M = 35.17 PHIOD(INITIAL PHI,DEGREES) = 0.
TP(PEAKING TIME,NANOSECONDS) = 0.213 GAMMA(GYRO RATIO) = 0.176E 08 MAX PI

ION — THIN FILM LONG. PICKUP SIGNAL
0E-00 0.480E-00 0.640E 00 0.800E 00 0.960E 00 0.112E 01 0.128E 01 0.144E 01 0.160E 01



0E-00 0.480E-00 0.640E 00 0.800E 00 0.960E 00 0.112E 01 0.128E 01 0.144E 01 0.160E 01
TIME(NANOSECONDS)
DPHI/DT)SIN(PHI) = 0.235(DPHI/DT)SIN(PHI)
= 25500. (FILM CROSS SECTION,SCM) = 0.129E-04
-04 LAMBDA(DAMPING,CPS) = 0.50E 09
080 DELTA = -0.930
ETA)35.17 SIGMA = (DELTA)0.85E 09
IAL PHI,DEGREES) = 0.
213 GAMMA(GYRO RATIO) = 0.176E 08 MAX PICKUP SIG. = 0.288E 02

Fig. 70



PICKUP VOLTS = (4)(3.1416)(S)(M)(DPHI/DT)SIN(PHI) = 0.235(DPHI/DT)SIN(PHI)

M(GAUSSES) = 1450. K(ERGS/CCM) = 25500. (FILM CROSS SECTION,SCM) = 0.12

LAMBDAS(MAGNETOSTRICTION) = 0.20E-04 LAMBDA(DAMPING,CPS) = 0.10E 09

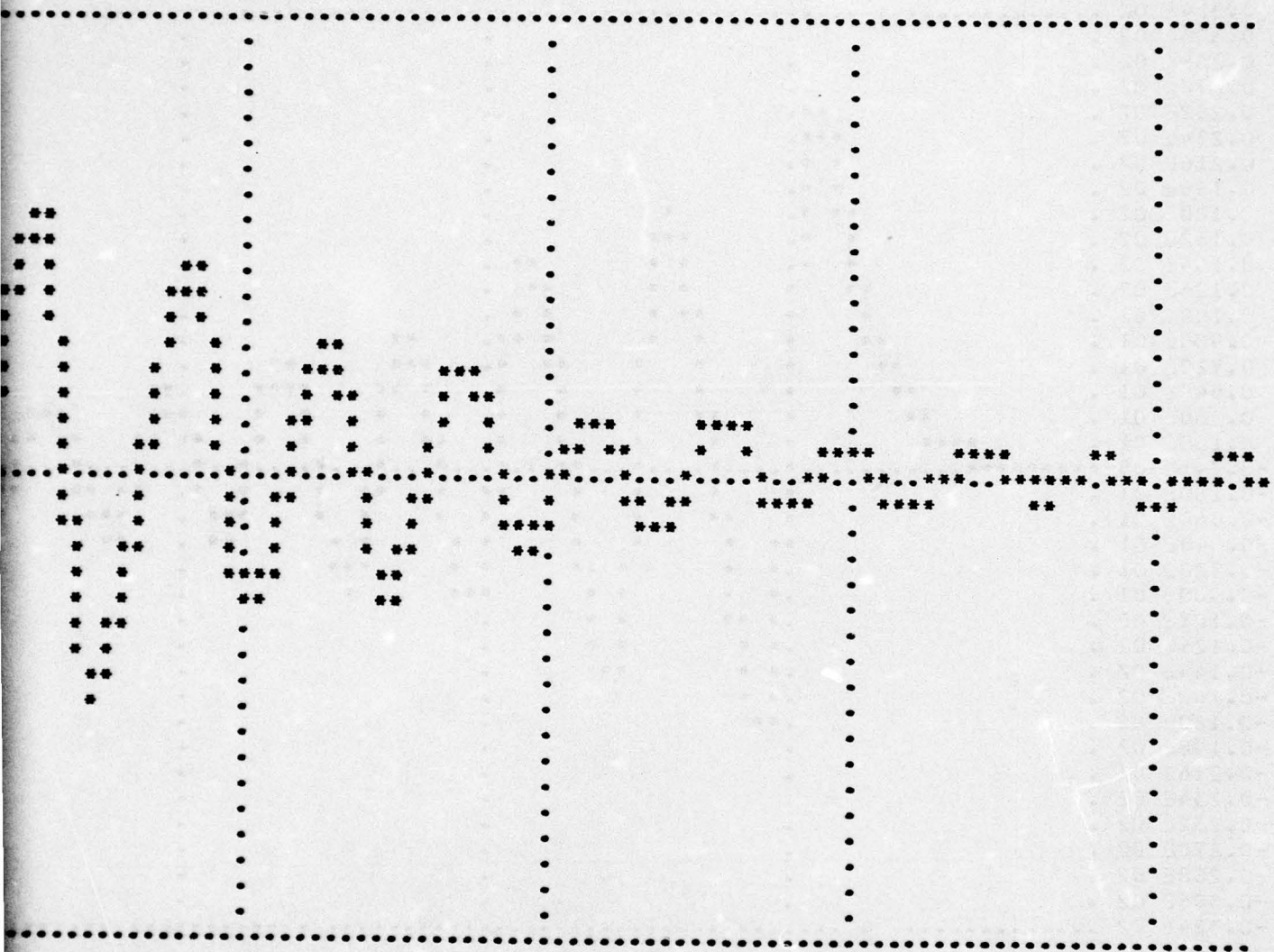
ALPHA = -1.000 BETA = 0.080 DELTA = -0.532

HSWCH = (ALPHA)35.17 HPERP = (BETA)35.17 SIGMA = (DELTA)0.85E 09

HANIS = 2K/M = 35.17 PHIOD(INITIAL PHI,DEGREES) = 0.

TP(PEAKING TIME,NANOSECONDS) = 0.242 GAMMA(GYRO RATIO) = 0.176E 08 MAX PIC

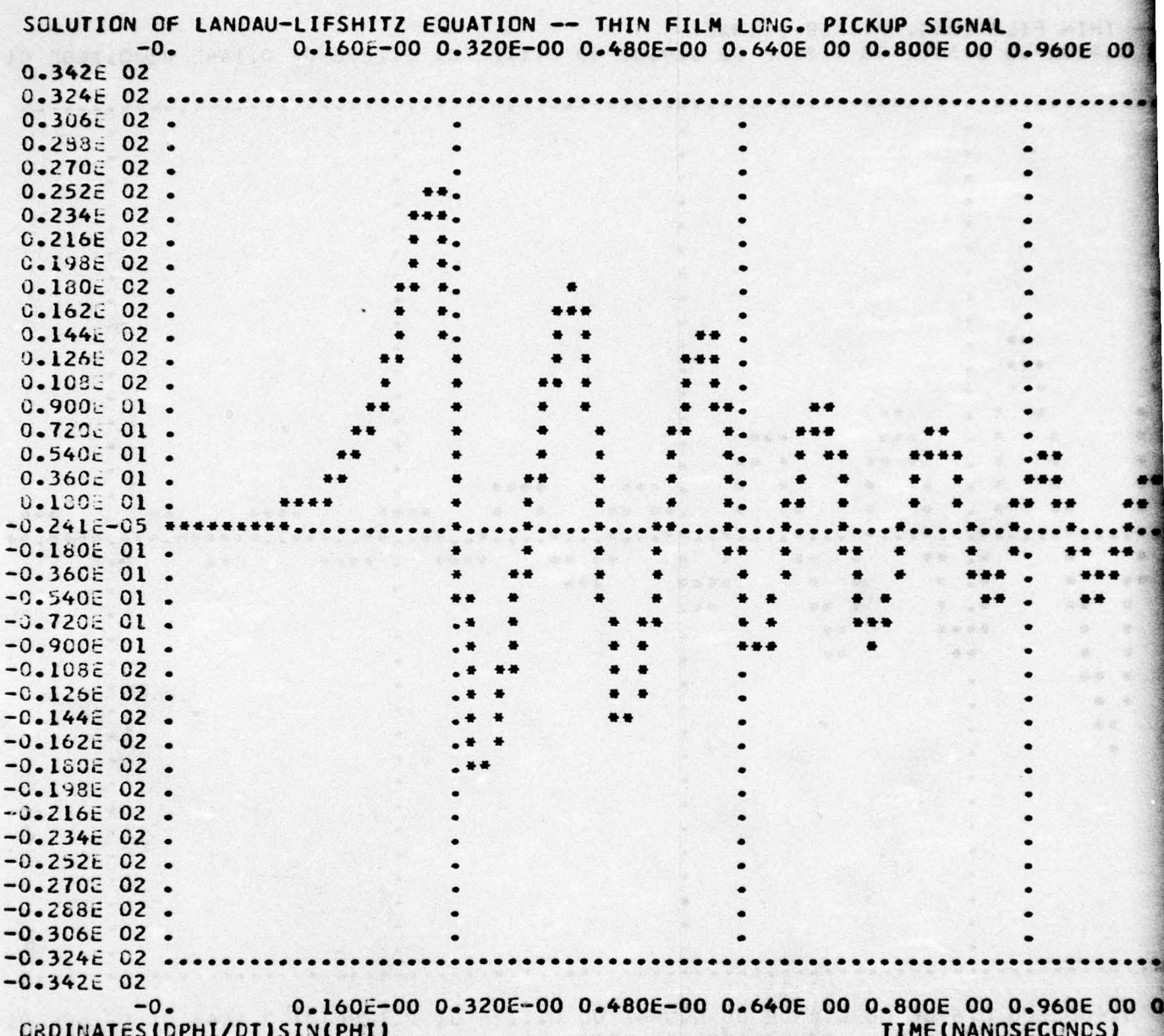
ON -- THIN FILM LONG. PICKUP SIGNAL
E-00 0.480E-00 0.640E 00 0.800E 00 0.960E 00 0.112E 01 0.128E 01 0.144E 01 0.160E 01



-00 0.480E-00 0.640E 00 0.800E 00 0.960E 00 0.112E 01 0.128E 01 0.144E 01 0.160E 01
TIME(NANOSECONDS)
HI/DT)SIN(PHI) = 0.235(DPHI/DT)SIN(PHI)
25500. (FILM CROSS SECTION,SCM) = 0.129E-04
4 LAMBDA(DAMPING,CPS) = 0.10E 09
0 DELTA = -0.532
A)35.17 SIGMA = (DELTA)0.85E 09
L PHI,DEGREES) = 0.
2 GAMMA(GYRO RATIO) = 0.176E 08 MAX PICKUP SIG. = 0.269E 02

Fig. 71

2



PICKUP VOLTS = (4)(3.1416)(S)(M)(DPHI/DT)SIN(PHI) = 0.235(DPHI/DT)SIN(PHI)

M(GAUSSES) = 1450. K(ERGS/CCM) = 25500. (FILM CROSS SECTION,SCM) = 0.129E

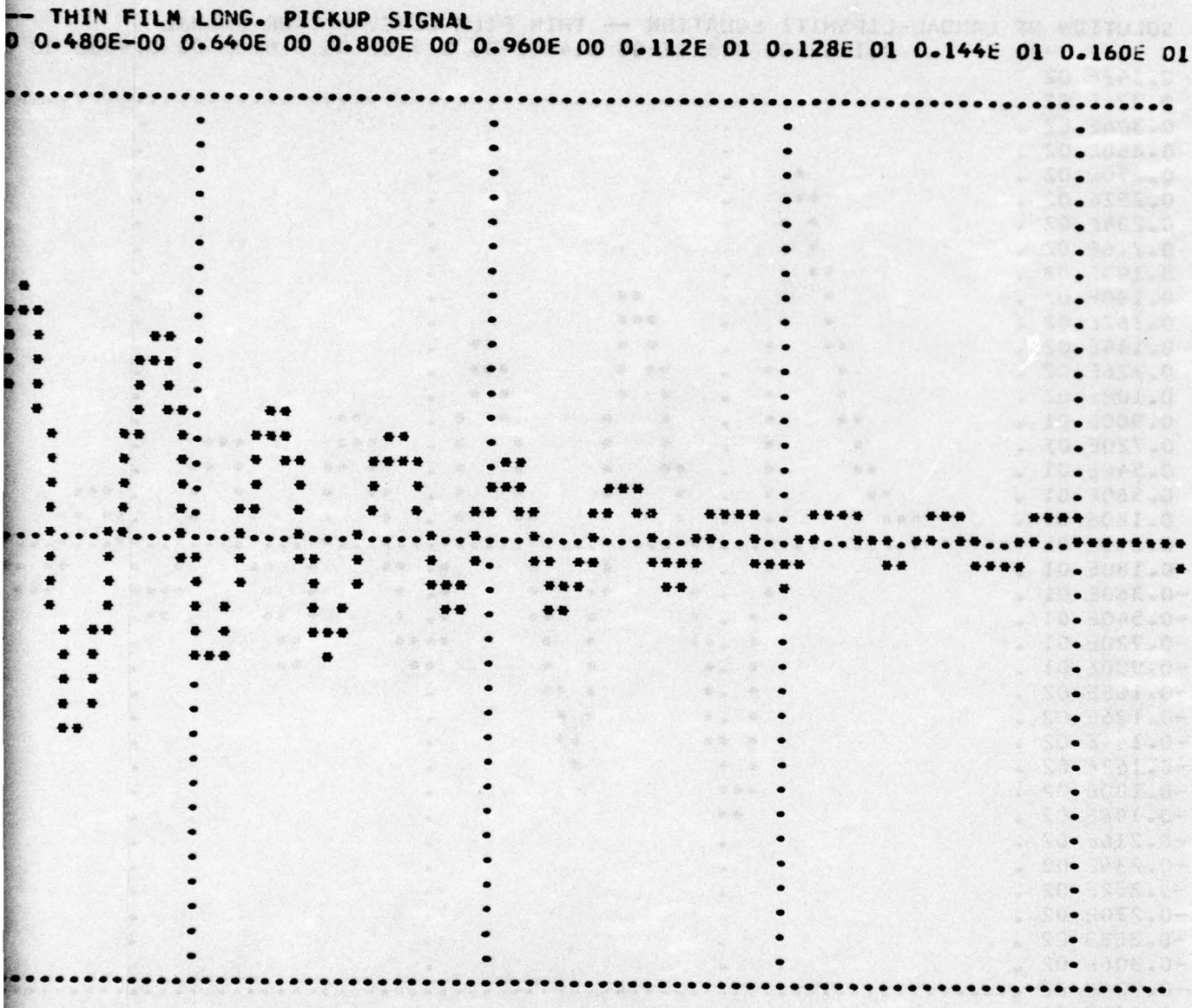
LAMBDAS(MAGNETOSTRICTION) = 0.20E-04 LAMBDA(DAMPING,CPS) = 0.10E 09

ALPHA = -1.000 BETA = 0.080 DELTA = -0.132

HSWCH = (ALPHA)35.17 HPERP = (BETA)35.17 SIGMA = (DELTA)0.85E 09

HANIS = 2K/M = 35.17 PHIOD(INITIAL PHI,DEGREES) = 0.

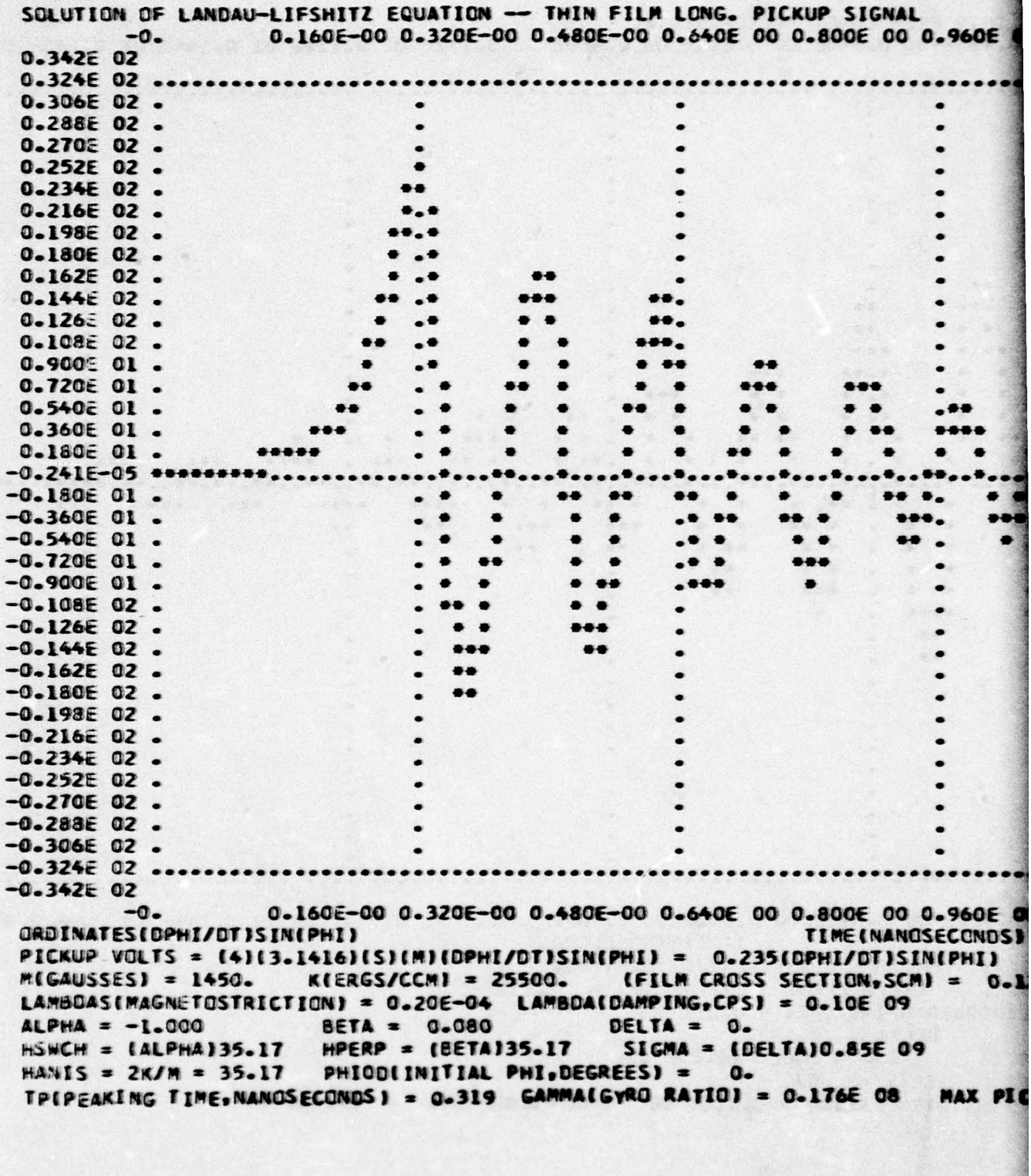
TP(PEAKING TIME,NANOSECONDS) = 0.291 GAMMA(GYRO RATIO) = 0.176E 08 MAX PICKUP

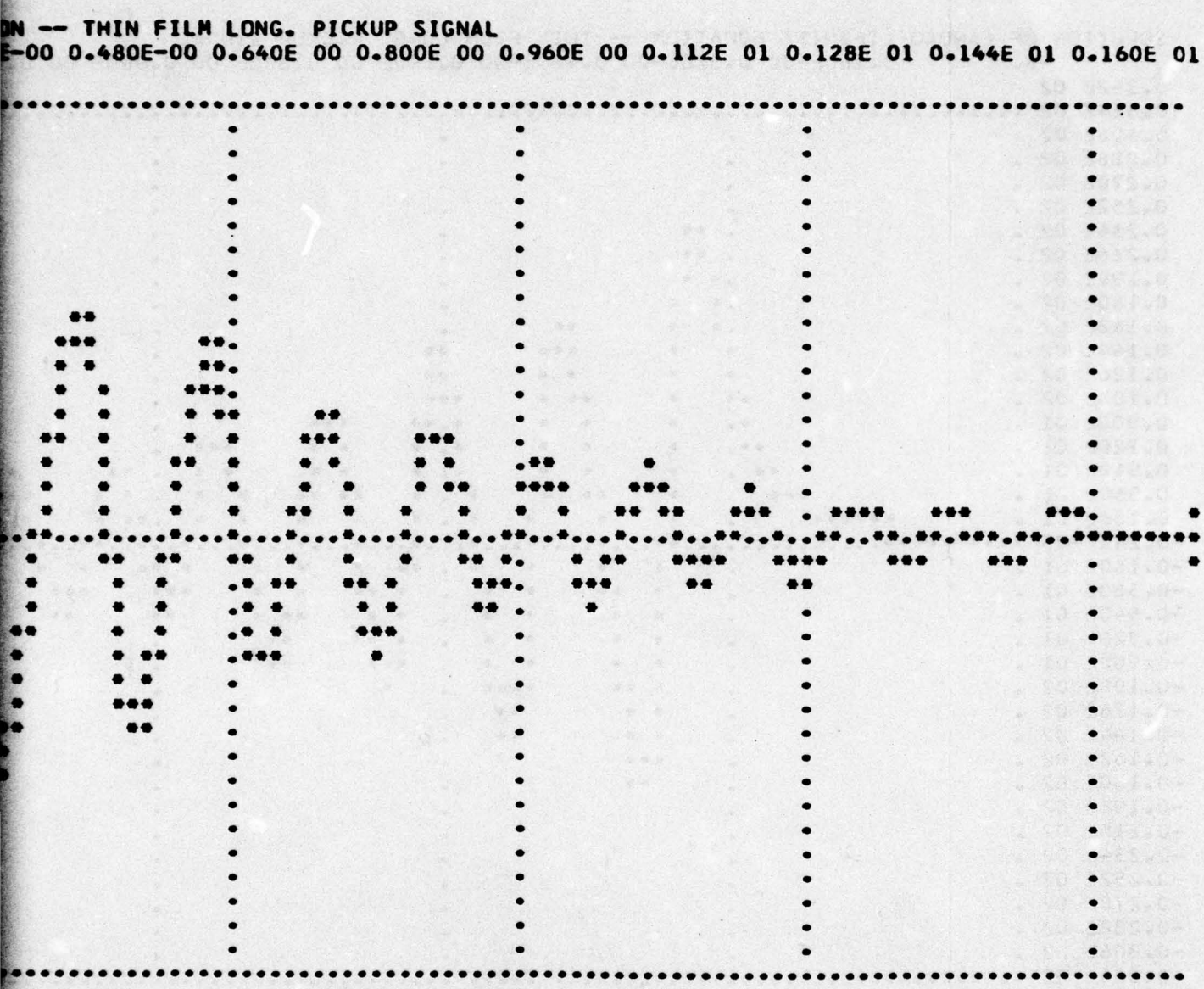


/DT)SIN(PHI) = 0.235(DPHI/DT)SIN(PHI)
1500. (FILM CROSS SECTION,SCM) = 0.129E-04
LAMBDA(DAMPING,CPS) = 0.10E 09
DELTA = -0.132
5.17 SIGMA = (DELTA)0.85E 09
NI,DEGREES) = 0.
GAMMA(GYRO RATIO) = 0.176E 08 MAX PICKUP SIG. = 0.252E 02

Fig. 72

2

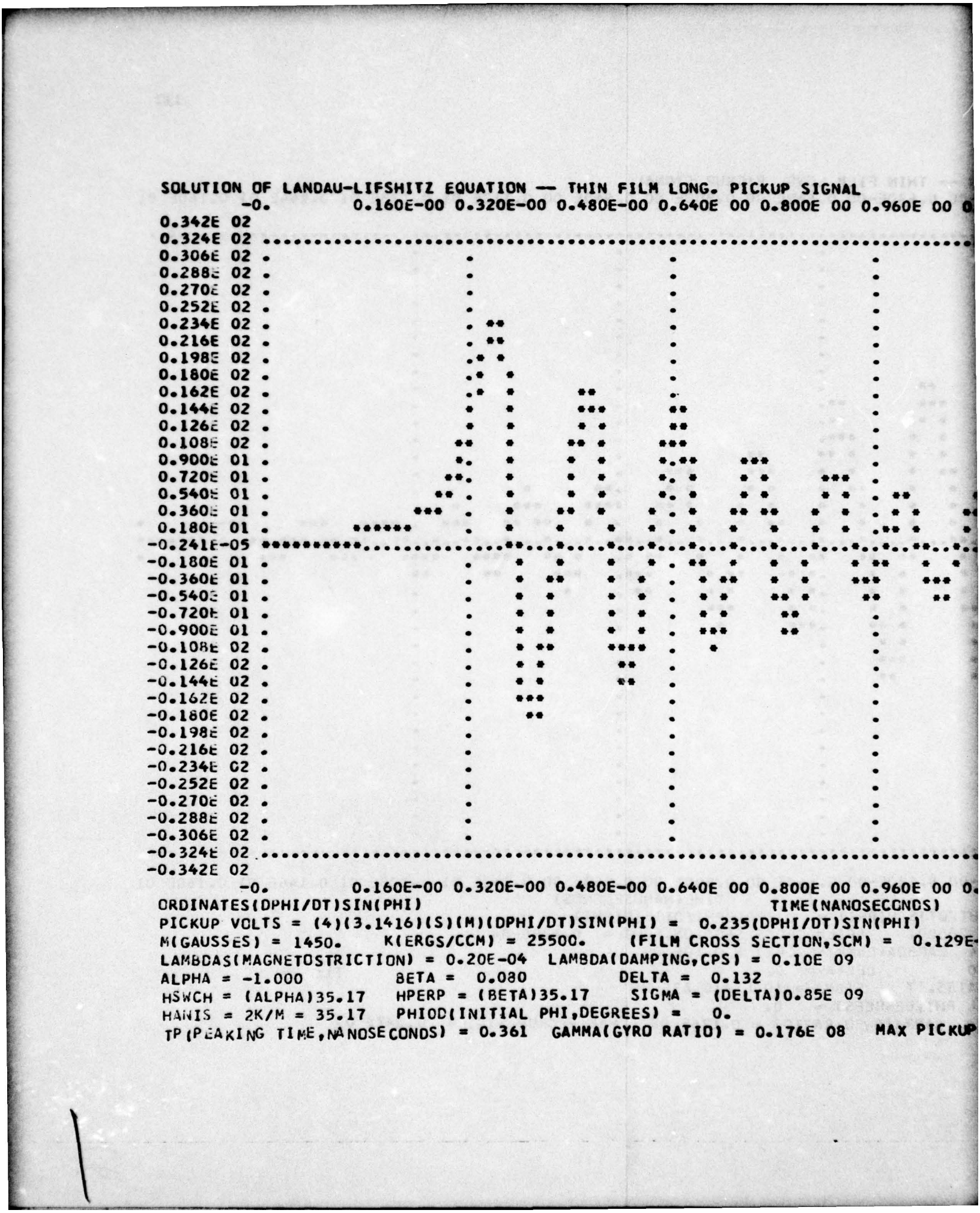

SOLUTION OF LANDAU-LIFSHITZ EQUATION -- THIN FILM LONG. PICKUP SIGNAL
-0. 0.160E-00 0.320E-00 0.480E-00 0.640E 00 0.800E 00 0.960E
0.342E 02
0.324E 02
0.306E 02
0.288E 02
0.270E 02
0.252E 02
0.234E 02
0.216E 02
0.198E 02
0.180E 02
0.162E 02
0.144E 02
0.126E 02
0.108E 02
0.900E 01
0.720E 01
0.540E 01
0.360E 01
0.180E 01
-0.241E-05
-0.180E 01
-0.360E 01
-0.540E 01
-0.720E 01
-0.900E 01
-0.108E 02
-0.126E 02
-0.144E 02
-0.162E 02
-0.180E 02
-0.198E 02
-0.216E 02
-0.234E 02
-0.252E 02
-0.270E 02
-0.288E 02
-0.306E 02
-0.324E 02
-0.342E 02
-0. 0.160E-00 0.320E-00 0.480E-00 0.640E 00 0.800E 00 0.960E
ORDINATES(DPHI/DT)SIN(PHI) TIME(NANOSECONDS)
PICKUP VOLTS = (4)(3.1416)(S)(M)(DPHI/DT)SIN(PHI) = 0.235(DPHI/DT)SIN(PHI)
M(GAUSSES) = 1450. K(ERGS/CCM) = 25500. (FILM CROSS SECTION,SCM) = 0.1
LAMBDAS(MAGNETOSTRICTION) = 0.20E-04 LAMBDA(DAMPING,CPS) = 0.10E 09
ALPHA = -1.000 BETA = 0.080 DELTA = 0.
HSWCH = (ALPHA)35.17 HPERP = (BETA)35.17 SIGMA = (DELTA)0.85E 09
HANIS = 2K/M = 35.17 PHIOD(INITIAL PHI,DEGREES) = 0.
TP(PEAKING TIME,NANOSECONDS) = 0.319 GAMMA(GYRO RATIO) = 0.176E 08 MAX PI



PHI/DT)SIN(PHI) = 0.235(DPHI/DT)SIN(PHI)
= 25500. (FILM CROSS SECTION,SCM) = 0.129E-04
04 LAMBDA(DAMPING,CPS) = 0.10E 09
00 DELTA = 0.
TA)35.17 SIGMA = (DELTA)0.85E 09
AL PHI,DEGREES) = 0.
19 GAMMA(GYRO RATIO) = 0.176E 08 MAX PICKUP SIG. = 0.247E 02

Fig. 73

2



PICKUP VOLTS = (4)(3.1416)(S)(M)(DPHI/DT)SIN(PHI) = 0.235(DPHI/DT)SIN(PHI)

M(GAUSSES) = 1450. K(ERGS/CCM) = 25500. (FILM CROSS SECTION,SCM) = 0.129E-

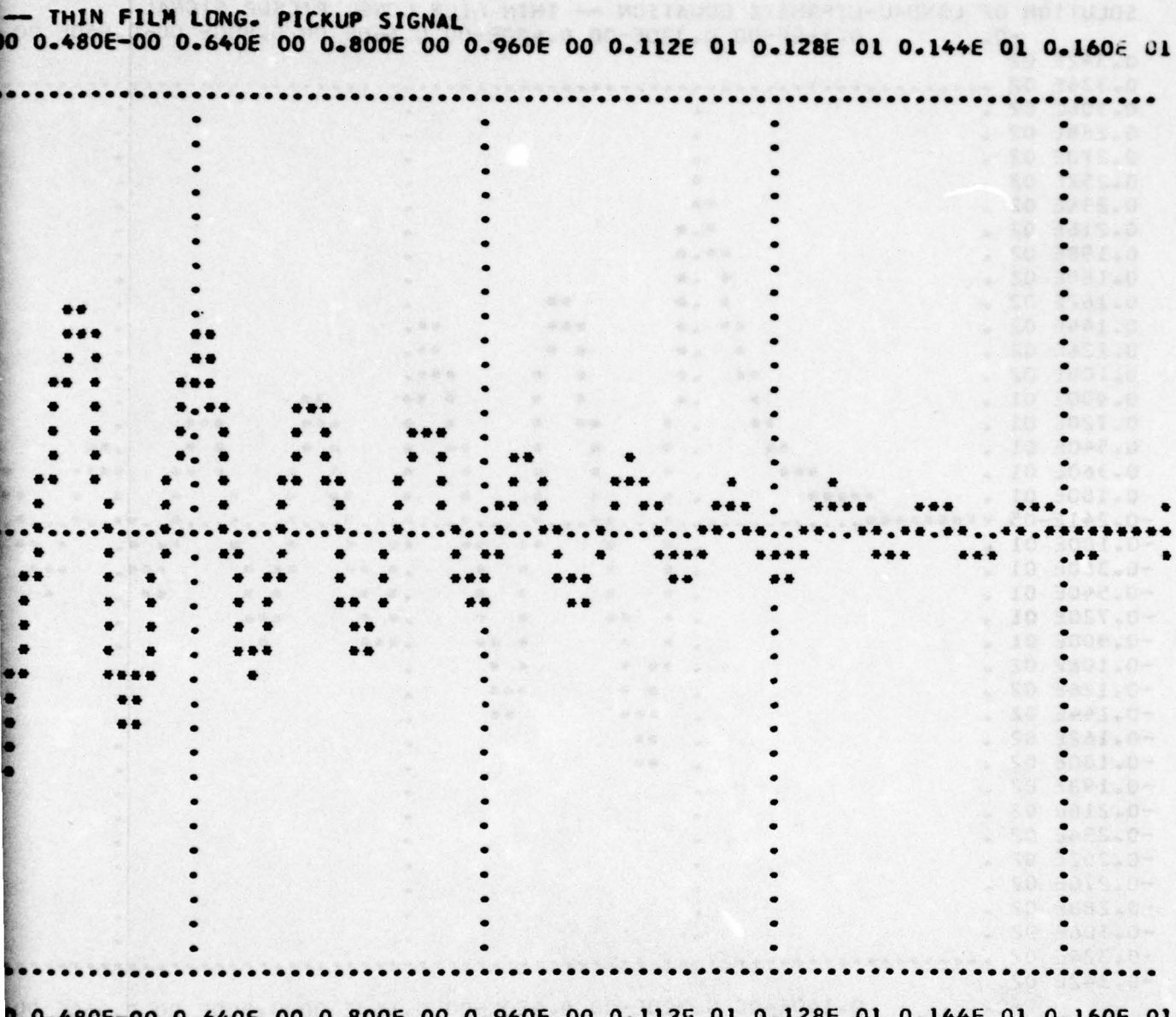
LAMBDAS(MAGNETOSTRICTION) = 0.20E-04 LAMBDA(DAMPING,CPS) = 0.10E 09

ALPHA = -1.000 BETA = 0.080 DELTA = 0.132

HSWCH = (ALPHA)35.17 HPERP = (BETA)35.17 SIGMA = (DELTA)0.85E 09

HANIS = 2K/M = 35.17 PHIOD(INITIAL PHI,DEGREES) = 0.

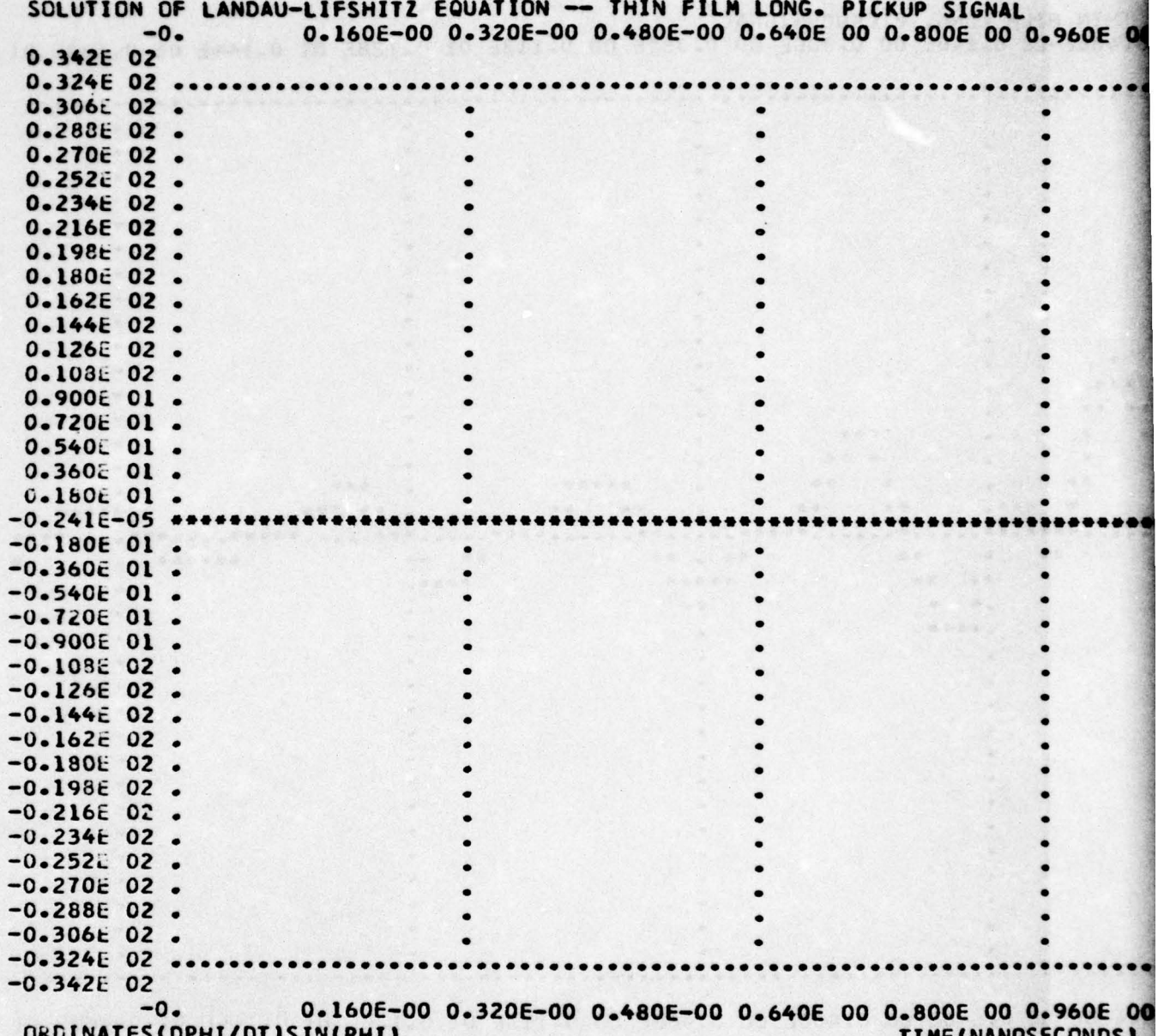
TP(PEAKING TIME,NANOSECONDS) = 0.361 GAMMA(GYRO RATIO) = 0.176E 08 MAX PICKUP



/DT)SIN(PHI) = 0.235(DPHI/DT)SIN(PHI)
3500. (FILM CROSS SECTION,SCM) = 0.129E-04
LAMBDA(DAMPING,CPS) = 0.10E 09
DELTA = 0.132
35.17 SIGMA = (DELTA)0.85E 09
PHI,DEGREES) = 0.
GAMMA(GYRO RATIO) = 0.176E 08 MAX PICKUP SIG. = 0.243E 02

Fig. 74

2



PICKUP VOLTS = (4)(3.1416)(S)(M)(DPHI/DT)SIN(PHI) = 0.235(DPHI/DT)SIN(PHI)

M(GAUSSES) = 1450. K(ERGS/CCM) = 25500. (FILM CROSS SECTION,SCM) = 0.12

LAMBDAS(MAGNETOSTRICTION) = 0.20E-04 LAMBDA(DAMPING,CPS) = 0.10E 09

ALPHA = -1.000 BETA = 0.080 DELTA = 0.532

HSWCH = (ALPHA)35.17 HPERP = (BETA)35.17 SIGMA = (DELTA)0.85E 09

HANIS = 2K/M = 35.17 PHIOD(INITIAL PHI,DEGREES) = 0.

TP(PEAKING TIME,NANOSECONDS) = 0.144 GAMMA(GYRO RATIO) = 0.176E 08 MAX PIC

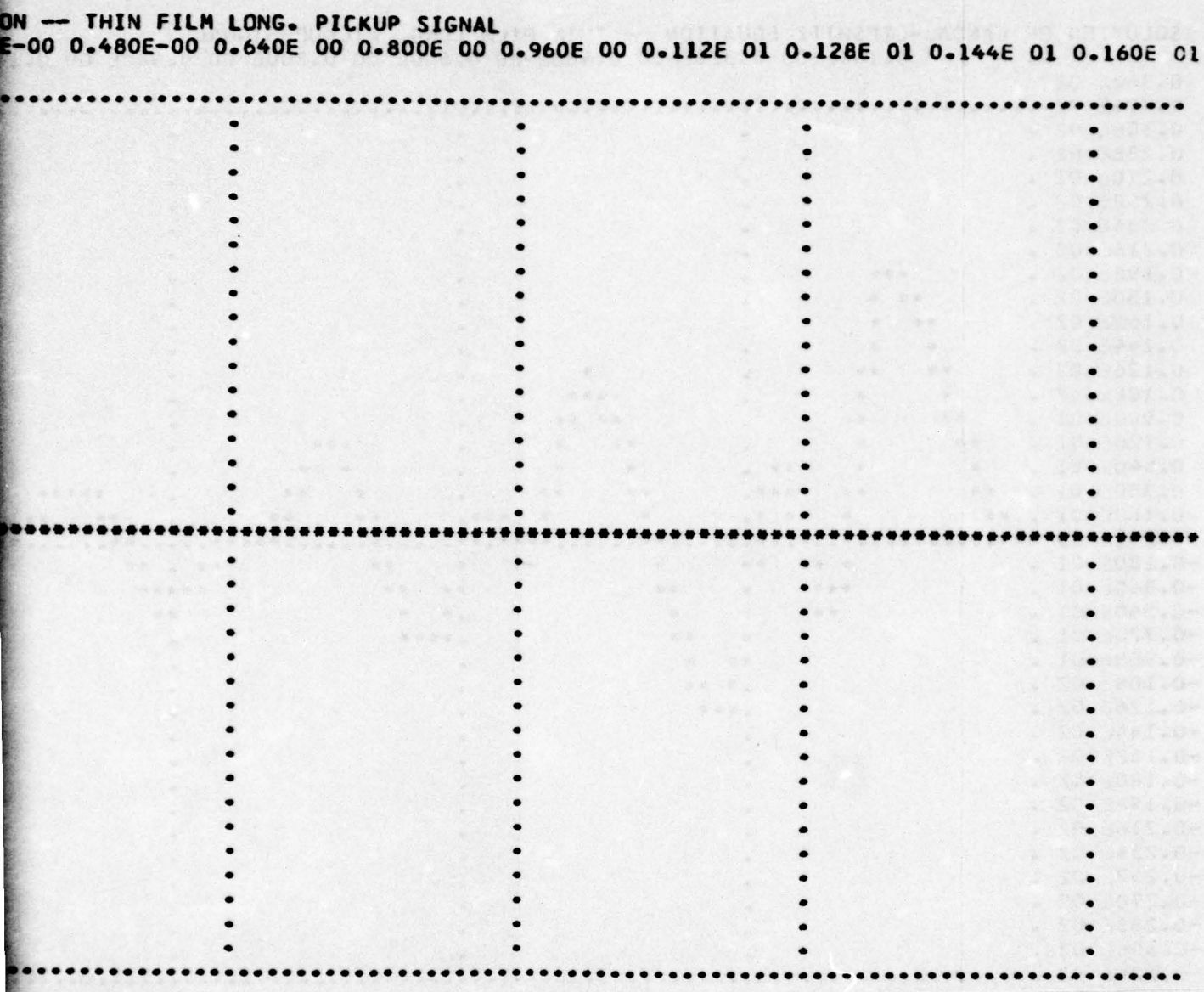
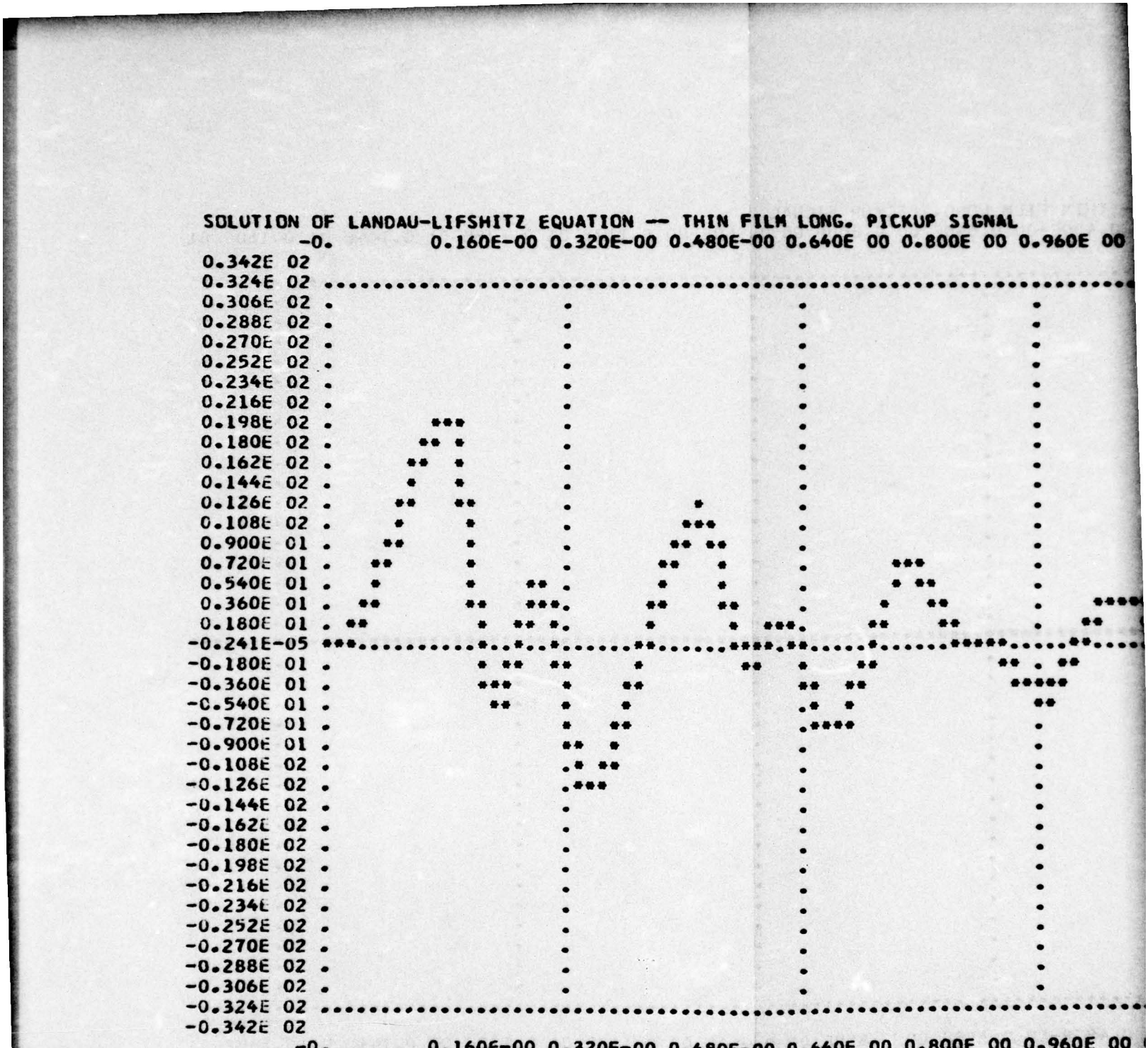

ON -- THIN FILM LONG. PICKUP SIGNAL
E-00 0.480E-00 0.640E 00 0.800E 00 0.960E 00 0.112E 01 0.128E 01 0.144E 01 0.160E 01
-00 0.480E-00 0.640E 00 0.800E 00 0.960E 00 0.112E 01 0.128E 01 0.144E 01 0.160E 01
TIME(NANOSECONDS)
MI/DT)SIN(PHI) = 0.235(DPHI/DT)SIN(PHI)
25500. (FILM CROSS SECTION,SCM) = 0.129E-04
LAMBDA(DAMPING,CPS) = 0.10E 09
DELTA = 0.532
A)35.17 SIGMA = (DELTA)0.85E 09
L PHI,DEGREES) = 0.
GAMMA(GYRO RATIO) = 0.176E 08 MAX PICKUP SIG. = 0.332E-00

Fig. 75

2



PICKUP VOLTS = (4)(3.1416)(S)(M)(DPHI/DT)SIN(PHI) = 0.235(DPHI/DT)SIN(PHI)

M(GAUSSES) = 1450. K(ERGS/CCM) = 25500. (FILM CROSS SECTION,SCM) = 0.129

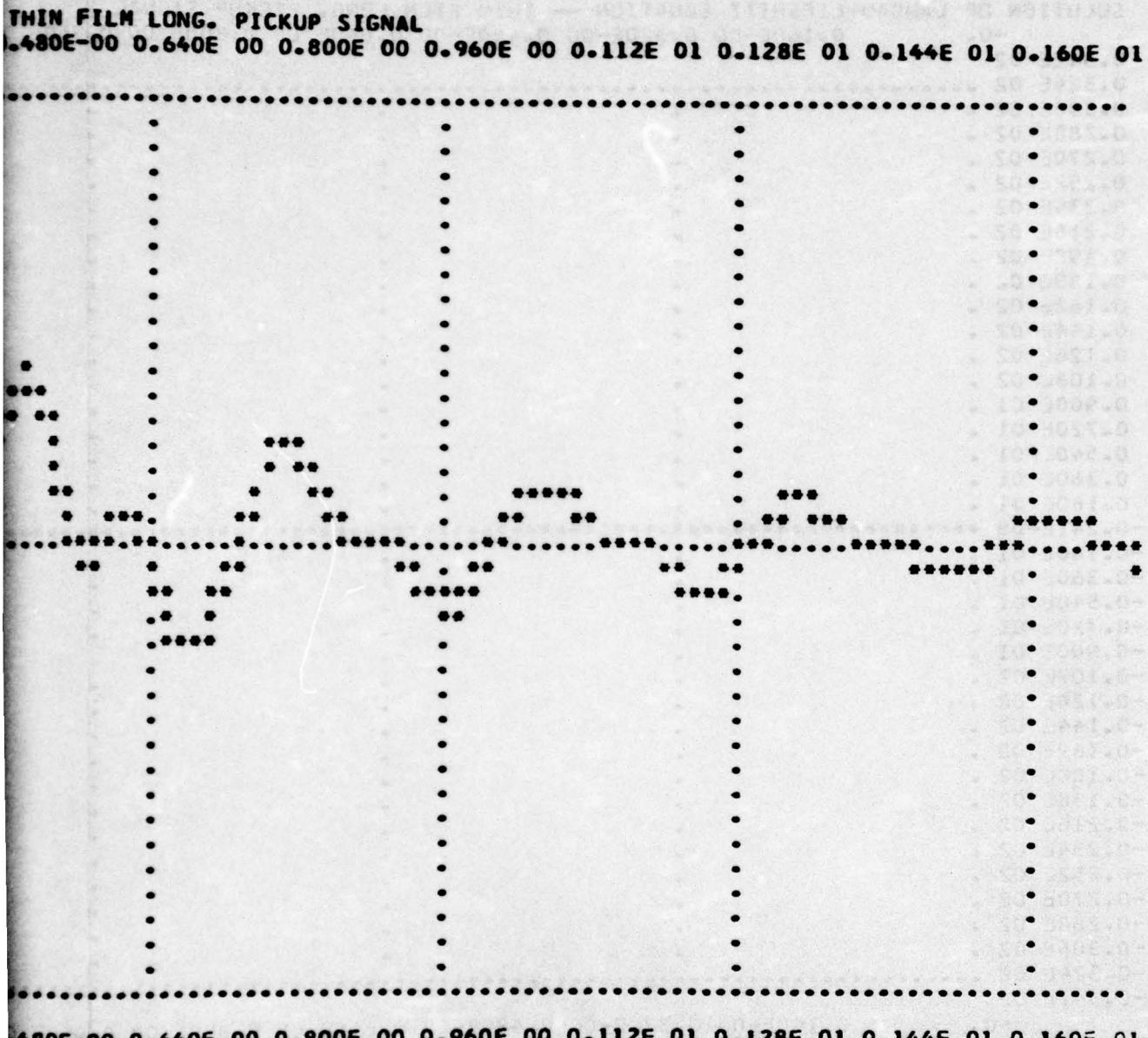
LAMBDAS(MAGNETOSTRICTION) = 0.20E-04 LAMBDA(DAMPING,CPS) = 0.10E 09

ALPHA = -0.500 BETA = 0.590 DELTA = 0.

HSWCH = (ALPHA)35.17 HPERP = (BETA)35.17 SIGMA = (DELTA)0.85E 09

HANIS = 2K/M = 35.17 PHIOD(INITIAL PHI,DEGREES) = 0.

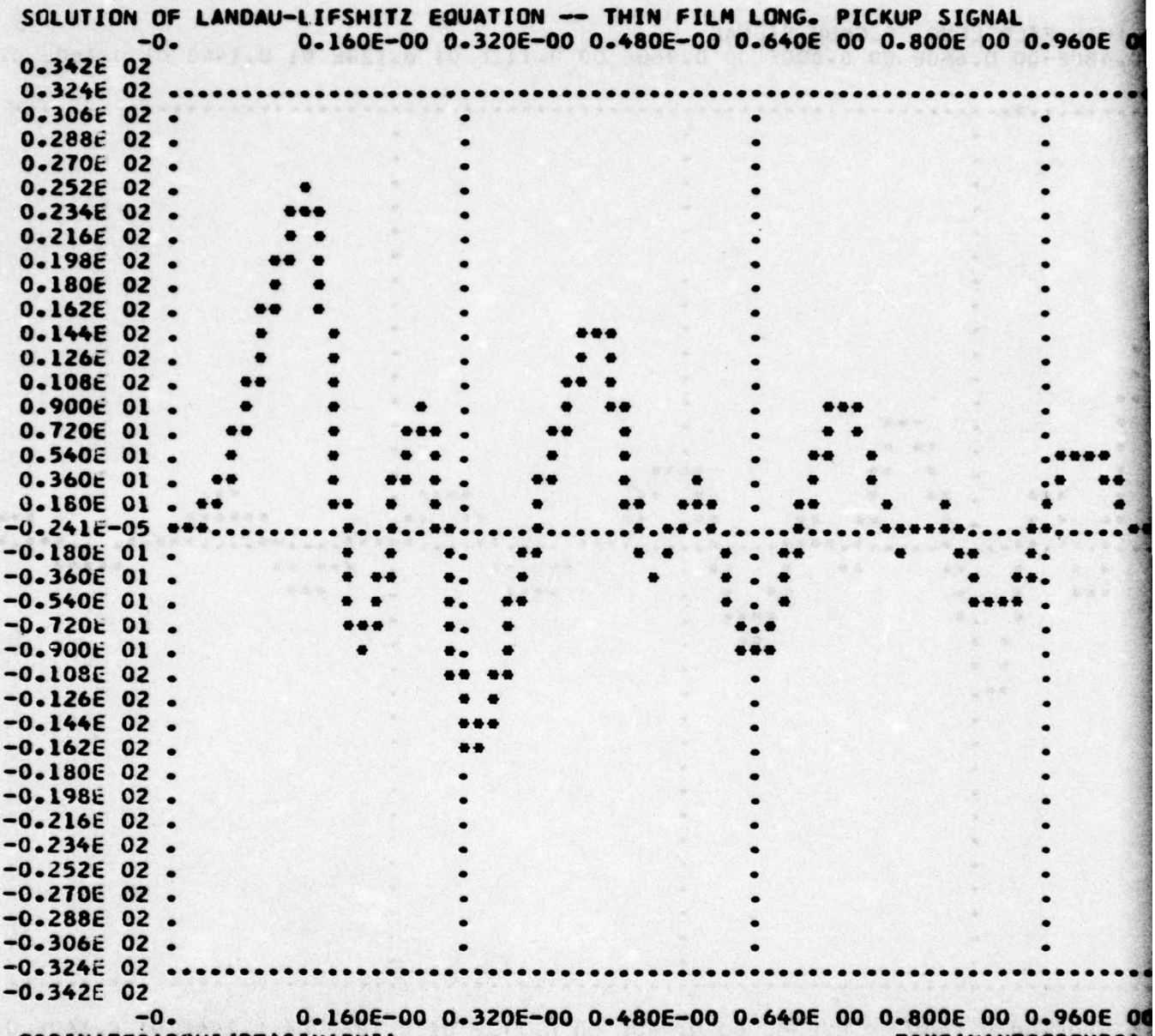
TP(PEAKING TIME,NANOSECONDS) = 0.157 GAMMA(GYRO RATIO) = 0.176E 08 MAX PICKU



SIN(PHI) = 0.235(DPHI/DT)SIN(PHI)
). (FILM CROSS SECTION,SCM) = 0.129E-04
BDA(DAMPING,CPS) = 0.10E 09
DELTA = 0.
17 SIGMA = (DELTA)0.85E 09
DEGREES) = 0.
A(GYRO RATIO) = 0.176E 08 MAX PICKUP SIG. = 0.206E 02

Fig. 76

2



PICKUP VOLTS = (4)(3.1416)(S)(M)(DPHI/DT)SIN(PHI) = 0.235(DPHI/DT)SIN(PHI)

M(GAUSSES) = 1450. K(ERGS/CCM) = 25500. (FILM CROSS SECTION,SCM) = 0.1

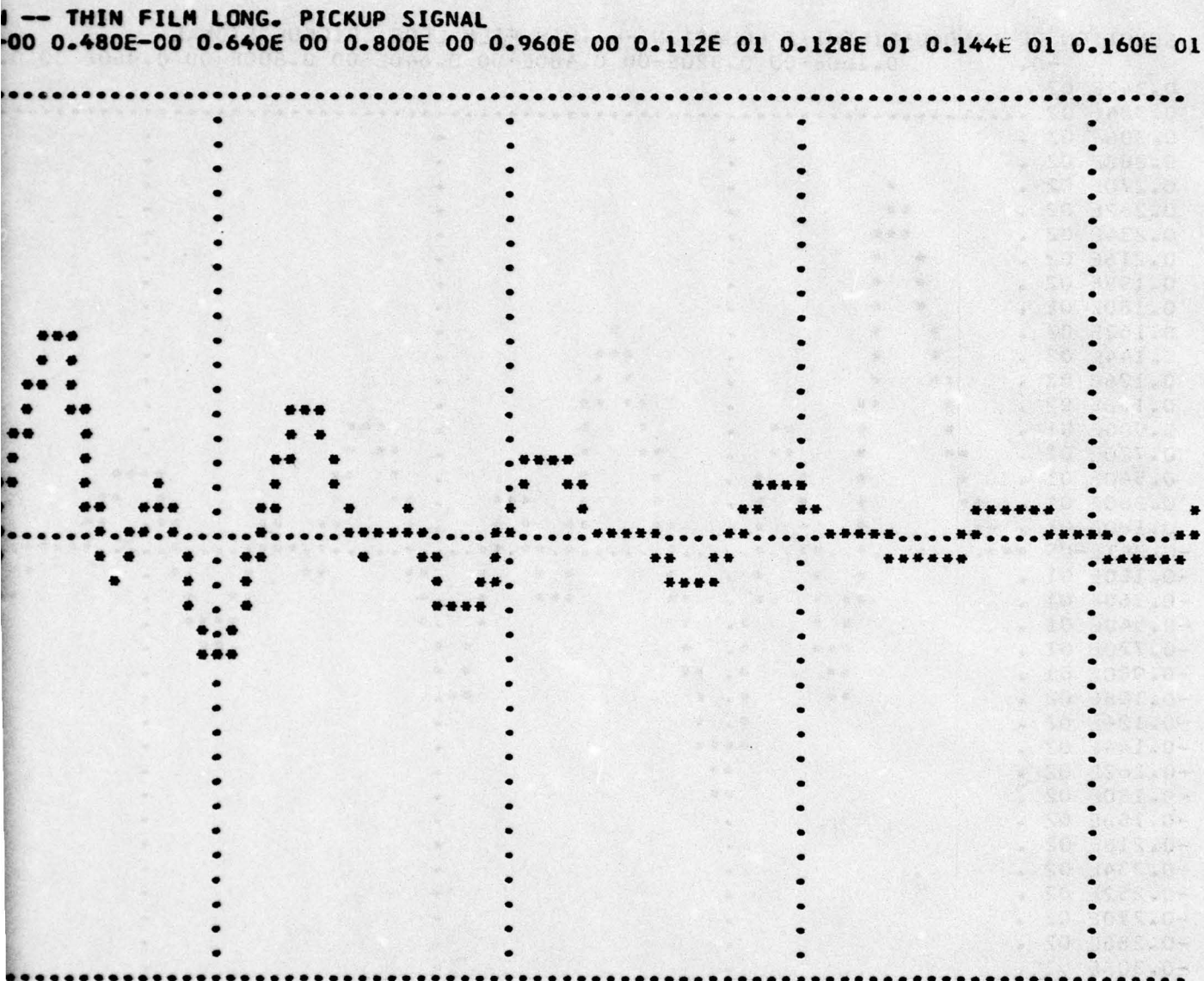
LAMBDAS(MAGNETOSTRICTION) = 0.20E-04 LAMBDA(DAMPING,CPS) = 0.10E 09

ALPHA = -0.700 BETA = 0.590 DELTA = 0.

HSWCH = (ALPHA)35.17 HPERP = (BETA)35.17 SIGMA = (DELTA)0.85E 09

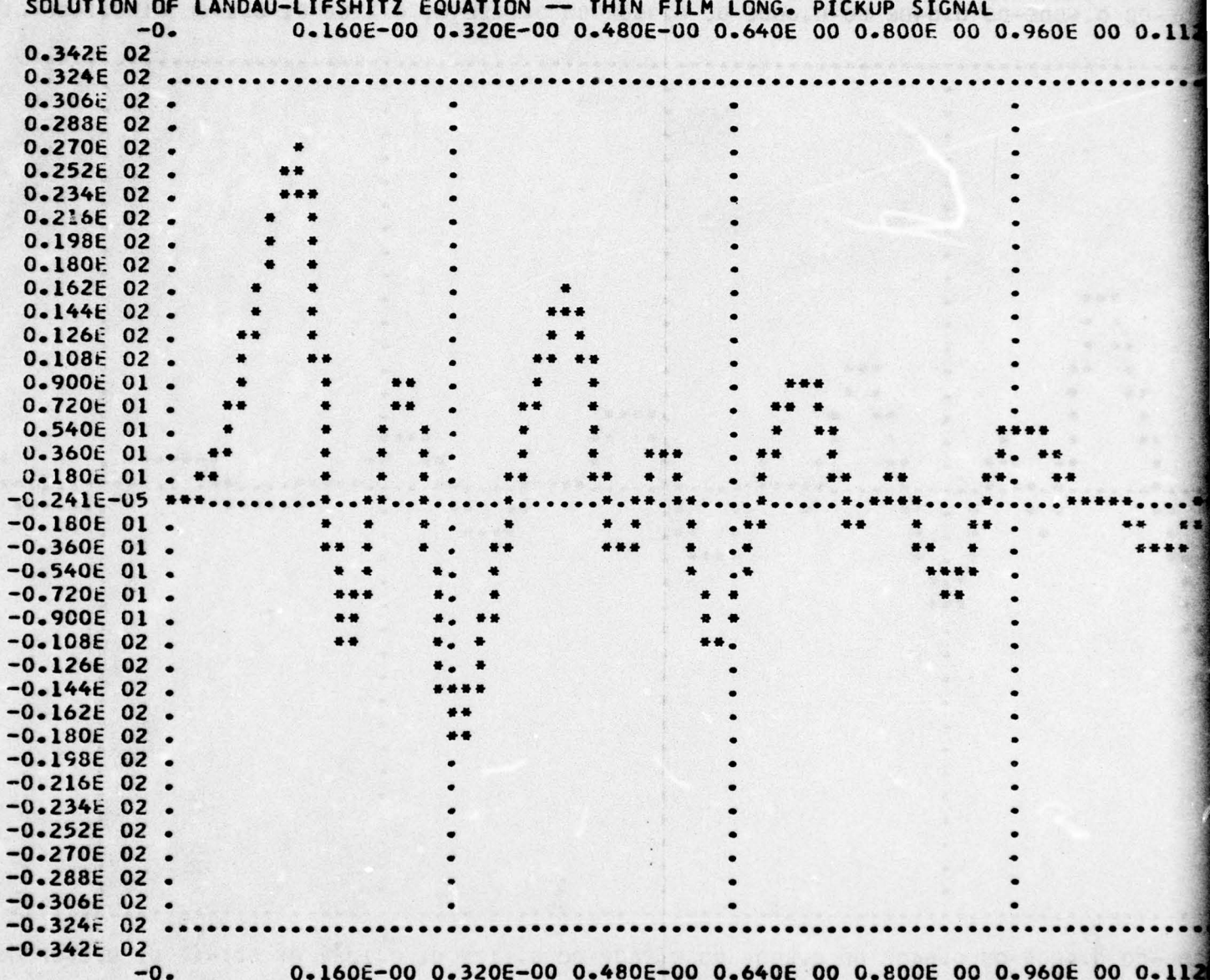
HANIS = 2K/M = 35.17 PHIOD(INITIAL PHI,DEGREES) = 0.

TP(PEAKING TIME,NANOSECONDS) = 0.145 GAMMA(GYRO RATIO) = 0.176E 08 MAX PIC



I/DT)SIN(PHI) = 0.235(DPHI/DT)SIN(PHI)
25500. (FILM CROSS SECTION,SCM) = 0.129E-04
LAMBDA(DAMPING,CPS) = 0.10E 09
DELTA = 0.
)35.17 SIGMA = (DELTA)0.85E 09
PHI,DEGREES) = 0.
GAMMA(GYRO RATIO) = 0.176E 08 MAX PICKUP SIG. = 0.244E 02

Fig. 77



PICKUP VOLTS = (4)(3.1416)(S)(M)(DPHI/DT)SIN(PHI) = 0.235(DPHI/DT)SIN(PHI)

M(GAUSSES) = 1450. K(ERGS/CCM) = 25500. (FILM CROSS SECTION,SCM) = 0.129E-04

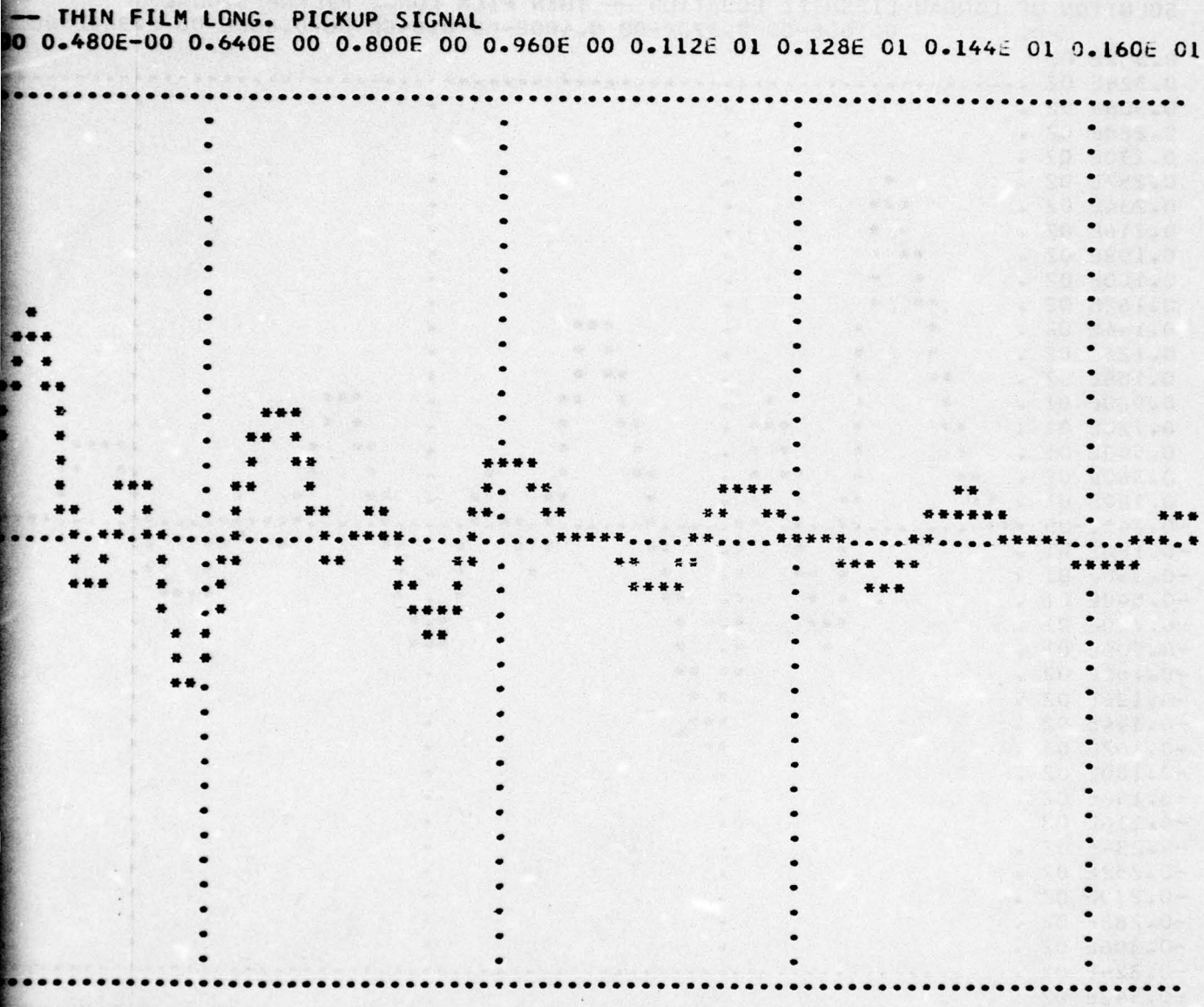
LAMBDAS(MAGNETOSTRICTION) = 0.20E-04 LAMBDA(DAMPING,CPS) = 0.10E 09

ALPHA = -0.800 BETA = 0.590 DELTA = 0.

HSWCH = (ALPHA)35.17 HPERP = (BETA)35.17 SIGMA = (DELTA)0.85E 09

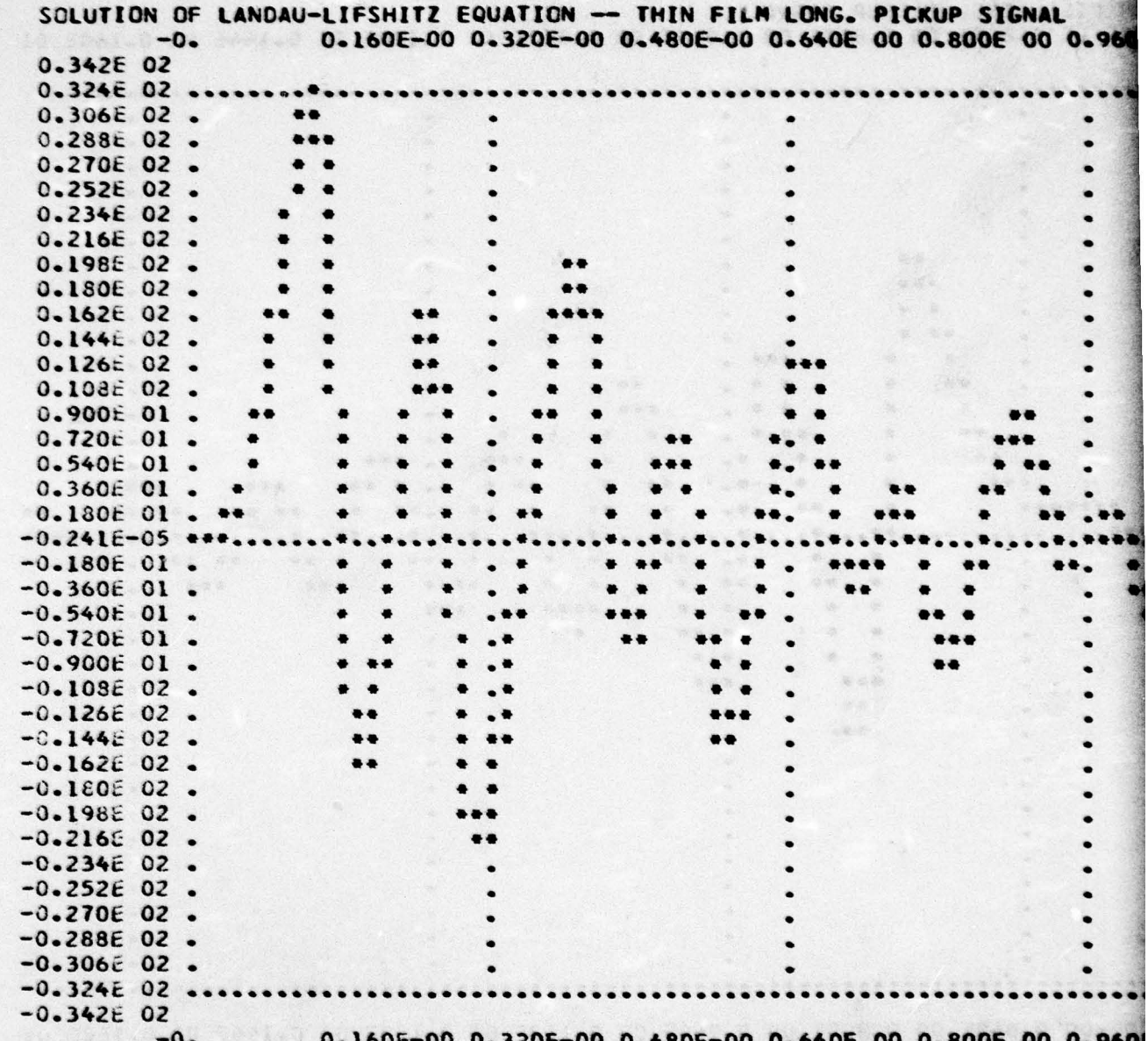
HANIS = 2K/M = 35.17 PHIOD(INITIAL PHI,DEGREES) = 0.

TP(PEAKING TIME,NANOSECONDS) = 0.140 GAMMA(GYRO RATIO) = 0.176E 08 MAX PICKUP SIG

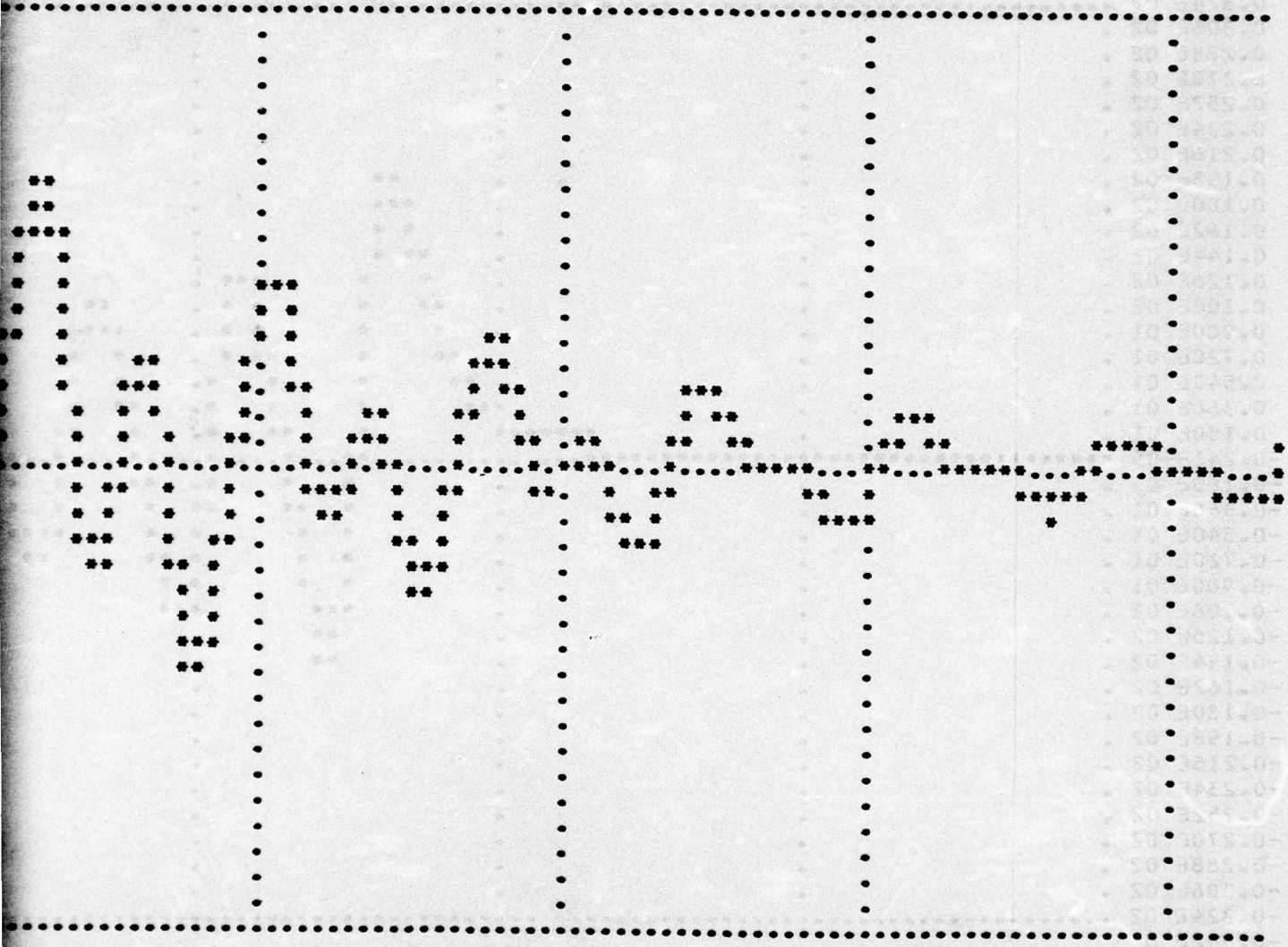


/DT)SIN(PHI) = 0.235(DPHI/DT)SIN(PHI)
3500. (FILM CROSS SECTION,SCM) = 0.129E-04
LAMBDA(DAMPING,CPS) = 0.10E 09
DELTA = 0.
35.17 SIGMA = (DELTA)0.85E 09
PHI,DEGREES) = 0.
GAMMA(GYRO RATIO) = 0.176E 08 MAX PICKUP SIG. = 0.261E 02

Fig. 78

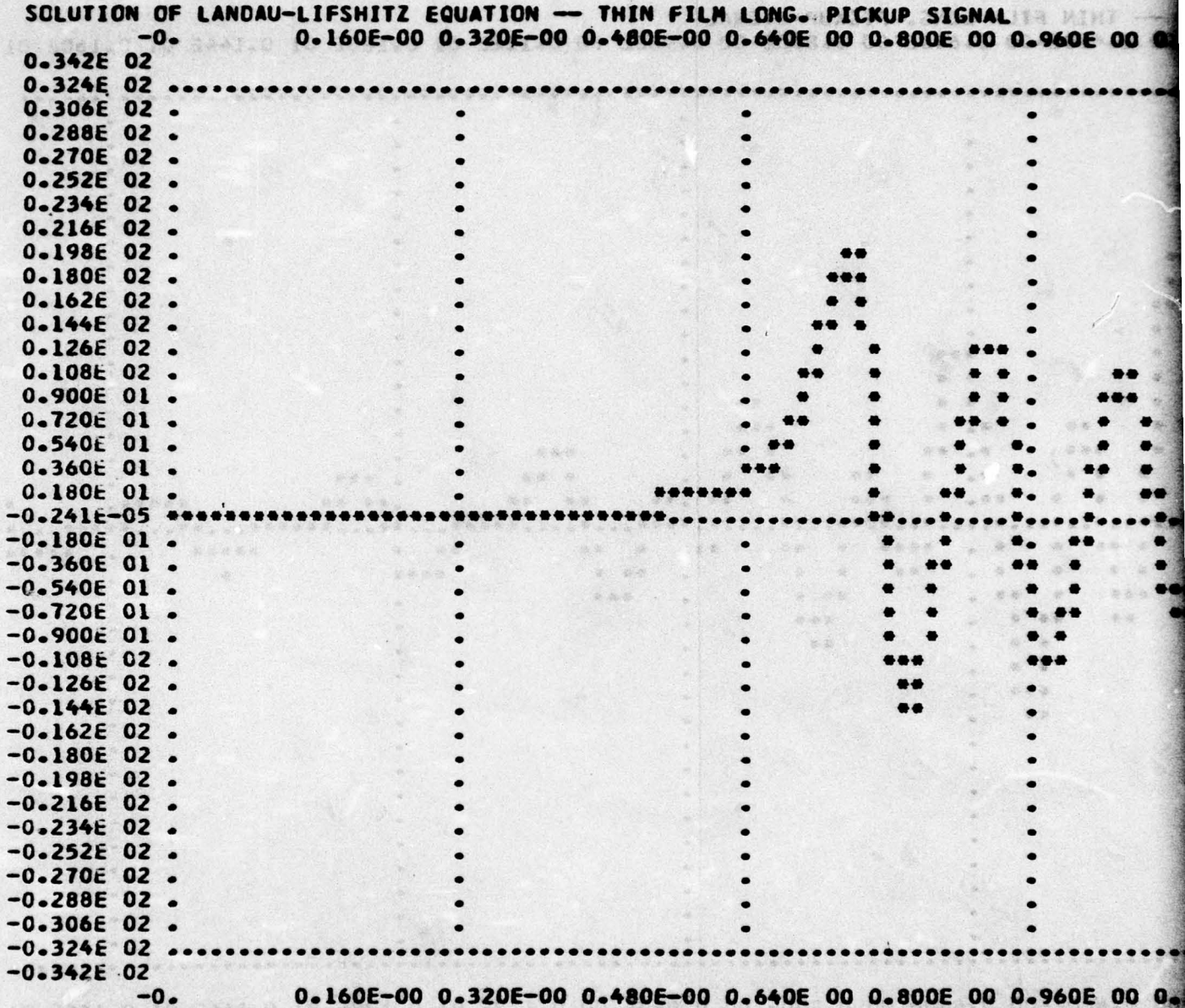

SOLUTION OF LANDAU-LIFSHITZ EQUATION -- THIN FILM LONG. PICKUP SIGNAL
-0. 0.160E-00 0.320E-00 0.480E-00 0.640E 00 0.800E 00 0.960
0.342E 02
0.324E 02
0.306E 02
0.288E 02
0.270E 02
0.252E 02
0.234E 02
0.216E 02
0.198E 02
0.180E 02
0.162E 02
0.144E 02
0.126E 02
0.108E 02
0.900E 01
0.720E 01
0.540E 01
0.360E 01
0.180E 01
-0.241E-05
-0.180E 01
-0.360E 01
-0.540E 01
-0.720E 01
-0.900E 01
-0.108E 02
-0.126E 02
-0.144E 02
-0.162E 02
-0.180E 02
-0.198E 02
-0.216E 02
-0.234E 02
-0.252E 02
-0.270E 02
-0.288E 02
-0.306E 02
-0.324E 02
-0.342E 02
-0. 0.160E-00 0.320E-00 0.480E-00 0.640E 00 0.800E 00 0.960
CRDINATES(DPHI/DT)SIN(PHI)
TIME(NANOSECON
PICKUP VOLTS = (4)(3.1416)(S)(M)(DPHI/DT)SIN(PHI) = 0.235(DPHI/DT)SIN(PHI
M(GAUSSES) = 1450. K(ERGS/CCM) = 25500. (FILM CROSS SECTION,SCM) =
LAMBDAS(MAGNETOSTRICTION) = 0.20E-04 LAMBDA(DAMPING,CPS) = 0.10E 09
ALPHA = -1.200 BETA = 0.590 DELTA = 0.
HSWCH = (ALPHA)35.17 HPERP = (BETA)35.17 SIGMA = (DELTA)0.85E 09
HANIS = 2K/M = 35.17 PHIOD(INITIAL PHI,DEGREES) = 0.
TP(PEAKING TIME,NANOSECONDS) = 0.127 GAMMA(GYRO RATIO) = 0.176E 08 MAX

ION -- THIN FILM LONG. PICKUP SIGNAL
DE-00 0.480E-00 0.640E 00 0.800E 00 0.960E 00 0.112E 01 0.128E 01 0.144E 01 0.160E 01



E-00 0.480E-00 0.640E 00 0.800E 00 0.960E 00 0.112E 01 0.128E 01 0.144E 01 0.160E 01
TIME(NANOSECONDS)
PHI/DT)SIN(PHI) = 0.235(DPHI/DT)SIN(PHI)
= 25500. (FILM CROSS SECTION,SCM) = 0.129E-04
04 LAMBDA(DAMPING,CPS) = 0.10E 09
90 DELTA = 0.
TA)35.17 SIGMA = (DELTA)0.85E 09
AL PHI,DEGREES) = 0.
27 GAMMA(GYRO RATIO) = 0.176E 08 MAX PICKUP SIG. = 0.321E 02

Fig. 79



ORDINATES(DPHI/DT)SIN(PHI) TIME(NANOSECONDS)

PICKUP VOLTS = (4)(3.1416)(S)(M)(DPHI/DT)SIN(PHI) = 0.235(DPHI/DT)SIN(PHI)

M(GAUSSES) = 1450. K(ERGS/CCM) = 25500. (FILM CROSS SECTION,SCM) = 0.129E-

LAMBDAS(MAGNETOSTRICTION) = 0.20E-04 LAMBDA(DAMPING,CPS) = 0.10E 09

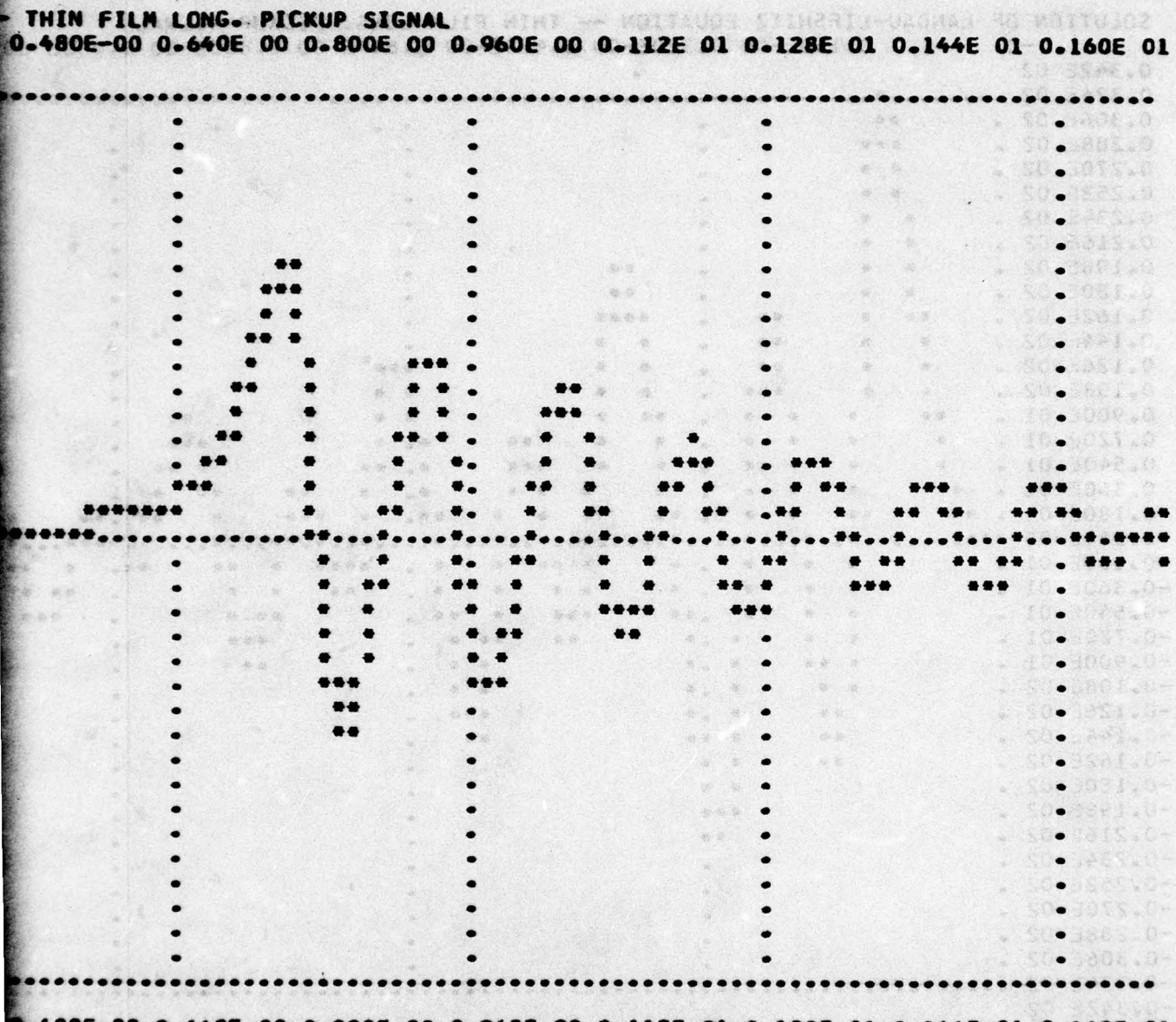
ALPHA = -0.700 BETA = 0.080 DELTA = 0.

H=WCH = (ALPHA)35.17 HPERP = (BETA)35.17 SIGMA = (DELTA)0.85E 09

HANIS = 2K/M = 35.17 PHIOD(INITIAL PHI,DEGREES) = 0.

TP(PEAKING TIME,NANOSECONDS) = 0.760 GAMMA(GYRO RATIO) = 0.176E 08 MAX PICKUP

- THIN FILM LONG. PICKUP SIGNAL



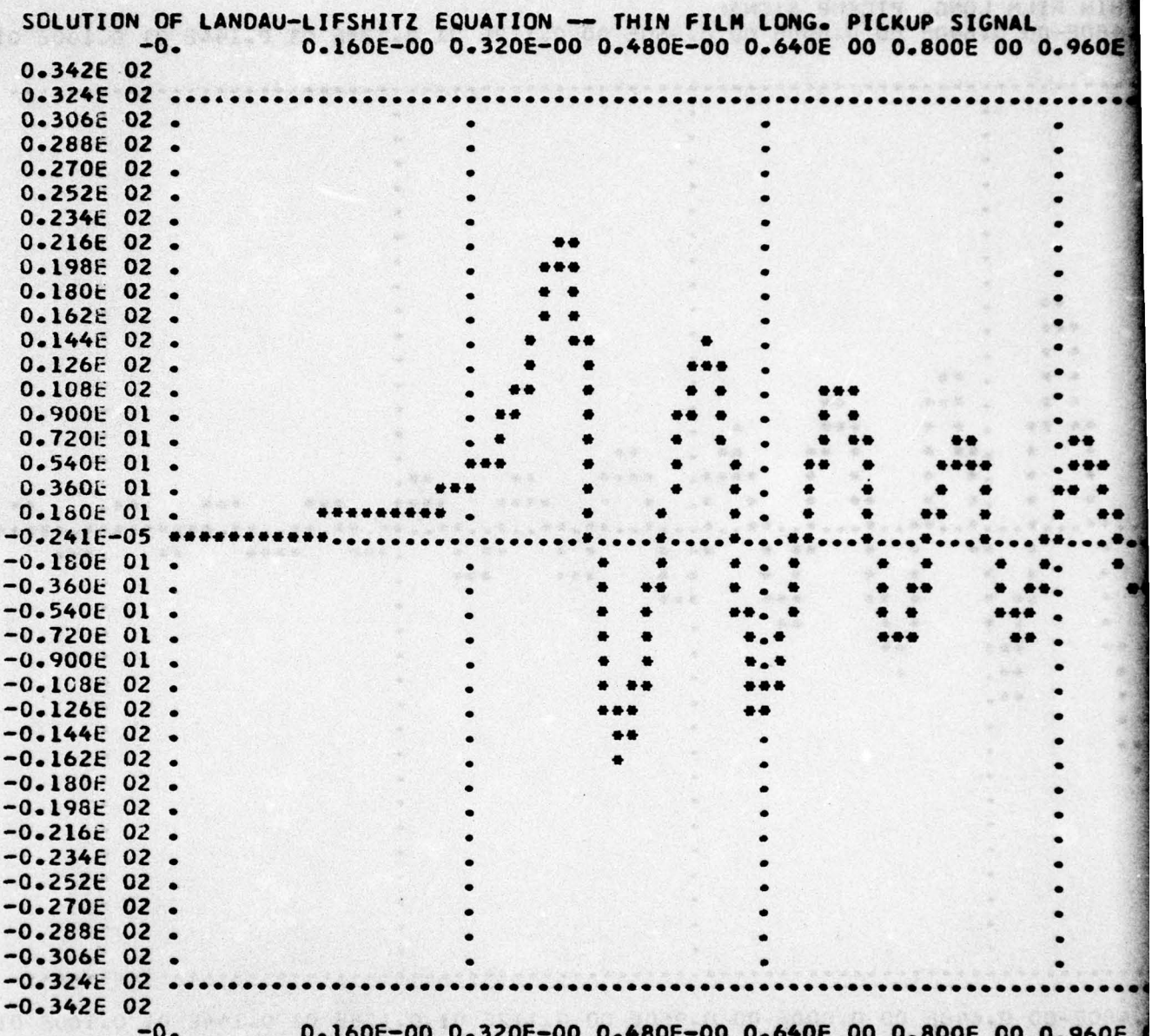
0.480E-00 0.640E 00 0.800E 00 0.960E 00 0.112E 01 0.128E 01 0.144E 01 0.160E 01

TIME(NANOSECONDS)

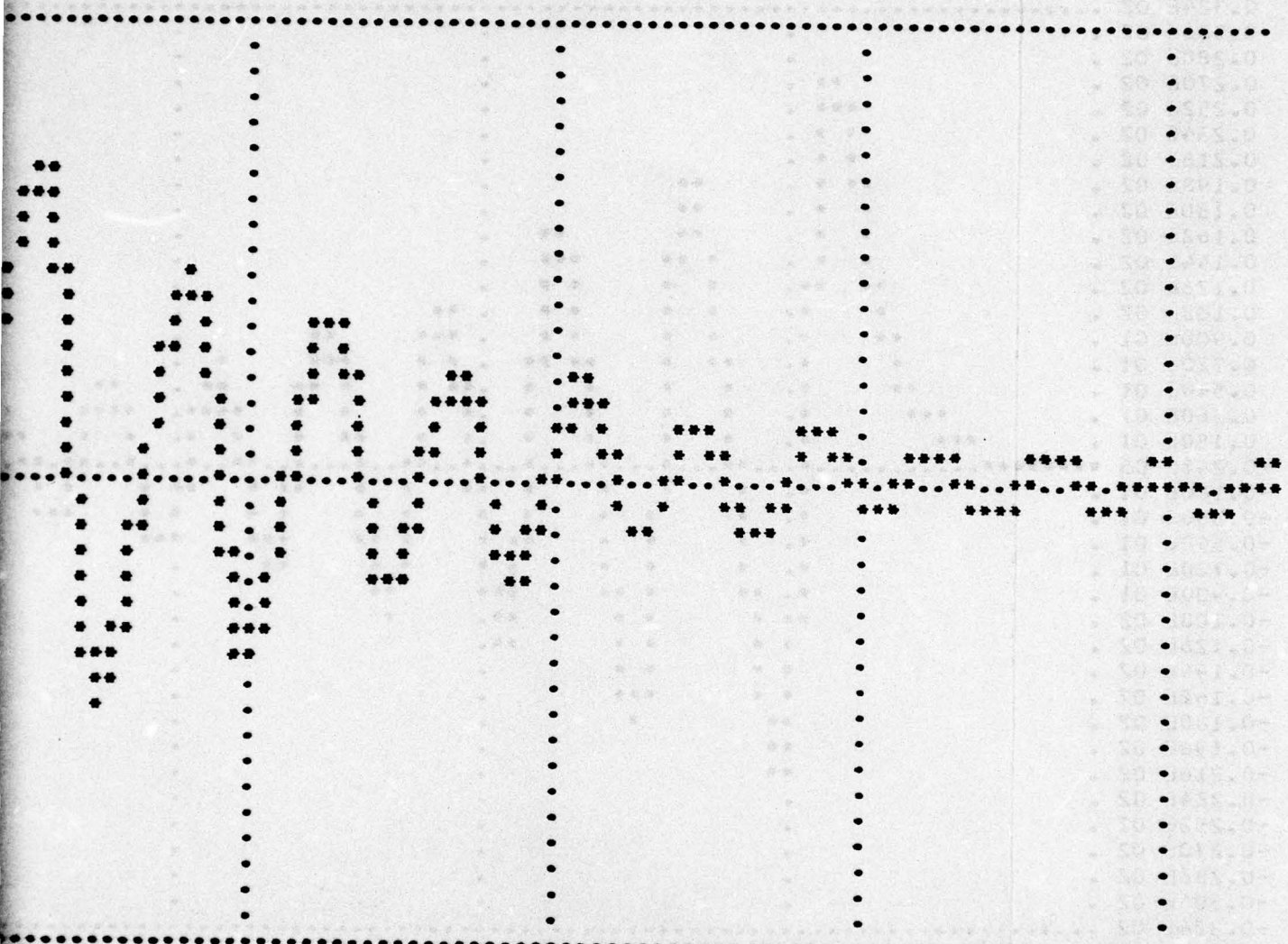
T)SIN(PHI) = 0.235(DPHI/DT)SIN(PHI)
00. (FILM CROSS SECTION,SCM) = 0.129E-04
MBDA(DAMPING,CPS) = 0.10E 09
DELTA = 0.
.17 SIGMA = (DELTA)0.85E 09
I,DEGREES) = 0.
MMA(GYRO RATIO) = 0.176E 08 MAX PICKUP SIG. = 0.194E 02

Fig. 80

2

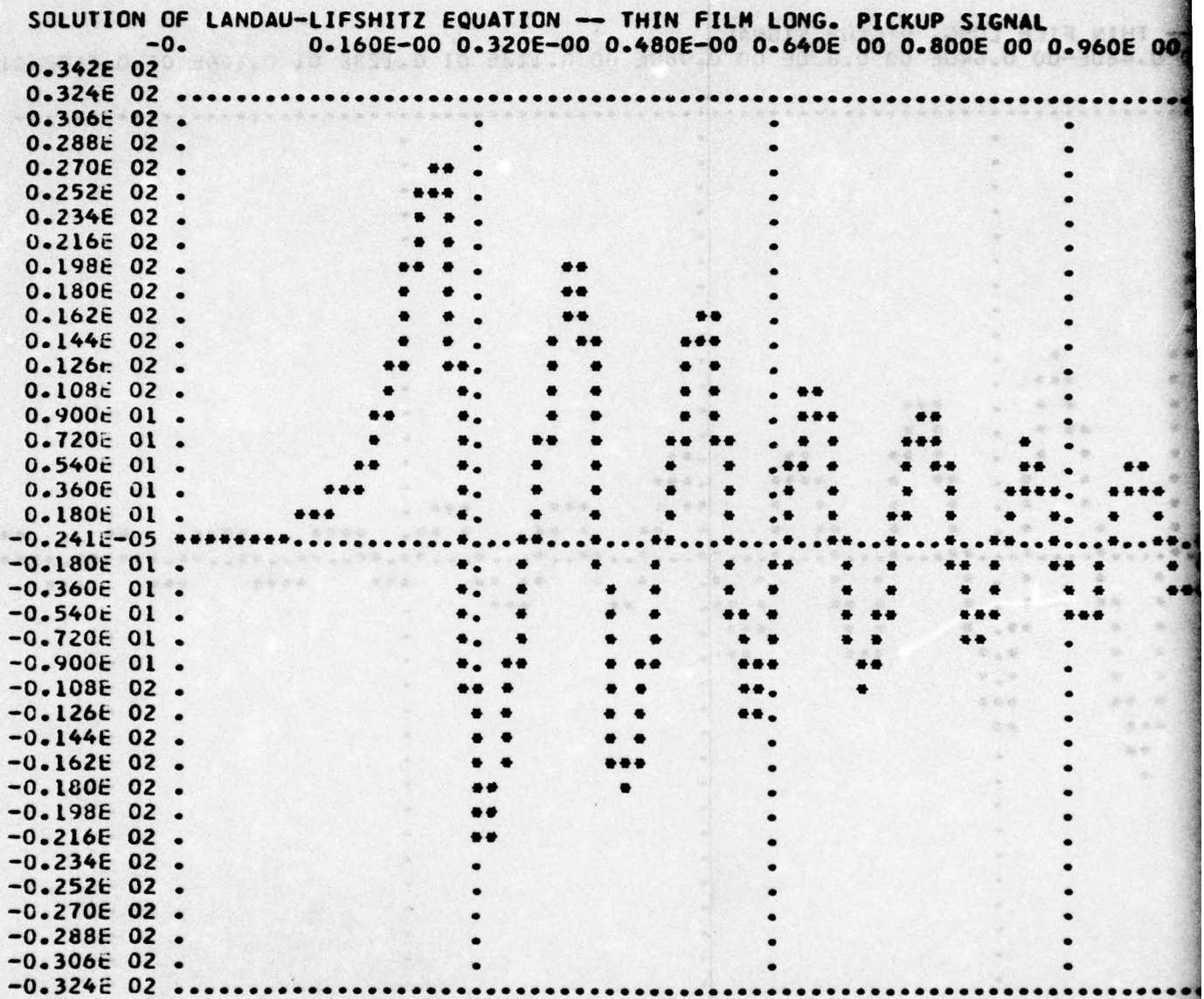

SOLUTION OF LANDAU-LIFSHITZ EQUATION -- THIN FILM LONG. PICKUP SIGNAL
-0. 0.160E-00 0.320E-00 0.480E-00 0.640E 00 0.800E 00 0.960E
0.342E 02
0.324E 02
0.306E 02
0.288E 02
0.270E 02
0.252E 02
0.234E 02
0.216E 02
0.198E 02
0.180E 02
0.162E 02
0.144E 02
0.126E 02
0.108E 02
0.900E 01
0.720E 01
0.540E 01
0.360E 01
0.180E 01
-0.241E-05
-0.180E 01
-0.360E 01
-0.540E 01
-0.720E 01
-0.900E 01
-0.108E 02
-0.126E 02
-0.144E 02
-0.162E 02
-0.180E 02
-0.198E 02
-0.216E 02
-0.234E 02
-0.252E 02
-0.270E 02
-0.288E 02
-0.306E 02
-0.324E 02
-0.342E 02
-0. 0.160E-00 0.320E-00 0.480E-00 0.640E 00 0.800E 00 0.960E
ORDINATES(DPHI/DT)SIN(PHI)
TIME(NANOSECONDS)
PICKUP VOLTS = (4)(3.1416)(S)(M)(DPHI/DT)SIN(PHI) = 0.235(DPHI/DT)SIN(PHI)
M(GAUSSES) = 1450. K(ERGS/CCM) = 25500. (FILM CROSS SECTION,SCM) = 0.
LAMBDAS(MAGNETOSTRICTION) = 0.20E-04 LAMBDA(DAMPING,CPS) = 0.10E 09
ALPHA = -0.800 BETA = 0.080 DELTA = 0.
HSWCH = (ALPHA)35.17 HPERP = (BETA)35.17 SIGMA = (DELTA)0.85E 09
HANIS = 2K/M = 35.17 PHIOD(INITIAL PHI,DEGREES) = 0.
TP(PEAKING TIME,NANOSECONDS) = 0.421 GAMMA(GYRO RATIO) = 0.176E 08 MAX PI

ON -- THIN FILM LONG. PICKUP SIGNAL
E-00 0.480E-00 0.640E 00 0.800E 00 0.960E 00 0.112E 01 0.128E 01 0.144E 01 0.160E 01

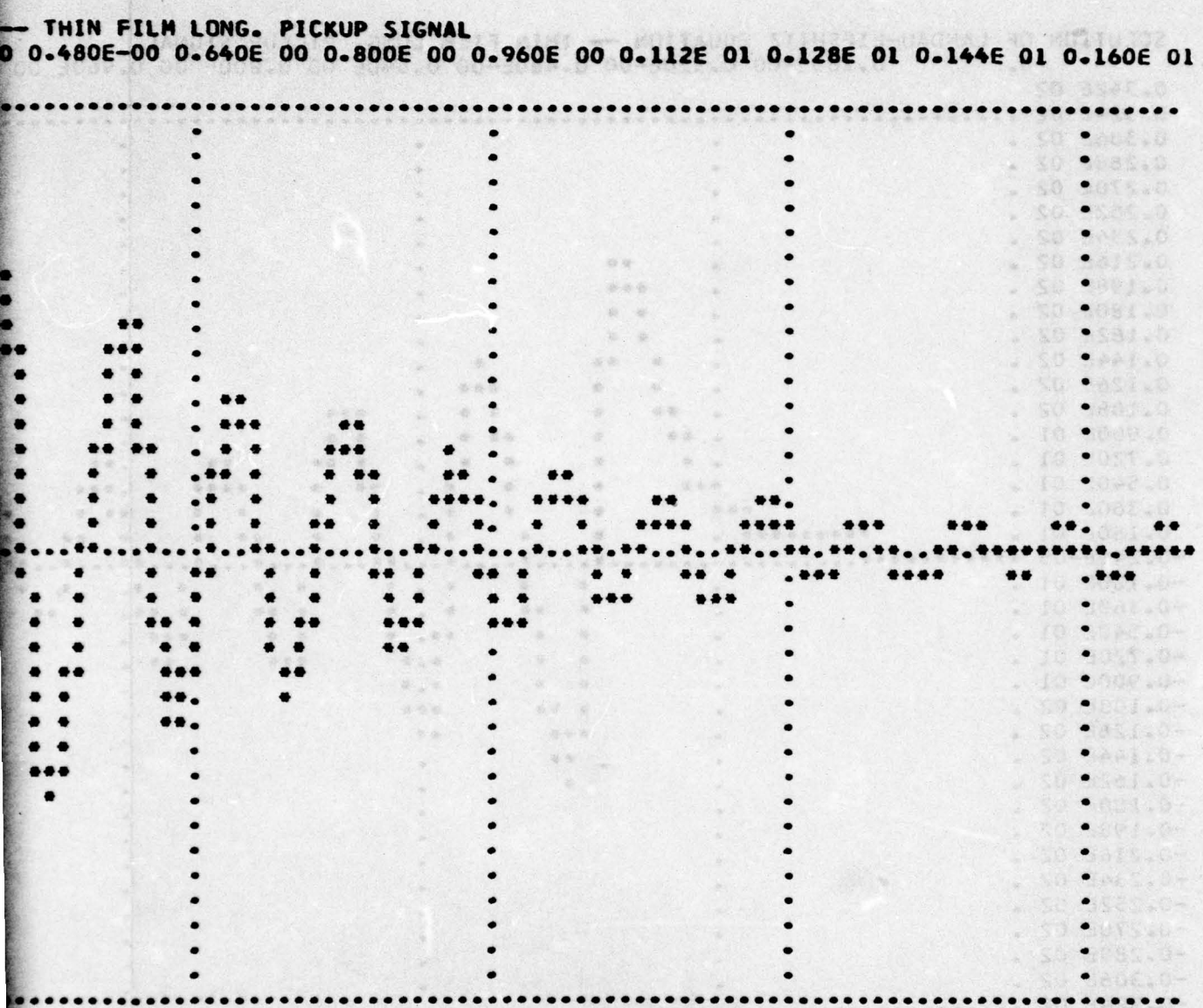


E-00 0.480E-00 0.640E 00 0.800E 00 0.960E 00 0.112E 01 0.128E 01 0.144E 01 0.160E 01
TIME(NANOSECONDS)
PHI/DT)SIN(PHI) = 0.235(DPHI/DT)SIN(PHI)
25500. (FILM CROSS SECTION,SCM) = 0.129E-04
04 LAMBDA(DAMPING,CPS) = 0.10E 09
10 DELTA = 0.
TA)35.17 SIGMA = (DELTA)0.85E 09
IL PHI,DEGREES) = 0.
21 GAMMA(GYRO RATIO) = 0.176E 08 MAX PICKUP SIG. = 0.213E 02

Fig. 81



PICKUP VOLTS = (4)(3.1416)(S)(M)(DPHI/DT)SIN(PHI) = 0.235(DPHI/DT)SIN(PHI)
M(GAUSSES) = 1450. K(ERGS/CCM) = 25500. (FILM CROSS SECTION,SCM) = 0.129
LAMBDAS(MAGNETOSTRICTION) = 0.20E-04 LAMBDA(DAMPING,CPS) = 0.10E 09
ALPHA = -1.200 BETA = 0.080 DELTA = 0.
HSWCH = (ALPHA)35.17 HPERP = (BETA)35.17 SIGMA = (DELTA)0.85E 09
HANIS = 2K/M = 35.17 PHIOD(INITIAL PHI,DEGREES) = 0.
TP(PEAKING TIME,NANOSECONDS) = 0.275 GAMMA(GYRO RATIO) = 0.176E 08 MAX PICKU



DT)SIN(PHI) = 0.235(DPHI/DT)SIN(PHI)
500. (FILM CROSS SECTION,SCM) = 0.129E-04
LAMBDA(DAMPING,CPS) = 0.10E 09

Fig. 82

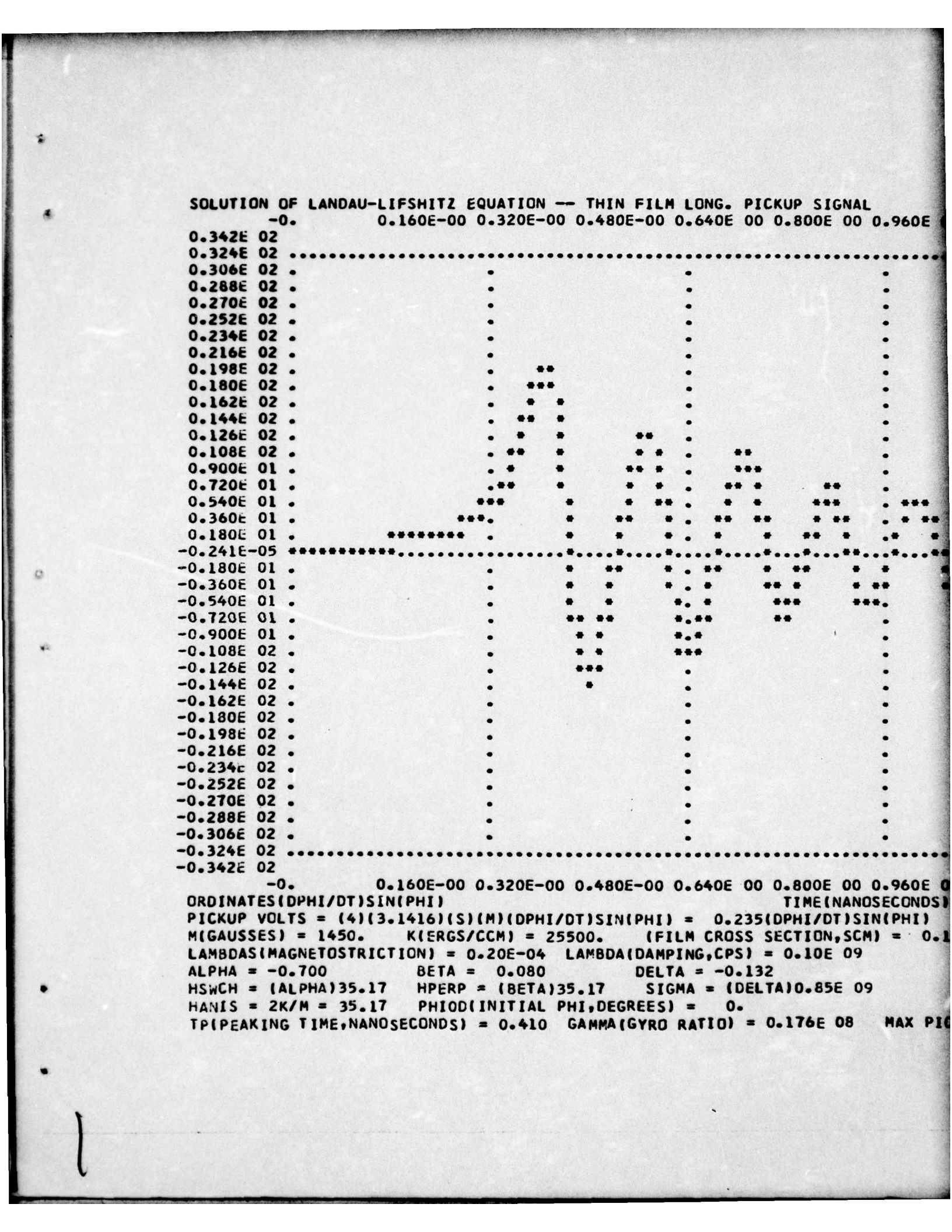
DELTA = 0.
3.17 SIGMA = (DELTA)0.85E 09
HI,DEGREES) = 0.
GAMMA(GYRO RATIO) = 0.176E 08 MAX PICKUP SIG. = 0.278E 02

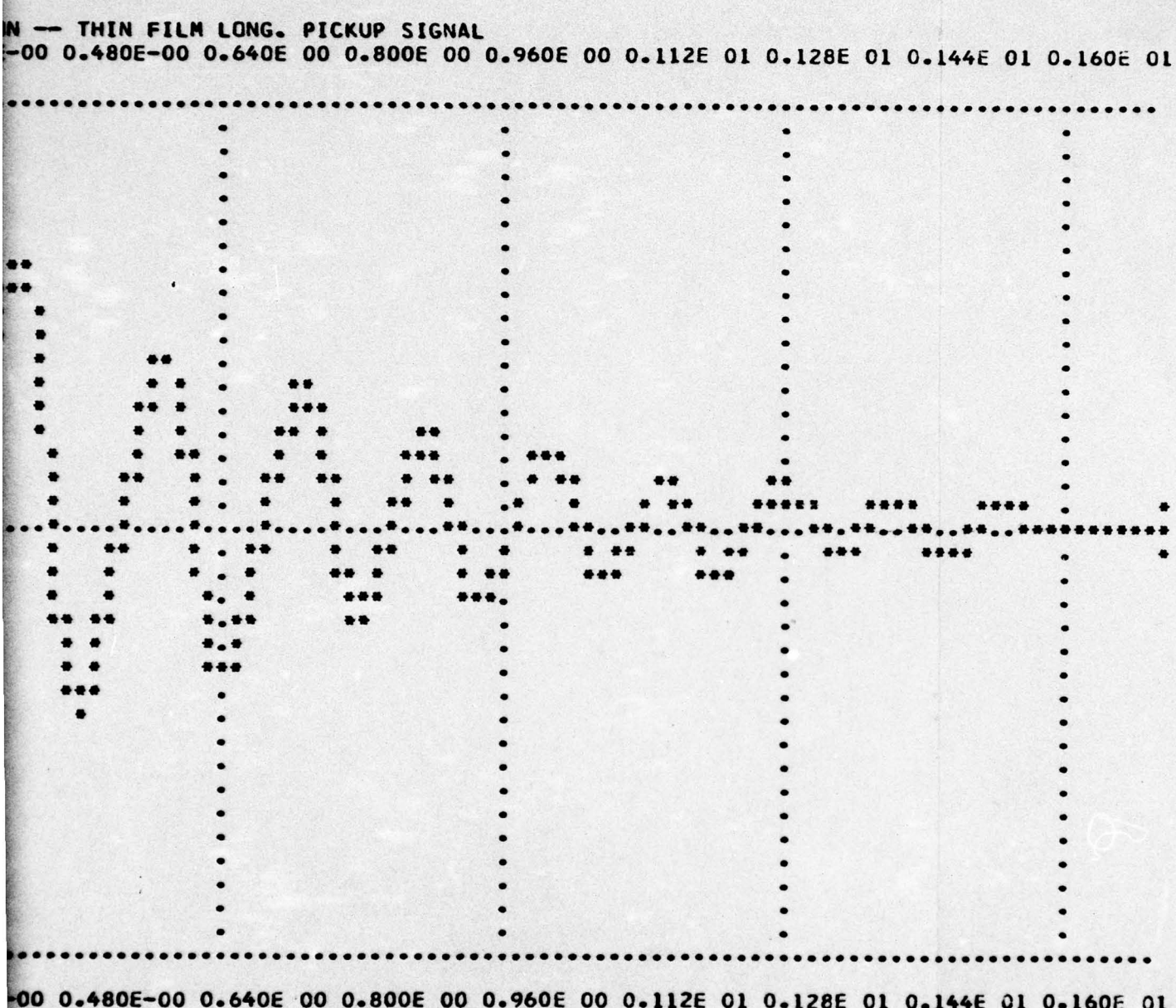
These observations show that there is little to be gained in the dynamic performance of the film beyond values of H_s and H_p, whose combined effects correspond to a switching speed in the neighborhood of 1/10 of a nanosecond.

These figures also show that the amplitude of the pickup signal increases as the switching field is increased and is higher for higher values of H_p.

Figures 83, 84, 85 and 86, 87, 88 inclusive

The dynamic responses represented by Figs. 83, 84, 85 correspond to the cases of Figs. 80, 81, 82 when a negative stress δ = - 0.132 is applied along H_p (compression). The time required for switching decreases and this decrease is more accentuated for lower values of switching field H_s. In the case of Figs. 86, 87, 88 a positive stress has been applied, Figs, 86 and 87 show that the magnetization does not reverse for H_s = - 24.5 oe (α = - 0.7) and H_s = 28.2 oe (α =-0.8), but a disturbed signal with peak occurring at 0.161 nsec. and 0.195 nsec respectively is registered in the plot description from the computation. The ordinate scale of the plot is too large to show the pickup signal corresponding to this disturbed condition. For a value of

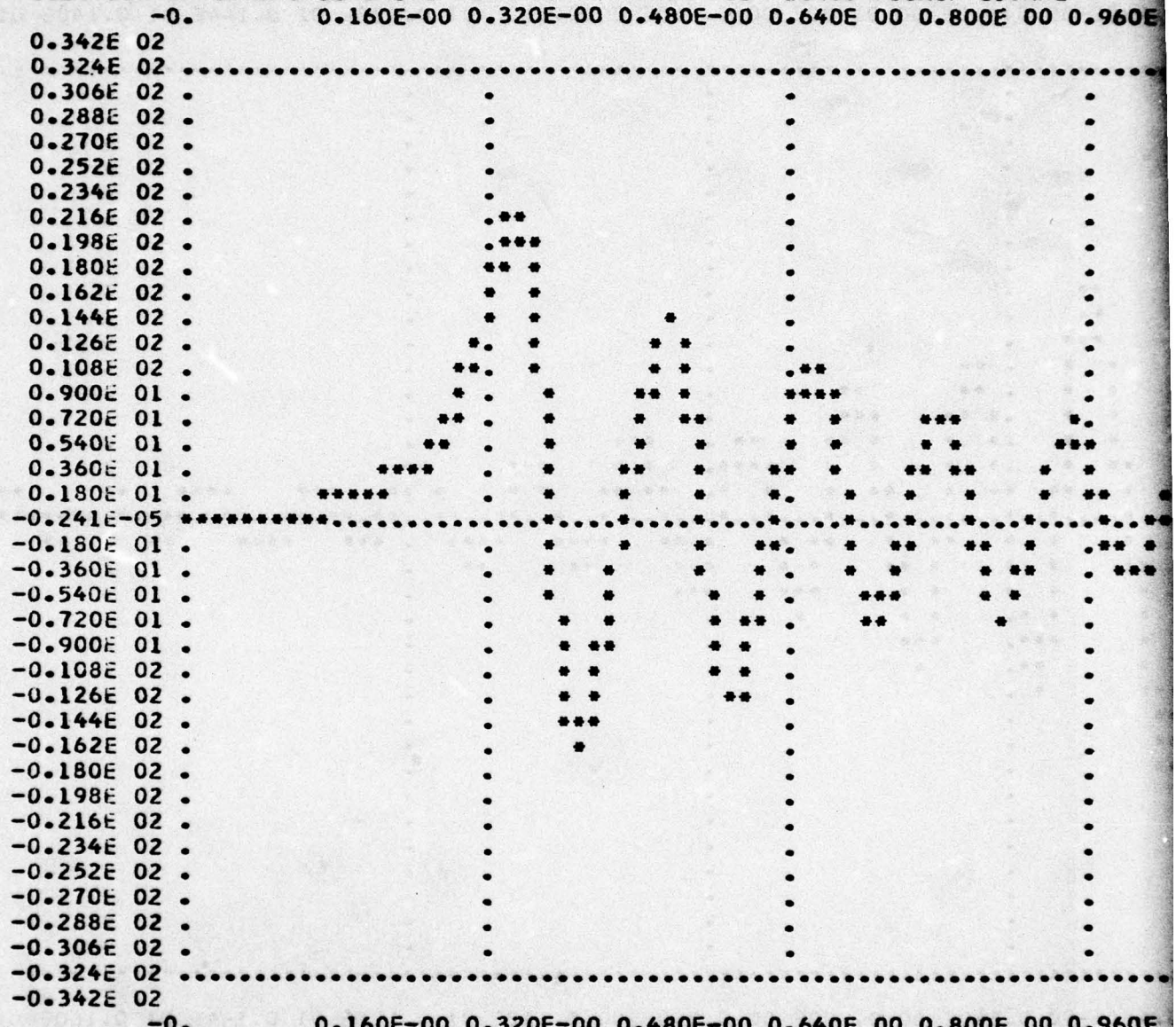

SOLUTION OF LANDAU-LIFSHITZ EQUATION -- THIN FILM LONG. PICKUP SIGNAL
-0. 0.160E-00 0.320E-00 0.480E-00 0.640E 00 0.800E 00 0.960E
0.342E 02
0.324E 02
0.306E 02
0.288E 02
0.270E 02
0.252E 02
0.234E 02
0.216E 02
0.198E 02
0.180E 02
0.162E 02
0.144E 02
0.126E 02
0.108E 02
0.900E 01
0.720E 01
0.540E 01
0.360E 01
0.180E 01
-0.241E-05
-0.180E 01
-0.360E 01
-0.540E 01
-0.720E 01
-0.900E 01
-0.108E 02
-0.126E 02
-0.144E 02
-0.162E 02
-0.180E 02
-0.198E 02
-0.216E 02
-0.234E 02
-0.252E 02
-0.270E 02
-0.288E 02
-0.306E 02
-0.324E 02
-0.342E 02
-0. 0.160E-00 0.320E-00 0.480E-00 0.640E 00 0.800E 00 0.960E 0
ORDINATES(DPHI/DT)SIN(PHI)
TIME(NANOSECONDS)
PICKUP VOLTS = (4)(3.1416)(S)(M)(DPHI/DT)SIN(PHI) = 0.235(DPHI/DT)SIN(PHI)
M(GAUSSES) = 1450. K(ERGS/CCM) = 25500. (FILM CROSS SECTION,SCM) = 0.1
LAMBDAS(MAGNETOSTRICTION) = 0.20E-04 LAMBDA(DAMPING,CPS) = 0.10E 09
ALPHA = -0.700 BETA = 0.080 DELTA = -0.132
HSWCH = (ALPHA)35.17 HPERP = (BETA)35.17 SIGMA = (DELTA)0.85E 09
HANIS = 2K/M = 35.17 PHIOD(INITIAL PHI,DEGREES) = 0.
TP(PEAKING TIME,NANOSECONDS) = 0.410 GAMMA(GYRO RATIO) = 0.176E 08 MAX PI



I/DT)SIN(PHI) = 0.235(DPHI/DT)SIN(PHI)
25500. (FILM CROSS SECTION,SCM) = 0.129E-04
LAMBDA(DAMPING,CPS) = 0.10E 09
DELTA = -0.132
)35.17 SIGMA = (DELTA)0.85E 09
PHI,DEGREES) = 0.
GAMMA(GYRO RATIO) = 0.176E 08 MAX PICKUP SIG. = 0.200E 02

Fig. 83

SOLUTION OF LANDAU-LIFSHITZ EQUATION -- THIN FILM LONG. PICKUP SIGNAL



ORDINATES(DPHI/DT)SIN(PHI) TIME(NANOSECONDS

PICKUP VOLTS = (4)(3.1416)(S)(M)(DPHI/DT)SIN(PHI) = 0.235(DPHI/DT)SIN(PHI)

M(GAUSSES) = 1450. K(ERGS/CCM) = 25500. (FILM CROSS SECTION,SCM) = 0.

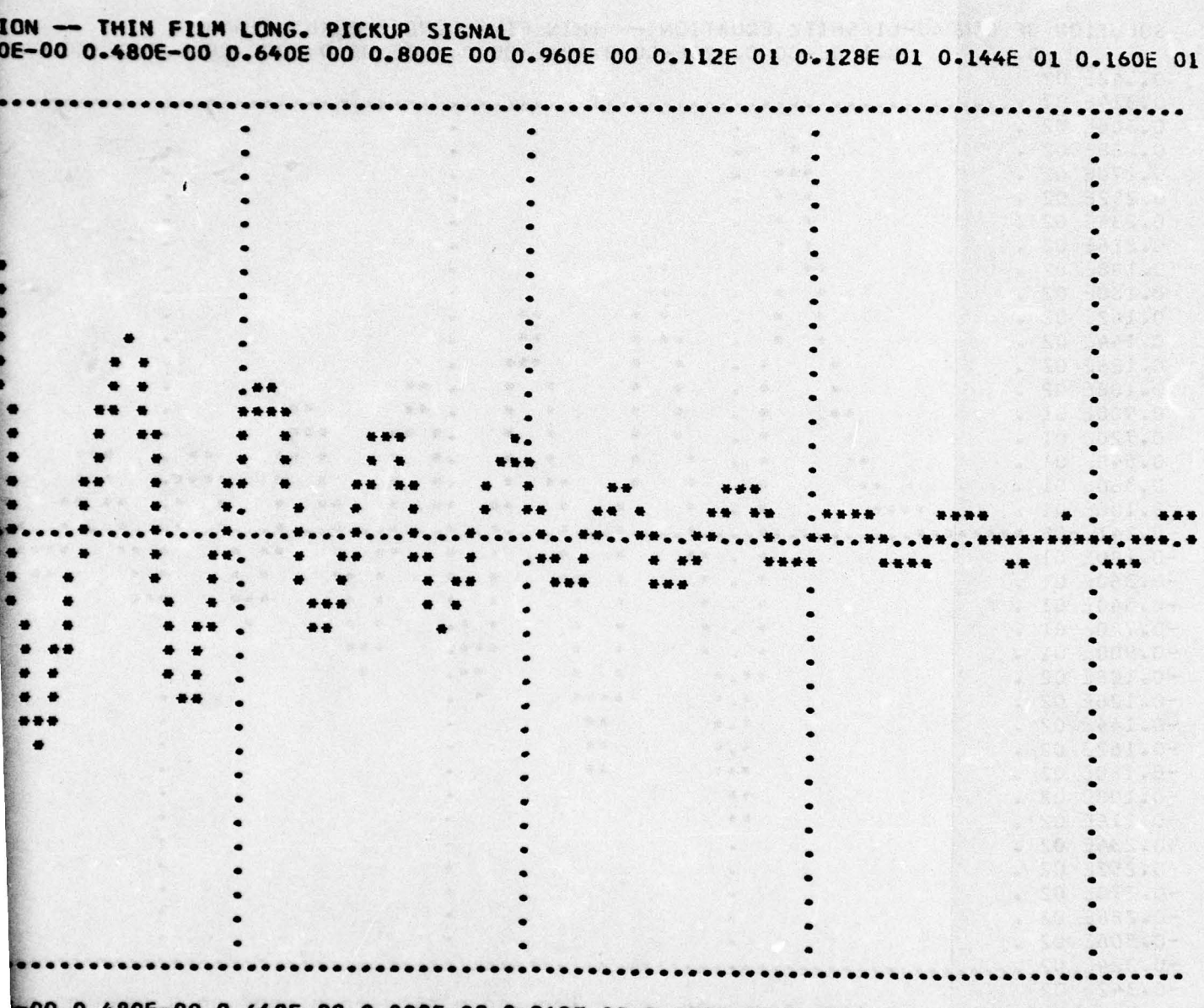
LAMBDAS(MAGNETOSTRICTION) = 0.20E-04 LAMBDA(DAMPING,CPS) = 0.10E 09

ALPHA = -0.800 BETA = 0.080 DELTA = -0.132

HSWCH = (ALPHA)35.17 HPERP = (BETA)35.17 SIGMA = (DELTA)0.85E 09

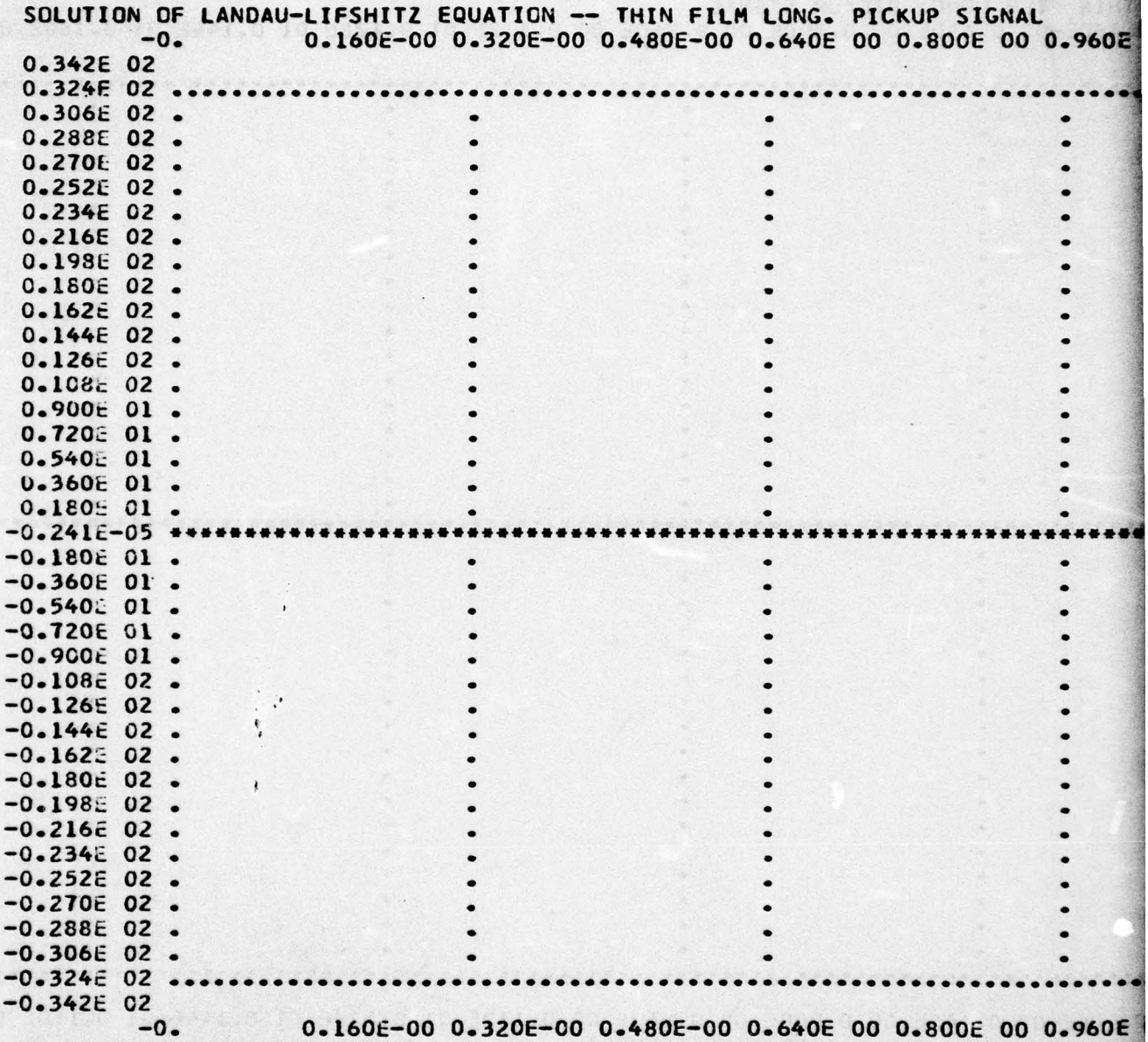
HANIS = 2K/M = 35.17 PHIOD(INITIAL PHI,DEGREES) = 0.

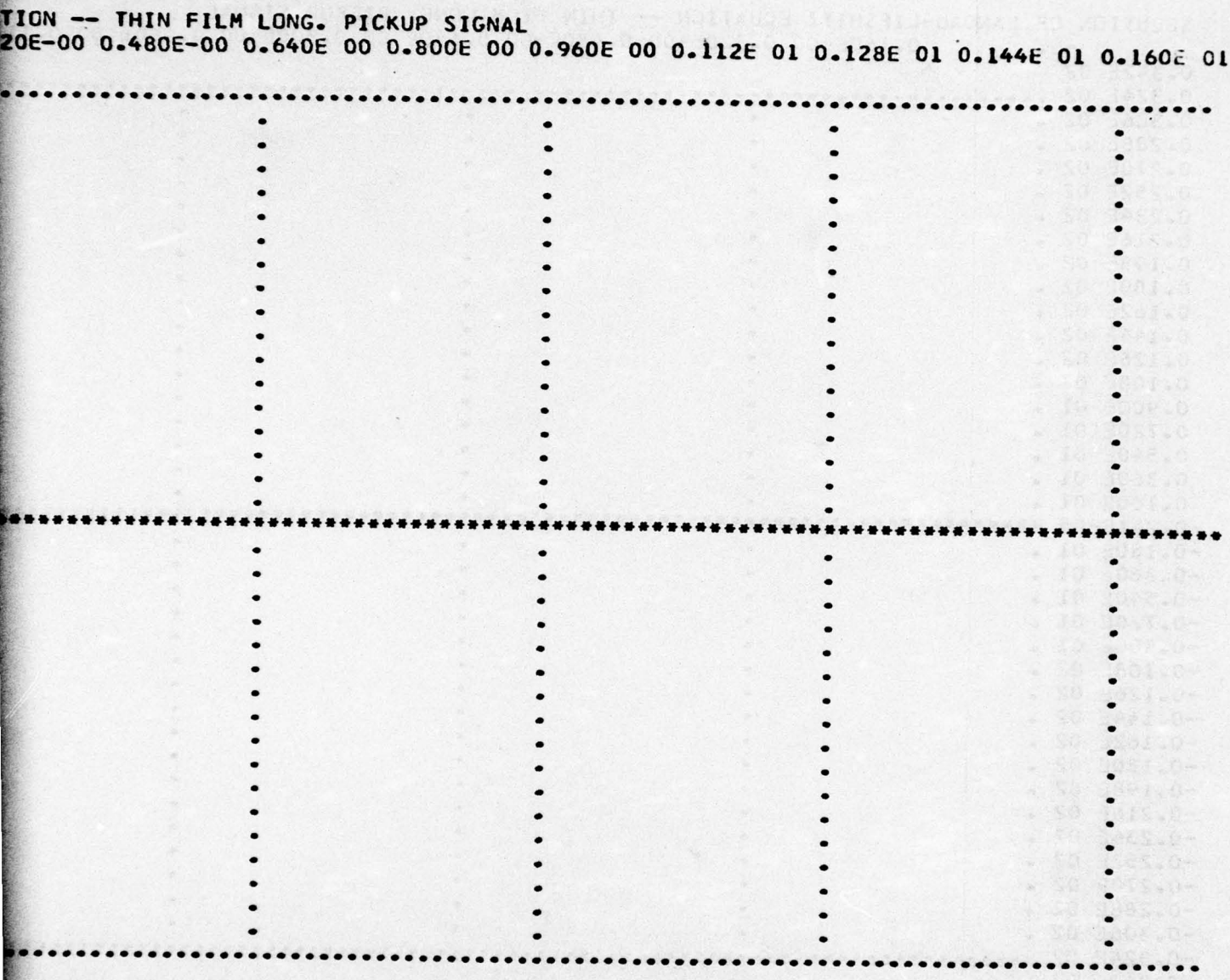
TP(PEAKING TIME,NANOSECONDS) = 0.350 GAMMA(GYRO RATIO) = 0.176E 08 MAX PI



HI/DT)SIN(PHI) = 0.235(DPHI/DT)SIN(PHI)
25500. (FILM CROSS SECTION,SCM) = 0.129E-04
LAMBDA(DAMPING,CPS) = 0.10E 09
DELTA = -0.132
A)35.17 SIGMA = (DELTA)0.85E 09
PHI,DEGREES) = 0.
GAMMA(GYRO RATIO) = 0.176E 08 MAX PICKUP SIG. = 0.218E 02

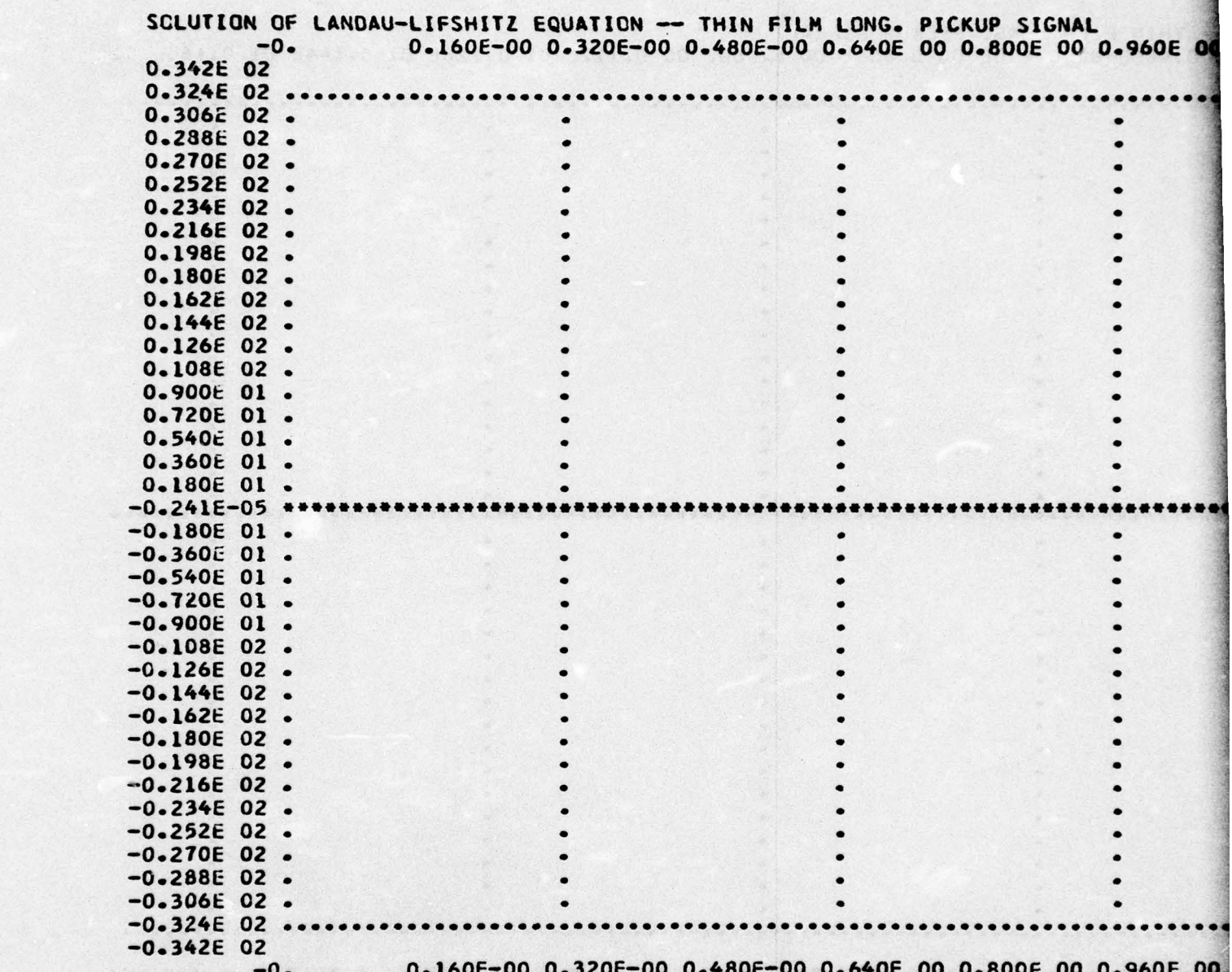
Fig. 84


SOLUTION OF LANDAU-LIFSHITZ EQUATION -- THIN FILM LONG. PICKUP SIGNAL
-0. 0.160E-00 0.320E-00 0.480E-00 0.640E 00 0.800E 00 0.960E
0.342E 02
0.324E 02
0.306E 02
0.288E 02
0.270E 02
0.252E 02
0.234E 02
0.216E 02
0.198E 02
0.180E 02
0.162E 02
0.144E 02
0.126E 02
0.108E 02
0.900E 01
0.720E 01
0.540E 01
0.360E 01
0.180E 01
-0.241E-05
-0.180E 01
-0.360E 01
-0.540E 01
-0.720E 01
-0.900E 01
-0.108E 02
-0.126E 02
-0.144E 02
-0.162E 02
-0.180E 02
-0.198E 02
-0.216E 02
-0.234E 02
-0.252E 02
-0.270E 02
-0.288E 02
-0.306E 02
-0.324E 02
-0.342E 02
-0. 0.160E-00 0.320E-00 0.480E-00 0.640E 00 0.800E 00 0.960E
ORDINATES(DPHI/DT)SIN(PHI)
TIME(NANOSECONDS
PICKUP VOLTS = (4)(3.1416)(S)(M)(DPHI/DT)SIN(PHI) = 0.235(DPHI/DT)SIN(PHI)
M(GAUSSES) = 1450. K(ERGS/CCM) = 25500. (FILM CROSS SECTION,SCM) = 0.
LAMBDAS(MAGNETOSTRICTION) = 0.20E-04 LAMBDA(DAMPING,CPS) = 0.10E 09
ALPHA = -0.700 BETA = 0.080 DELTA = 0.132
HSWCH = (ALPHA)35.17 HPERP = (BETA)35.17 SIGMA = (DELTA)0.85E 09
HANIS = 2K/M = 35.17 PHIOD(INITIAL PHI,DEGREES) = 0.
TP(PEAKING TIME,NANOSECONDS) = 0.161 GAMMA(GYRO RATIO) = 0.176E 08 MAX PI



PHI/DT)SIN(PHI) = 0.235(DPHI/DT)SIN(PHI)
= 25500. (FILM CROSS SECTION,SCM) = 0.129E-04
-04 LAMBDA(DAMPING,CPS) = 0.10E 09
080 DELTA = 0.132
ETA)35.17 SIGMA = (DELTA)0.85E 09
IAL PHI,DEGREES) = 0.
161 GAMMA(GYRO RATIO) = 0.176E 08 MAX PICKUP SIG. = 0.444E-00

Fig. 86



PICKUP VOLTS = (4)(3.1416)(S)(M)(DPHI/DT)SIN(PHI) = 0.235(DPHI/DT)SIN(PHI)

M(GAUSSES) = 1450. K(ERGS/CCM) = 25500. (FILM CROSS SECTION,SCM) = 0.12

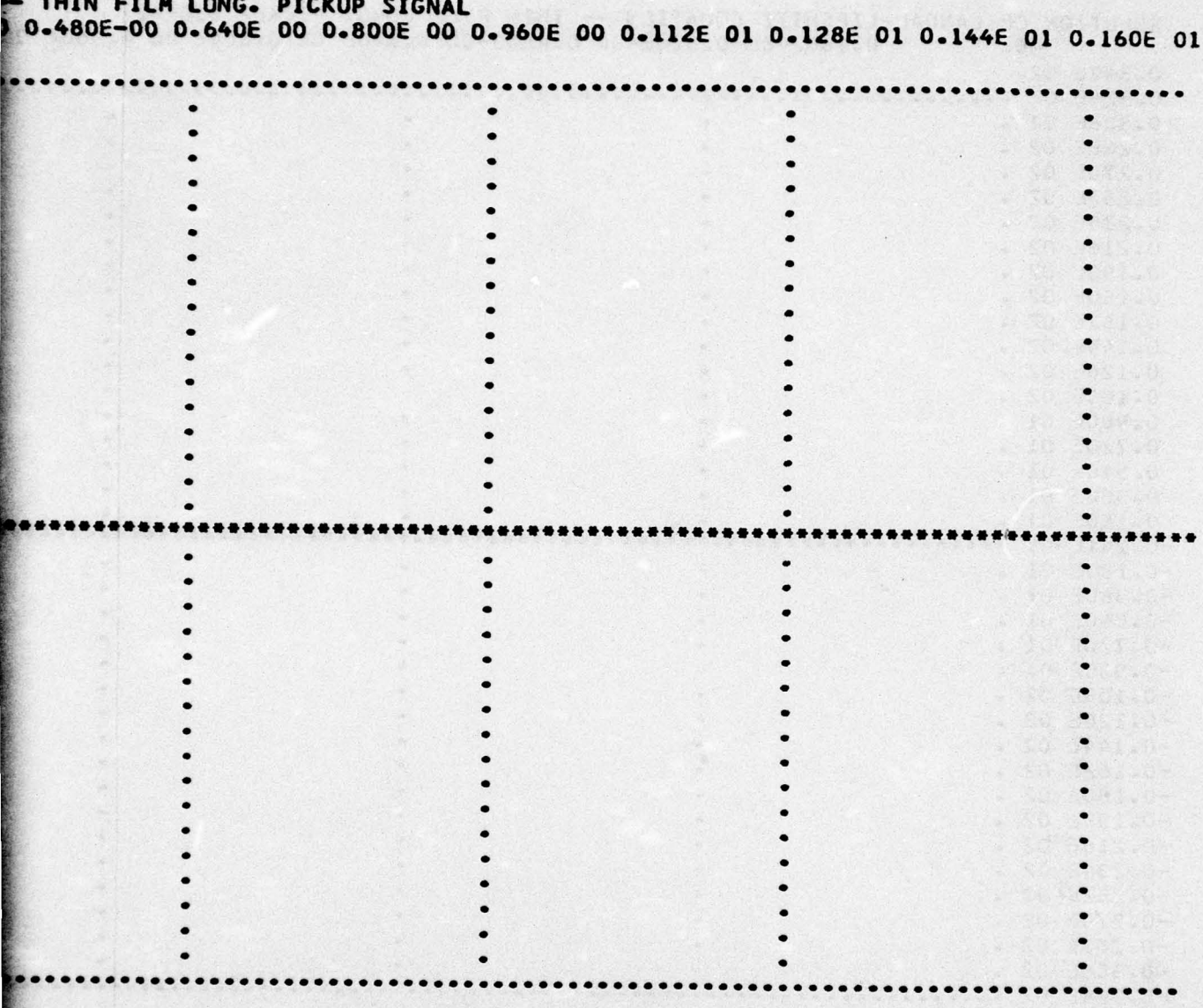
LAMBDAS(MAGNETOSTRICTION) = 0.20E-04 LAMBDA(DAMPING,CPS) = 0.10E 09

ALPHA = -0.800 BETA = 0.080 DELTA = 0.132

HSWCH = (ALPHA)35.17 HPERP = (BETA)35.17 SIGMA = (DELTA)0.85E 09

HANIS = 2K/M = 35.17 PHIOD(INITIAL PHI,DEGREES) = 0.

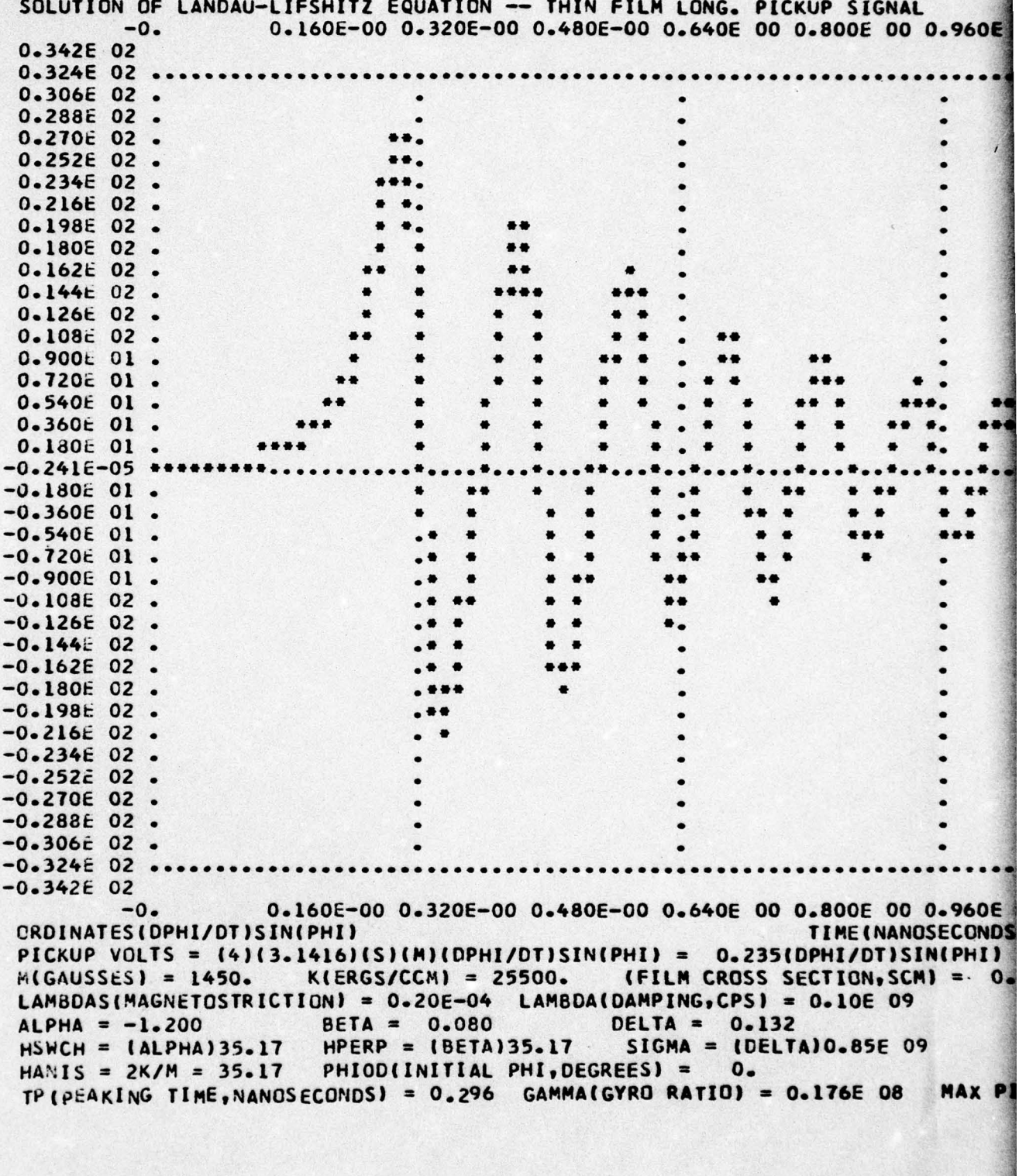
TP(PEAKING TIME,NANOSECONDS) = 0.195 GAMMA(GYRO RATIO) = 0.176E 08 MAX PICK

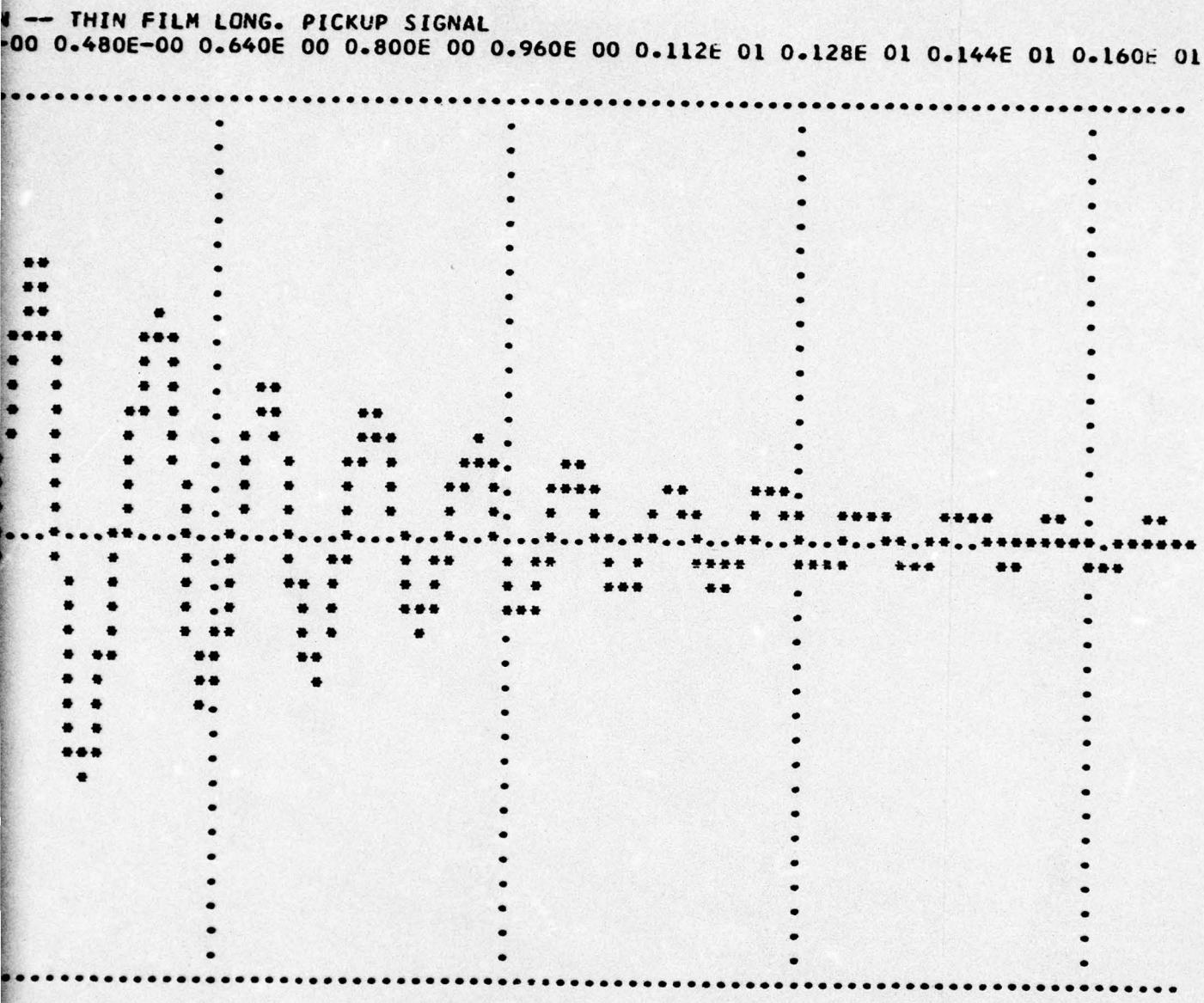


T)SIN(PHI) = 0.235(DPHI/DT)SIN(PHI)
00. (FILM CROSS SECTION,SCM) = 0.129E-04
AMBDA(DAMPING,CPS) = 0.10E 09
DELTA = 0.132
.17 SIGMA = (DELTA)0.85E 09
I,DEGREES) = 0.
AMMA(GYRO RATIO) = 0.176E 08 MAX PICKUP SIG. = 0.674E 00

Fig. 87

2


SOLUTION OF LANDAU-LIFSHITZ EQUATION -- THIN FILM LONG. PICKUP SIGNAL
-0. 0.160E-00 0.320E-00 0.480E-00 0.640E 00 0.800E 00 0.960E
0.342E 02
0.324E 02
0.306E 02
0.288E 02
0.270E 02
0.252E 02
0.234E 02
0.216E 02
0.198E 02
0.180E 02
0.162E 02
0.144E 02
0.126E 02
0.108E 02
0.900E 01
0.720E 01
0.540E 01
0.360E 01
0.180E 01
-0.241E-05
-0.180E 01
-0.360E 01
-0.540E 01
-0.720E 01
-0.900E 01
-0.108E 02
-0.126E 02
-0.144E 02
-0.162E 02
-0.180E 02
-0.198E 02
-0.216E 02
-0.234E 02
-0.252E 02
-0.270E 02
-0.288E 02
-0.306E 02
-0.324E 02
-0.342E 02
-0. 0.160E-00 0.320E-00 0.480E-00 0.640E 00 0.800E 00 0.960E
ORDINATES(DPHI/DT)SIN(PHI)
TIME(NANOSECONDS
PICKUP VOLTS = (4)(3.1416)(S)(M)(DPHI/DT)SIN(PHI) = 0.235(DPHI/DT)SIN(PHI)
M(GAUSSES) = 1450. K(ERGS/CCM) = 25500. (FILM CROSS SECTION,SCM) = 0.
LAMBDAS(MAGNETOSTRICTION) = 0.20E-04 LAMBDA(DAMPING,CPS) = 0.10E 09
ALPHA = -1.200 BETA = 0.080 DELTA = 0.132
HSWCH = (ALPHA)35.17 HPERP = (BETA)35.17 SIGMA = (DELTA)0.85E 09
HANIS = 2K/M = 35.17 PHIOD(INITIAL PHI,DEGREES) = 0.
TP(PEAKING TIME,NANOSECONDS) = 0.296 GAMMA(GYRO RATIO) = 0.176E 08 MAX PI



I/DT)SIN(PHI) = 0.235(DPHI/DT)SIN(PHI)
25500. (FILM CROSS SECTION,SCM) = 0.129E-04
LAMBDA(DAMPING,CPS) = 0.10E 09
DELTA = 0.132
)35.17 SIGMA = (DELTA)0.85E 09
PHI,DEGREES) = 0.
GAMMA(GYRO RATIO) = 0.176E 08 MAX PICKUP SIG. = 0.274E 02

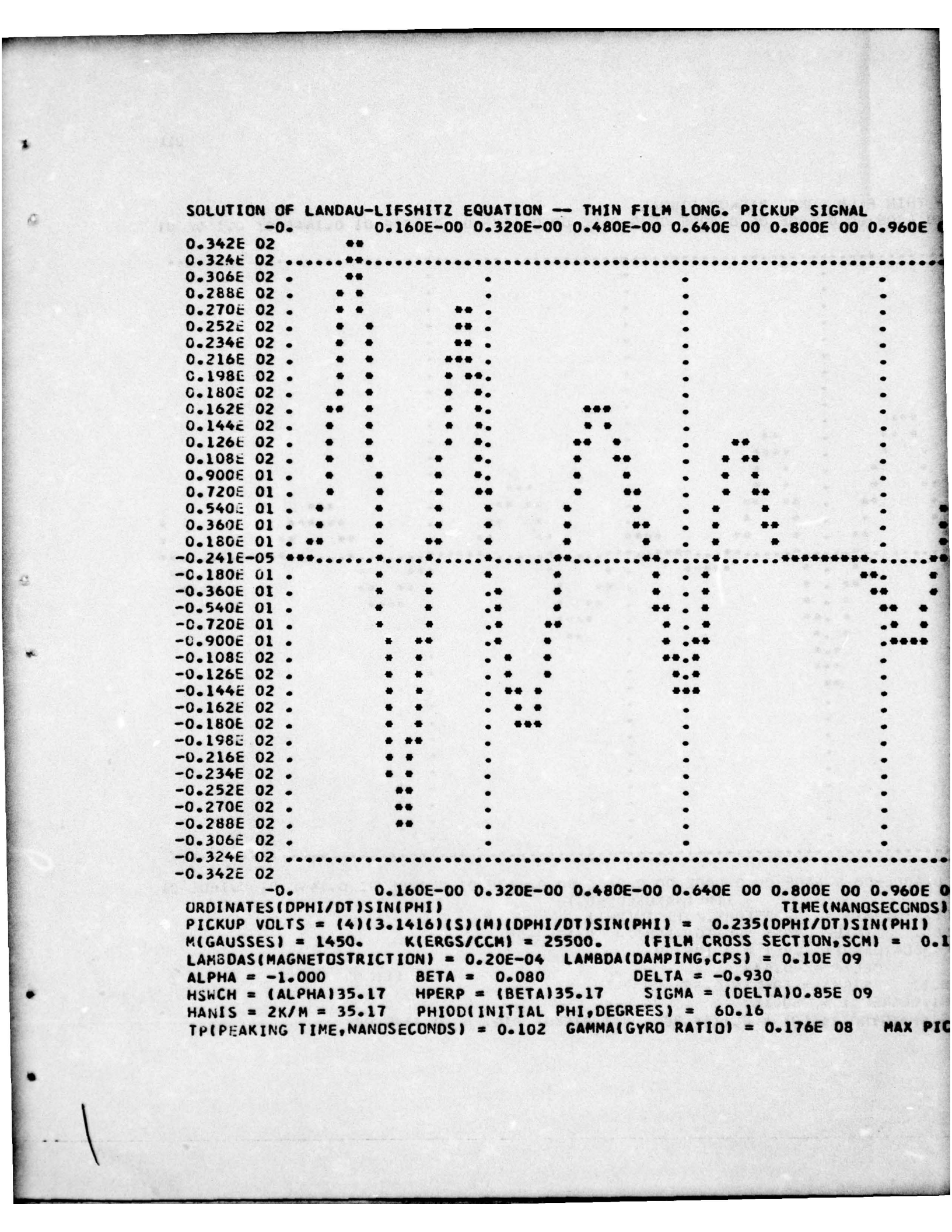
Fig. 88

H_s between - 28.2 oe and - 42 oe the peaking time occurs at 0.296 nsec.

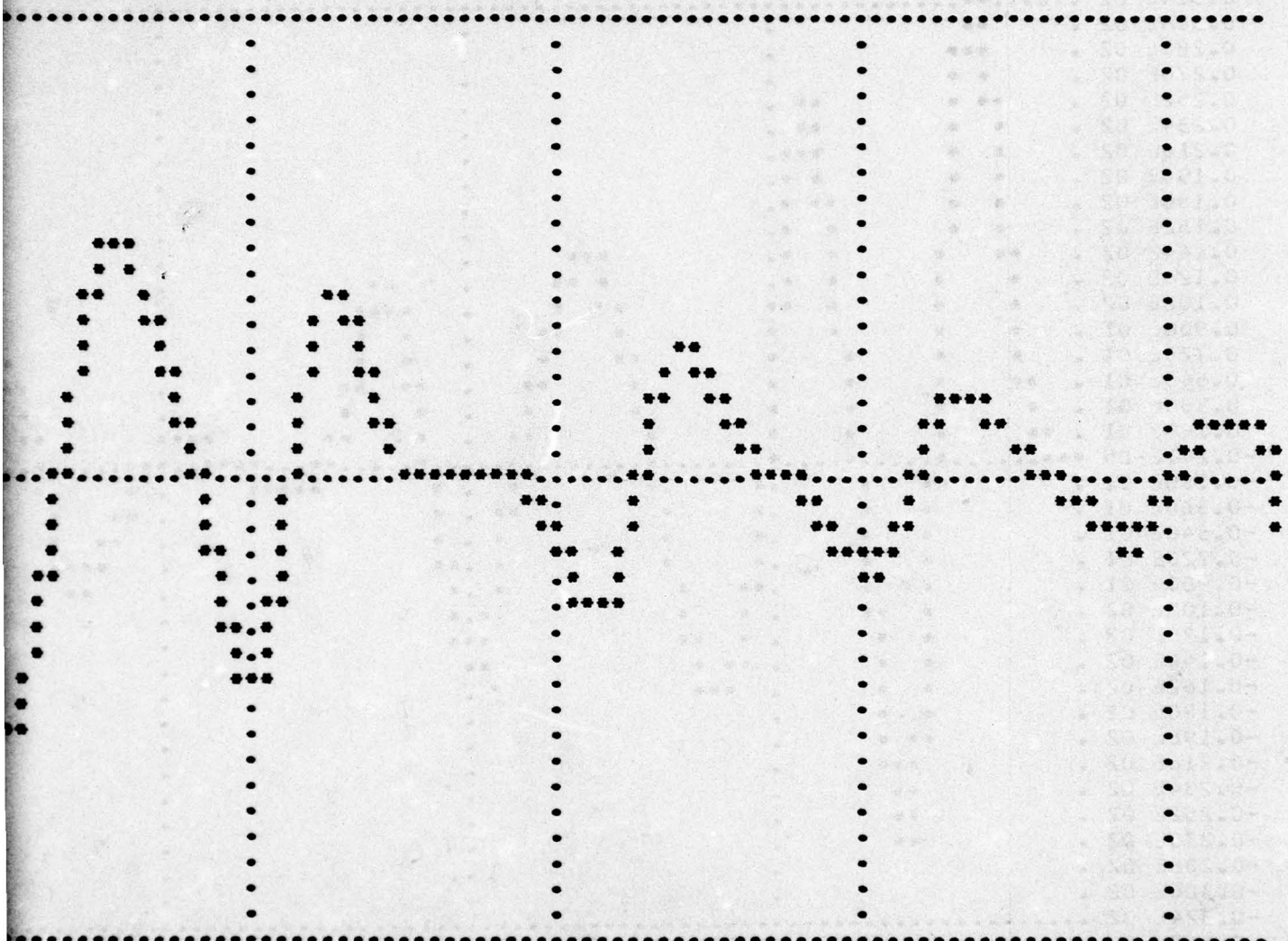
These observations show the effect of an applied stress in changing the switching threshold of the film. This is to be expected since the anisotropy constant of the film depends upon the sign and the magnitude of an applied stress, for a given value of the magnetostriction coefficient. The possibility of controlling the switching threshold by an applied stress would be of interest in applications requiring controlled changes from non destructive to destructive read operation and vice versa.

Figures 89, 90, 91 inclusive.

In the figures the initial angle ϕ_o has been made equal to 60° and the normalized stress δ is decreased from - 0.930 to - 0.132 with a perpendicular field β = 0.08 and the switching field kept at α = - 1. Comparing these plots to identical cases in Figs. 70, 71, 72, except for the value of ϕ_o = 0, it is apparent that as ϕ_o is increased the pickup signal is higher and switching is faster. This observation is reasonable considering that as ϕ_o increases the initial torque acting on M is higher and switching must consequently be faster, all other conditions remaining the same.

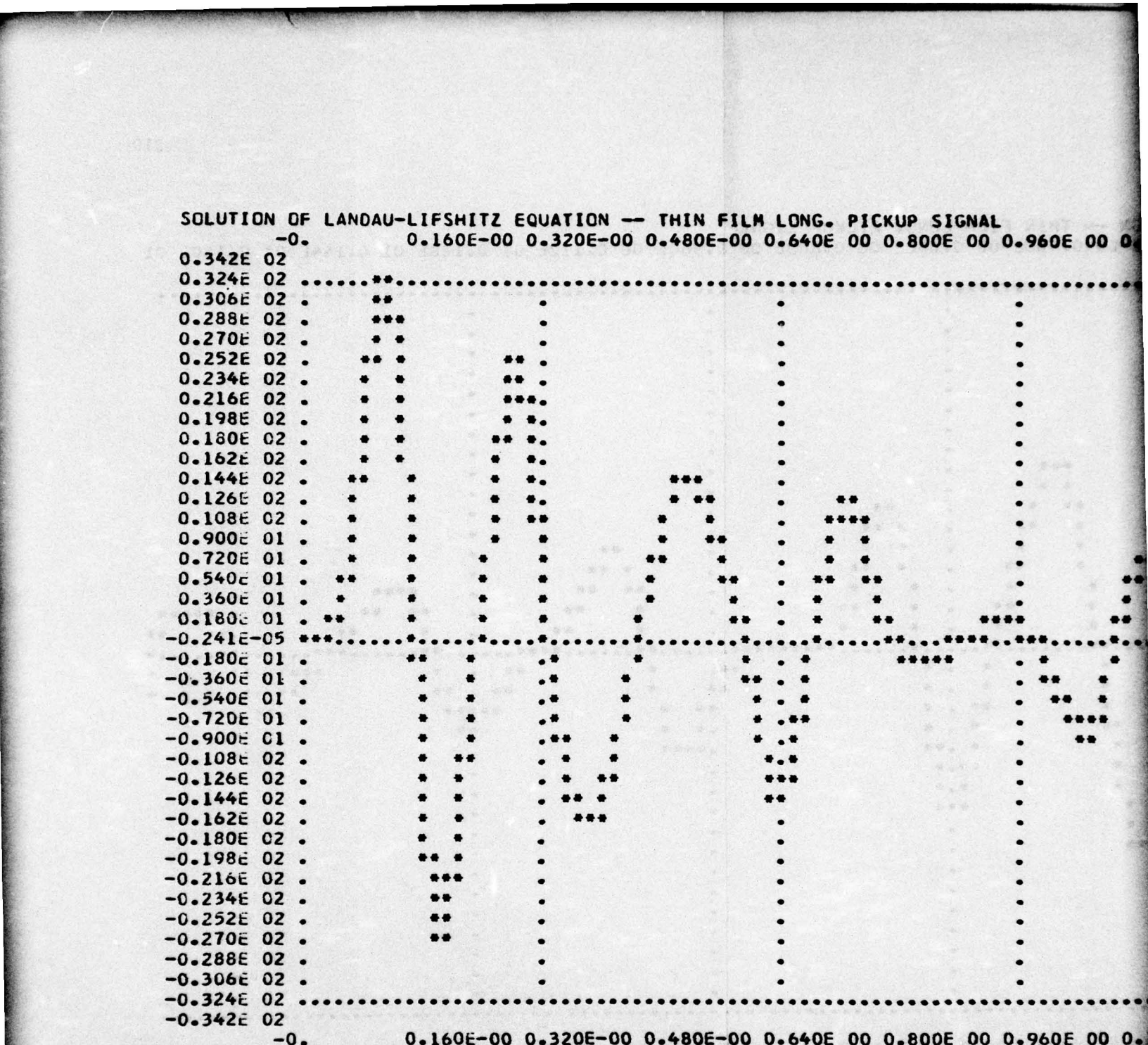

SOLUTION OF LANDAU-LIFSHITZ EQUATION -- THIN FILM LONG. PICKUP SIGNAL
-0. 0.160E-00 0.320E-00 0.480E-00 0.640E 00 0.800E 00 0.960E
0.342E 02
0.324E 02
0.306E 02
0.288E 02
0.270E 02
0.252E 02
0.234E 02
0.216E 02
0.198E 02
0.180E 02
0.162E 02
0.144E 02
0.126E 02
0.108E 02
0.900E 01
0.720E 01
0.540E 01
0.360E 01
0.180E 01
-0.241E-05
-0.180E 01
-0.360E 01
-0.540E 01
-0.720E 01
-0.900E 01
-0.108E 02
-0.126E 02
-0.144E 02
-0.162E 02
-0.180E 02
-0.198E 02
-0.216E 02
-0.234E 02
-0.252E 02
-0.270E 02
-0.288E 02
-0.306E 02
-0.324E 02
-0.342E 02
-0. 0.160E-00 0.320E-00 0.480E-00 0.640E 00 0.800E 00 0.960E 0
ORDINATES(DPHI/DT)SIN(PHI) TIME(NANOSECONDS)
PICKUP VOLTS = (4)(3.1416)(S)(M)(DPHI/DT)SIN(PHI) = 0.235(DPHI/DT)SIN(PHI)
M(GAUSSES) = 1450. K(ERGS/CCM) = 25500. (FILM CROSS SECTION,SCM) = 0.1
LAMBDAS(MAGNETOSTRICTION) = 0.20E-04 LAMBDA(DAMPING,CPS) = 0.10E 09
ALPHA = -1.000 BETA = 0.080 DELTA = -0.930
HSWCH = (ALPHA)35.17 HPERP = (BETA)35.17 SIGMA = (DELTA)0.85E 09
HANIS = 2K/M = 35.17 PHIOD(INITIAL PHI,DEGREES) = 60.16
TP(PEAKING TIME,NANOSECONDS) = 0.102 GAMMA(GYRO RATIO) = 0.176E 08 MAX PIC

ON — THIN FILM LONG. PICKUP SIGNAL
E-00 0.480E-00 0.640E 00 0.800E 00 0.960E 00 0.112E 01 0.128E 01 0.144E 01 0.160E 01



E-00 0.480E-00 0.640E 00 0.800E 00 0.960E 00 0.112E 01 0.128E 01 0.144E 01 0.160E 01
TIME(NANOSECONDS)
HI/DT)SIN(PHI) = 0.235(DPHI/DT)SIN(PHI)
25500. (FILM CROSS SECTION,SCM) = 0.129E-04
4 LAMBDA(DAMPING,CPS) = 0.10E 09
0 DELTA = -0.930
A)35.17 SIGMA = (DELTA)0.85E 09
L PHI,DEGREES) = 60.16
2 GAMMA(GYRO RATIO) = 0.176E 08 MAX PICKUP SIG. = 0.354E 02

Fig. 89



PICKUP VOLTS = (4)(3.1416)(S)(M)(DPHI/DT)SIN(PHI) = 0.235(DPHI/DT)SIN(PHI)

M(GAUSSES) = 1450. K(ERGS/CCM) = 25500. (FILM CROSS SECTION,SCM) = 0.129E-

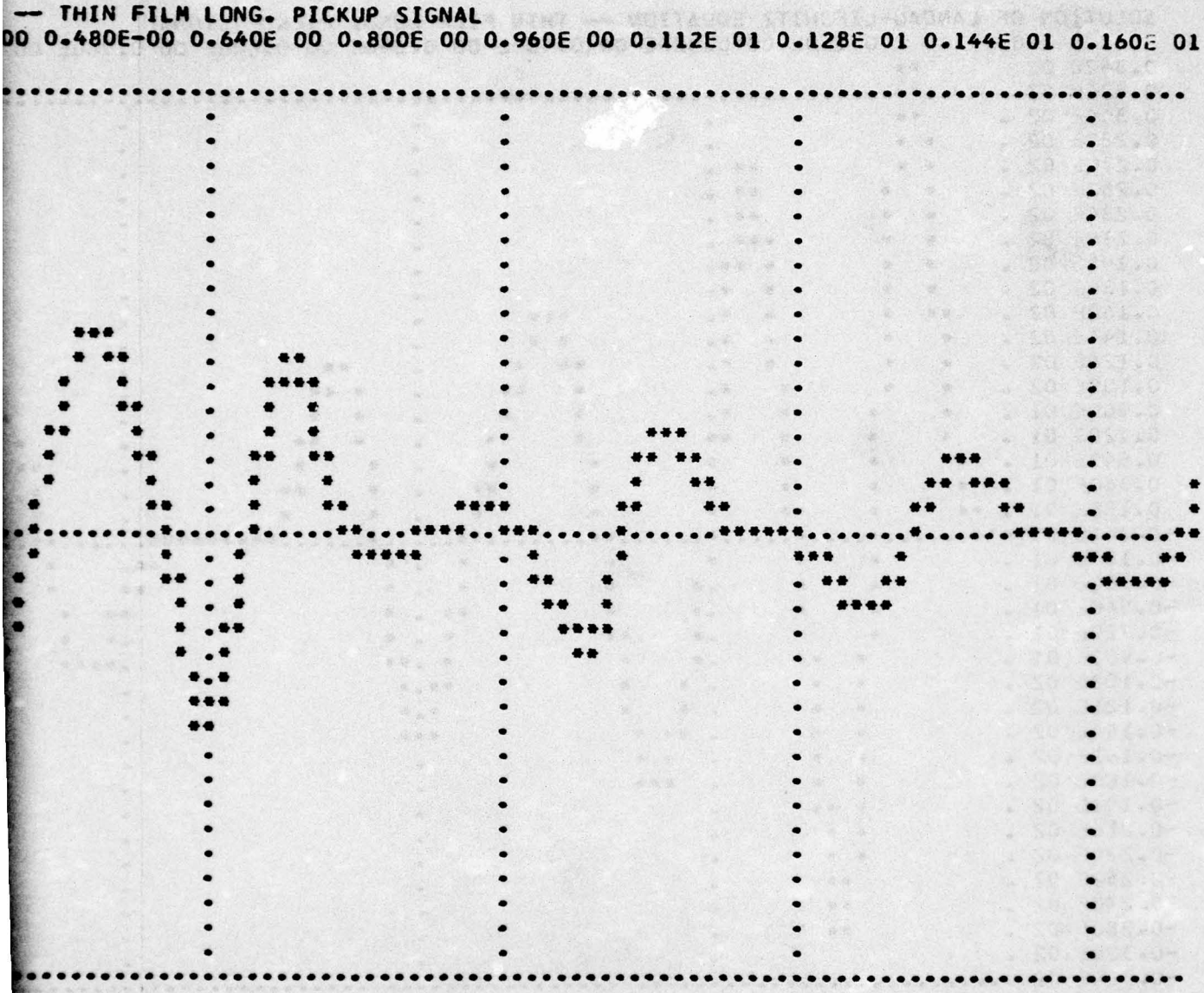
LAMBDAS(MAGNETOSTRICTION) = 0.20E-04 LAMBDA(DAMPING,CPS) = 0.10E 09

ALPHA = -1.000 BETA = 0.080 DELTA = -0.532

HSWCH = (ALPHA)35.17 HPERP = (BETA)35.17 SIGMA = (DELTA)0.85E 09

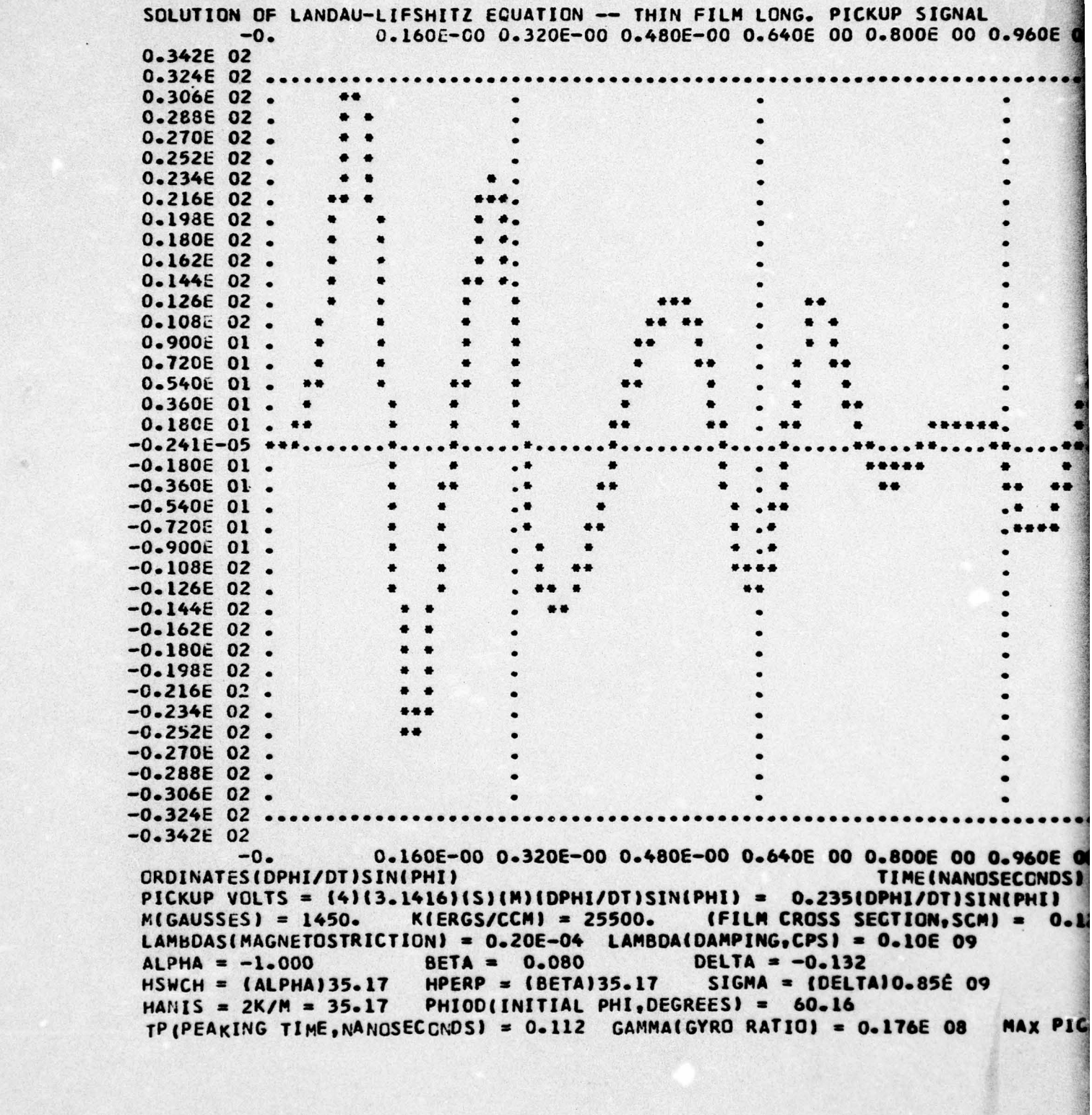
HANIS = 2K/M = 35.17 PHIOD(INITIAL PHI,DEGREES) = 60.16

TP(PEAKING TIME,NANOSECONDS) = 0.107 GAMMA(GYRO RATIO) = 0.176E 08 MAX PICKUP



(DT)SIN(PHI) = 0.235(DPHI/DT)SIN(PHI)
500. (FILM CROSS SECTION,SCM) = 0.129E-04
LAMBDA(DAMPING,CPS) = 0.10E 09
DELTA = -0.532
5.17 SIGMA = (DELTA)0.85E 09
HI,DEGREES) = 60.16
GAMMA(GYRO RATIO) = 0.176E 08 MAX PICKUP SIG. = 0.333E 02

Fig. 90



PICKUP VOLTS = (4)(3.1416)(S)(M)(DPHI/DT)SIN(PHI) = 0.235(DPHI/DT)SIN(PHI)

M(GAUSSES) = 1450. K(ERGS/CCM) = 25500. (FILM CROSS SECTION,SCM) = 0.1

LAMBDAS(MAGNETOSTRICTION) = 0.20E-04 LAMBDA(DAMPING,CPS) = 0.10E 09

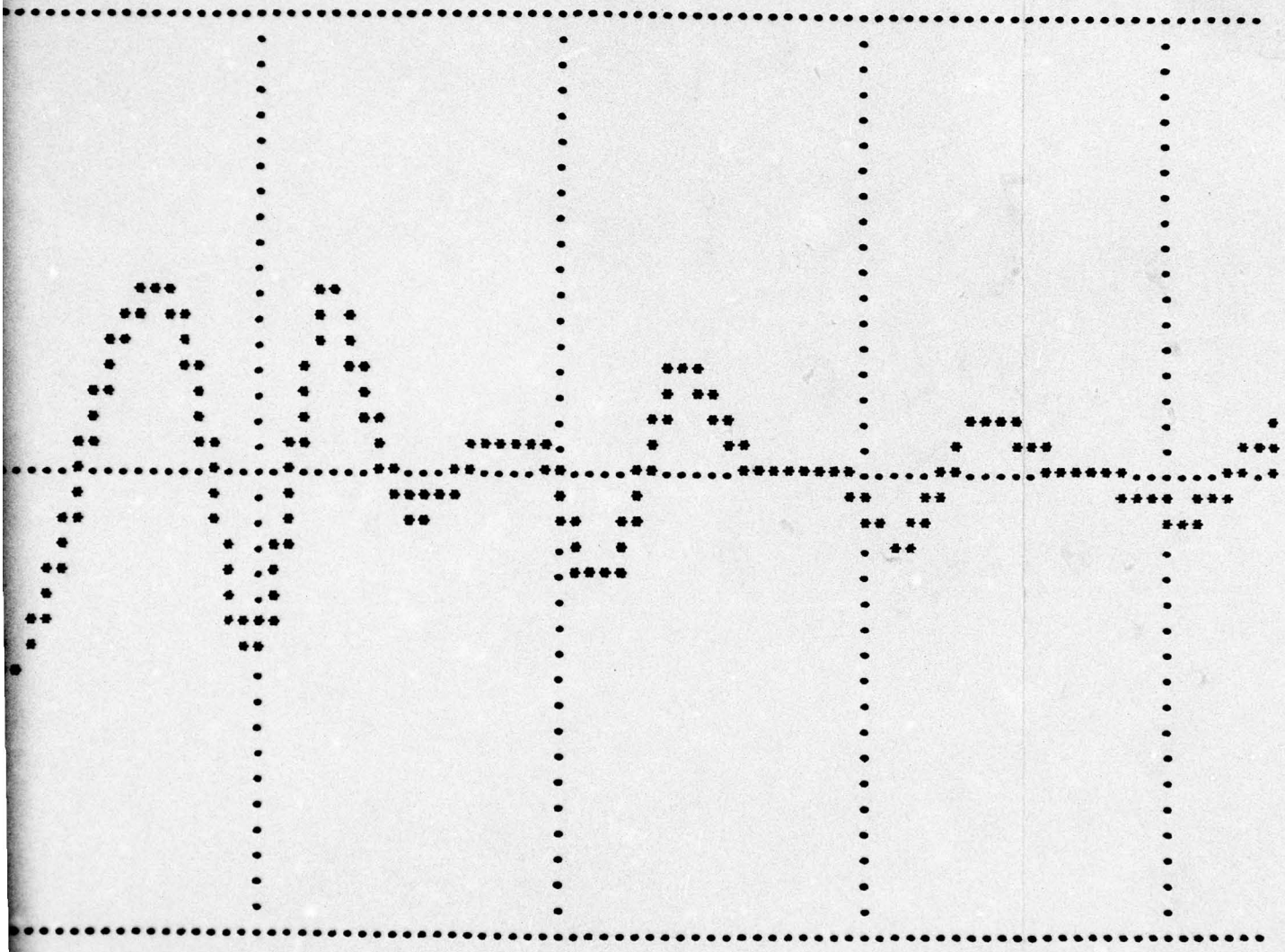
ALPHA = -1.000 BETA = 0.080 DELTA = -0.132

HSWCH = (ALPHA)35.17 HPERP = (BETA)35.17 SIGMA = (DELTA)0.85E 09

HANIS = 2K/M = 35.17 PHIOD(INITIAL PHI,DEGREES) = 60.16

TP(PEAKING TIME,NANOSECONDS) = 0.112 GAMMA(GYRO RATIO) = 0.176E 08 MAX PIC

ION -- THIN FILM LONG. PICKUP SIGNAL
0E-00 0.480E-00 0.640E 00 0.800E 00 0.960E 00 0.112E 01 0.128E 01 0.144E 01 0.160E 01



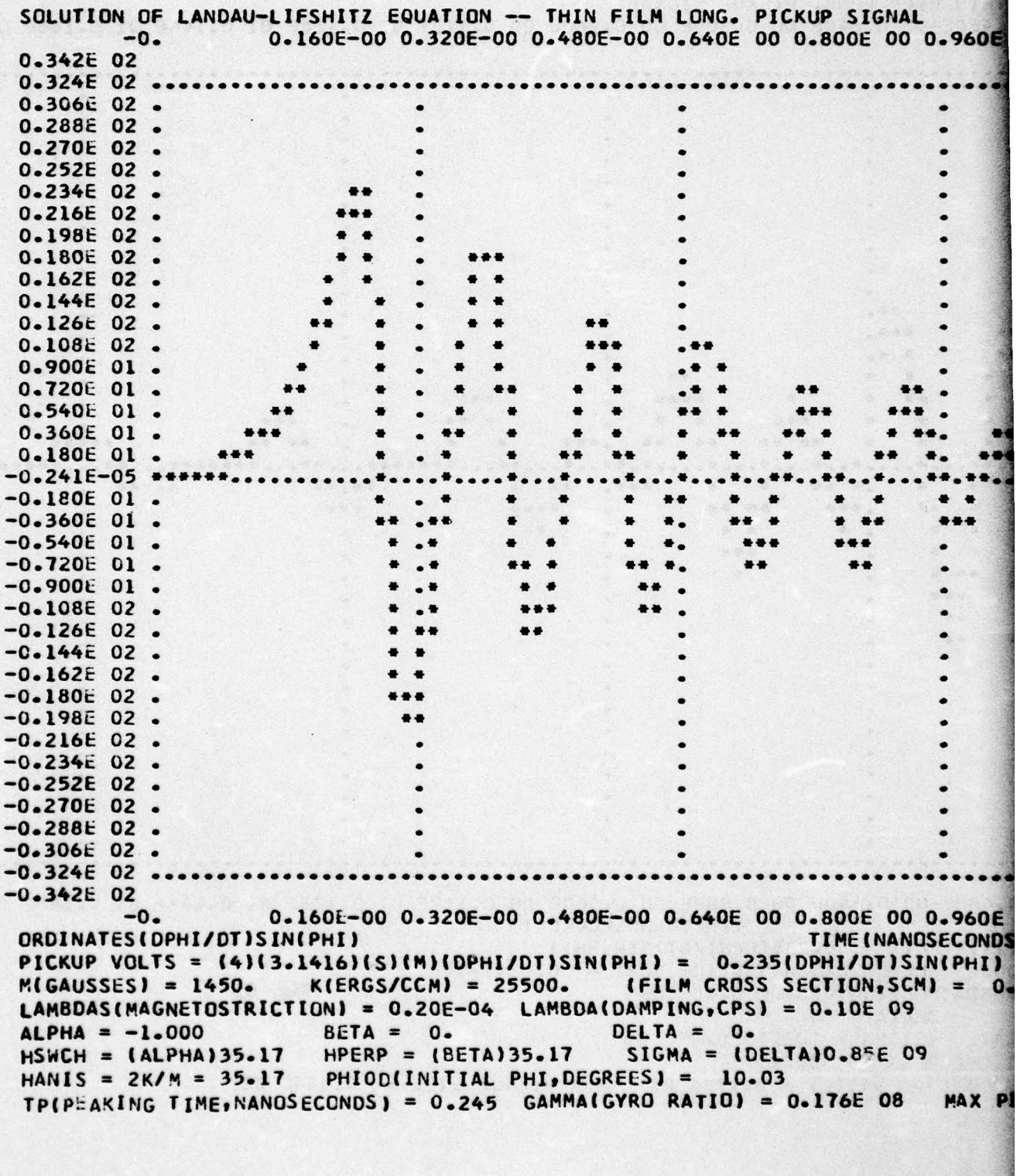
E-00 0.480E-00 0.640E 00 0.800E 00 0.960E 00 0.112E 01 0.128E 01 0.144E 01 0.160E 01
TIME(NANOSECONDS)
PHI/DT)SIN(PHI) = 0.235(DPHI/DT)SIN(PHI)
= 25500. (FILM CROSS SECTION,SCM) = 0.129E-04
04 LAMBDA(DAMPING,CPS) = 0.10E 09
00 DELTA = -0.132
TA)35.17 SIGMA = (DELTA)0.85E 09
AL PHI,DEGREES) = 60.16
12 GAMMA(GYRO RATIO) = 0.176E 08 MAX PICKUP SIG. = 0.310E 02

Fig. 91

Figures 92, 93, 94, 95 inclusive.

The conclusions suggested by the previous figures are confirmed in these cases, where ϕ_o is increased progressively through 10°, 30°, 45° and 60°. The perpendicular field has been made equal to zero and it may be concluded that the effect of increasing ϕ_o in the absence of β is equivalent to increasing β when ϕ_o is kept at zero. As evidenced by Figs. 76 and 93, the peaking time observed with $\alpha = -0.5$, $\beta = 0.590$ and $\phi_o = 0$ is the same as that observed with $\alpha = -1.0$, $\beta = 0$, $\phi_o = 30°$. This shows that with proper setting of ϕ_o the same switching time corresponding to a high value of β may be obtained with half the value of the switching field. The voltage induced due to ferromagnetic oscillation is larger with $\phi_o = 30°$ than it is with $\beta = 0.590$. The dynamic responses characterizing the cases in these figures show a relative increase in ferromagnetic resonance effects as ϕ_o is increased.

Figures 96 to 104 inclusive. The plots in these figures show the effect of changing the damping constant λ for negative applied stress, no stress, and positive applied stress, with $H_p = 2.8$ oe ($\beta = 0.08$),



PICKUP VOLTS = (4)(3.1416)(S)(M)(DPHI/DT)SIN(PHI) = 0.235(DPHI/DT)SIN(PHI)

M(GAUSSES) = 1450. K(ERGS/CCM) = 25500. (FILM CROSS SECTION,SCM) = 0.

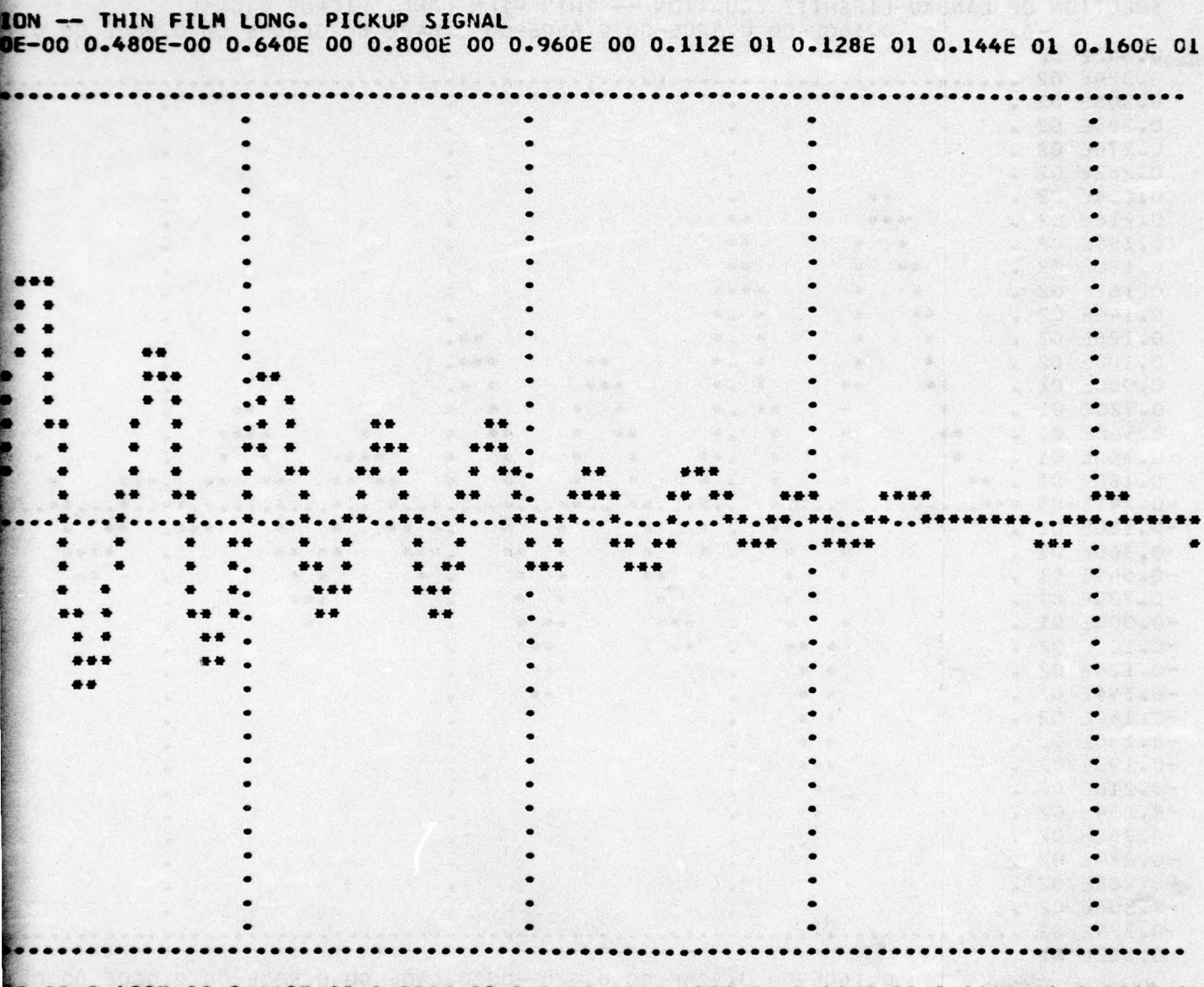
LAMBDAS(MAGNETOSTRICTION) = 0.20E-04 LAMBDA(DAMPING,CPS) = 0.10E 09

ALPHA = -1.000 BETA = 0. DELTA = 0.

HSWCH = (ALPHA)35.17 HPERP = (BETA)35.17 SIGMA = (DELTA)0.85E 09

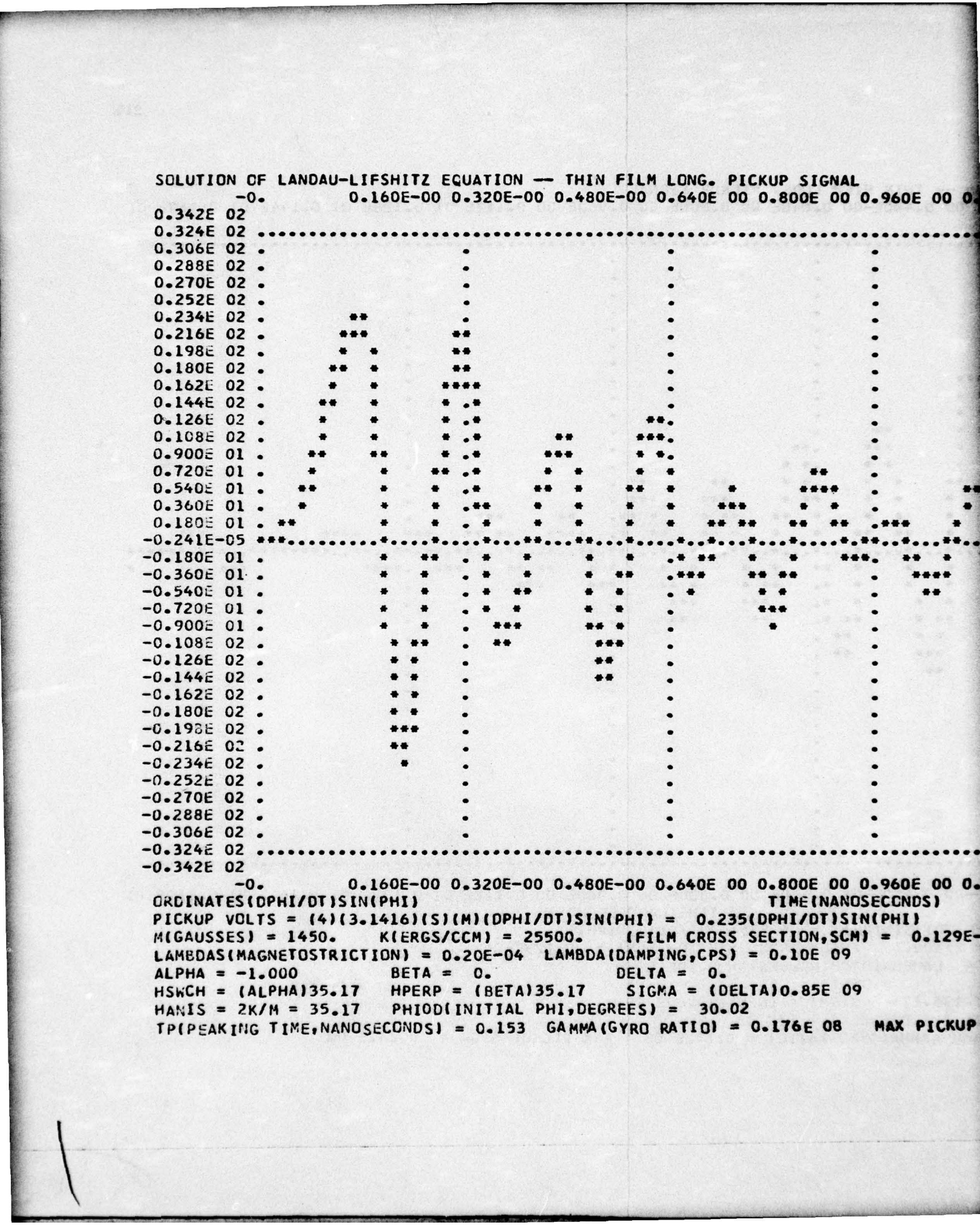
HANIS = 2K/M = 35.17 PHIOD(INITIAL PHI,DEGREES) = 10.03

TP(PEAKING TIME,NANOSECONDS) = 0.245 GAMMA(GYRO RATIO) = 0.176E 08 MAX P



PHI/DT)SIN(PHI) = 0.235(DPHI/DT)SIN(PHI)
= 25500. (FILM CROSS SECTION,SCM) = 0.129E-04
-04 LAMBDA(DAMPING,CPS) = 0.10E 09
DELTA = 0.
TA)35.17 SIGMA = (DELTA)0.85E 09
AL PHI,DEGREES) = 10.03
245 GAMMA(GYRO RATIO) = 0.176E 08 MAX PICKUP SIG. = 0.232E 02

Fig. 92



PICKUP VOLTS = (4)(3.1416)(S)(M)(DPHI/DT)SIN(PHI) = 0.235(DPHI/DT)SIN(PHI)

M(GAUSSES) = 1450. K(ERGS/CCM) = 25500. (FILM CROSS SECTION,SCM) = 0.129E-

LAMBDAS(MAGNETOSTRICTION) = 0.20E-04 LAMBDA(DAMPING,CPS) = 0.10E 09

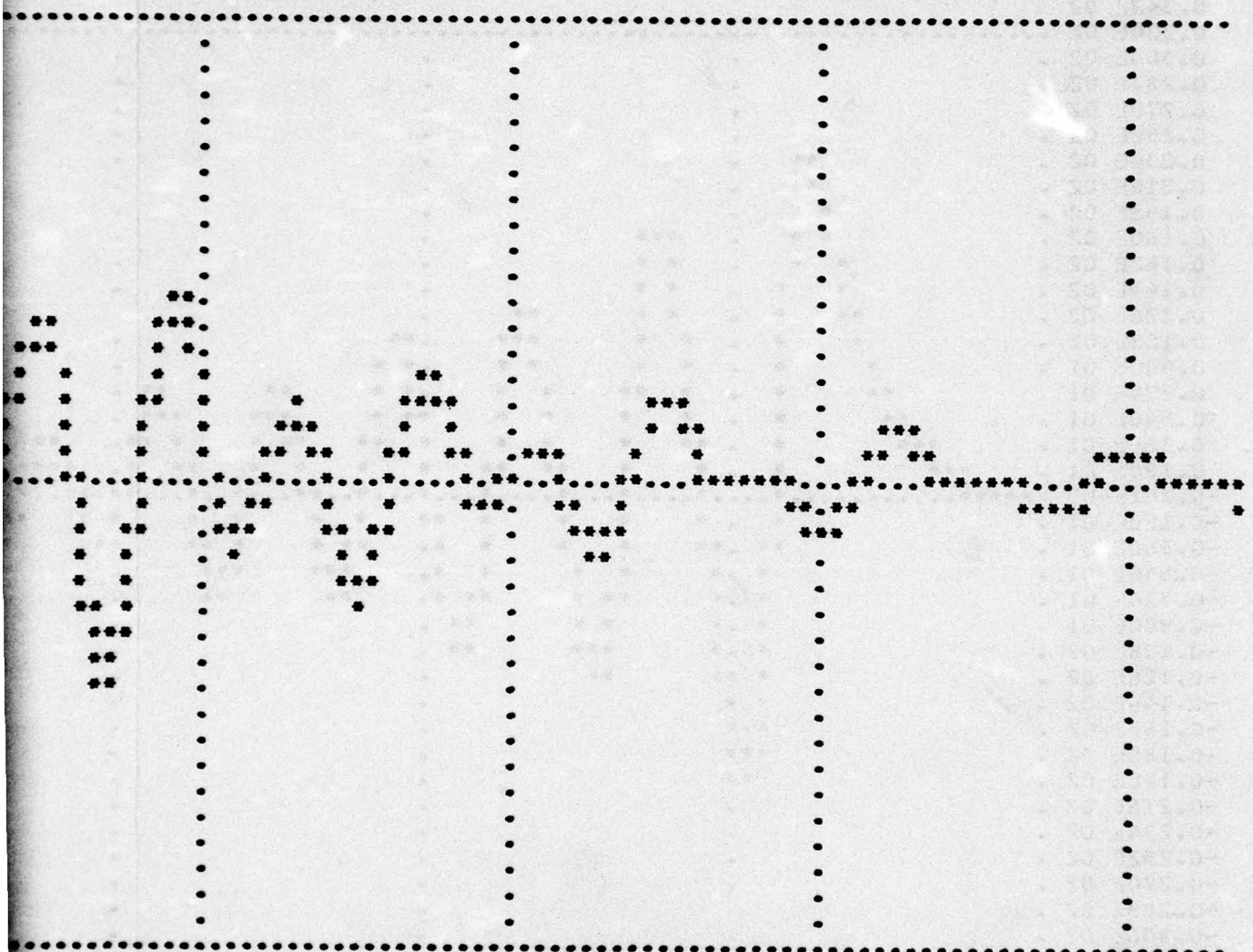
ALPHA = -1.000 BETA = 0. DELTA = 0.

HSWCH = (ALPHA)35.17 HPERP = (BETA)35.17 SIGMA = (DELTA)0.85E 09

HANIS = 2K/M = 35.17 PHIOD(INITIAL PHI,DEGREES) = 30.02

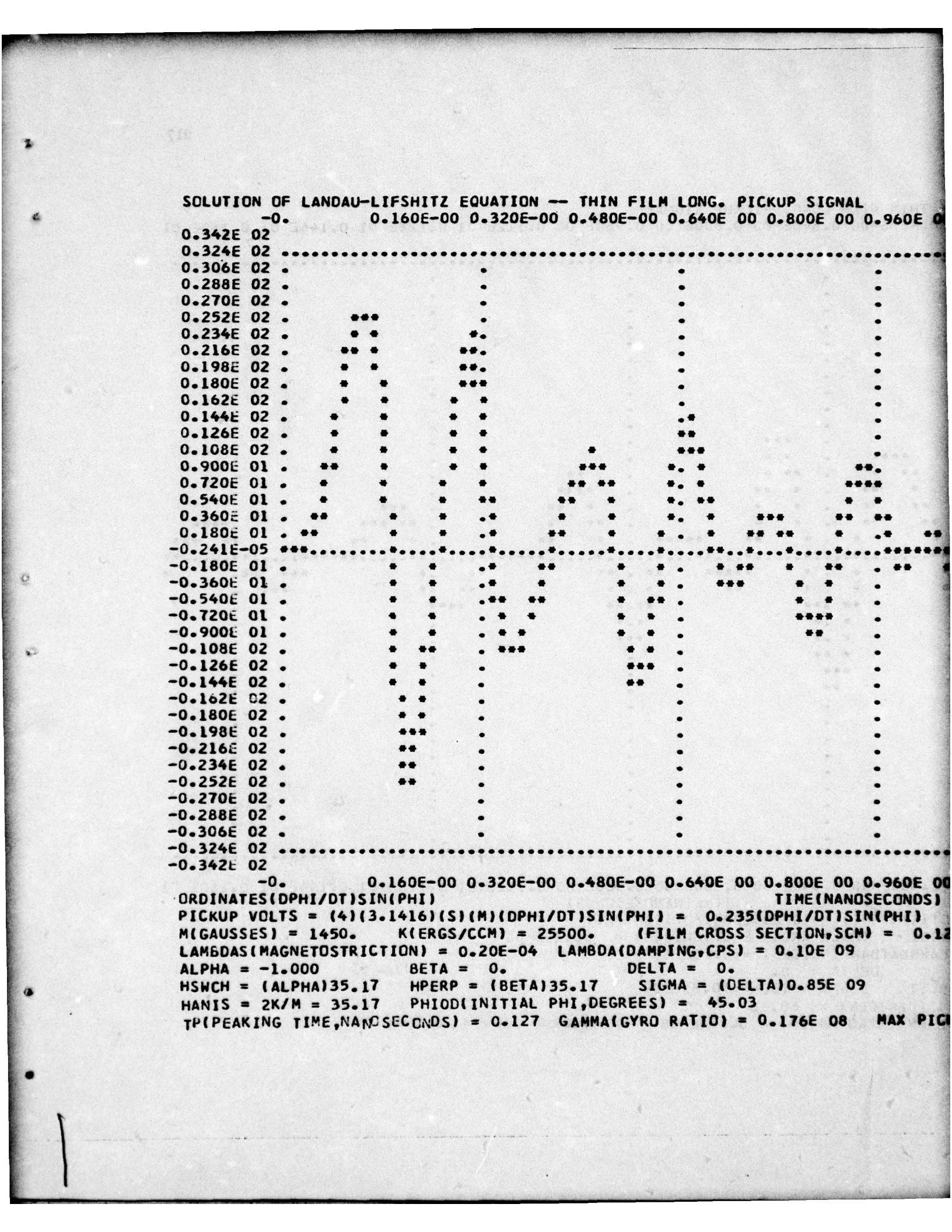
TP(PEAKING TIME,NANOSECONDS) = 0.153 GAMMA(GYRO RATIO) = 0.176E 08 MAX PICKUP

— THIN FILM LONG. PICKUP SIGNAL
0 0.480E-00 0.640E 00 0.800E 00 0.960E 00 0.112E 01 0.128E 01 0.144E 01 0.160E 01

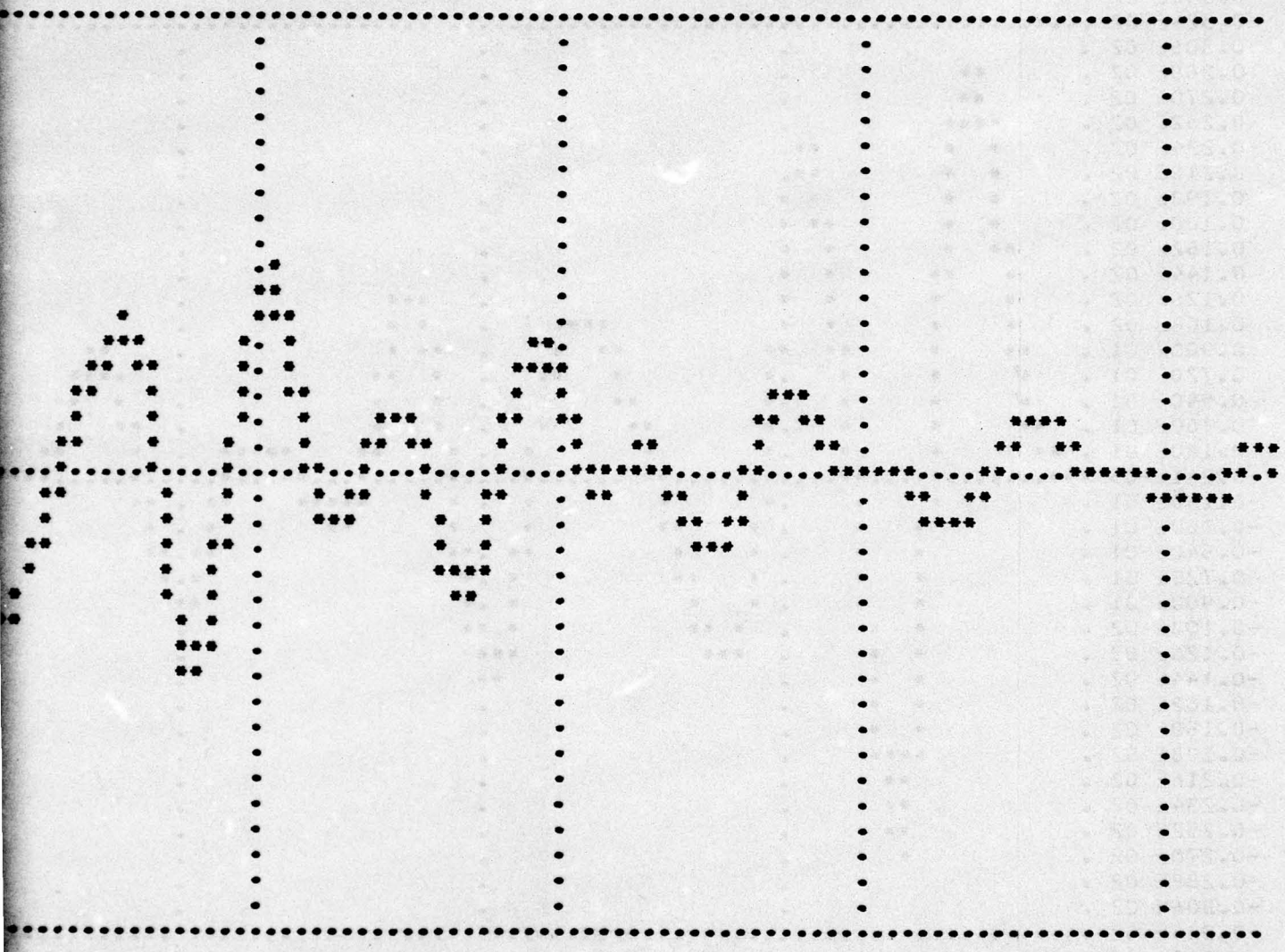


0.480E-00 0.640E 00 0.800E 00 0.960E 00 0.112E 01 0.128E 01 0.144E 01 0.160E 01
TIME(NANOSECONDS)

DT)SIN(PHI) = 0.235(DPHI/DT)SIN(PHI)
300. (FILM CROSS SECTION,SCM) = 0.129E-04
LAMBDA(DAMPING,CPS) = 0.10E 09 Fig. 93
DELTA = 0.
3.17 SIGMA = (DELTA)0.85E 09
HI,DEGREES) = 30.02
GAMMA(GYRO RATIO) = 0.176E 08 MAX PICKUP SIG. = 0.234E 02


SOLUTION OF LANDAU-LIFSHITZ EQUATION -- THIN FILM LONG. PICKUP SIGNAL
-0. 0.160E-00 0.320E-00 0.480E-00 0.640E 00 0.800E 00 0.960E 0
0.342E 02
0.324E 02
0.306E 02
0.288E 02
0.270E 02
0.252E 02
0.234E 02
0.216E 02
0.198E 02
0.180E 02
0.162E 02
0.144E 02
0.126E 02
0.108E 02
0.900E 01
0.720E 01
0.540E 01
0.360E 01
0.180E 01
-0.241E-05
-0.180E 01
-0.360E 01
-0.540E 01
-0.720E 01
-0.900E 01
-0.108E 02
-0.126E 02
-0.144E 02
-0.162E 02
-0.180E 02
-0.198E 02
-0.216E 02
-0.234E 02
-0.252E 02
-0.270E 02
-0.288E 02
-0.306E 02
-0.324E 02
-0.342E 02
-0. 0.160E-00 0.320E-00 0.480E-00 0.640E 00 0.800E 00 0.960E 00
ORDINATES(DPHI/DT)SIN(PHI) TIME(NANOSECONDS)
PICKUP VOLTS = (4)(3.1416)(S)(M)(DPHI/DT)SIN(PHI) = 0.235(DPHI/DT)SIN(PHI)
M(GAUSSES) = 1450. K(ERGS/CCM) = 25500. (FILM CROSS SECTION,SCM) = 0.12
LAMBDAS(MAGNETOSTRICTION) = 0.20E-04 LAMBDA(DAMPING,CPS) = 0.10E 09
ALPHA = -1.000 BETA = 0. DELTA = 0.
HSWCH = (ALPHA)35.17 HPERP = (BETA)35.17 SIGMA = (DELTA)0.85E 09
HANIS = 2K/M = 35.17 PHIOD(INITIAL PHI,DEGREES) = 45.03
TP(PEAKING TIME,NANOSECONDS) = 0.127 GAMMA(GYRO RATIO) = 0.176E 08 MAX PIC

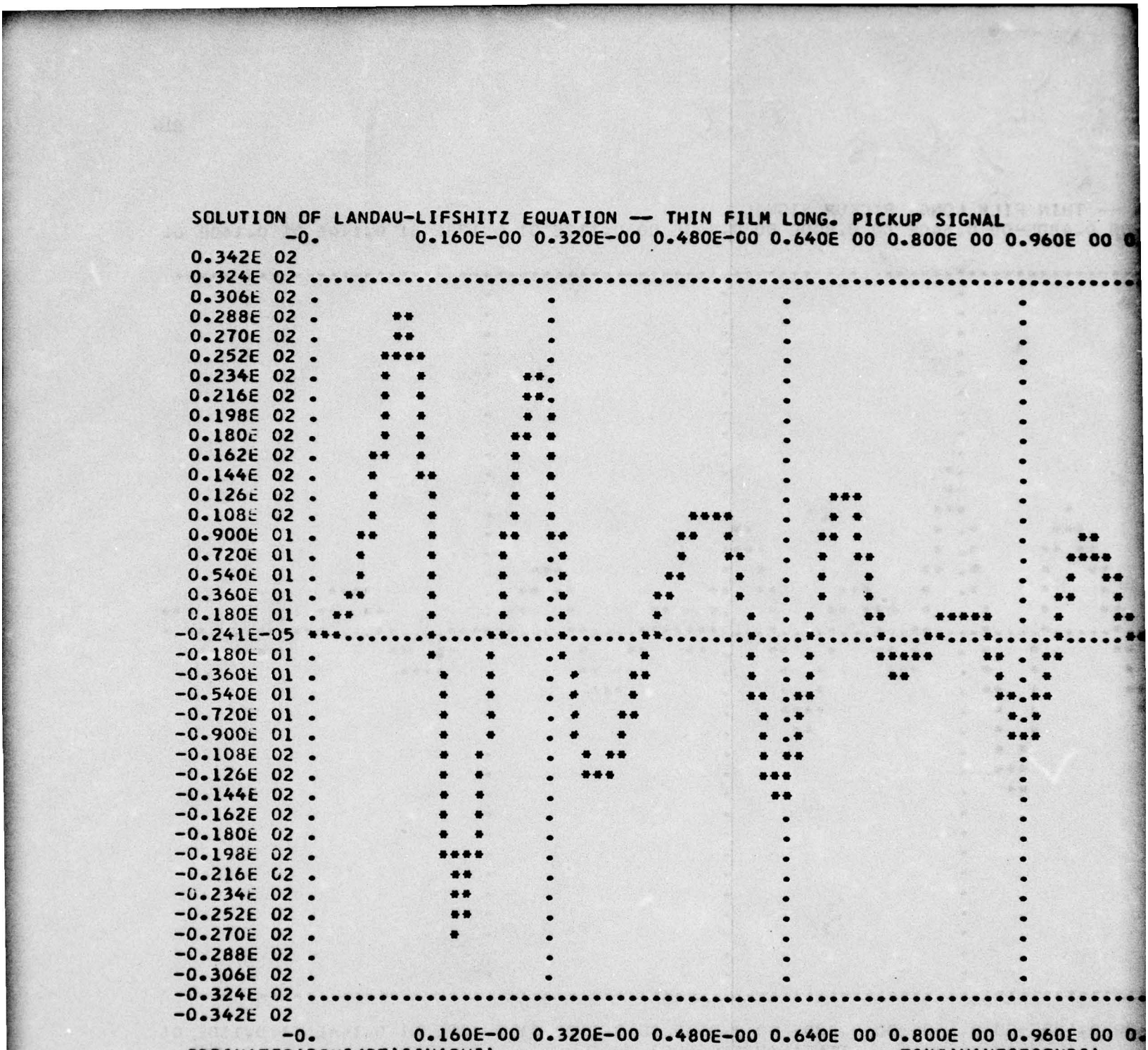
ION -- THIN FILM LONG. PICKUP SIGNAL
0E-00 0.480E-00 0.640E 00 0.800E 00 0.960E 00 0.112E 01 0.128E 01 0.144E 01 0.160E 01



E-00 0.480E-00 0.640E 00 0.800E 00 0.960E 00 0.112E 01 0.128E 01 0.144E 01 0.160E 01
TIME(NANOSECONDS)
PHI/DT)SIN(PHI) = 0.235(DPHI/DT)SIN(PHI)
= 25500. (FILM CROSS SECTION,SCM) = 0.129E-04
04 LAMBDA(DAMPING,CPS) = 0.10E 09
DELTA = 0.
TA)35.17 SIGMA = (DELTA)0.85E 09
AL PHI,DEGREES) = 45.03
27 GAMMA(GYRO RATIO) = 0.176E 08 MAX PICKUP SIG. = 0.261E 02

Fig. 94

2



PICKUP VOLTS = (4)(3.1416)(S)(M)(DPHI/DT)SIN(PHI) = 0.235(DPHI/DT)SIN(PHI)

M(GAUSSES) = 1450. K(ERGS/CCM) = 25500. (FILM CROSS SECTION,SCM) = 0.129E-

LAMBDAS(MAGNETOSTRICTION) = 0.20E-04 LAMBDA(DAMPING,CPS) = 0.10E 09

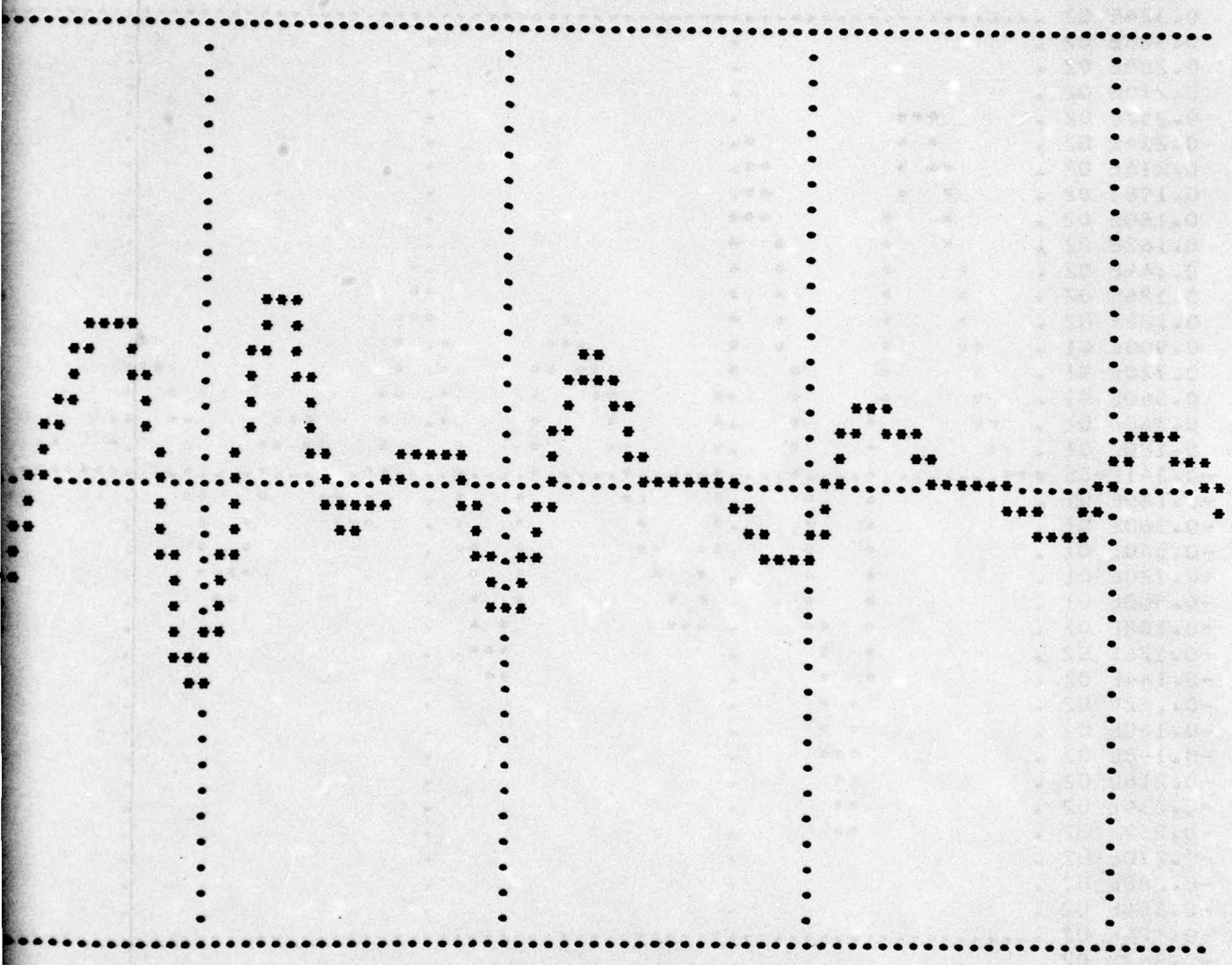
ALPHA = -1.000 BETA = 0. DELTA = 0.

HSWCH = (ALPHA)35.17 HPERP = (BETA)35.17 SIGMA = (DELTA)0.85E 09

HANIS = 2K/M = 35.17 PHIOD(INITIAL PHI,DEGREES) = 60.16

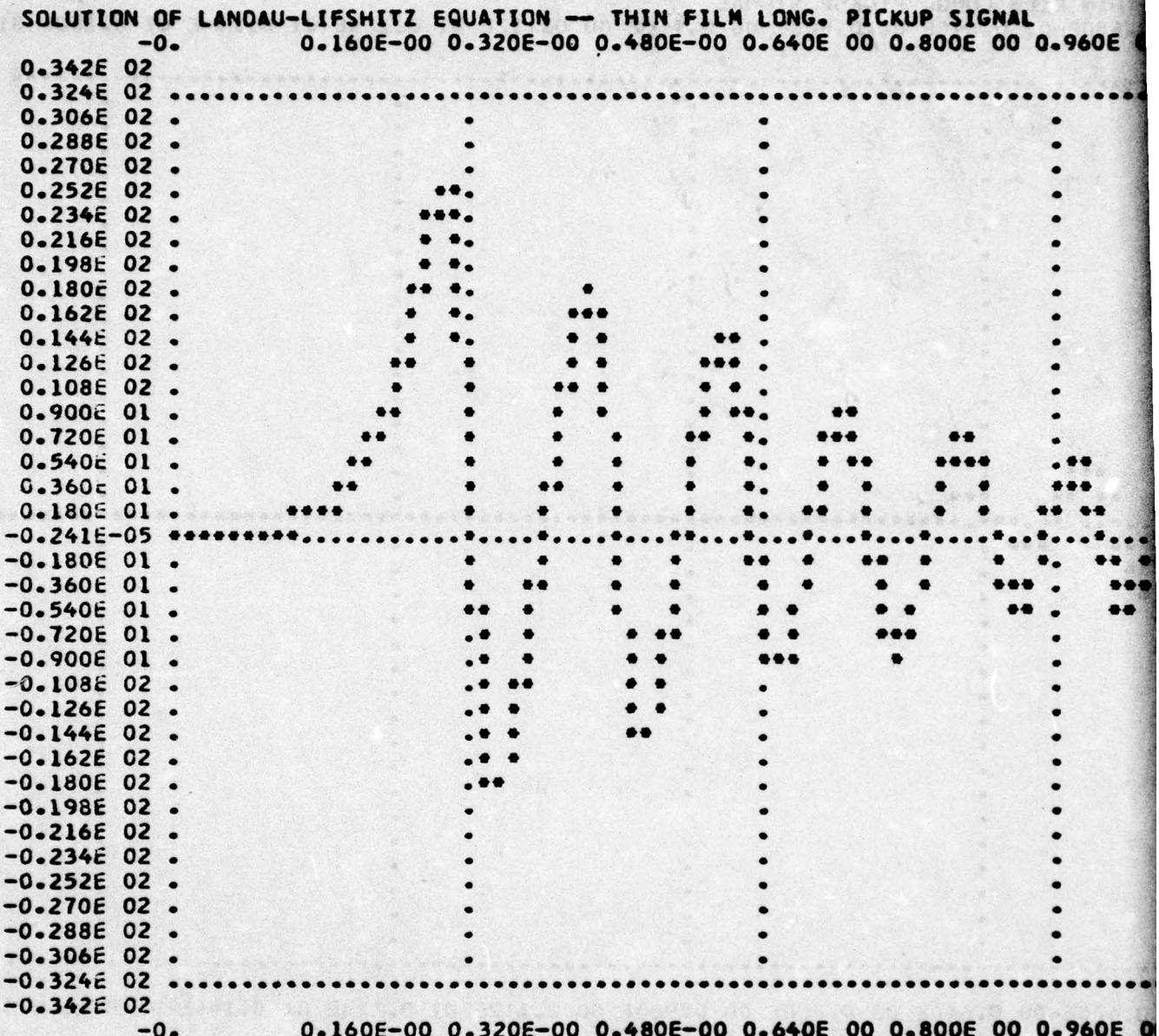
TP(PEAKING TIME,NANOSECONDS) = 0.122 GAMMA(GYRO RATIO) = 0.176E 08 MAX PICKUP

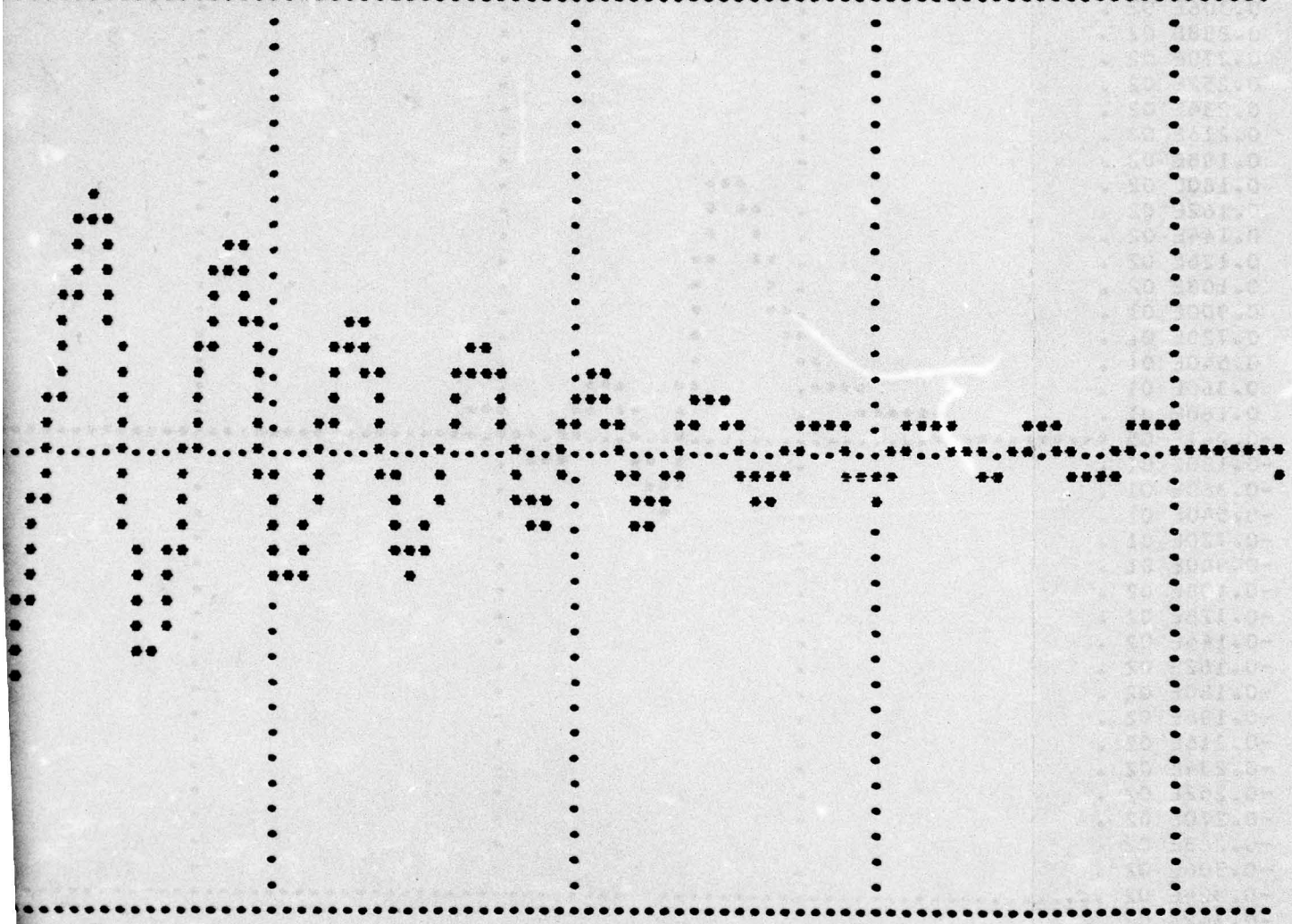
— THIN FILM LONG. PICKUP SIGNAL
00 0.480E-00 0.640E 00 0.800E 00 0.960E 00 0.112E 01 0.128E 01 0.144E 01 0.160E 01



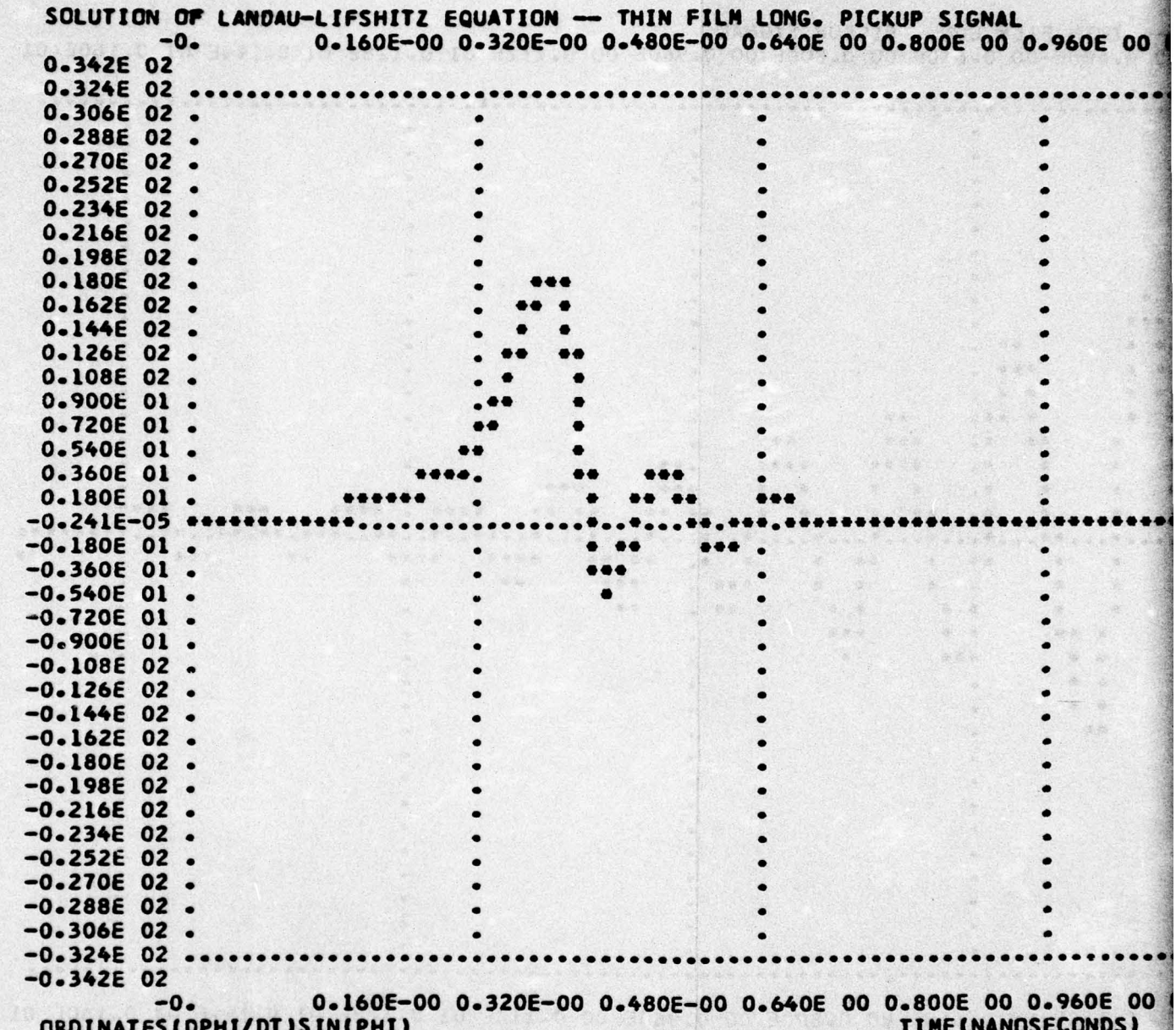
0 0.480E-00 0.640E 00 0.800E 00 0.960E 00 0.112E 01 0.128E 01 0.144E 01 0.160E 01
TIME(NANOSECONDS)
(DT)SIN(PHI) = 0.235(DPHI/DT)SIN(PHI)
3500. (FILM CROSS SECTION,SCM) = 0.129E-04
LAMBDA(DAMPING,CPS) = 0.10E 09
DELTA = 0.
35.17 SIGMA = (DELTA)0.85E 09
PHI,DEGREES) = 60.16
GAMMA(GYRO RATIO) = 0.176E 08 MAX PICKUP SIG. = 0.294E 02

Fig. 95


SOLUTION OF LANDAU-LIFSHITZ EQUATION -- THIN FILM LONG. PICKUP SIGNAL
-0. 0.160E-00 0.320E-00 0.480E-00 0.640E 00 0.800E 00 0.960E
0.342E 02
0.324E 02
0.306E 02
0.288E 02
0.270E 02
0.252E 02
0.234E 02
0.216E 02
0.198E 02
0.180E 02
0.162E 02
0.144E 02
0.126E 02
0.108E 02
0.900E 01
0.720E 01
0.540E 01
0.360E 01
0.180E 01
-0.241E-05
-0.180E 01
-0.360E 01
-0.540E 01
-0.720E 01
-0.900E 01
-0.108E 02
-0.126E 02
-0.144E 02
-0.162E 02
-0.180E 02
-0.198E 02
-0.216E 02
-0.234E 02
-0.252E 02
-0.270E 02
-0.288E 02
-0.306E 02
-0.324E 02
-0.342E 02
-0. 0.160E-00 0.320E-00 0.480E-00 0.640E 00 0.800E 00 0.960E 0
ORDINATES(DPHI/DT)SIN(PHI) TIME(NANOSECONDS)
PICKUP VOLTS = (4)(3.1416)(S)(M)(DPHI/DT)SIN(PHI) = 0.235(DPHI/DT)SIN(PHI)
M(GAUSSES) = 1450. K(ERGS/CCM) = 25500. (FILM CROSS SECTION,SCM) = 0.1
LAMBDAS(MAGNETOSTRICTION) = 0.20E-04 LAMBDA(DAMPING,CPS) = 0.10E 09
ALPHA = -1.000 BETA = 0.080 DELTA = -0.132
HSWCH = (ALPHA)35.17 HPERP = (BETA)35.17 SIGMA = (DELTA)0.85E 09
HANIS = 2K/M = 35.17 PHIOD(INITIAL PHI,DEGREES) = 0.
TP(PEAKING TIME,NANOSECONDS) = 0.291 GAMMA(GYRO RATIO) = 0.176E 08 MAX PIC



PHI/DT)SIN(PHI) = 0.235(DPHI/DT)SIN(PHI)
= 25500. (FILM CROSS SECTION,SCM) = 0.129E-04
04 LAMBDA(DAMPING,CPS) = 0.10E 09 Fig. 96
80 DELTA = -0.132
TA)35.17 SIGMA = (DELTA)0.85E 09
AL PHI,DEGREES) = 0.
91 GAMMA(GYRO RATIO) = 0.176E 08 MAX PICKUP SIG. = 0.252E 02



PICKUP VOLTS = (4)(3.1416)(S)(M)(DPHI/DT)SIN(PHI) = 0.235(DPHI/DT)SIN(PHI)

M(GAUSSES) = 1450. K(ERGS/CCM) = 25500. (FILM CROSS SECTION,SCM) = 0.129

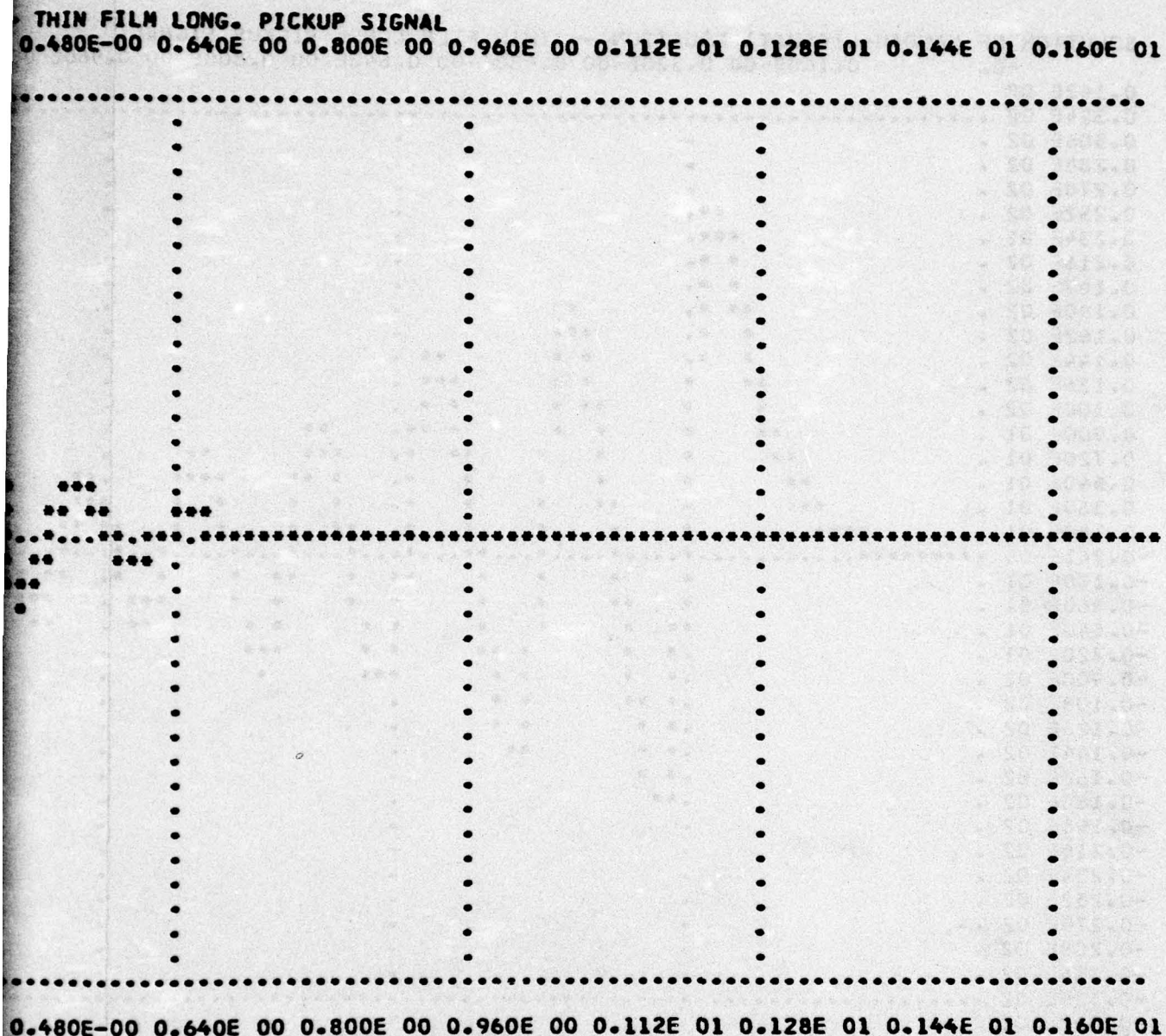
LAMBDAS(MAGNETOSTRICTION) = 0.20E-04 LAMBDA(DAMPING,CPS) = 0.50E 09

ALPHA = -1.000 BETA = 0.080 DELTA = -0.132

HSWCH = (ALPHA)35.17 HPERP = (BETA)35.17 SIGMA = (DELTA)0.85E 09

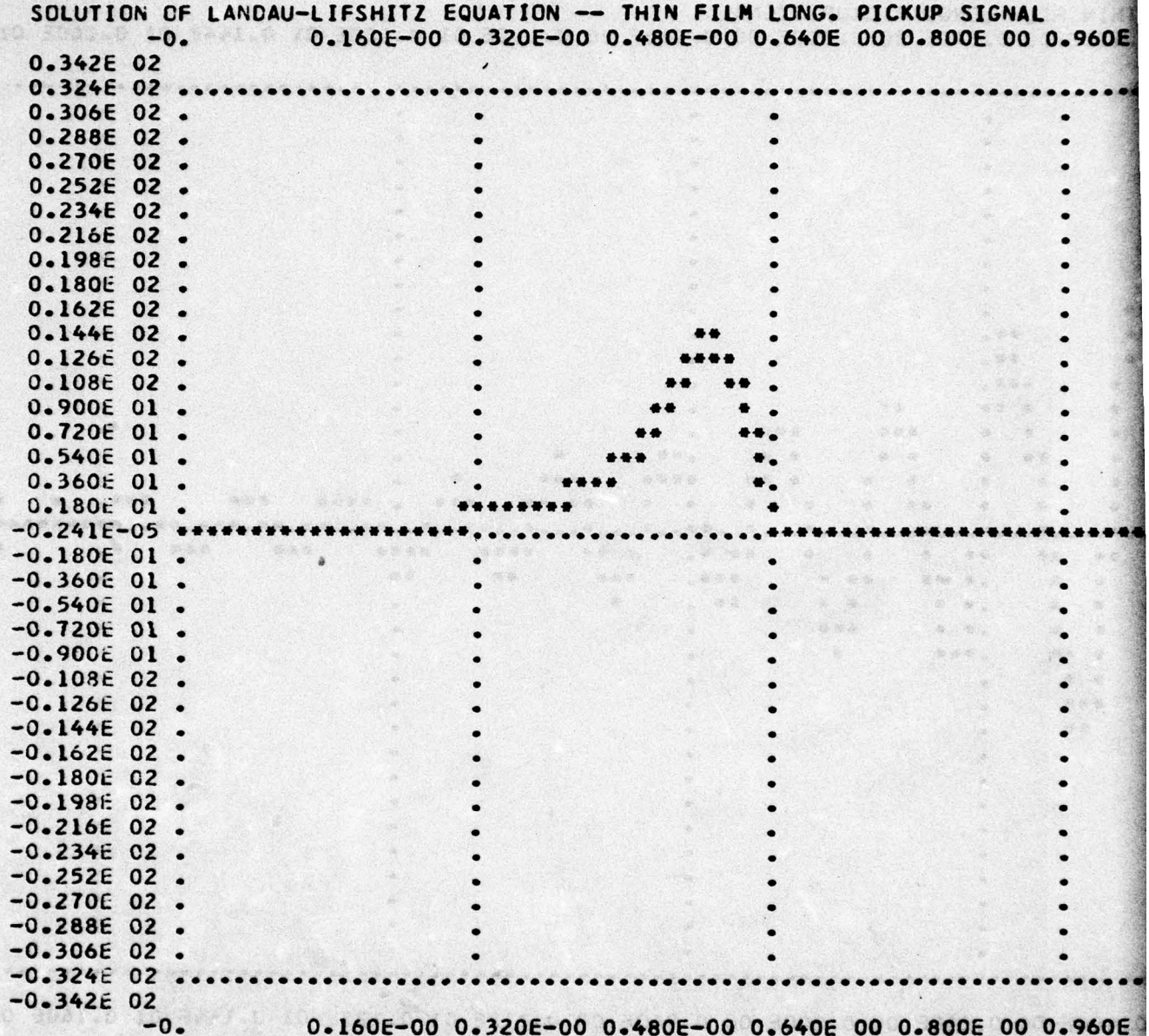
HANIS = 2K/M = 35.17 PHIOD(INITIAL PHI,DEGREES) = 0.

TP(PEAKING TIME,NANOSECONDS) = 0.400 GAMMA(GYRO RATIO) = 0.176E 08 MAX PICKU

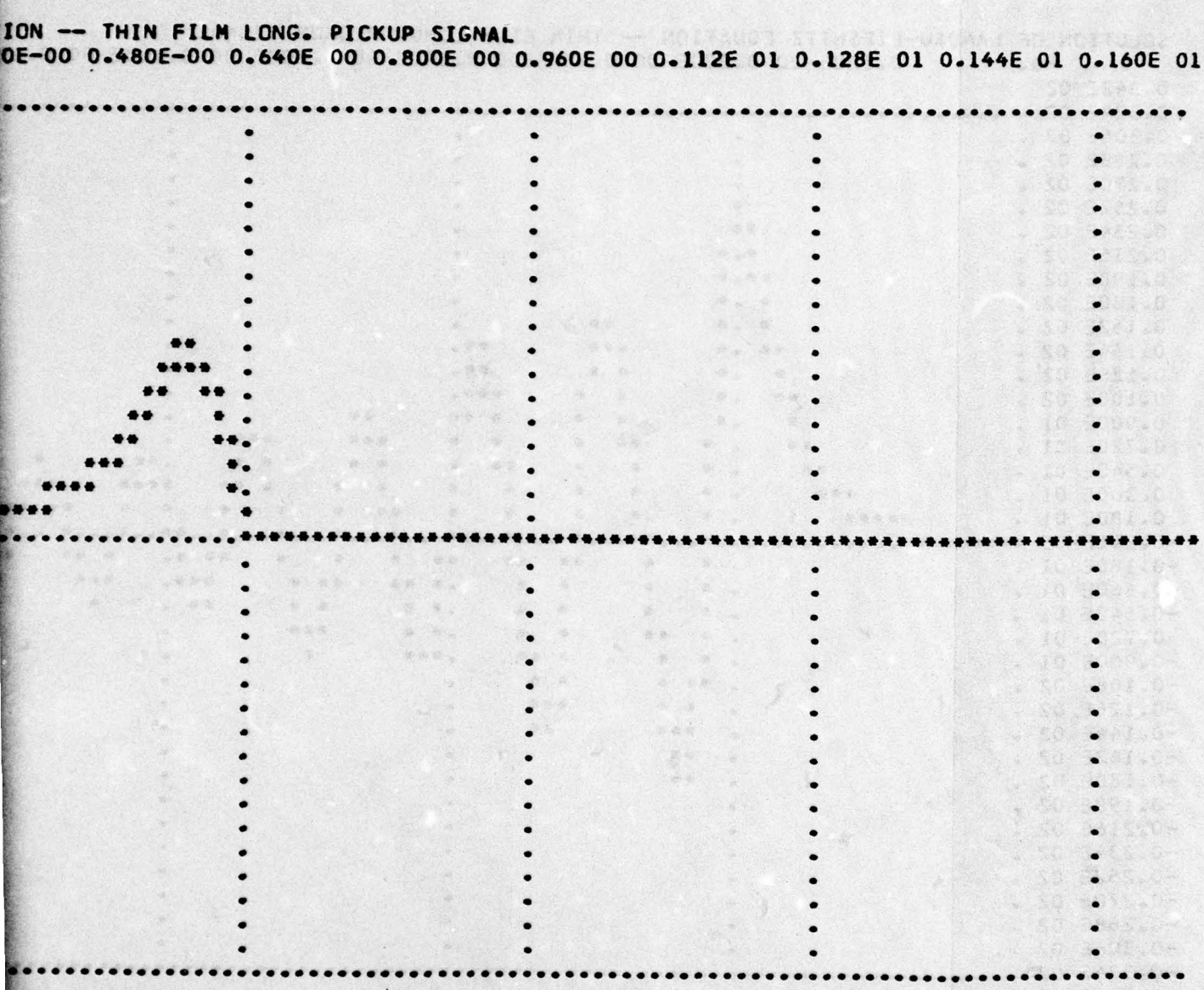


T)SIN(PHI) = 0.235(DPHI/DT)SIN(PHI)
00. (FILM CROSS SECTION,SCM) = 0.129E-04
AMBDA(DAMPING,CPS) = 0.50E 09
DELTA = -0.132
.17 SIGMA = (DELTA)0.85E 09
1,DEGREES) = 0.
AMMA(GYRO RATIO) = 0.176E 08 MAX PICKUP SIG. = 0.188E 02

Fig. 97



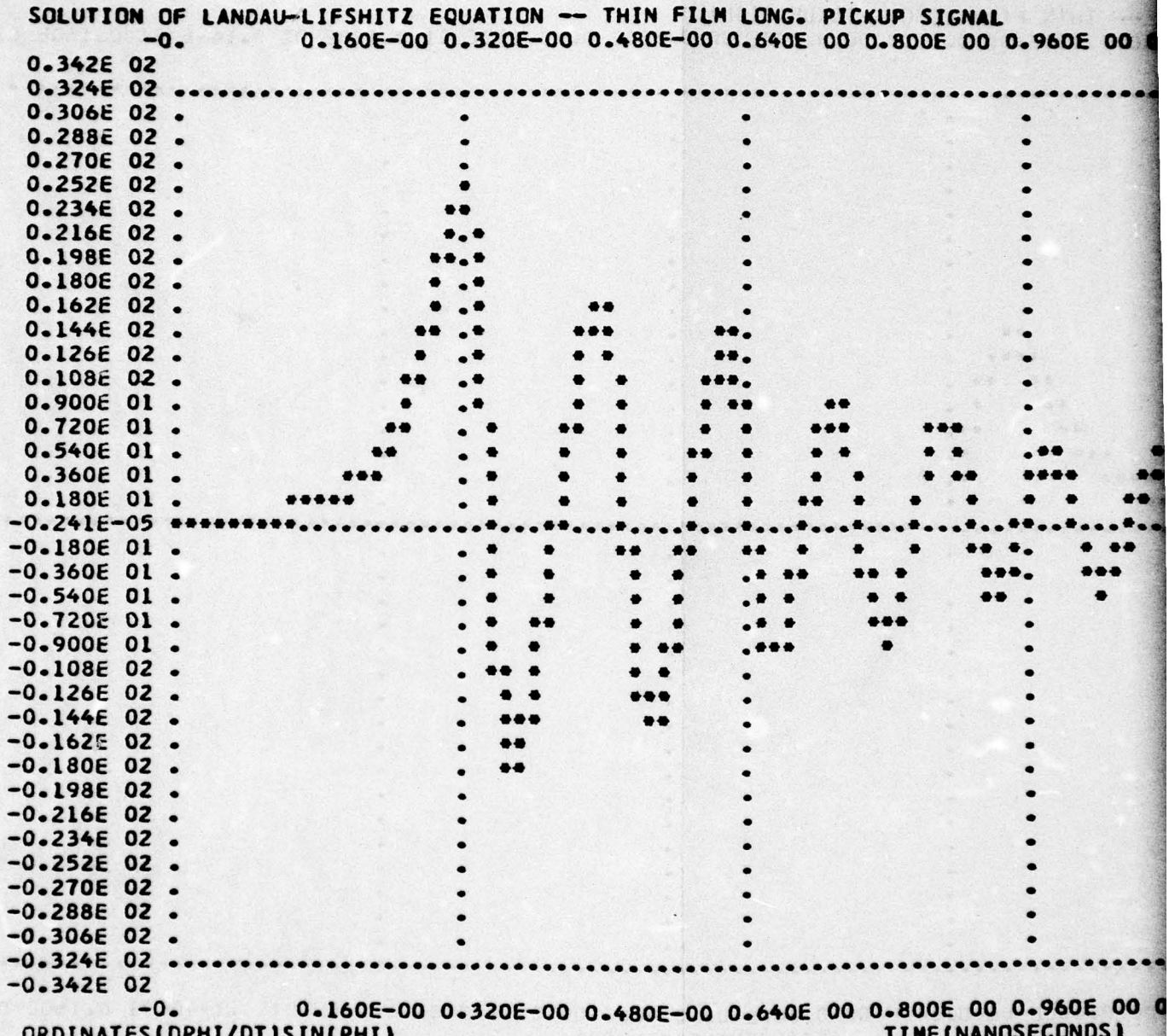
PICKUP VOLTS = (4)(3.1416)(S)(M)(DPHI/DT)SIN(PHI) = 0.235(DPHI/DT)SIN(PHI)
M(GAUSSES) = 1450. K(ERGS/CCM) = 25500. (FILM CROSS SECTION,SCM) = 0.
LAMBDAS(MAGNETOSTRICTION) = 0.20E-04 LAMBDA(DAMPING,CPS) = 0.10E 10
ALPHA = -1.000 BETA = 0.080 DELTA = -0.132
HSWCH = (ALPHA)35.17 HPERP = (BETA)35.17 SIGMA = (DELTA)0.85E 09
HANIS = 2K/M = 35.17 PHIOD(INITIAL PHI,DEGREES) = 0.
TP(PEAKING TIME,NANOSECONDS) = 0.573 GAMMA(GYRO RATIO) = 0.176E 08 MAX PI



PHI/DT)SIN(PHI) = 0.235(DPHI/DT)SIN(PHI)
= 25500. (FILM CROSS SECTION,SCM) = 0.129E-04
04 LAMBDA(DAMPING,CPS) = 0.10E 10
30 DELTA = -0.132
TA)35.17 SIGMA = (DELTA)0.85E 09
AL PHI,DEGREES) = 0.
73 GAMMA(GYRO RATIO) = 0.176E 08 MAX PICKUP SIG. = 0.137E 02

Fig. 98

7



PICKUP VOLTS = (4)(3.1416)(S)(M)(DPHI/DT)SIN(PHI) = 0.235(DPHI/DT)SIN(PHI)

M(GAUSSES) = 1450. K(ERGS/CCM) = 25500. (FILM CROSS SECTION,SCM) = 0.129E

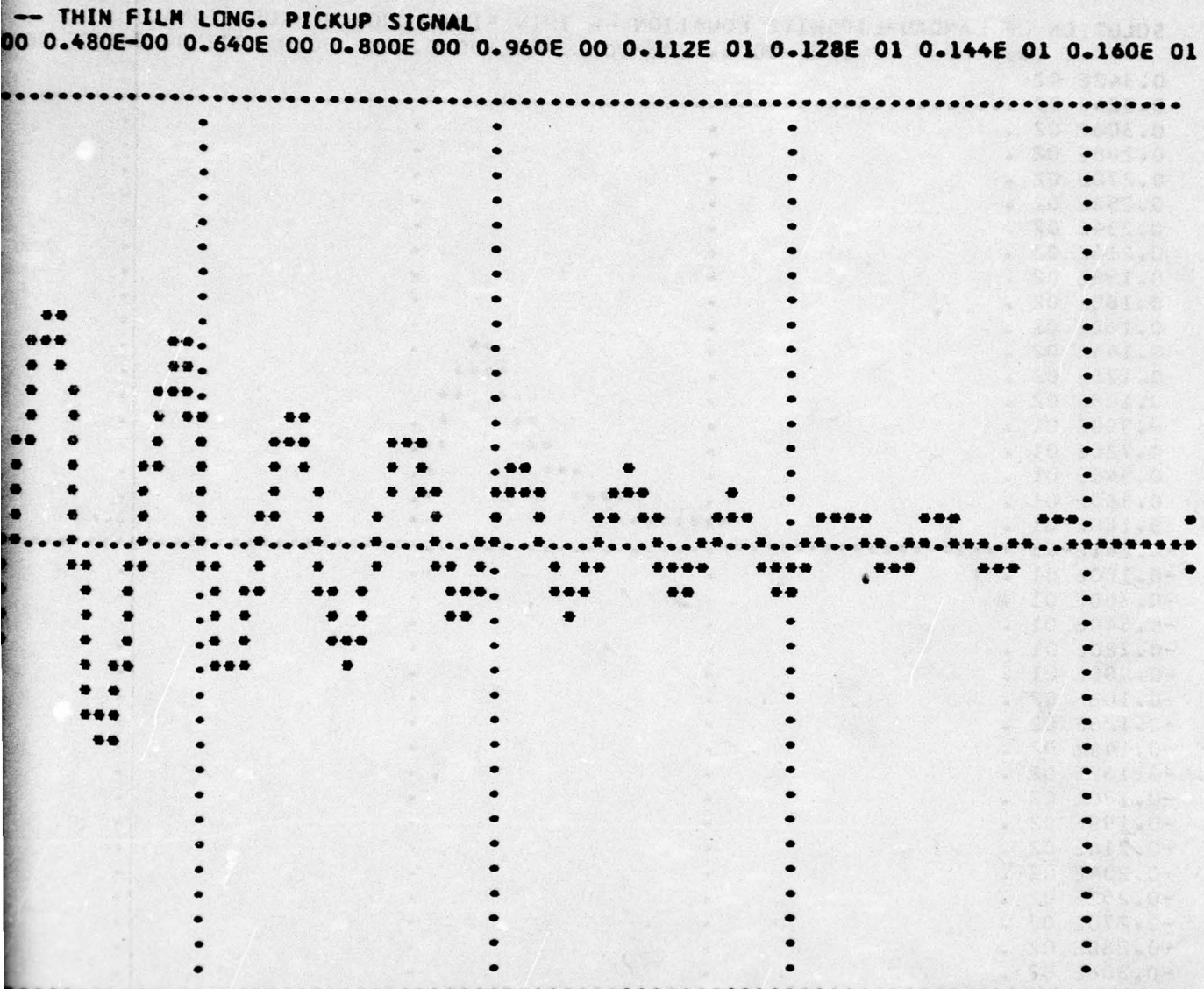
LAMBDAS(MAGNETOSTRICTION) = 0.20E-04 LAMBDA(DAMPING,CPS) = 0.10E 09

ALPHA = -1.000 BETA = 0.080 DELTA = 0.

HSWCH = (ALPHA)35.17 HPERP = (BETA)35.17 SIGMA = (DELTA)0.85E 09

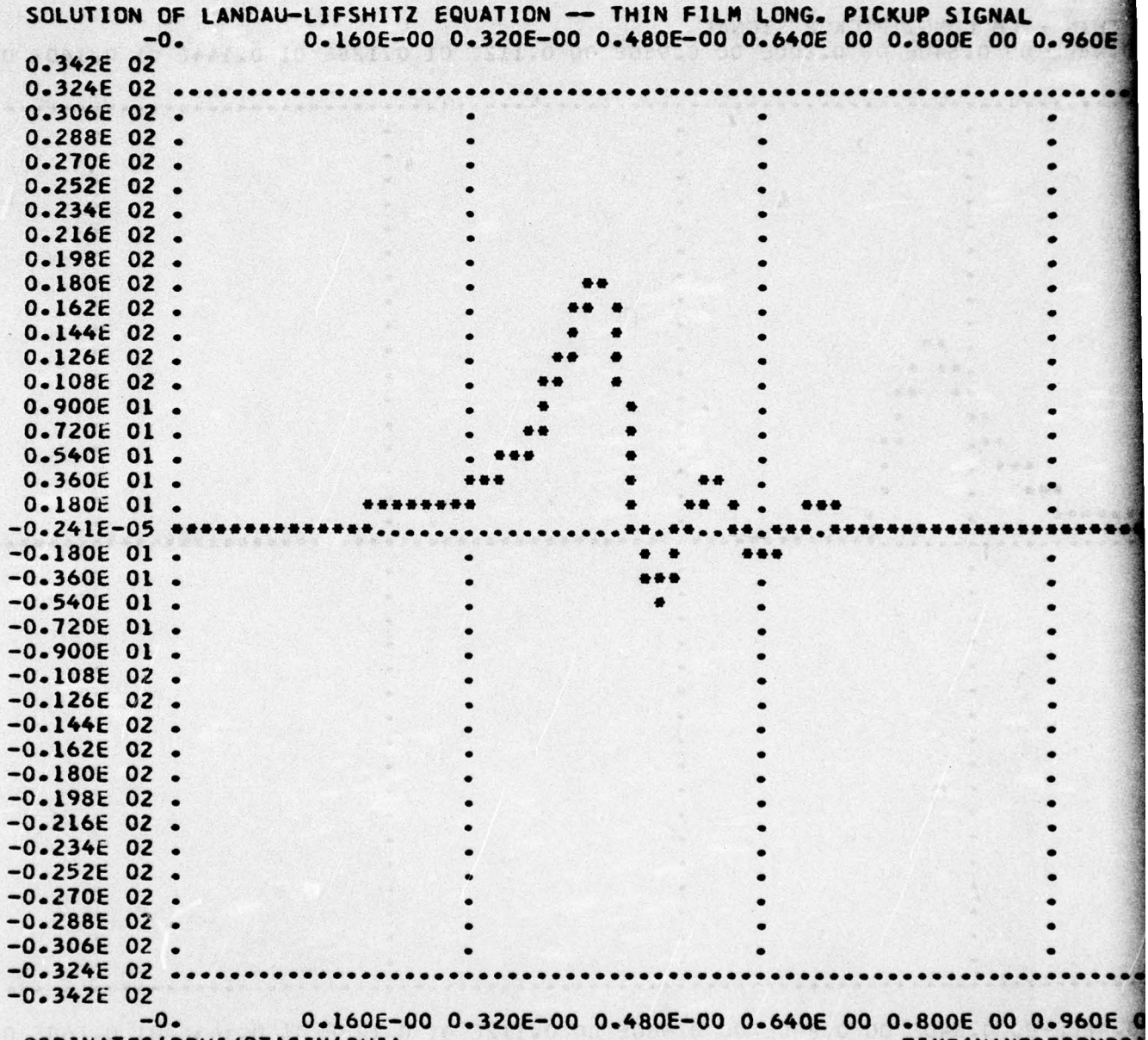
HANIS = 2K/M = 35.17 PHIOD(INITIAL PHI,DEGREES) = 0.

TP(PEAKING TIME,NANOSECONDS) = 0.319 GAMMA(GYRO RATIO) = 0.176E 08 MAX PICKU



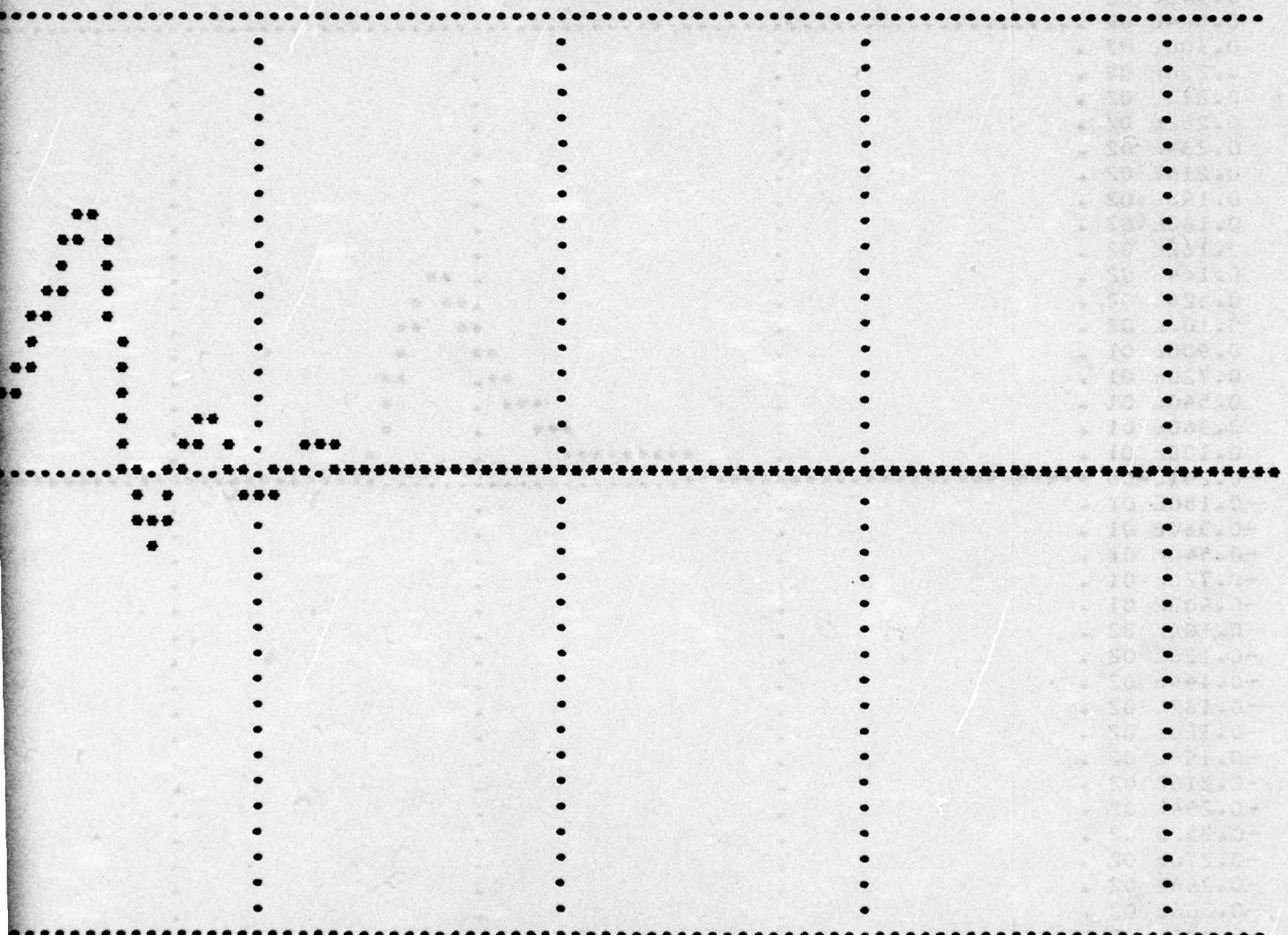
DT)SIN(PHI) = 0.235(DPHI/DT)SIN(PHI)
000. (FILM CROSS SECTION,SCM) = 0.129E-04
LAMBDA(DAMPING,CPS) = 0.10E 09
DELTA = 0.
0.17 SIGMA = (DELTA)0.85E 09
HI,DEGREES) = 0.
GAMMA(GYRO RATIO) = 0.176E 08 MAX PICKUP SIG. = 0.247E 02

Fig. 99



PICKUP VOLTS = (4)(3.1416)(S)(M)(DPHI/DT)SIN(PHI) = 0.235(DPHI/DT)SIN(PHI)
M(GAUSSES) = 1450. K(ERGS/CCM) = 25500. (FILM CROSS SECTION,SCM) = 0.1
LAMBDAS(MAGNETOSTRICTION) = 0.20E-04 LAMBDA(DAMPING,CPS) = 0.50E 09
ALPHA = -1.000 BETA = 0.080 DELTA = 0.
HSWCH = (ALPHA)35.17 HPERP = (BETA)35.17 SIGMA = (DELTA)0.85E 09
HANIS = 2K/M = 35.17 PHIOD(INITIAL PHI,DEGREES) = 0.
TP(PEAKING TIME,NANOSECONDS) = 0.460 GAMMA(GYRO RATIO) = 0.176E 08 MAX PI

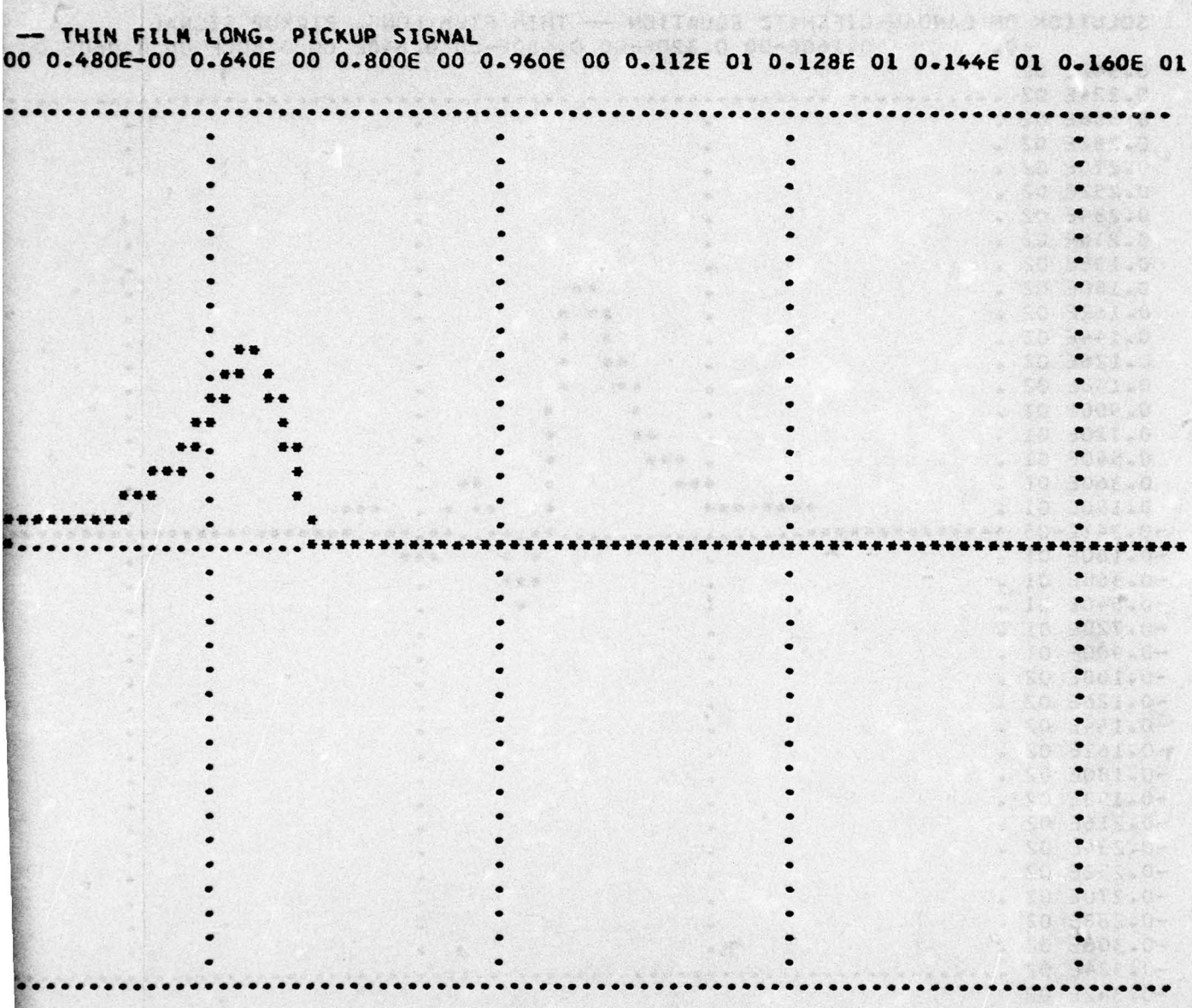
ION — THIN FILM LONG. PICKUP SIGNAL
0E-00 0.480E-00 0.640E 00 0.800E 00 0.960E 00 0.112E 01 0.128E 01 0.144E 01 0.160E 01



E-00 0.480E-00 0.640E 00 0.800E 00 0.960E 00 0.112E 01 0.128E 01 0.144E 01 0.160E 01
TIME(NANOSECONDS)
PHI/DT)SIN(PHI) = 0.235(DPHI/DT)SIN(PHI)
= 25500. (FILM CROSS SECTION,SCM) = 0.129E-04
04 LAMBDA(DAMPING,CPS) = 0.50E 09
80 DELTA = 0.
TA)35.17 SIGMA = (DELTA)0.85E 09
AL PHI,DEGREES) = 0.
60 GAMMA(GYRO RATIO) = 0.176E 08 MAX PICKUP SIG. = 0.187E 02

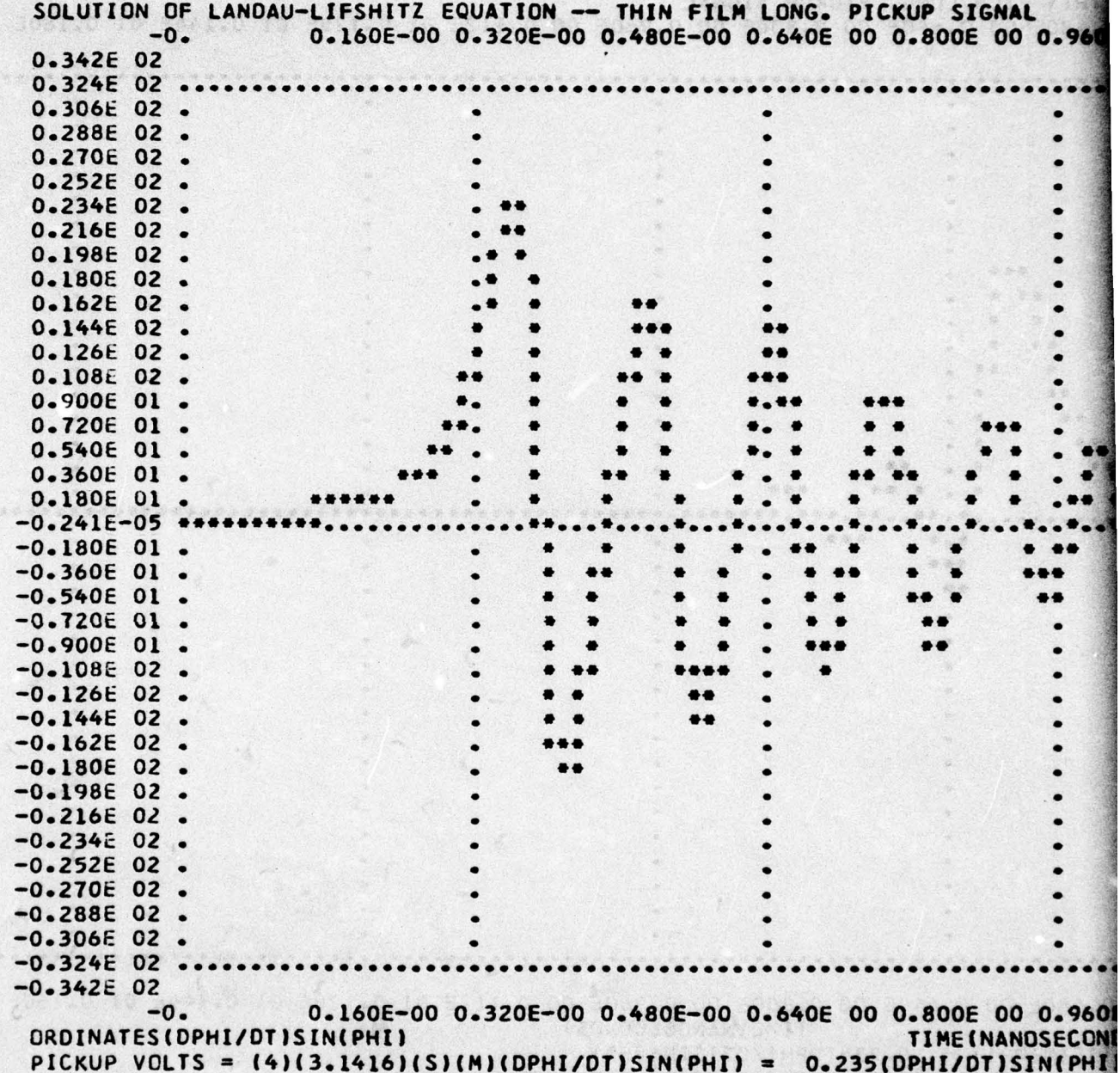
Fig. 100

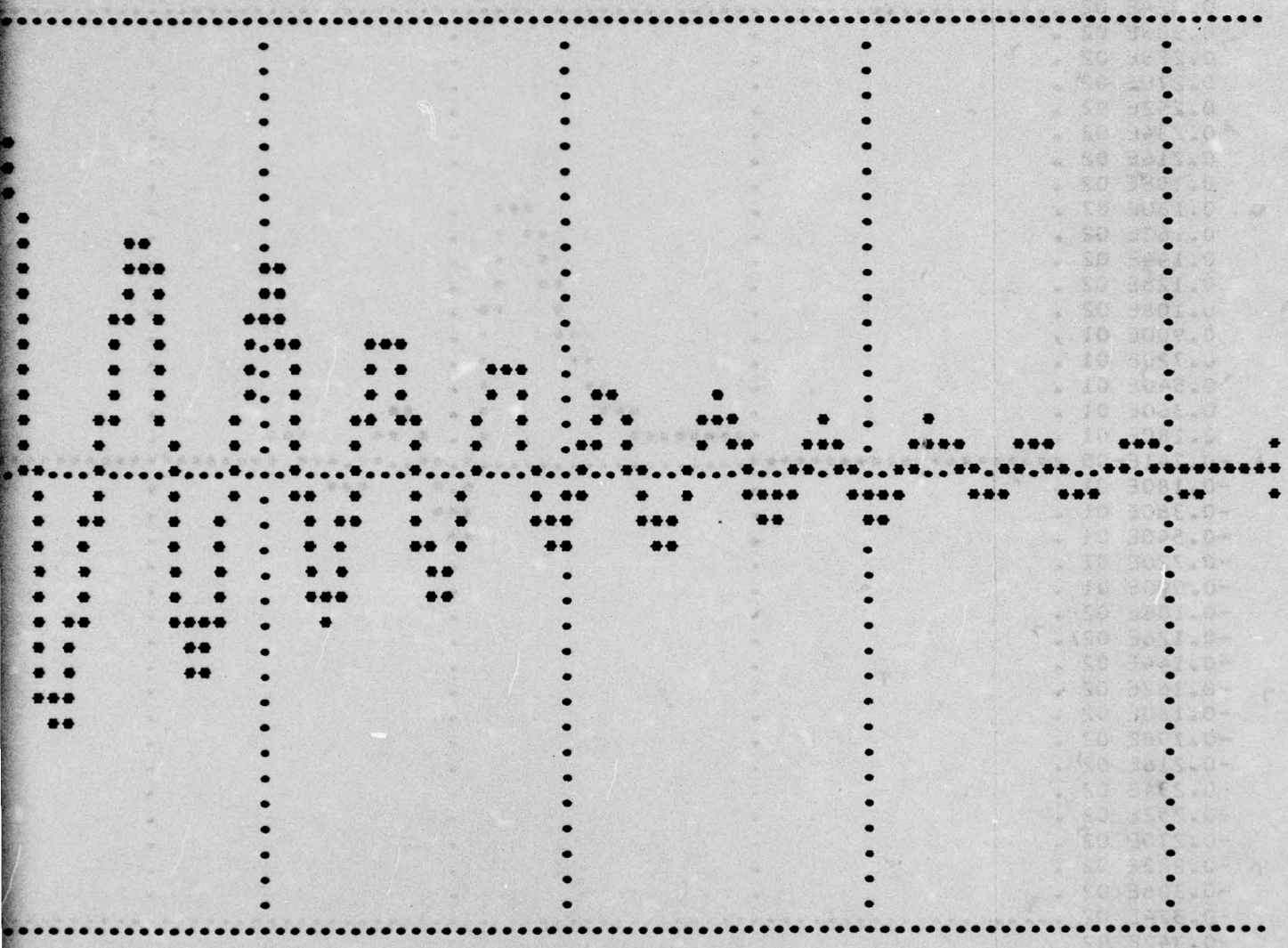
PICKUP VOLTS = (4)(3.1416)(S)(M)(DPHI/DT)SIN(PHI) = 0.235(DPHI/DT)SIN(PHI)
M(GAUSSES) = 1450. K(ERGS/CCM) = 25500. (FILM CROSS SECTION,SCM) = 0.129E
LAMBDAS(MAGNETOSTRICTION) = 0.20E-04 LAMBDA(DAMPING,CPS) = 0.10E 10
ALPHA = -1.000 BETA = 0.080 DELTA = 0.
HSWCH = (ALPHA)35.17 HPERP = (BETA)35.17 SIGMA = (DELTA)0.85E 09
HANIS = 2K/M = 35.17 PHIOD(INITIAL PHI,DEGREES) = 0.
TP(PEAKING TIME,NANOSECONDS) = 0.688 GAMMA(GYRO RATIO) = 0.176E 08 MAX PICKU



/DT)SIN(PHI) = 0.235(DPHI/DT)SIN(PHI)
3500. (FILM CROSS SECTION,SCM) = 0.129E-04
LAMBDA(DAMPING,CPS) = 0.10E 10
DELTA = 0.
35.17 SIGMA = (DELTA)0.85E 09
PHI,DEGREES) = 0.
GAMMA(GYRO RATIO) = 0.176E 08 MAX PICKUP SIG. = 0.138E 02

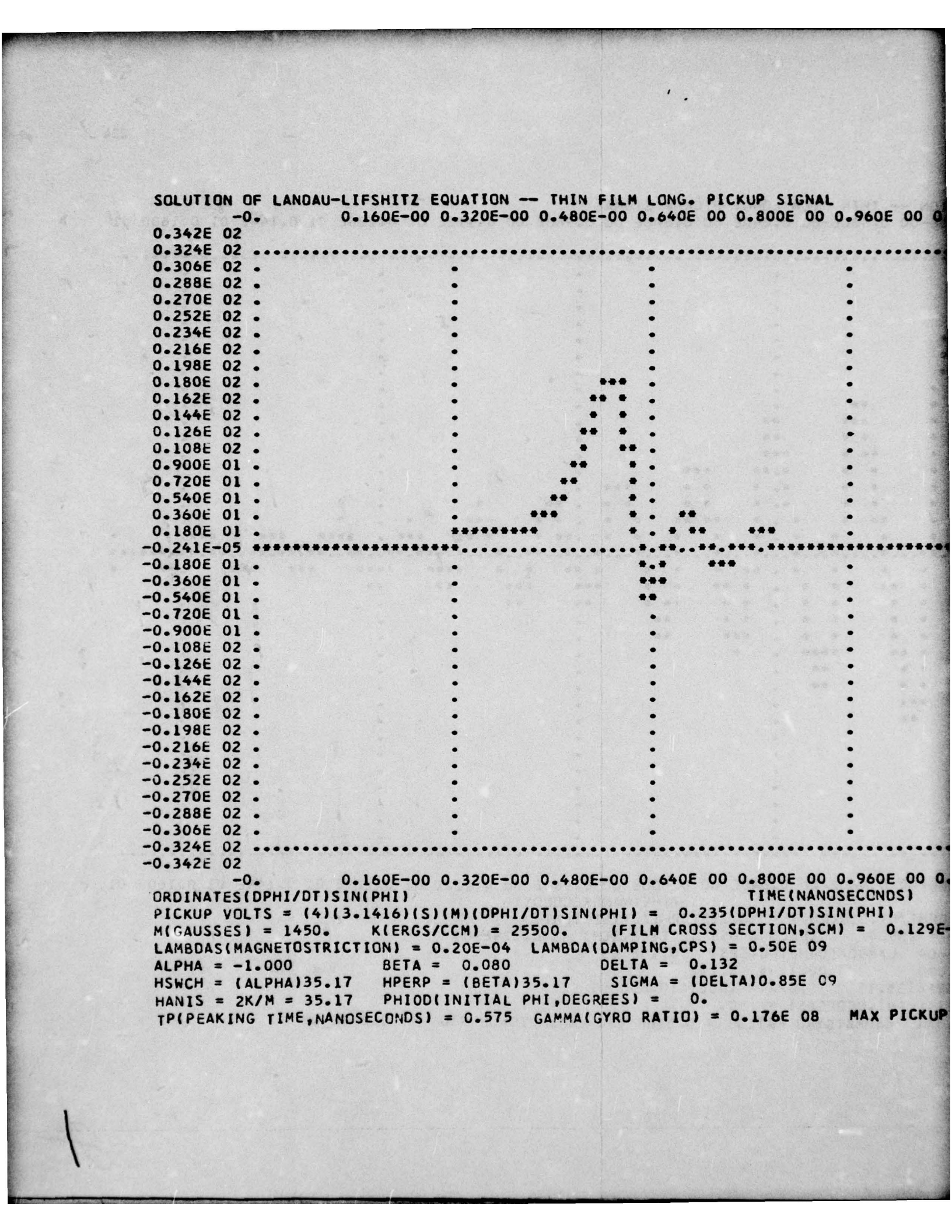
Fig. 101


SOLUTION OF LANDAU-LIFSHITZ EQUATION -- THIN FILM LONG. PICKUP SIGNAL
-0. 0.160E-00 0.320E-00 0.480E-00 0.640E 00 0.800E 00 0.960
0.342E 02
0.324E 02
0.306E 02
0.288E 02
0.270E 02
0.252E 02
0.234E 02
0.216E 02
0.198E 02
0.180E 02
0.162E 02
0.144E 02
0.126E 02
0.108E 02
0.900E 01
0.720E 01
0.540E 01
0.360E 01
0.180E 01
-0.241E-05
-0.180E 01
-0.360E 01
-0.540E 01
-0.720E 01
-0.900E 01
-0.108E 02
-0.126E 02
-0.144E 02
-0.162E 02
-0.180E 02
-0.198E 02
-0.216E 02
-0.234E 02
-0.252E 02
-0.270E 02
-0.288E 02
-0.306E 02
-0.324E 02
-0.342E 02
-0. 0.160E-00 0.320E-00 0.480E-00 0.640E 00 0.800E 00 0.960
ORDINATES(DPHI/DT)SIN(PHI)
TIME(NANOSECONI
PICKUP VOLTS = (4)(3.1416)(S)(M)(DPHI/DT)SIN(PHI) = 0.235(DPHI/DT)SIN(PHI
M(GAUSSES) = 1450. K(ERGS/CCM) = 25500. (FILM CROSS SECTION,SCM) =
LAMBDAS(MAGNETOSTRICTION) = 0.20E-04 LAMBDA(DAMPING,CPS) = 0.10E 09
ALPHA = -1.000 BETA = 0.080 DELTA = 0.132
HSWCH = (ALPHA)35.17 HPERP = (BETA)35.17 SIGMA = (DELTA)0.85E 09
HANIS = 2K/M = 35.17 PHIOD(INITIAL PHI,DEGREES) = 0.
TP(PEAKING TIME,NANOSECONDS) = 0.361 GAMMA(GYRO RATIO) = 0.176E 08 MAX



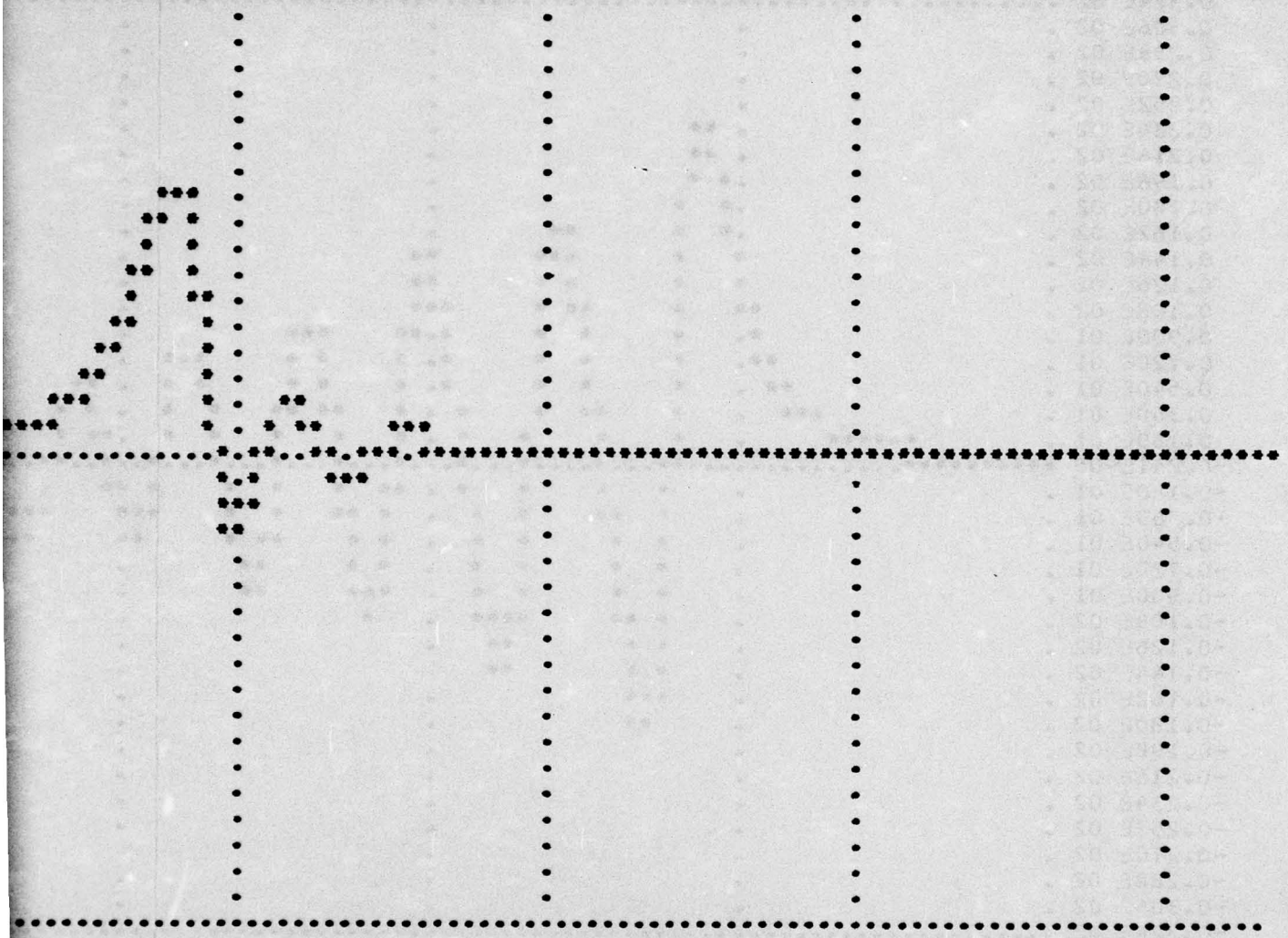
DPHI/DT)SIN(PHI) = 0.235(DPHI/DT)SIN(PHI)
= 25500. (FILM CROSS SECTION,SCM) = 0.129E-04
-04 LAMBDA(DAMPING,CPS) = 0.10E 09
080 DELTA = 0.132
ETA)35.17 SIGMA = (DELTA)0.85E 09
IAL PHI,DEGREES) = 0.
361 GAMMA(GYRO RATIO) = 0.176E 08 MAX PICKUP SIG. = 0.243E 02

Fig. 102



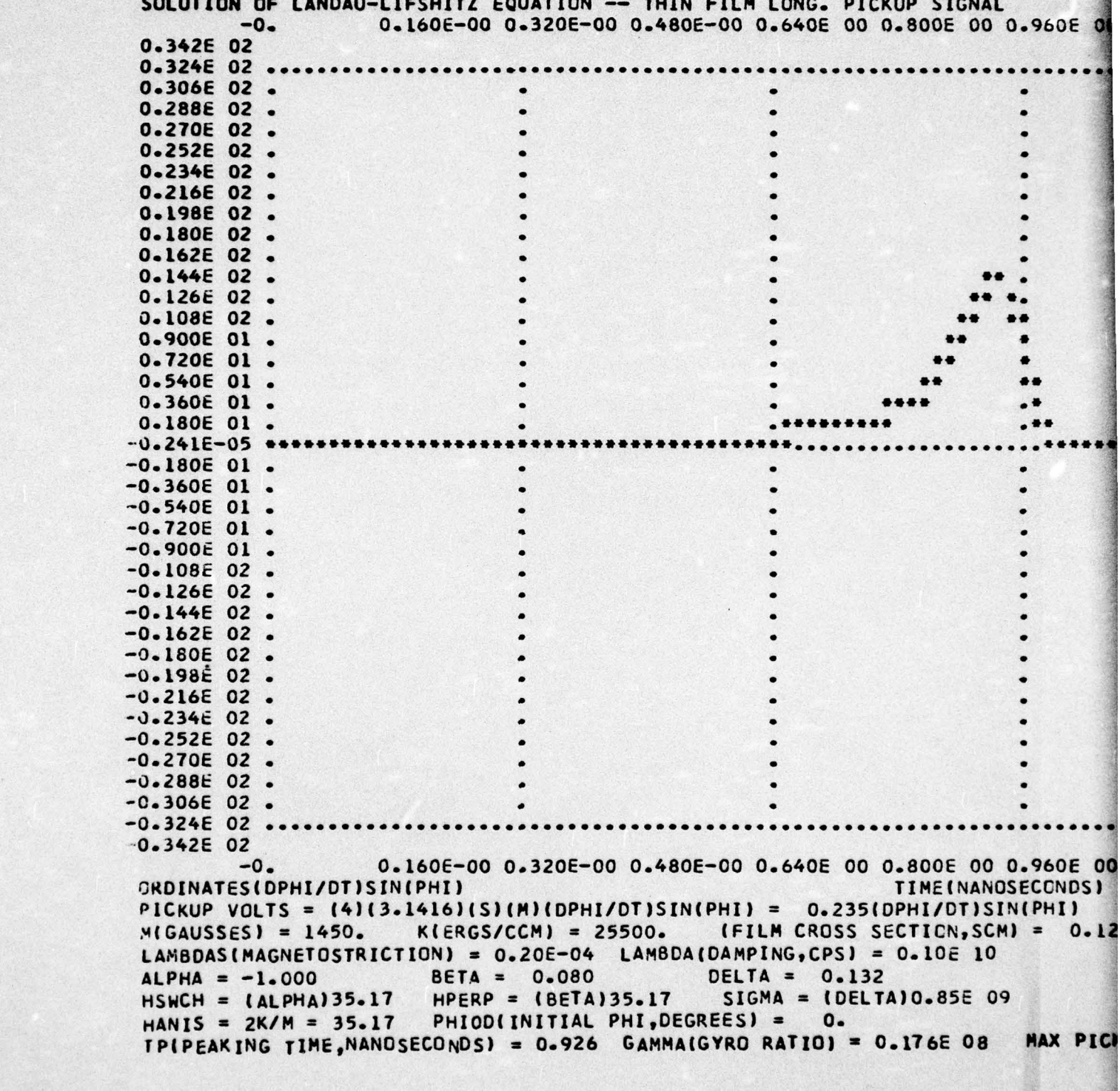
PICKUP VOLTS = (4)(3.1416)(S)(M)(DPHI/DT)SIN(PHI) = 0.235(DPHI/DT)SIN(PHI)
M(GAUSSES) = 1450. K(ERGS/CCM) = 25500. (FILM CROSS SECTION,SCM) = 0.129E-
LAMBDAS(MAGNETOSTRICTION) = 0.20E-04 LAMBDA(DAMPING,CPS) = 0.50E 09
ALPHA = -1.000 BETA = 0.080 DELTA = 0.132
HSWCH = (ALPHA)35.17 HPERP = (BETA)35.17 SIGMA = (DELTA)0.85E 09
HANIS = 2K/M = 35.17 PHIOD(INITIAL PHI,DEGREES) = 0.
TP(PEAKING TIME,NANOSECONDS) = 0.575 GAMMA(GYRO RATIO) = 0.176E 08 MAX PICKUP

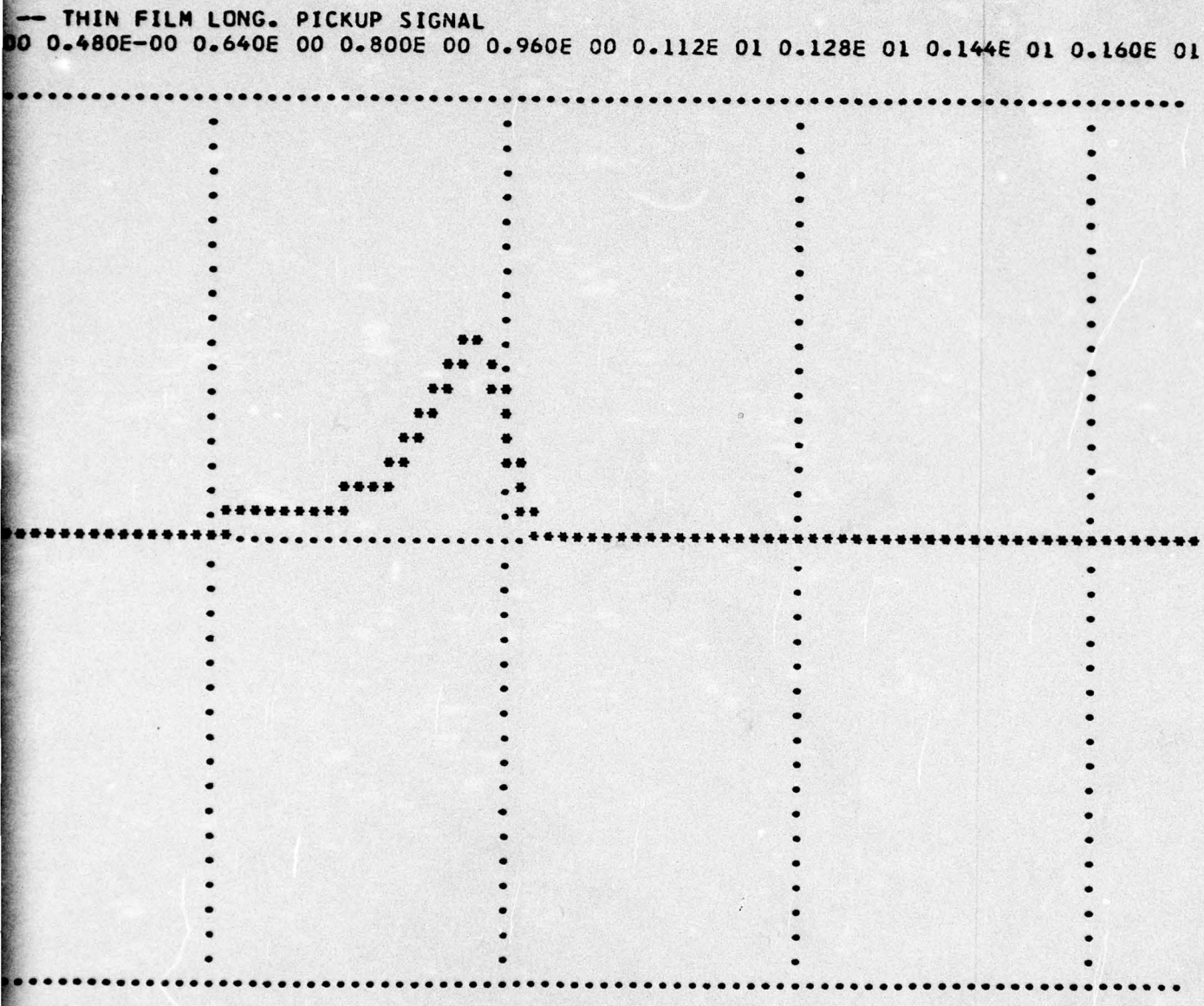
N -- THIN FILM LONG. PICKUP SIGNAL
-00 0.480E-00 0.640E 00 0.800E 00 0.960E 00 0.112E 01 0.128E 01 0.144E 01 0.160E 01



00 0.480E-00 0.640E 00 0.800E 00 0.960E 00 0.112E 01 0.128E 01 0.144E 01 0.160E 01
TIME(NANOSECONDS)
I/DT)SIN(PHI) = 0.235(DPHI/DT)SIN(PHI)
25500. (FILM CROSS SECTION,SCM) = 0.129E-04
LAMBDA(DAMPING,CPS) = 0.50E 09
DELTA = 0.132
)35.17 SIGMA = (DELTA)0.85E 09
PHI,DEGREES) = 0.
GAMMA(GYRO RATIO) = 0.176E 08 MAX PICKUP SIG. = 0.187E 02

Fig. 103


SOLUTION OF LANDAU-LIFSHITZ EQUATION -- THIN FILM LONG. PICKUP SIGNAL
-0. 0.160E-00 0.320E-00 0.480E-00 0.640E 00 0.800E 00 0.960E 0
0.342E 02
0.324E 02
0.306E 02
0.288E 02
0.270E 02
0.252E 02
0.234E 02
0.216E 02
0.198E 02
0.180E 02
0.162E 02
0.144E 02
0.126E 02
0.108E 02
0.900E 01
0.720E 01
0.540E 01
0.360E 01
0.180E 01
-0.241E-05
-0.180E 01
-0.360E 01
-0.540E 01
-0.720E 01
-0.900E 01
-0.108E 02
-0.126E 02
-0.144E 02
-0.162E 02
-0.180E 02
-0.198E 02
-0.216E 02
-0.234E 02
-0.252E 02
-0.270E 02
-0.288E 02
-0.306E 02
-0.324E 02
-0.342E 02
-0. 0.160E-00 0.320E-00 0.480E-00 0.640E 00 0.800E 00 0.960E 00
ORDINATES(DPHI/DT)SIN(PHI)
TIME(NANOSECONDS)
PICKUP VOLTS = (4)(3.1416)(S)(M)(DPHI/DT)SIN(PHI) = 0.235(DPHI/DT)SIN(PHI)
M(GAUSSES) = 1450. K(ERGS/CCM) = 25500. (FILM CROSS SECTION,SCM) = 0.12
LAMBDAS(MAGNETOSTRICTION) = 0.20E-04 LAMBDA(DAMPING,CPS) = 0.10E 10
ALPHA = -1.000 BETA = 0.080 DELTA = 0.132
HSWCH = (ALPHA)35.17 HPERP = (BETA)35.17 SIGMA = (DELTA)0.85E 09
HANIS = 2K/M = 35.17 PHIOD(INITIAL PHI,DEGREES) = 0.
TP(PEAKING TIME,NANOSECONDS) = 0.926 GAMMA(GYRO RATIO) = 0.176E 08 MAX PIC



I/DT)SIN(PHI) = 0.235(DPHI/DT)SIN(PHI)
25500. (FILM CROSS SECTION,SCM) = 0.129E-04
LAMBDA(DAMPING,CPS) = 0.10E 10
DELTA = 0.132
035.17 SIGMA = (DELTA)0.85E 09
PHI,DEGREES) = 0.
GAMMA(GYRO RATIO) = 0.176E 08 MAX PICKUP SIG. = 0.140E 02

Fig. 104

H_s = - 35 oe (α = - 1.0).

Figures 96, 97, 98 refer to the case of a negative stress δ = - 0.132. As the damping is increased from $\lambda = 10^8$ to 5×10^8 and to 10×10^8 cps, the amplitude of the first pickup voltage overshoot, due to the ferromagnetic oscillation, decreases from "0.7 x peaking voltage" to zero. The value of the peaking voltage is reduced by 50%. The disappearance of the oscillation would make an increase in damping desirable in thin film digital applications. However, in addition to the decrease in pickup signal, damping has the undesirable feature of increasing switching time as a comparison between Figs. 96 and 98 shows. As the damping constant is increased from 10^8 to 10×10^8 cps, peaking time increases from 0.291 nsec. to 0.573 nsec. A curve showing the increase in peaking time (or the decrease in peaking volts) as the damping constant is increased would be of interest and could be easily obtained with a slight modification of the program written for solving the Landau-Lifshitz equation. This study has not been included in the extensive digital computation reported in this investigation and is merely suggested as an extension of this work.

Figures 99, 100, 101 inclusive and 102, 103, 104 inclusive refer to cases in which all parameters are

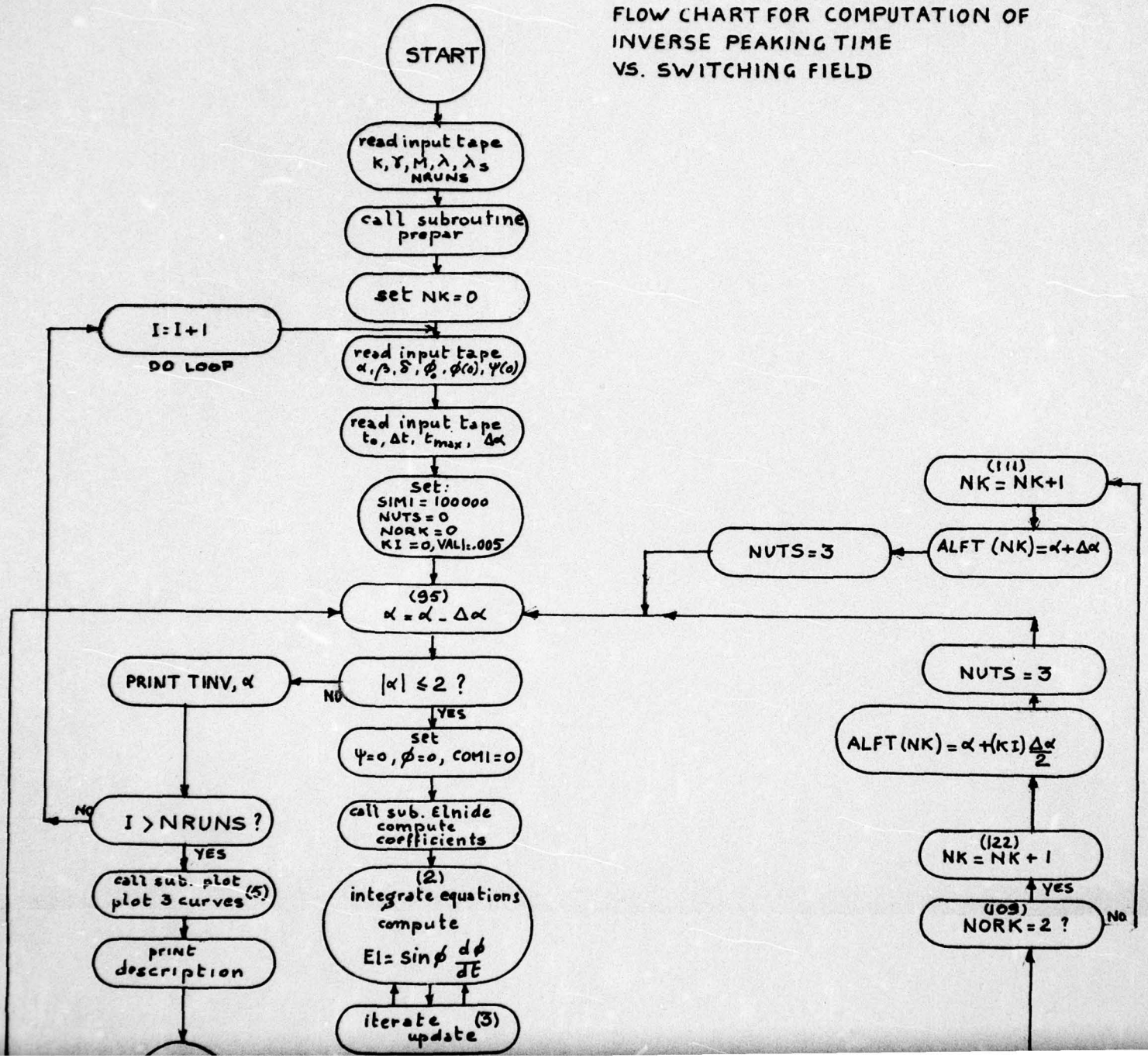
left equal to those in preceding Figs. 96, 97, 98, except the stress δ . In the case of Figs. 99, 100, 101, δ is zero, while in the case of Figs. 102 to 104, is made positive. The effects of increased damping when $\delta = 0$ or $\delta > 0$ is the same as for $\delta < 0$. From the nine plots in Figs. 96 to 104 an important observation may be made: as the stress is increased from negative values to positive values, the delay caused by increased damping increases. An examination of the switching responses in Figs. 98, 101, 104 shows that the curves have the same amplitude, no overshoot, but different switching delays. For example, as δ is increased from - 0.132 (Fig. 98) to + 0.132 (Fig. 104) peaking time increases from 0.573 nsec. to 0.926, with the same pickup signal amplitude and no overshoot. The possibility of increased damping acting on the composition by small additions of other elements combined with metallurgical treatment seems to be worthy of investigation. Also, the application of a compression along the direction of H_p or a tension along H_s tends to offset the increase in switching delay caused by increased damping.

(2) Inverse peaking time vs. switching field magnitude for constant β or constant δ .

As done by other investigators,[6, 7] the dynamic

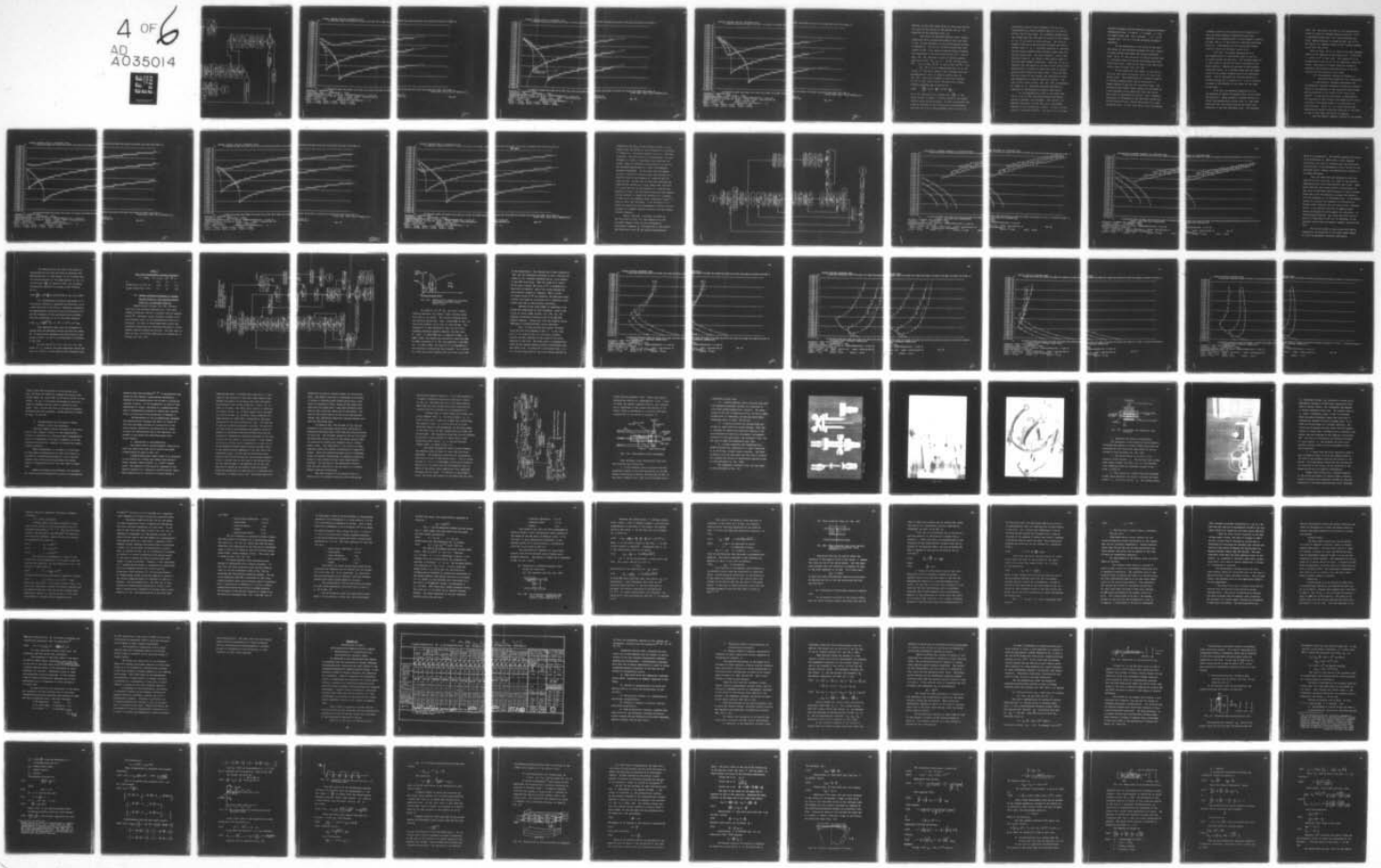
FIG. 105

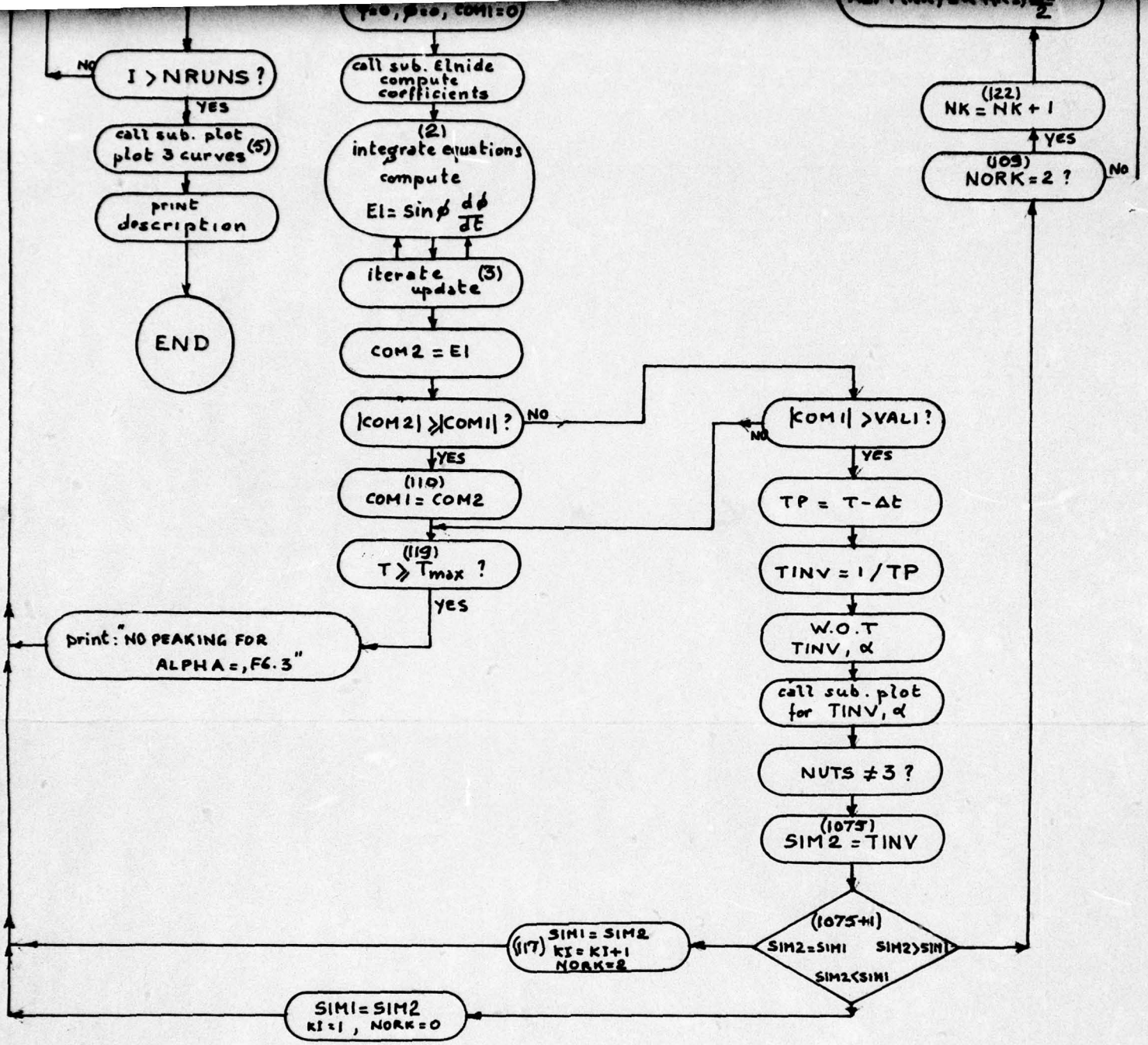
FLOW CHART FOR COMPUTATION OF INVERSE PEAKING TIME VS. SWITCHING FIELD

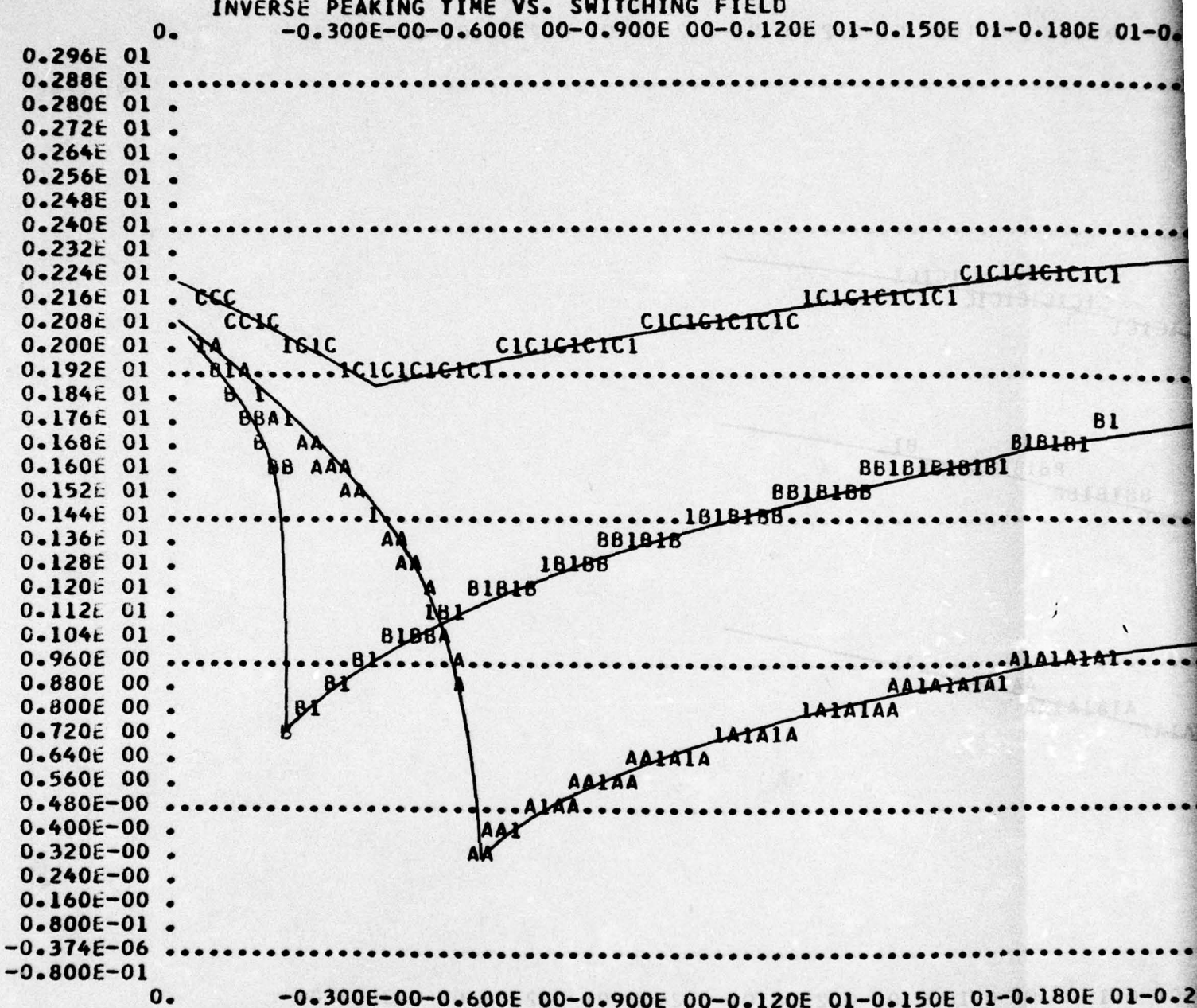


AD-A035 014 CALIFORNIA UNIV LOS ANGELES DEPT OF ENGINEERING F/G 20/2
ON THE USE OF PIEZOELECTRIC-MAGNETOSTRICTIVE COUPLING IN DIGITA--ETC(U)
AUG 62 A A BORSEI NONR-233(52)
UNCLASSIFIED UCLA62-37 NL

4 OF 6
AD
A035014




I > NRUNS ?
NO
YES
call sub. plot
plot 3 curves (5)
print
description
END
call sub. Elnide
compute
coefficients
(2)
integrate equations
compute
El = Sin φ dφ/dE
iterate
update (3)
COM2 = El
|COM2| ≥ |COM1| ?
NO
YES
(110)
COM1 = COM2
(119)
T ≫ Tmax ?
yes
print: "NO PEAKING FOR
ALPHA =, F6.3"
(122)
NK = NK + 1
YES
(109)
NORK = 2 ?
NO
|COM1| > VAL1 ?
NO
YES
TP = T - Δt
TINV = 1/TP
W.O.T
TINV, α
call sub. plot
for TINV, α
NUTS ≠ 3 ?
(1075)
SIM2 = TINV
(1075+11)
SIM2 = SIM1
SIM2 > SIM1
SIM2 < SIM1
(117) SIM1 = SIM2
KI = KI + 1
NORK = 2
SIM1 = SIM2
KI = 1 , NORK = 0



ORDINATES = 1/PEAKING TIME
M(GAUSSES)= 860. K(ERGS/CCM) = 1290.
LAMBDAS(MAGNETOSTRICTION) = 0.19E-04 LAMBDA(DAMPING,CPS) = 0.10E 09
GAMMA(GYRO RATIO) = 0.176E 08 DELTA = -0.200 SIGMA = (DELTA)0.45E 08
HSWCH = (ALPHA) 3.00 HPERP = (BETA) 3.00
HANIS = 2K/M = 3.00 PHIOD(INITIAL PHI,DEGREES) = 0.
BETA1 = 0.080 BETA2 = 0.500 BETA3 = 1.000
ALFT1 = -0.6506 ALFT2 = -0.270 ALFT3 = -0.530

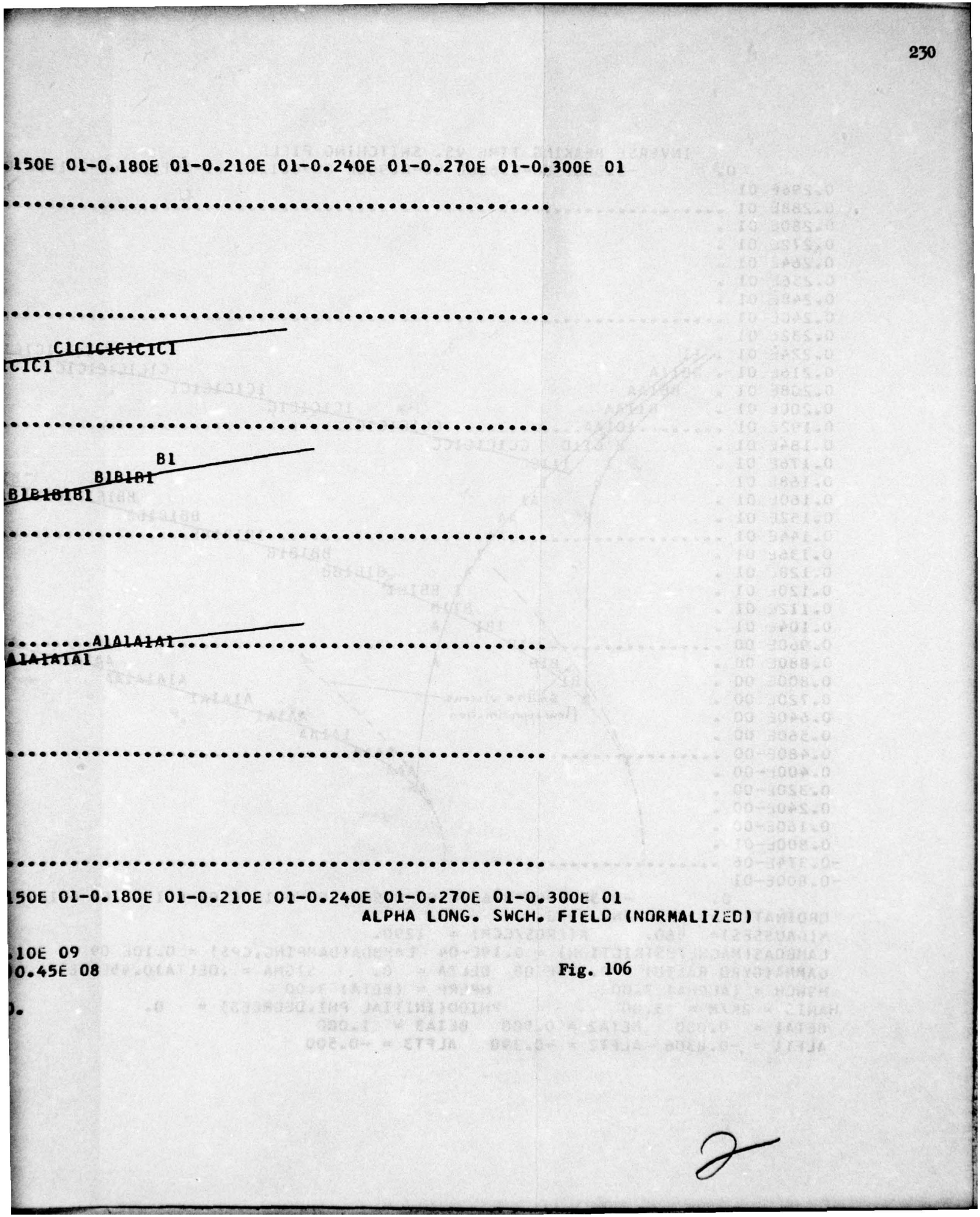
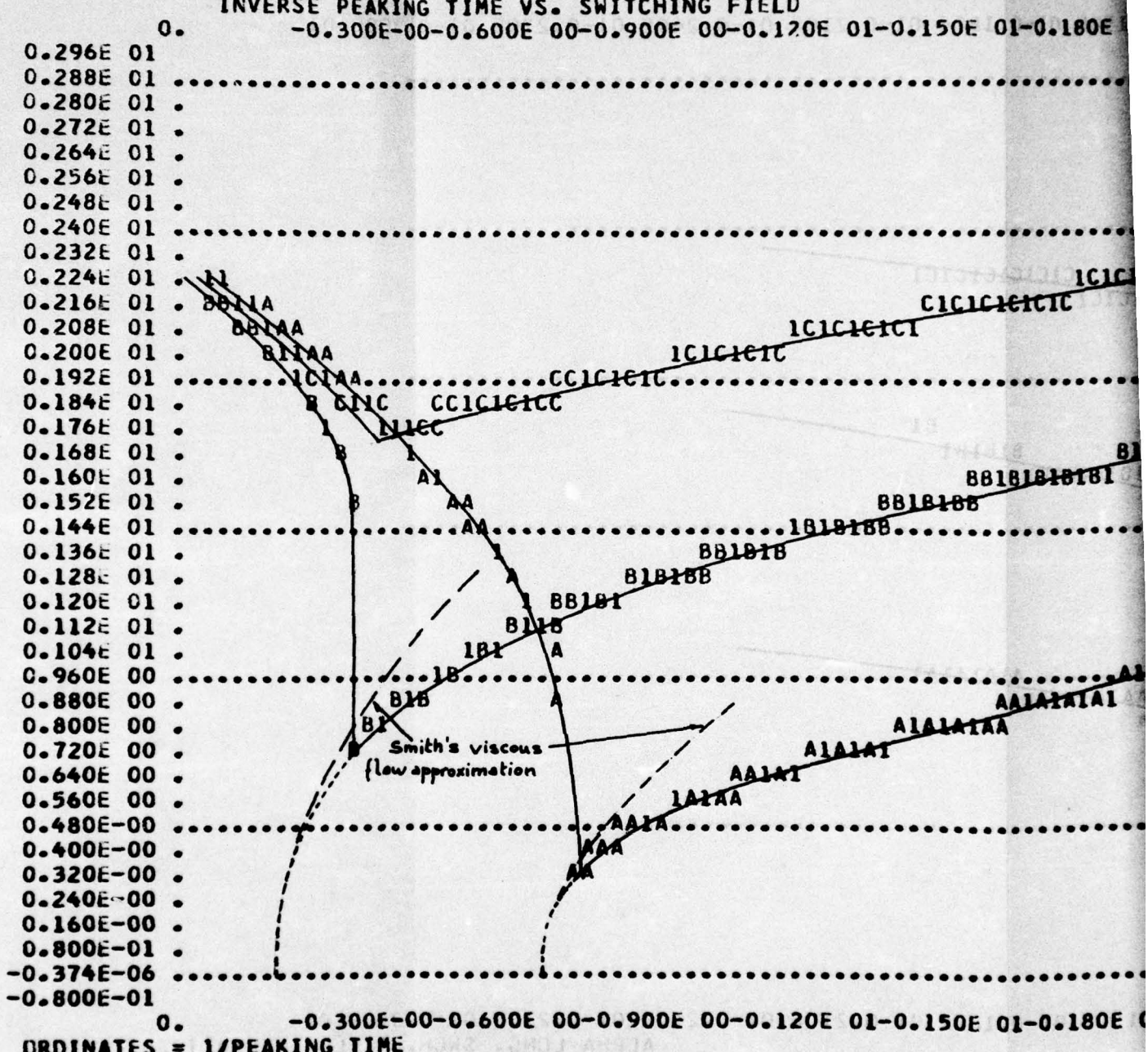

.150E 01-0.180E 01-0.210E 01-0.240E 01-0.270E 01-0.300E 01
C1C1C1C1C1C1
1C1C1
B1
B1B1B1
1B1B1B1B1
A1A1A1A1
1A1A1A1A1
150E 01-0.180E 01-0.210E 01-0.240E 01-0.270E 01-0.300E 01
ALPHA LONG. SWCH. FIELD (NORMALIZED)
.10E 09
)0.45E 08
).

Fig. 106


INVERSE PEAKING TIME VS. SWITCHING FIELD
0.
-0.300E-00-0.600E 00-0.900E 00-0.120E 01-0.150E 01-0.180E
0.296E 01
0.288E 01
0.280E 01
0.272E 01
0.264E 01
0.256E 01
0.248E 01
0.240E 01
0.232E 01
0.224E 01
0.216E 01
0.208E 01
0.200E 01
0.192E 01
0.184E 01
0.176E 01
0.168E 01
0.160E 01
0.152E 01
0.144E 01
0.136E 01
0.128E 01
0.120E 01
0.112E 01
0.104E 01
0.960E 00
0.880E 00
0.800E 00
0.720E 00
0.640E 00
0.560E 00
0.480E-00
0.400E-00
0.320E-00
0.240E-00
0.160E-00
0.800E-01
-0.374E-06
-0.800E-01
Smith's viscous flow approximation
ORDINATES = 1/PEAKING TIME
M(GAUSSES)= 860. K(ERGS/CCM) = 1290.
LAMBDAS(MAGNETOSTRICTION) = 0.19E-04 LAMBDA(DAMPING,CPS) = 0.10E 09
GAMMA(GYRO RATIO) = 0.176E 08 DELTA = 0. SIGMA = (DELTA)0.45E 08
HSWCH = (ALPHA) 3.00 HPERP = (BETA) 3.00
HANIS = 2K/M = 3.00 PHIOD(INITIAL PHI,DEGREES) = 0.
BETA1 = 0.080 BETA2 = 0.500 BETA3 = 1.000
ALFT1 = -0.8306 ALFT2 = -0.390 ALFT3 = -0.500

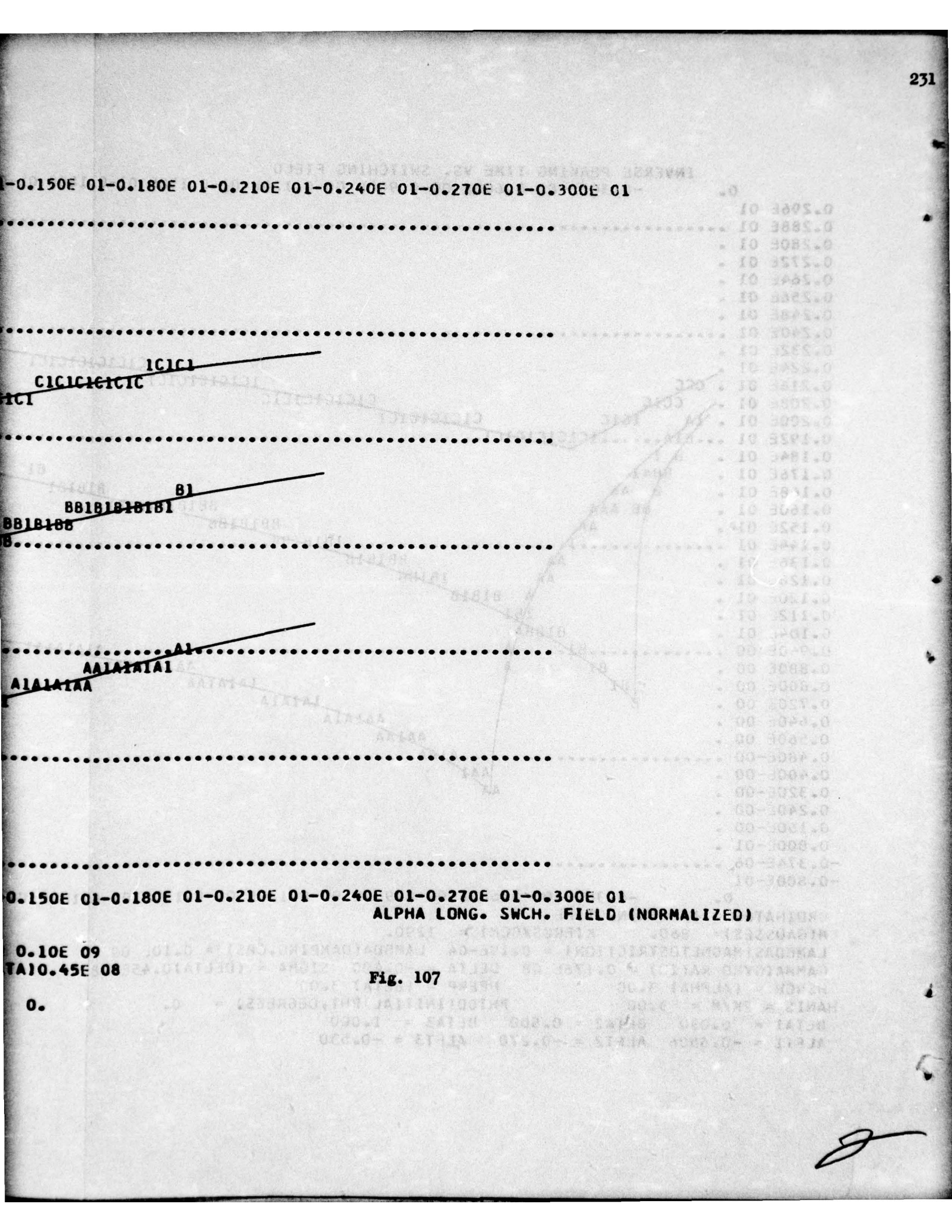
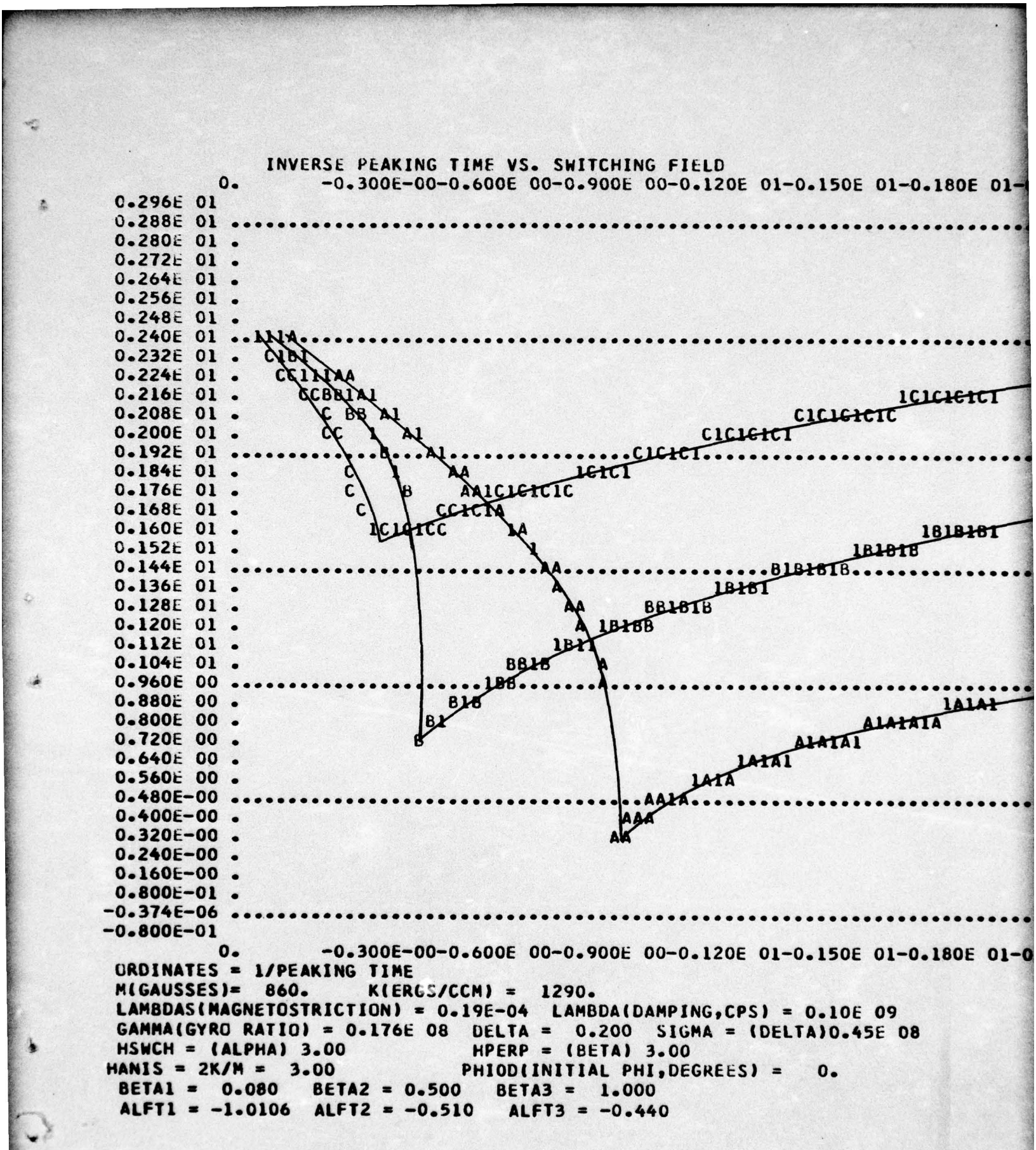

-0.150E 01-0.180E 01-0.210E 01-0.240E 01-0.270E 01-0.300E 01
1C1C1
C1C1C1C1C1C
1C1
B1
BB1B1B1B1B1
BB1B1B8
A1
AA1A1A1A1
A1A1A1AA
0.150E 01-0.180E 01-0.210E 01-0.240E 01-0.270E 01-0.300E 01
ALPHA LONG. SWCH. FIELD (NORMALIZED)
0.10E 09
TA)0.45E 08
0.

Fig. 107


INVERSE PEAKING TIME VS. SWITCHING FIELD
0. -0.300E-00-0.600E 00-0.900E 00-0.120E 01-0.150E 01-0.180E 01-
0.296E 01
0.288E 01
0.280E 01
0.272E 01
0.264E 01
0.256E 01
0.248E 01
0.240E 01
0.232E 01
0.224E 01
0.216E 01
0.208E 01
0.200E 01
0.192E 01
0.184E 01
0.176E 01
0.168E 01
0.160E 01
0.152E 01
0.144E 01
0.136E 01
0.128E 01
0.120E 01
0.112E 01
0.104E 01
0.960E 00
0.880E 00
0.800E 00
0.720E 00
0.640E 00
0.560E 00
0.480E-00
0.400E-00
0.320E-00
0.240E-00
0.160E-00
0.800E-01
-0.374E-06
-0.800E-01
0. -0.300E-00-0.600E 00-0.900E 00-0.120E 01-0.150E 01-0.180E 01-0
ORDINATES = 1/PEAKING TIME
M(GAUSSES)= 860. K(ERGS/CCM) = 1290.
LAMBDAS(MAGNETOSTRICTION) = 0.19E-04 LAMBDA(DAMPING,CPS) = 0.10E 09
GAMMA(GYRO RATIO) = 0.176E 08 DELTA = 0.200 SIGMA = (DELTA)0.45E 08
HSWCH = (ALPHA) 3.00 HPERP = (BETA) 3.00
HANIS = 2K/M = 3.00 PHIOD(INITIAL PHI,DEGREES) = 0.
BETA1 = 0.080 BETA2 = 0.500 BETA3 = 1.000
ALFT1 = -1.0106 ALFT2 = -0.510 ALFT3 = -0.440

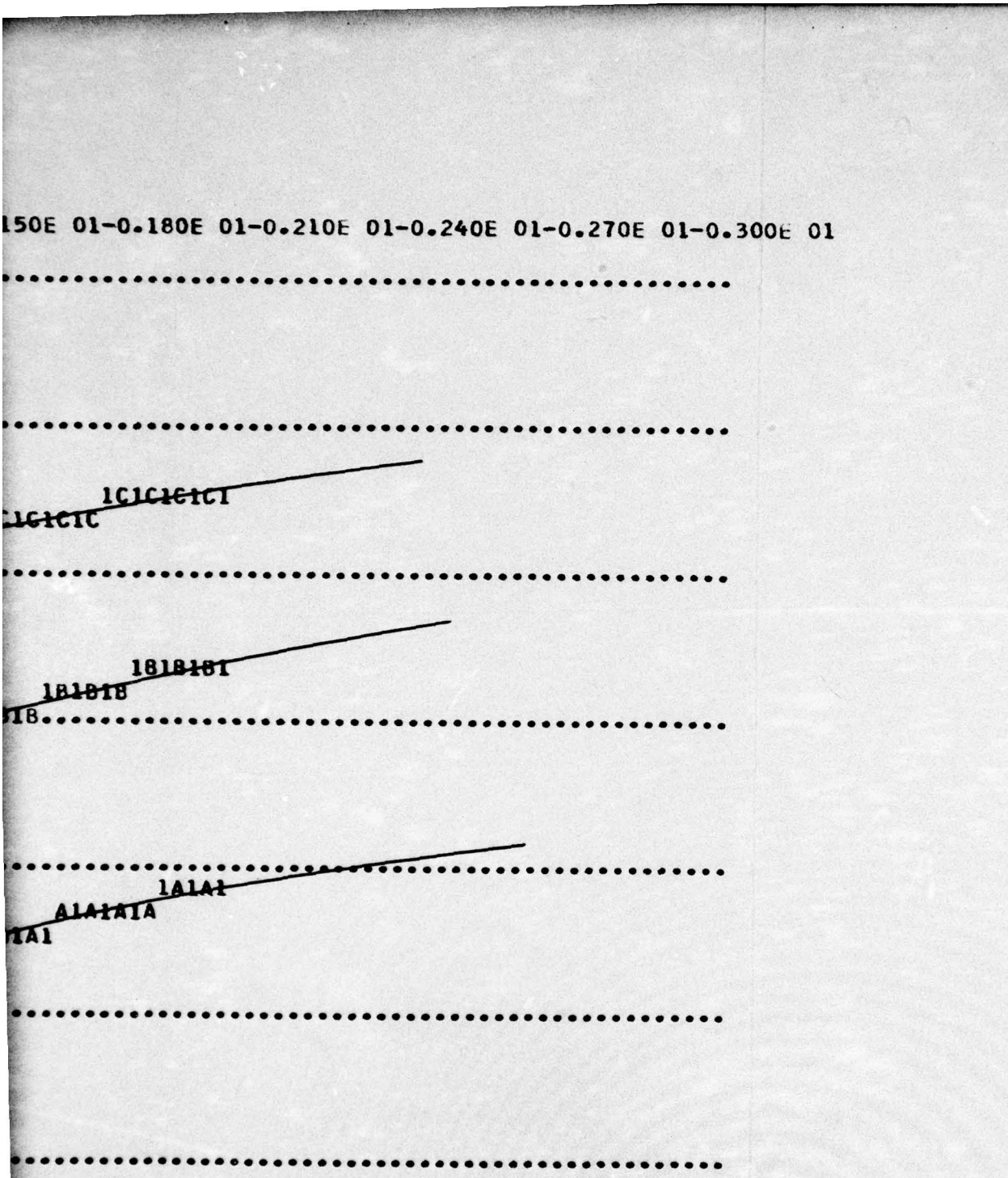

150E 01-0.180E 01-0.210E 01-0.240E 01-0.270E 01-0.300E 01
1C1C1C1C1
1B1B1B1
1A1A1
A1A1A1A
50E 01-0.180E 01-0.210E 01-0.240E 01-0.270E 01-0.300E 01
ALPHA LONG. SWCH. FIELD (NORMALIZED)
10E 09
0.45E 08

Fig. 108

behavior of the films under study has been characterized by a plot of the inverse of the peaking time vs. the magnitude of the switching field H_s.

Such plots are obtained directly from a digital computation with a program described by the flow chart in Fig. 105 and referenced to the corresponding listing in Appendix 8. The case of the 80-20 nickel-iron film studied in Ref. 6 was again considered before extending the computation to the 44-56 nickel-iron film. Each of Figs. 106, 107, 108 shows 3 plots of inverse peaking time vs α for β = .08, .5, 1.0. In Fig. 106 the stress δ = - 0.2, in Fig. 107 δ = 0, and in Fig. 108 δ = + 0.2.

Fig. 107 is to be compared with Fig. 10, p. 271 of Ref. 6. The curves shown in the reference have been extrapolated to zero, as shown in dotted lines in Fig. 107. Also, the statement is made that assuming $4\pi M << 2K/M$ and $\lambda << \gamma M$ the two scalar Landau-Lifshitz equations may be reduced to:

$$(108) \qquad \frac{d^2\phi}{dt^2} + 4\pi\lambda \frac{d\phi}{dt} + 4\pi\gamma^2 \frac{dE}{d\phi} = 0$$

If in this equation it is assumed that $\frac{d^2\phi}{dt^2} = 0$, the author in Ref. 6 obtains a viscous motion of the magnetization vector during reversal. He then investigates the range of validity of this "viscous flow approximation" and finds it to be in good agreement with the exact so-

lution when reversal occurs between 5 and 10 nsec., corresponding to inverse peaking times of 0.2, and 0.1 in Fig. 107 of this study. It is however evident from this figure that the film does not switch in this region as H_s is too small to cause reversal. The curve is actually limited by the switching threshold and below a certain value of H_s a disturbed condition is observed, and the inverse peaking time increases rather than continuing toward zero. The curve presents a cusp at the threshold value of H_s, which is the coercive force of the film under dynamic conditions. From Fig. 107 it is apparent that the region of validity of the viscous flow approximation is restricted below the value of inverse peaking time at which the cusp occurs. Since the film does not switch in this region, the usefulness of this approximation is of limited practical interest. The part of the curves in Figs. 106, 107, 108, corresponding to values of H_s below the switching threshold is important in non-destructive readout applications.

As the perpendicular field is increased from .08 to .5 to 1.0 the switching threshold decreases, reaches a minimum, and increases. This behavior is apparent from Figs. 106 and 107, but is influenced strongly by the presence of a stress. In fact, if the stress is increased from δ = - 0.2 to 0, to + 0.2, the

minimum disappears and the switching threshold decreases continuously from = 0.08 to = 1.0 when = + 0.2, as shown in Fig. 108. For a constant , as is increased from - 0.2 to + 0.2 the switching threshold decreases.

In the description at the bottom of the plots the values of the switching threshold for the 3 curves is given and has been named ALFT (alpha threshold). Figs. 109 to 111 show the plots of inverse peaking time vs. switching field for the positive magnetostriction nickel-iron film. These curves lead to the same observations made for Figs. 106, 107, 108.

In the region near the origin, at the left of the cusp, the curves in figures 106 to 111 have a negative slope. The significance of a negative slope in an "inverse peaking curve" may be discussed in a manner similar to the case of a positive slope. The presence of two stable states implies the existence of a high energetic level separating these two states. This level is represented by the hard axis of magnetization and is originated by the anisotropy forces and the DC external forces, before application of a step switching field. To this high energy level corresponds

a dynamic coercive force defined as the magnitude of the step field capable of impressing sufficient momentum to the magnetization to cause magnetic reversal. In Figs. 106 to 111 the values of normalized switching field α_T corresponding to the cusp are the dynamic coercive forces for different values of β.

If $\alpha > \alpha_T$ the moment impressed by α to the magnetization is sufficiently high to cause it to rotate beyond the hard axis. The "peaking time" Δt is then taken to signify the time to accomplish complete reversal. Beyond the position of hard magnetization the vector M is guided toward the new stable state by the residual momentum and by the anisotropy field. If α is increased the residual momentum increases causing Δt to decrease and $1/\Delta t$ to increase, as shown by the branches of the curves at the right of the cusp.

If $\alpha < \alpha_T$ the momentum impressed by α is insufficient to rotate the magnetization vector beyond the hard axis. After reaching a maximum angular rotation the magnetization rotates back to a new state different from the original one by the static contribution of the step switching field. The "peaking

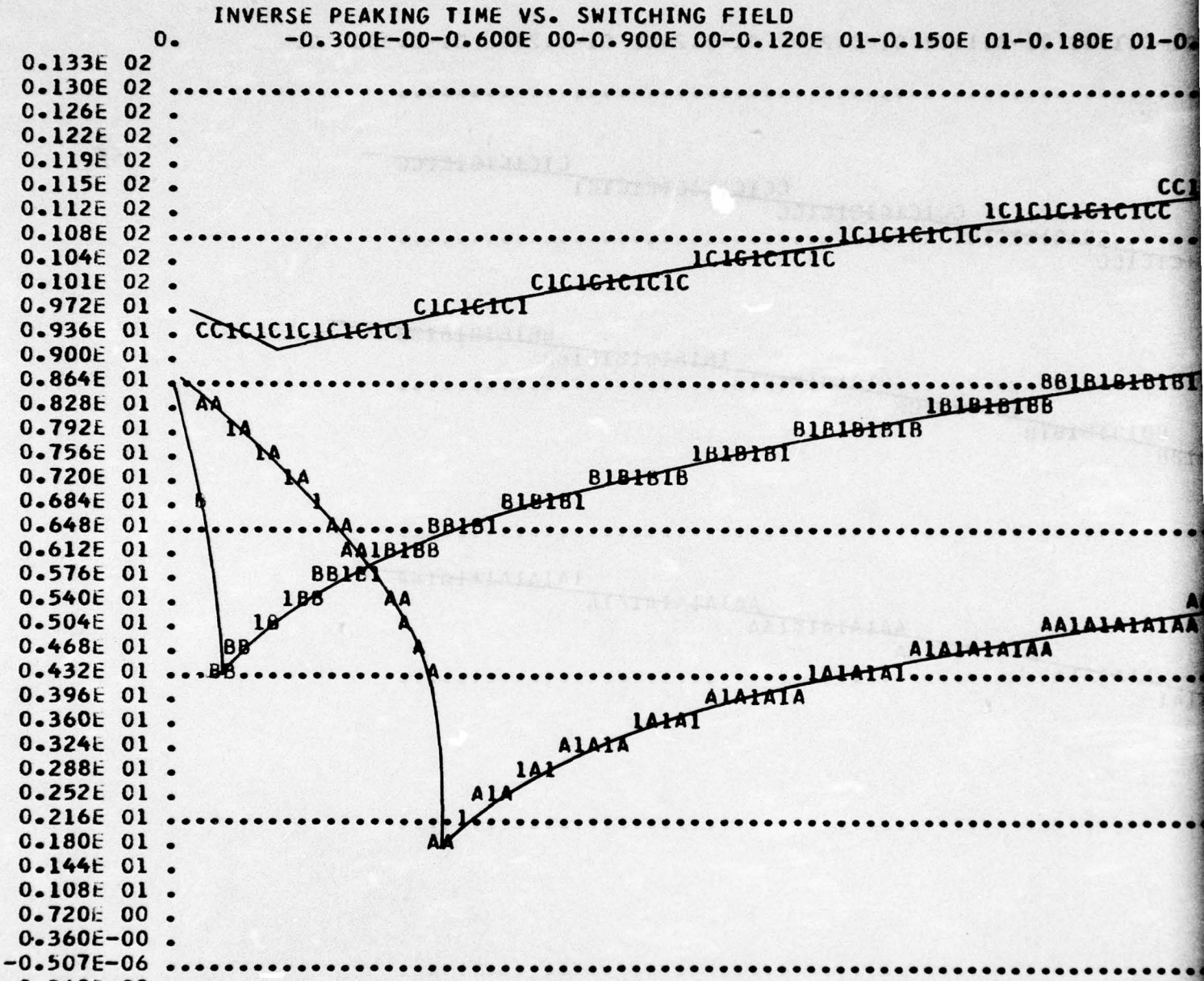
time" Δt represents the time for the magnetization vector to reach its maximum angular excursion. As α is decreased toward zero Δt should decrease and $1/\Delta t$ should increase, as shown by Figs. 106 to 111. The result is a negative slope for the "inverse peaking curve" near the origin.

Plots in Figs. 106 to 111 show a very small negative number at the ordinate of the origin (e.g. - 0.773 E-07 = $- 0.773 \times 10^{-7}$ in Fig. 106). This number is to be interpreted as zero and is due to computation round off errors. The negative ordinate below the origin is entered by the plotting subroutine and is to be disregarded for the purpose of this study.

(3) Ferromagnetic resonance frequency vs. switching field magnitude, for constant β, δ.

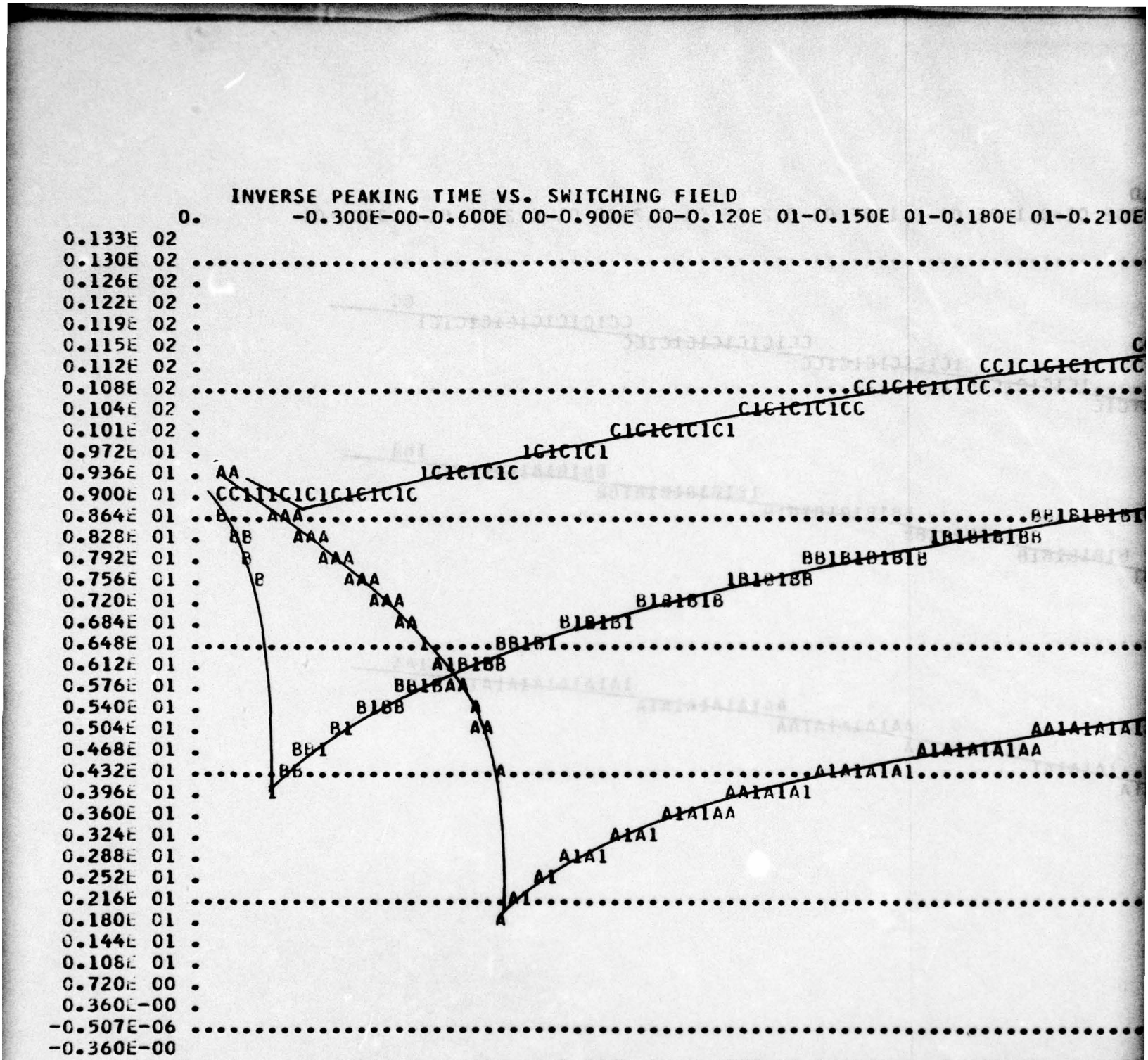
In ferromagnetic resonance experiments the ferromagnetic resonance frequency is found to be proportional to the magnitude of the applied DC field around which precession of the magnetization vector takes place[13]. In the case of thin films, as mentioned at the beginning of this chapter, the magnetization vector initiates a precessing motion as it approaches H_s after reversal. Since H_s is a step function the magnetization spirals around the direction of the field to come to rest under the effect of damping.

From the digital computer solution of the dynamic


INVERSE PEAKING TIME VS. SWITCHING FIELD
0. -0.300E-00-0.600E 00-0.900E 00-0.120E 01-0.150E 01-0.180E 01-0.
0.133E 02
0.130E 02
0.126E 02
0.122E 02
0.119E 02
0.115E 02
0.112E 02
0.108E 02
0.104E 02
0.101E 02
0.972E 01
0.936E 01
0.900E 01
0.864E 01
0.828E 01
0.792E 01
0.756E 01
0.720E 01
0.684E 01
0.648E 01
0.612E 01
0.576E 01
0.540E 01
0.504E 01
0.468E 01
0.432E 01
0.396E 01
0.360E 01
0.324E 01
0.288E 01
0.252E 01
0.216E 01
0.180E 01
0.144E 01
0.108E 01
0.720E 00
0.360E-00
-0.507E-06
-0.360E-00
0. -0.300E-00-0.600E 00-0.900E 00-0.120E 01-0.150E 01-0.180E 01-0.
ORDINATES = 1/PEAKING TIME
M(GAUSSES)= 1450. K(ERGS/CCM) = 25500.
LAMBDAS(MAGNETOSTRICTION) = 0.19E-04 LAMBDA(DAMPING,CPS) = 0.10E 09
GAMMA(GYRO RATIO) = 0.176E 08 DELTA = -0.200 SIGMA = (DELTA)0.89E 09
HSWCH = (ALPHA)35.17 HPERP = (BETA)35.17
HANIS = 2K/M = 35.17 PHIOD(INITIAL PHI,DEGREES) = 0.
BETA1 = 0.080 BETA2 = 0.500 BETA3 = 1.000
ALFT1 = -0.5506 ALFT2 = -0.090 ALFT3 = -0.200

0.150E 01-0.180E 01-0.210E 01-0.240E 01-0.270E 01-0.300E 01
CC
CC1C1C1C1C1C1C1C1
CC1C1C1C1C1C1CC
1C1C1C1C1C1CC
C1C1C1C
1BB
BB1B1B1B1B1B1B
1B1B1B1B1BB
BB1B1B1B1B1B
1B1B1B1BB
B1B
1A1AA
1A1A1A1A1A1A1A
AA1A1A1A1A1A
AA1A1A1A1AA
A1A1A1A1AA
A1
0.150E 01-0.180E 01-0.210E 01-0.240E 01-0.270E 01-0.300E 01
ALPHA LONG. SWCH. FIELD (NORMALIZED)
0.10E 09
A)0.89E 09
0.

Fig. 109


INVERSE PEAKING TIME VS. SWITCHING FIELD
0.
-0.300E-00-0.600E 00-0.900E 00-0.120E 01-0.150E 01-0.180E 01-0.210E
0.133E 02
0.130E 02
0.126E 02
0.122E 02
0.119E 02
0.115E 02
0.112E 02
0.108E 02
0.104E 02
0.101E 02
0.972E 01
0.936E 01
0.900E 01
0.864E 01
0.828E 01
0.792E 01
0.756E 01
0.720E 01
0.684E 01
0.648E 01
0.612E 01
0.576E 01
0.540E 01
0.504E 01
0.468E 01
0.432E 01
0.396E 01
0.360E 01
0.324E 01
0.288E 01
0.252E 01
0.216E 01
0.180E 01
0.144E 01
0.108E 01
0.720E 00
0.360E-00
-0.507E-06
-0.360E-00
0.
-0.300E-00-0.600E 00-0.900E 00-0.120E 01-0.150E 01-0.180E 01-0.210E
ORDINATES = 1/PEAKING TIME
M(GAUSSES)= 1450. K(ERGS/CCM) = 25500.
LAMBDAS(MAGNETOSTRICTION) = 0.19E-04 LAMBDA(DAMPING,CPS) = 0.10E 09
GAMMA(GYRO RATIO) = 0.176E 08 DELTA = 0. SIGMA = (DELTA)0.89E 09
HSWCH = (ALPHA)35.17 HPERP = (BETA)35.17
HANIS = 2K/M = 35.17 PHIOD(INITIAL PHI,DEGREES) = 0.
BETA1 = 0.080 BETA2 = 0.500 BETA3 = 1.000
ALFT1 = -0.7306 ALFT2 = -0.170 ALFT3 = -0.210

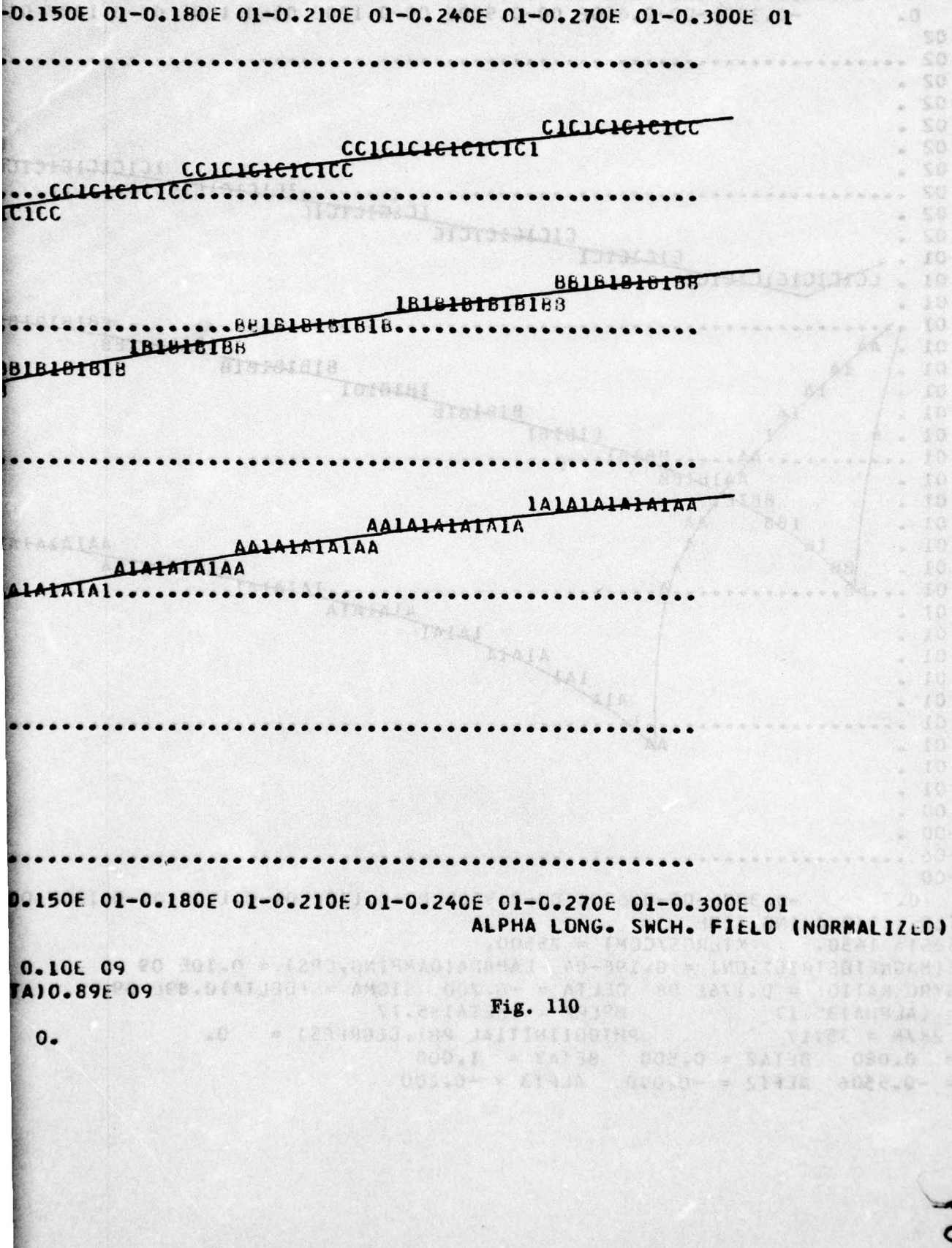
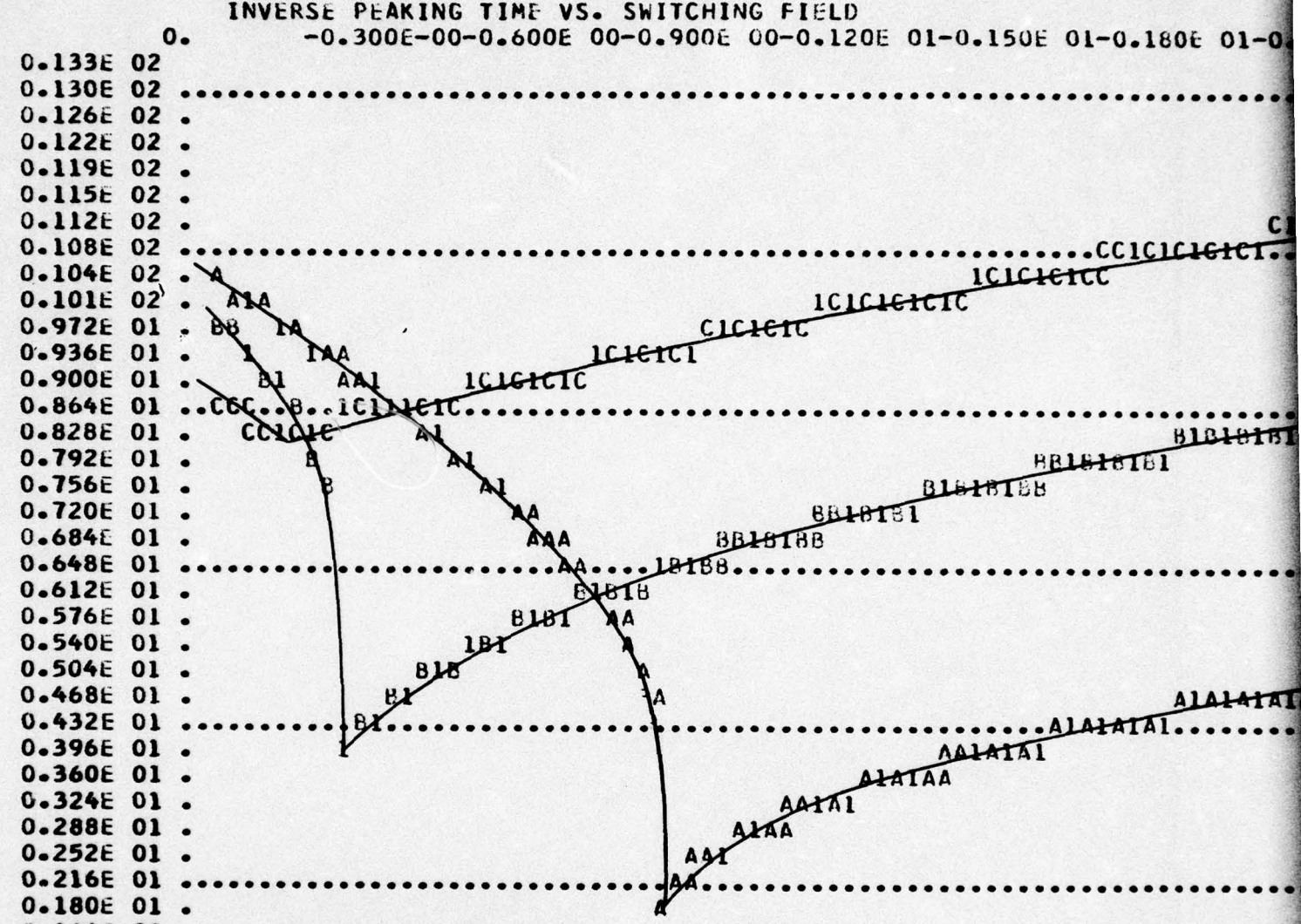

-0.150E 01-0.180E 01-0.210E 01-0.240E 01-0.270E 01-0.300E 01
0.150E 01-0.180E 01-0.210E 01-0.240E 01-0.270E 01-0.300E 01
ALPHA LONG. SWCH. FIELD (NORMALIZED)
0.10E 09
0.89E 09
0.

Fig. 110



ORDINATES = 1/PEAKING TIME
M(GAUSSES)= 1450. K(ERGS/CCM) = 25500.
LAMBDAS(MAGNETOSTRICTION) = 0.19E-04 LAMBDA(DAMPING,CPS) = 0.10E 09
GAMMA(GYRO RATIO) = 0.176E 08 DELTA = 0.200 SIGMA = (DELTA)0.89E 09
HSWCH = (ALPHA)35.17 HPERP = (BETA)35.17
HANIS = 2K/M = 35.17 PHIOD(INITIAL PHI,DEGREES) = 0.
BETA1 = 0.080 BETA2 = 0.500 BETA3 = 1.000
ALFT1 = -0.9106 ALFT2 = -0.290 ALFT3 = -0.200

01-0.150E 01-0.180E 01-0.210E 01-0.240E 01-0.270E 01-0.300E 01
C1C1CC
C1C1C1C1C1C1C1
C1C1C1C1C1C1
CC1C1C1C1C1
1C1C1C1CC
1C1C
BB1BB
B1B1B1B1B1B1BB
BB1B1B1B1B1
B1B1B1B1BB
BB1B1B1B1
B1B1B1BB
1
1A1A1AA
AA1A1A1A1A1A
AA1A1A1A1AA
A1A1A1A1AA
A1A1A1A1
AA1A1A1
1AA
01-0.150E 01-0.180E 01-0.210E 01-0.240E 01-0.270E 01-0.300E 01
ALPHA LONG. SWCH. FIELD (NORMALIZED)
) = 0.10E 09
DELTA)0.89E 09
= 0.

Fig. 111

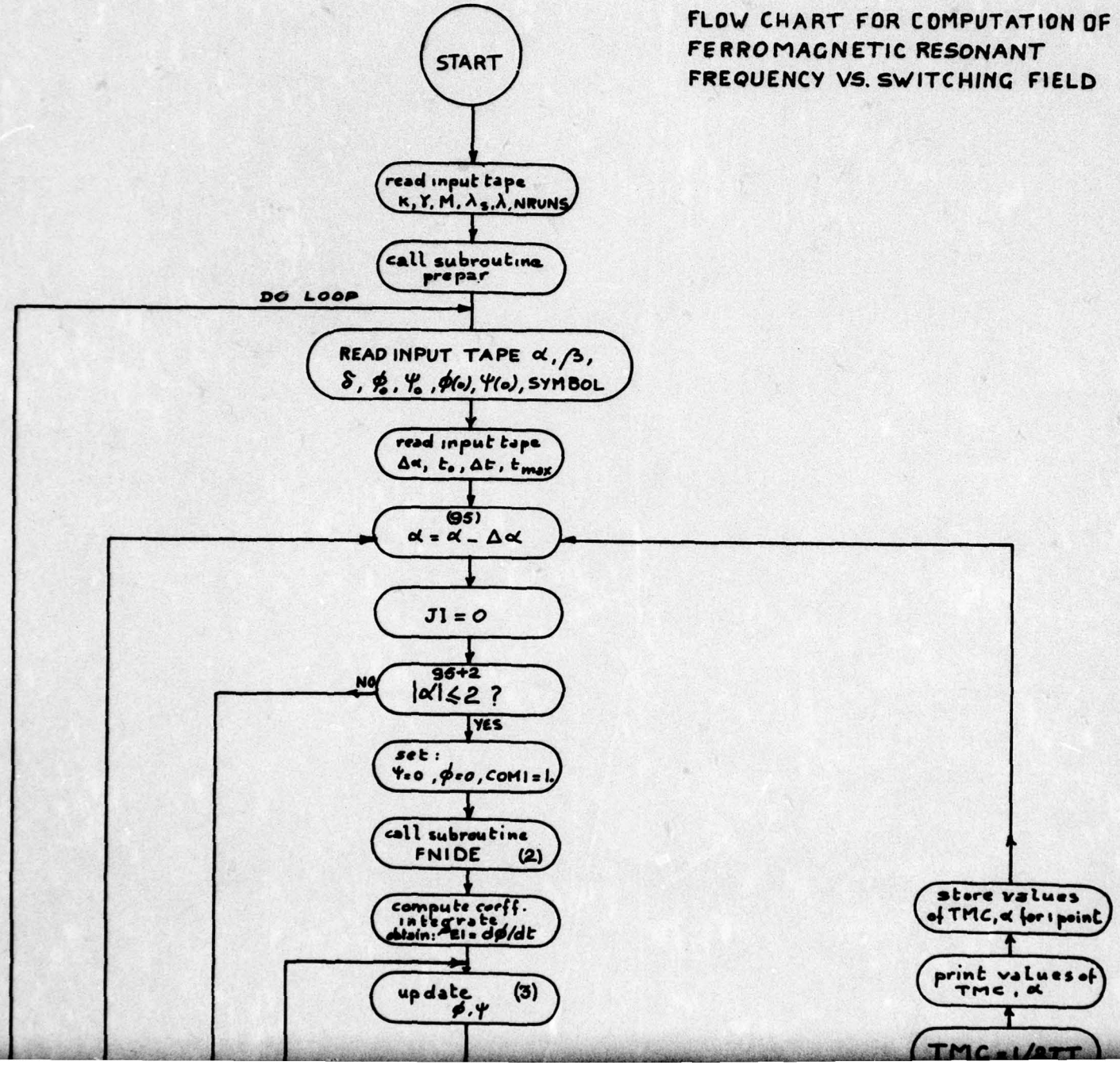
2

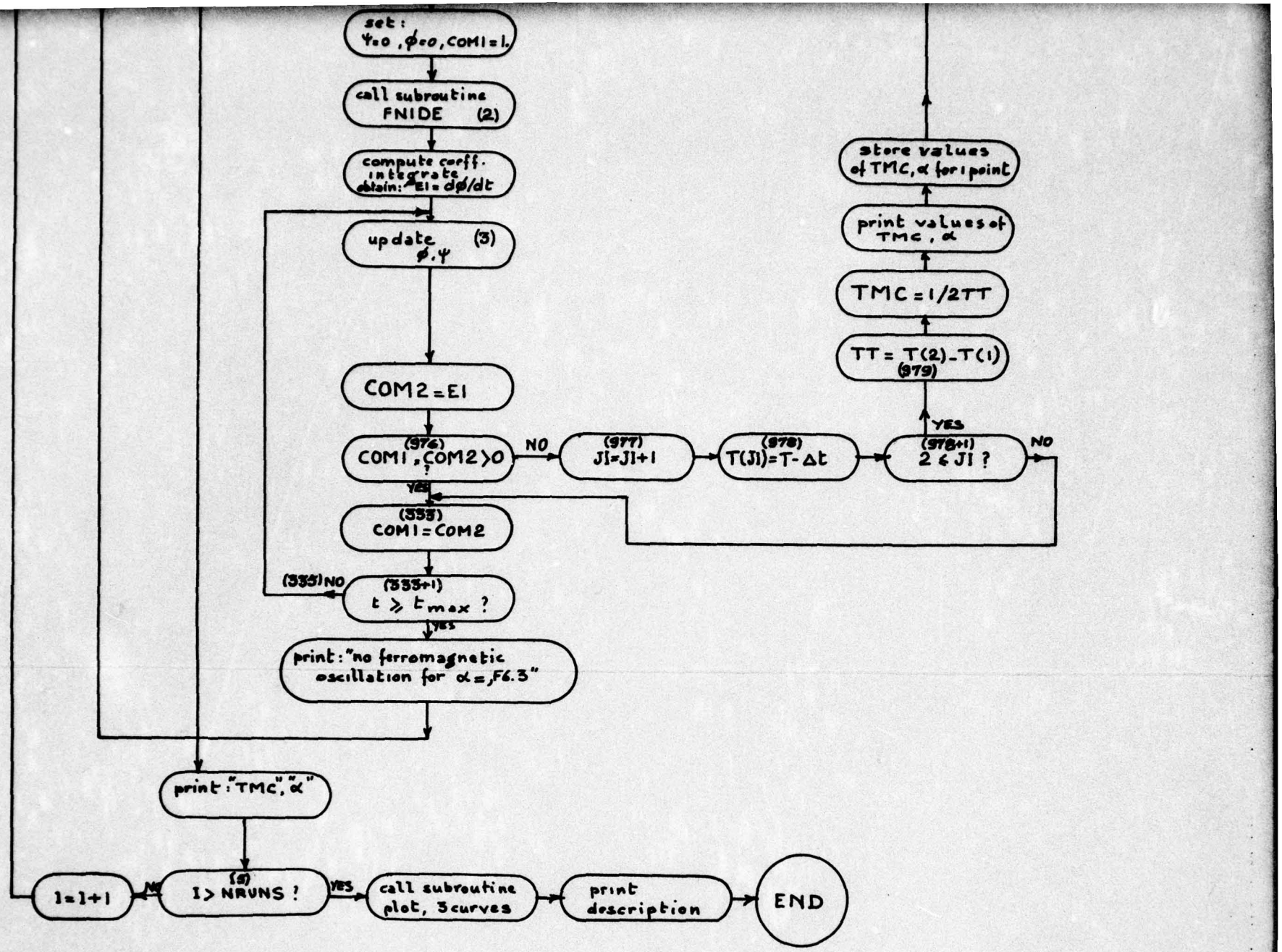
response of the film, it was observed earlier in this chapter that the period of the ferromagnetic oscillation is larger for a disturbed condition than for a switched condition. The variation of the ferromagnetic resonant frequency as stress or switching field magnitude are varied, cannot be predicted analytically as it may for the situation encountered in a usual ferromagnetic resonance experiment. In the usual case the magnetization is caused to precess around the direction of a fixed DC field in the presence of a weak RF field directed at 90°. In the case of thin film switching the magnetization rotates by a large angle under the drive of a step function, in the presence of a constant perpendicular field. The oscillation observed after magnetization reversal is damped and therefore its frequency is affected by the damping, which, experience shows,[6] is small in thin film switching. It is therefore of interest to study thin film ferromagnetic resonance effects by means of a digital computer directly from the Landau-Lifshitz equation.

Toward that end a program, described by the flow chart in Fig. 112, was prepared and used to obtain computer plots of the ferromagnetic oscillation frequency vs. the magnitude of the switching field with stress δ and applied perpendicular

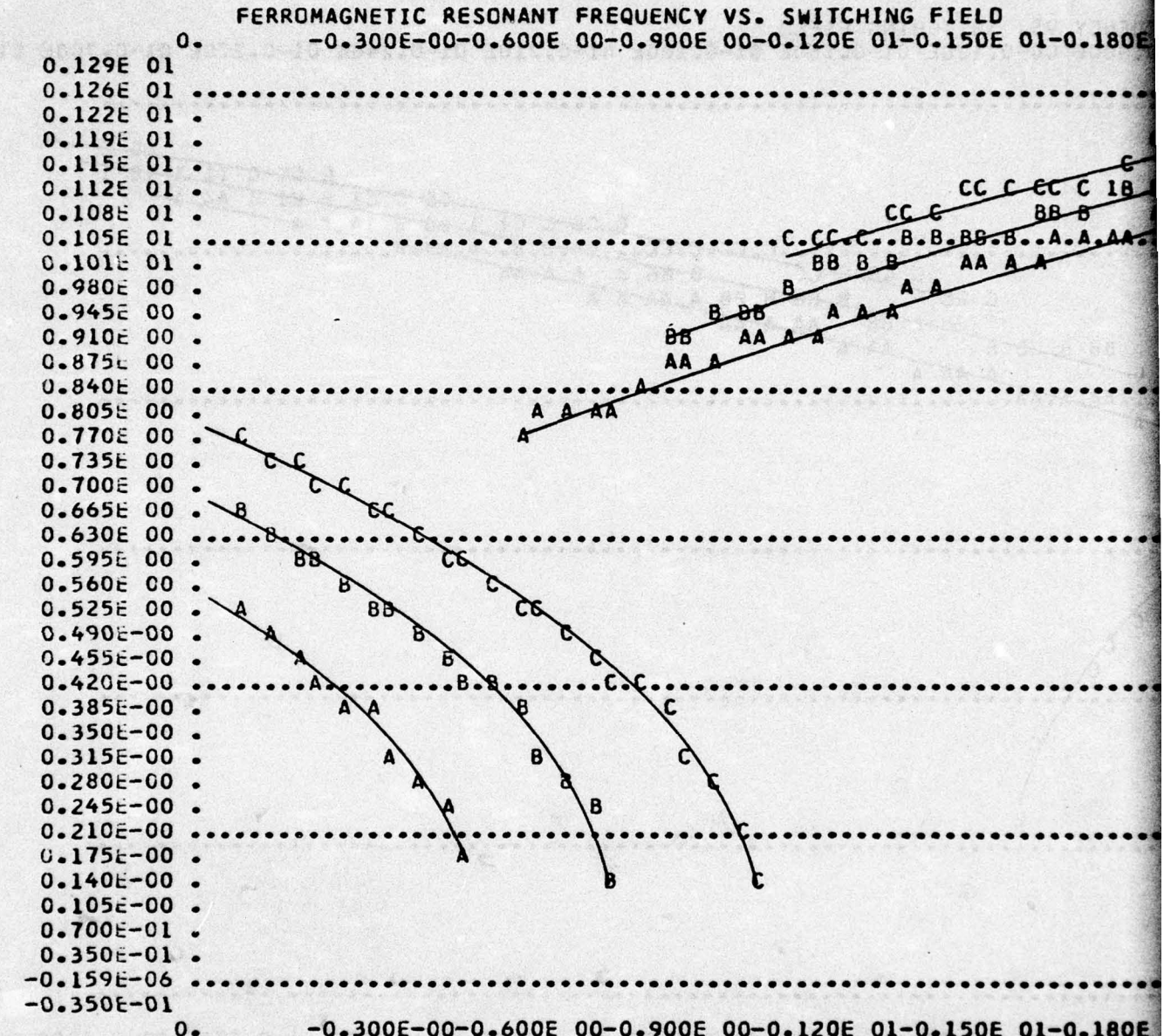
FIG. 112

FLOW CHART FOR COMPUTATION OF FERROMAGNETIC RESONANT FREQUENCY VS. SWITCHING FIELD




set:
Ψ=0, φ=0, COM1=1.
call subroutine FNIDE (2)
compute coeff. integrate obtain: E1 = dφ/dt
update φ, Ψ (3)
COM2 = E1
(976) COM1, COM2 > 0
NO
(977) J1 = J1+1
(978) T(J1) = T - Δt
(978+1) 2 < J1 ?
NO
YES
YES
(333) COM1 = COM2
(333) NO
(333+1) t ≥ t max ?
YES
print: "no ferromagnetic oscillation for α =, F6.3"
store values of TMC, α for 1 point
print values of TMC, α
TMC = 1/2TT
TT = T(2) - T(1) (979)
print: "TMC", "α"
(5) I > NRUNS ?
NO
YES
I = I+1
call subroutine plot, 3 curves
print description
END

FERROMAGNETIC RESONANT FREQUENCY VS. SWITCHING FIELD



ORDINATES = FERROMAG. RES. FREQUENCY (KMC)
M(GAUSSES) = 860. K(ERGS/CCM) = 1290.
LAMBDAS(MAGNETOSTRICTION) = 0.19E-04 LAMBDA(DAMPING,CPS) = 0.10E 09
GAMMA(GYRO RATIO) = 0.176E 08
HSWCH = (ALPHA) 3.00 HPERP = (BETA) 3.00 SIGMA = (DELTA)0.45E 08
HANIS = 2K/M = 3.00 PHIOD(INITIAL PHI,DEGREES) = 0.
DELTA1 = -0.300 DELTA2 = 0. DELTA3 = 0.300 BETA

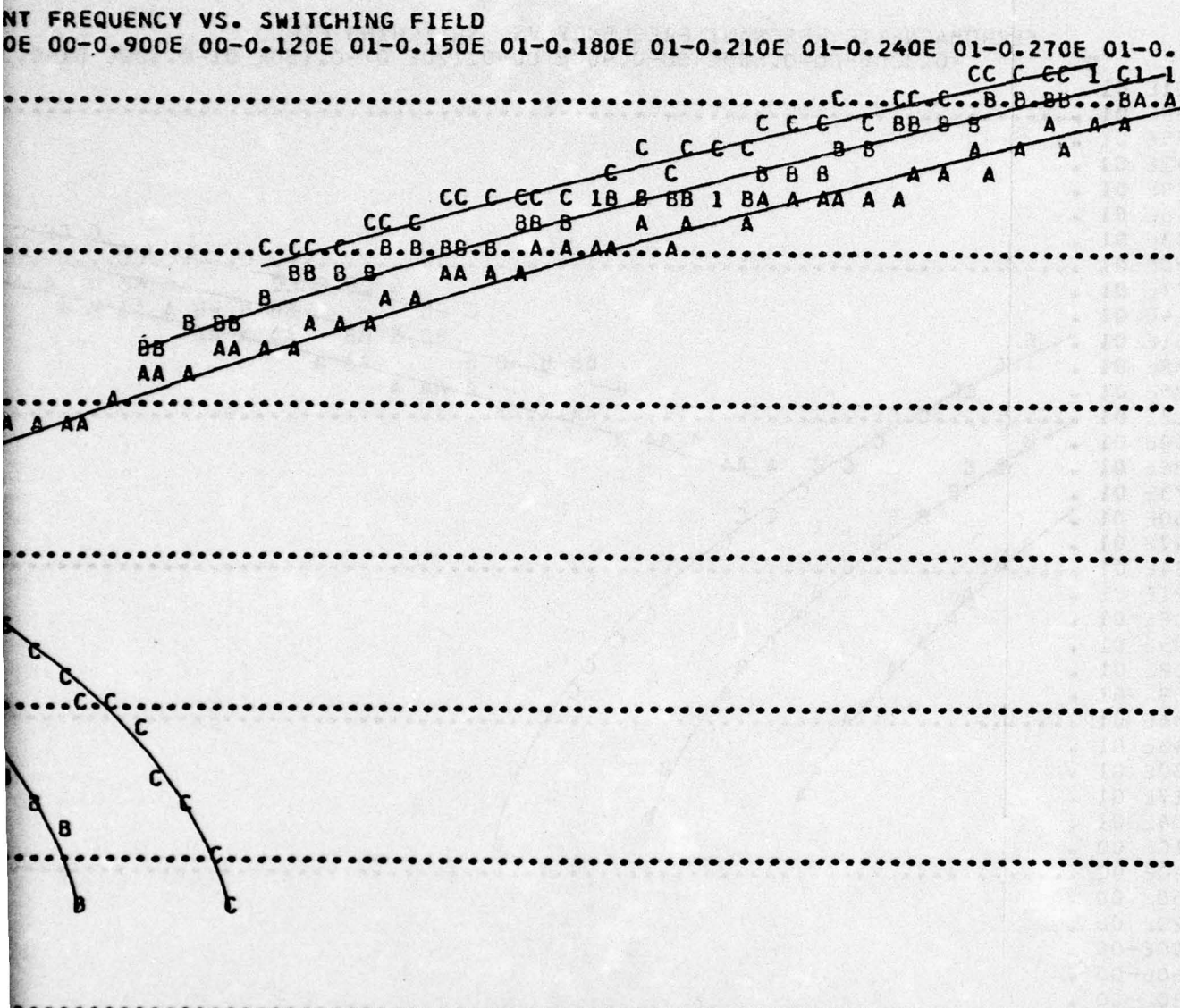
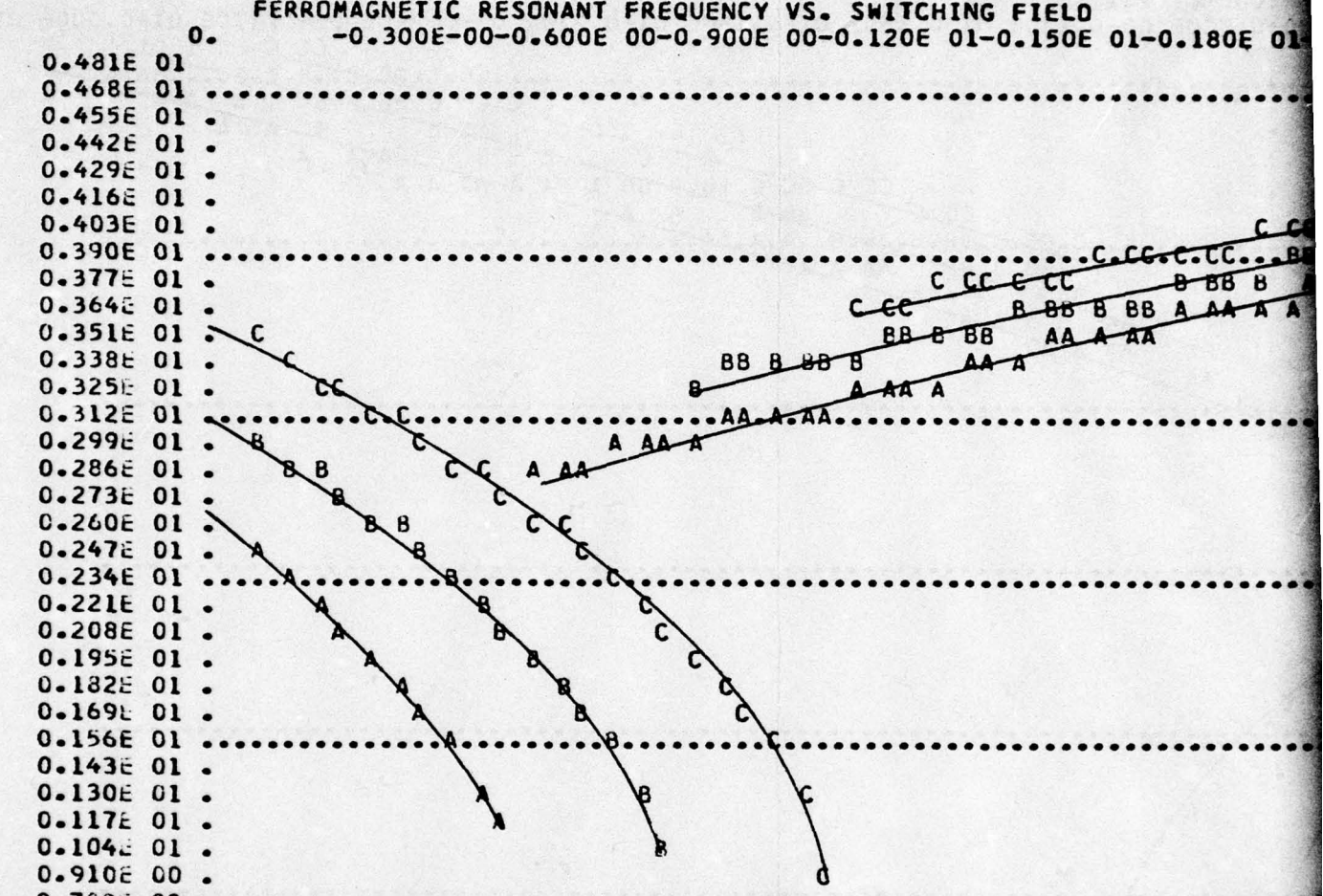
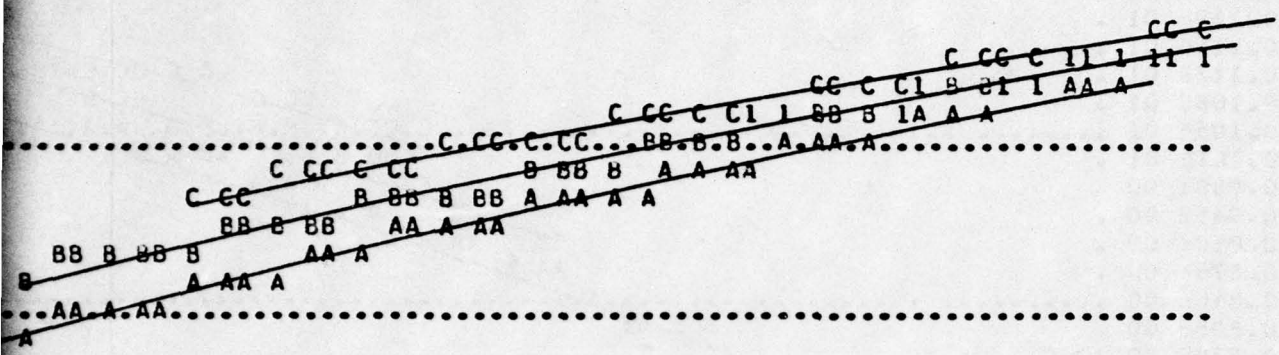

NT FREQUENCY VS. SWITCHING FIELD
0E 00-0.900E 00-0.120E 01-0.150E 01-0.180E 01-0.210E 01-0.240E 01-0.270E 01-0.300E 01
E 00-0.900E 00-0.120E 01-0.150E 01-0.180E 01-0.210E 01-0.240E 01-0.270E 01-0.300E 01
= LONG.SWCH.FIELD (NORMALIZED)
(KMC)
1290.
LAMBDA(DAMPING,CPS) = 0.10E 09
TA) 3.00 SIGMA = (DELTA)0.45E 08
AL PHI,DEGREES) = 0.
DELTA3 = 0.300 BETA = 0.020

Fig. 113



ORDINATES = FERROMAG. RES. FREQUENCY (KMC)
M(GAUSSES) = 1450. K(ERGS/CCM) = 25500.
LAMBDAS(MAGNETOSTRICTION) = 0.19E-04 LAMBDA(DAMPING,CPS) = 0.10E 09
GAMMA(GYRO RATIO) = 0.176E 08
HSWCH = (ALPHA)35.17 HPERP = (BETA)35.17 SIGMA = (DELTA)0.89E 09
HANIS = 2K/M = 35.17 PHIOD(INITIAL PHI,DEGREES) = 0.
DELTA1 = -0.300 DELTA2 = 0. DELTA3 = 0.300 BETA =

QUENCY VS. SWITCHING FIELD
0.900E 00-0.120E 01-0.150E 01-0.180E 01-0.210E 01-0.240E 01-0.270E 01-0.300E 01





0.900E 00-0.120E 01-0.150E 01-0.180E 01-0.210E 01-0.240E 01-0.270E 01-0.300E 01
G.SWCH.FIELD (NORMALIZED)
)
0.
BDA(DAMPING,CPS) = 0.10E 09

.17 SIGMA = (DELTA)0.89E 09 Fig. 114
I,DEGREES) = 0.
DELTA3 = 0.300 BETA = 0.020

2

field β as parameters. The machine computes the period of an oscillation of $d\emptyset/dt$ after a first complete oscillation, in order to ascertain that the period computed pertains to the gyromagnetic effect and not to the switching effect, whether the magnetization switches or is simply disturbed.

Fig. 113 shows the plot obtained for the film reported in Ref. 6 and Fig. 114 refers to the positive magnetostriction film investigated in this study. These plots show that the curves present a discontinuity at the value of switching field necessary to cause reversal. Below this point the frequency decreases non linearly with the magnitude of the switching field. If the magnetization is reversed the frequency of oscillation increases almost linearly with the value of the switching field. It is observed also that an applied stress causes an increase in the frequency of oscillation. In the disturbed condition, the curves show that the frequency is lower than in the case of switching, as was observed earlier from the dynamic response curves of the film.

The results shown by these curves will now be compared to the prediction of the small signal theory of usual ferromagnetic resonance experiments.

The expression for the total free energy, E, associated with the film was given by equation (93). Differentiating E with respect to ϕ, assuming that the initial position of the magnetization is $\phi_o = 0$, substituting $\frac{\partial E}{\partial \phi}$ in equation (108), the following differential equation is obtained, after dividing by 2 K:

$$(109)\quad \frac{d^2\phi}{dt^2} + 4\pi\lambda \frac{d\phi}{dt} + 8\,K\pi\gamma^2(1+\delta+\alpha)\,\phi = 8\,K\pi\gamma^2\beta$$

In a ferromagnetic resonance experiment α is a DC field, constant in amplitude and direction, β is a small RF field at 90° from α. Under these conditions the magnetization precesses around the direction of α and the frequency of this precession may be written from the coefficient of ϕ in the above equation:

$$(110)\quad f_n = \left(\frac{2K}{\pi}\right)^{1/2} \gamma\ (1+\delta+\alpha)^{1/2} \times 10^{-9}\ \text{Kmc}$$

This expression shows that the frequency increases with the switching field α and with the stress δ, in qualitative agreement with the portion of the curves in Figs. 113 and 114 corresponding to switching of the film.

For the cases $\delta = 0$, $\alpha = 0.9, 2.1, 3.0$ the values of f_n given by the above expression and by the curve B in Fig. 114 are shown in the following table.

TABLE V

Thin film ferromagnetic resonant frequency:

$K = 25500$, $\gamma = 0.176 \times 10^8$, $\delta = 0$

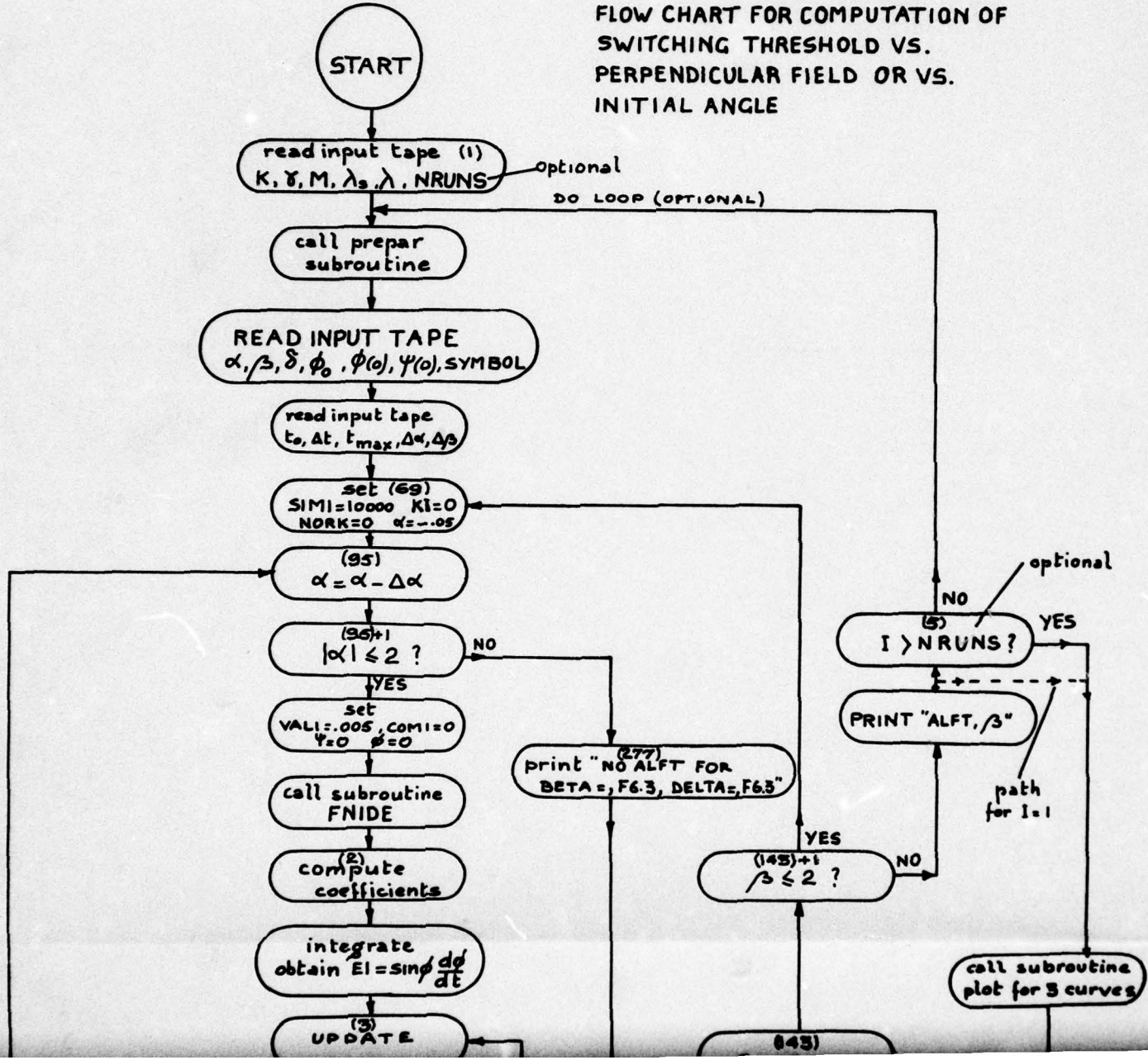
α	0.9	2.1	3
f_n(Kmc) Curve B, Fig. 94	3.25	3.9	4.3
f_n(Kmc) Expression (110)	2.1	3.1	3.8

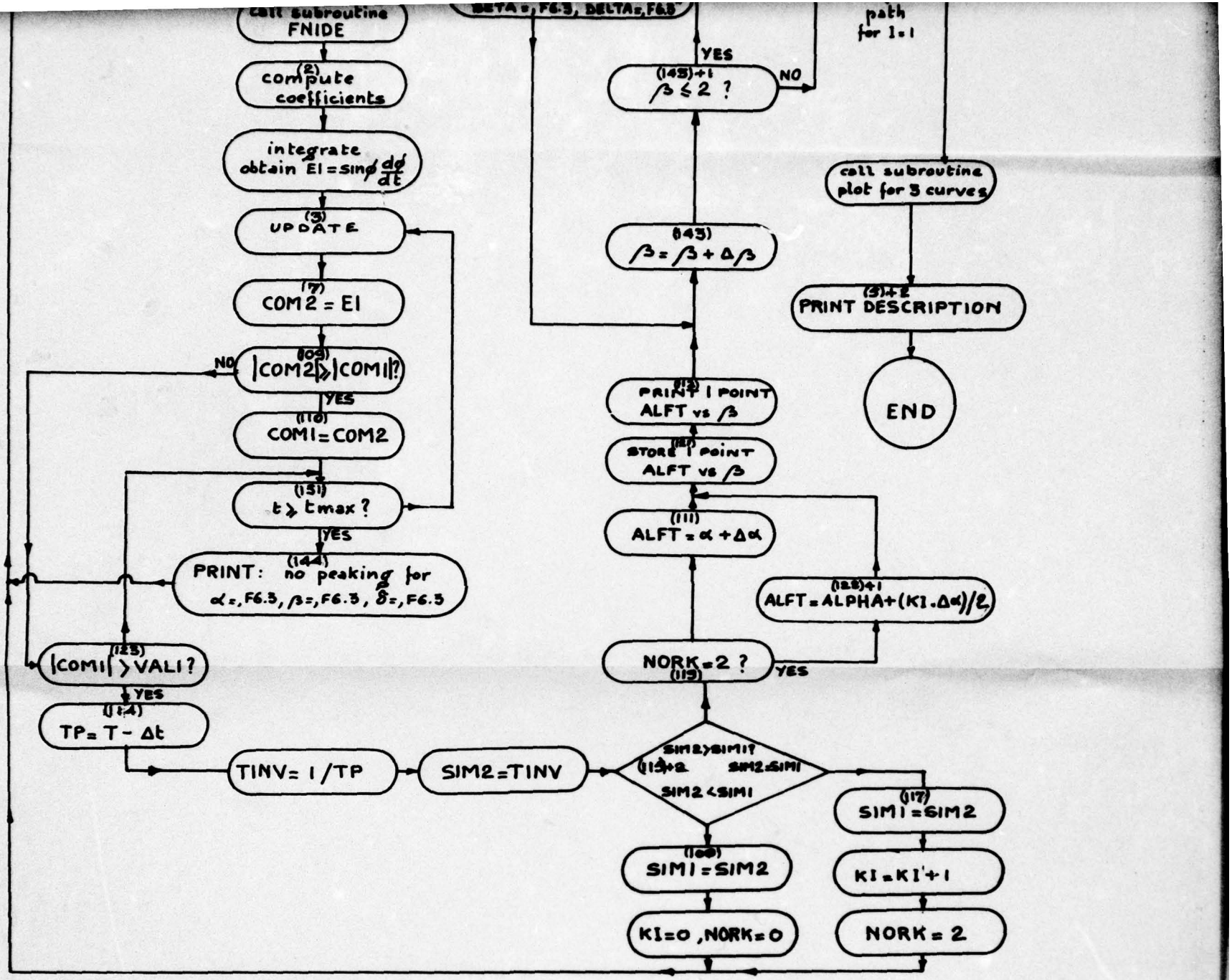
(4) Dynamic switching threshold vs. perpendicular field β, for constant initial angle ϕ_o or constant stress δ.

Computer plots in Figs. 106, 107, 108 have shown that the switching threshold of a film under dynamic conditions, and for a constant value of applied stress δ, decreases, passes through a minimum value and increases again, as the perpendicular field β is increased. In order to investigate more closely the parameters influencing the switching threshold a special digital computer program was written. The flow chart is shown in Fig. 115 and the computation is carried out as follows (cf. Fig. 116)

FIG. 115

FLOW CHART FOR COMPUTATION OF SWITCHING THRESHOLD VS. PERPENDICULAR FIELD OR VS. INITIAL ANGLE




call subroutine FNIDE
(2) compute coefficients
integrate obtain E1 = sinφ dφ/dt
(3) UPDATE
(7) COM2 = E1
(109) |COM2| ≥ |COM1| ?
NO
YES
(110) COM1 = COM2
(151) t ≥ tmax ?
YES
(144) PRINT: no peaking for α=, F6.3, β=, F6.3, δ=, F6.5
(125) |COM1| > VALI ?
YES
(114) TP = T - Δt
TINV = 1/TP
SIM2 = TINV
(119) NORK = 2 ?
YES
(111) ALFT = α + Δα
(112) PRINT 1 POINT ALFT vs β
(121) STORE 1 POINT ALFT vs β
(143) β = β + Δβ
(145)+1 β ≤ 2 ?
NO
YES
(128)+1 ALFT = ALPHA + (K1 . Δα)/2
SIM2 > SIM1 ?
(115)+2 SIM2 = SIM1
SIM2 < SIM1
(117) SIM1 = SIM2
K1 = K1 + 1
NORK = 2
(100) SIM1 = SIM2
K1 = 0 , NORK = 0
path for I = 1
call subroutine plot for 3 curves
(3)+2 PRINT DESCRIPTION
END

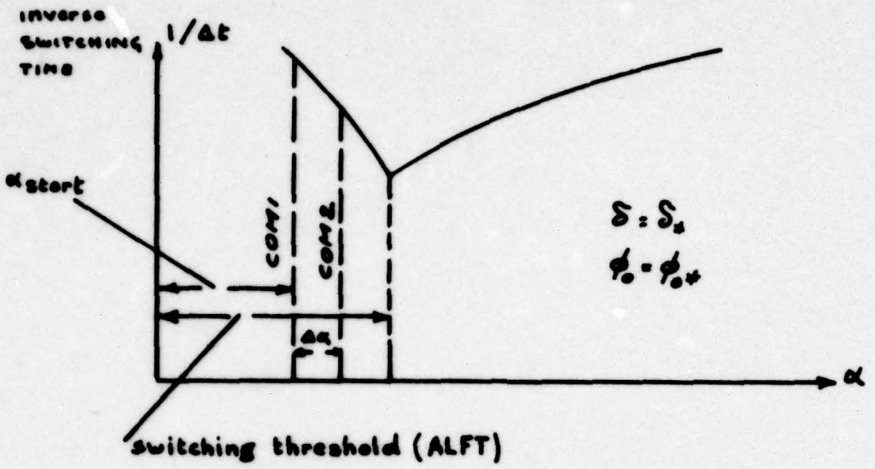


Fig. 116: Computational scheme for obtaining the dynamic switching curve (ALFT vs. β)

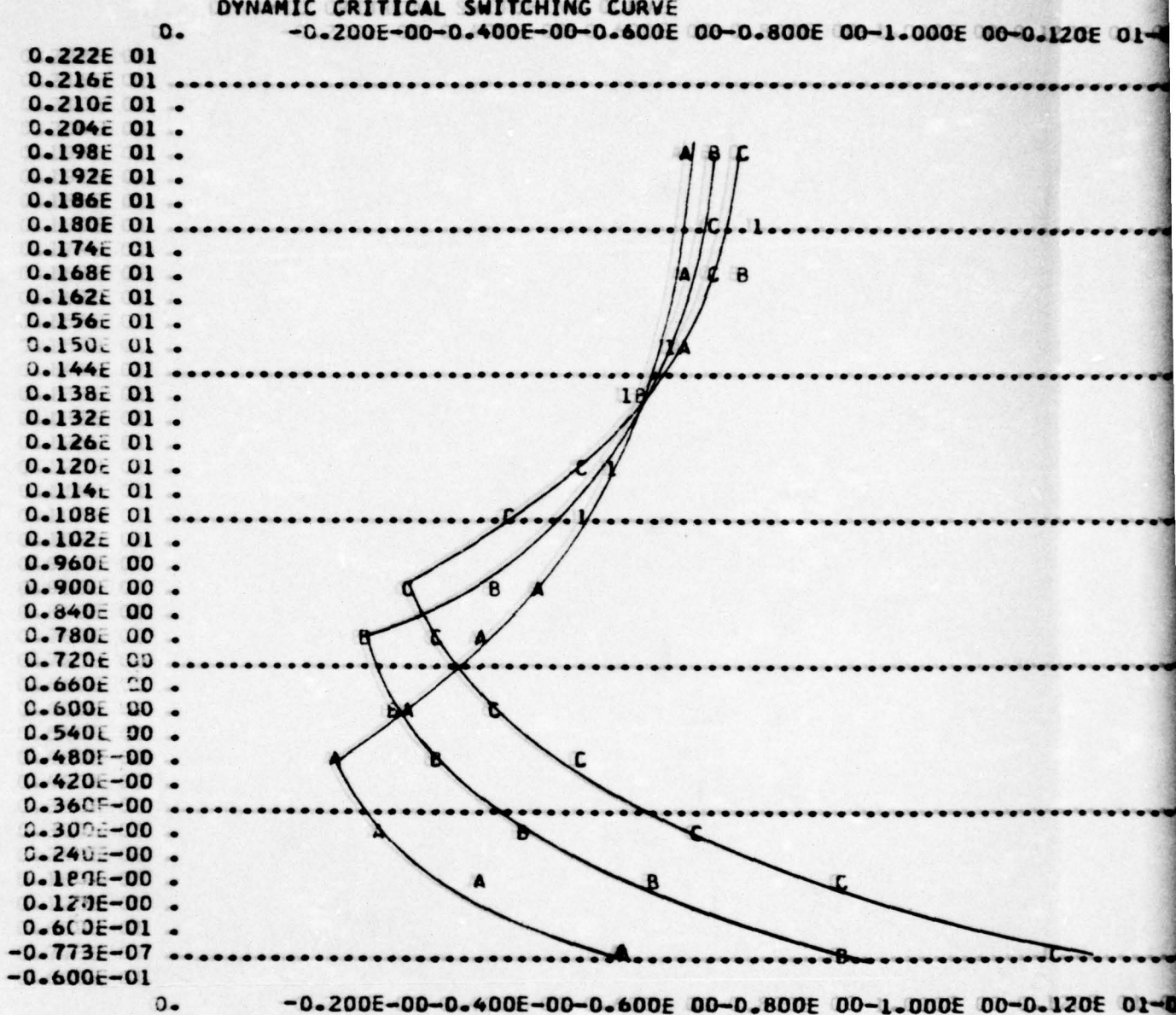
For given α, β, δ, ϕ_0 the scalar Landau-Lifshitz equations are solved; small starting values of α and β are chosen. The solution obtained gives the inverse peaking time $1/\Delta t$, called COM1 in Fig. 116 and in the program, and is kept in core storage. The variable α is then advanced by $\Delta\alpha$ and the corresponding switching response computed, the new value of $1/\Delta t$ is named COM2 and is compared to COM1. If COM2 < COM1, the computation proceeds by replacing COM1 by COM2, advancing α by $\Delta\alpha$ and computing a new COM2, etc. If COM2 > COM1, the value of α corresponding to the switching threshold has been reached. It is stored in a 3000 word array together with the value of β used

in the computation. The variable β is then advanced by $\Delta\beta$ and the computation restarts to give a new pair of values of the switching threshold and β, to be stored in the 3000 word array. When the range of α and of β has been covered, the value of δ is changed and a new curve (in which α and β are varied through the same previous ranges) is computed. When 3 curves, for three values of δ are obtained, the 3000 word array contains the graph to be plotted and is therefore transferred onto tape by the plotting subroutine.

Because of the large number of equations to be solved the computation is time consuming. Each of the 3 sets of curves shown in Figs. 117, 118, 119, 120 requires 30 minutes of machine time on an IBM 7090 digital computer. During this time the computer solves 5400 pairs of Landau-Lifshitz scalar equations.

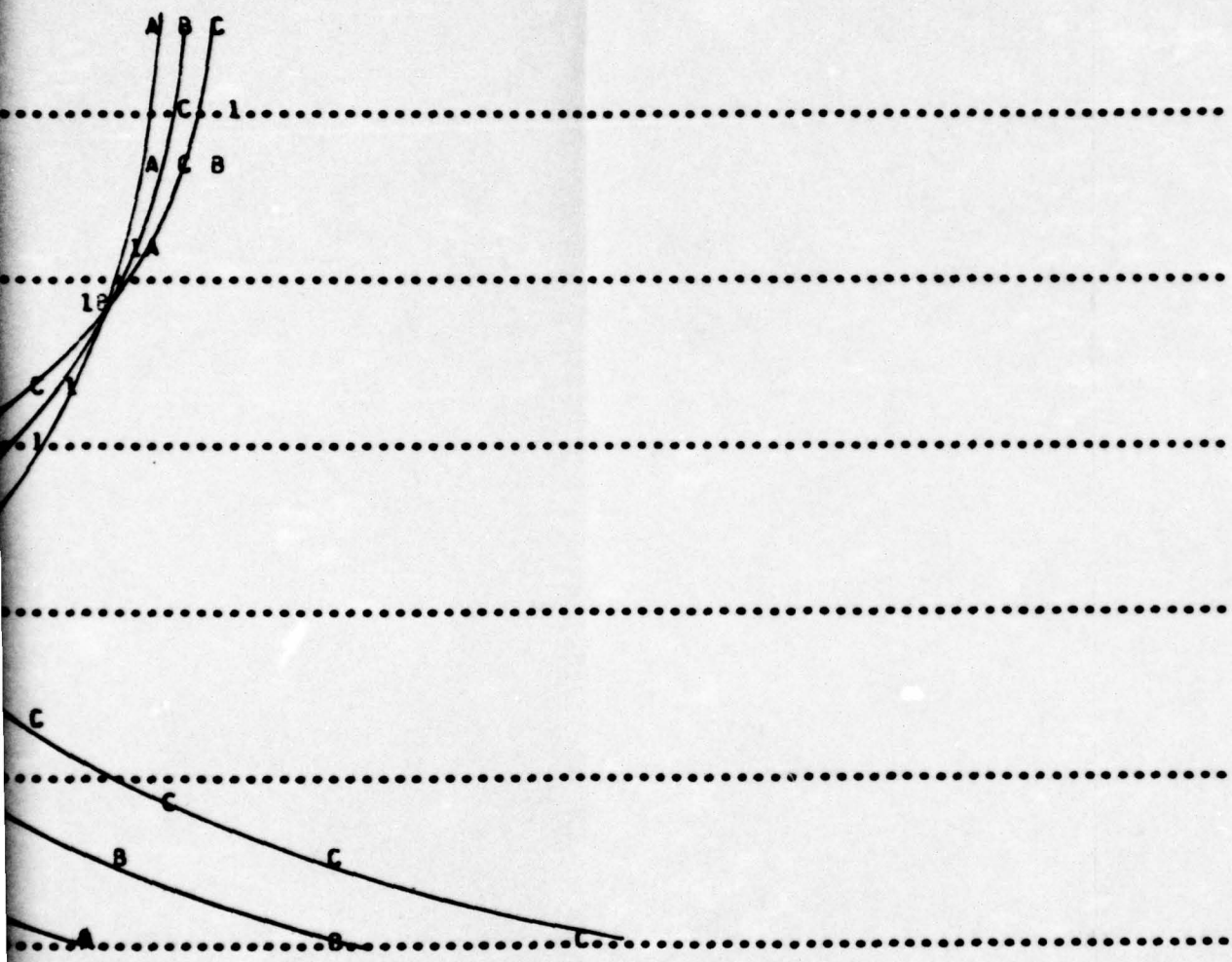
Figs. 117 and 118 show the dynamic switching curve for the film reported in Ref. 6. In the lower part of the graph in Fig. 117 the curves resemble astroid branches obtained in the study of the static behavior of the film. For high values of perpendicular field β the dynamic behavior differs considerably from the static case. As stress δ is increased from - 0.3 to + 0.3 the lower part of the curves moves parallel to

DYNAMIC CRITICAL SWITCHING CURVE



ORDINATES = PERP. FIELD (NORMALIZED)
M(GAUSSES) = 860. K(ERGS/CCM) = 1290.
LAMBDAS(MAGNETOSTRICTION) = 0.19E-04 LAMBDA(DAMPING,CPS) = 0.10E 09
GAMMA(GYRO RATIO) = 0.176E 08
HSWCH = (ALPHA) 3.00 HPERP = (BETA) 3.00 SIGMA = (DELTA)0.45E 08
HANIS = 2K/M = 3.00 PHIOD(INITIAL PHI,DEGREES) = 0.
DELTA1 = -0.300 DELTA2 = 0. DELTA3 = 0.300

ING CURVE
00-0.600E 00-0.800E 00-1.000E 00-0.120E 01-0.140E 01-0.160E 01-0.180E 01-0.200E 01

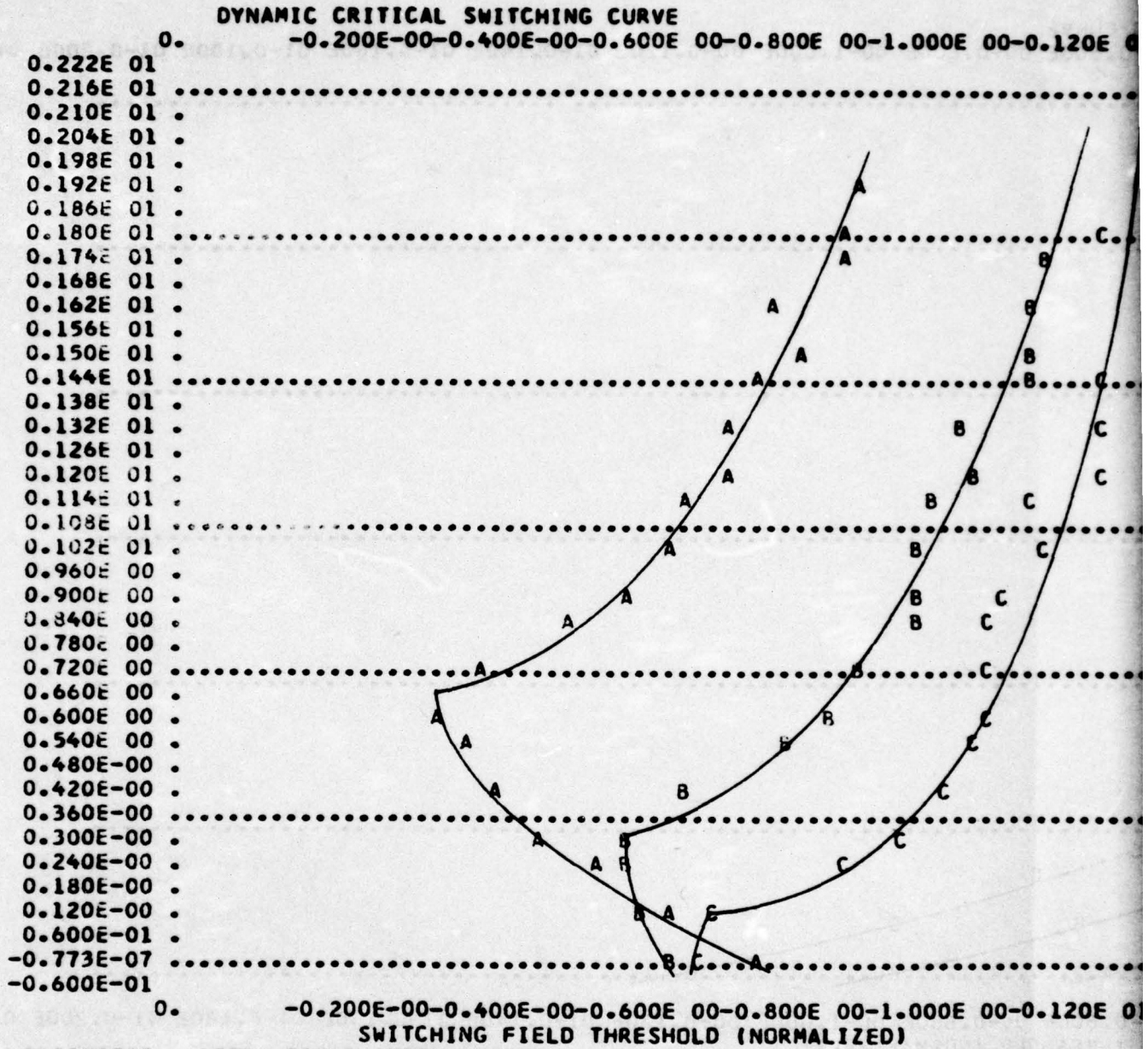


00-0.600E 00-0.800E 00-1.000E 00-0.120E 01-0.140E 01-0.160E 01-0.180E 01-0.200E 01
D THRESHOLD (NORMALIZED)

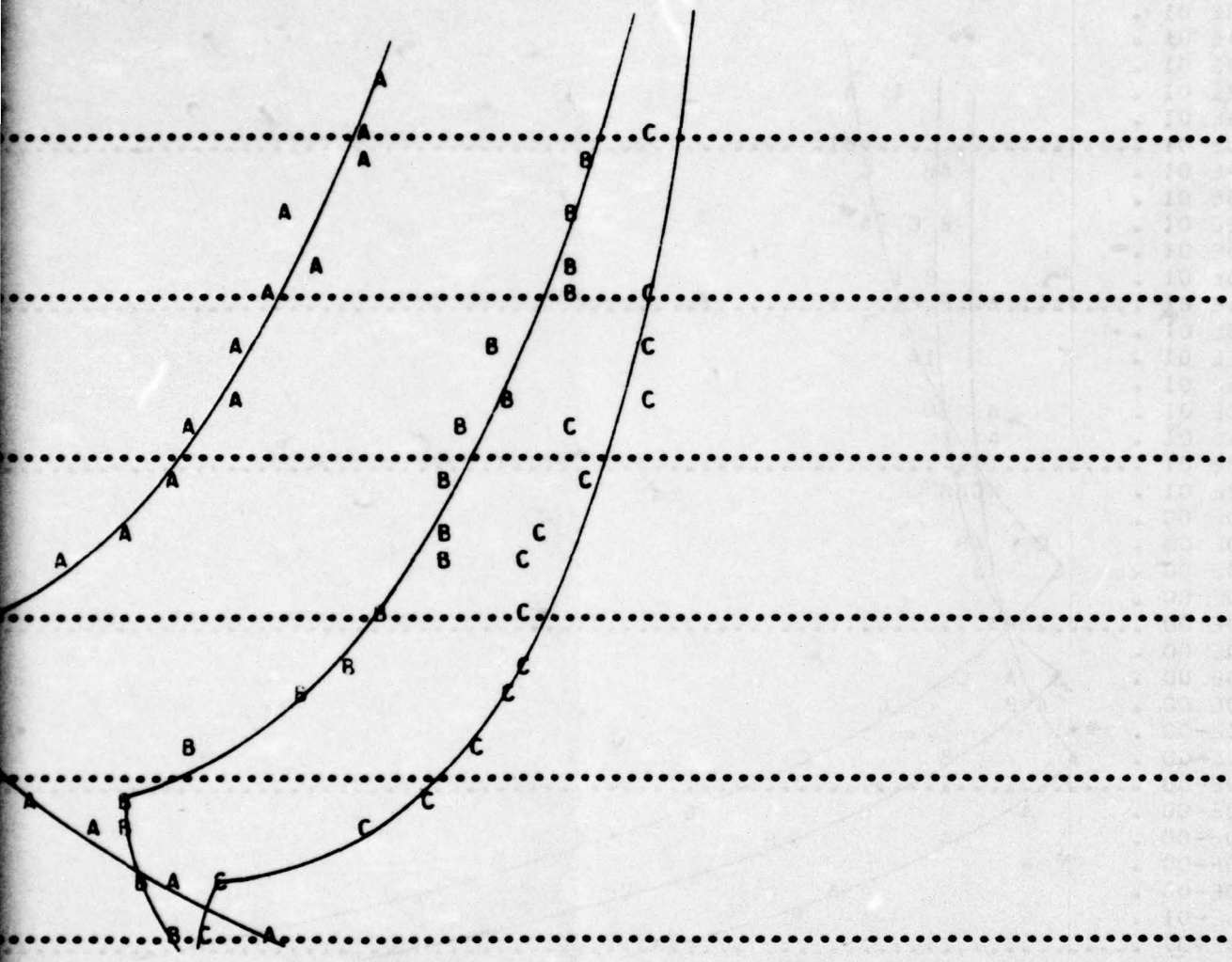
1290.
LAMBDA(DAMPING,CPS) = 0.10E 09

3.00 SIGMA = (DELTA)0.45E 08
PHI,DEGREES) = 0.
DELTA3 = 0.300

Fig. 117


DYNAMIC CRITICAL SWITCHING CURVE
0. -0.200E-00-0.400E-00-0.600E 00-0.800E 00-1.000E 00-0.120E 0
0.222E 01
0.216E 01
0.210E 01
0.204E 01
0.198E 01
0.192E 01
0.186E 01
0.180E 01
0.174E 01
0.168E 01
0.162E 01
0.156E 01
0.150E 01
0.144E 01
0.138E 01
0.132E 01
0.126E 01
0.120E 01
0.114E 01
0.108E 01
0.102E 01
0.960E 00
0.900E 00
0.840E 00
0.780E 00
0.720E 00
0.660E 00
0.600E 00
0.540E 00
0.480E-00
0.420E-00
0.360E-00
0.300E-00
0.240E-00
0.180E-00
0.120E-00
0.600E-01
-0.773E-07
-0.600E-01
0. -0.200E-00-0.400E-00-0.600E 00-0.800E 00-1.000E 00-0.120E 0
SWITCHING FIELD THRESHOLD (NORMALIZED)
ORDINATES = PERP. FIELD (NORMALIZED)
M(GAUSSES) = 860. K(ERGS/CCM) = 1290.
LAMBDAS(MAGNETOSTRICTION) = 0.19E-04 LAMBDA(DAMPING,CPS) = 0.10E 09
GAMMA(GYRO RATIO) = 0.176E 08
HSWCH = (ALPHA) 3.00 HPERP = (BETA) 3.00 SIGMA = (DELTA)0.45E 08
HANIS = 2K/M = 3.00 DELTA = 0.
PHIOD1= 4.98 PHIOD2= 20.00 PHIOD3 = 29.97

CHING CURVE
E-00-0.600E 00-0.800E 00-1.000E 00-0.120E 01-0.140E 01-0.160E 01-0.180E 01-0.200E 01



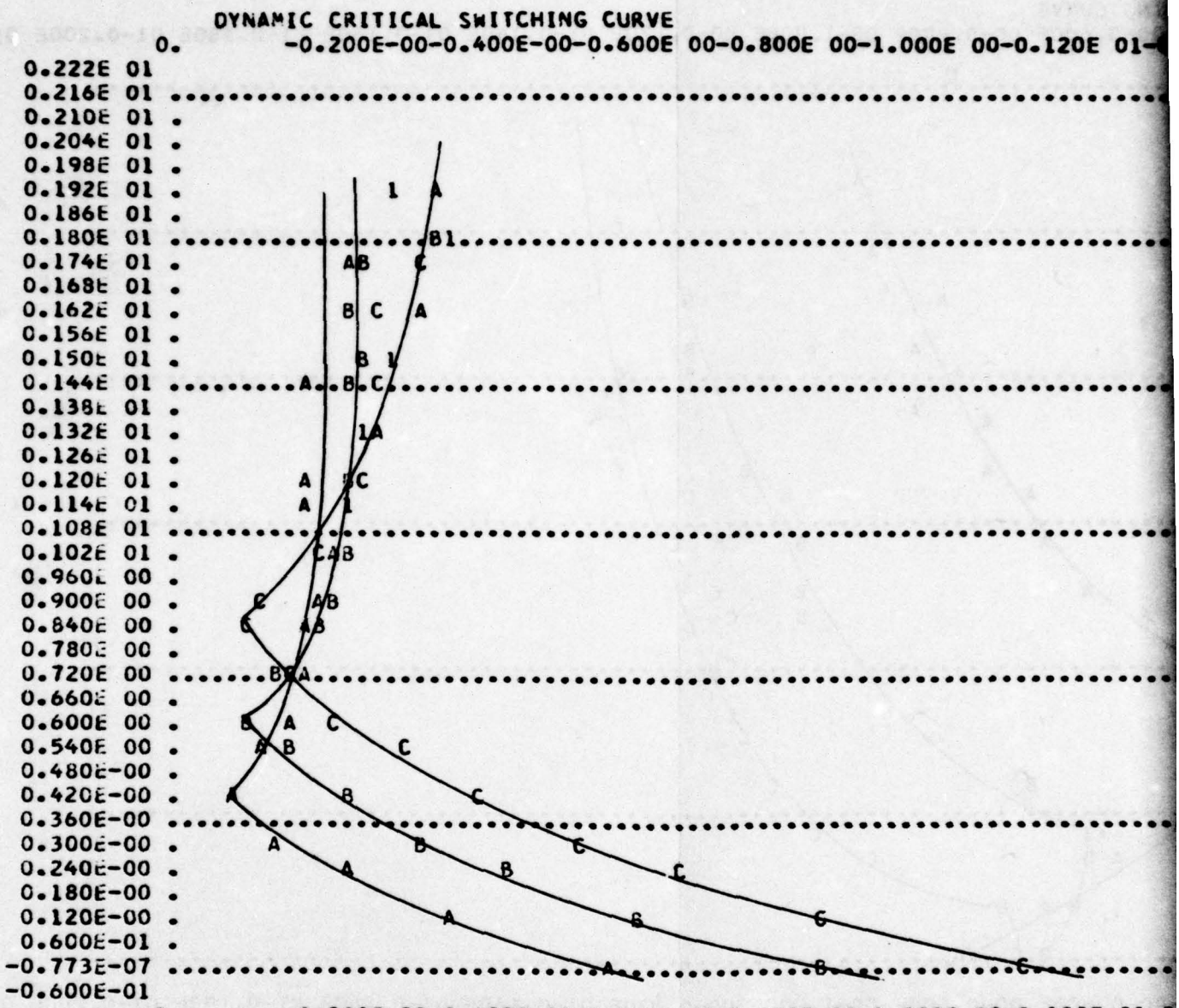
E-00-0.600E 00-0.800E 00-1.000E 00-0.120E 01-0.140E 01-0.160E 01-0.180E 01-0.200E 01
FIELD THRESHOLD (NORMALIZED)
D)
= 1290.
04 LAMBDA(DAMPING,CPS) = 0.10E 09

ETA) 3.00 SIGMA = (DELTA)0.45E 08

.00 PHIOD3 = 29.97

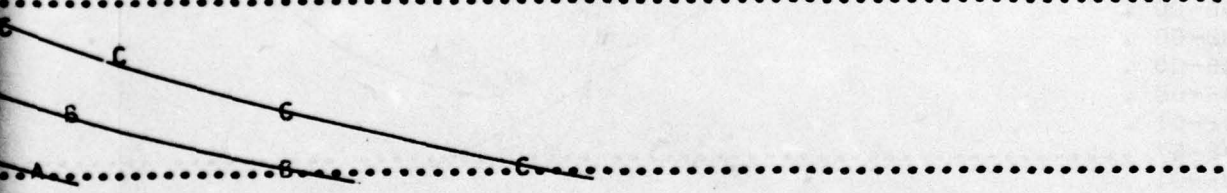
Fig. 118

2



ORDINATES = PERP. FIELD (NORMALIZED)
M(GAUSSES) =1450. K(ERGS/CCM) = 25500.
LAMBDAS(MAGNETOSTRICTION) = 0.19E-04 LAMBDA(DAMPING,CPS) = 0.10E 09
GAMMA(GYRO RATIO) = 0.176E 08
HSWCH = (ALPHA)35.17 HPERP = (BETA)35.17 SIGMA = (DELTA)0.89E 09
HANIS = 2K/M = 35.17 PHIOD(INITIAL PHI,DEGREES) = 0.
DELTA1 = -0.300 DELTA2 = 0. DELTA3 = 0.300

CURVE
0.600E 00-0.800E 00-1.000E 00-0.120E 01-0.140E 01-0.160E 01-0.180E 01-0.200E 01

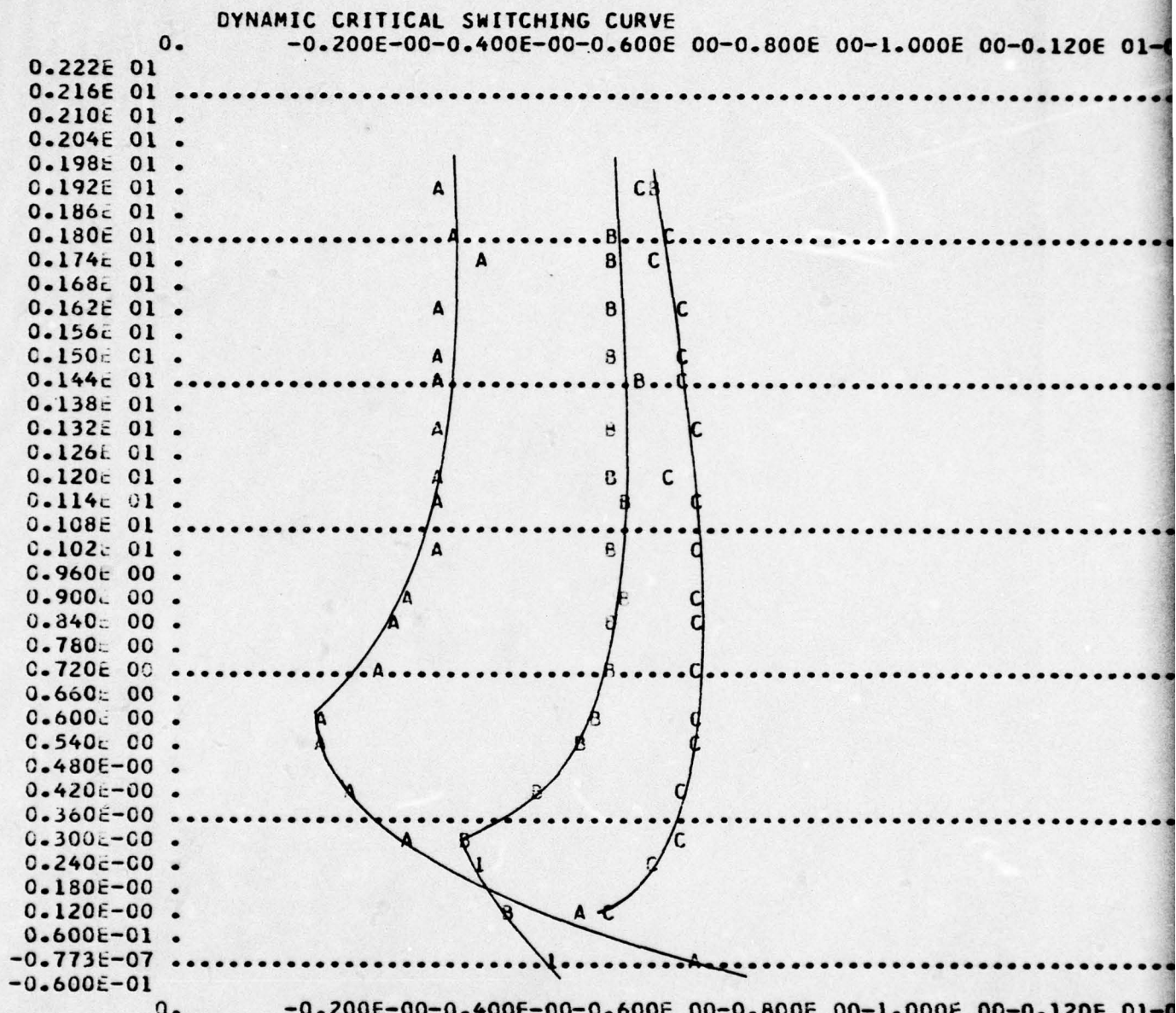


-0.600E 00-0.800E 00-1.000E 00-0.120E 01-0.140E 01-0.160E 01-0.180E 01-0.200E 01
THRESHOLD (NORMALIZED)

500.
LAMBDA(DAMPING,CPS) = 0.10E 09

5.17 SIGMA = (DELTA)0.89E 09
HI,DEGREES) = 0.
DELTA3 = 0.300

Fig. 119



ORDINATES = PERP. FIELD (NORMALIZED)

M(GAUSSES) =1450. K(ERGS/CCM) = 25500.

LAMBDAS(MAGNETOSTRICTION) = 0.19E-04 LAMBDA(DAMPING,CPS) = 0.10E 09

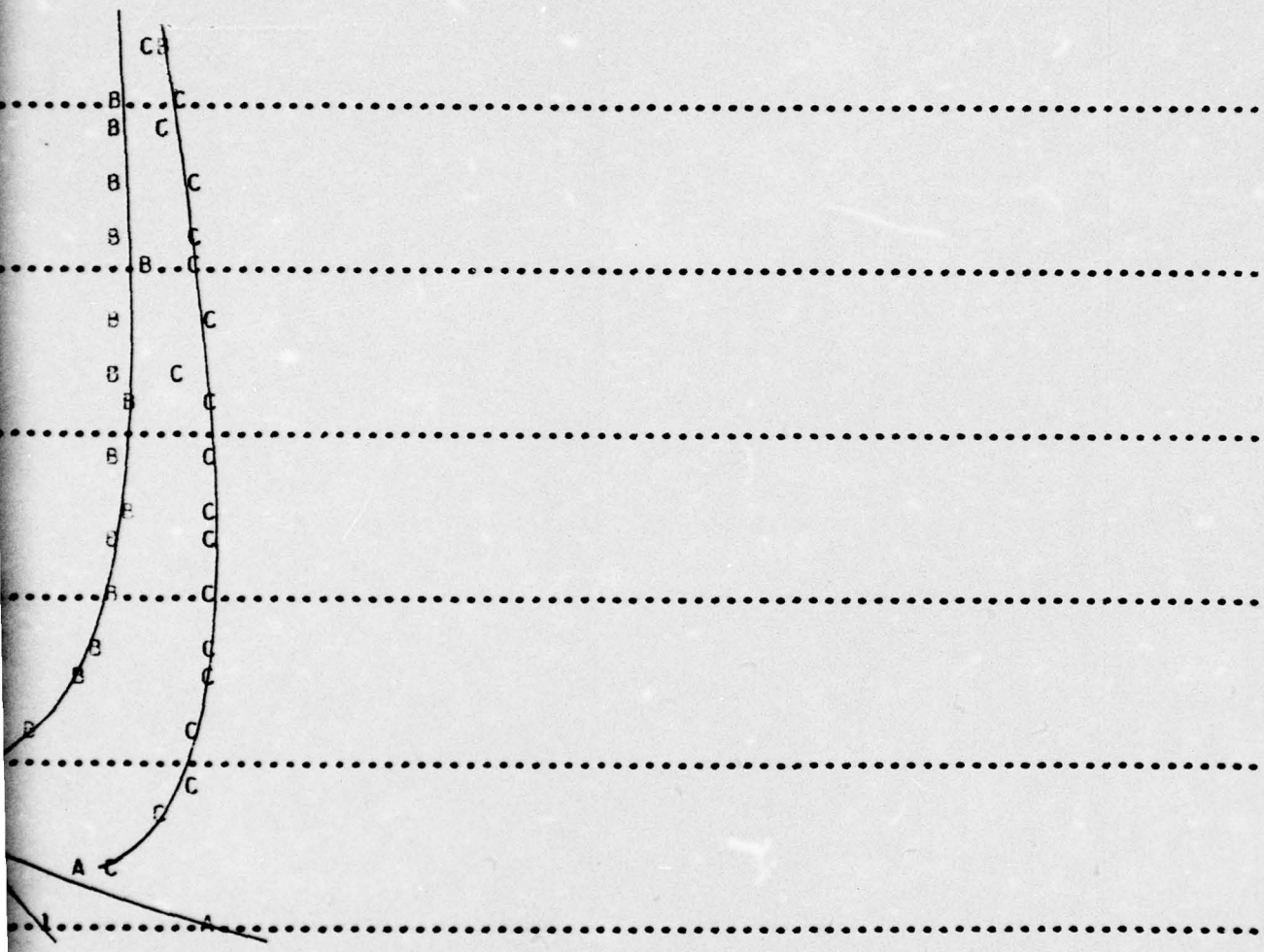
GAMMA(GYRO RATIO) = 0.176E 08

HSWCH = (ALPHA)35.17 HPERP = (BETA)35.17 SIGMA = (DELTA)0.89E 09

HANIS = 2K/M = 35.17 DELTA = 0.

PHIOD1= 4.98 PHIOD2= 20.00 PHIOD3 = 29.97

TCHING CURVE
0E-00-0.600E 00-0.800E 00-1.000E 00-0.120E 01-0.140E 01-0.160E 01-0.180E 01-0.200E 01



E-00-0.600E 00-0.800E 00-1.000E 00-0.120E 01-0.140E 01-0.160E 01-0.180E 01-0.200E 01
IELD THRESHOLD (NORMALIZED)
0)
= 25500.
04 LAMBDA(CAMPING,CPS) = 0.10E 09

TA)35.17 SIGMA = (DELTA)0.89E 09

00 PHI003 = 29.97

Fig. 120

itself, away from the origin as in the static case. Fig. 118 shows the effect of changing the value of the initial angle ϕ_o from 4.98° to 20° and to 29.97° at zero stress. As ϕ_o is increased the minimum in the curve tends to disappear and the curve is shifted to the right. Figs. 119 and 120 refer to the positive magnetostriction film with parameter values identical to those in Figs. 117 and 118.

2. Instrumentation for the study of stress effects on thin film switching

From the computer results discussed in the first part of this chapter, reversal of the magnetization occurs in a fraction of a nanosecond when a hypothetical pulse of instantaneous rise time is applied, as in the situation simulated by a computer in solving the Landau-Lifshitz equation.

When an experiment is designed it is necessary to find means of producing pulses with rise times of a fraction of a nanosecond (possibly 0.1 nsec.) and the response time of the oscilloscope where the pickup signal is displayed must be of the same order of magnitude.

Modern techniques and instruments are available for constructing instrumentation suitable to experimental

study of thin film switching.[61, 62] As discussed in the course of this chapter, subnanosecond switching is obtained if the magnetization can be made to reverse by coherent rotation. At low frequencies, in spite of the application of stress, switching of a magnetostrictive film is predominantly governed by domain wall coercive force, as discussed in the second part of Chapter I.

The description of the instrumentation designed and constructed for studying the effect of stress on thin film switching includes an illustration of the entire system, followed by the discussion of design criteria for dimensioning some of the important components in the system and predicting pickup loop output signals.

a. Description of instrumentation.

The system used to produce magnetic field pulses with very short rise times and to record very short voltage pulses is shown in Fig. 121.

A high-voltage power supply (5000 V) is connected to one contact of a single pole double throw mercury relay, through a short section C_1 of RG 9 coaxial cable. The armature of the relay is connected to the central conductor of a section of an RG 9 coaxial cable, whose opposite end is connected to ground through a

high-voltage diode D (2500V) and a resistor, R. The value of the resistor is such that, when added to the forward resistance of the diode, the total resistance from ground to the central conductor of cable C_2 is equal to 50 ohms. The other relay contact is connected to a short section C_1 of RG-9 coaxial cable followed by a 65 ft section C_3 of RG-19 cable, connected to a short section of RG-9 cable, terminated at the input connector of the strip transmission line. The line may or may not be short-circuited at the end. In the first case the current, and therefore the magnetic field, is maximum at the shorted end but reflected waves must be absorbed if repeated and undesired switching of the film located near the short is to be avoided. In the second case the end of the line is connected to a cable and to an RF termination power resistor with resistance equal to the characteristic impedance of the line and of the connecting cable. In this case no reflection takes place at the end of the line but the available magnetic field is smaller than in the case of the shorted line, for the same voltage at the opposite end of the line. The film is placed on the central strip line plate, below the pickup wire, in the case of a 3 conductor configuration, as shown in Fig. 122. The pickup wire is U-

shaped and is made of tungsten (gauge 51) coated with gold. The shape of the wire is preserved by inserting it inside a capillary pyrex tubing coated with a thin layer of evaporated silver, except in the region just above the film where only a very thin filiform silver film is left along the outer side of the tubing. The role of the silver film is to act as an electrostatic shield, thus decreasing capacitive coupling between the line and the pickup loop.

As shown in Fig. 122 the ends of the loop are inserted in an insulating teflon block, which may be displaced vertically about 1/32" from the center position on each side. The voltages induced by the air flux above and below the central plate in the pickup loop may then be cancelled by turning the extended stem of a micrometric screw. This adjustment is also useful in using inductive pickup for partial cancellation of capacitive pickup. These two undesired pickups occur at different times, but partial cancellation of remaining capacitive pickup by this method has been found experimentally possible. The two ends of the gold-plated tungsten wire are then connected to the two inputs of a Hewlett Packard sampling oscilloscope.

The glass envelope of the mercury relay is removed from its pronged receptacle after heating the

the sealing compound around it. It is then mounted in a coaxial T-shaped enclosure for coupling to cables C_1, C_1', C_2. The relay must be of the "break-before-make" type and the cylindrical section enclosing its armature must be surrounded by an energizing coil.

A pickup loop is placed around the central conductor between cable C_1 and relay contact t_2 in order to pick off a signal to trigger the oscilloscope. The length of cable C_3 must be such as to allow sufficient delay in the propagation of the pulse going to the strip line, for the trigger pulse to strobe the oscilloscope. The triggering signal may also be obtained by placing a large resistor in series with a cable connecting relay contact t_2 to the oscilloscope trigger input, as shown in Fig. 121.

The strip transmission line is placed between two Helmoltz coils in order to reset the film after switching. The resetting action must be synchronized with the operation of the mercury relay. This is accomplished by means of a programmed current pulse generator which drives the relay coil and the Helmoltz coils by means of two pulses, whose repetition rate, amplitude and phase may be varied. In addition to the Helmoltz coils, the strip line support is provided with two coils

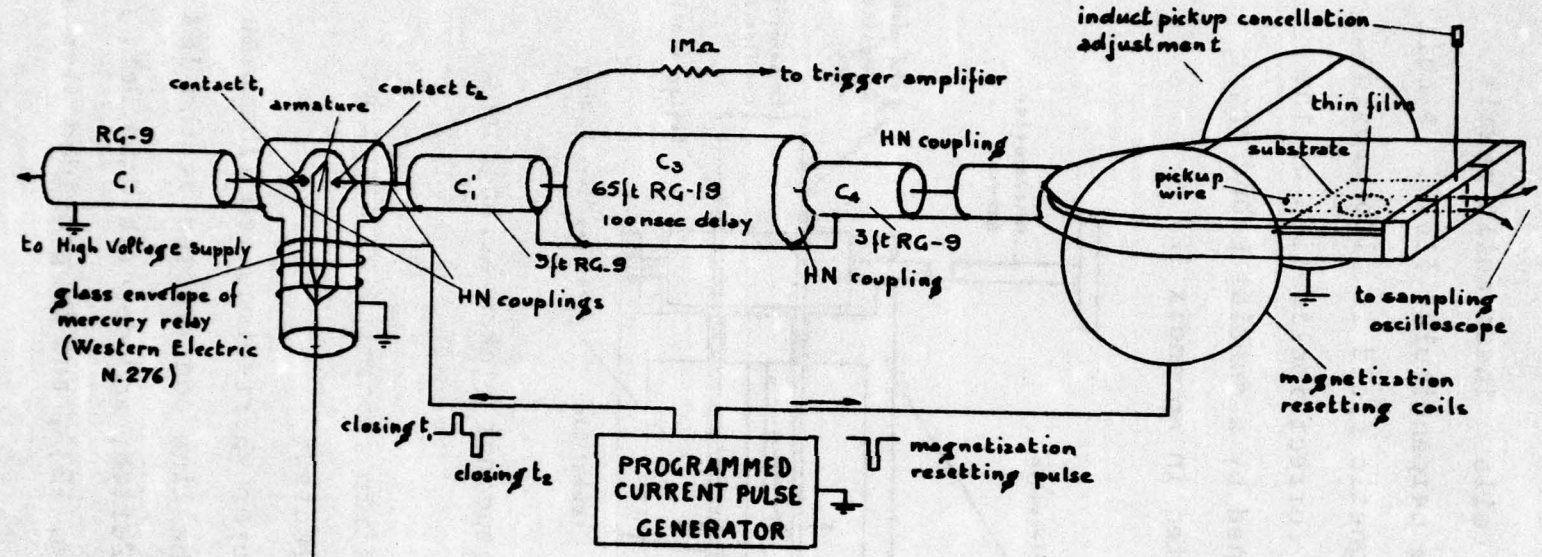


FIG. 121 EXPERIMENTATION FOR THIN FILM PULSE SWITCHING

at 90° from the Helmoltz coils. These coils permit studying the effects of a perpendicular field. A coil to cancel the earth's magnetic field is also provided and is adjustable to the correct inclination of the earth's field as determined by a special probe whose construction is illustrated in Appendix 12.

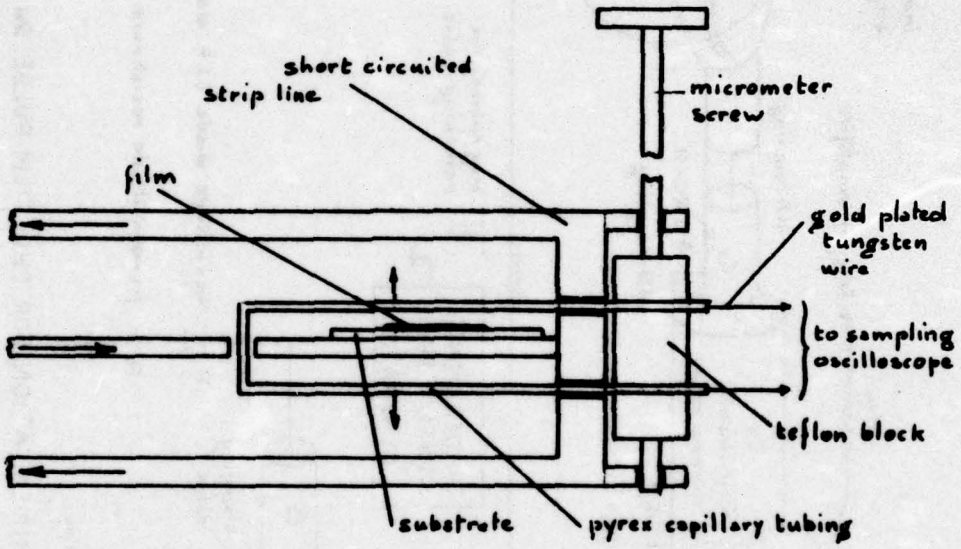


Fig. 122: Longitudinal pickup arrangement

Four different strip transmission lines have been designed and constructed:

1. A two conductor short-circuited line with dimensions similar to the line constructed at the IBM Research Laboratory in Zurich, and described in Ref. 61. The line is shown in Fig. 123A, and is provided with a

longitudinal pickup loop.

2. A three-conductor short circuited line with wide interplate spacing, suitable for insertion of thick-film coated piezoelectric crystals. The termination of the line is sketched in Fig. 122 and is shown mounted with its resetting, biasing and earth field cancelling coils, in Figs. 124 and 125.

3. A short-circuited line having three conductors of equal width and narrow spacing. This line is suitable for impressing mechanical bending to the film substrate by means of a micrometric arrangement connected to the upper plate, and sketched in Fig. 126. The line is shown disassembled in Fig. 123C.

4. A three conductor line terminated by a GR-874 connector for connection to a cable terminated by an RF 50 ohm, 20 watt coaxial resistor. The three conductors have the same width and the line is suitable for studying the effects of mechanically applied stress on film switching (cf. Fig. 123B).

The components sketched in Fig. 121 are shown in the photograph in Fig. 127.

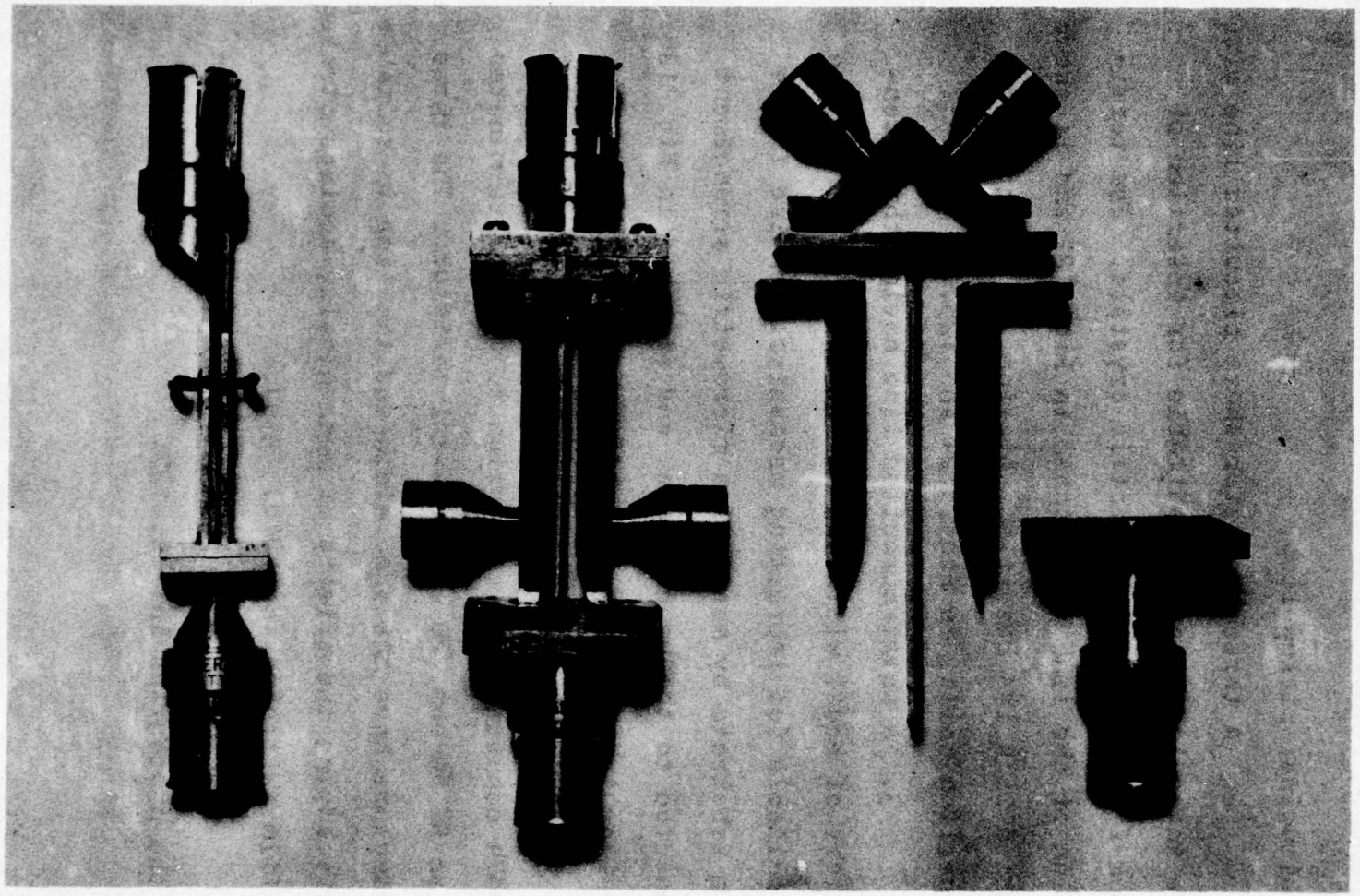


Fig. 123A Fig. 123B Fig. 123C

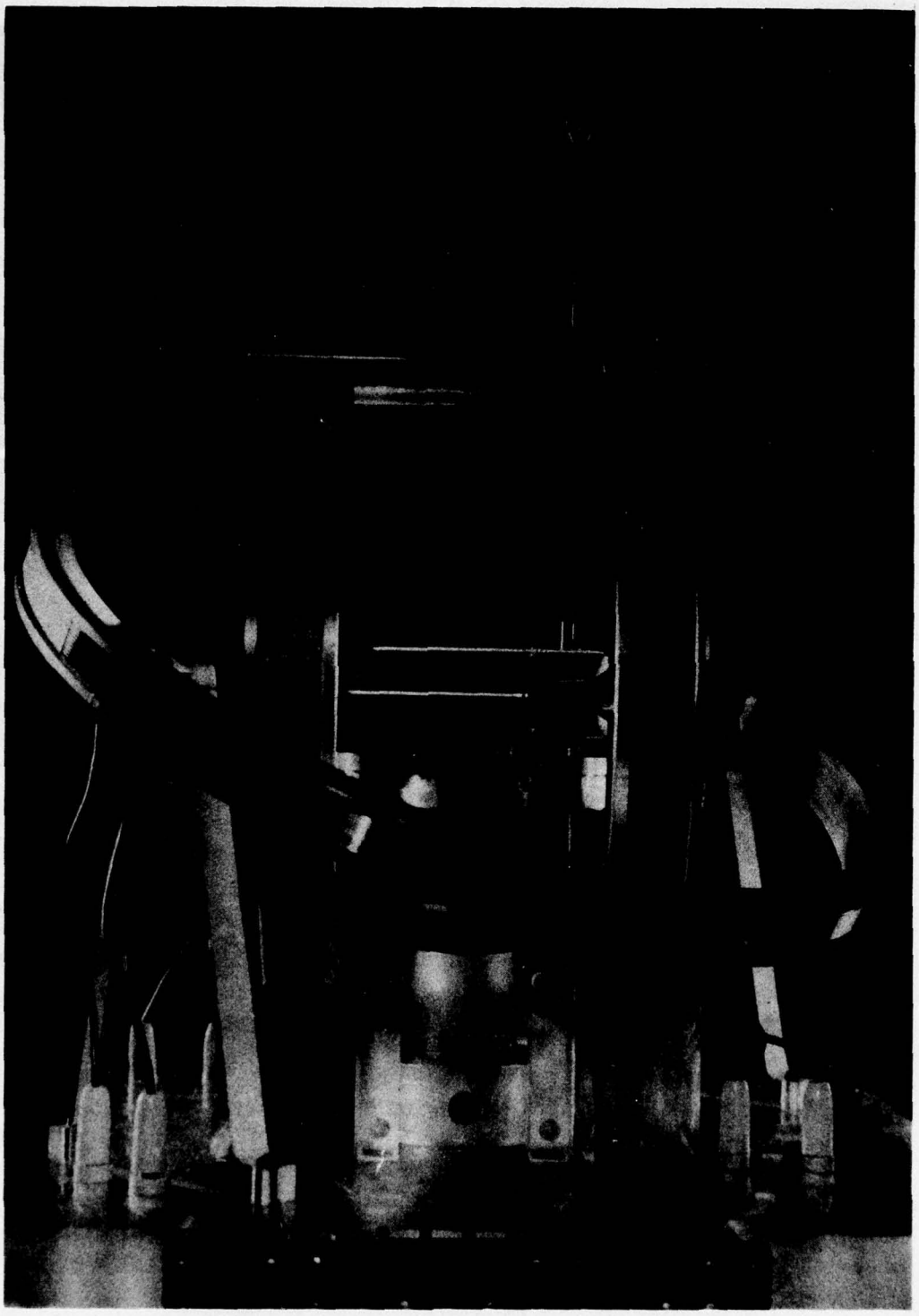


Fig. 124

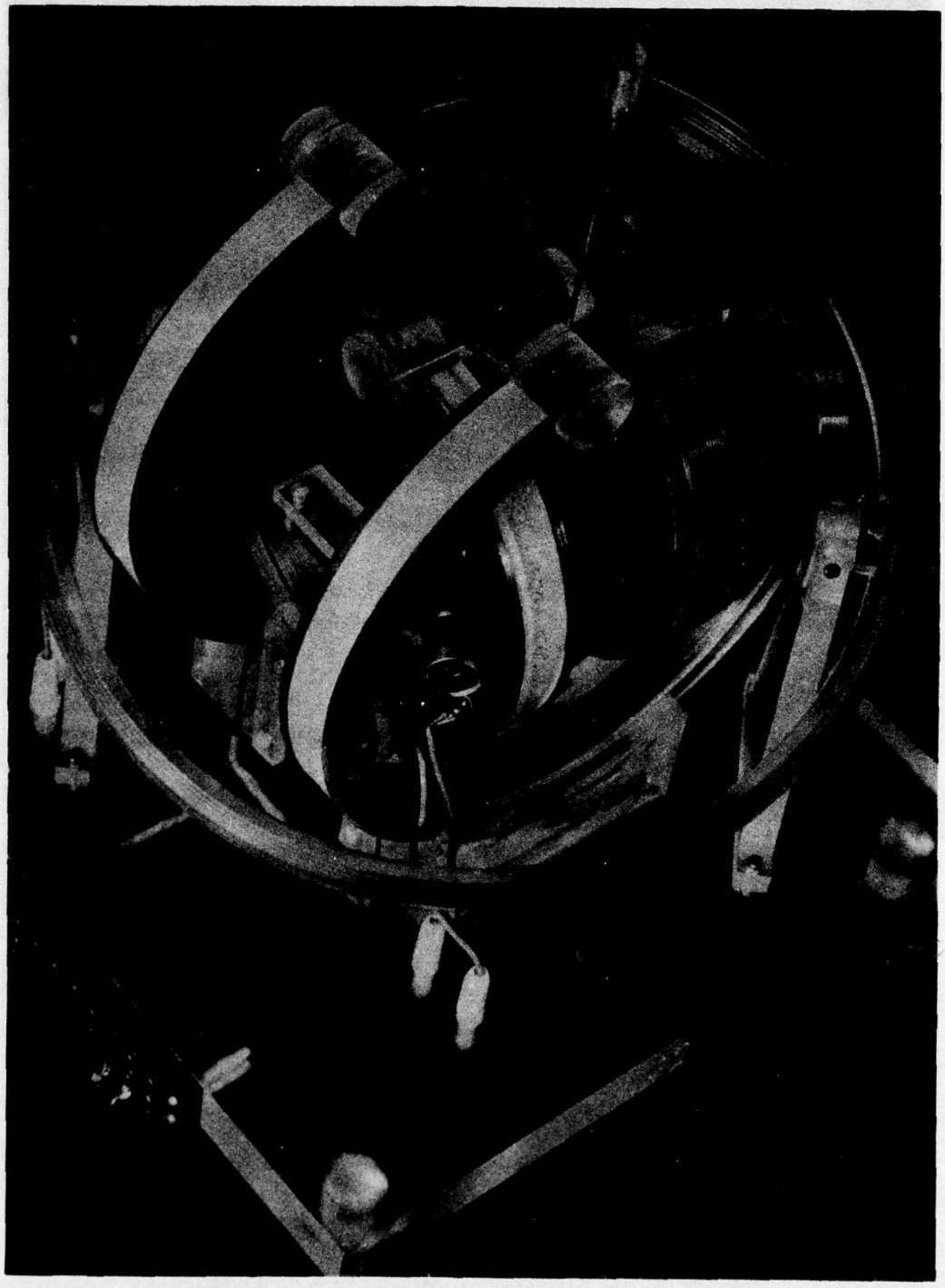


Fig. 125

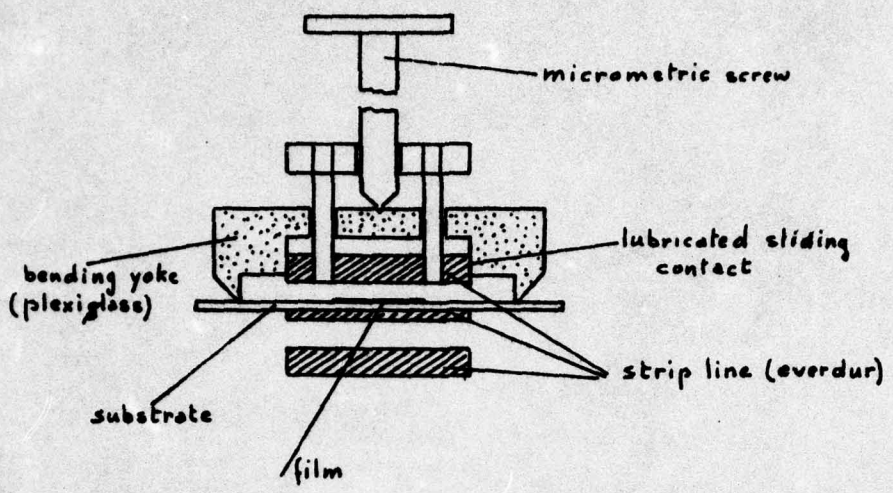


Fig. 126: Arrangement for mechanical film stressing

b. Operation and design considerations.

The operation of the system may be described by following the sequence of events taking place from the generation of very short rise time pulses to the recording of film switching (cf. Fig. 120).

1. The mercury relay is at first in its normally closed position t_1. The positive high voltage power supply charges the cable C_2 to a few thousand volts remaining below the breakdown voltage of the diode D (2500 V).

2. Upon receiving a signal from the programmed current pulse generator the relay is actuated and opens contact t_1 and closes contact t_2. The charging cable

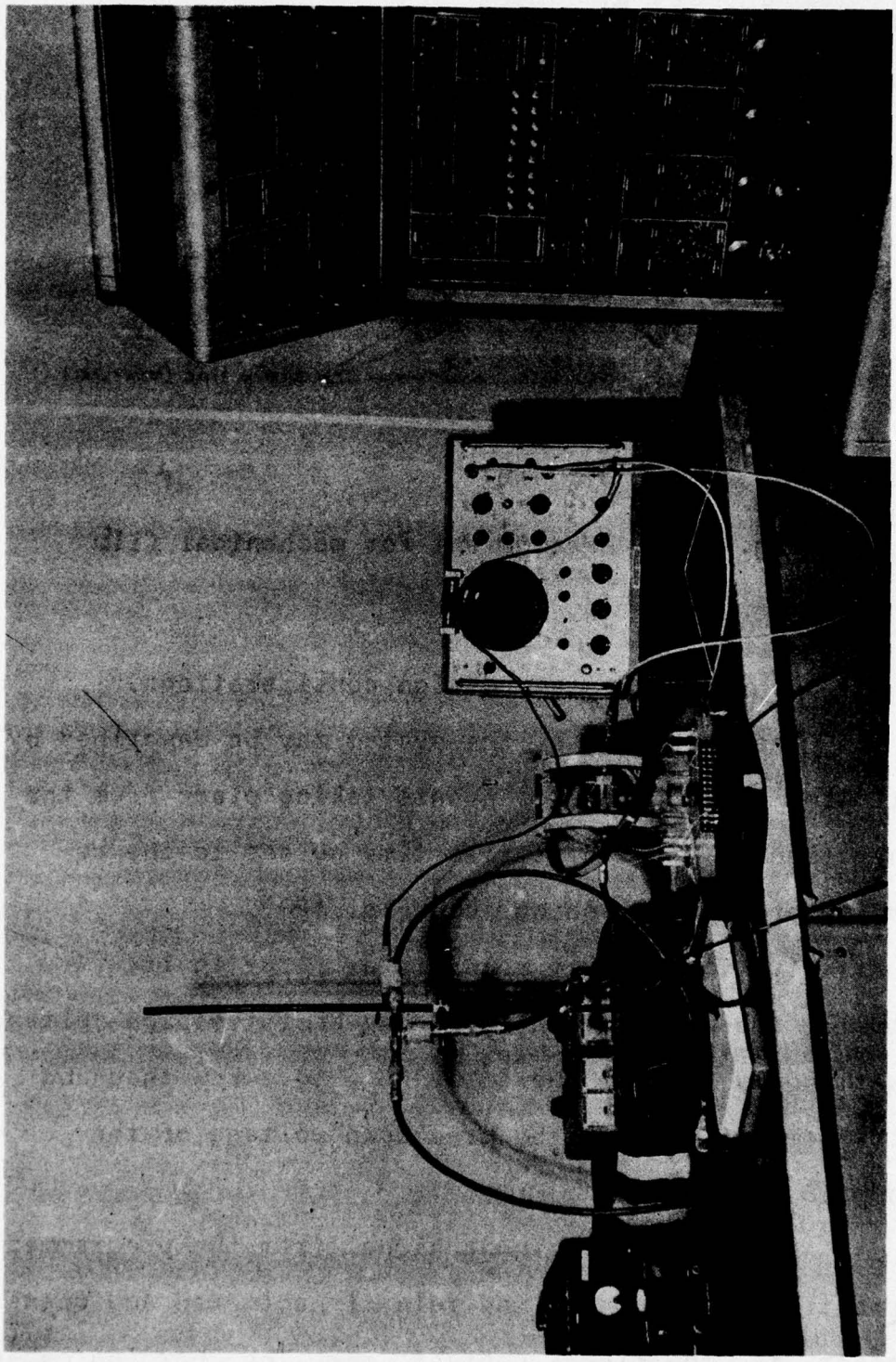


Fig. 127

C_2 discharges through t_2, producing a current pulse propagating through a 50 ohm mixed transmission line made of coaxial cables, HN connectors, and shorted or 50-ohm terminated strip line. The voltage surge at t_2 sends a triggering signal to the oscilloscope, while the pulse proceeding toward the strip line is sufficiently delayed (100 nsec) through cable C_3 to reach the oscilloscope in a strobed condition. The current pulse through the line causes the film magnetization to reverse and a voltage pulse is induced in the pickup loop and displayed on the sampling oscilloscope CRT. The relay is actuated in the reverse direction, to close contact t_1 and recharge the cable by an opposite polarity pulse from the programmed current pulse generator.

3. A signal from the pulse generator causes a pair of Helmoltz coils to reset the magnetization of the film to the original state and the process is repeated. The three pulses controlling the opening and the resetting of the relay, and the resetting of the magnetization must be properly synchronized.

Rather than carrying out a detailed analysis of the system to predict its behavior when a subnanosecond rise-time pulse propagates through it, the configuration is optimized experimentally after designing

the most important components from known microwave techniques.

(1) Strip line design

Several papers have been published in recent years on the design of strip transmission lines for microwave applications.[3, 4, 5, 6] This type of transmission line operates in the TEM mode,[7] for which the characteristic impedance, phase constant and velocity of propagation are given by:

(111) $$Z_o = (L/C)^{1/2}$$

(112) $$\beta = \omega (LC)^{1/2}$$

(113) $$V = 1/(LC)^{1/2}$$

The velocity of propagation is equal to the velocity of light propagating in free space, since the line has two conductors and the dielectric is air. The velocity is then given by

(114) $$V = 1/(\mu_o \cdot \varepsilon_o)^{1/2}$$

The expression for the characteristic impedance becomes:

(115) $$Z_o = 1/V\,C = 1/3 \times 10^8\,C \quad \text{ohms}$$

where the capacitance C per unit length of line is the sum of the capacitance between the central conductor and the ground plane and a term due to the fringing field capacitance, which is a substantial part of the total capacitance for characteristic impedances above

25 ohms.[63] The line is to be designed for a characteristic impedance of 50 ohm to match the connecting cable.

The method suggested in Ref. 69 for the design of strip transmission lines is applied for determining the cross sectional dimensions of strip lines. In the case of the strip line shown in Figs. 122, 124, 125 and mentioned in paragraph 2 of the previous section, the line is to be used to test the effects of a piezoelectrically applied stress on a thin film. A spacing of 1/2" between central conductor and ground plane is considered suitable for the insertion of piezoelectric crystals. Also, as reported in Ref. 70, it is desirable to minimize the effects of current relaxation in the ground planes on the film by making the strip-to-ground plane separation as large as possible. Finally, a total separation of 1" between ground planes is convenient for welding the line to an Amphenol UG-495 A/U 50 ohm connector. Selecting a strip thickness of 1 mm and using Everdur (a strong bronze alloy) sufficient rigidity is given to the central conductor while its thickness is kept at a minimum. From the diagram on p. 124, Ref. 69, a strip thickness-to-ground plane separation of 1/25.4 = 0.04 with a characteristic impedance of 50 ohms gives a strip width of 3.4 cm. The specifications of the strip line

are then:

- ground plane separation: 2.54 cm
- strip width: 3.4 cm
- strip thickness: 1 mm
- length: 10 cm
- ground plane width: 9 cm.

The last dimension is selected in order to minimize the effects of fringing due to ground plane width. The curve on p. 18, Ref. 66, shows that with the above dimensions the capacitance of the line may be considered equal to that of an identical line with infinite ground plane widths, within graphical errors. This strip line is shown in Figs. 122, 124, 125.

The three-conductor strip line with narrow spacing is dimensioned with a similar procedure. In this case the three conductors have the same width in order to use the arrangement shown in Fig. 126 for stressing the film through mechanical bending. The use of GR connectors type 874 is desirable as they cause minimum mismatch among other existing types of connectors. Such a connector has a diameter of 1 cm and a similar ground plane spacing would allow a minimum mismatch. The thickness of the central connector is chosen as in the previously-designed line: 1 mm. From Ref. 69, it

is found that a ratio of strip thickness to ground plane spacing of 1/10 corresponds to a strip width of 1.15 cm, at a characteristic impedance of 50 ohms. Such a width would not accommodate a one cm diameter film in a region of uniform magnetic field, inside the line. A width of 1.5 cm is considered more suitable, working backwards in the above mentioned diagram one finds a ground plane separation of 1.25 cm. The final dimensions of the line are then:

- ground plane separation: 1.25 cm
- strip width: 1.5 cm
- strip thickness: 1 mm.
- ground plane width: 1.5 cm
- length: 7 cm

The effects of finite ground plane width on the characteristic impedance may be checked from the diagram on p. 18 of Ref. 66. It is found that Z_o would have the value pertaining to an identical line with infinite ground plane width, within graphical accuracy.

The attenuation in the two above-discussed lines has been found negligible, using the curves in Fig. 6, p. 125 of Ref. 69.

The two-conductor strip line mentioned in paragraph 1 of the previous section will now be discussed.

In this case again, the characteristic impedance is given by:

$$Z_o = (L/C)^{1/2}$$

Let s be the separation between the two plates and w their width, the capacitance and inductance per unit length are given by:

(116) $$C = \varepsilon_o \, w/s \quad , \quad L = \mu_o \, s/w$$

substituting into the expression for Z_o yields:

(117) $$Z_o = (\mu_o/\varepsilon_o)^{1/2} \, (s/w) = 377 \, s/w$$

The effects of fringing have been assumed negligible. This is true[71] if $s/w < 0.1$. Choosing $Z_o = 50$ ohms, $w = 1.5$ cm (sufficient to place a 1 cm. diameter film in a uniform field, the conductor separation is obtained: $s = 0.2$ cm. The fringing effects are negligible at $s/w = 0.13$. In fact, using the graph in Fig. 6, p. 18 of Ref. 66, the effects of fringing may be estimated by reading the capacitance of the three-conductor line having spacing 0.4 cm instead of 0.2, width 1.5, and dividing this capacitance by 2. The result is 66 $\mu\mu$F/unit length, corresponding to $Z_o = 50$ ohms. This shows that, within graphical errors, the ratio $s/w = 0.13$ allows one to neglect fringing effects. The final dimensions of the two conductor parallel plate line are thus:

- conductor separation: 0.2 cm
- conductor width: 1.5 cm
- length: 7 cm

The length of the lines has been established in order to obtain a rigid configuration easily mounted in the center of the two pairs of Helmoltz coils; it is too small to cause appreciable attenuation, as was checked earlier for a three-conductor configuration, using the curves found in Ref. 69.

The characteristic impedance of strip transmission lines may be measured using a Q-meter and a standard capacitor. The method is simple and is explained in Ref. 63, pp. 3 and 7.

(2) Estimation of available magnetic field inside the strip line

(a) Two conductor line (cf. Fig. 128)

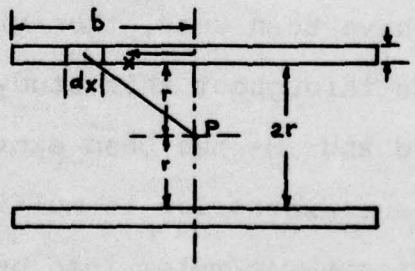


Fig. 128: Two conductor transmission line cross section. Computation of magnetic field intensity at P.

Assuming the current pulse I uniformly distributed across a line of infinite length in the direction perpendicular to the plane of the figure, the magnetic field at the center P of the line, due to an element dx, is given by:

$$(118) \qquad d H_p = \frac{dI}{2 \pi a} = \frac{it}{\pi} \frac{dx}{a} = \frac{it}{\pi} (r^2 + x^2)^{-1/2} dx$$

where I is the total current in the line, i is the current density in ampere/m^2. Integrating from 0 to b, and substituting (2it) by I/b gives:

$$(119) \qquad H_{2p} = \frac{I}{\pi b} \ln \frac{b + (b^2 + r^2)^{1/2}}{r}$$

Let V be the instantaneous voltage across the line. The current through the line is:

$$I = V/Z_o,$$

Substituting in the expression for H_{2p} gives:

$$(120) \qquad H_{2p} = \frac{V}{\pi b Z_o} \ln \frac{b + (b^2 + r^2)^{1/2}}{r}$$

in which MKS units have been used, thus giving H_{2p} in ampere/meter. Since throughout this study the emu system has been used and H has been expressed in oersteds, the previous expression is multiplied by $4 \pi 10^{-3}$ to convert amperes/meter into oersteds; the expression is also multiplied by 1000 and V is expressed in KV.

The value of the magnetic field expressed in oersteds, at the center of a 50 ohm, two conductor parallel-plate line with separation 2r and width 2b, when V K volts are impressed across the conductors, is then:

$$(121) \qquad H_{2p} = \frac{0.08}{b} \ln \frac{b + (b^2 + r^2)^{1/2}}{r} V$$

where b and r are expressed in meters

V is expressed in Kvolts

For V = 1 KV, b = 0.0075 m, r = 0.001 m (case of the two-plate line discussed in preceding paragraph 2); the natural logarithm in the preceding expression is equal to 2.71 and one obtains:

$$(122) \qquad H_{2p} = 29 \text{ oersteds/KV}$$

The intensity of the magnetic field observed is considerably smaller than the prediction of expression (121). Losses caused by reflections, by the generation of the relay and attenuation in the cabling reduce the voltage at the line to one half the value at the power supply. If the line is short-circuited at the end, the available magnetic field near the short is twice as high.[61, 62]

(b) Three conductor line: (cf. Fig. 129)

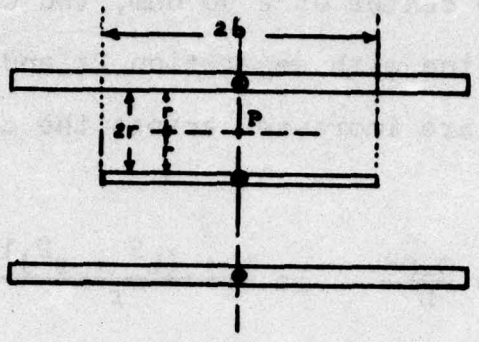


Fig. 129: Three conductor line cross section, computation of magnetic field intensity at P .

Expression (121) may be used to obtain the intensity of the magnetic field at the center P between the strip and one of the ground planes. The line impedance between these two conductors is however 100 ohms, as the total impedance is 50 ohms. It is found that:

$$H_{2p} = 4 \text{ oe/KV}$$

In this case again the available field may be increased by shorting the line at the end and placing the film near the short.

(3) Estimation of film pickup voltage in sensing loop.

An approximate evaluation of the pickup voltage when the actual distance between the pickup wire and the

film is taken into account, may be carried out, using the results of a theoretical analysis supported by experiment and reported in Ref. 72.

If an infinite rectilinear wire is placed in a position parallel to the plane of a square film, a distance c above the center and perpendicular to the direction of easy magnetization assumed along the direction of two parallel edges, the flux enclosing the wire is related to the flux in the film by the expression:[72]

$$\Phi_w = \frac{\Phi_F}{2} \left(1 - \frac{4c}{\pi l}\right) \tag{123}$$

where

$$\Phi_F = M S \tag{124}$$

S being the cross-section area of the film. Expression (123) is obtained assuming rectilinear magnetic poles at two opposite edges of the film and expanding the results of a conformal mapping into a series. If the film is circular this assumption is not valid and the flux distribution must be determined using two semi-circular magnetic pole distributions. However, if the pickup wire is placed above the center of a circular film, such that $c \ll 1$, along a direction parallel to the substrate plane and perpendicularly to

the film easy axis, the expression (123) may be used as an approximating value for computing the voltage induced in the wire. For a pickup loop indefinitely close to the film the emf induced was obtained from a computer solution of the equation of Landau and Lishitz, assuming a switching pulse of zero rise time. The following expression was found for the emf induced (cf. expression (103)),

$$e = 4\pi M S \frac{d\phi}{dt} \sin \phi \tag{125}$$

From (125) and (123), the emf induced in a wire placed above the film, at the position of the upper side of the pickup loop shown in Fig. 122, is given by the expression:

$$e_i = \frac{1}{2} \left(1 - \frac{4c}{\pi l}\right) e \tag{126}$$

where e (max. pickup sig.) may be read from any one of the description computer plots for the film dynamic response and for a given set of parameters. No emf is induced in the lower side of the loop shown in Fig. 122 because of the screening action of the line central conductor and of the silver electrostatic shield surrounding the pickup wire.

With $c = 1$ mm and $l = 10$ mm, expression (126) becomes:

(127) $$e_i = 0.44\ e$$

4. Mercury relay, coaxial cables, connectors.

Mercury relay

High-speed mercury relays suitable for the severe voltage and current requirements of this experiment are not available commercially. Western Electric relays type 275 and 276 are the best substitutes and their nominal 1000 hours life is reduced to less than 15 hours of intermittent operation.

The requirements of the mercury relay are determined as follows:

- The charging cable length is selected in order to give a pulse of a few hundred nanoseconds with a reasonable attenuation. The repetition rate is then fixed in order to operate the relay at a low duty cycle, but still sufficiently high so as to give close sample traces on the oscilloscope display; from experience 500 pulses per seconds is considered satisfactory. The duty cycle when operating at 2000 volts through 50 ohms would correspond to an average current of 0.5 m for a pulse width of 25 nsec. The average current is very low, but the instantaneous value is 40 amperes. A pulse width of 25 nsec is determined

from a maximum acceptable attenuation of 5 db at 3 Kmc and from the velocity of propagation (65.9% of the free space velocity of light) for the cable chosen (RG-19U).

- When the relay contact connected to the high voltage supply closes, the cable is charged to 2000 V and the current rate of increase on closure may be determined by evaluating the charging time constant and should be kept below 25 amperes per microseconds for Western Electric relays type 275 and 276. The same limitation holds when the relay armature closes on the contact t_2 connected to the delay cable and a current pulse with a rise time of several amperesnin a fraction of a nanosecond is produced.

The instantaneous voltage across the relay open contacts should not exceed 500 volts in the case of Western Electric relays mentioned earlier. Such voltages reach a few thousand volts in this application (2000 V in this experiment).

- The relay must have a coaxial mount and its contacts must be insulated from ground to several thousand volts. This may be accomplished by removing the glass envelope from its metallic case, inserting the envelope in a coaxial mount, potting and insulating it with epoxy and teflon. The relay-operating coil

must be reconstructed around the coaxial enclosure and should be designed for at least 300 ampere turns to provide high-speed operation of the relay on closing and opening.

Coaxial cables.

The delay cable should have low attenuation as it may be required to provide a delay of several hundred nanoseconds. The best delay line is a rigid air tubing, a section of cable type RG-19U has been used in experiments reported in Ref. 2 as it has the advantage of being flexible. The attenuation of such a cable is 7.7 db per 100 ft at 3 Kmc. A section of cable RG-9U (attenuation: 15 db per 100 ft at 3 Kmc) has been used as charging cable; the attenuation requirement on this cable is not so severe as for the delay cable, since a shorter length is required.

Connectors.

If the system is to be operated at 2000 volts or above, HN type connectors are required and will not arc up to 6000 V, although their nominal peak limitation is 5000 V. Ref. 73 (p. 5, Fig. 6) gives the measured value of VSWR for an HN connector. The graph in the figure shows that the Voltage Standing Wave Ratio does not exceed 1.1 up to 3 Kmc. From the knowledge of the

VSWR the reflection loss RL in db may be obtained, for a particular connection, from the expression:[74]

$$(128) \qquad RL = 10 \log_{10}\left[1/\left(1 - \frac{VSWR - 1}{VSWR + 1}\right) \right] \text{ db}$$

At lower operating voltages (1000 volts) GR connectors type 874 may be used, preferably.

The connection of the delay cable to the short sections of RG-9U cables connecting to the strip line on one side of the delay cable and to the relay/on the opposite side presents a special problem because of the difference in cable diameters (cf. Fig.121). Reflection losses at these two connections should be measured; to this purpose a PRD 219 Rotary Standing Wave Indicator may be used conveniently up to a frequency of 2 Kmc, instead of a slotted line.

An upper bound for the attenuation of the cables and connectors at 3 Kmc from the relay to the strip transmission line may be obtained using expression (128) and cable attenuation data. This line includes:

4 HN connectors	1 db ea.	4.0
6 ft RG-9 cable	15 db/100 ft	0.9
65 ft RG-19 "	7.7 db/1000 ft	5.0
		9.9 db at 3 Kmc

In this computation a high value of VSWR (1.5) has been substituted in expression (128) as three HN connectors are not mated to their standard counterpart.

This estimate of attenuation in the coaxial cabling shows the detrimental effect of reflection losses caused by mismatch and by excessive lengths of coaxial cables.

The design and contruction of the instrumentation for studying the dynamic behavior of films under stress is to be followed by a checkout phase leading to the final display of pickup waveforms on the sampling oscilloscope. This final phase of the experimental investigation of stress effects on dynamic switching is proposed as a continuation of this work, in which emphasis is placed on the static magnetic behavior.

As mentioned in the introduction, the effects of isotropic stresses on low frequency switching of magnetic films are studied by coupling the film to piezoelectric ceramics. Coupling to particular cuts of single piezoelectric crystals is also of interest and is included in this study. Before considering the stressing of a film by a piezoelectric substrate it is in order to evaluate the magnitude of strains available

from piezoelectrics. For this reason the next chapter begins with the presentation of a table containing data on electrostrictive and piezoelectric crystals, as well as information on the suitability of these materials to form a film substrate.

CHAPTER III

Piezoelectric crystals and piezoelectric-magnetostrictive coupling

1. Characteristics of piezoelectric and electrostrictive crystals, Table.

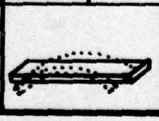
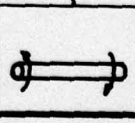
As mentioned in the introduction this Chapter is concerned with the evaluation of strains available from piezoelectric substrates and their effects on the switching properties of magnetostrictive films. A combination of modes of motion, materials and geometries are considered. Table VI summarizes the information useful in determining the suitability of several piezoelectric substrates for depositing magnetostrictive thin films with acceptable switching properties (magnetic anisotropy). Surface strains produced by a specified electric field (500 volts across 0.010"), for a specified mode, are included in the Table and are considered in selecting crystals to be coupled to magnetic films.

These strains correspond to drives with DC electric fields and are evaluated from the piezoelectric equations of state or from the steady state solutions of the differential equations of motion.

Table VI is the result of theoretical pre-

TABLE

CHARACTERISTICS OF ELECTROSTRICTIVE AND PIEZOELECT

	ELECTROSTRICTIVE CERAMI															
	BAR								DISC		ROD		CYLINDER			
	col.1 LONG MODE		col.2 THICKNESS MODE		col.3 SHEAR MODE		col.4 BENDING MODE bimorph		col.5 RADIAL MODE		col.6 TORSION. MODE		col.7 RADIAL MODE		col.8 SPLIT FLEXUR MODE	
	$BaTiO_3$	PZT-5	$BaTiO_3$	PZT-5	$BaTiO_3$	PZT-5	$BaTiO_3$	PZT-5	$BaTiO_3$	PZT-5	$BaTiO_3$	PZT-5	$BaTiO_3$	PZT-5	$BaTiO_3$	PZ
piezoelectric constant $\times 10^{-12}$ m/V	d_{31} -58	d_{31} -140	d_{33} 149	d_{33} 320	d_{15} 205	d_{15} 495	d_{31} -58	d_{31} -140	d_{31} -58	d_{31} -140	d_{15} 205	d_{15} 495	d_{31} -58	d_{31} -140	d_{31} -58	d_3 -14
electromechanical coupling coefficient	0.185	0.318	0.46	0.675	0.44	0.635	0.185	0.318	0.185	0.318	0.44	0.655	0.185	0.318	0.185	0.3
resonant frequency cps	$\frac{n}{2L}\left[\frac{E}{\delta}\right]^{\frac{1}{2}}$		$\frac{1.11}{2t}\left[\frac{E}{\delta}\right]^{\frac{1}{2}}$		$\frac{0.63n}{2t}\left[\frac{E}{\delta}\right]^{\frac{1}{2}}$		$\frac{1.29t}{L^2}\left[\frac{E}{\delta}\right]^{\frac{1}{2}}$		$\frac{0.34}{R}\left[\frac{E}{\delta}\right]^{\frac{1}{2}}$		$\frac{0.63n}{2L}\left[\frac{E}{\delta}\right]^{\frac{1}{2}}$		$\frac{1}{2\pi R}\left[\frac{E}{\delta}\right]^{\frac{1}{2}}$		$\frac{10t}{L^2}\left[\frac{E}{\delta}\right.$	
available strain μin/in 500V. across 0.01"	-113	-270	293	630	405	970	-113	-270	-113	-270	405	970	-113	-270	-113	-27
surface smoothness	← POOR															
Curie point °C	100	300	100	300	100	300	100	300	100	300	100	300	100	300	100	30
mechanical Q	500	75	500	75	500	75	500	75	500	75	500	75	500	75	500	75
maximum safe relative humidity	← 100%															
density gr/cm³	5.5	7.5	5.5	7.5	5.5	7.5	5.5	7.5	5.5	7.5	5.5	7.5	5.5	7.5	5.5	7.5
Young's modulus $E=1/s_{11}^E$, $\times 10^{11}$ dynes/cm²	11.6	7.5	11.6	7.5	11.6	7.5	11.6	7.5	11.6	7.5	11.6	7.5	11.6	7.5	11.6	7.5
geometry																

t = thickness of plate or bar or cylinder wall.
n = order of vibrational mode

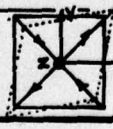
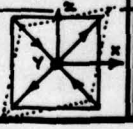
LE VI

PIEZOELECTRIC MATERIALS

ERAMICS								PIEZOELECTRIC CRYSTALS		ELECTROSTRICT.	
CYLINDER				MISC. SHAPES				PLATE		SPLIT CYLINDER	
col. 7 RADIAL MODE		col. 8 SPLIT CYL. FLEXURAL MODE		col. 9 HELICAL FLEXURAL MODE		col. 10 SPIRAL LONG. MODE		col. 11 FACE SHEAR MODE Z-cut	col. 12 FACE SHEAR MODE Y-cut	col. 13 GAP VARIATIONS TRANSVERSE MODE	
$BaTiO_3$	PZT-5	$BaTiO_3$	PZT-5	$BaTiO_3$	PZT-5	$BaTiO_3$	PZT-5	Ammonium dihydrogen phosphate ADP	quartz	$BaTiO_3$	PZT-5
d_{31} -58	d_{31} -140	d_{31} -58	d_{31} -140	d_{31} -58	d_{31} -140	d_{31} -58	d_{31} -140	d_{36} 48 (0°Z)	d_{14} 0.85 (0°Y)	d_{31} -58	d_{31} -140
0.185	0.318	0.185	0.318	0.185	0.318	0.185	0.318	0.28	0.14	0.185	0.318
$\frac{1}{2\pi R}\left[\frac{E}{\delta}\right]^{\frac{1}{2}}$		$\frac{10t}{L^2}\left[\frac{E}{\delta}\right]^{\frac{1}{2}}$		-		-		-	-	$\frac{10t}{L^2}\left[\frac{E}{\delta}\right]^{\frac{1}{2}}$	
-113	-270	-113	-270	-113	-270	-113	-270	24	1.7	gap variation for V=1000 V. R_1=0.5cm, t=0.08cm: theory 1.7×10^{-4}; expt. 2.4×10^{-4}	theory 4.1×10^{-4}; expt. 6.8×10^{-4}
								FAIR	GOOD	POOR	POOR
100	300	100	300	100	300	100	300	max allow. temp. 100°C	max allow. temp. 550°C	100	300
500	75	500	75	500	75	500	75	-	-	500	75
								94%	100%	100%	100%
5.5	7.5	5.5	7.5	5.5	7.5	5.5	7.5	1.8	2.65	5.5	7.5
11.6	7.5	11.6	7.5	11.6	7.5	11.6	7.5	5.9	7.8	1.6	7.5






dictions and experiments reported in this chapter and information collected from the literature.[89, 90, 93, 95, 98, 100]

Properties desired from a piezoelectric substrate are listed hereafter and are helpful in the selection of the best possible piezoelectric material, geometry and driving mode. A piezoelectric substrate must obey the following requirements in order to confer acceptable magnetic properties to the film and the ability of transmitting strains.

a) High Curie point and temperature stability (above 200°C, temperature of magnetic annealing of the film).

b) Absence of hygroscopicity (to avoid outgassing effects in vacuum and deterioration of the surface).

c) Smooth plane surface, i.e. minimization of microscopic irregularities.

d) Absence of chemical or physical reaction with nickel-iron alloys.

e) High piezoelectric constant, combined with high dielectric and mechanical strength (to produce strains between 100 and 1000 micro in/in with reasonable applied voltages, 500 to 1000 volts).

2. Theoretical models of piezoelectric and electrostrictive behavior

a) General method of analysis, piezoelectric equations of state, equation of motion, magnitude of piezoelectric constant d.

The detailed description of the method to be followed to obtain stresses, strains, electric displacements and electric fields, in a given piezoelectric or electrostrictive configuration is given in two classic books by Mason (cf. Refs. 89 and 90). Only a brief outline is given in this section.

Among the four possible variables, strain, stress, electric displacement, electric field, two are selected as dependent and two as independent, according to the nature of the driving forces applied to the crystal. The dependent variables are written in generalized tensor notation (Ref. 89, p. 38).

From the knowledge of the crystallographic class to which the crystal belongs, multirank tensors relating the dependent and independent variables are obtained (Ref. 89, p. 40).

The tensors are related to or are exactly the coefficients available from the crystal manufacturer.

If components of the dependent variables along

directions other than the crystallographic axes are desired, the tensors must be referred to the new axes by use of standard formulas (Cf. Ref. 89, p. 455).

When electric fields are applied to a free crystal, strains and electric displacements are produced. The independent variables are the stresses (equal to zero at the boundary if the crystal is free) and the applied electric fields. The dependent variables are the strains S_i and the electric displacements δ_m. The general expressions are (Ref. 89, p. 39):

$$(129)\quad S_i = s^E_{i1} T_1 + s^E_{i2} T_2 + s^E_{i3} T_3 + s^E_{i4} T_4 + s^E_{i5} T_5 + s^E_{i6} T_6 + d_{1i} E_1 + d_{2i} E_2 + d_{3i} E_3$$

$$(130)\quad \delta_m = d_{m1} T_1 + d_{m2} T_2 + d_{m3} T_3 + d_{m4} T_4 + d_{m5} T_5 + d_{m6} T_6 + \frac{\varepsilon^T_{m1}}{4\pi} E_1 + \frac{\varepsilon^T_{m2}}{4\pi} E_2 + \frac{\varepsilon^T_{m3}}{4\pi} E_3$$

Static strains for a free crystal are given by expression (129) with $T_i = 0$. For a given driving mode and a given crystal the strains S_i are obtained from the knowledge of applied electric fields E_1, E_2, E_3 and the piezoelectric constants d_{1i}, d_{2i}, d_{3i}. Expression (130) is of no interest in this study.

If the transient response of the crystal is desired when the applied voltage varies with time, the

equation of motion must be considered and the displacement of a point or the strain at a point may be obtained by solving the differential equation of motion.

Newton's differential equation of motion is combined with the piezoelectric equations of state (129) and (130). The resulting differential equation is solved after imposing proper boundary conditions. The strains and the displacements are then found as a function of time, space and the applied electric field. The differential equation may be conveniently solved in Laplace transform space when the applied electric field is a step or a pulse. If the electric drive is sinusoidal the displacement time dependency may be represented by

$$\xi_1 = \xi e^{j\omega t}$$

The strains are then expressed as a function of the frequency ω and an equivalent circuit for the piezoelectric crystal may be obtained. When solving the differential equation of motion in the Laplace transform space, use of the final value theorem yields the steady state response readily.

The piezoelectric equation of state (129) is used in this Chapter to obtain the DC strains entered in Table VI. The complete response to a step voltage is derived for one configuration.

An order of magnitude of piezoelectrically produced strains to stress a film deposited on a crystal is given by experimental studies reported in Ch. I, Part 2, for the 44-56 nickel-iron film having a magnetostriction constant of 20×10^{-6}. It was found that anisotropic strains between 100 and 1000 micro-in/in induced sufficient stresses in a film deposited on a glass substrate to cause considerable changes in hysteresis loop characteristics. Theoretical predictions illustrated by the curves in Fig. 34 led to the same conclusions.

For all piezoelectric modes and geometries described, interelectrode spacing is kept at minimum standard values and voltages less than 1000 V. are applied

b) Electrostrictive bar, length mode, DC strains, (cf. Fig. 130 and Table VI, Col. 1).

For such a configuration the voltage is applied along the axis 3 and the strain is obtained along axis 1. For a Lead Zirconate Titanate ceramic (PZT-5) the piezoelectric constant d_{31} controlling this mode is: $d_{31} = -140$ m/V. With 500 V across 0.010" the resulting strain is

$$S_1 = d_{31} \frac{V}{t} = 270 \times 10^{-6} \text{ (PZT-5)}$$

For Barium Titanate $d_{31} = -58$, S_1 becomes: 113×10^{-6}

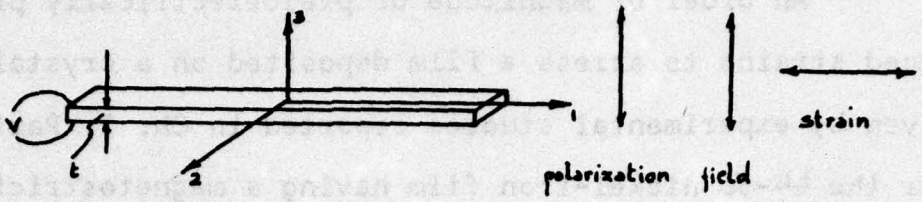


Fig. 130 Length mode of electrostrictive bar

Strains of 113 and 270 micro in/in for 500 V. applied across 0.010" indicate that electrostrictive ceramics are suitable to obtain strains between 100 and 1000 micro in/in with reasonable voltages impressed across practical values of interelectrode spacings. Also the high Curie point (300°C for PZT-5) allows deposition of the film at annealing temperatures between 200 and 300°C necessary to obtain a high degree of magnetic anisotropy.

The surface of the ceramic makes however a poor substrate for a magnetic film and must be changed to eliminate microscopic irregularities. This question will be examined further while discussing coupling of films to electrostrictive substrates. The high mechanical Q of Barium Titanate and Lead Zirconate Titanate makes these materials suitable to impress large alternating strains upon films at the piezoelectric resonant frequency (cf. Table VI).

The previously calculated strains are obtained from a polarized ceramic. If a film is deposited on an unpolarized ceramic, a permanent strain may be obtained in the film by polarizing the polycrystal after the deposition of the film. In the case of PZT-5 the residual strain may be as high as 2000 x 10^{-6}, as has been measured in experiments reported in Part 3 of this Chapter.

c) Electrostrictive bar, thickness mode, transient and DC strains (cf. Fig. 131 and Table VI, Col. 2)

In the thickness mode the polarization, the applied field and the strains are parallel.

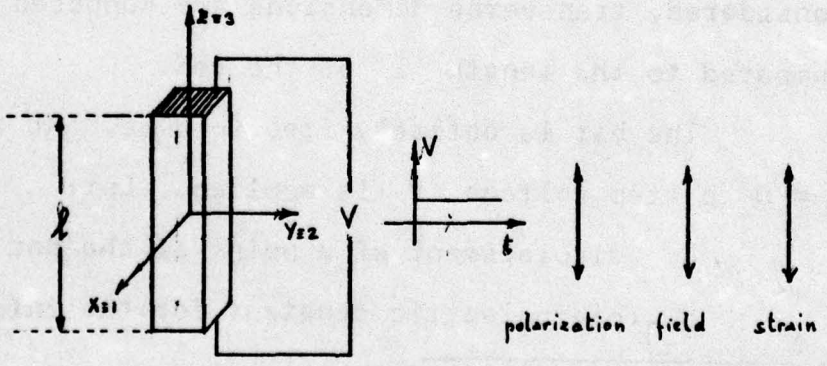


Fig. 131 Thickness mode of piezoelectric bar

The piezoelectric constant d_{33} controls the strains along the "3" axis when the polarization and

the applied field are also directed along "3". In the case of a plate having a thickness $t = 0.010"$, with 500 V. across the electrodes the strain S_3 is:

$$S_3 = d_{33} \frac{V}{t} = 630 \times 10^{-6} \text{ for PZT-5,}$$

$$(d_{33} = 320 \times 10^{-12} \text{ m/V})$$

$$S_3 = 295 \times 10^{-6} \text{ for Barium Titanate,}$$

$$(d_{33} = 149 \times 10^{-12} \text{ m/V})$$

The case of a bar driven in the thickness mode is studied next, and transient and DC strains produced by a step voltage are evaluated.*

Consider a piezoelectric bar oriented along the z-axis (Fig. 131), with the origin of coordinates at its center. Only stresses and strains along z are considered, transverse dimensions are supposed small as compared to the length l of the rod.

The bar is entirely free to move. At time $t = 0$ a step voltage V is applied. Let:

u: displacement of a point of the bar along z

d_{33}: piezoelectric constant for the thickness mode

---

*This dissertation study was originally intended to include an investigation of the application of voltage pulses to a piezoelectric crystal coupled to a magnetostrictive film. The preliminary theoretical study, partially reported in this section, showed the propagation of reflected pulses in a crystal would cause undesirable coupling to the ferromagnetic film. This study was carried out in 1959 and published in Annual

(Footnote continued next page)

S_3: strain $\frac{\partial u}{\partial z}$ along the direction of z coinciding with axis "3"

T_3: stress along z-axis

Y : Young's modulus

ρ : density

The equation of motion is:

$$\frac{\partial^2 u}{\partial z^2} = \frac{1}{\alpha^2} \ddot{u} , \tag{131}$$

where

$$1/\alpha^2 = \rho / Y. \tag{132}$$

At $z = 0$ and for all time:

$$u = 0, \frac{\partial u}{\partial t} = 0 . \tag{133}$$

At $z = -1/2$ and $z = 1/2$:

$$\frac{\partial u}{\partial z} = d_{33} E(t), \tag{134}$$

where $E(t)$ is the applied electric field

In Laplace transform space Eq. (131) becomes:

$$\frac{d^2 U}{dz^2} = \frac{s^2}{\alpha^2} U \quad \text{(all initial conditions are zero)} \tag{135}$$

---

*Summary Report N° 60-82 of investigations in digital technology research, June 1, 1959 to May 31, 1960. Independently, a similar investigation published in the Journal of Applied Physics in July 1960, Vol. 31 N° 7, was undertaken by Leo Levi. The findings reported by the two investigators on the piezoelectric response were essentially the same.

The solution is:

$$U = A\, e^{zs/\alpha} + B\, e^{-zs/\alpha}$$

After determination of constants from boundary conditions:

$$(136)\quad U(s) = \alpha\, d_{33}\, \frac{E(s)}{s}\, e^{zs/\alpha} - ls/2\alpha\, \frac{1 - e^{2zs/\alpha}}{1 + e^{-ls/\alpha}}$$

Case of an applied step function: $E(s) = E/s$. Eq. (136) becomes:

$$(137)\quad U(s) = \frac{\alpha d_{33} E}{s^2} \times$$

$$\left\{ e^{-\frac{s}{\alpha}(\frac{l}{2} - z)} - \left[e^{-\frac{s}{\alpha}(\frac{3l}{2} - z)} + e^{-\frac{s}{\alpha}(\frac{l}{2} + z)} \right] + \right.$$

$$+ \left[e^{-\frac{s}{\alpha}(\frac{3l}{2} + z)} + e^{-\frac{s}{\alpha}(\frac{5l}{2} - z)} \right] -$$

$$\left. - \left[e^{-\frac{s}{\alpha}(\frac{5l}{2} + z)} + e^{-\frac{s}{\alpha}(\frac{5l}{2} - z)} \right] + \ldots \right\}$$

Transformation into the time domain yields:

$$(138)\quad u(t) = \alpha d_{33} E \left\{ \left[t - \frac{1}{\alpha}(\frac{l}{2} - z) \right] . u \left[t - \frac{1}{\alpha}(\frac{l}{2} - z) \right] - \right.$$

$$- \left[t - \frac{1}{\alpha}(\frac{3l}{2} - z) \right] . u \left[t - \frac{1}{\alpha}(\frac{3l}{2} - z) \right] -$$

$$\left. - \left[t - \frac{1}{\alpha}(\frac{l}{2} + z) \right] . u \left[t - \frac{1}{\alpha}(\frac{l}{2} + z) \right] + \right.$$

$$+\left[t - \frac{1}{\alpha}\left(\frac{3l}{2} + z\right)\right] . u\left[t - \frac{1}{\alpha}\left(\frac{3l}{2} + z\right)\right] + \ldots \Bigg\}$$

From Eq. (138) the displacements at $z = \pm 1/2$ may be obtained and are plotted vs. time in Fig. 132.

The strains are given by:

$$(139) \quad \frac{dU}{dz} = d_{33} E \sum_{1}^{n} \frac{e^{-\frac{s}{\alpha}\left(n\frac{l}{2} + z\right)}}{s}$$

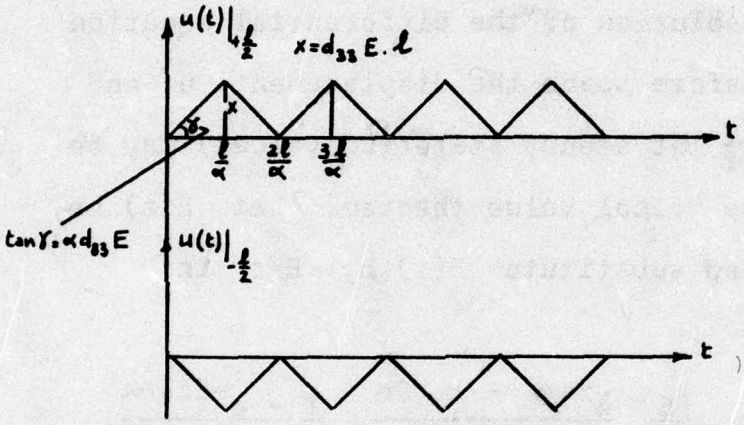


Fig. 132 End displacement of electrostrictive bar (thickness mode)

In Eq. (139) terms in the summation are transformed into the time domain by:

$$(140) \quad \mathcal{L}^{-1} \frac{e^{-as}}{s} = u(t - a)$$

Using (140) the strain at $z = 0$ is obtained:

$$(141) \quad S\big|_{z=0} = \frac{\partial u}{\partial z}\Big|_{z=0} = d_{33} E \sum_{n=0}^{n} u\left(t - \frac{(2n+1)l}{2a}\right)$$

Equation (141) is plotted in Fig. 133

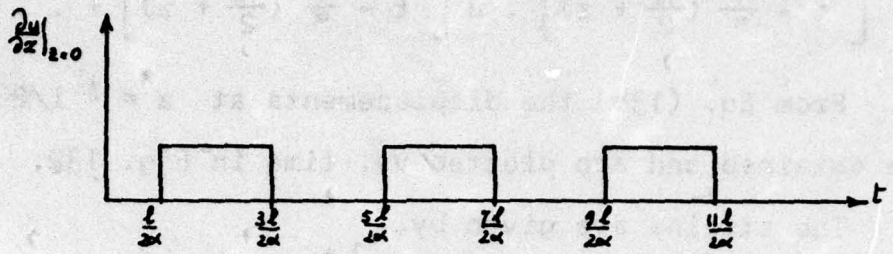


Fig. 133 Strains in electrostrictive bar at z = 0 (thickness mode)

From the solution of the differential equation of motion in transform space the displacement u and the strain $S = \frac{\partial u}{\partial z}$ at steady state (DC values) may be obtained using the "final value theorem". Let E(s) be a step function and substitute E(s) by E/s in Eq. (136):

$$(142)\quad U(s) = \alpha d_{33} \frac{E}{s^2} \frac{e^{zs/\alpha} - 1s/2\alpha}{1 + e^{-1s/\alpha}} \frac{1 - e^{-2zs/\alpha}}{s^2}$$

Using the final value theorem (multiply by s and let $s \longrightarrow 0$), Eq. (142) becomes:

$$(143)\qquad \lim_{s\to 0} \; s \,.\, U(s) = \alpha d_{33} E \frac{1}{2} \frac{0}{0} \,.$$

Using l'Hopital's rule:

$$\lim_{s\to 0} \frac{1 - e^{2zs/\alpha}}{s^2} = \frac{2}{\alpha} z$$

Eq. (143) becomes:

$$\lim_{s\to 0} \; s \,.\, U(s) = d_{33} E z$$

Let $z = \pm 1/2$ and transform back into the time domain:

$$u\Big|_{\pm 1/2} = \pm d_{33} \; E \frac{1}{2}$$

The strain is:

$$S_3 = \frac{\Delta u}{\Delta z} = \frac{u\Big|_{\pm 1/2}}{1/2} = \pm d_{33} \; E \; ,$$

equal to the DC value given by the piezoelectric equation of state.

A general method to obtain the transient and the steady state response for a voltage step producing a field step $E(t)$, is to obtain the response to an impulsive field. In this case $E(s) = E$ and since the system under study is linear, the response to a step is given by the time integral of the response to an impulse E.

Figures (132) and (133) show that in the assumed absence of dissipation, waves travel along the bar with velocity

$$v = \left[\frac{Y}{\rho}\right]^{1/2} ,$$

causing oscillations of the film domain walls. The reflected waves could be absorbed by proper terminations at the ends of the crystal or by proper shaping of the applied step voltage. Because these possibilities are considered impractical, the treatment of the problem

of piezoelectrically-induced stress is confined to the steady state response of a DC electric field.

d) Electrostrictive bar, bending mode, DC strains (cf. Fig. 134) and Table VI, Col. 4)

As stated by Petermann,[95] "the largest motion amplitudes are obtained with transducers operating in flexural or torsional modes." A composite electrostrictive bar capable of large motion is obtained by cementing two electrostrictive ceramics with a conductive glue. The transducer thus obtained is called a "bimorph" and is polarized and driven as shown in Fig. 134.

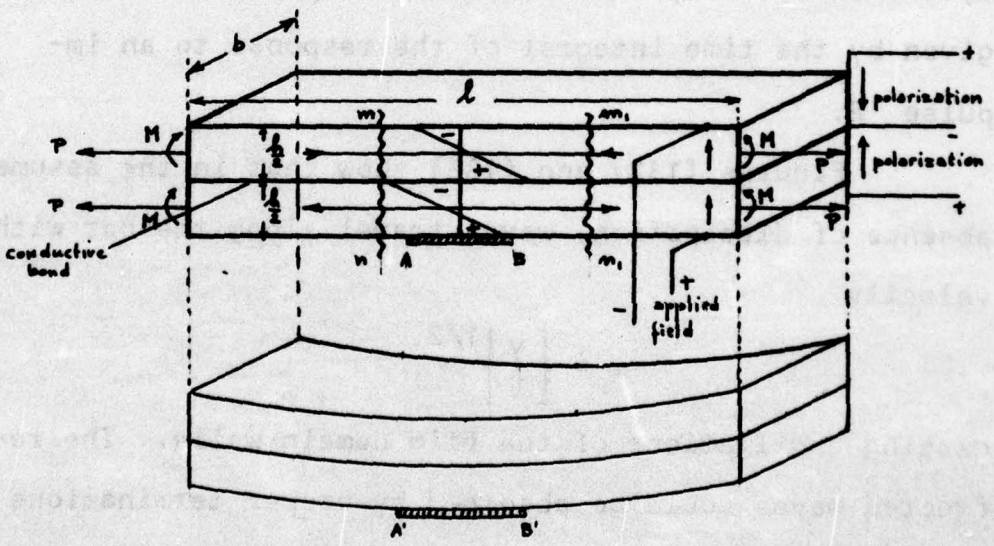


Fig. 134 Bending mode of electrostrictive bar (bimorph)

If a thin film is evaporated on the lower electrode with the polarization and the field directions as shown, the film will be subjected to an anisotropic tension. Strains produced in the film by a given applied voltage may be obtained following the analysis of the bimetallic strip, as treated by Timoshenko.[96]

Let $h/2$ be the thickness of each electrostrictive bar, b their width, V the applied voltage, r the radius of curvature, d_{31} the piezoelectric constant, YI the flexural rigidity of the polycrystalline ceramic. Consider a strip cut out by two adjacent cross sections $m\ n$ and $m_1\ n_1$ (Fig. 134). The internal forces over the cross section can be reduced to a tensile force P and a moment M for the upper bar and identically for the lower bar. For equilibrium:

(144) $$\frac{Ph}{2} = 2\,M$$

The moment M is related to the radius of curvature by:

(145) $$M = \frac{YI}{r}$$

From (144) and (145):

(146) $$P = 4\,\frac{YI}{hr}$$

Since at the joining surface the expansion of the upper bar must be equal to the contraction of the lower bar, the total strains along such surface must also be

equal. The total strain is the sum of the strains due to the electric field, the force P and the moment M. These strains are given by the following expressions:

Strain due to E: $d_{31} E$

Strain due to P: $\frac{P}{(h/2)\, bY}$

Strain due to M: $\frac{\sigma}{Y} = M \frac{h/4}{YI} = \frac{YI}{r} \frac{h/4}{YI} = \frac{h}{4r}$

The sign of the strain in the upper bar is opposite to that in the lower bar. Equating the total strains, in the upper and in the lower bars, yields:

$$- d_{31} E + \frac{2P}{bhY} + \frac{h}{4r} = d_{31} E - \frac{2P}{bhY} - \frac{h}{4r}$$

(147) $$\frac{4P}{bhY} = 2 d_{31} E - \frac{h}{2r}$$

Substituting P from (146) into (147) and I by $(bh^3/96)$, yields:

(148) $$\frac{h}{6r} = 2 d_{31} E - \frac{h}{2r}$$

Equation (148) yields the curvature $\frac{1}{r}$:

(149) $$\frac{1}{r} = \frac{3}{h} d_{31} E$$

Substituting I by $(bh^3/96)$ and $1/r$ by expression (149), (146) becomes:

$$P = \frac{Ybh}{8} d_{31} E$$

The maximum strain at the surface is obtained by adding the strain due to P to the strain due to

the curvature $\frac{1}{r}$:

(150) $$S_{max} = \frac{2P}{bhY} + \frac{h}{4r}$$

Substituting P from (146) into (150) and I by $bh^3/96$, yields:

(151) $$S_{max} = \frac{1}{r} \frac{h}{3}$$

Substituting $\frac{1}{r}$ from (149) into (151) yields:

(152) $$S_{max} = d_{31} E$$

Expression (152) shows that the strain obtained at the surface of the bimorph is equal to that given by a bar of the same width driven in the thickness mode. The bimorph does not present advantages as compared to the single polycrystalline element for stressing a thin film. Transversal motion of one end when the other end is clamped is however relatively large, as the following derivation shows (Fig. 135).

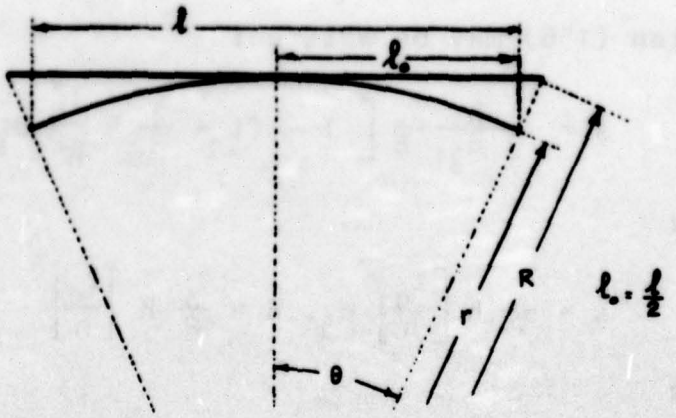


Fig. 135 Flexural displacement of bimorph

The transversal displacement is given by:

(153) $$s = (R - r)\cos\theta$$

where $$\cos\theta = r/R = r/(l_o^2 + r^2)^{1/2}$$

Expression (153) becomes

(154) $$s = r\left[1 - \frac{r}{(l_o^2 + r^2)^{1/2}}\right] = r\left[1 - \frac{1}{\left[\frac{l_o^2}{r^2} + 1\right]^{1/2}}\right]$$

From equation (149):

(155) $$\frac{l_o^2}{r^2} = 9\,\frac{l_o^2}{h^2}\,d_{31}\,E = 9\,\frac{l_o^2}{h^2}\,S_{max}$$

(154) becomes:

(156) $$s = \frac{h}{3\,d_{31}\,E}\left[1 - \frac{1}{(9\,\frac{l_o^2}{h^2}\,d_{31}^2\,E^2 + 1)^{1/2}}\right]$$

If

(157) $$(3\,\frac{l_o}{h}\,d_{31}\,E)^2 \ll 1,$$

expression (156) may be written:

(158) $$s = \frac{h}{3\,d_{31}\,E}\left[1 - (1 - \tfrac{1}{2}\,9\,\frac{l_o^2}{h^2}\,d_{31}^2\,E^2)\right]$$

Finally:

(159) $$s = \tfrac{3}{2}\,h\left[\frac{l_o}{h}\right]^2 d_{31}\,E = \tfrac{3}{2}\,h\left[\frac{l_o}{h}\right]^2 S_{max}$$

Example:

Let $\frac{l}{h} = 100$, $d_{31} = 140 \times 10^{-12}$ (PZT-5),

$$\frac{l_o}{h} = \frac{l}{2h} = 50$$

$$E = \frac{V}{h/2} = \frac{1000\ V}{0.010 \times 2.54 \times 10^{-2}\ m},$$

The maximum strain is:

$$S_{max} = d_{31}\ E = 550 \times 10^{-6}$$

The transversal displacement, as given by (159) is:

(160) $$s = \frac{3}{2} \times 0.020 \times 2500 \times 550 \times 10^{-6} = 0.410"$$

Such a large displacement would not be allowed by the limited mechanical strength of the ceramic but if instead of 1000 V across 0.010", one were to apply 100 V only, the displacement would be:

$$s = 0.041",$$

which is not excessive.

For this example condition (157) gives, for 100 V across 0.010":

$$(3\ \frac{l_o}{h}\ d_{31}\ E)^2 = (3 \times 50 \times 55 \times 10^{-6})^2 = 0.08 << 1,$$

which shows the validity of (158) in this case.

e) Electrostrictive disc, radial mode, DC strains (cf. Fig. 136 and Table VI, col. 5)

In the case of a polarized electrostrictive disc driven in the radial mode the cartesian tensor

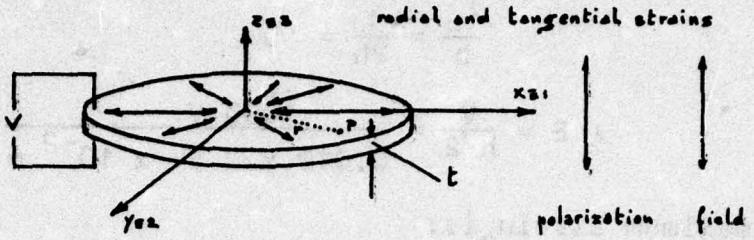


Fig. 136 Radial mode of electrostrictive disc

equations must be transformed into cylindrical coordinates. This transformation is carried out in detail by Mason in Ref. 89, p. 486. The derivation of the classical equation of motion is also shown and applied to the case of a sinusoidal driving function E_z. This study is concerned with the derivation of the steady state strains after application of a pulse. The equation of motion will therefore be taken from the literature (Ref. 89, p. 491) and a step voltage will be applied. The steady state response is obtained by passing to the limit as $s \longrightarrow 0$.

The equation of motion is:

$$(161) \quad \frac{\partial^2 u_r}{\partial r^2} + \frac{1}{r}\frac{\partial u_r}{\partial r} - \frac{u_r}{r^2} = \frac{1}{v^2}\frac{\partial^2 u_r}{\partial t^2}$$

where u_r = displacement at radius r

$v = Y/(1 - \sigma^2)\rho$

Y = Young's modulus

σ = Poisson's ratio

ρ = density

In cylindrical coordinates the radial and tangential strains are given by:

$$(162) \qquad S_{rr} = \frac{\partial u_r}{\partial r} \qquad S_{\theta\theta} = \frac{u_r}{r}$$

Taking the Laplace transform of (161):

$$(163) \qquad \frac{dU_r}{dr^2} + \frac{1}{r}\frac{dU_r}{dr} - \frac{U_r}{r^2} = \frac{1}{r^2} s^2 U_r$$

or

$$(164) \qquad \frac{dU_r}{dr^2} + \frac{1}{r}\frac{dU_r}{dr} + \left(-\frac{s^2}{v^2} - \frac{1}{r^2}\right) U_r = 0$$

The solution of this Bessel equation includes modified Bessel functions, with argument:

$$\frac{sr}{v}$$

The solution is:

$$(165) \qquad U_r = A\, I_1 \left(\frac{sr}{v}\right) \quad \text{(The } K_n \text{ functions are zero)}$$

From Eqs. (162) in transform space:

$$(166) \quad \begin{cases} S_{\theta\theta} = \dfrac{A}{r} I_1 \left(\dfrac{sr}{v}\right) \\ S_{rr} = A\left[\dfrac{s}{v} I_o \left(\dfrac{sr}{v}\right) - \dfrac{I_1\left(\frac{sr}{v}\right)}{r}\right] \end{cases}$$

From the electromechanical equations applied to cylindrical coordinates, the radial stress is (Ref. 89, p. 491):

$$(167)\qquad T_{rr} = \frac{Y}{1-\sigma^2}\left[S_{rr} - S_{\theta\theta}\right] - d_{31}\frac{E_z\,Y}{1-\sigma}$$

Since T_{rr} must be zero at the edge $r = a$ of the disc:

$$(168)\qquad A = \frac{d_{31}\,E_z\,(1+\sigma)}{\frac{s}{v}I_o - \frac{1-\sigma}{a}I_1}$$

Substituting A from (168) into Eqs. (166)

$$(169)\qquad \begin{cases} S_{\theta\theta} = d_{31}\dfrac{E_z\,(1+\sigma)}{r}\dfrac{I_1(\frac{sr}{v})}{\frac{s}{v}I_o(\frac{sa}{v}) - \frac{1-\sigma}{a}I_1(\frac{sa}{v})} \\ S_{rr} = d_{s1}\,E_z\,(1+\sigma)\dfrac{\frac{s}{v}I_o(\frac{sr}{v}) - \frac{I_1}{r}(\frac{sr}{v})}{\frac{s}{r}I_o(\frac{sa}{v}) - \frac{1-\sigma}{a}I_1(\frac{sa}{v})} \end{cases}$$

Using the properties:

$$(170)\qquad \lim_{s\to o} I_o(\frac{sr}{r}) = 1$$

$$\lim_{s\to o} I_1(\frac{sr}{v}) = \frac{sr}{2v}$$

Equations (169) become at the limit:

$$(171)\qquad S_{\theta\theta} = -d_{31}\,E_z$$

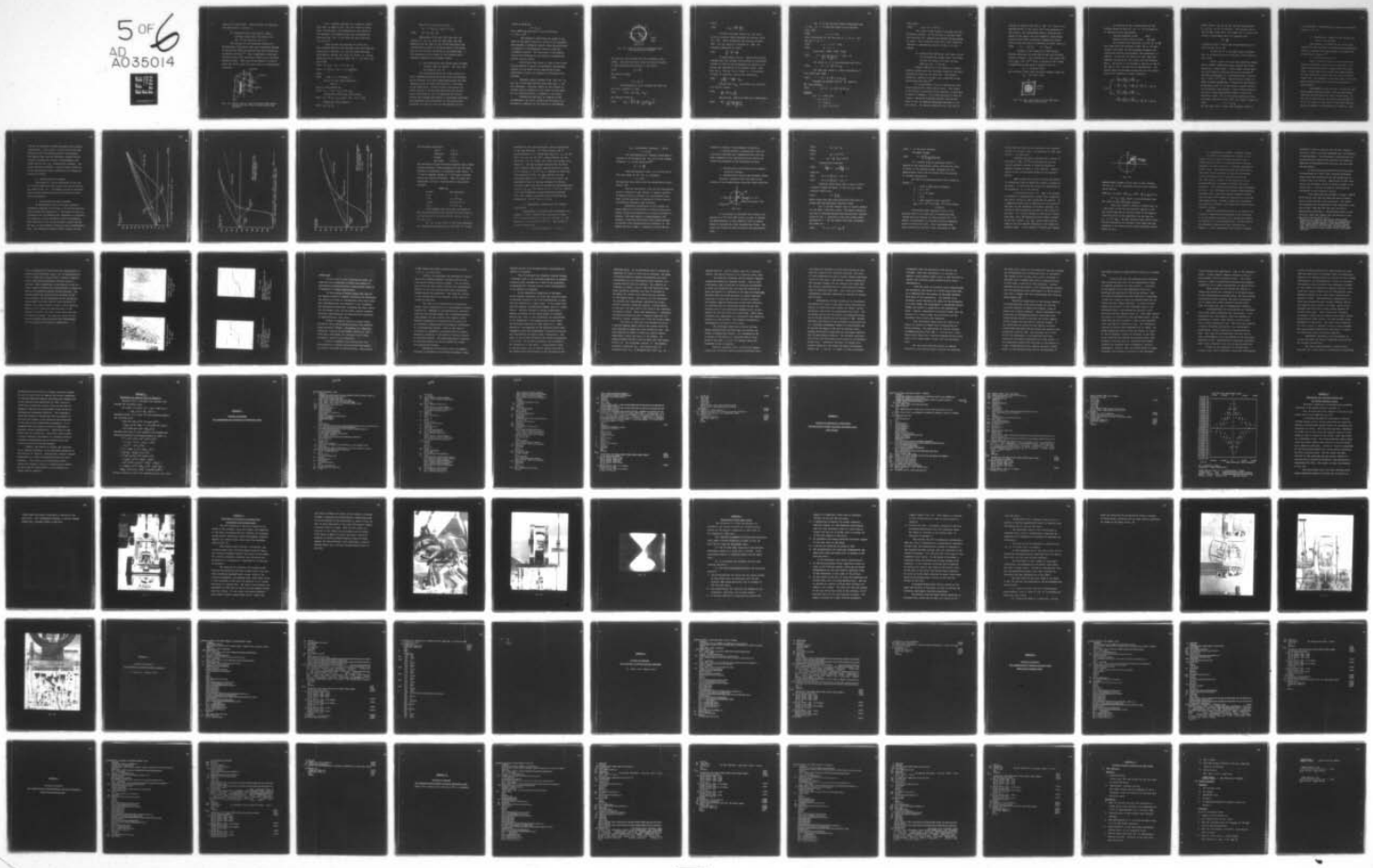
$$S_{rr} = -d_{31}\,E_z$$

Equations (171) show that the radial strain and the tangential strain are equal and independent of the distance r from the center to any point P on the disc.

The strains given by Eqs. (171) are the same as

AD-A035 014 CALIFORNIA UNIV LOS ANGELES DEPT OF ENGINEERING F/G 20/2
ON THE USE OF PIEZOELECTRIC-MAGNETOSTRICTIVE COUPLING IN DIGITA--ETC(U)
AUG 62 A A BORSEI NONR-233(52)
UNCLASSIFIED UCLA62-37 NL

5 OF 6
AD
A035014



those for a length mode. Expected orders of magnitude have been given in section b.

f) Electrostrictive thin walled, closed cylinder, radial mode, DC strains (cf. Fig. 137 and Table VI, col. 7)

The analysis of the vibrations induced in a ferroelectric cylindrical shell with transverse isotropy in the case of radial polarization has been carried out by Haskins and Walsh.[94] These investigators have been concerned mainly with vibrations induced by a sinusoidal driving voltage. Their results may however be used to obtain DC strains along the axial and the circumferential directions.

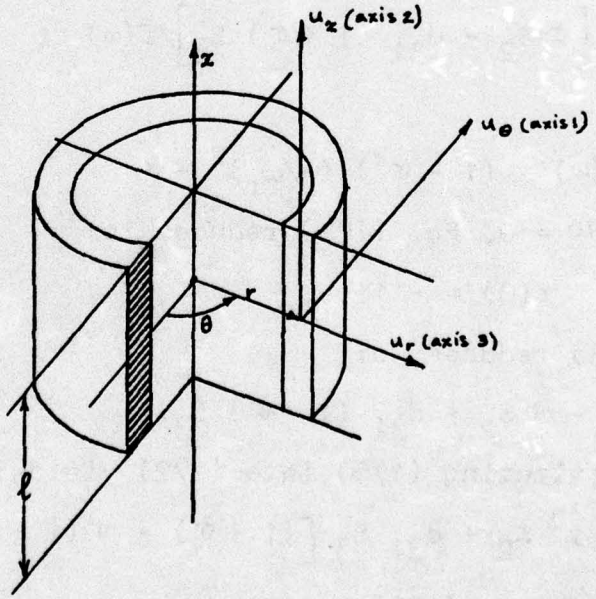


Fig. 137 Radial mode of electrostrictive thin walled closed cylinder (Figure after Haskins and Walsh[94])

For a cylinder referred to a system of coordinate axes, as shown in Fig. 137, the strains of interest, in stressing a film deposited on the surface of the cylinder, are directed along the circumferential direction (u_θ, axis 1) and along the axial direction (u_z, axis 2).

After writing the equations of motion for a free cylinder driven in the thickness mode and using the piezoelectric equations of state the above-mentioned investigators derived the values of strains S_1 and S_2 along the θ and z directions (Ref. 94, p. 732, Eqs.(6.5) and (6.6)):

$$S_2 + \sigma S_1 - d_{31} (1 + \sigma) E_3 = 0 \tag{172}$$

$$S_1 = \left[\sigma S_2 - d_{31} (1 + \sigma) E_3\right] / f(\omega) \tag{173}$$

where

$$f(\omega) = (1 - \sigma^2) (\omega/\omega_r)^2 - 1 \tag{174}$$

Let $\omega = 0$, Eq. (174) reduces to:

$$f(0) = - 1$$

and eq. (173) reduces to:

$$S_1 = - \sigma S_2 + d_{31} (1 + \sigma) E_3. \tag{175}$$

Substituting (175) into (172) yields:

$$S_2 = \sigma^2 S_2 + d_{31} E_3 \left[(1 + \sigma) - \sigma(1 + \sigma)\right] \tag{176}$$

Expression (176) becomes:

$$S_2 = d_{31} E_3 \tag{177}$$

Substituting (177) into (175):

$$S_1 = -\sigma d_{31} E_3 + d_{31}(1 + \sigma) E_3$$

$$S_1 = d_{31} E_3 = S_2 \tag{178}$$

Expressions (177) and (178) show that the strains S_1 and S_2 have the same sign, the same magnitude and are equal to the strain obtainable from a piezoelectric plate of thickness equal to the thickness of the cylinder and driven in the length mode. A film deposited on the surface of the cylinder would therefore experience an isotropic stress.

g) Electrostrictive thin walled split cylinder, flexural mode, DC strains. (Cf. Fig. 138 and Table VI, Col. 8)

The strain produced on the outer surface of a split cylinder polarized and driven along the thickness may be obtained, in a first approximation, from the same expression used to obtain the strain of a bar driven in the length mode. A more accurate calculation requires the use of curved beam theory but for the purpose of obtaining an order of magnitude for surface strains the straight beam theory is considered sufficient. All assumptions and derivations for the piezoelectric equations of state of a bar are then applied and the

strain is given by:

$$S = d_{31} E$$

For a PZT-5 bar 500 volts across 0.010" gives $S = 270 \times 10^{-6}$.

The problem of predicting the change in gap width as the split cylinder is driven in the thickness mode assumes a particular interest when the polycrystal is coupled to a ferromagnetic material along one cylindrical surface. The reluctance of the magnetic circuit thus obtained may be changed by changing the applied electric field.

Rectilinear beam theory is used in the following derivations to derive an approximate relationship between the gap width and the applied DC voltage. Experimental results are compared to theoretical predictions.

Consider a split cylinder (Fig. 138), let R_1 and R_2 be the inner and the outer radii and t the wall thickness. The axial length of the cylinder is assumed large as compared to the radius and the thickness is considered small as compared to the radius.

Assuming the gap small as compared to the circumference, the split cylinder may be treated as a cylindrical condenser for the purpose of determining

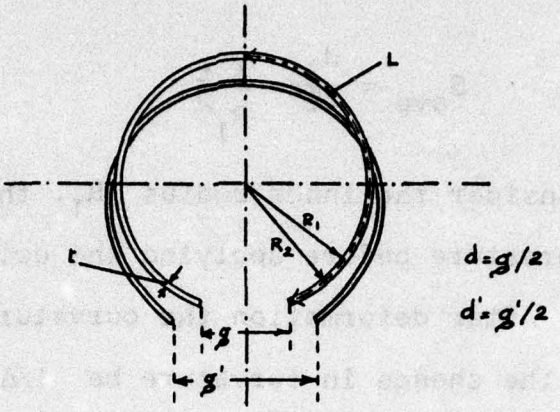


Fig. 138 Flexural mode of electrostrictive thin walled split cylinder

the electric field between the two cylindrical electrodes. The electric field along the radial direction is then inversely proportional to the radius:

(179) $$E_r = \frac{K}{R}$$

The strain is then:

(180)

$$S_r = d_{31} E_r$$

The differential strain between the inner and the outer cylinders is then:

(181) $$\Delta S_r = d_{31} (E_{R_1} - E_{R_2})$$

The average strain is:

(182) $$S_{ave} = \frac{d_{31}}{2} \left[\frac{K}{R_1} - \frac{K}{R_1 (1 + \frac{t}{R_1})} \right],$$

hence:

(183) $$S_{ave} = \frac{d_{31}}{2} \frac{K\,t}{R_1^2}$$

Consider the inner radius R_1, the corresponding curvature before applying the driving fields is: $1/R_1$. After deformation the curvature becomes $1/R_1'$. Let the change in curvature be $1/\Delta R$, the following expression is valid:

(184) $$\frac{1}{R_1'} = \frac{1}{R_1} - \frac{1}{\Delta R}$$

An approximate value of $1/\Delta R$ may be obtained assuming that the cylinder cross section is rectilinear instead of circular and determining its change in curvature upon application of an external field. From Ref. 96, p. 219, Eq. (d), a strain S is related to a change in curvature $1/\Delta R$ by the expression:

(185) $$\frac{16}{bt^2\Delta R} I + \frac{t}{2\Delta R} = S_{ave}$$

Substituting S_{ave} from (183) into (185) and I by $bt^3/16$, yields:

(186) $$\frac{1}{\Delta R} = \frac{3}{4} d_{31} \frac{K}{R_1^2}$$

Substituting $1/\Delta R$ from (186) into (184) gives:

(187) $$R_1' = \frac{1}{\frac{1}{R_1} - \frac{3}{4} \frac{K}{R_1^2} d_{31}}$$

Let g be the gap width before deformation and $d = g/2$. If L is half the length of the cylinder (Fig. 138),

(188) $$L + d = \pi R_1$$

After deformation let the new value of L be L' and the new d be d'

(189) $$L' = L + d' = \pi R_1' .$$

(190) $$d' = L' - L$$

From (187), (188), (189), (190):

(191) $$d' = \frac{}{\frac{1}{R_1} - \frac{3}{4}\frac{K}{R_1^2} d_{31}} - (\pi R_1 - d)$$

The change in d is then obtained from (191):

(192) $$d' - d = \frac{3}{4} \pi K d_{31}$$

The total gap change is, after substituting K from (179) into (192):

(193) $$g' - g = \frac{3}{2} \pi R_1 E_r d_{31}$$

Consider an average value of E_r given by $\frac{V}{t}$, (193) becomes:

(194) $$\Delta g = g' - g = \frac{3}{2} \pi R_1 \frac{V}{t} d_{31}$$

Example:

Let $V = 1000$ volts

$R_1 = 0.5$ cm

$t = 0.08$ cm

$d = 140 \times 10^{-12}$ m/V

From (194):

(195) $\Delta g = 4.1 \times 10^{-4}$ cm

This value of gap change is obtained from the polarized cylinder. If the voltage is applied across the electrodes of a depolarized cylinder the gap change is larger. Gap variations predicted in this study are compared to experimental results in Part 3 of this Chapter.

h) Piezoelectric ADP plate, face shear (z-cut) and piezoelectric quartz plate, face shear (y-cut), DC strains (cf. Fig. 139 and Table VI, Col. 11 and 12).

Strains induced in a film coupled to a piezoelectric ceramic disc are isotropic because of the polycrystalline nature of the substrate. The electromechanical coupling is in this case originated by the electrostrictive effect.[89]

If an anisotropic strain is desired the first order piezoelectric effect must be used. This effect is not present in polycrystalline materials as they have a center of symmetry. It is then necessary to have recourse to naturally polarized crystals and from the table in Ref. 93 Ammonium Dihydrogen Phosphate is the best choice. The general properties for this type of

crystal are given in Ref. 89, p. 138. If a slab is cut perpendicularly to the Z-axis and a film deposited on one surface, the longitudinal motion, along the diagonals of the square cut, will impress a longitudinal tensile strain with a transverse compressive strain. These strains are equal in magnitude and their value is:

$$S_1 = - d_{36} E_3 , \qquad S_2 = d_{36} E_3 \tag{196}$$

Because of the fragility of ADP crystals thicker plates must be used than in the case of piezoelectric ceramics. For a thickness of 1 mm, with a 45°-Z cut ($d_{36} = 48 \times 10^{-12}$ m/V), a voltage of 500 V gives a compressive strain along a diagonal equal to:

$$S_1 = - 24 \text{ micro in/in.}$$

and a tensile strain along the other diagonal equal to:

$$S_2 = + 24 \text{ micro in/in.}$$

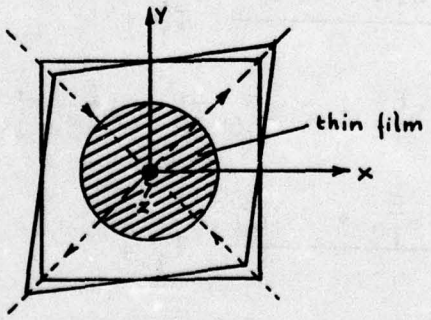


Fig. 139 Face shear mode of Z-cut ADP plate and Y-cut quartz plate

In addition to the characteristics of ADP crystals given in Table VI, col. 11, the following is of interest in this application.

Voltage breakdown (V/mm) 6400

Breaking strain (micro in/in) 500-1000

The piezoelectric equations of state for an ADP face shear mode are developed in Ref. 89, p. 457 when stresses and fields are the dependent variables and strains and electric displacements the independent variables. In the case of interest in this study the dependent variables are the strains and the displacements. The method to be followed is similar to that of Ref. 89, p. 457, and need not be repeated here. The results give the following expressions for the strains after a 45° rotation of tensors involved:

$$(197)\quad \begin{cases} S_1' = \dfrac{s_{11}^E + s_{12}^E + 2\,s_{66}^E}{2}\,T_1' + \\ \quad + s_{11}^E + s_{12}^E + 2\,s_{66}^E\,T_2' + s_{13}^E\,T_3' - d_{36}\,E_3 \\ S_2' = \dfrac{s_{11}^E + s_{12}^E + 2\,s_{66}^E}{2}\,T_1' + \\ \quad + \dfrac{s_{11}^E + s_{12}^E + 2\,s_{66}^E}{2}\,T_2' + s_{13}^E\,T_3' + d_{36}\,E_3 \end{cases}$$

Other strains S_3', S_4', S_5', S_6' and the displacements δ_1, δ_2, δ_3 are of no interest. The notation used is that of Mason (Ref. 89); the symbol δ is used for the electric displacement and it is intended that:

$$\delta = \frac{D}{4\pi}$$

A complete table of units used in piezoelectricity is found in Ref. 90, p. 58.

In the case of a free ADP crystal subjected only to an applied electric field Eqs. (197) reduce to Eqs. (196).

Quartz crystal cuts have high operating temperatures (550°C), which makes them suitable for vacuum deposition of thin films. A very smooth surface and a very good film-to-substrate bond may be obtained.[76] The main disadvantage is a low piezoelectric constant ($d_{14} = 0.85 \times 10^{-12}$ m/V). Unless they are driven at their resonant frequencies, in which case the motion is multiplied by the Q of the crystal, quartz crystals do not produce large strains. Static strains would be too low to cause appreciable changes in thin film hysteresis loops. For a Y-cut plate operating in the face shear mode (as in Fig. 139), the strain is given by

$$S = - d_{14} E_y \tag{198}$$

For 500 volts across 0.010" the available strain is

1.7 microin/in. The properties of quartz are given in Table VI, col. 12.

3. Experimental studies on electrostrictive ceramics (DC strains)

Measurements of strains by the strain gage method have been performed on polarized and unpolarized ceramics, together with measurements of resonant and anti-resonant frequency.[97]

a. Electrostrictive disc:

Discs of Barium Titanate and Lead Zirconate Titanate available commercially are polarized. The samples were depolarized by heating above the Curie point. Strain gages were applied and repolarization was done while the crystals were in a bath of transformer oil. The thickness of the discs was 0.25 cm for Barium Titanate and 0.317 cm for Lead Zirconate Titanate PZT-5.

Experimental curves in Figs. 140 and 141 show that maximum available strains from the unpolarized state are 260 and 2130 micro in/in respectively. In the case of PZT ceramics the crystal must be kept in oil if DC strains of the order of 1000 micro in/in or above are desired, at thicknesses of interest. Figs.

140 and 141 show also strains obtainable from a polarized crystal. These strains are 200 micro in/in and 830 micro in/in for $BaTiO_3$ and PZT-5 respectively. The figures also show the deviations between strains actually recorded and strains corresponding to the linear law for the d_{31} piezoelectric constant. The large deviation represents a safety factor introduced by the manufacturer (Solar Electronics for $BaTiO_3$ and Clevite for PZT-5).

b. Electrostrictive cylinder

Measurement of strains obtainable in the case of a PZT cylinder have been carried out and the results are shown in Fig. 142. The maximum strain is 935 micro in/in from the unpolarized state and 455 micro in/in after polarization.

c. Electrostrictive split cylinder

An experimental study of the gap variations obtained by applying a DC voltage to an electrostrictive split cylinder was carried out. The purpose of this investigation was to determine the variations of reluctance in a magnetic circuit including a thick ferromagnetic film deposited on the outside cylinder surface and the air gap, as the cylinder is driven in the circumferential mode. The cylinder was made of PZT-5 ceramic and had

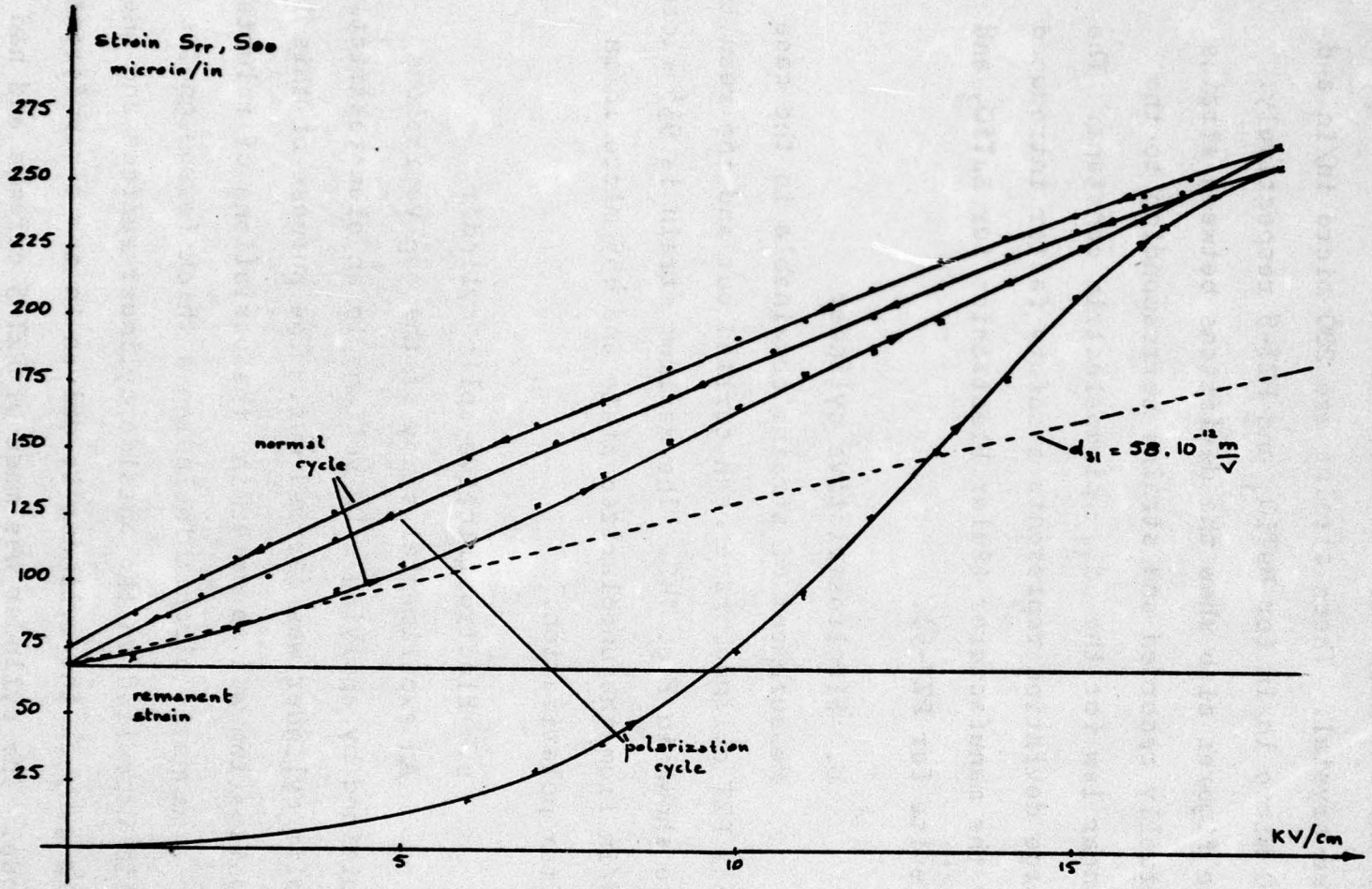


FIG. 140 BARIUM TITANATE POLARIZATION CURVE, DISC

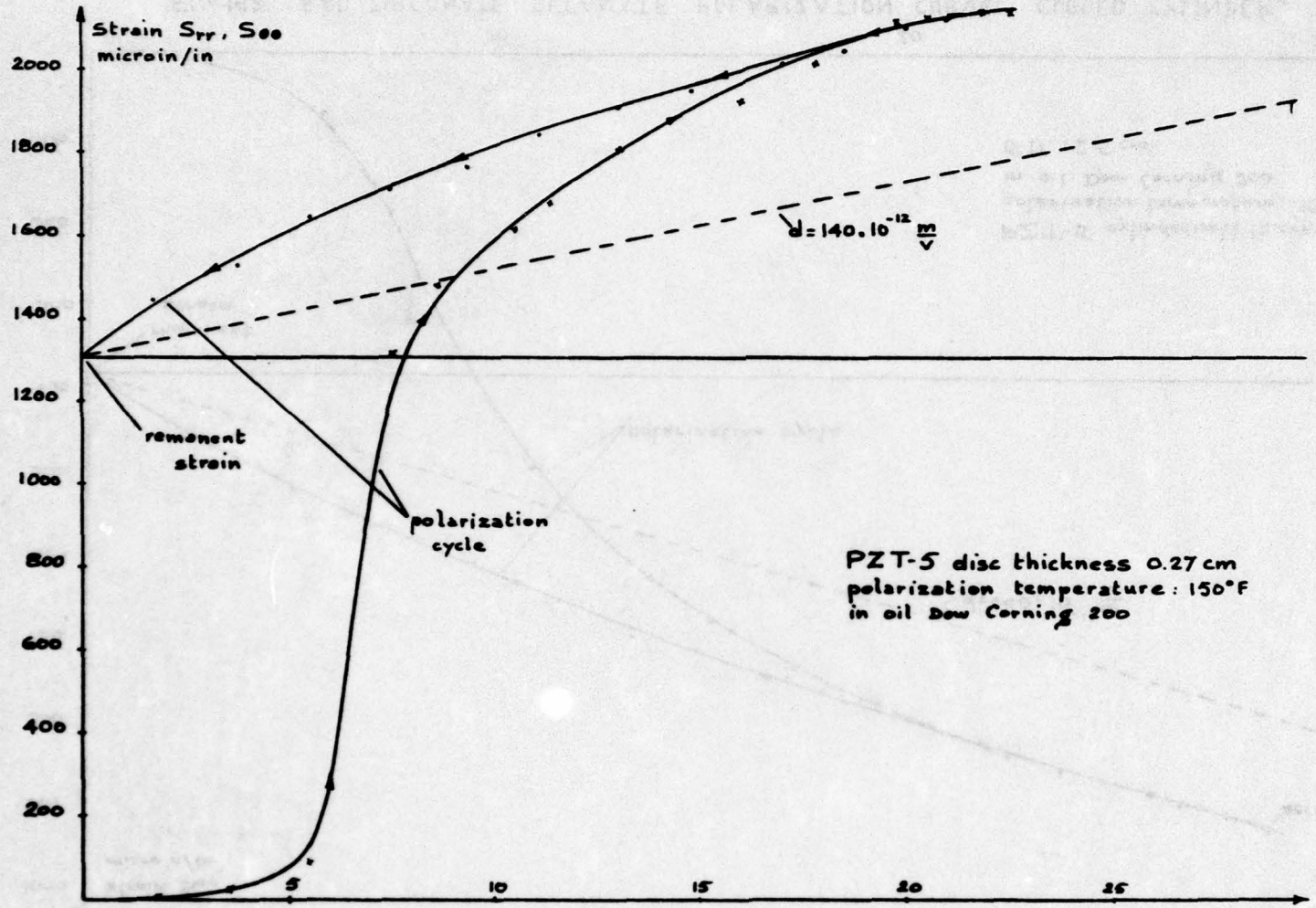


FIG. 141 LEAD ZIRCONATE TITANATE POLARIZATION CURVE, DISC.

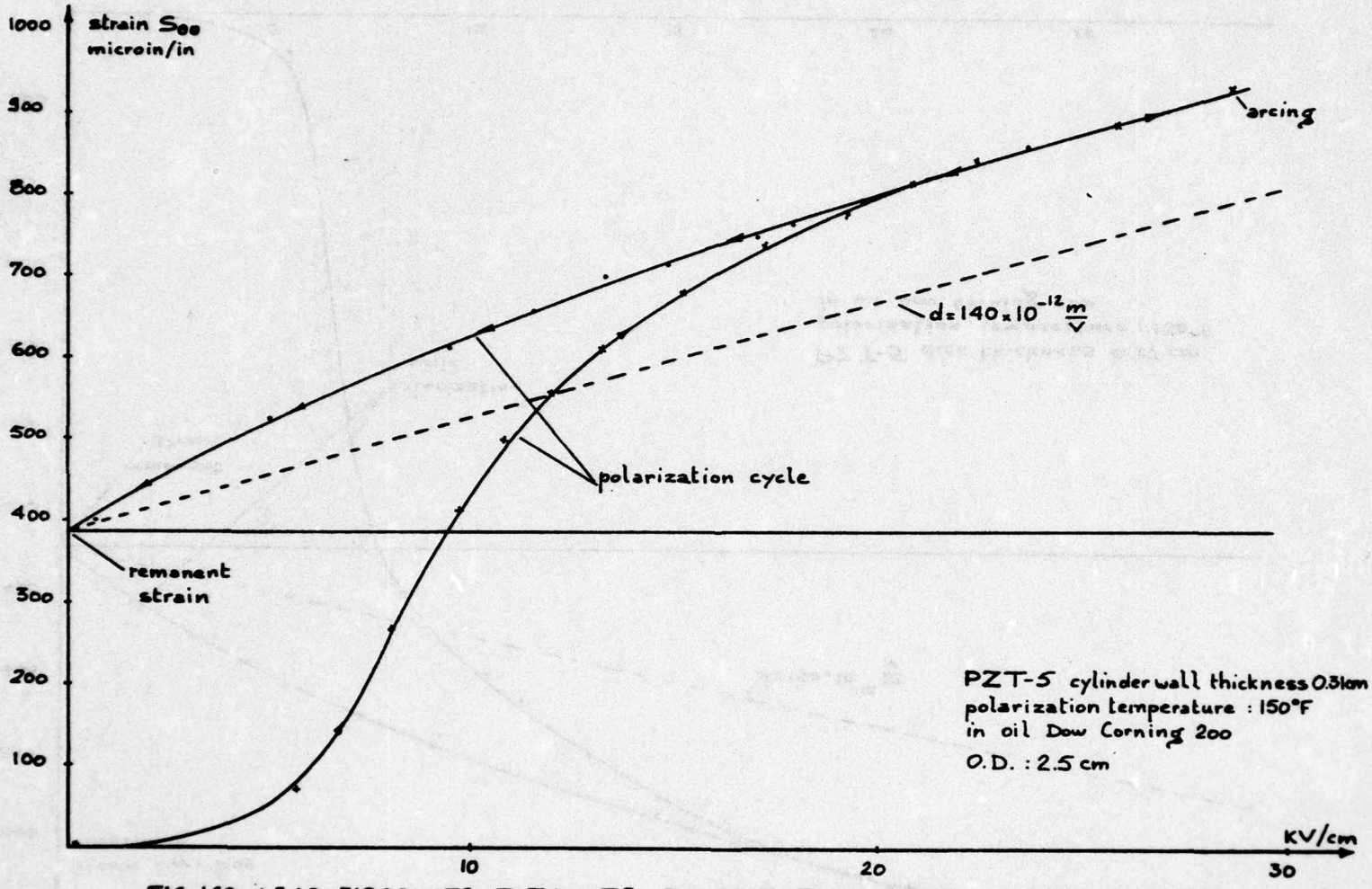


FIG. 142 LEAD ZIRCONATE TITANATE POLARIZATION CURVE, CLOSED CYLINDER.

the following dimensions:

radius	0.5 cm.
thickness:	0.08 cm.
length:	1 cm.
gap width:	0.15 cm.

The variations in gap width were measured using a Kodak contour projector, which magnified the gap 100 times and gave a projection on a graduated rigid screen. At a value of applied voltage of 1.5 KV arcing occurred across the crystal electrodes. Table VII shows the experimental results, starting from an unpolarized cylinder.

TABLE VII

K Volts	Gap variations
0 KV	0
1 KV	3×10^{-3} cm.
1.3 KV	5.35×10^{-3} cm.
0 KV	2×10^{-3} cm.

From straight beam theory the gap change in this electrostrictive split cylinder has been found to be proportional to the piezoelectric strain $E_3 d_{31}$ (cf. Eq. 194).

Let p_E be the ratio of the strain developed in a depolarized polycrystal by a DC field E to that

developed in the same polycrystal, after polarization, by the same DC field. For 1000 V across 0.08 cm (corresponding to 12.5 KV/cm) the values of p_E for the PZT-5 disc and for the PZT-5 closed cylinder are respectively: 6.8, 4.0 (Figs. 141, 142), the average value being 5.2. The gap variation measured for the PZT-5 split cylinder (depolarized sample) driven by a field of 12.5 KV/cm is 3×10^{-3} cm, as reported in Table VII. From expression (194), the gap variation for the polarized sample is 4.1×10^{-4} cm at 12.5 KV/cm. An approximate value of the gap variation for the unpolarized sample may then be obtained by multiplying this value by $p_{E\ ave}$, the result is 2.13×10^{-3} cm. Considering the assumptions and approximations involved, this value compares favorably with the measured gap variation of 3×10^{-3} cm, at 12.5 KV.

d. Experimental determination of coupling coefficient.

Measurements on resonant and antiresonant frequencies of PZT-5 crystals were carried out on the PZT-5 cylinder mentioned in previous section b. The method used is described in Ref. 97. The results of the measurement are:

f_r = Resonant frequency: 121 KC

f_{ar} = antiresonant frequency: 134 KC

f = 13 KC

The electromechanical coupling coefficient is related to the frequency gap Δf and to the resonant frequency f_r by the expression:[89]

$$k^2 = 2.5 \frac{\Delta f}{f_r}$$

From manufacturer's data $k = 0.54$ for PZT-5. From the values of Δf and f_r measured:

$$k = 0.52$$

The measured value checks with the manufacturer's data within 3.7%.

From the theoretical study and the experimental results contained in this chapter it appears possible to induce isotropic stresses in a ferromagnetic thin film, of the same order of magnitude as those induced by mechanical bending of the substrate.

Theoretical predictions in this chapter indicate that it is not possible to produce large anisotropic strains with piezoelectric crystals available at present. The only types of crystallographic cuts capable of inducing sufficiently high strains pertain to crystals with low piezoelectric constants d. Rochelle salt has a high d constant, but must be re-

jected for reasons of environmental instability.

A coupling between a piezoelectric (electrostrictive) substrate and a magnetostrictive film has been attempted in the laboratory and the results obtained are presented in the forthcoming section.

4. Piezoelectric (electrostrictive) magnetostrictive coupling.

a. Piezoelectric uniaxial and isotropic stress.

Consider a magnetic thin film with its direction of easy magnetization along the Y-axis (Fig.143)

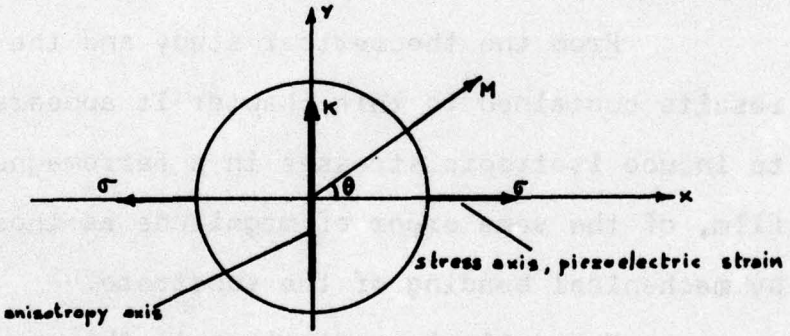


Fig. 143

It is proposed to determine the voltage to be applied to a 45° Z-cut ADP crystal in order to reverse the magnetization, on the assumption that an initial torque is provided by a weak perpendicular field. The total free energy includes anisotropy and magnetostriction:

(199) $$E_t = E_K + E_\sigma$$

where:

(200) $$E_K = K \cos^2 \theta$$

(201) $$E_\sigma = \frac{3}{2} \lambda_s \sigma \sin^2 \theta$$

Imposing the conditions

(202) $$\frac{\partial E_t}{\partial \theta} = 0 \quad \text{and} \quad \frac{\partial^2 E_t}{\partial \theta^2} > 0$$

leads to:

(203) $$\sin 2\theta \left(\frac{3}{2} \lambda_s \sigma - K\right) = 0$$

(204) $$\cos 2\theta \left(\frac{3}{2} \lambda_s \sigma - K\right) > 0$$

Condition (203) shows that in order to have a magnetic change the angle θ must be zero, then condition (204) gives:

(205) $$\sigma > \frac{2}{3} \frac{K}{\lambda_s}$$

which states that the stress effective field must be larger than the anisotropy effective field.

Let Y be the average value of Young's modulus for the film, ν Poisson's ratio. The stress induced in the film is obtained equating the piezoelectric uniaxial strain in the x direction to the film strain corresponding to σ. For the longitudinal mode considered the stress is:

(206) $$\sigma = (1 + \nu)\, Y\, d'_{36} \frac{V}{t}$$

where t is the plate thickness.

From (205) and (206):

$$V > \frac{2}{3} \frac{K_t}{\lambda_s} \frac{1}{d'_{36}\, Y\, (1+\nu)} \tag{207}$$

If a voltage given by expression (207) is applied to the piezoelectric plate, reversal will occur by effect of the applied stress, assuming that the magnetization vector may be started from its position of unstable equilibrium.

For the 44-56 magnetostrictive film studied in Chapter I:

t = 0.001 m (ADP plate thickness)

$\lambda_s = 20 \times 10^{-6}$

$Y = 13 \times 10^{9}$ Kg/m^2

$\nu = 0.28$

$K = 2550$ Joule/m^2 (25500 ergs/cm^3)

$d'_{36} = 24 \times 10^{-12}$ m/V (ADP 45° Z-cut piezoel. constant).

Substituting these numerical values in expression (207) it is found that an exceedingly high voltage would be required to cause reversal (21×10^4 volts), corresponding to a piezoelectrically impressed strain of 6000 micro in/in. From experiments with glass substrate on the 44-56 film, variations of 10%

in the coercive force of the hysteresis loop required strains of 100 micro in/in, corresponding to 3500 volts across a 1 mm ADP plate.

Rochelle salt has a piezoelectric constant of the order of 500×10^{-12} m/v and would be the only crystal presently capable of inducing significant magnetic changes by means of a DC coupling. Unfortunately it must be discarded because of its hygroscopicity.

ADP crystals may be used to study the effects of alternating stresses where the crystal is driven at resonance. In this case the strains are multiplied by the mechanical Q of the crystal.

As discussed in Sec. 2.e when a DC voltage is applied to a piezoelectric ceramic disc, tangential and radial strains of equal magnitude are induced. If a magnetostrictive film is deposited on the surface of the disc, on the assumption of perfect coupling, the strains in the film should be equal to the strains in the disc. If a surface element of the film is considered (Fig. 144), the magnetostrictive effects induced by the two stresses S_{rr}, $S_{\theta\theta}$ should cancel one another if the film behaves according to the simple rotational model. In the absence of domain wall motion,

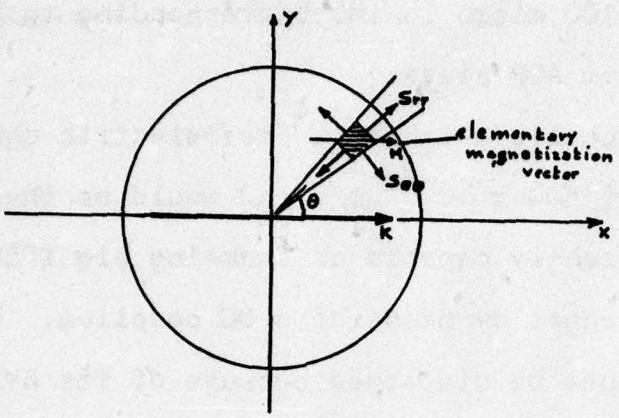


Fig. 144

magnetization changes are due only to spin rotation. The sum E_t of the anisotropy and the stress energies would then be:

$$(208)\quad E_t = K \sin^2\theta + \frac{3}{2}\lambda_s S_{rr} \cos^2\theta + \frac{3}{2}\lambda_s S_{\theta\theta} \sin^2\theta$$

If $S_{rr} = S_{\theta\theta}$ there is no contribution from the stress to the anisotropy constant.

There are, however, motions of domain walls in a thin film, as has been discussed in Chapter I, and the torque impressed on the wall spins by the magnetostriction forces is not expected to be the same for S_{rr} as for $S_{\theta\theta}$. The wall coercive force should therefore be affected by an isotropic stress while the contribution to the coercive force from rotational effects should be zero.

b. Experimental studies. Isotropic stress.

In order to investigate the effects of isotropic stresses induced piezoelectrically upon a magnetostrictive film, a 44-56 nickel-iron film was deposited by evaporation upon a polished electrode of a PZT-5 disc. The electrode had to be covered with a thin layer of SiO in order to close the microscopic surface irregularities in the silver electrode. Fig. 145a shows a replica of the surface of an unpolished PZT disc, obtained by lifting the silver electrode. The surface irregularities appear magnified 25 times. Fig. 145b shows the surface after mechanical polishing with a very fine lapping compound (alumina abrasive type 0.05 B Linde Air Products Co.), with the same magnification. Further studies and experiments are required to obtain a film substrate surface microscopically smooth.

When the film magnetization is reversed at low frequency, imperfections originated in the substrate or in the magnetic material act as nucleation centers for domains of reverse magnetization. In the light of the theories of Kersten and Néel, discussed in Chapter I, and of experimental observations on Bitter

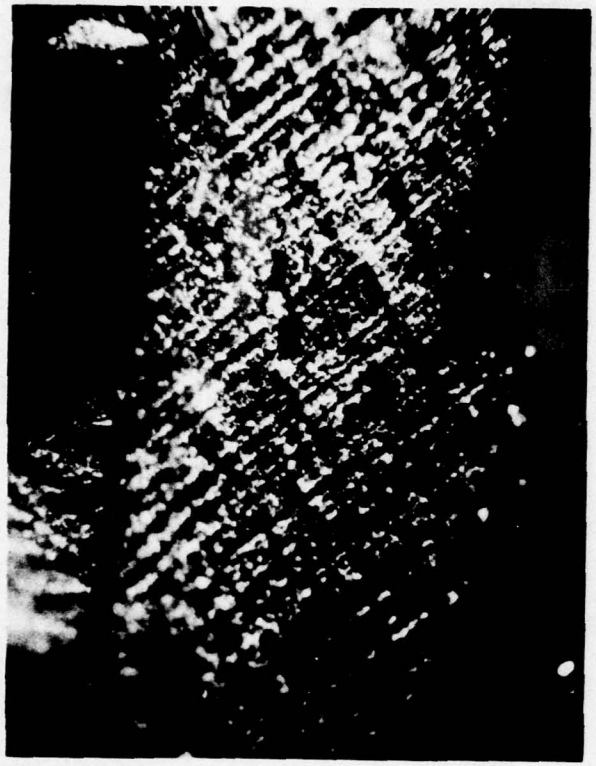
patterns* it may be asserted that the wall coercive force in a film is strongly dependent upon the presence of imperfections. The microscopic irregularities in a polycrystalline ceramic film substrate are therefore important in determining the film wall coercive force and anisotropy.

In the previously-mentioned 44-56 nickel-iron film deposited on a PZT-5 disc, observed hysteresis loops along the longitudinal and the transversal directions were very similar. Application of 5000 volts across the electrodes caused no visible changes in coercive force. The lack of magnetic anisotropy was attributed to poor substrate surface.

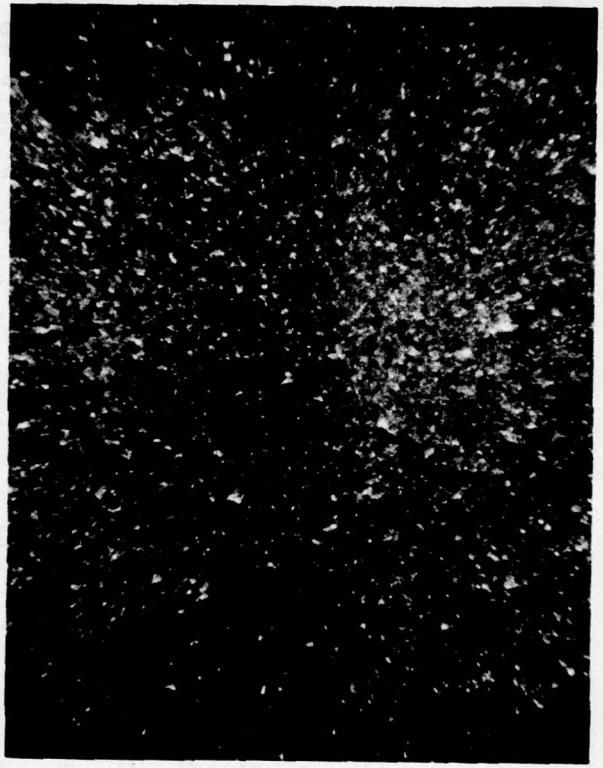
A new experiment was designed in which a 1200 Å 80-20 nickel-iron film was deposited upon a thicker layer of SiO covering a disc electrode. The differences between the two hysteresis loops displayed at the top of Figs. 146a and 146b show that the film is magnetically anisotropic. Oscilloscope traces at the bottom of these two figures show the effects of iso-

*Reference 101 contains some of the first Bitter pattern photographs on the effects of inclusions on domain wall configurations. They represented the first experimental confirmation of Neel's theory. Figs. 48 and 50 in Ch. I of this dissertation also show the presence of Neel spikes around film imperfections.

tropic piezoelectric strains upon the longitudinal and perpendicular hysteresis loops. For an applied electric field of 1000 volts across 0.010" a change of approximately 10% in the longitudinal coercive force is observed. More information on the effects of the isotropic stress on domain wall configurations is necessary and may be obtained by Bitter pattern displays. The perpendicular loop coercive force increases by 5% approximately. If the polarities of the voltage are interchanged, the high electric field necessary to produce any visible magnetic changes causes depolarization of the crystal and repolarization in the opposite direction, the final result being the same: an isotropic tension. The quadratic nature of the electrostrictive effect does not allow observation of effects due to an isotropic compression.



surface replica, unpolished
$BaTiO_3$ crystal
FIG. 145a



polished $BaTiO_3$ surface
(mechanical polishing)
FIG. 145b

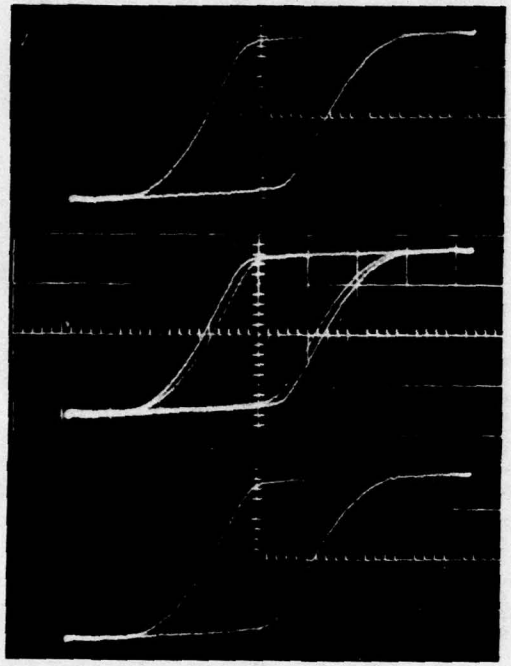


FIG. 146a

isotropic stress
grounded film, opposite electrode: -1000V
$BaTiO_3$ thickness: 0.010"
Long. Loop, 80-20 Ni-Fe
Horiz: 1cm = 3.46 oe.
Vert: 1cm = 550 gausses

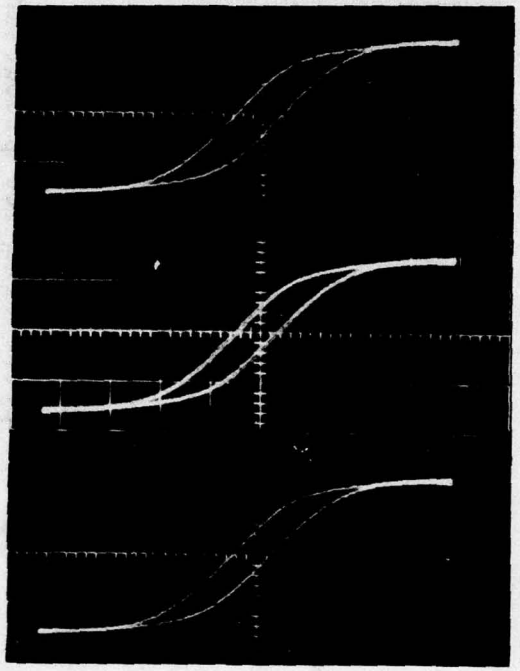


FIG. 146b

Isotropic stress
grounded film, opposite electrode: -1000V
$BaTiO_3$ thickness: 0.010"
Perp. Loop 80-20 Ni-Fe
Horiz: 1cm = 3.46 oe
Vert: 1cm = 550 gausses

CONCLUSIONS

At the start of this dissertation study, an objective was established to define the effects of piezoelectric-magnetostrictive coupling which might be of interest in digital applications.

In the process of moving toward that goal it was found necessary to improve procedures for predicting the effects of stress on ferromagnetic thin films since this information was not available in the literature. The theoretical predictions considered the quasi static and the dynamic cases and the models adopted required extensive experimentation for measuring the properties of magnetostrictive thin films.

Effects of applied stresses on quasi static hysteresis loops and on Bitter patterns were observed using mechanical strains. Instruments for observing effects of stresses on the dynamic behavior of thin films were constructed, but extensive use of these instruments remains to be undertaken.

Strains obtainable from piezoelectric and electrostrictive crystals were predicted from theory for several materials and driving modes. Observations

of DC strains were made on polycrystalline electrostrictive configurations.

Finally, an experiment was performed to observe the actual coupling between a magnetostrictive thin film and an electrostrictive ceramic. The relatively poor surface of the ceramic affected the switching properties of the film and prevented close correlation between theory and experiment. The study was limited to the transmission of an isotropic strain from the crystal to the film.

The study of the transmission of mechanical strains from a piezoelectric to a ferromagnetic material requires the knowledge of electromechanical relationships for the driving element and of magnetomechanical relationships for the receiver (the magnetic film). Abundant information is available on the effects of an electrical stimulus upon the mechanical deformation of a piezoelectric crystal. Most of this body of literature is confined to the application of electromechanical equations to the motion of crystals driven by sinusoidal inputs. The same piezoelectric equation of state may however be used to predict DC strains from applied DC voltages.

Information on the pseudo static and dynamic switching of magnetostrictive films has, however, been

missing and had to be obtained before considering the effects of coupling.

This dissertation has therefore evolved through a thorough study of the switching properties of magnetostrictive films followed by a study on the properties of piezoelectric crystals and by a final investigation on the effects of coupling.

In the theoretical prediction of the quasi static magnetic properties of films the classical model of coherent rotation of the film magnetization is used, with the addition of a stress term. It is assumed that the film magnetic configuration remains that of a single domain. Through a process of energy minimization a general polynomial of the fourth degree is obtained. Certain real roots of this polynomial are proportional to the components of the magnetization vector along the switching field and at right angle to it. When plotted vs. the magnitude of the switching field these components yield the "longitudinal" hysteresis loop and the "transversal" hysteresis loop, respectively. The shape of these loops determines the switching properties of the film. All possible parameters are included in the formulation of the model; a perpendicular field, an applied stress, and an initial angular position of the magnetization with respect to the direction of the

switching field. As the switching field is changed in magnitude the locus of roots may be followed. By using a criterion based on energy considerations the roots corresponding to the film magnetization component in a certain direction may be obtained. The complete information to obtain a plot of the film hysteresis loop under specified conditions may then be obtained by following the correct roots along the real branches of the complex plane. The process of root extraction and plotting was considerably simplified by using a special protractor called the spirule, a device which, in the past, has been used in the study of the stability of control systems. After some experience, a hysteresis loop may be plotted in about 15 minutes under any conditions of stress, perpendicular field and initial angle.

The locus of roots was also obtained by use of a digital computer which selects the correct roots and plots directly on paper the final hysteresis loop. The time required to obtain a hysteresis loop by digital computation, using root locus, is 50 seconds. By simply punching two data cards in which the film magnetization M, the anisotropy constant K, the magnetostriction coefficient λ_s, the initial value of switching field H_s, of perpendicular field H_p, of

applied stress σ , and of initial angle γ , a new hysteresis loop may be obtained in a relatively short time.

The graphical technique and the digital computer program may however be improved further. Time to plot a hysteresis loop by hand may be decreased considerably if rules for sketching root loci when the position of poles and zeroes is a function of the gain are established. Existing rules for fixed positions of zeroes and poles allow one to sketch the root loci by hand in seconds. The digital computer program may be made more efficient by confining the root extraction process to the real branches and by using previously computed roots as best guesses for the next roots to be extracted. Under these conditions the computation of a hysteresis loop should be reduced to a few seconds. This improved procedure is recommended as an item of future study.

The rotational model used to write the free energy associated with the film does not consider the effects of domain wall motion. If a mathematical description of the effects of inclusions may be introduced in the model, a closer fit between theory and experiment would be obtained.

Critical switching curves in which the magnetization has an initial angular position different from

zero cannot be obtained in closed form because of the implicit nature of the variables involved. The locus of roots method may be used to obtain critical switching curves in such cases. The digital computer program has been changed slightly and the computer plot shows that the critical switching curve is tilted when the initial angle is different from zero. This curve has assumed considerable practical importance in relation to digital applications.

Experimental studies carried out to investigate the effects of stress on the quasi static switching properties of films have been carried out using a special hysteresis loop tester for magnetostrictive films. The instrument may be used to measure film magnetostriction by the Villari effect with an accuracy of 20%. Another important new feature of the instrument is the provision of a switching arrangement capable of interchanging the AC and the DC supply to two sets of Helmoltz coils, keeping the AC drive tuned with the same power amplifier and the same tuning condenser. The switching operation also causes the film output to be sensed by two different pickup coils. Additional circuitry for making calibrations identical, for making the phase relationship between the x and the y signal to the oscilloscope

independent from the operation of the switch, are included. With this instrument it is possible to impress a pure bending moment across a thin film and to control the resulting strain within 40 micro in/in. approximately.

From the study of hysteresis loops obtained with the hysteresis loop tester on a 44-56 nickel-iron film, it is observed that the results of the model disagree with those of the experiments. The addition of an isotropic stress decreases the extent of the difference. As is well known, the disagreement is originated because domain wall motion is neglected in the mathematical model. However, experimental observation shows that the presence of a stress brings the predictions and the experiment more closely into agreement.

This observation agrees with the study of the effect of stresses on domain wall configurations by Bitter patterns. The application of tensile stresses on magnetostrictive films (89.3 - 10.7 and 77.5 - 22.5 nickel-iron) shows that a positive magnetostrictive film under stress behaves more closely like the rotational model.

The above mentioned measurement of magnetostriction by the Villari effect consisted in stressing

the film until closure of the transverse loop was obtained and extrapolating the oscilloscope trace to saturation. This method is not accurate and a better technique is desirable and is needed since data on magnetostriction of thin films is missing in the literature. Results obtained during the course of this investigation indicate that the magnetostriction coefficient of a 44-56 nickel-iron film is higher than the corresponding bulk alloy by approximately 30%.

Theoretical predictions on the dynamic behavior of magnetostrictive films were carried out from the classical equation of Landau and Lifshitz, using an analog and a digital computer. Results published in the literature on non-magnetostrictive films were first duplicated and served to evaluate the analog computer circuit diagram and the digital computer program. It was found that the analog and the digital solutions agreed with each other and were within the previous computational result by 15%. The constants for a 44-56 Ni-Fe film evaporated in the laboratory were then entered in the digital computation and from results of the computation predictions were made on the effects of stress, perpendicular field, damping constant, initial angle, on the switching time, and on the magnitude of

the signal induced by magnetization reversal in a pickup loop.

It was found that the switching delay decreased when increasing the value of the perpendicular field, as reported previously by other workers. A decrease in the applied stress had comparable effects but increased the amplitude of the pickup voltage. When the applied switching field was decreased in amplitude, a point was reached at which the magnetization did not reverse but was simply disturbed. In order to investigate the variation of this threshold value of the switching field, a new program was devised to plot directly from the computer curves of $1/\Delta t$ (Δt: switching time), as a function of the switching field. It was found that the curve presents a cusp at the threshold value and does not continue to zero. This finding is contrary to earlier work reported by D. O. Smith. Another program was used to study the effects of stress on the ferromagnetic resonance frequency of the film. It was observed that beyond the threshold value, the frequency increases with the switching field almost linearly, in agreement with ferromagnetic resonance experiments. However, when the magnetization is simply disturbed, the frequency decreases as the switching

field increases and experiences a jump at the threshold point. A final digital computer program is used to plot dynamic critical switching curves. This information is useful in predicting switching under dynamic conditions, for a given configuration of applied forces.

These studies do not include the effects of domain wall motion and, although it is recognized that, in the subnanosecond switching region, the film reverses essentially by spin rotation, the small contribution due to domain wall motion should be derived from a model including this type of magnetization reversal.

Instrumentation for the prediction of switching times under stress conditions was constructed. A subnanosecond rise time magnetic field was obtained by discharging a coaxial cable through a mercury relay into a strip transmission line. The strip line supports a jig for stressing substrates or may accommodate a piezoelectric crystal supporting a magnetostrictive film. This type of instrumentation has been used by other investigators, only the addition of the stressing mechanism is new. Measurements on high-speed switching under stress conditions have not yet been carried out.

Studies on the properties of piezoelectric crystals under static conditions follow the investigation

on the switching properties of magnetostrictive films. From the examination of different modes and geometries, materials and configurations are selected and are studied theoretically and experimentally in order to determine the maximum strains available from reasonable voltages. In the studies on mechanically applied stresses it was found that strains between 100 and 1000 μin/in. cause important changes in the quasi static switching properties of films. From theoretical predictions it is found that electrostrictive ceramics ($BaTiO_3$, PZT) in the shape of discs, plates, cylinders, driven in the expander mode will give strains ranging between 100 and 800 micro in/in. These strains are isotropic; anisotropic strains may be obtained from single crystal piezoelectrics (ADP, quartz), but with maximum strain amplitudes of 48 μin/in. The quasi static behaviors of a bar, a disc, a cylinder, a ring, a split cylinder were investigated theoretically and values of strains for 1000 volts across 0.01" were tabulated.

Experiments performed on the measurement of strains confirmed the order of magnitude predicted for the cylinder and the disc.

The final coupling between a piezoelectric substrate and a thin film was accomplished by depositing

an 80-20 nickel-iron film on a $BaTiO_3$ substrate flashed by a thin layer of SiO to improve the surface conditions. A film with definite magnetic anisotropy was obtained and it was observed that application of 1000 V across a 0.010" disc caused the coercive force of the film to change by 10% along the longitudinal direction and by 5% along the transverse direction. This experiment shows that energy is transmitted from the crystal to the film but changes in the switching characteristics of the film are not sufficiently pronounced. It is suggested that the coupling surface be improved to minimize surface irregularities. Experiments on ADP should also be carried out. Since this crystal makes a better substrate, the effects of isotropic stresses on domain configurations may be observed with such crystals by means of Bitter patterns.

Finally, the effects of driving the substrate at its resonant frequency, on the switching properties of the film are of interest. Piezoelectric crystals respond efficiently to a band of frequencies below the first resonance. The effects of an alternating stress, induced by coupling a film to a piezoelectric crystal, on the motion of domain walls is also proposed as a future item of research.

APPENDIX 1

Derivation of equation (25) in Chapter I

Equation (25) is obtained from equation (21) through the following steps:

$$2K \sin(\phi - \gamma) \cos(\phi - \gamma) - 3\lambda_s \sigma \sin\phi \cos\phi - $$
$$- MH_p \cos\phi + MH_s \sin\phi = 0$$

Expanding $\sin(\phi - \gamma)$, $\cos(\phi - \gamma)$ and factoring $\sin\phi$ at the left-hand side:

$$\sin\phi\,(2K \cos\phi \cos^2\gamma - 2K \cos\phi \sin^2\gamma -$$
$$- 3\lambda_s\sigma \cos\phi + MH_s) = - 2K \sin^2\phi \sin\gamma \cos\gamma +$$
$$+ 2K \cos^2\phi \sin\gamma \cos\gamma + MH_p \cos\phi$$

Squaring both sides of this equation and ordering the resulting equation in decreasing powers of $\cos\phi = s$:

$$s^4 (- 4K^2 \cos^4\gamma - 8K^2 \sin^2\gamma \cos^2\gamma +$$
$$+ 12 K\lambda_s\sigma \cos^2\gamma - 12K\lambda_s\sigma \sin^2\gamma -$$
$$- 9\lambda_s^2\sigma^2 - 4K^2 \sin^4\gamma) +$$
$$+ s^3 (- 4KMH_s \cos^2\gamma + 4KMH_s \sin^2\gamma +$$
$$+ 6\lambda_s\sigma MH_s - 8KH_pM \sin\gamma \cos\gamma) +$$
$$+ s^2 (4K^2 \cos^2\gamma + 8K^2 \sin^2\gamma \cos^2\gamma -$$
$$- 12K\lambda_s\sigma \cos^2\gamma + 12K\lambda_s\sigma \sin^2\gamma +$$
$$+ 4K^2 \sin^4\gamma + 9\lambda_s^2\sigma^2 - M^2H_s^2 - M^2H_p^2) +$$
$$+ s (4KMH_s \cos^2\gamma - 4KMH_s \sin^2\gamma - 6\lambda_s\sigma MH_s +$$
$$+4KMH_p \sin\gamma \cos\gamma) + M^2H_s^2 - 4K\sin^2\gamma \cos^2\gamma = 0$$

Dividing through by $(2K)^2$ and simplifying gives eq. (25).

APPENDIX 2

Listing of program

for computation and plotting of hysteresis loops

```
THIN FILM HYSTERESIS LOOP
*       FORTRAN
        DIMENSION PHONY(1083),R2(2,4),PRDR(3),PRDI(3),SMR(3),SMI(3)
        DIMENSION SDEV(4),R3(4),R4(4)
        COMMON PHONY,PRDR,SMR,SMI
 1      READ INPUT TAPE 5,300,EM,CAY,ELAMS
        READ INPUT TAPE 5,302,DELA,DELY,SYMBOL
 2      READ INPUT TAPE 5,301, ALFFA,BETA,GAMMA,DELTA
 300    FORMAT(F10.0,F10.0,E10.2)
 301    FORMAT(4F10.3)
 302    FORMAT(2F10.4,A6)
 7      FORMAT(2F15.6)
        BAC=2.*CAY/EM
        BAD=2.0*CAY/(3.0*ELAMS)
        IOD=GAMMA
        GAMMA = GAMMA*3.14159265/180.
        SGAM=SINF(GAMMA)
        CGAM=COSF(GAMMA)
        MP=3
        IS=1
        ALPHA=ALFFA
        CALL PREPAR(43,37,1.26,-.06,-ALFFA,ALFFA/18.,0,0,-1,20,17,0.,0.)
 10     F=1.+DELTA**2-2.*DELTA*(CGAM**2-SGAM**2)
        B=4.*BETA*SGAM*CGAM+2.*ALPHA*(CGAM**2-SGAM**2-DELTA)
        C=-(F-ALPHA**2-BETA**2)
        D=-(B-2.*BETA*SGAM*CGAM)
        E=-ALPHA**2+(SGAM**2)*(CGAM**2)
        CALL LLNPRC (SMI(3))
        CALL ROOTR(F,B,C,D,E,R2,KK,PRDR,PRDI,SMR,SMI)
        IF(KK)45,15,45
 15     DO 19 I=1,4
        SDEV(I)=0.
        IF(R2(2,I))19,18,19
  18    SDEV(I)=((4.*F*R2(1,I)+3.*B)*R2(1,I)+2.*C)*R2(1,I)+D
 19     CONTINUE
        WRITE OUTPUT TAPE 6,9753,(R2(1,I),I=1,4),(R2(2,I),I=1,4)
 9753   FORMAT(4(10X,F20.9)/4(10X,F20.9))
        GO TO (50,200,25),MP
 25     LR=0
        DO 30 I=1,4
        IF(R2(2,I))30,27,30
 27     LR=LR+1
        R3(LR)=R2(1,I)
 30     CONTINUE
        IF(LR-4)35,75,35
 35     IP=1
        GO TO (351,352),IS
 351    IF(R3(1)-R3(2))36,37,37
 36     Y1=R3(1)
```

```
      GO TO 38
37     Y1=R3(2)
38    CALL POINT(Y1,ALPHA,SYMBOL)
      WRITE OUTPUT TAPE 6,7,Y1,ALPHA
      IS=2
      GO TO 45
352   CALL COMPAR(Y1,R3,2,YP)
      Y1=YP
      CALL POINT(YP,ALPHA,SYMBOL)
      WRITE OUTPUT TAPE 6,7,YP,ALPHA
      IF(ALPHA-1.0E-5)39,39,45
39    XMRU=YP
      XMRL=YP
45    ALPHA=ALPHA+DELA
      MP=1
      GO TO 10
50    LR=0
      DO 55 I=1,4
      IF(R2(2,I))55,52,55
52    LR=LR+1
      R3(LR)=R2(1,I)
55    CONTINUE
      IF (LR-4)60,150,150
60    GO TO(65,605,620),IP
65    CALL COMPAR(Y1,R3,2,YP)
      Y1=YP
      CALL POINT(YP,ALPHA,SYMBOL)
      WRITE OUTPUT TAPE 6,7,YP,ALPHA
      IF (ALPHA+ALFFA)70,6051,6051
6051  XMRU=0.
      XMRL=0.
      HCR=0.
      HCL=0.
      GO TO 70
605    MP=2
      ALPHA=ALPHA-DELA
      GO TO 200
70    IF(ALPHA+ALFFA)45,500,500
75    IP=2
      Y2=MAX1F(R3(1),R3(2),R3(3),R3(4))
      Y1=MIN1F(R3(1),R3(2),R3(3),R3(4))
      CALL POINT(Y1,ALPHA,SYMBOL)
      WRITE OUTPUT TAPE 6,7,Y1,ALPHA
      CALL POINT(Y2,ALPHA,SYMBOL)
      WRITE OUTPUT TAPE 6,7,Y2,ALPHA
      GO TO 45
80    IF(ALPHA+ALFFA)85,500,500
85    CALL COMPAR(Y1,R3,4,YP1)
      CALL COMPAR(Y2,R3,4,YP2)
```

```
      CALL POINT(YP1,ALPHA,SYMBOL)
      WRITE OUTPUT TAPE 6,7,YP1,ALPHA
      CALL POINT(YP2,ALPHA,SYMBOL)
      WRITE OUTPUT TAPE 6,7,YP2,ALPHA
      Y1=YP1
      Y2=YP2
      IF(ALPHA-1.0E-5)86,86,87
 86    XMRU=Y2
      XMRL=Y1
87    GO TO 45
150   IF(IP-1)80,90,80
90    DO 95 I=1,4
      R4(I)=999.9
      IF(SDEV(I))95,95,93
93    R4(I)=SDEV(I)
95    CONTINUE
      Y2=MIN1F(R4(1),R4(2),R4(3),R4(4))
      DO 97 I=1,4
      IF(R4(I)-Y2)97,96,97
96    Y2=R3(I)
97    CONTINUE
100   CALLCOMPAR(Y1,R3,4,YP1)
      Y1=YP1
      CALL POINT(Y1,ALPHA,SYMBOL)
      WRITE OUTPUT TAPE 6,7,Y1,ALPHA
        CALL POINT(Y2,ALPHA,SYMBOL)
      WRITE OUTPUT TAPE 6,7,Y2,ALPHA
      MM=(Y2-Y1)/DELY
      DO 105 I=1,MM
      XI=I
      YY=Y1+XI*DELY
      CALL POINT(YY,ALPHA,SYMBOL)
      WRITE OUTPUT TAPE 6,7,YY,ALPHA
105   CONTINUE
      HCL=ALPHA
      IP=2
      GO TO 80
200   MM=(Y2-Y1)/DELY
      DO 205 I=1,MM
      XI=I
      YY=Y1+XI*DELY
      CALL POINT(YY,ALPHA,SYMBOL)
      WRITE OUTPUT TAPE 6,7,YY,ALPHA
205   CONTINUE
      HCR=ALPHA
      IP=3
      GO TO 45
620   CALL COMPAR(Y2,R3,2,YP2)
      Y2=YP2
```

```
      CALL POINT(YP2,ALPHA,SYMBOL)
      WRITE OUTPUT TAPE 6,7,YP2,ALPHA
      IF(ALPHA-1.0E-5)621,621,70
 621  XMRU=Y2
      XMRL=Y2
      GO TO 70
 500  CALL PLOT
      WRITE OUTPUT TAPE  6,864,EM,BAC,BETA,DELTA,IOD,EM,CAY,ELAMS,BAC,BA
     1D,XMRU,XMRL,HCR,HCL
      WRITE OUTPUT TAPE 15,864,EM,BAC,BETA,DELTA,IOD,EM,CAY,ELAMS,BAC,BA
     1D,XMRU,XMRL,HCR,HCL
  864 FORMAT(20X,32HNORMALIZED MAGNETIZATION = MNORM//34H MAGNETIZATION
     1(GAUSSES) = (MNORM),F6.0/42H HSWCH (OERSTEDS) =  ALPHA(2K/M) = (AL
     2PHA),F5.2/9H  BETA = ,F5.3,14X,8HDELTA = ,F6.3/22H GAMMA(INITIAL P
     3HI) = ,I3,2X,17HM (SATURATION) = ,F6.0/15H K(ERGS/CCM) = ,F6.0,6X,
     422HLAMBDAS(MAGSTRICTION)=,E8.2/15H HPERP = (BETA),F5.2,7X,22HSIGMA
     5(DYN/SCM)=(DELTA),E8.2/8H XMRU = ,F6.4,13X,7HXMRL = ,F7.4/7H HCR =
     6 ,F6.4,14X,6HHCL = ,F7.4)
      GO TO 2
      END                                                          0164
*     FORTRAN
      SUBROUTINE COMPAR(Y,A,N,Z)
      DIMENSION A(4),B(4)
      L=0
      DO 10 I=1,N
      B(I)=A(I)-Y
      IF(B(I))10,4,4
 4    L=L+1
      IF(L-1)5,5,6
 5    Z=A(I)
      GO TO 10
 6    IF(A(I)-Z)7,10,10
 7    Z=A(I)
 10   CONTINUE
      RETURN
      END
*     FORTRAN
*TBP                                                             0163
      SUBROUTINE TBP(TBNK1,TBNK2,TBNK3,TBNK4,IBNK1,IBNK2)          61244
      GO TO(20,21,22),IBNK2                                        61246
   20 WRITE OUTPUT TAPE 6 ,83
      WRITE OUTPUT TAPE 15,83
      WRITE OUTPUT TAPE6,82
      WRITE OUTPUT TAPE 15,82
      GO TO 12                                                     61249
   21 WRITE OUTPUT TAPE 6 ,77,TBNK1,
     1(IBNK1(I),I=1,19)
      WRITE OUTPUT TAPE 15,77,TBNK1,
     1(IBNK1(I),I=1,19)
```

```
      GO TO 12                                                          61252
   22 TA=0.960
      TB=0.480
      TC=0.000
      TD=-0.480
      TE=-.960
      WRITE OUTPUT TAPE 6,80,TA,TB,TC,TD,TE
      WRITE OUTPUT TAPE15,80,TA,TB,TC,TD,TE
      12 RETURN                                                         61255
      77 FORMAT(1H  E10.3,18A6,A1)                                      61256
   80 FORMAT(14X,F5.3,3X,F5.3,3X,F5.3,2X,F6.3,2X,F6.3)
    82 FORMAT(14X,25HTHIN FILM HYSTERESIS LOOP)
      83 FORMAT(1H1)                                                    61259
      DIMENSION IBNK1(19)                                               61260
      DIMENSION TBNK3(11)                                               61261
      END                                                               0164
*     BINARY
```

APPENDIX 3

Listing of program for computation and plotting of static critical switching curve with example

```
STATIC CRITICAL SWITCHING CURVE - ASTROID
*      FORTRAN
       DIMENSION GEORGE(12),PANCHO(12),PEDRO(12),PATTY(12),SYMBOL(12)
       DIMENSION SDEV(4),Y(200),X(200)
       DIMENSION PHONY(1083),R2(2,4),PRDR(3),PRDI(3),SMR(3),SMI(3)        00000010
       COMMON PHONY,PRDR,PRDI,SMR,SMI                                        20
    55 FORMAT(5F12.6)
       READ INPUT TAPE 5,101,EM,CAY,ELAMS
   101 FORMAT(3F12.5)
       N=1
       CALL PREPAR(49,37,-1.200,.050,1.170,-.065,0,0,1,23,17,0.,0.)
       I=1
    10 READ INPUT TAPE 5,102,GEORGE(I),PANCHO(I),PEDRO(I),PATTY(I),SYMBOL
      1(I)
   102 FORMAT(4F10.4,A6)
       I=I+1
       IF(I-12)10,10,1
 1     I=0
 2     I=I+1
 3     DELTA=PATTY(I)
       BETA=PANCHO(I)
 4     ALPHA=GEORGE(I)
       GAMMA=PEDRO(I)
       IGAMM=GAMMA
       BAC=2.*CAY/EM
       BAD=2.*CAY/3.*ELAMS
       GAMMA = GAMMA*3.14159265/180.
       SGAM=SINF(GAMMA)
       CGAM=COSF(GAMMA)
       CAROL=1.0
       F=1.+DELTA**2-2.*DELTA*(CGAM**2-SGAM**2)
   11  B=4.*BETA*SGAM*CGAM+2.*ALPHA*(CGAM**2-SGAM**2-DELTA)
       C=-(F-ALPHA**2-BETA**2)
       D=-(B-2.*BETA*SGAM*CGAM)
       E=-ALPHA**2+(SGAM**2)*(CGAM**2)
       CALL LLNPRC(SMI(3))
       CALL ROOTR(F,B,C,D,E,R2,KK,PRDR,PRDI,SMR,SMI)
       IF(KK)45,2025,45
  45   WRITE OUTPUT TAPE 6,48
  48   FORMAT (45H ROOT PROGRAM FAILED FOR FOLLOWING POLYNOMIAL  )
2025   IF(R2(2,1))212,117,212
 117   IF(R2(2,2))212,118,212
 118   IF(R2(2,3))212,119,212
 119   IF(R2(2,4))212,120,212
  212  IF(CAROL-2.0)213,127,213
  213  WRITE OUTPUT TAPE 6,214,BETA
  214  FORMAT(18HNEVER 4 REAL ROOTS,F10.5)
       GO TO 22
  120  IF(ABSF(ALPHA)-1.0001)968,969,969
```

```
 969  WRITE OUTPUT TAPE 6,674,BETA
 674  FORMAT(19HALWAYS 4 REAL ROOTS,F10.4)
 968  IF(ALPHA)972,972,973
 972  ALPHA=ALPHA-.02
      CAROL=2.
      GO TO 11
 973  ALPHA=ALPHA+.02
      CAROL=2.
      GO TO 11
 127  X(N)=ALPHA
      Y(N)=BETA
      WRITE OUTPUT TAPE 6,55,ALPHA,BETA,DELTA,X(N),Y(N)
      CALL POINT(X(N),Y(N),SYMBOL(I))
      N=N+1
 22   CAROL=1.
      IF(ABSF(BETA)-1.005)842,843,843
 843  CALL SAVE
      IF(I-12)2,982,982
 842  IF(BETA)844,844,845
 844  BETA=BETA-.1
      GO TO 4
 845  BETA=BETA+.1
      GO TO 4
 982  WRITE OUTPUT TAPE 6,53
 53   FORMAT(1H1)
      CALL PLOT
      WRITE OUTPUT TAPE 6,222,BAC,IGAMM,EM,CAY,ELAMS,BAC,BAD,PATTY(1),PA
     1TTY(2),PATTY(3)
      WRITE OUTPUT TAPE15,222,BAC,IGAMM,EM,CAY,ELAMS,BAC,BAD,PATTY(1),PA
     1TTY(2),PATTY(3)
 222  FORMAT(28X,29H NORM COERCIVE FIELD (ALPHAC)//16H  HC = (ALPHAC)(,F
     15.2,4H)   /30H  ORDINATES = NORM HPERP(BETA)//22H  GAMMA(INITIAL P
     2HI) =,I1,19H  M (SATURATION) = ,F5.0/16H  K(ERGS/CCM) = ,F6.0,25H
     3  LAMBDAS(MAGSTRICTION)=,E8.2/17H  HPERP = (BETA)(,F5.2,3H)  ,22HS
     4IGMA(DYN/SCM)=(DELTA),E8.2/10H  DELTA1 =,F5.2,12H    DELTA2 =,F5.2
     5,12H    DELTA3 =,F5.2)
      CALL EXIT
      END
*     FORTRAN
*TBP                                                                  0163
      SUBROUTINE TBP(TBNK1,TBNK2,TBNK3,TBNK4,IBNK1,IBNK2)             61244
      GO TO(20,21,22),IBNK2                                           61246
   20 WRITE OUTPUT TAPE 6 ,83
      WRITE OUTPUT TAPE 15,83
      WRITE OUTPUT TAPE6,82
      WRITE OUTPUT TAPE 15,82
      GO TO 12                                                        61249
   21 WRITE OUTPUT TAPE 6 ,77,TBNK1,
     1(IBNK1(I),I=1,19)
```

```
      WRITE OUTPUT TAPE 15,77,TBNK1,
     1(IBNK1(I),I=1,19)
      GO TO 12                                                    61252
 22   TA=-1.000
      TB=-0.500
      TC=0.000
      TD=0.500
      TE=1.000
      WRITE OUTPUT TAPE 6,80,TA,TB,TC,TD,TE
      WRITE OUTPUT TAPE15,80,TA,TB,TC,TD,TE
   12 RETURN                                                      61255
   77 FORMAT(1H  E10.3,18A6,A1)                                   61256
 80   FORMAT(13X,F6.3,4X,F6.3,3(5X,F5.3))
 82   FORMAT(14X,29HFILM CRITICAL SWITCHING CURVE)
   83 FORMAT(1H1)                                                 61259
      DIMENSION IBNK1(19)                                         61260
      DIMENSION TBNK3(11)                                         61261
      END                                                         0164
*      BINARY
```

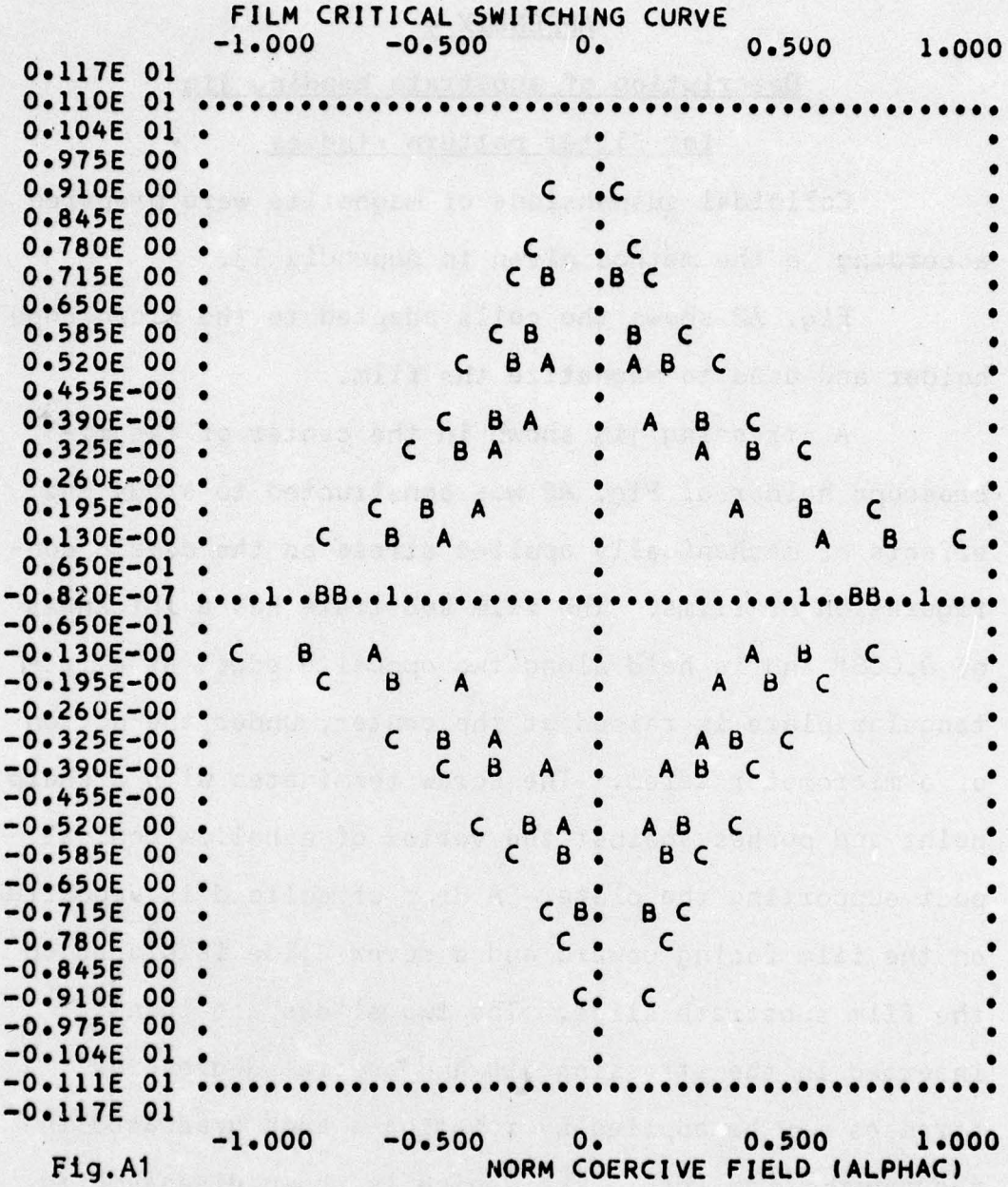


Fig.A1

HC = (ALPHAC)(0.69)
ORDINATES = NORM HPERP(BETA)

GAMMA(INITIAL PHI) =5 M (SATURATION) = 1450.
K(ERGS/CCM) = 500. LAMBDAS(MAGSTRICTION)=0.20E-04
HPERP = (BETA)(0.69) SIGMA(DYN/SCM)=(DELTA)0.67E-02
DELTA1 = 0.20 DELTA2 =-0. DELTA3 =-0.20

APPENDIX 4

Description of substrate bending jig for Bitter pattern studies

Colloidal suspensions of magnetite were prepared according to the method given in Appendix 13.

Fig. A2 shows the coils adapted to the microscope holder and used to magnetize the film.

A stressing jig shown in the center of the microscope holder of Fig. A2 was constructed to study the effects of mechanically applied stress on the domain configuration of films. The film substrate has a thickness of 0.006" and is held along two opposite edges as a rectangular plate is raised at the center, under the action of a micrometer screw. The screw terminates with a sharp point and pushes against the vertex of a hollow conical post supporting the plate. A drop of colloid is deposited on the film facing upward and a cover slide is placed on the film substrate slide. The two slides are then inserted in the stressing jig and several degrees of stresses may be applied by rotating a knob graduated in thousandths of an inch. The device is shown disassembled in Fig. A9c.

The plate which raises the film substrate moves upward remaining parallel to itself and constantly in

contact with the slide, as pressure is exerted at one point only. This arrangement provides a constant bending moment and a constant stress in the film.

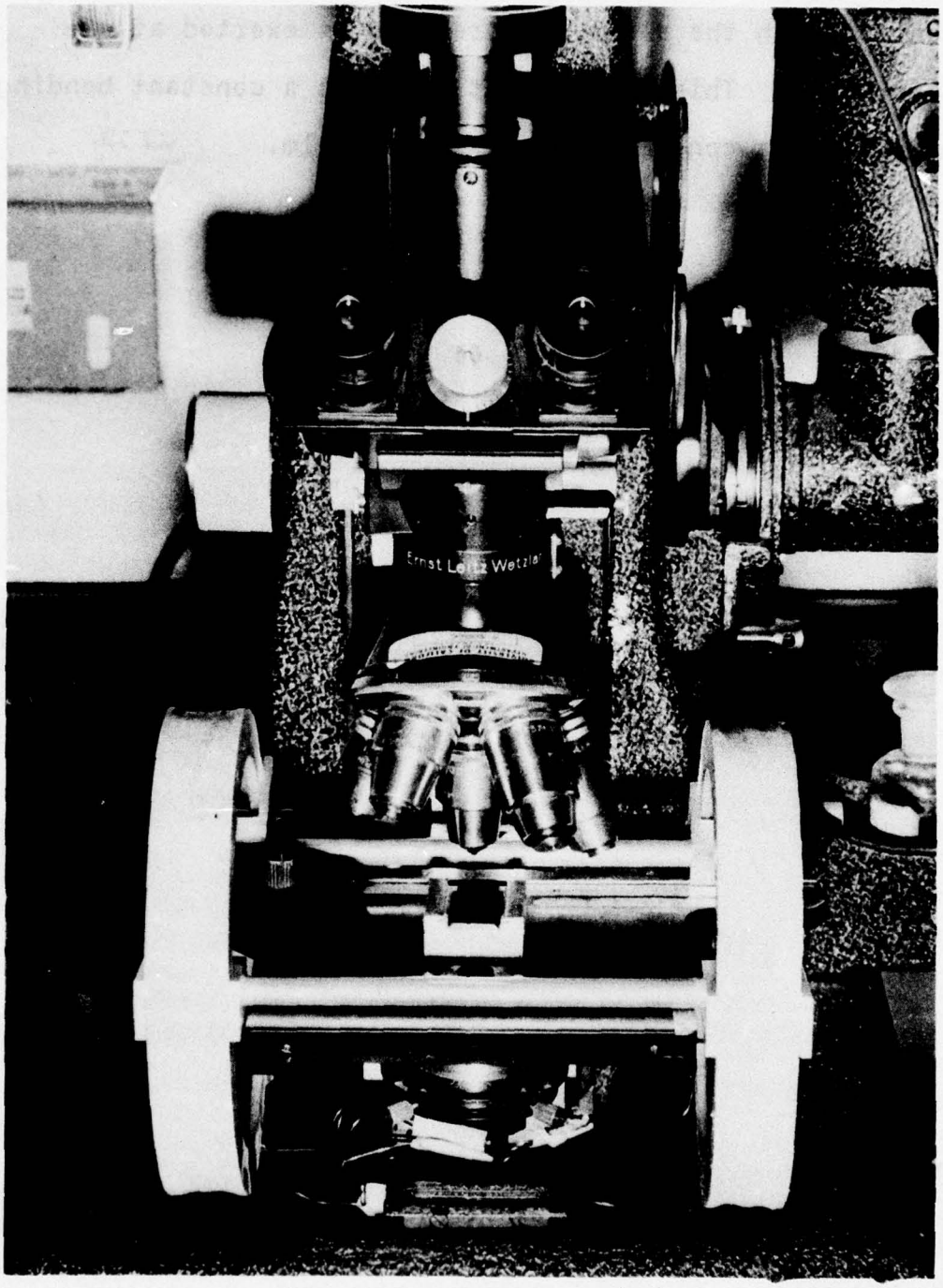


Fig. A2

APPENDIX 5

Description of device for bending film substrates in B-H loop tester

The film substrate is bent by a pyrex bar inserted in the coilform, above the sample, and supported at the ends, protruding from the coilform, by a plastic, spring loaded, vertically sliding arrangement connected rigidly to a central shaft shown under the plexiglass table in Fig. A4.

This central shaft includes a micrometer and a plastic wheel (Fig. A4) whose manual rotation lowers the sliding arrangement against the action of the spring. This feature eliminates backlash, and controlled displacements of a fraction of a thousandth of an inch may be obtained.

The pyrex bar is initially set resting on the film and the points of two (one on each side of the coilform) accurately machined ivory screws, fixed to the sliding arrangement, are adjusted until they barely touch a line inscribed on the glass bar parallel to its length and along its central line. Two small silver mirrors are evaporated at both ends of the bar on the surfaces facing the ivory screws. As the screws are turned clockwise their points advance toward their mirror images and

the contact between the object and its image is observed through a measuring microscope having a magnifying power of 36 and mounted on the instrument, as shown in Fig. A3. Fig. A5 shows the point of the screw (the object) coming in contact with its image. When the two screws are adjusted in this manner the micrometer may be turned. Under these conditions the glass bar moves vertically parallel to itself, pressing equally along two edges against the film substrate, thus impressing a constant bending moment and a constant unidirectional stress to the film.

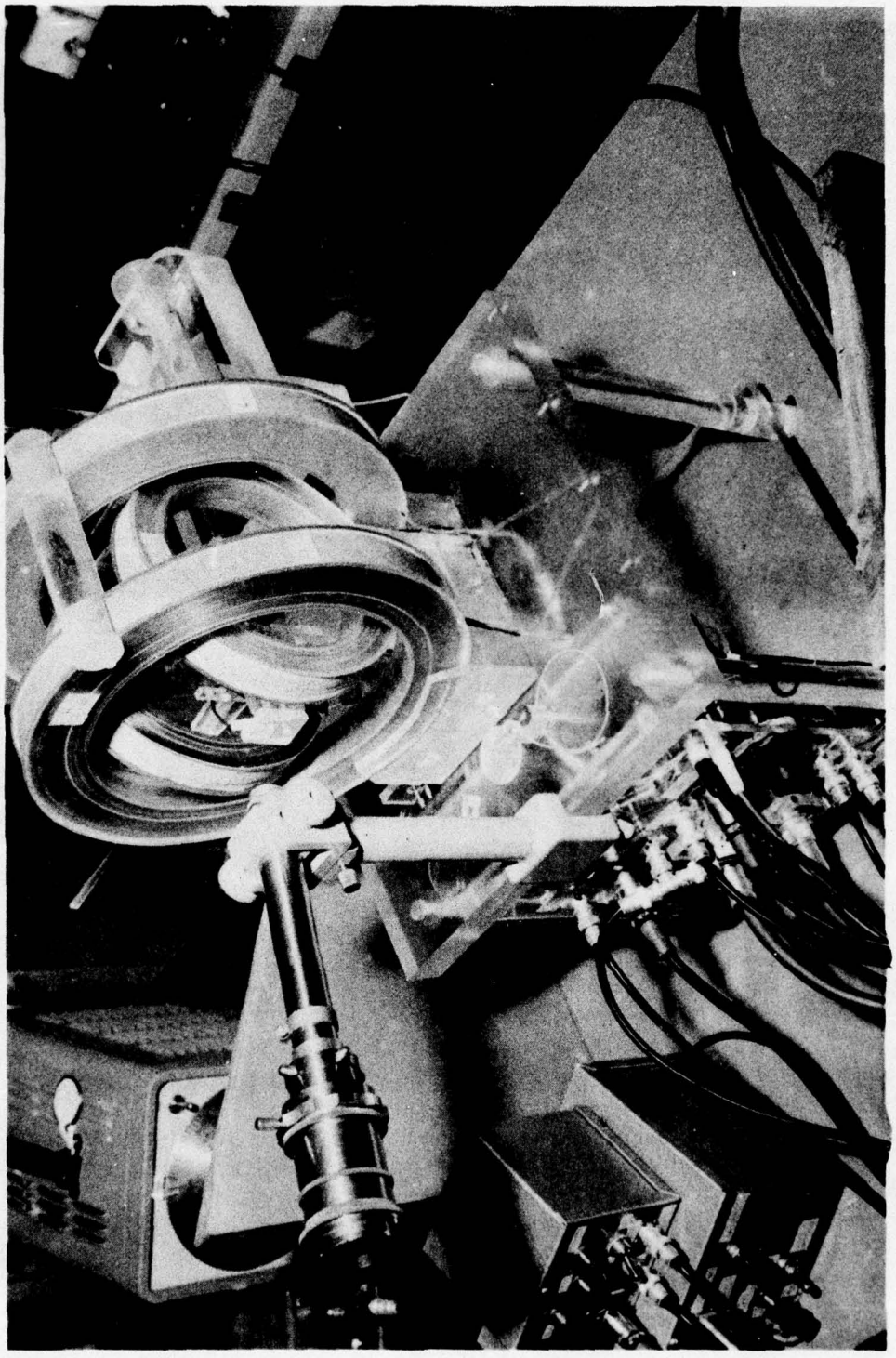


Fig. A3

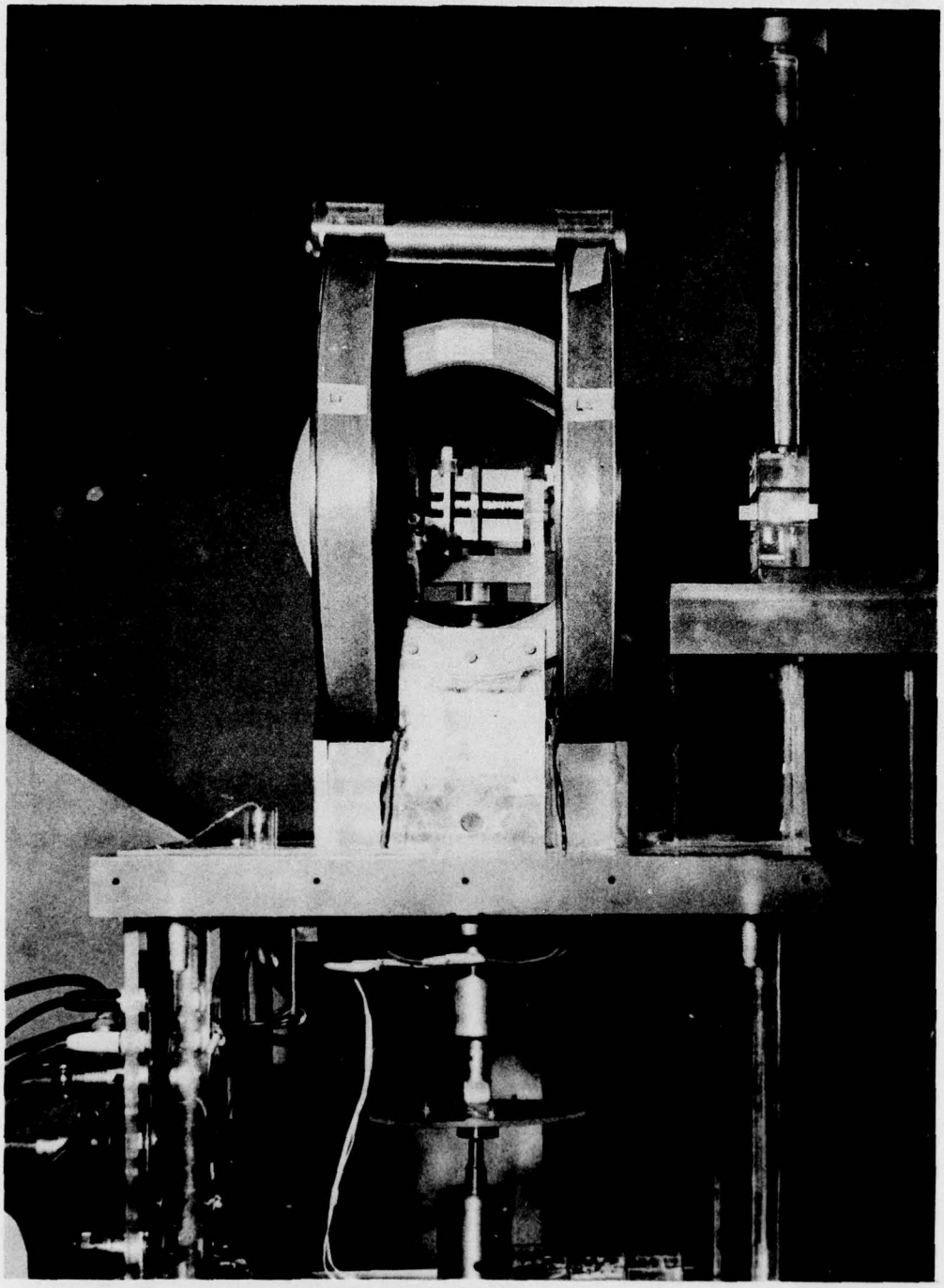


Fig. A4

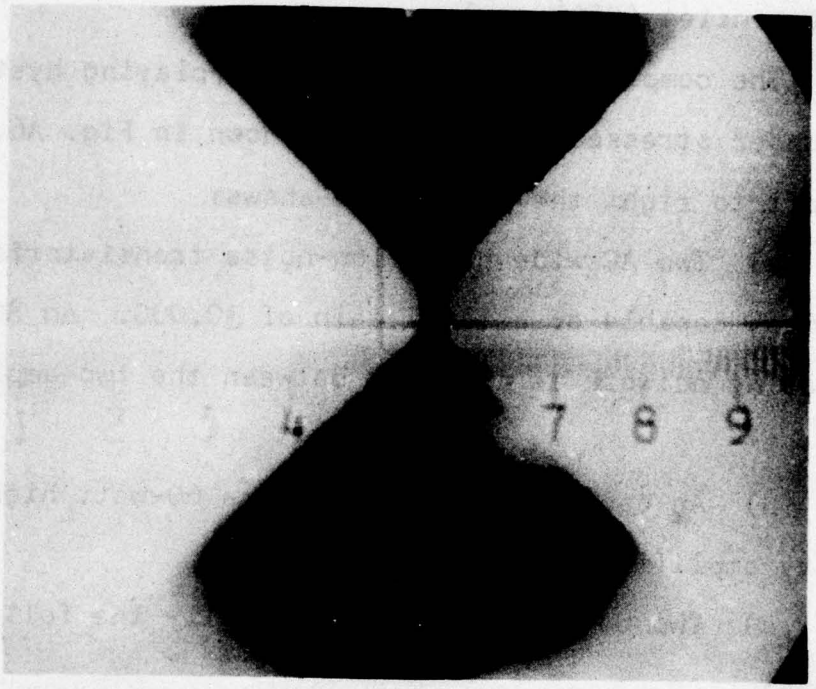


Fig. A5

APPENDIX 6

Description of B-H loop tester

The following is a brief description of a hysteresis loop tester suitable for studying stress effects on the magnetic properties of thin films at low frequencies (2500 cps).

The complete arrangement for displaying hysteresis loops under stressed conditions is shown in Fig. A6. From left to right the photograph shows:

a) Two AC wide band, low-noise transistorized amplifiers capable of a total gain of 30,000. An RC integrating network is inserted between the two amplifiers.

b) An oscillator for driving a 60-watt high fidelity amplifier.

c) Two boxes displaying frontally the following controls:

1. Two potentiometers for cancelling the signal present in the pickup coil, in quadrature with the emf induced, when using one pickup coil or another at 90° from the first.
2. One potentiometer for adjusting the damping of the integrated, amplified, and filtered signal.
3. A variable inductor for adjusting the cutoff fre-

quency of a high pass filter used to eliminate flicker, 60 cps and 180 cps noise.

4. A compensated attenuator for making identical, vertical signals on a 545 Tektronix oscilloscope, when the same hysteresis loop of a given film is viewed from one set of pickup coils or another set at 90° with respect to the first.
5. An attenuator for making identical horizontal signals in the same sense as the above.
6. A switch for reversing the phase by 180°.
7. Two potentiometers for adjusting independently the phase when using one pickup coil or another at 90° from the first.

d) The hysteresis loop tester consisting of:

1. An elevated plexiglass table supporting 2 pairs of coils at 90° from one another, which may be driven independently by the high fidelity amplifier shown in the background, at the right of the picture.
2. In the center of the sets of coils just mentioned are located three sets of pickup-bucking coils. One set is mounted on a hollow coilform which receives the sample to be studied. The other two sets are mounted on the top and on the bottom of the coilform, at 90° from the first set and are disposed in series. The sample is placed on a small circular plexiglass

support shown in Fig. A7. This support is inserted in the coilform which is made of thick pyrex for rigidity.

3. A device for inducing uniaxial stresses in the film by bending mechanically the film substrate, while the sample is inserted in the pickup coils, is described in Appendix 5.

The stresses may also be impressed isotropically when the film is evaporated on a piezoelectric substrate. In this case, the piezoelectric crystal is inserted in the coilform and high voltage leads are connected to the crystal electrodes. Fig. A8 shows the front panel of the hysteresis loop tester; in the center of the panel a conductor brings the polarizing voltage through an HN connector, to two terminals insulated with plexiglass and teflon and shown on the right on the plastic table. At the left of the table, two spring-loaded terminals are used to attach leads connected to metal strain gages glued on the piezoelectric crystal on the face not covered by the film.

A multipole double-throw switch, visible on the lower left portion of the panel, is used to perform the following simultaneous switching operations.

The AC drive from the high fidelity amplifier is switched from a first set of coils to a second at 90°

from the first.

The DC drive from a separate supply (used to provide a biasing perpendicular field) is switched from the second set of coils to the first.

The horizontal input to the oscilloscope is switched from a circuit configuration, requiring the insertion of an attenuator to another not requiring any attenuation.

The input to the AC amplifier is switched from one set of pickup coils to another.

In the foreground and at the left of Fig. A7 are located two plexiglass posts supporting two fine adjustment coils, one for each driving condition.

The instrument is thus capable of displaying longitudinal and perpendicular hysteresis loops while the film is under stress. Instead of rotating the film, the instrumentation around it has been "rotated" by switching from one configuration to the other.

The knob shown on the upper right of the panel in Fig. A8 controls the magnitude of the DC perpendicular biasing field.

e) A pair of large coils for cancelling the earth magnetic field is shown in Fig. A6 surrounding the hysteresis loop tester.

f) A precision VTVM for calibration, a DC am-

meter for measuring the perpendicular field, a battery of three tuning condensers and the high fidelity amplifier, are shown at the right of Fig. A6.

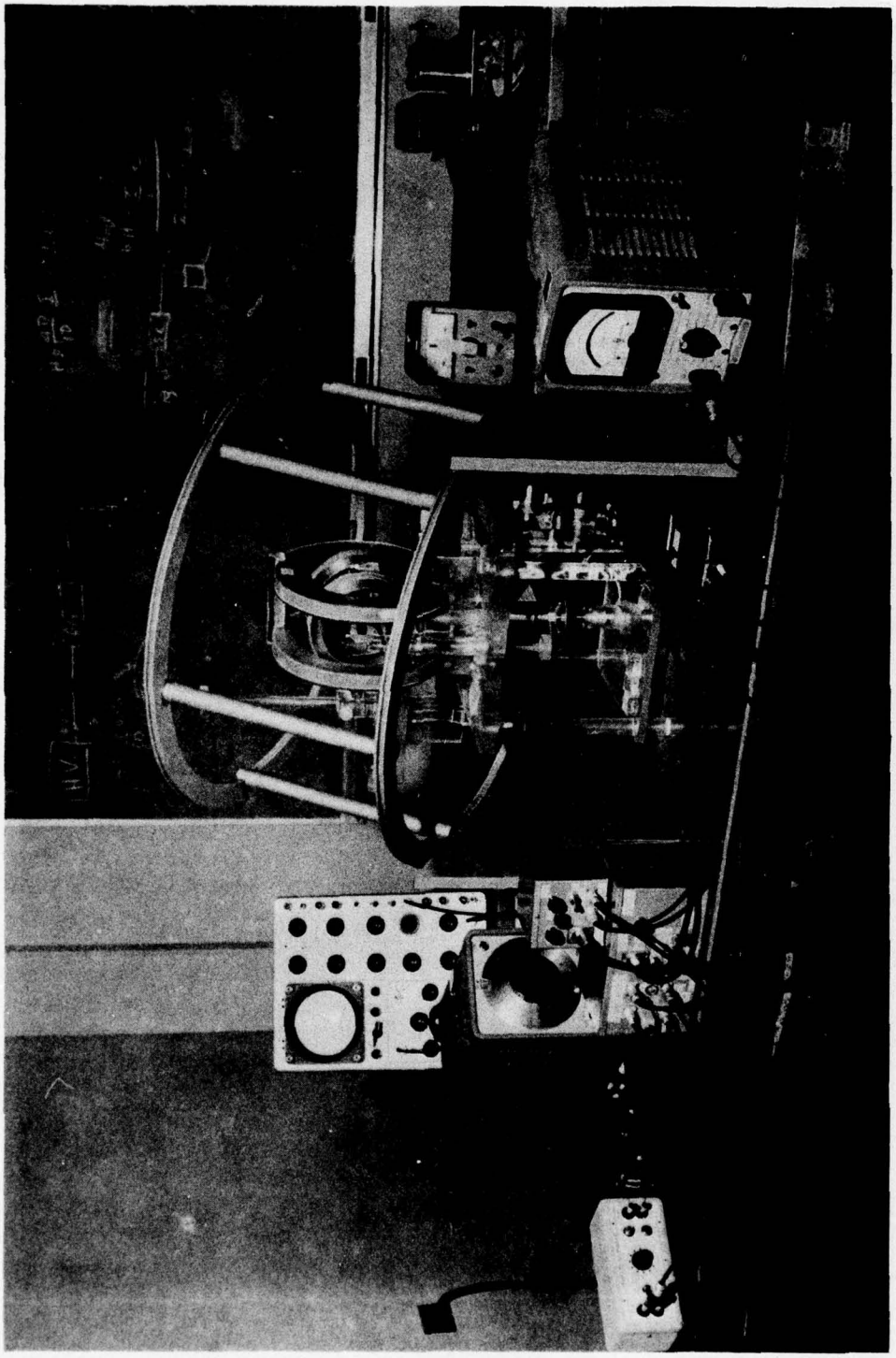


Fig. A6

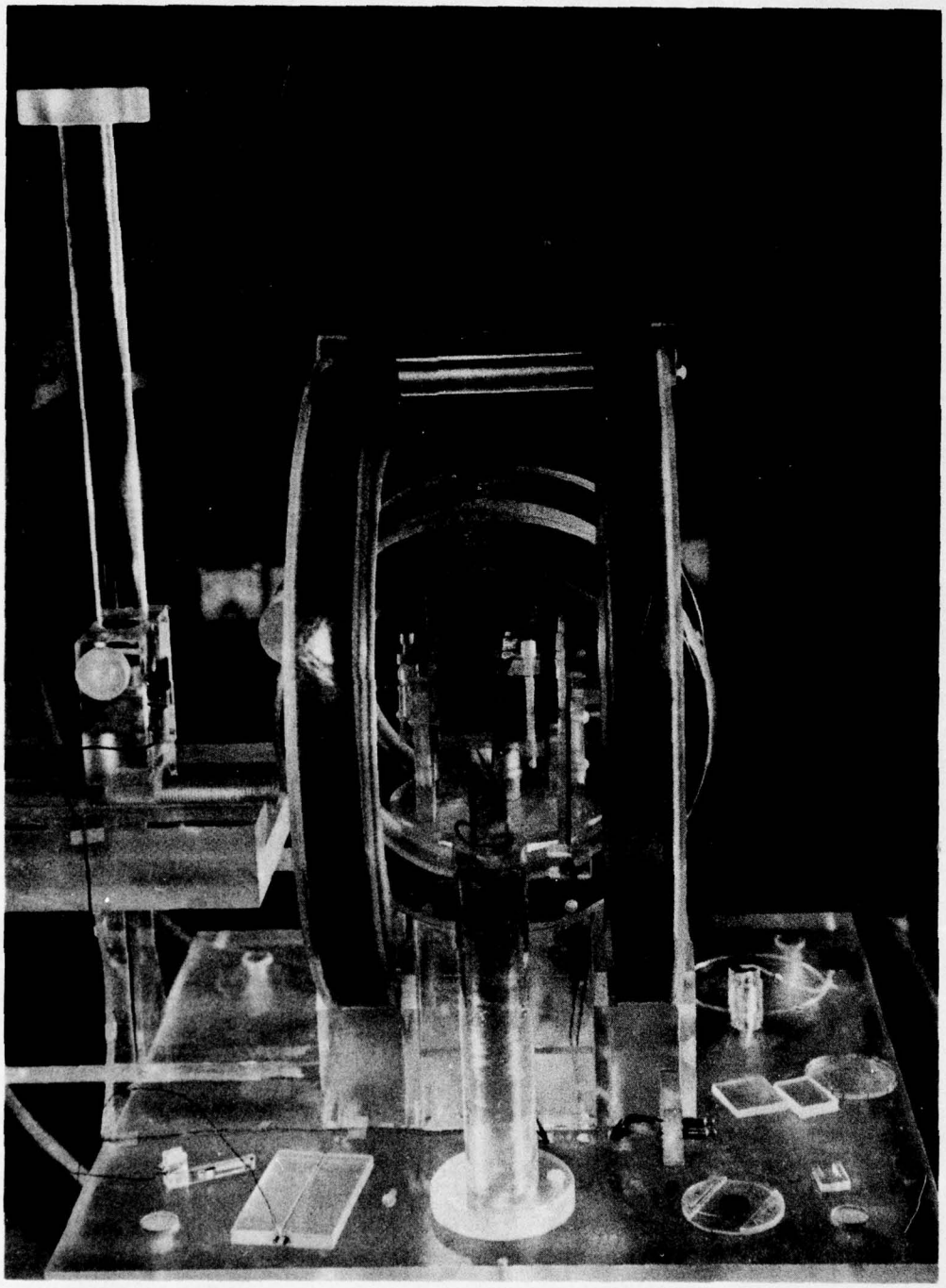


Fig. A7

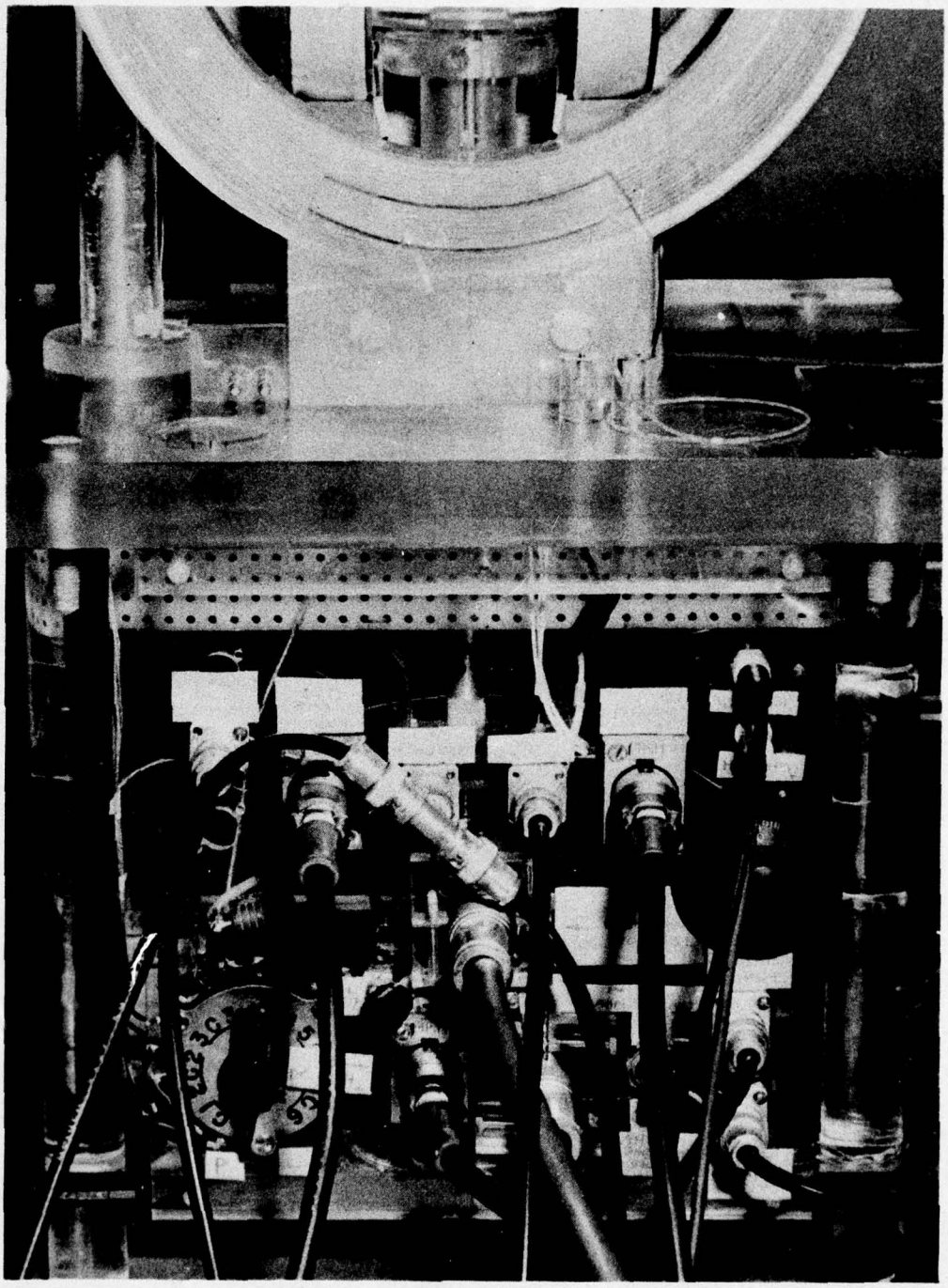


Fig. A8

APPENDIX 7

Listing of program

for solution of Landau-Lifshitz equation

a) One curve computer plot

```
LANDAU-LIFSHITZ EQUATIONS BORSEI FILM NON-DESTR. READ
*       FORTRAN
        DIMENSION VAR(12)
        EQUIVALENCE (VAR(3),PHI),(VAR(6),DPHI),(VAR(9),PSI),(VAR(12),DPSI)
        ZERO=0.
        READ INPUT TAPE 5,583,ESS
  583   FORMAT(E10.3)
 1      READ INPUT TAPE 5,100,CAY,GAMMA,EM,ELAMS,ELAMDA,NRUNS
        PI = 3.14159265
        EPSLON = 4.*PI*EM**2/CAY
 100    FORMAT(F10.0,E10.2,F10.0,E10.2,E10.2,I10)
        DO 5 I=1,NRUNS
        READ INPUT TAPE 5,101,ALPHA,BETA,DELTA,PHI0,PHI,PSI
 101    FORMAT(6F10.0)
        READ INPUT TAPE 5,102,T0,DELTAT,TMAX
 102    FORMAT(F10.0,F10.2,F10.0)
        GEORGE=4.*3.14159*EM*ESS
        BAC=2.*CAY/EM
        BAD=2.0*CAY/(3.0*ELAMS)
        PHI0D=PHI0*180./3.14159265
        IA=0
        N1=0
        N2=0
        MART=1
        CALL GBN(IA,N1,T,E1,N2)
        COM1=0.
        CALL FNIDE(DELTAT,T0,100,.006)
        C1=(2.*CAY*GAMMA*1.0E-9)/EM
        C2=(2.*CAY*ELAMDA*1.0E-9)/EM**2
 2      SPSI=SINF(PSI)
        CPSI=COSF(PSI)
        SPHI=SINF(PHI)
        CPHI=COSF(PHI)
        A1=ALPHA*SPHI-BETA*CPHI+DELTA*SINF(2.*PHI)/2.
       1+SINF(2.*(PHI-PHI0))/2.*COSF(PSI)
        A2=SPSI*(ALPHA*CPHI+BETA*SPHI-DELTA/2.*(SINF(PHI))**2)
        A3=SPSI*CPSI
        DPSI=C1*A1-C2*A2-C2*EPSLON*A3
        DPHI=-(C2*A1+C1*A2+C1*EPSLON*A3)/CPSI
        E1 =     SPHI*DPHI
 3      CALL FINTEG(DPSI,PSI)
        CALL FINTEG(DPHI,PHI)
        CALL FUPDAT(VAR,4,L1,T)
        GO TO (2,3,4,4,4),L1
 4      CONTINUE
        IA=1
        CALL GBN(IA,N1,T,E1,N2)
 201    FORMAT(8E15.4)
        GO TO (98,45),MART
```

```
  98  COM2=E1
      IF(COM2-COM1)12,12,10
  10  COM1=COM2
      GO TO 45
  12  TP=T-DELTAT
      SIG=COM1
      MART=2
      GO TO 45
  45  IF(T-TMAX) 3,51,51
 51   IA=2
      CALL GBN(IA,N1,T,E1,N2)
      WRITE OUTPUT TAPE 6,7654,GEORGE,EM,CAY,ESS,ELAMS,ELAMDA,ALPHA,BETA
     1,DELTA,BAC,BAC,BAD,BAC,PHI0D,TP,GAMMA,SIG
      WRITE OUTPUT TAPE15,7654,GEORGE,EM,CAY,ESS,ELAMS,ELAMDA,ALPHA,BETA
     1,DELTA,BAC,BAC,BAD,BAC,PHI0D,TP,GAMMA,SIG
 7654 FORMAT(34H  ORDINATES(DPHI/DT)SIN(PHI)      ,28X,18HTIME(NANOSECON
     1DS) /2X,52HPICKUP VOLTS = (4)(3.1416)(S)(M)(DPHI/DT)SIN(PHI) = ,F6
     2.3,17H(DPHI/DT)SIN(PHI)/15H  M(GAUSSES) = ,F5.0,18H    K(ERGS/CCM)
     3 = ,F6.0,31H    (FILM CROSS SECTION,SCM) = ,E10.3
     4  /30H  LAMBDAS(MAGNETOSTRICTION) = ,E8.2,24H  LAMBDA(DAMPING,CPS)
     5 = ,E8.2/10H  ALPHA = ,F6.3,16H         BETA = ,F6.3,17H         D
     6ELTA = ,F6.3/17H  HSWCH = (ALPHA),F5.2,17H   HPERP = (BETA),F5.2,1
     79H    SIGMA = (DELTA),E8.2/17H  HANIS = 2K/M = ,F5.2,32H   PHI0D(I
     8NITIAL PHI,DEGREES) = ,F6.2/33H  TP(PEAKING TIME,NANOSECONDS) = ,F
     95.3,22H  GAMMA(GYRO RATIO) = ,E9.3,21H   MAX PICKUP SIG. = ,E10.3)
 5    CONTINUE
      GO TO 1
      END
*     FORTRAN                                                          0162
*TBP                                                                  0163
      SUBROUTINE TBP(TBNK1,TBNK2,TBNK3,TBNK4,IBNK1,IBNK2)              61244
      GO TO(20,21,22),IBNK2                                            61246
   20 WRITE OUTPUT TAPE  6,83
      WRITE OUTPUT TAPE 15,83
      WRITE OUTPUT TAPE  6,82
      WRITE OUTPUT TAPE 15,82
      GO TO 12                                                         61249
   21 WRITE OUTPUT TAPE  6,77,TBNK1,
     1(IBNK1(I),I=1,19)                                                61251
      WRITE OUTPUT TAPE 15,77,TBNK1,
     1(IBNK1(I),I=1,19)
      GO TO 12                                                         61252
   22 WRITE OUTPUT TAPE  6,80,
     1(TBNK3(I),I=1,11)                                                61254
      WRITE OUTPUT TAPE 15,80,
     1(TBNK3(I),I=1,11)
   12 RETURN                                                           61255
   77 FORMAT(1H  E10.3,18A6,A1)                                        61256
   80 FORMAT(E20.3,10E10.3)                                            61257
```

```
   82 FORMAT(71H  SOLUTION OF LANDAU-LIFSHITZ EQUATION -- THIN FILM LONG
     1. PICKUP SIGNAL)
   83 FORMAT(1H1)                                                        61259
      DIMENSION IBNK1(19)                                                61260
      DIMENSION TBNK3(11)                                                61261
      END                                                                0164
*     LABEL
*     FAP
       COUNT 40
       ENTRY GBN
GBN    CLA   1,4
       STA   GBNA
GBNA   CLA   0
       ARS   18
       STO   TB+10
       CLA   2,4
       STA   GBNB
GBNB   CLA   0
       STO   TB+13
       CLA   3,4
       STA   GBNC
GBNC   CLA   0
       STO   TB+18
       CLA   4,4
       STA   GBND
GBND   CLA   0
       STO   TB+19
       CLA   5,4
       STA   GBNE
GBNE   CLA   0
       STO   TB+22
       SXD   IR4,4
TB     CALL  TBN
       DEC   109,39,-.016,.016,34.20,-1.80,0,0,-1
       PZE   0
       DEC   20,18
       PZE   0
       PZE   K1
       PZE   K1+3000
       DEC   0
       BCD 100000.
       PZE   0
       PZE   0
       BCD 100000*
       DEC   0
       PZE   0
       LXD   IR4,4
       TRA   6,4
K1     BSS   3000
```

```
IR4     DEC   0

        END
*       BINARY
```

APPENDIX 7

Listing of program
for solution of Landau-Lifshitz equating

b) Three curve computer plot

```
LANDAU-LIFSHITZ EQUATIONS SMITH FILM 3 CURVES
*       FORTRAN
        DIMENSION VAR(12),SYMBOL(10),XBETA(3),TP(3),PKV(3)
        EQUIVALENCE (VAR(3),PHI),(VAR(6),DPHI),(VAR(9),PSI),(VAR(12),DPSI)
        ZERO=0.
        READ INPUT TAPE 5,583,ESS
  583   FORMAT(E10.3)
  1     READ INPUT TAPE 5,100,CAY,GAMMA,EM,ELAMS,ELAMDA,NRUNS
        PI = 3.14159265
        EPSLON = 4.*PI*EM**2/CAY
  100   FORMAT(F10.0,E10.2,F10.0,E10.2,E10.2,I10)
        CALL PREPAR(103,39,-.05,.05,5.00,-.20,0,0,-1,20,12,0.,0.)
        KN=0
        DO 5 I=1,NRUNS
        READ INPUT TAPE 5,101,ALPHA,BETA,DELTA,PHI0,PHI,PSI,SYMBOL(I)
  101   FORMAT(F10.2,F10.2,F10.1,3F10.0,A6)
        XBETA(I)=BETA
        READ INPUT TAPE 5,102,T0,DELTAT,TMAX
  102   FORMAT(F10.0,F10.2,F10.0)
        GEORGE=4.*3.14159*EM*ESS
        BAC=2.*CAY/EM
        BAD=2.0*CAY/(3.0*ELAMS)
        PHI0D=PHI0*180./3.14159265
        MART=1
        COM1=0.
        CALL FNIDE(DELTAT,T0,100,.006)
        C1=(2.*CAY*GAMMA*1.0E-9)/EM
        C2=(2.*CAY*ELAMDA*1.0E-9)/EM**2
  2     SPSI=SINF(PSI)
        CPSI=COSF(PSI)
        SPHI=SINF(PHI)
        CPHI=COSF(PHI)
        A1=ALPHA*SPHI-BETA*CPHI+DELTA*SINF(2.*PHI)/2.
       1+SINF(2.*(PHI-PHI0))/2.*COSF(PSI)
        A2=SPSI*(ALPHA*CPHI+BETA*SPHI-DELTA/2.*(SINF(PHI))**2)
        A3=SPSI*CPSI
        DPSI=C1*A1-C2*A2-C2*EPSLON*A3
        DPHI=-(C2*A1+C1*A2+C1*EPSLON*A3)/CPSI
        E1 =     SPHI*DPHI
  3     CALL FINTEG(DPSI,PSI)
        CALL FINTEG(DPHI,PHI)
        CALL FUPDAT(VAR,4,L1,T)
        GO TO (2,3,4,4,4),L1
  4     CONTINUE
        CALL POINT(T,E1,SYMBOL(I))
  201   FORMAT(8E15.4)
        GO TO (98,45),MART
   98   COM2=E1
        IF(COM2-COM1)12,12,10
```

```
   10  COM1=COM2
       GO TO 45
   12  KN=KN+1
       TP(KN)=T-DELTAT
       PKV(KN)=COM1
       MART=2
       GO TO 45
   45  IF(T-TMAX) 3,51,51
   51  CONTINUE
    5  CONTINUE
       CALL PLOT
       WRITE OUTPUT TAPE 6,7654,GEORGE,EM,CAY,ESS,ELAMS,ELAMDA,ALPHA,GAMM
      1A,DELTA,BAC,BAC,BAD,BAC,PHI0D
       WRITE OUTPUT TAPE15,7654,GEORGE,EM,CAY,ESS,ELAMS,ELAMDA,ALPHA,GAMM
      1A,DELTA,BAC,BAC,BAD,BAC,PHI0D
 7654  FORMAT(34H  ORDINATES(DPHI/DT)SIN(PHI)       ,28X,18HTIME(NANOSECON
      1DS) /2X,52HPICKUP VOLTS = (4)(3.1416)(S)(M)(DPHI/DT)SIN(PHI) = ,F6
      2.3,17H(DPHI/DT)SIN(PHI)/15H  M(GAUSSES) = ,F5.0,18H    K(ERGS/CCM)
      3 = ,F6.0,31H    (FILM CROSS SECTION,SCM) = ,E10.3
      4  /30H  LAMBDAS(MAGNETOSTRICTION) = ,E8.2,24H  LAMBDA(DAMPING,CPS)
      5 = ,E8.2/10H  ALPHA = ,F6.3,22H  GAMMA(GYRO RATIO) = ,E10.3,10H  D
      6ELTA = ,F6.3/17H  HSWCH = (ALPHA),F5.2,17H   HPERP = (BETA),F5.2,1
      79H    SIGMA = (DELTA),E8.2/17H  HANIS = 2K/M = ,F5.2,32H   PHI0D(I
      8NITIAL PHI,DEGREES) = ,F6.2)
       WRITE OUTPUT TAPE6,7655,XBETA(1),TP(1),PKV(1),XBETA(2),TP(2),PKV(2
      1),XBETA(3),TP(3),PKV(3)
 7655  FORMAT(7H BETAX=,F6.3,4H TP=,F6.3,5H PKV=,E10.3,8H, BETAY=,F6.3,4H
      1 TP=,F6.3,5H PKV=,E10.3,8H, BETAZ=,F6.3,4H TP=,F6.3,5H PKV=,E10.3)
       GO TO 1
       END
*      FORTRAN                                                          0162
*TBP                                                                   0163
       SUBROUTINE TBP(TBNK1,TBNK2,TBNK3,TBNK4,IBNK1,IBNK2)              61244
       GO TO(20,21,22),IBNK2                                            61246
   20  WRITE OUTPUT TAPE  6,83
       WRITE OUTPUT TAPE 15,83
       WRITE OUTPUT TAPE  6,82
       WRITE OUTPUT TAPE 15,82
       GO TO 12                                                         61249
   21  WRITE OUTPUT TAPE  6,77,TBNK1,
      1(IBNK1(I),I=1,19)                                                61251
       WRITE OUTPUT TAPE 15,77,TBNK1,
2     1(IBNK1(I),I=1,19)
       GO TO 12                                                         61252
   22  WRITE OUTPUT TAPE  6,80,
      1(TBNK3(I),I=1,11)                                                61254
       WRITE OUTPUT TAPE 15,80,
      1(TBNK3(I),I=1,11)
   12  RETURN                                                           61255
```

```
   77 FORMAT(1H  E10.3,18A6,A1)                                          61256
   80 FORMAT(E20.3,10E10.3)                                              61257
   82 FORMAT(71H  SOLUTION OF LANDAU-LIFSHITZ EQUATION -- THIN FILM LONG
     1. PICKUP SIGNAL)
   83 FORMAT(1H1)
      DIMENSION IBNK1(19)                                                61259
      DIMENSION TBNK3(11)                                                61260
      END                                                                61261
*      BINARY                                                           0164
```

APPENDIX 8

Listing of program for computation of "unverse peaking time", three curve computer plot

```
INVERSE PEAKING TIME-BORSEI FILM
*      FORTRAN
       DIMENSION VAR(12),SYMBOL(10),XBETA(3),ALFT(3)
       EQUIVALENCE (VAR(3),PHI),(VAR(6),DPHI),(VAR(9),PSI),(VAR(12),DPSI)
       ZERO=0.
 1     READ INPUT TAPE 5,100,CAY,GAMMA,EM,ELAMS,ELAMDA,NRUNS
       PI = 3.14159265
       EPSLON = 4.*PI*EM**2/CAY
 100   FORMAT(F10.0,E10.2,F10.0,E10.2,E10.2,I10)
       BAC=2.*CAY/EM
       BAD=2.*CAY/(3.*ELAMS)
       CALL PREPAR(103,39,.03,-.03,2.96,-.08,0,0,1,120,6,0.,0.)
       NK=0
       DO 5 I=1,NRUNS
       READ INPUT TAPE 5,101,ALPHA,BETA,DELTA,PHI0,PHI,PSI,SYMBOL(I)
 101   FORMAT(F10.2,F10.2,F10.1,3F10.0,A6)
       PHI0D=PHI0*180./3.1416
       XBETA(I)=BETA
        READ INPUT TAPE 5,102,T0,DELTAT,TMAX,DELA
       SIM1=100000.
       NUTS=0
       NORK=0
       KI=0
  95   ALPHA=ALPHA-DELA
       IF (ABSF(ALPHA)-2.0) 96,96,51
  96   CONTINUE
 102   FORMAT(F10.0,F10.2,F10.0,F10.5)
       PSI=0.
       PHI=0.
       COM1=0.
       VAL1=0.005
       CALL FNIDE(DELTAT,T0,100,.006)
       C1=(2.*CAY*GAMMA*1.0E-9)/EM
       C2=(2.*CAY*ELAMDA*1.0E-9)/EM**2
 2     SPSI=SINF(PSI)
       CPSI=COSF(PSI)
       SPHI=SINF(PHI)
       CPHI=COSF(PHI)
       A1=ALPHA*SPHI-BETA*CPHI+DELTA*SINF(2.*PHI)/2.
      1+SINF(2.*(PHI-PHI0))/2.*COSF(PSI)
       A2=SPSI*(ALPHA*CPHI+BETA*SPHI-DELTA/2.*(SINF(PHI))**2)
       A3=SPSI*CPSI
       DPSI=C1*A1-C2*A2-C2*EPSLON*A3
       DPHI=-(C2*A1+C1*A2+C1*EPSLON*A3)/CPSI
       E1 =     SPHI*DPHI
 3     CALL FINTEG(DPSI,PSI)
       CALL FINTEG(DPHI,PHI)
       CALL FUPDAT(VAR,4,L1,T)
       GO TO (2,3,4,4,4),L1
```

```
  4  CONTINUE
  7  COM2=E1
     IF(ABSF(COM2)-ABSF(COM1))112,110,110
 110 COM1=COM2
119  IF(T-TMAX)3,223,223
112  IF(ABSF(COM1)-VAL1)119,119,114
114  TP=T-DELTAT
 115 TINV=1./TP
     CALL POINT(ALPHA,TINV,SYMBOL(I))
     IF(NUTS-3)1075,95,1075
1075 SIM2=TINV
     IF(SIM2-SIM1)108,117,109
 108 SIM1=SIM2
     KI=0
     NORK=0
      GO TO 95
117  SIM1=SIM2
     KI=KI+1
     NORK=2
     GO TO 95
109  IF(NORK-2)111,122,111
122  XKI=KI
     NK=NK+1
     ALFT(NK)=ALPHA+(XKI*DELA)/2.
     NUTS=3
     GO TO 95
 111 NK=NK+1
     ALFT(NK)=ALPHA
     NUTS=3
     GO TO 95
 13  FORMAT(20X,4HTINV,20X,5HALPHA)
 14  FORMAT(11X,E13.5,15X,E13.5)
 51  CONTINUE
5    CONTINUE
     CALL PLOT
     WRITE OUTPUT TAPE 6,653,EM,CAY,ELAMS,ELAMDA,GAMMA,DELTA,BAD,BAC,BA
    1C,BAC,PHI0D,XBETA,ALFT
     WRITE OUTPUT TAPE15,653,EM,CAY,ELAMS,ELAMDA,GAMMA,DELTA,BAD,BAC,BA
    1C,BAC,PHI0D,XBETA,ALFT
 653 FORMAT(50H  ORDINATES = 1/PEAKING TIME                          ,46X,3
    16HALPHA LONG. SWCH. FIELD (NORMALIZED)/14H  M(GAUSSES)= ,F5.0,19H
    2    K(ERGS/CCM) = ,F6.0/30H  LAMBDAS(MAGNETOSTRICTION) = ,E8.2,24H
    3  LAMBDA(DAMPING,CPS) = ,E8.2/22H  GAMMA(GYRO RATIO) = ,E9.3,10H
    4DELTA = ,F6.3,17H  SIGMA = (DELTA),E8.2/17H  HSWCH = (ALPHA),F5.2,
    525H           HPERP = (BETA),F5.2/16H HANIS = 2K/M = ,F5.2,40H
    6       PHI0D(INITIAL PHI,DEGREES) = ,F6.2/10H  BETA1 = ,F6.3,11H
    7 BETA2 = ,F5.3,11H   BETA3 = ,F6.3/10H  ALFT1 = ,F6.3,11H6  ALFT2
    8= ,F6.3,11H   ALFT3 = ,F6.3)
     GO TO 1
```

```
 223  CONTINUE
 227  FORMAT(34H            NO PEAKING FOR ALPHA = ,F6.3)
      GO TO 95
      END
*     FORTRAN                                                          0162
*TBP                                                                   0163
      SUBROUTINE TBP(TBNK1,TBNK2,TBNK3,TBNK4,IBNK1,IBNK2)              61244
      GO TO(20,21,22),IBNK2                                            61246
   20 WRITE OUTPUT TAPE  6,83
      WRITE OUTPUT TAPE 15,83
      WRITE OUTPUT TAPE  6,82
      WRITE OUTPUT TAPE 15,82
      GO TO 12                                                         61249
   21 WRITE OUTPUT TAPE  6,77,TBNK1,
     1(IBNK1(I),I=1,19)                                                61251
      WRITE OUTPUT TAPE 15,77,TBNK1,
     1(IBNK1(I),I=1,19)
      GO TO 12                                                         61252
   22 WRITE OUTPUT TAPE  6,80,
     1(TBNK3(I),I=1,11)                                                61254
      WRITE OUTPUT TAPE 15,80,
     1(TBNK3(I),I=1,11)
   12 RETURN                                                           61255
   77 FORMAT(1H  E10.3,18A6,A1)                                        61256
   80 FORMAT(E20.3,10E10.3)                                            61257
 82   FORMAT(15X,40HINVERSE PEAKING TIME VS. SWITCHING FIELD)
   83 FORMAT(1H1)                                                      61259
      DIMENSION IBNK1(19)                                              61260
      DIMENSION TBNK3(11)                                              61261
      END                                                              0164

*     BINARY
```

APPENDIX 9

Listing of program

for computation of "ferromagnetic resonant frequency",

three curve computer plot

```
FERROMAGNETIC RESONANT FREQUENCY-BORSEI FILM
*       FORTRAN
        DIMENSION VAR(12),SYMBOL(10)
        DIMENSION T(2),XDELTA(3)
        EQUIVALENCE (VAR(3),PHI),(VAR(6),DPHI),(VAR(9),PSI),(VAR(12),DPSI)
        ZERO=0.
 1      READ INPUT TAPE 5,100,CAY,GAMMA,EM,ELAMS,ELAMDA,NRUNS
        PI = 3.14159265
        EPSLON = 4.*PI*EM**2/CAY
 100    FORMAT(F10.0,E10.2,F10.0,E10.2,E10.2,I10)
        BAC=2.*CAY/EM
        BAD=2.*CAY/(3.*ELAMS)
        CALLPREPAR(103,39,.03,-.03,4.81,-.13,0,0,1,120,6,0.,0.)
        DO 5 I=1,NRUNS
        READ INPUT TAPE 5,101,ALPHA,BETA,DELTA,PHI0,PHI,PSI,SYMBOL(I)
 101    FORMAT(F10.2,F10.2,F10.1,3F10.0,A6)
        PHI0D=PHI0*180./3.1416
        XDELTA(I)=DELTA
         READ INPUT TAPE 5,102,T0,DELTAT,TMAX,DELA
  95    ALPHA=ALPHA-DELA
        JI=0
        IF (ABSF(ALPHA)-3.0) 96,96,51
  96    CONTINUE
 102    FORMAT(F10.0,F10.2,F10.0,F10.5)
        PSI=0.
        PHI=0.
        COM1=1.
        CALL FNIDE(DELTAT,T0,100,.006)
        C1=(2.*CAY*GAMMA*1.0E-9)/EM
        C2=(2.*CAY*ELAMDA*1.0E-9)/EM**2
 2      SPSI=SINF(PSI)
        CPSI=COSF(PSI)
        SPHI=SINF(PHI)
        CPHI=COSF(PHI)
        A1=ALPHA*SPHI-BETA*CPHI+DELTA*SINF(2.*PHI)/2.
       1+SINF(2.*(PHI-PHI0))/2.*COSF(PSI)
        A2=SPSI*(ALPHA*CPHI+BETA*SPHI-DELTA/2.*(SINF(PHI))**2)
        A3=SPSI*CPSI
        DPSI=C1*A1-C2*A2-C2*EPSLON*A3
        DPHI=-(C2*A1+C1*A2+C1*EPSLON*A3)/CPSI
        E1=DPHI
 3      CALL FINTEG(DPSI,PSI)
        CALL FINTEG(DPHI,PHI)
        CALL FUPDAT(VAR,4,L1,TX)
        GO TO (2,3,4,4,4),L1
   4    CONTINUE
        COM2=E1
 976    IF(COM1*COM2)977,977,333
 333    COM1=COM2
```

```
      IF(TX-TMAX)335,223,223
  335 GO TO 3
  977 JI=JI+1
  978 T(JI)=TX-DELTAT
      IF(2-JI)979,979,333
  979 TT=T(2)-T(1)
      TMC=1./(2.*TT)
      CALL POINT(ALPHA,TMC,SYMBOL(I))
      GO TO 95
   13 FORMAT(20X,3HTMC,20X,5HALPHA)
   14 FORMAT(11X,E13.5,15X,E13.5)
   51 CONTINUE
    5 CONTINUE
      CALL PLOT
      WRITE OUTPUT TAPE 6,653,EM,CAY,ELAMS,ELAMDA,GAMMA,BAC,BAC,BAD,BAC,
     1PHIOD,XDELTA,BETA
      WRITE OUTPUT TAPE15,653,EM,CAY,ELAMS,ELAMDA,GAMMA,BAC,BAC,BAD,BAC,
     1PHIOD,XDELTA,BETA
  653 FORMAT(66H                                    ALPHA = LONG.SWCH.FIELD (N
     1ORMALIZED)/43HORDINATES = FERROMAG. RES. FREQUENCY (KMC) /13HM(GAU
     2SSES) = ,F5.0,19H     K(ERGS/CCM) = ,F6.0/28HLAMBDAS(MAGNETOSTRICT
     3ION) = ,E8.2,24H  LAMBDA(DAMPING,CPS) = ,E8.2/20HGAMMA(GYRO RATIO)
     4 = ,E9.3/17H  HSWCH = (ALPHA),F5.2,17H   HPERP = (BETA),F5.2,19H
     5  SIGMA = (DELTA),E8.2/17H  HANIS = 2K/M = ,F5.2,32H   PHIOD(INITI
     6AL PHI,DEGREES) = ,F6.2/9HDELTA1 = ,F6.3,17H        DELTA2 = ,F6.3
     7,19H          DELTA3 = ,F6.3,17H          BETA = ,F6.3)
      GO TO 1
  223 CONTINUE
  227 FORMAT(48H           NO FERROMAG. OSCILLATION FOR ALPHA = ,F6.3)
      GO TO 95
      END
*     FORTRAN                                                          0162
*TBP                                                                   0163
      SUBROUTINE TBP(TBNK1,TBNK2,TBNK3,TBNK4,IBNK1,IBNK2)              61244
      GO TO(20,21,22),IBNK2                                            61246
   20 WRITE OUTPUT TAPE  6,83
      WRITE OUTPUT TAPE 15,83
      WRITE OUTPUT TAPE  6,82
      WRITE OUTPUT TAPE 15,82
      GO TO 12                                                         61249
   21 WRITE OUTPUT TAPE  6,77,TBNK1,
     1(IBNK1(I),I=1,19)                                                61251
      WRITE OUTPUT TAPE 15,77,TBNK1,
     1(IBNK1(I),I=1,19)
      GO TO 12                                                         61252
   22 WRITE OUTPUT TAPE  6,80,
     1(TBNK3(I),I=1,11)                                                61254
      WRITE OUTPUT TAPE 15,80,
     1(TBNK3(I),I=1,11)
```

```
   12 RETURN                                                              61255
   77 FORMAT(1H  E10.3,18A6,A1)                                           61256
   80 FORMAT(E20.3,10E10.3)                                               61257
82    FORMAT(15X,52HFERROMAGNETIC RESONANT FREQUENCY VS. SWITCHING FIELD
     1)
   83 FORMAT(1H1)                                                         61259
      DIMENSION IBNK1(19)                                                 61260
      DIMENSION TBNK3(11)                                                 61261
      END                                                                 0164
*     BINARY
```

APPENDIX 10

Listing of program

for computation of dynamic critical switching curve, three curve computer plot with ϕ_o or δ as a parameter

```
DYNAMIC SWITCHING CURVE-BORSEI FILM PHI
*       FORTRAN
        DIMENSION VAR(12),SYMBOL(10),XPHI0D(3)
        EQUIVALENCE (VAR(3),PHI),(VAR(6),DPHI),(VAR(9),PSI),(VAR(12),DPSI)
        ZERO=0.
 1      READ INPUT TAPE 5,100,CAY,GAMMA,EM,ELAMS,ELAMDA,NRUNS
        PI = 3.14159265
        EPSLON = 4.*PI*EM**2/CAY
 100    FORMAT(F10.0,E10.2,F10.0,E10.2,E10.2,I10)
        BAC=2.*CAY/EM
        BAD=2.*CAY/(3.*ELAMS)
        CALLPREPAR(103,39,.02,-.02,2.22,-.06,0,0,1,120,6,0.,0.)
        DO 5  I=1,NRUNS
        READ INPUT TAPE 5,101,XALPHA,BETA,DELTA,PHI0,PHI,PSI,SYMBOL(I)
  101   FORMAT(F10.2,F10.2,F10.1,3F10.0,A6)
        PHI0D=PHI0*180./3.1416
        XPHI0D(I)=PHI0D
         READ INPUT TAPE 5,102,T0,DELTAT,TMAX,DELA,DELB
 69     SIM1=10000.
        KI=0
        NORK=0
        ALPHA=-0.05
        ALPHA=XALPHA+DELA
  95    ALPHA=ALPHA-DELA
        IF(ABSF(ALPHA)-2.0)96,96,277
  96    CONTINUE
  102   FORMAT(F10.0,F10.2,F10.0,2F10.5)
        VAL1=0.005
        COM1=0.
        PSI=0.
        PHI=0.
        CALL FNIDE(DELTAT,T0,100,.006)
        C1=(2.*CAY*GAMMA*1.0E-9)/EM
        C2=(2.*CAY*ELAMDA*1.0E-9)/EM**2
 2      SPSI=SINF(PSI)
        CPSI=COSF(PSI)
        SPHI=SINF(PHI)
        CPHI=COSF(PHI)
        A1=ALPHA*SPHI-BETA*CPHI+DELTA*SINF(2.*PHI)/2.
       1+SINF(2.*(PHI-PHI0))/2.*COSF(PSI)
        A2=SPSI*(ALPHA*CPHI+BETA*SPHI-DELTA/2.*(SINF(PHI))**2)
        A3=SPSI*CPSI
        DPSI=C1*A1-C2*A2-C2*EPSLON*A3
        DPHI=-(C2*A1+C1*A2+C1*EPSLON*A3)/CPSI
        E1 =     SPHI*DPHI
 3      CALL FINTEG(DPSI,PSI)
        CALL FINTEG(DPHI,PHI)
        CALL FUPDAT(VAR,4,L1,T)
        GO TO (2,3,4,4,4),L1
```

```
   4  CONTINUE
   7 COM2=E1
 109 IF(ABSF(COM2)-ABSF(COM1))123,110,110
 110 COM1=COM2
151  IF(T-TMAX)3,144,144
144  CONTINUE
147  FORMAT(34H            NO PEAKING FOR ALPHA = ,F6.3,9H  BETA = ,F6.3
    1,10H  DELTA = ,F6.3)
     GO TO 95
123  IF(ABSF(COM1)-ABSF(VAL1))151,151,114
114  TP=T-DELTAT
 115 TINV=1./TP
     SIM2=TINV
     IF(SIM2-SIM1)108,117,119
117  SIM1=SIM2
     KI=KI+1
     NORK=2
     GO TO 95
119  IF(NORK-2)111,122,111
122  XKI=KI
     ALFT=ALPHA+(XKI*DELA)/2.
     GO TO 121
 108 SIM1=SIM2
     KI=0
     NORK=0
     GO TO 95
 111 ALFT=ALPHA+DELA
121  CALL POINT(ALFT,BETA,SYMBOL(I))
112  CONTINUE
143  BETA=BETA+DELB
     IF(BETA-2.)69,69,51
  13 FORMAT(20X,4HBETA,20X,4HALFT)
 14  FORMAT(11X,E13.5,15X,E13.5)
 51  CONTINUE
 55  CONTINUE
5    CONTINUE
     CALL PLOT
     WRITE OUTPUT TAPE 6,653,EM,CAY,ELAMS,ELAMDA,GAMMA,BAC,BAC,BAD,BAC,
    1DELTA,XPHIOD
     WRITE OUTPUT TAPE15,653,EM,CAY,ELAMS,ELAMDA,GAMMA,BAC,BAC,BAD,BAC,
    1DELTA,XPHIOD
 653 FORMAT(64H                              SWITCHING FIELD THRESHOLD (NORM
    1ALIZED) /39H  ORDINATES = PERP. FIELD (NORMALIZED) /14H  M(GAUSSES
    2) =,F5.0,19H      K(ERGS/CCM) = ,F6.0/30H  LAMBDAS(MAGNETOSTRICTION
    3) = ,E8.2,24H  LAMBDA(DAMPING,CPS) = ,E8.2/22H  GAMMA(GYRO RATIO)
    4= ,E9.3/17H  HSWCH = (ALPHA),F5.2,17H   HPERP = (BETA),F5.2,18H
    5SIGMA = (DELTA),E8.2/17H  HANIS = 2K/M = ,F5.2,11H   DELTA = ,F6.3
    6/10H  PHIOD1= ,F6.2,16H        PHIOD2= ,F6.2,16H       PHIOD3 = ,F
    76.2)
```

```
      GO TO 1
  277 CONTINUE
  281 FORMAT(30H           NO ALFT FOR BETA = ,F6.3,10H  DELTA = ,F6.3)
      GO TO 143
      END
*     FORTRAN                                                          0162
*TBP                                                                   0163
      SUBROUTINE TBP(TBNK1,TBNK2,TBNK3,TBNK4,IBNK1,IBNK2)              61244
      GO TO(20,21,22),IBNK2                                            61246
   20 WRITE OUTPUT TAPE  6,83
      WRITE OUTPUT TAPE 15,83
      WRITE OUTPUT TAPE  6,82
      WRITE OUTPUT TAPE 15,82
      GO TO 12                                                         61249
   21 WRITE OUTPUT TAPE  6,77,TBNK1,
     1(IBNK1(I),I=1,19)                                                61251
      WRITE OUTPUT TAPE 15,77,TBNK1,
     1(IBNK1(I),I=1,19)
      GO TO 12                                                         61252
   22 WRITE OUTPUT TAPE  6,80,
     1(TBNK3(I),I=1,11)                                                61254
      WRITE OUTPUT TAPE 15,80,
     1(TBNK3(I),I=1,11)
   12 RETURN                                                           61255
   77 FORMAT(1H  E10.3,18A6,A1)                                        61256
   80 FORMAT(E20.3,10E10.3)                                            61257
  82  FORMAT(15X,32HDYNAMIC CRITICAL SWITCHING CURVE)
   83 FORMAT(1H1)                                                      61259
      DIMENSION IBNK1(19)                                              61260
      DIMENSION TBNK3(11)                                              61261
      END                                                              0164
*     BINARY
```

```
DYNAMIC SWITCHING CURVE-BORSEI FILM DELTA
*       FORTRAN
        DIMENSION VAR(12),SYMBOL(10),XDELTA(3)
        EQUIVALENCE (VAR(3),PHI),(VAR(6),DPHI),(VAR(9),PSI),(VAR(12),DPSI)
        ZERO=0.
 1      READ INPUT TAPE 5,100,CAY,GAMMA,EM,ELAMS,ELAMDA,NRUNS
        PI = 3.14159265
        EPSLON = 4.*PI*EM**2/CAY
 100    FORMAT(F10.0,E10.2,F10.0,E10.2,E10.2,I10)
        BAC=2.*CAY/EM
        BAD=2.*CAY/(3.*ELAMS)
        CALLPREPAR(103,39,.02,-.02,2.22,-.06,0,0,1,120,6,0.,0.)
        DO 5   I=1,NRUNS
        READ INPUT TAPE 5,101,XALPHA,BETA,DELTA,PHI0,PHI,PSI,SYMBOL(I)
  101   FORMAT(F10.2,F10.2,F10.1,3F10.0,A6)
        PHI0D=PHI0*180./3.1416
        XDELTA(I)=DELTA
         READ INPUT TAPE 5,102,T0,DELTAT,TMAX,DELA,DELB
 69     SIM1=10000.
        KI=0
        NORK=0
        ALPHA=-0.05
        ALPHA=XALPHA+DELA
  95    ALPHA=ALPHA-DELA
        IF(ABSF(ALPHA)-2.0)96,96,277
  96    CONTINUE
  102   FORMAT(F10.0,F10.2,F10.0,2F10.5)
        VAL1=0.005
        COM1=0.
        PSI=0.
        PHI=0.
        CALL FNIDE(DELTAT,T0,100,.006)
        C1=(2.*CAY*GAMMA*1.0E-9)/EM
        C2=(2.*CAY*ELAMDA*1.0E-9)/EM**2
 2      SPSI=SINF(PSI)
        CPSI=COSF(PSI)
        SPHI=SINF(PHI)
        CPHI=COSF(PHI)
        A1=ALPHA*SPHI-BETA*CPHI+DELTA*SINF(2.*PHI)/2.
       1+SINF(2.*(PHI-PHI0))/2.*COSF(PSI)
        A2=SPSI*(ALPHA*CPHI+BETA*SPHI-DELTA/2.*(SINF(PHI))**2)
        A3=SPSI*CPSI
        DPSI=C1*A1-C2*A2-C2*EPSLON*A3
        DPHI=-(C2*A1+C1*A2+C1*EPSLON*A3)/CPSI
        E1 =     SPHI*DPHI
 3      CALL FINTEG(DPSI,PSI)
        CALL FINTEG(DPHI,PHI)
        CALL FUPDAT(VAR,4,L1,T)
        GO TO (2,3,4,4,4),L1
```

```
   4  CONTINUE
   7 COM2=E1
 109 IF(ABSF(COM2)-ABSF(COM1))123,110,110
 110 COM1=COM2
151  IF(T-TMAX)3,144,144
144  CONTINUE
147  FORMAT(34H            NO PEAKING FOR ALPHA = ,F6.3,9H  BETA = ,F6.3
    1,10H  DELTA = ,F6.3)
     GO TO 95
123  IF(ABSF(COM1)-ABSF(VAL1))151,151,114
114  TP=T-DELTAT
 115 TINV=1./TP
     SIM2=TINV
     IF(SIM2-SIM1)108,117,119
117  SIM1=SIM2
     KI=KI+1
     NORK=2
     GO TO 95
119  IF(NORK-2)111,122,111
122  XKI=KI
     ALFT=ALPHA+(XKI*DELA)/2.
     GO TO 121
 108 SIM1=SIM2
     KI=0
     NORK=0
     GO TO 95
 111 ALFT=ALPHA+DELA
121  CALL POINT(ALFT,BETA,SYMBOL(I))
112  CONTINUE
143  BETA=BETA+DELB
     IF(BETA-2.)69,69,51
  13 FORMAT(20X,4HBETA,20X,4HALFT)
 14  FORMAT(11X,E13.5,15X,E13.5)
 51  CONTINUE
 55  CONTINUE
5    CONTINUE
     CALL PLOT
     WRITE OUTPUT TAPE 6,653,EM,CAY,ELAMS,ELAMDA,GAMMA,BAC,BAC,BAD,BAC,
    1PHIOD,XDELTA
     WRITE OUTPUT TAPE15,653,EM,CAY,ELAMS,ELAMDA,GAMMA,BAC,BAC,BAD,BAC,
    1PHIOD,XDELTA
 653 FORMAT(64H                                SWITCHING FIELD THRESHOLD (NORM
    1ALIZED) /39H  ORDINATES = PERP. FIELD (NORMALIZED) /14H  M(GAUSSES
    2) =,F5.0,19H     K(ERGS/CCM) = ,F6.0/30H  LAMBDAS(MAGNETOSTRICTION
    3) = ,E8.2,24H  LAMBDA(DAMPING,CPS) = ,E8.2/22H  GAMMA(GYRO RATIO)
    4= ,E9.3/17H  HSWCH = (ALPHA),F5.2,17H   HPERP = (BETA),F5.2,18H
    5SIGMA = (DELTA),E8.2/17H  HANIS = 2K/M = ,F5.2,32H   PHIOD(INITIAL
    6 PHI,DEGREES) = ,F6.2/11H  DELTA1 = ,F6.3,17H         DELTA2 = ,F6.
    73,16H       DELTA3 = ,F6.3)
```

```
      GO TO 1
  277 CONTINUE
  281 FORMAT(30H           NO ALFT FOR BETA = ,F6.3,10H  DELTA = ,F6.3)
      GO TO 143
      END
*     FORTRAN                                                          0162
*TBP                                                                   0163
      SUBROUTINE TBP(TBNK1,TBNK2,TBNK3,TBNK4,IBNK1,IBNK2)              61244
      GO TO(20,21,22),IBNK2                                            61246
   20 WRITE OUTPUT TAPE  6,83
      WRITE OUTPUT TAPE 15,83
      WRITE OUTPUT TAPE  6,82
      WRITE OUTPUT TAPE 15,82
      GO TO 12                                                         61249
   21 WRITE OUTPUT TAPE  6,77,TBNK1,
     1(IBNK1(I),I=1,19)                                                61251
      WRITE OUTPUT TAPE 15,77,TBNK1,
     1(IBNK1(I),I=1,19)
      GO TO 12                                                         61252
   22 WRITE OUTPUT TAPE  6,80,
     1(TBNK3(I),I=1,11)                                                61254
      WRITE OUTPUT TAPE 15,80,
     1(TBNK3(I),I=1,11)
   12 RETURN                                                           61255
   77 FORMAT(1H  E10.3,18A6,A1)                                        61256
   80 FORMAT(E20.3,10E10.3)                                            61257
  82  FORMAT(15X,32HDYNAMIC CRITICAL SWITCHING CURVE)
   83 FORMAT(1H1)                                                      61259
      DIMENSION IBNK1(19)                                              61260
      DIMENSION TBNK3(11)                                              61261
      END                                                              0164
*     BINARY
```

APPENDIX 11

Absolute chemical analysis of thin films

I. Iron Analysis

Reagents

1. Chloride Buffer

   16.2ml conc. HC1 and 23.3gms KC1 per one liter of distilled water.

2. Thiocyanate - Acetone solution

   Add 150ml acetone and 20 gm NH_4SCN in 250 ml volumetric flask and bring up to the mark with distilled water.

Procedures

1. Heat to dissolve the thin-film material on a sample glass-slide specimen, size approximately 4 cm^2, in approximately 1/2 cc of conc. HNO_3.
2. Carefully heat to near dryness with constant shaking.
3. Add approximately 8 cc of distilled water (save 3 cc for the nickel analysis).
4. Pipet exactly 1 cc (or some other appropriate volume) into a 25 ml volumetric flask.
5. Add 5cc buffer solution and 5 cc Thiocyanate - Acetone solution. Bring up to the mark with distilled water.

6. Run a blank.
7. Read the optical density at 520 mc, using the blank as a reference.
8. Calculations:

   Opt. Dens. x 64.4 = μgm Iron

   $\frac{(\mu\text{gm Iron})}{\text{Sample volume}}$ = μgm Iron per ml sample.

II. Nickel Analysis

Reagents

1. 20% Tartaric acid
2. 2% $K_2S_2O_4$
3. 50% Nitric acid
4. 6N N_aOH
5. 1% Dimethyl-glyoxime (in methyl alcohol or ethanol)

Procedure

In 25 ml volumetric flask

1. Sample size 25-75 μgm 1cc.
2. Add sample (1cc) to vol. flask.
3. Add 2cc. tartaric acid, 2cc $K_2S_2O_8$, 5cc 6N N_aOH and 2cc dimethy-glyoxime.
4. Heat for two minutes at 60-70°C; cool and add water to mark.
5. Read at 530 mc using a reagent blank.

   Calculation opt. dens. x 69 = μgm Ni

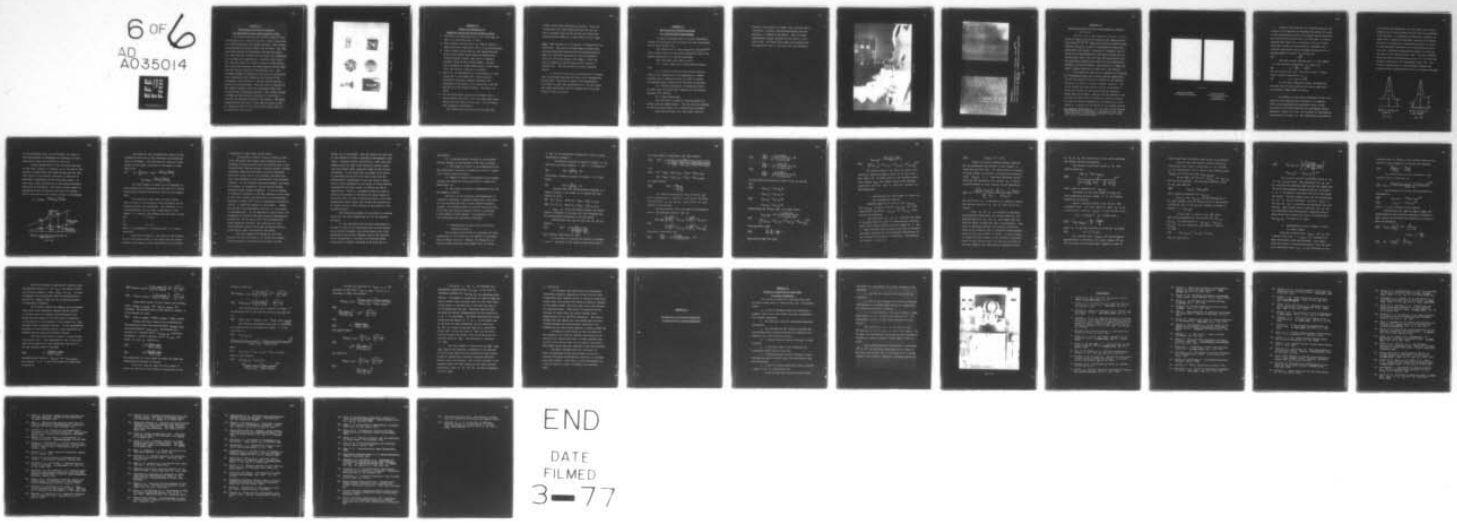
$$\frac{\mu gm\ Nickel}{Sample\ volume} = \mu gm\ Ni\ per\ ml\ sample.$$

$$\frac{[\mu gm\ Fe/ml] \times 100}{[\mu gm\ Fe/ml] + [\mu gm\ Ni/ml]} = \%\ Fe$$

$$\frac{[\mu gm\ Ni/ml] \times 100}{[\mu gm\ Fe/ml] + [\mu gm\ Ni/ml]} = \%\ Ni$$

AD-A035 014 CALIFORNIA UNIV LOS ANGELES DEPT OF ENGINEERING F/G 20/2
ON THE USE OF PIEZOELECTRIC-MAGNETOSTRICTIVE COUPLING IN DIGITA--ETC(U)
AUG 62 A A BORSEI NONR-233(52)
UNCLASSIFIED UCLA62-37 NL

6 OF 6
AD
A035014



END

DATE
FILMED
3-77

APPENDIX 12

Description of probe to determine the direction of the earth's magnetic field

In order to position the earth's magnetic field cancellation coils shown in Fig. A6, a device consisting of a small plexiglass air turbine driving a small pickup coil has been constructed (Figs. A9a and A9b). Fig. A9b shows the turbine air distributor and the back plate, Fig. A9a shows the turbine with the small coil terminated by two rings and supported by a stainless steel shaft. Fig. A9a also shows the turbine casing in which exhaust ducts have been machined and supporting two brushes which pick off the emf induced in the rotating coil. The assembled turbine is mounted at the end of a long plastic tube, connected to the compressed air system of the laboratory, and containing a coaxial cable to be connected to an oscilloscope. When the tube is parallel to the earth's magnetic field the sinusoidal signal displayed on the oscilloscope vanishes. The turbine rotates at 20000 rpm and the local direction of the earth's field may be determined within a few degrees. The power supply feeding the coils is then adjusted until a compass needle located at the loop tester pickup coils is in indifferent equilibrium.

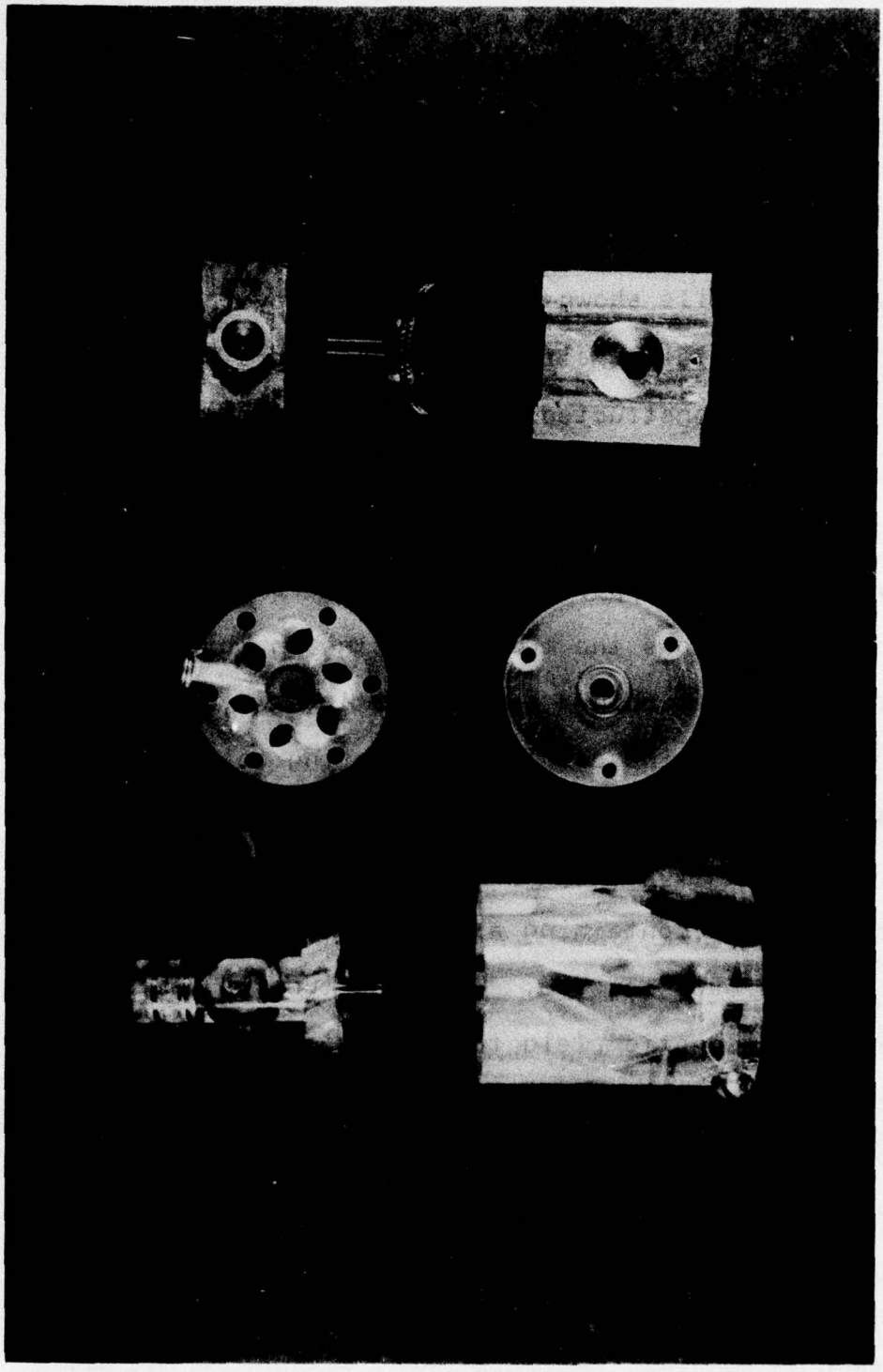


Fig. A9a Fig. A9b Fig. A9c

APPENDIX 13

Method of preparation of magnetite colloid for Bitter pattern studies

1. Dissolve 2 gr $FeCl_2.4H_2O$ and 5.4 gr. $FeCl_3.6H_2O$ in 300 cc of distilled water at 70°C.
2. With constant stirring add 5 gr. NaOH in pellets which have been dissolved in 50 cc of distilled water.
3. Using a paper filter separate the liquid from the muddy black deposit which should be washed with distilled water several times until it becomes neutral (check Ph with litmus paper). The best way of washing is to keep adding water to the filter until the neutral condition is obtained.
4. Add 2 gr. of Dodecylamine to 16 milliliters of one-normal HCl (a one-normal HCl solution may be obtained by diluting standard laboratory Hcl according to the ratio 11 vol. water per 1 vol HCl. Add 20 cc of the washed filtrate. Add 150 cc of water.
5. Put the black heavy liquid thus obtained into a Waring Blender and beat it at slow speed until foam reaches the top (about 20 minutes). Let set until foam disappears (overnight).

The colloid may be tested now on a thin film

using a dark field microscope, possibly. Since the colloid may still have large particles one may add 200 cc of water, let set for one day and decant the large particles which go to the surface of the liquid.

Note: When testing it is convenient to demagnetize the film first. This may be accomplished by magnetizing the film along the direction of hard magnetization by means of a DC field supplied by a pair of Helmoltz coils in a B-H loop tester, for example. After the film is magnetized the DC supply plate voltage is switched off. The film breaks into many elongated domains.

If the film domain wall coercive force is larger than the maximum available DC field, an AC demagnetizer may be used. The field is held in the demagnetizer coil with its hard axis perpendicular to the coil plane and slowly moved away from the demagnetizer along the normal to the coil plane.

APPENDIX 14

Description of Tolansky's method for film thickness measurements

A simple instrumentation to obtain interference fringes for measuring film thickness has been constructed and is shown in Fig. A10.

The method used is that proposed by Tolansky[37,38] and is widely known for measuring thicknesses from a few hundred Angstroms up to several thousands.

Fig. A10 shows from right to left:

a) A power supply for a high pressure mercury lamp.

b) A 100 watt high pressure mercury lamp enclosed in an aluminum box, and supported by a holder provided with a spherical mirror in order to obtain the maximum light intensity into the Leitz microscope.

c) A holder supporting a 77A Wratten filter to admit only the green light component of the mercury spectrum (λ = 5460 Å).

d) A Leitz microscope.

Fig. A2 shows a closeup of the microscope objective and the sample holder. The two coils are mounted on the microscope holder for studying Bitter patterns.

Near the left hand coil, the holder used for

thickness measurements is shown. The silvered film is covered by a dichroic semi-silvered mirror and this ensemble is clamped in the holder. Fig. A11 shows interference fringes obtained in the case of a circular film. The figure also shows the procedure and the expression used to calculate the film thickness.

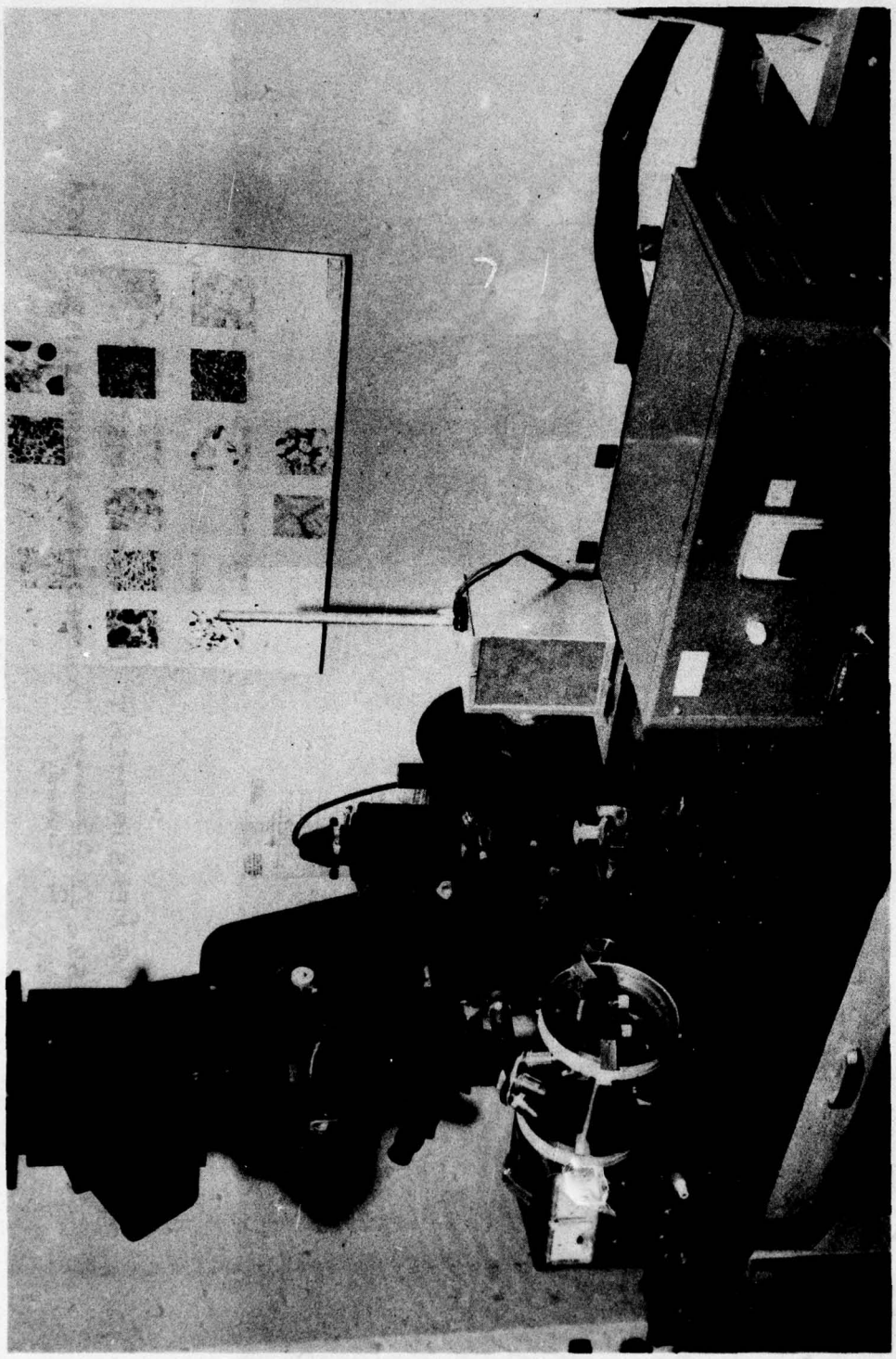
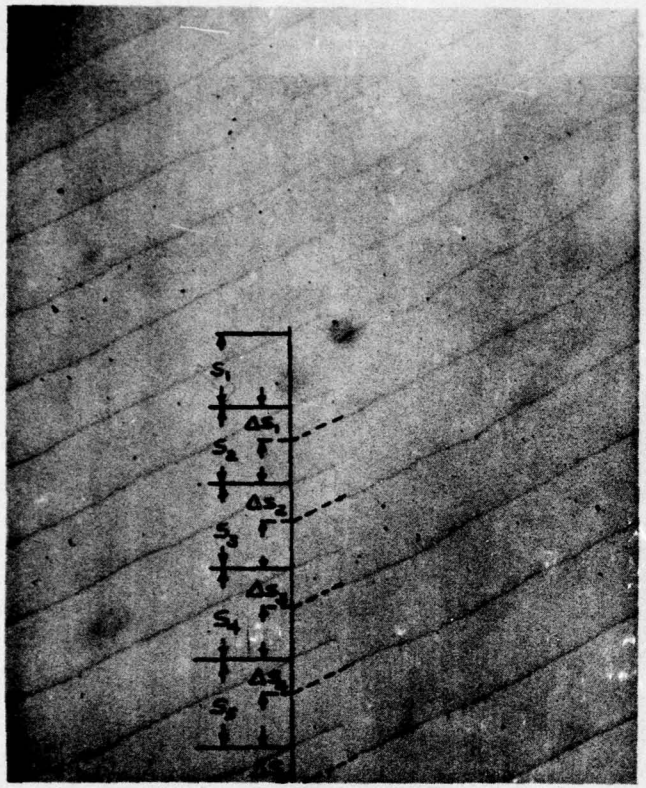
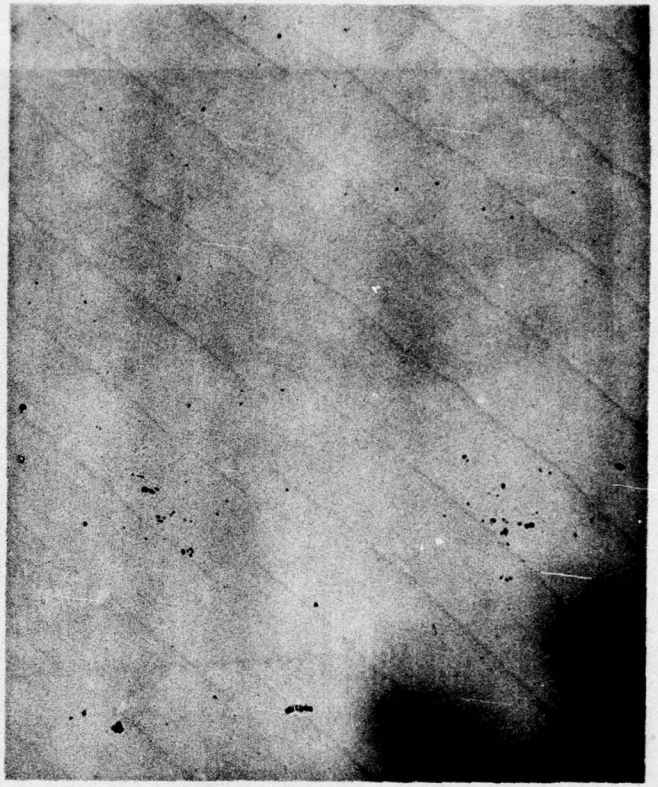


Fig. A10





APPENDIX 14

FILM THICKNESS MEASUREMENT (TOLANSKY METHOD[37.38])

FILM THICKNESS = $\frac{\lambda}{2} \frac{\Delta S_{average}}{S_{average}}$, $\lambda = 5460 Å \pm 4\%$, EXAMPLE: $1290 Å \pm 45 Å$

Fig. A11

APPENDIX 15*

Statistical errors in X-ray spectrochemical analysis

1. Introduction

Non-destructive spectrochemical analysis of thin films is widely used for determining the composition of thin films.[82, 83, 84] Compared to the wet chemical quantitative analysis, it has the advantages of being non-destructive and faster. Exposure of a magnetic film to X-rays for a few minutes does not alter visibly the coercive force (Fig. A12), and once the fluorescence unit and recording equipment have been set for quantitative analysis of certain elements, processing of a sample becomes a simple operation lasting only a few minutes.

This method of analysis is, however, not absolute, as it determines only the relative percent composition and not the absolute content by weight of the elements involved, as given by a purely chemical analysis. The latter method has been used by several researchers to check the accuracy of the spectrochemical analysis. Rhodin has, for example, compared the two methods in the analysis of thin films of austenitic stainless alloys. He found excellent agreement with differences of a few tenths of a percent of the amount of any element present and standard deviations of less than 5% for both methods.

*The numbers of the equations in Appendix 15 are underlined in order to distinguish them from those in the main body of the dissertation.

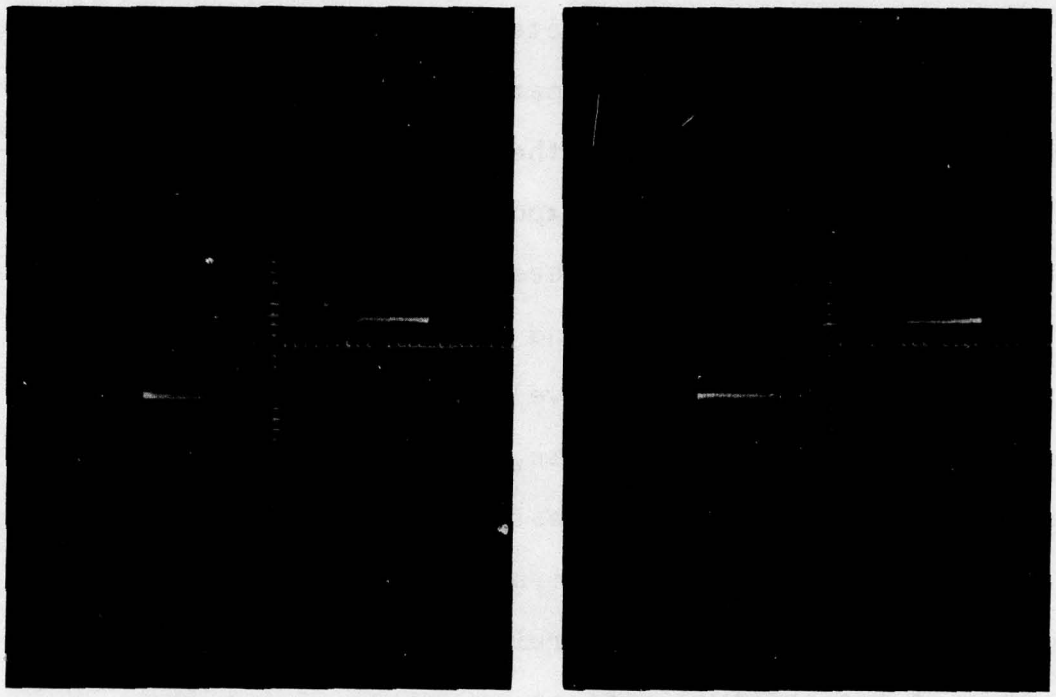


Fig. A12

Hysteresis loop of 80-20
Ni-Fe film before X-ray exposure

Hysteresis loop after
3 min. film exposure to X-rays.
45 ma 50 KV
Machlett AEG 50 Tube

Because X-ray emission is a Gaussian process, the accuracy to be expected in measuring the number of counts at the characteristic line of an element may be predicted and controlled by proper choice of the number of counts. Assuming that there are no systematic errors or deviations due to drift in the electronic equipment, the absolute statistical errors (standard deviation) on an average number of counts $\bar{N}$ is given by:

(1) $$s = \sqrt{\bar{N}}$$

The error in the counting rate $n = N/t$, where t is the time for accumulating N counts, is:

(2) $$s_n = \sqrt{N}/t = \sqrt{n/t}$$

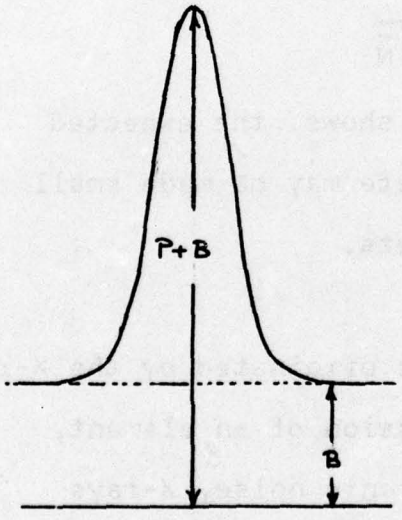
and the relative per unit statistical error S (fractional standard deviation), is:

(3) $$s_n = s_n/n = 1/\sqrt{\bar{N}}$$

As the latter expression shows, the expected relative error on the counting rate may be made small by choosing a high number of counts.

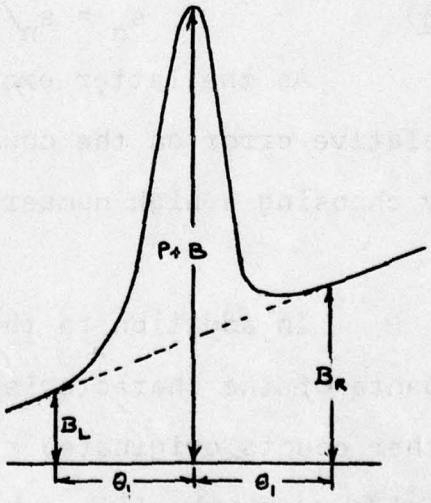
In addition to the counts originated by the X-ray quanta of the characteristic emission of an element, other counts originated by electronic noise, X-rays scattered by the film substrate and surrounding instrumentation, cosmic rays, etc. are included in the observed total number of counts N. This undesirable contribution

constitutes the background, and its effect may be minimized by use of pulse height analysis and low scattering film substrate. A background reading must, however, be taken, and a complete measurement consists of recording the time to accumulate a predetermined number of counts at the goniometer position of the characteristic emission and a different predetermined number of counts on any side of the characteristic line. The first reading gives the "Peak-plus-Background level" (P + B) while the second reading gives the "Background level" (B). The desired counting rate is the difference between the counting rates corresponding to the two readings (Fig.A13).



Element counting rate
$(P+B)-B$

Fig. A13



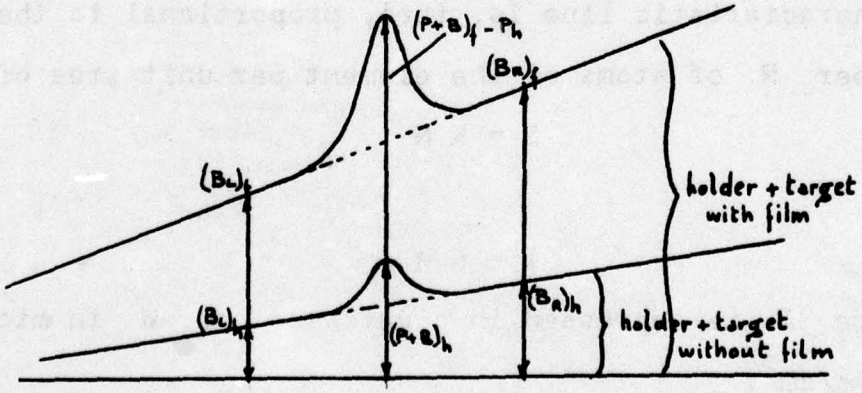
Element counting rate
$(P+B)-\frac{B_L+B_R}{2}$

Fig. A14

If the background level is not constant, its value at the peak position is determined by averaging two readings, one on each side (Fig.A14) of the peak.

In the determination of the counting rates due to very small amounts of elements, as is the case in the analysis of thin films, the sample holder used may contain traces of the elements involved, or these may be contained as impurities in the X-ray tube target. In such cases, their contribution to the observed counting rates must be determined. The holder without sample is introduced in the fluorescence unit and the counting rate of the amount of the element present is determined:

$$P_t = (P+B)_h - \frac{(P+B_L)_h + (P+B_R)_h}{2}$$



Element being analyzed present as holder and target impurities

Fig. A15

The sample is then inserted and, because of the scattering effect due to the substrate, the background level is different. The counting rate relative to the amount of the element contained in the sample is then (Fig. A15):

$$(4) \qquad P_f = \left\{ \left[(P+B_f) + P_h \right] - \frac{(B_L)_f + (B_R)_f}{2} \right\} - \left[(P+B)_h - \frac{(B_L)_t + (B_R)_h}{2} \right]$$

The total number of counts to be accumulated at each reading must be determined on the basis of a chosen desired final expected statistical error on the composition.

The analysis of thin films by X-ray fluorescence is based on the assumption that absorption and enhancement effects are negligible. The intensity, I, of a characteristic line is, then, proportional to the number N of atoms of the element per unit area of film:

$$(5) \qquad I = K N$$

or

$$(6) \qquad I = K W$$

where I is expressed in counts/sec and W in micrograms/cm^2.

Under this assumption the atoms of each element in the film absorb primary X-ray quanta and emit characteristic X-ray quanta without influencing the absorption

or emission of other atoms in the matrix.

If one were to direct a beam of primary X-rays on an infinitely thin sample whose thickness kept increasing, one would notice that the counting rate of the characteristic emission becomes constant beyond a certain thickness, which has been named "critical thickness". Below this value, and as the thickness increases from zero, the intensity of the characteristic line increases linearly. As the thickness increases further, the intensity assumes an exponential law and finally becomes constant beyond critical thickness. If one is willing to tolerate a deviation of 1% from linearity as the limit of the linear region, one finds that the corresponding thickness is about 10^{-5} cm for an exponential constant of 1000 p, p being the density of the element. Rhodin has plotted, from experimental results, surface density in micrograms/cm^2. In the experiments reported here, the assumption of linearity has been observed experimentally to hold for Ni, Fe, up to about 180 micrograms/cm^2, within graphical accuracy. The statistics of X-ray spectrochemical analysis have been discussed previously by Parrish, Mack and Spielberg and others.

The same concepts are applied to thin film analysis for the case where small amounts of elements being analyzed are considered to be present in the

holder and in the target. This was found to be the case in the analysis of Fe-Ni contained in ferromagnetic thin films. A special holder covered with a 1/16" very pure Cadmium plate was made after discarding several other very pure metals which contained larger traces of iron and nickel. It was found that the amount of Fe and Ni in the holder and in the X-ray tube target gave net characteristic intensities of the same order of magnitude as those originated by the amount of these elements contained in the films alone, for 10% Fe and 10% Ni compositions. Finally, a graphical method was used to speed up the process of selecting the proper number of counts in order to reach a certain accuracy in the final composition, while taking into account the discrete set of values of total count settings on the console of the counter-recorder.

The following procedure is considered in reaching values for the final composition and for the expected accuracy:

a) The expression for the final composition is written in terms of the proportionality factors between characteristic intensity and surface density for films evaporated from the pure elements, and of the characterictic intensities of the film to be analyzed (peak, background for element contained in the film and in

the target).

b) A desired overall accuracy of the measured percent contents of one element in the film is chosen.

c) The number of counts to be accumulated in all the observations involved is computed in order to guarantee a certain desired accuracy.

d) Number of counts corresponding to the counter settings are chosen as close as possible to those computed under (c).

e) The overall accuracy is redetermined from the new number of counts.

The drift in the electronic instrumentation is recorded by inserting a standard sample every five minutes and recording the time of each standard intensity reading. The intensity drift is plotted versus the time of the day and the best straight line fit is obtained by the method of least squares. The readings on the film intensities are corrected accordingly.

.2 Determination of composition with preset statistical error.

The procedure illustrated for obtaining the final compositions in thin films will be applied to the binary alloy of Nickel and Iron. However, for generality in treating binary mixtures, the elements will be called

X and Y, and the method outlined will refer to these hypothetical elements.

The percent contents by weight of element X in the film containing elements X and Y is defined as:

$$(7) \qquad W_X\% = \frac{W_X}{W_X + W_Y} \; 100$$

The percent contents by weight of element Y is, similarly:

$$(8) \qquad W_Y\% = \frac{W_Y}{W_X + W_Y} \; 100$$

Assuming that the characteristic intensity is a linear function of the weight of an element per unit surface of film:

$$(9) \quad W_X = K_X I_X \quad \text{where } I_X = (I_{P+B} - I_B)_X \text{ in film}$$

$$(10) \quad W_Y = K_Y I_Y \quad \text{where } I_Y = (I_{P+B} - I_B)_Y \text{ in film}$$

$I_{P+B} - I_B$ is the difference between the characteristic intensity of the peak plus the background and the characteristic intensity of the background.

Substituting eqs. (9) and (10) into eq. (7) one obtains:

$$(11) \qquad W_X\% = \frac{100}{1 + \dfrac{K_X (I_{P+B} - I_B)_Y}{K_Y (I_{P+B} - I_B)_X}}$$

and a similar expression for $W_Y\%$.

If one wishes to include the amounts of elements X and Y contained in the sample holder and in the X-

ray tube target as impurities, eq. (11) becomes:

$$(12) \qquad W_X\% = \frac{100}{1 + \frac{K_X}{K_Y} \frac{(I_{P+B} - I_B)_{Y\ film} - (I_{P+B} - I_B)_{Y\ holder}}{(I_{P+B} - I_B)_{X\ film} - (I_{P+B} - I_B)_{X\ holder}}}$$

Let:

$$(13) \qquad M_Y = (I_{P+B} - I_B)_{Y\ film} - (I_{P+B} - I_B)_{Y\ holder}$$

$$M_X = (I_{P+B} - I_B)_{X\ film} - (I_{P+B} - I_B)_{X\ holder}$$

eq. (13) becomes:

$$(15) \qquad W_X\% = \frac{100}{1 + \frac{K_X}{K_Y} \frac{M_Y}{M_X}}$$

The absolute statistical error affecting $W_X\%$ will be expressed as a function of the errors affecting the quantities K_X, K_Y, M_Y, M_X. These errors are independent of one another.

From the general rules for combining independent errors, the absolute error on $W_X\%$ is:

$$(16) \qquad S_{abs\ W_X\%} = \left[\left(\frac{W_X\%}{K_X}\right)^2 S^2_{abs\ K_X} + \left(\frac{W_X\%}{K_Y}\right)^2 S^2_{abs\ K_Y} + \left(\frac{W_X\%}{M_Y}\right)^2 S^2_{abs\ M_Y} + \left(\frac{W_X\%}{M_X}\right)^2 S^2_{abs\ M_X}\right]$$

The partial derivatives are:

$$(17) \qquad \frac{\partial W_X}{\partial K_X} = - \frac{M_Y/K_Y M_X}{(1 + K_X\ M_Y/K_Y\ M_X)^2} \quad 100$$

$$(17) \qquad \frac{\partial W_X}{\partial K_Y} = \frac{K_X M_Y / K_Y^2 M_X}{(1 + K_X M_Y / K_Y M_X)^2} \; 100$$

$$(18) \qquad \frac{\partial W_X}{\partial M_Y} = - \frac{K_X / K_Y M_X}{(1 + K_X M_Y / K_Y M_X)^2} \; 100$$

$$\frac{\partial W_X}{\partial M_X} = \frac{K_X M_Y / M_X^2 K_Y}{(1 + K_X M_Y / K_Y M_X)^2} \; 100$$

and the absolute statistical errors on K_X, K_Y, M_Y, M_X are:

$$(19) \qquad S_{abs\ K_X} = S_{rel\ K_X} K_X,$$

$$S_{abs\ K_Y} = S_{rel\ K_Y} K_Y$$

$$(20) \qquad S_{abs\ M_Y} = S_{rel\ M_Y} M_Y,$$

$$S_{abs\ M_X} = S_{rel\ M_X} M_X$$

Substituting (7) through (20) into (16) yields:

$$(21) \qquad S_{abs\ W_X\%} = 100 \frac{K_X M_Y / K_Y M_X}{(1 + K_X M_Y / K_Y M_X)^2} \times \left[S^2_{rel\ K_X} + S^2_{rel\ K_Y} + S^2_{rel\ M_Y} + S^2_{rel\ M_X} \right]^{1/2}$$

From expression (15):

$$(22) \qquad \frac{K_X}{K_Y} \frac{M_Y}{M_X} = \frac{100}{W_X\%} - 1$$

Substituting (22) into (21):

$$S_{abs\ W_X\%} = \frac{W_X\%\ (100 - W_X\%)}{100} \times$$

(23)
$$\times \left[S^2_{rel\ K_X} + S^2_{rel\ K_Y} + S^2_{rel\ M_Y} + S^2_{rel\ M_X} \right]^{1/2}$$

The largest value of the factor in front of the radical in expression (23) is equal to 25, and occurs when $W_X\% = 50$. At fixed values of the relative statistical errors S_{rel}, the largest value of the absolute statistical error for $W_X\%$ is, therefore, obtained at a 50% composition.

3 Determination of Total number of counts for pure calibration samples.

Equation (23) will be used to find $S_{rel\ M_Y}$ and $S_{rel\ M_X}$ assuming a desired $S_{abs\ W_X\%}$ and a 50% composition, and knowing $S_{rel\ K_X}$ and $S_{rel\ K_Y}$ which will now be evaluated.

The quantities K_X and K_Y represent the slopes of straight lines in a plot of characteristic intensity versus film surface density for pure samples of X and Y. These straight lines intersect the axis of ordinates and points representing the background contributions to the recorded characteristic intensities. The equation for element X will be:

(24) $$(I_{P+B})_X = B + K_X W_X$$

Samples of several measured surface densities W_X are evaporated from amounts of pure element X, using the same film mask. The characteristic intensity of these samples is recorded, including the background level, $(I_{P+B})_X$. If k films with different surface densities are considered, the constant K_X is given, using the method of least squares, by the expression:

(25) $$K_X = \frac{k\sum_{n=1}^{k}\left[W_X\,(I_{P+B})_X\right]_n - \sum_{n=1}^{k} W_{X,n} \sum_{n=1}^{k} (I_{P+B})_n}{k\sum_{n=1}^{k} W_{X,n}^2 - (\sum W_{X,n})^2}$$

The coefficient K_Y is obtained in an identical manner. The absolute errors on K_X and K_Y will now be evaluated.

Since K_X and K_Y are obtained by measuring characteristic intensities and surface densities, the absolute errors on K_X and K_Y will depend upon the absolute errors on these two sets of measurements. However, as mentioned earlier, the absolute statistical error on the intensity may be controlled through proper choice of the total number of counts. If such a number is chosen in order to make all the absolute statistical errors on the counting rates the same for all films of the same element, then the absolute statistical error

on K_X or K_Y will depend only on the errors affecting the surface density measurements.

The absolute statistical errors on K_X will then be given by:

$$S_{abs\ K_X} = S_{abs\ (I_{P+B})_X} \left[\frac{k^2}{(k-1)\left[k \sum_{n=1}^{k} (W_X)^2_n - \sum_{n=1}^{k} (W_X)^2_n \right]} \right]^{1/2} \quad (26)$$

with a similar expression for $S_{abs\ K_Y}$.

The choice of the total number of counts for films containing the pure element X is, for example, carried out as follows.

Assume a relative percent error 1% and a 99% confidence level. The total number of counts N_X to be accumulated in recording $(I_{P+B})_X$ is then obtained from:

$$0.33 = 100/(N_X)^{1/2}, \quad N_X = 91{,}809 \text{ counts}$$

$$S_{abs\ (I_{P+B})_X} = \frac{N_X}{t_X} = \frac{(I_{P+B})}{N_X} \quad (27)$$

where t_X is the time recorded to accumulate N_X counts

$$N_X = t_X\ (I_{P+B})_X \quad (28)$$

The counting rates $(I_{P+B})_X$ are first measured approximately by selecting total counts between 10^4 and 10^5, for times not exceeding three minutes in order to

avoid appreciable electronic drift during a measurement.

The film with the smallest surface density is chosen first and, using a total count of $N_X = 91{,}809$, t_X are obtained and used to obtain final counting rates $(I_{P+B})_X$, all having the same $S_{abs\ (I_{P+B})_X}$.

By eq. (26), the value of $S_{abs\ K_X}$ and $S_{abs\ K_Y}$ may now be calculated. The relative statistical error on K_X will then be:

(29) $$S_{rel\ K_X} = S_{abs\ K_X}/K_X$$

with a similar expression for $S_{rel\ K_Y}$.

$S_{rel\ K_X}$ and $S_{rel\ K_Y}$ are now substituted in eq. (23) together with the desired value of the absolute statistical error on the percent contents in weight of element X : $S_{abs\ W_X\%}$.

A value $W_X\%$ is chosen in eq. (23) since this value corresponds to the smallest sum $S^2_{rel\ M_Y} + S^2_{rel\ M_X}$ for given values of $S_{abs\ W_X\%}$, $S_{rel\ K_X}$, $S_{rel\ K_Y}$. If, for simplicity, one assumes to make in eq. (23):

(30) $$S_{rel\ M_X,\ M_Y} = S_{rel\ M_Y} = S_{rel\ M_X}$$

then eq. (23) gives:

$$(31) \qquad S_{rel\ M_X,\ M_Y} = \left\{ \frac{1}{2} \left[\frac{S_{abs}\ W_X\%}{\frac{W_X\%\ (100 - W_X\%)}{100}} \right]^2 - \right.$$

$$\left. - (S_{rel\ K_X})^2 - (S_{rel\ K_Y})^2 \right\}^{1/2}$$

The value of relative statistical errors on M_X and M_Y are now known. The expressions for M_X and M_Y are given by equations (13) and (14) and depend upon the peak and background counting rates for the element X or Y contained in the mixed film and in the holder and target. The pure sample films used for determining K_X and K_Y are now discarded; the ratio K_X/K_Y in eq. (15) for $W_X\%$ is now known and represents the calibration. When a mixed film is analyzed, M_X and M_Y are determined from characteristic intensity measurements whose total counts will now be calculated from $S_{rel\ M_X,\ M_Y}$, as given by eq. (31).

4 Determination of total number of counts for mixed samples.

Given two counting rates $I_{(P+B)}$ and I_B and a limited total time $T = t_{(P+B)} + t_B$ available for their measurement, Mack and Spielberg have shown, using the method of Lagrange Multipliers, that the relative statistical error S_{rel} in the difference of the

counting rates is minimum if the counting times are selected in such a manner as to satisfy the equation:

$$\frac{\partial S_{rel}}{\partial t_{(P+B)}} = \frac{\partial S_{rel}}{\partial t_{(B)}} \qquad (32)$$

The relative error in the difference of the counting rates is expressed by:

$$S_{rel\ P} = \frac{\left[(I_{P+B}\ S_{rel\ (P+B)})^2 + (I_B\ S_{rel\ B})^2\right]^{1/2}}{I_{P+B} - I_B} \qquad (33)$$

The relative error in the two measurements is expressed by:

$$S_{rel\ P+B} = C/(I_{P+B}\ t_{P-B})^{1/2} \qquad (34)$$

$$S_{rel\ P} = C/(I_B\ t_B)^{1/2} \qquad (35)$$

where C is the confidence level desired.

Substituting eqs. (34) and (35) in (33), and differentiating the resulting expression according to (32), yields the following two expressions obtained by Mack and Spielberg:

$$N_{P+B} = \left(\frac{C}{S_{rel}}\right)^2 r^{2/3} \frac{r^{\frac{1}{2}} + 1}{(r-1)^2} \qquad (36)$$

where: $r = \frac{I_{P+B}}{I_B}$

$$N_B = \left(\frac{C}{S_{rel}}\right)^2 \frac{r^{\frac{1}{2}} + 1}{(r-1)^2} \qquad (37)$$

From the knowledge of approximate counting rates and desired values of C and S_{rel}, one obtains values for the total number of counts N_{P+B} and N_B. In order to expedite the calculations, Mack and Spielberg have plotted eqs. (36) and (37) and the resulting procedure is essentially graphical.

In the case in which the samples are so dispersed (thin films with thicknesses between 100 and 1500 Å) as to make traces of elements being detected in the holder and tube target of the same order of magnitude as the amounts of such elements in the sample, eqs. (36) and (37) cannot be applied directly. In the measurements mentioned in the following section, these equations are modified and the resulting procedure follows:

First, the holder with no sample is placed in the fluorescence unit. Using approximate rates of the positions of the peak and of the background, the ratio of the two counting rates is obtained:

(38) $$r_3 = \frac{(I_{P+B})_{X,\ holder}}{(I_B)_{X,\ holder}}$$

and with preset values of C_{holder} and $S_{rel\ holder}$ for elements X or Y, the total number of counts will be given by:

$$(39)\quad N_{(P+B)X,\ holder} = \left(\frac{C_{X,\ holder}}{S_{rel\ X,\ holder}}\right)^2 r_3^{3/2}\ \frac{r_3^{1/2}+1}{r_3-1)^2}$$

$$(40)\quad N_{(B)\ X,\ holder} = \left(\frac{C_{X,\ holder}}{S_{rel\ X,\ holder}}\right)^2 \cdot \frac{r_3^{1/2}+1}{(r_3-1)^2}$$

Using these values of total counts, the counting rates $I_{(P+B)\ X,\ holder}$ and $I_{(B)\ X,\ holder}$ are obtained. The counting rate of the amount of element X in the holder is, then:

$$(41)\quad I_{(P)\ X,\ holder} = I_{P+B)X,\ holder} - I_{(B)X,\ holder}$$

Second, the total counts to be accumulated at the positions of the film intensity peak $I_{(P+B)X,\ film}$ and the background $I_{(B)X,\ film}$ are obtained as a function of a relative error: $S_{rel\ M_X,\ M_Y}$ previously determined, a preset confidence level $C_{X,\ film}$ and ratios r_1 and r_2 defined by:

$$(42)\quad r_1 \triangleq \frac{I_{(P)X,\ film}}{I_{(P)X,\ holder}}$$

$$(43)\quad r_2 \triangleq \frac{(I_{P+B})_{X,\ film}}{(I_B)_{X,\ film}}$$

The expressions of total number of counts for these two intensities are derived as follows.

Using eqs. (36) and (37) the total number of counts for the film in the absence of impurities in the

holder is given by:

$$(44)\quad N_{(P+B)X,\ film} = \left(\frac{C_{X,\ film}}{S_{rel\ X,\ film}}\right)^2 r_2^{3/2}\ \frac{r_2^{1/2}+1}{(r_2-1)^2}$$

$$(45)\quad N_{(B)X,film} = \left(\frac{C_{X,\ film}}{S_{rel\ X,\ film}}\right)^2\ \frac{r_2^{1/2}+1}{(r_2-1)^2}$$

The counting rates due to amounts of element X in the holder and in the film are given by eq. (41) and by:

$$(46)\quad I_{(P)X,\ film} = I_{(P+B)X,\ film} - I_{(B)X,\ film},$$ respectively

The relative statistical error made in measuring the intensity due to the amount of element X in the film alone is:

$$(47)\quad S_{rel\ M_X,\ M_Y} = \frac{\left[(I_{(P)X,film}\ S_{rel\ X,film})^2 + (I_{(P)X,holder}\ S_{rel\ X,hold.})^2\right]^{\frac{1}{2}}}{I_{(P)X,\ film} - I_{(P)X,\ holder}}$$

When:

$$(48)\quad S_{rel\ X,f,h} = S_{rel\ X,\ film} = S_{rel\ X,\ holder},$$

then eq. (43) becomes:

$$(49)\quad S_{rel\ M_X,\ M_Y} = S_{rel\ X,f,h}\ \frac{\left[I^2_{(P)X,\ film} + I^2_{(P)X,\ holder}\right]^{1/2}}{I_{(P)X,\ film} - I_{(P)X,\ holder}}$$

Solving this equation for $S_{rel\ X,\ f,\ h}$ and replacing in (44) where $S_{rel\ X,\ film} = S_{rel\ X,\ f,\ h'}$ according to (48), one obtains:

$$N_{(P+B)X,\ film} = \frac{I^2_{(P)X,\ film} + I^2_{(P)X,\ holder}}{(I_{(P)X,\ film} - I_{(P)X,\ holder})^2} \times$$

(50)

$$\left(\frac{C_{X,\ film}}{S_{rel\ M_X,\ M_Y}}\right)^2 \quad r_2^{3/2} \quad \frac{r_2^{1/2} + 1}{(r_2 - 1)^2}$$

Let:

(51) $$r_1 = \frac{I_{(P)X,\ film}}{I_{(P)X,\ holder}}$$

Then (50) becomes:

$$N_{(P+B)X,\ film} = \frac{r_1^2 + 1}{(r_1 - 1)^2} \quad \frac{r_2^{1/2} + 1}{(r_2 - 1)^2} \times$$

(52)

$$r_2^{3/2} \left(\frac{C_{X,\ film}}{S_{rel\ M_X,\ M_Y}}\right)^2$$

and similarly:

$$N_{(B)X,\ film} = \frac{r_1^2 + 1}{(r_1 - 1)^2} \quad \frac{r_2^{1/2} + 1}{(r_2 - 1)^2} \times$$

(53)

$$\left(\frac{C_{X,\ film}}{S_{rel\ M_X,\ M_Y}}\right)^2$$

The ratios r_1 and r_2 are obtained from approximate counting rates, $C_{X,\ film}$ is the level of confidence desired and $S_{rel}\ M_X,\ M_Y$ was determined previously. The number of counts given by (52) and (53) are used to obtain final counting rates for all mixed composition films, at the position of the peak (Eq. 52) or of the background (Eq. 53). Equations (39) and (40) are used for similar determinations for the contents of X or Y in the holder. The final characteristic intensities for the amounts of X or Y in the holder and in the film are then determined, and the quantities M_X and M_Y given by (13) and (14) to be substituted in Eq. (15) to find the value of $W_X\%$ are now known and will satisfy the preset value of the absolute statistical error on $W_X\%$. The procedure is identical for $W_Y\%$.

The total number of counts given by (39), (40), (52), (53) do not generally correspond to the settings of total counts which may be accumulated by the counter stages on commercially available recorders (Phillips Norelco unit, for example). The closest settings to the computed values are then chosen and the final relative statistical errors on W_X and W_Y are then recomputed, using Eq. (33).

4. Conclusion

The procedure described above for determining the percent chemical composition of thin film by X-ray fluorescence with expected values of relative statistical errors takes into account the effect of impurity contents in the sample holder, the X-ray tube target and surrounding instrumentation. Such effect is important in the analysis of sample with low surface density (from approximately 100 to 1000 Å in thickness). The method assumes that the samples are thin enough that the relationship between the characteristic intensity of an element and the film surface density is linear, within 1%.

A graphical method based on this procedure has been worked out in order to expedite the process of obtaining final compositions with a certain expected statistical error and has been used to analyze the nickel-iron films used in the work reported in this dissertation.

The final counting rates are corrected for drift, as mentioned in the introduction, by use of a standard film whose characteristic intensity is recorded every five minutes. This film is placed permanently in a special holder in order to minimize the placement order.

APPENDIX 16

Description of system for production of thin films by vacuum evaporation

APPENDIX 16

System for production of thin films by vacuum evaporation

The system assembled for producing thin films by vacuum evaporation is shown in Fig. A16. The picture shows:

a. A pair of Helmholtz coils for producing a magnetic field to be used during and after evaporation for magnetic annealing.

b. An eight pol plug for connecting measuring instruments.

c. Two fittings for $\frac{1}{4}$" tubing to provide the installation with circulating water for cooling or for eventual use of RF induction heating.

d. A shutter operated manually through a rotary coupling.

e. A film mask shown on the foreground for evaporating eight films at one time.

f. A sliding shutter operated through a rotary coupling and used to obtain three film thicknesses with one evaporation.

g. A film resistance monitoring slide to provide a rough control of evaporation rate.

A high voltage glow discharge ring located

just under the film holder for further cleaning of the substrate.

i. Two 400 amp couplings for using boats or filaments.

j. Six 75 amp couplings for heating or driving small motors or providing high voltage for evaporation on stressed piezoelectric crystals.

k. A large stainless steel post holding a copper block heated by four 150 watt cartridge heaters. The film holder is fixed to this block and heated by conduction.

The figure also shows the controls for the 400 amp supply, the DC supply and the 75 amp supply. The DC supply was obtained by rectifying the line voltage and filtering in order to obtain a final ripple factor of 0.25%.

The vacuum equipment used provides a vacuum from 10^{-6} to 10^{-7} mm Hg before evaporation and is shown in the lower half of Fig. A16. It consists of a 4" system assembled from standard components purchased separately.

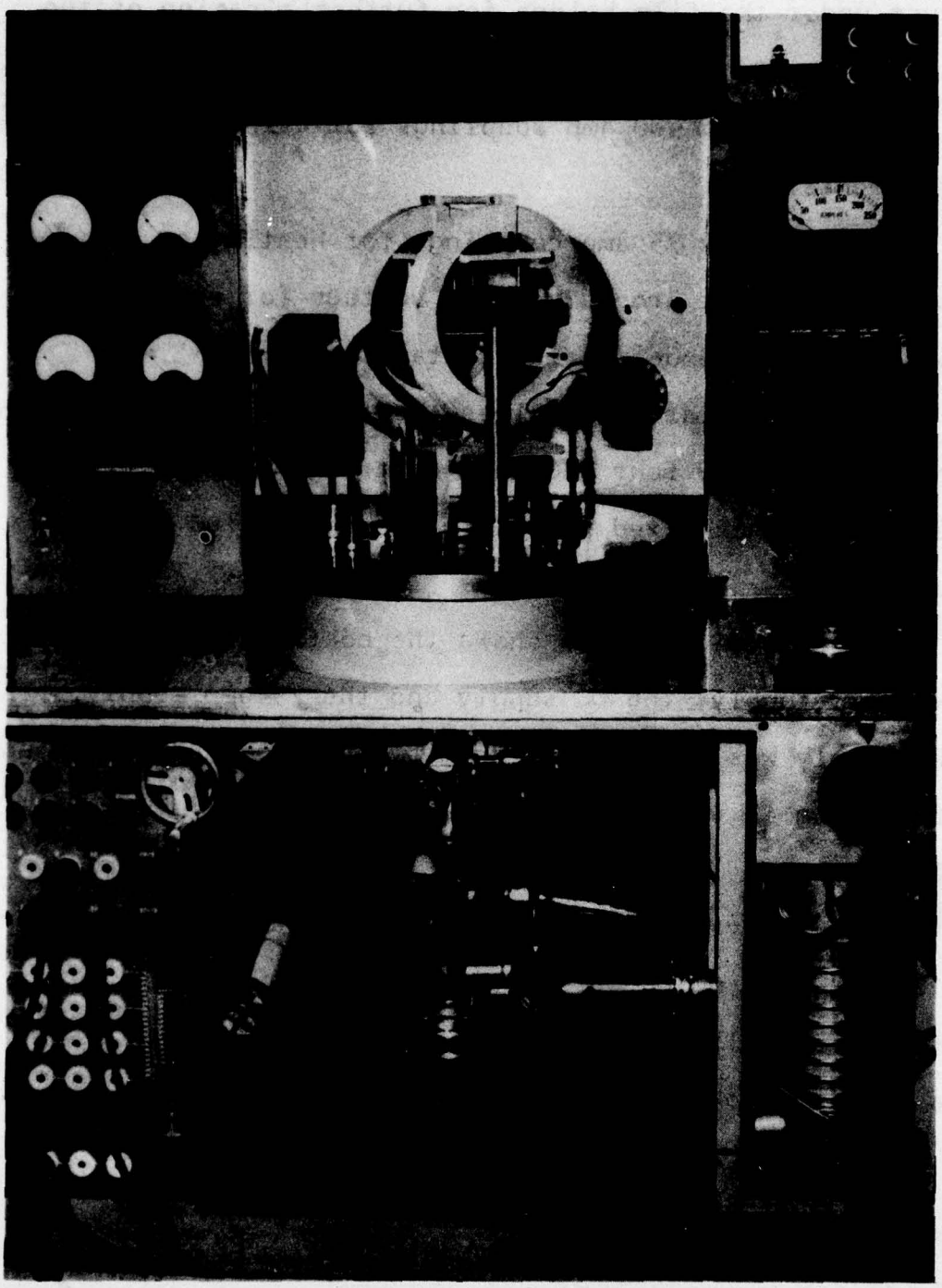


Fig. A16

BIBLIOGRAPHY

1. Joule, J. P. On a new class of magnetic forces. Ann. Electr. Magn. Chem. 8, 1842.

2. Joule, J. P. On the effects of magnetism upon the dimensions of steel bars. Phil. Mag. 30, 76-77, pp. 225-241, 1847.

3. Villari E. Change of magnetization by tensions and by electric current. Ann. Phys. Chem. 126, pp. 87-122, 1865.

4. Bozorth, R. M. et Al. Magnetic properties of metals and alloys. Book published by the American Society of Metals, from a seminar on magnetic properties of metals and alloys, National Metal Congress and Exposition, Cleveland, Oct. 25-26, 1958. Ch. 10 and pp. 246-250.

5. Remington Rand Progress Reports on deposited core matrix, N° 1-10, St. Paul, 1956.

6. Smith, D. O. Static and dynamic behavior of thin permalloy films. J. Appl. Phys. 29, N° 3, March 1958.

7. Olson, C. D. and Pohm, A. V. Flux reversal in thin films of 82% Ni, 18% Fe, J. Appl. Phys. 29, N° 3, March, 1958.

8. Chu, K. and Singer, J. R. Thin film magnetization analysis. Proc. IRE, 47, New York, July 1959.

9. Bradley, E. M., Prutton, M. Rotation and wall motion in thin films of nickel-iron alloys. J. of electronics and control, VI, p. 81, 1959.

10. Bozorth, R. M. Ferromagnetism (book) pp. 476-484, Van Nostrand, 1951.

11. Kittel, C. Physical theory of ferromagnetic domains, Rev. of Mod. Physics, 21, N° 4, Oct. 1949.

12. Kittel C. Theory and structure of ferromagnetic domains in films and small particles. Phys. Review, 70, N° 11-12, Dec. 1946.

13. Prache, P. M. Structures granulaires ferromagnétiques (book) Dunod Editeur, Paris, France, 1957.

14. Bloch, F. On the theory of exchange problems. Z. Physik, 74, p. 295, 1932.

15. Lifshitz, E. On the magnetic structure of iron. J. Phys. USSR 8, p. 337, 1944.

16. Néel, L. Some properties of elementary ferromagnetic domain walls. Cahiers de Physique, 25, p. 1, 1944.

17. Lilley, B. Energies and widths of domain boundaries in ferromagnetics. Phil. Mag. 41, p. 792, 1950.

18. Landau, L. and Lifshitz, E. On the theory of the dispersion of magnetic permeability in ferromagnetic studies. Physik Z. Sowjetunion 8, p. 153, 1935.

19. Gilbert, T. A. Report N° 11 Armour research foundation, Jan. 25, 1935.

20. Weiss, P. Molecular field hypothesis and ferromagnetic properties. J. de Physique et le Radium, 6, p. 661, Dec. 1907.

21. Blois, M. S. Preparation of thin films and their properties. J. Appl. Phys. 26, p. 975, 1955.

22. Van Vleck, J. H. The theory of electric and magnetic susceptibilities (book) Oxford University Press, 1932.

23. Becker, R. and Doring, W. Ferromagnetismus(book) Springer, Berlin, 1939.

24. Vautier, R. Thesis, University of Paris, 1953.

25. MacDonald, J. R. Stress in evaporated ferromagnetic films. Phys. Rev., 106, N° 5, June 1957.

26. Baltzer, P. K. Effective magnetic anisotropy and magnetostriction of monocrystals. Phys. Rev., 108, N° 3, Nov. 1957.

27. Blades, J. D. Stress anisotropy in Ni-Fe thin films, J. Appl. Phys. Suppl. to Vol. 30, N° 4, Apr. 1959, p. 260 S.

28. Conger, R. L. and Essig, F. C. Resonance and reversal phenomenon in ferromagnetic films. Phys. Rev. 104, p. 915, Nov. 1956.

29. Gyorgy, E. M. Flux reversal in soft ferromagnetics. J. Appl. Phys. Suppl. to Vol. 31, N° 5, May 1960.

30. Humphrey, F. B. Transverse flux change in soft ferromagnetics. J. Appl. Phys. 29, N° 4, p. 284, 1958.

31. Kikuchi, R. On the minimum of magnetization reversal time. J. Appl. Phys. 27, Part 2, p. 1352, 1956.

32. Evans, W. R. Control system dynamics (book) McGraw-Hill, 1954, and Spirule Co., Whittier, Calif.

33. Savant, C. J. Jr. Basic Feedback Control System Design (book) McGraw-Hill, p. 114, 1958.

34. Truxal, J. G. Feedback Control System (book) McGraw-Hill, p. 242, 1958.

35. Harloff, N. J. and Kayser, W. Pulse measurements on thin magnetic films. Elektron. Rechenanlagen, 1961, 3, N° 3, pp. 113-118.

36. von W. Kolb Display of critical field characteristics in thin magnetic films. Elektron. Rechenanlagen, 1961, 3, N° 3, pp. 110-113.

37. Tolansky, S. Multiple beam interferometry of surfaces and films (book) 1st Ed. Clarendon Press (Oxford), 1948.

38. Holland L. Vacuum deposition of thin films (book) pp. 224-231, Wiley, 1958.

39. Spain, R. J. and Rubinstein, H. Thin film switching in the hard direction by wall motion. J. Appl. Phys. Suppl. to Vol. 32, N° 3, p. 288S, March 1961.

40. Kriessman, C. J., Belson, H. S. and Edelman, F. H. Anisotropy and coercivity in thin films. J. Appl. Phys. Suppl. to Vol. 30, N° 4, p. 262S, April 1959.

41. Smith, D. O. and Weiss, G. P. Steady-state and pulse measurement techniques for thin magnetic films in the vhf-uhf range. J. Appl. Phys., Vol. 29 N° 3, March 1958.

42. Dijkstra, L. J. and Martius, U. M., Domain pattern in silicon iron under stress, Reviews of Modern Physics, Vol. 25, p. 146, 1956.

43. Neel, L. Remarques sur la theorie des proprietes magnetiques des couches minces et des grains fins. J. Phys. et le Radium, Vol. 17, p. 250, 1956.

44. Bloch, F. Zur Theorie des Austauschproblems und der Remanenzerscheinung der Ferromagnetika. Z. Physik, Vol. 74, p. 295, February 1932.

45. Huber, E. E., Smigh, D. O., Goodenough, J. B. Domain-Wall structure in Permalloy films. J. Appl. Phys. Vol. 29, p. 294, 1958.

46. Smith, D. O. and Harte, K. J. Non-coherent switching in permalloy films. Report N° 53 G-0061, Contract AF 19(604)-7400, M.I.T. Lincoln Laboratory, Lexington, Mass.

47. Fuller, Harrison W. and Rubinstein, Harvey. Observations made on domain walls in thin films. J. Appl. Phys. Suppl. to Vol. 30, N° 4, April 1959.

48. Smith, D. O., Huber, E. E., Cohen, M. S., Weiss, G. P. Anisotropy and inversion in permalloy films. J. Appl. Phys. Suppl. to Vol. 31, N° 5, May 1960.

49. Staudhammer, J. Measurement of magnetostriction, M.S. thesis in Engineering, University of California at Los Angeles, 1956.

50. Smith, D. O., Anisotropy in permalloy films. J. Appl. Phys. Suppl. to Vol. 30, N° 4, pp. 264S-265S, April 1959.

51. Néel, L. Effet des cavités et des inclusions sur le champ coercitif. Cahiers de Physique N° 25, 24 pages, December 1944.

52. Néel, L. Quelques propriétés des parois des domaines élémentaires ferromagnetiques. Cahiers de Physique, N° 25, 20 pages, December 1944.

53. Kersten, M., Zur Theorie der ferromagnetischen Hysterese und der Anfangspermeabilitat. Phys. Z. 1943 Vol.44,p.63, reprinted by J.W.Edwards, Ann Arbor, Mich., 1943.

54. Kittel, C. On the theory of ferromagnetic resonance absorption. Physical Review, January 1948.

55. Landau, L. and Lifshitz, E. On the theory of the dispersion of magnetic permeability in ferromagnetic bodies. Physik. Zeits. Sowjetunion, Vol. 8, 153-169, 1935.

56. Gilbert, T. A. Armour Research Foundation, Report N° 11, January 1955.

57. Polder, D. On the theory of ferromagnetic resonance. Philosophical Magazine, January 1949.

58. Gillette, P. R. and Oshima, K. Magnetization reversal by rotation. J. Appl. Phys. Vol. 29, N° 3, p. 529, March 1958.

59. Anderson, H. H. and Johnson, T. R. Numerical integration of differential equations on the 704 EDPM Technical Report CODE 011.070.592, IBM Poughkeepsie, New York, January 1956.

60. Haynes, M. K. Differential equation solving subroutine group, PK NIDE Report D2, IBM Computing Center, Poughkeepsie, New York, April 2, 1957.

61. Dietrich, W., Proebster, W. E., Wolf, P. Nanosecond switching in thin magnetic films. IBM Journal of Research and Development, p. 189, April 1960.

62. Dietrich, W. Proebster, W. E. Measuring switching speed of magnetic films. Electronics, p. 79, June 3, 1960.

63. Barrett, R. M. Microwave printed circuits, a historical survey. IRE Trans. on Microwave Theory and Techniques, Vol. MTT-3, N° 2, March 1955.

64. Begovitch, Nicholas A. Capacity and characteristic impedance of strip transmission lines with rectangular inner conductors. IRE Trans. on Microwave Theory and Techniques. Vol. MTT-3, N° 2, March 1955.

65. Park, D. Planar transmission lines. IRE Trans. on Microwave Theory and Techniques, Vol. MTT-3, N° 2, March 1955.

66. Hayt, W. H. Jr. Potential solution of a Homogeneous strip line of finite width. IRE Trans. on microwave theory and techniques. Vol. MTT-3, N° 2, March 1955.

67. Ramo, S., Whinnery, J. R. Fields and waves in modern ratio (book) p. 319, Wiley 1953.

68. Packard, S. K. Optimum impedance and dimensions for strip transmission lines. IRE Trans. MTT October 1957.

69. Cohn, S. B. Problems in strip transmission lines. IRE Trans. MTT N° 2, March 1955.

70. Remington Rand Univac, Quarterly Report, Vol. II, 1960. Px 1599-1 Sperry Rand Corp. St. Paul, Minn.

71. International Telegraph and Telephone Co. Reference Data for Radio Engineers (book) p. 591. American Book - Stratford Press, 4th Ed., 1961 printing.

72. Oguey, H. J. Sensitive flux measurements of thin magnetic films. The Review of Scientific Instruments, Vol. 31, N° 7, July 1960.

73. Sweet, L. and Lebowitz, R. A. Measurement of VSWR in coaxial systems PRD Reports, Vol. 7, N° 3, July 1961. PRD Electronics Inc. Inglewood, Calif.

74. General Radio Company. The measurement of cable characteristics. Reprint N.E.-104, West Concord, Mass. February 1958.

75. Winningstad, C. N. Nanosecond pulse measurements. Reprint of 1961 Wescon paper. Tektronix Inc. Box 500, Beaverton, Oregon.

76. Bömmel H. and Dransfeld, K. Excitation of hypersonic waves by ferromagnetic resonance. Phys. Rev. Letters, Vol. 3, N° 2, July 15, 1959.

77. Brown, William Fuller. Magnetic energy formulas and their relation to magnetization theory. Reviews of Modern Physics, Vol. 25, N° 1, January 1953.

78. Brillouin, L. Les tenseurs en mécanique et en Elasticite. (Book) Dover, pp. 11,216-217. 1946.

79. Sokolnikoff, I. S. Mathematical theory of elasticity (Book) McGraw-Hill, p. 43. 1946.

80. Harrington, J. V. On the statics and dynamics of magnetic domain boundaries. Lincoln Laboratory Technical Report N° 166. M.I.T. January 1958.

81. Smith, D. O., Weiss, G. P. Isotropic stress measurements in permalloy films. J. Appl. Phys. Suppl. to Vol. 33, N° 3, March 1962.

82. Rhodin, T. N. Chemical analysis of thin films by X-ray emission spectography, Anal. Chem. 27, 1857 (1955).

83. Liebhafsky and Zemany, Film Thickness by X-Ray Emission Spectography, Anal. Chem. Vol. 28, p. 455.

84. Liebhafsky, Pfeiffer, Winslow, Zemany, X-ray absorption and emission in analytical chemistry (book) pp. 153-158, Wiley, 1960.

85. Beers, Y. Introduction to the theory of error, pp. 48-49. Addison Wesley, 1953-1957.

86. Parrish, W. X-ray intensity measurements with counter tubes. Philips Technical Rev. 1956, 17, 206.

87. Mack, M. and Spielberg, Statistical factors in X-ray intensity measurements. Spectrochimica Acta, Vol. 12, pp. 169-178, 1958.

88. Hoel, P. G. Introduction to Mathematical statistics Book), pp. 32, 130, Wiley, 1947.

89. Mason, W. P. Piezoelectric crystals and their applications to ultrasonics (Book) Van Nostrand, 1950.

90. Mason, W. P. Physical acoustics and the properties of solids (Book) Van Nostrand, 1958.

91. Katz, H. W. Solid state magnetic and dielectric devices (Book) Wiley, 1959.

92. Cady, W. G. Piezoelectricity (Book) McGraw-Hill, 1946.

93. Piezotronic Technical Data, p. 17, Brush Electronics Company, Cleveland, Ohio.

94. Haskins, J. F. and Walsh, J. L. Vibrations of ferroelectric cylindrical shells with transverse isotropy. I) Radially Polarized case. J. Acoust. Soc. Am. Vol. 29, N° 6, p. 729, July 1957.

95. Petermann, L. A. Producing motion with magnetostrictive and piezoelectric transducers. Electrical Manufacturing. p. 99, December 1955.

96. Timoshenko, S. Strength of Materials, Part I (book) II ed., 1949, pp. 217-219.

97. Bogue Electric Manufacturing Co. Internal memorandum A-39543, electrical test procedure for ceramic transducers (crystals). July 1959, Paterson, N.J.

98. Clevite Electronic Components Division Modern piezoelectric ceramics, Bulletin N° 9244. Clevite Corp. Cleveland, Ohio.

99. Clevite Electronic Research Div. PZT-5 Specifications based on laboratory experience, Internal memorandum April 27, 1959, Clevite Corp., Cleveland, Ohio.

100. Solar Manufacturing Corp. Piezoelectric ceramic crystals, Bulletin N° PL-55160, Los Angeles, Calif.

101. Williams, H. J., R. N. Bozorth, W. Shockley, magnetic domains in single crystals of silicon iron, Phys. Reviews Vol. 75, N° 1, p. 55, Jan. 1, 1949.